ELECTRONIC STRUCTURE OF MOLECULES: STUDIES BY PHOTOELECTRON SPECTROSCOPY AND AB INITIO CALCULATIONS

by

Isobel Simpson

Thesis Presented for the
Degree of Doctor of Philosophy

University of Edinburgh

October 1980

For

my Mum, Brother and Percy Browne

Acknowledgements

I would like to express my grateful thanks to Dr. Michael Palmer for his guidance, help, encouragement and friendship during the course of this study.

In addition I would also like to thank Dr. Ian Gosney and his research group, expecially Alan Aitken, for providing samples for part of my experimental work, and Mrs. Jane Gorrie for her skill and patience in typing this manuscript.

Postgraduate Courses Attended

1.	Scientific German	(2 units)	German Department
2.	Molecular Spectroscopy	(2 units)	Dr. S. Cradock and Dr. D. Rankin
3.	Flash Vacuum Pyrolysis	(1 unit)	Dr. H. McNab
4.	Colloids	(1 unit)	Dr. D. Cooper
5.	The Chemistry of Dyes	(1 unit)	ICI Organic Division - a departmental symposium
6.	Introduction to Fortran	(1 unit)	Dr. C.N.M. Pounder
7.	Neutron Diffraction	(1 unit)	Dr. G.S. Pawley - a departmental symposium

"The principle of science, the definition almost, is the following:

The test of all knowledge is experiment. Experiment is the sole judge of scientific "truth". But what is the source of knowledge? Where do the laws that are to be tested come from? Experiment, itself, helps to produce these laws, in the sense that it gives us hints. But also needed is imagination to create from these hints the great generalizations - to guess at the wonderful, simple, but very strange patterns beneath them all, and then to experiment to check again to see whether we have made the right guess."

Feynmann

Abstract

The electronic structures of several series of molecules, mainly nitrogen heterocycles, have been investigated by Photoelectron Spectroscopy and ab initio calculations.

Calculations of the molecular electronic ground states have been used for interpretation of experimental nuclear quadrupole coupling data for the 5-membered ring azoles and their N-methyl derivatives. Photoelectron spectroscopy has been used to investigate vapour phase tautomerism of the triazoles and tetrazoles, and He(I) and He(II) photoelectron spectra for the complete azole and N-methyl azole series have been assigned.

Ab initio calculations, using both minimal basis and double zeta basis sets, for the ground states of the azines, naphthalene and the mono- and di-azanaphthalenes have been performed both to investigate the effect of aza substitution in the cyclic system and as an aid to assignment of the He(I) and He(II) photoelectron spectra. Unrestricted Hartree Fock (UHF) open shell calculations for the radical anions of the complete molecular series, and cations of the azines, have been performed to investigate the effect of the size of basis set used on the UHF wavefunction, and for interpretation and assignment of data from electron spin resonance spectroscopic studies.

Photoelectron spectroscopic studies have been performed on a series of bicyclic alkenes to interpret the observed reactiviti of the ethylenic group. Similar experimental studies have been used to interpret and predict (where data is lacking) possible molecular conformations and reactivities of a series of unusual bridged ring dienes.

CONTENTS

CHAPTER 1

(i) THE THEORETICAL METHOD - Ab Initio Calculations

Historical Background

In 1900 Max Planck presented at a meeting of the German Physical Society an empirical formula which attempted to bridge the gap between the Rayleigh-Jeans law and Wein's law of blackbody radiation. The former described the connection between wavelength and intensity correctly at long wavelength, the latter gave a correct description in the limit of short wavelengths. Planck's formula, which was a purely empirical interpolation formula between two well-known laws, fitted the precise measurements that were then available with great accuracy. This inspired Planck to search for a rigorous derivation of his formula.[1]

And "after a few weeks of the most strenuous work of [his] life, the darkness lifted and an unexpected vista began to appear..." This happened, however not until he had been forced to "...an act of desperation."

The act of desperation was the assumption that an oscillator could absorb and emit energy only in the form of quanta of energy $E = h\nu$. Planck's revolutionary assumption was ignored by most physicists and even attacked by some, even Planck himself spent the following 15 years trying to derive his results without assuming the quantization of the oscillators. He concluded "...that the elementary quantum of action played a far more significant part in physics than (he) had initially been inclined to suspect..."

Albert Einstein, in 1905 realised the sweeping significance of the assumption that Planck had made so reluctantly. He concluded[2] that Planck's "... determination of the quantum is to a certain degree independent of his theory of Blackbody

radiation..." He then showed that Planck's "light quantum hypothesis" if generalised by assuming that all light can be emitted or absorbed only in the form of quanta of the energy

$$E = h\nu$$

explained not only Stokes law of fluorescence but also Lenard's recent measurements of the photoeffect. Einstein's equation $E = h\nu$ of course specifies only that light cannot be emitted continuously. It was not initially interpreted as meaning that light quanta are discrete particles that are emitted in a well-defined direction. This final conclusion was drawn by Einstein in 1909.

The notion that atoms are the building blocks of all matter had been firmly established during the nineteenth century; however the structure of the atoms remained a complete mystery. Without any notion of atomic structure, it was of course impossible to apply the new quantum hypothesis to the Atom - its proper realm. The situation suddenly changed in 1911 when Rutherford[3] discovered that all the positive charge and almost all the mass of an atom are concentrated in an extremely small nucleus surrounded by an almost massless negative cloud. In 1912 a young Danish physicist Niels Bohr met Rutherford and one year later he had abstracted from Rutherford's discovery a theory of the structure of the hydrogen atom.[4] Bohr's model of the hydrogen atom had the electron circle the nucleus in allowed orbits whose angular momenta were quantized. The energy difference between two orbits was to be equal to the energy of the photon emitted in the transition of an electron from one orbit to another.

During the next ten years Bohr's theory was generalised and refined and by 1923 it had been formed into what is now known as the old quantum theory. This theory was capable of explaining most of the observed features of atomic spectra qualitatively - some quantitatively, but it was obvious this was not the whole story.

The next hurdle was overcome by Prince Louis de Broglie[5] who proposed, based on relativistic considerations, that particles should be assigned a wavelength

$$h = \frac{\lambda}{p}$$

known as the de Broglie wavelength. This sparked an explosive development in the field. In July 1925, Werner Heisenberg[6] published a paper entitled "Über die quanten theoretische Undeutung Kinenatischer und mechanischer Beziehungen" (on the quantum theoretical representation of kinematical and mechanical relations).

In this paper he proposed a quantum theory that did away with all such classical concepts as velocity and location of electrons in an atom that could not be measured in any conceivable way, and replaced them with relations between observable quantities. The algebraic rules that connected the observables Heisenberg invented as he went along - these were shown by Born and Jordan[7] to be the rules of matrix algebra.

In January 1926 Erwin Schroedinger[8] introduced his postulates for the transition from classical mechanics to quantum mechanics, and derived the Schroedinger equation of the hydrogen atom. In March 1926 Schroedinger[9] showed the equivalence of his theory and Heisenberg's matrix mechanics.

In January 1928 Paul Adrienne Mainie Dirac at Cambridge published[10] "The Quantum Theory of the Electron" which reconciled quantum mechanics with the special theory of relativity. He effectively put the finishing touches to an intellectual monolith that had taken less than three years to be constructed, and provides the foundation of our understanding of the electronic structure of atoms and molecules.

(ii) Quantum Chemical Calculations

The major application of quantum mechanics in chemistry has been the attempt to calculate molecular energies, geometries and accurate molecular wavefunctions. Early calculations, which were restricted to H, H_2^+ and H_2 met with considerable success and provided a basis for the qualitative understanding of the electronic structure of molecules.

The classical equation of motion of a particle in a potential is

$$E = \frac{p^2}{2m} + V(\underline{r}) \qquad (1)$$

If we change this equation into an operator equation by replacing E by $i\hbar(\partial/\partial t)$ and replacing p by operator $-i\hbar\nabla$ and applying the resulting operator equation to a wave function and solve for it, we obtain the Schrödinger equation:

$$i\hbar \frac{\partial \Psi}{\partial t} = -\frac{\hbar^2}{2m} \nabla^2 \Psi + V(C)\Psi \qquad (2)$$

In the case of the hydrogen atom, the potential energy is given by Coulomb's law:

$$V(\underline{r}) = V(r) = -\frac{e^2}{r} \qquad (3)$$

Substituting this into (2) gives

$$i\hbar \frac{\partial \Psi}{\partial t} = -\frac{\hbar^2}{2m} \nabla^2 \Psi - \frac{e^2 \Psi}{r} \qquad (4)$$

This is the famous Schroedinger equation of the hydrogen atom which, when solved, gives complete agreement between experimental values for energy levels of H atom and values calculated using (4).

The application of the same procedure to other systems also leads to agreement with the experimental results and the Schroedinger postulates are the key to a complete description of quantum phenomena if:

a) we can overcome the mathematical difficulties involved in solving the Schroedinger equation,

b) we know the force law applicable to the situation.

For more than 2 particles, the mathematical difficulties are often considerable, just as in the case of a classical many-body problem. There exist, however, very powerful approximate methods for dealing with more complicated problems.

Equation (2) is a partial differential equation and can be solved by writing the wave function as a product of a function $u(r)$ which depends only on $\underline{r}$, and $\varphi(t)$ which depends only on t.

$$\Psi(\underline{r},t) = \varphi(t)\, u(\underline{r})$$

hence

$$i\hbar u(\underline{r}) \frac{\partial \varphi}{\partial t} = -\frac{\hbar^2}{2m} \varphi(t)\, \nabla^2 u(\underline{r}) + V(\underline{r})\, \varphi(t)\, u(\underline{r}) \qquad (5)$$

$\therefore$ ÷ by $\Psi(\underline{r},t)$ to obtain

$$\frac{i\hbar}{\varphi(t)} \frac{d\varphi}{\partial t} = -\frac{\hbar^2}{2mu(\underline{r})} \nabla^2 u(\underline{r}) + V(\underline{r}) \qquad (6)$$

since the left side of this equation does not depend on $\underline{r}$,

and the right side does not depend on t, both sides must be equal to the same constant.

Hence

$$\frac{i\hbar\partial\varphi}{\varphi\,\partial t} = E \text{ or, } \varphi = u_o e^{-iE\,t/\hbar} \tag{7}$$

and

$$Eu(\underline{r}) = -\frac{\hbar^2}{2m}\nabla^2 u(\underline{r}) + V(\underline{r})u(\underline{r}) \tag{8}$$

(8) is usually called the time independent Schroedinger equation. Obviously the separation cannot be carried out if V is time dependent. Since $Et/\hbar$ in equation (7) must be dimensionless E must have the dimension of energy $w = E/h$ = frequency, and as E is constant, w is constant.

$$\therefore \Psi(\underline{r},t) = \varphi(t)u(\underline{r}) = e^{-iwt}\,u(\underline{r}) \tag{9}$$

This is a wave function which describes a monochromatic standing wave whose amplitude u is a function of r.

The Schroedinger equation is a homogeneous differential equation and leaves a constant factor in its solutions undetermined. The normalisation of the wavefunction $\int u^*(r)u(r)d\tau = 1$ allows us to determine this factor and to calculate the absolute probability densities.

The time independent Schroedinger equation

$$Eu = -\frac{\hbar^2}{2m}\nabla^2 u + Vu \tag{10}$$

is often written as an operator equation

$$Eu = \left(-\frac{\hbar^2}{2m}\nabla^2 + V\right)u = Au \tag{11}$$

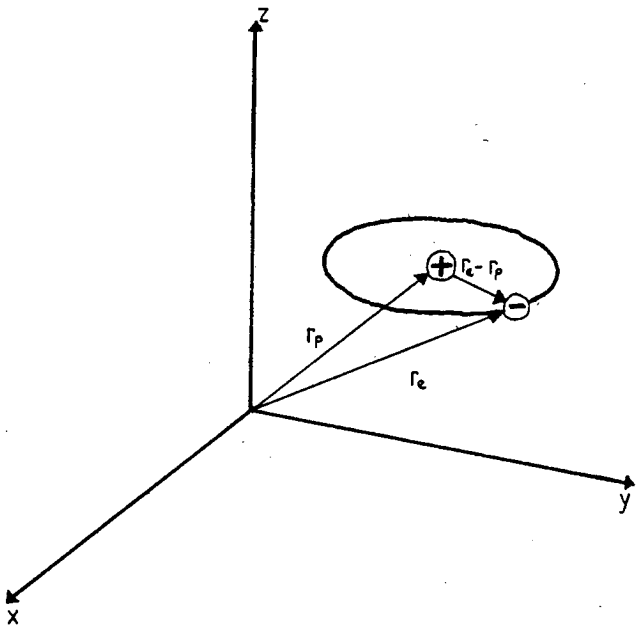

FIG 1 CLASSICAL PICTURE OF A HYDROGEN ATOM AS DESCRIBED IN A CARTESIAN COORDINATE SYSTEM

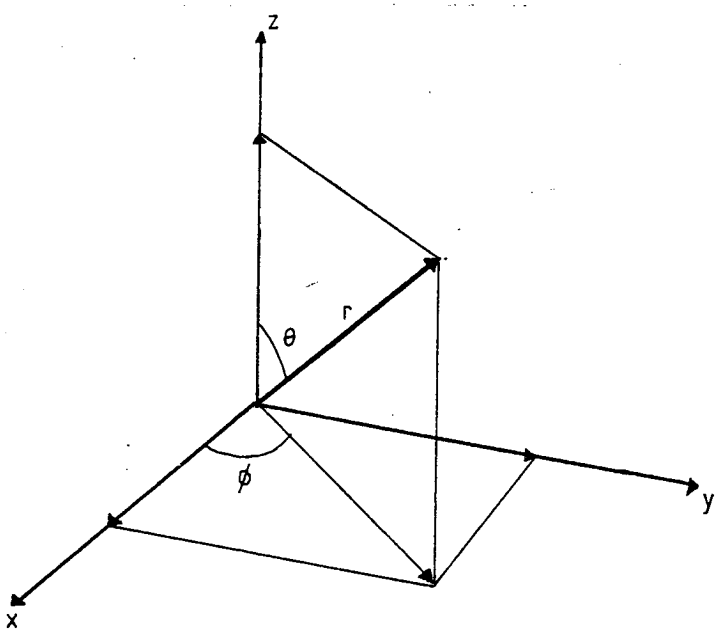

FIG 2 SPHERICAL POLAR COORDINATES

The operator

$$H = -\frac{\hbar^2}{2m}\nabla^2 + V \qquad (12)$$

is called the Hamiltonian operator or the Hamiltonian. The eigenvalues E of the Hamiltonian are the possible energy values of the system.

(iii) The Hydrogen Atom

A hydrogen atom consists of a proton and electron held together by electrostatic attraction. Classical physics would give the energy of the system as:

$$E = \frac{\underline{p}_e^2}{2m_e} + \frac{\underline{p}_p^2}{2m_p} - \frac{e^2}{|\underline{r}_e - \underline{r}_p|} \qquad (13)$$

See Figure 1

total energy = kinetic energy of electron + kinetic energy of proton + potential energy of proton and electron due to their mutual coulomb attraction

$\underline{p}_e$ = momentum of electron $\quad$ $\underline{p}_p$ = momentum of proton

m_e = electron mass $\quad$ m_p = proton mass

$|\underline{r}_e - \underline{r}_p|$ = distance between electron + proton

From this the following Hamiltonians are obtained.

$$H = -\frac{\hbar^2}{2m_e}\nabla e^2 - \frac{\hbar^2}{2m_p}\nabla p^2 - \frac{e^2}{\underline{r}_e - \underline{r}_p} \qquad (14)$$

The operator ∇e^2 operates only on the electron coordinates; the operator ∇p^2 operates only on the proton coordinates.

This Hamiltonian describes the system completely. It describes not only the behaviour of the electron and proton

due to the coulomb interaction but also any motion the atom as a whole might make. This unnecessary information can be removed by transforming to a centre-of-mass coordinate system. Whence the Hamiltonian becomes

$$H = -\frac{\hbar^2}{2m_e}\left(\frac{m}{m_p}\nabla_R + \nabla\right)^2 - \frac{\hbar^2}{2m_p}\left(\frac{m}{m_e}\nabla_R - \right)^2 - \frac{e^2}{r} \qquad (15)$$

$$m = \frac{m_e m_p}{m_e + m_p}\ ;\ \nabla_e = \frac{m}{m_p}\nabla_R + \nabla ; \nabla_p = \frac{m}{m_e}\nabla_R - \nabla$$

∇_R operates only on the coordinates of the centre of mass, and $\underline{R}$ the coordinate vector of centre of mass,

$$\underline{R} = \begin{pmatrix} X \\ Y \\ Z \end{pmatrix} = \frac{m_e \underline{r}_e + m_p \underline{r}_p}{m_e + m_p}$$

(15) is an operator equation hence

$$H = -\frac{\hbar^2}{2m_e}\left[\frac{m^2}{m_p^2}\nabla_R^2 + \frac{m}{m_p}(\nabla_R\nabla - \nabla\nabla_R) + \nabla^2\right] \qquad (16)$$

$$-\frac{\hbar^2}{2m_p}\left[\frac{m^2}{m_e}\nabla^2_R - \frac{m}{m_e}(\nabla_R\nabla - \nabla_R\nabla_R) + \nabla^2\right] - \frac{e^2}{r}$$

or $$H = -\frac{\hbar^2}{2(m_e+m_p)}\nabla^2_R - \frac{h^2}{2m}\nabla^2 - \frac{e^2}{r} \qquad (17)$$

This Hamiltonian is the sum of 2 parts, one depending on R only and the other on r only. As this is so we can separate the Schrödinger equation by substituting

$$\psi(r,R) = \Phi(R)u(r) \qquad (18)$$

into equation (18) into (17) we obtain

$$-\frac{\hbar^2}{2(m_e+m_p)}u\nabla^2_R\Phi - \frac{\hbar^2}{2m}\Phi\nabla^2 u - \frac{e^2}{r}u\Phi = Etu\Phi \qquad (19)$$

dividing through by $u\Phi$ gives

$$-\frac{\hbar^2}{2(m_e+m_p)}\nabla^2_R\Phi - \frac{\hbar^2}{2mu}\nabla^2_u - \frac{e^2}{r} = Et \tag{20}$$

$$-\frac{\hbar^2}{2(m_e+m_p)\Phi}\nabla^2_R\Phi = Ec = \frac{\hbar^2}{2mu}\nabla^2_u - \frac{e^2}{r} + Et \tag{21}$$

$$-\frac{\hbar^2}{2(m_e+m_p)}\nabla^2_R\Phi = Ec\Phi \tag{22}$$

using $E = Et - Ec$ (23)

$$-\frac{\hbar^2}{2m}\nabla^2_u - \frac{e^2u}{r} = Eu \tag{24}$$

The solution of (22) is a plane wave describing whatever motion the centre of mass (i.e. the atom as a whole) makes. Equation (24) is the Schrödinger equation of a particle moving in a fixed potential.

(iv) Separation of the Schrödinger equation in Spherical Polar Coordinates

Since the potential of the hydrogen atom has spherical symmetry it is appropriate to transform to spherical polar coordinates before attempting a solution. The coordinate system used is shown below, see also Figure 2.

now $\nabla^2 = \frac{\partial^2}{\partial x^2} + \frac{\partial^2}{\partial y^2} + \frac{\partial^2}{\partial z^2}$ becomes in spherical polar coords

$$\nabla^2 = \frac{1}{r^2}\frac{\partial}{\partial r}\left(r^2\frac{\partial}{\partial r}\right) + \frac{1}{r^2\sin\theta}\frac{\partial}{\partial\theta}\left(\sin\theta\frac{\partial}{\partial\theta}\right) + \frac{1}{r^2\sin^2\theta}\frac{\partial^2}{\partial\phi^2} \tag{25}$$

substituting into (24) yields

$$\frac{1}{r^2}\frac{\partial}{\partial r}\left(r^2\frac{\partial u}{\partial r}\right)+\frac{1}{r^2\sin\theta}\frac{\partial}{\partial\theta}\left(\sin\theta\frac{\partial u}{\partial\theta}\right)$$

$$+\frac{1}{r^2\sin^2\theta}\frac{\partial^2 u}{\partial\phi^2}+\frac{2m}{\hbar^2}\left(\frac{e^2}{r}+E\right)u=0 \qquad (26)$$

substituting

$$u(r) = X(r)\,Y(\theta,\phi)$$

$$Y\frac{\partial}{\partial r}\left(r^2\frac{\partial X}{\partial r}\right)+\frac{X}{\sin\theta}\frac{\partial}{\partial\theta}\left(\sin\theta\frac{\partial Y}{\partial\theta}\right)+\frac{X}{\sin^2\theta}\frac{\partial^2 Y}{\partial\phi^2}$$

$$+\frac{2mr^2}{\hbar^2}\left(\frac{e^2}{r}+E\right)XY=0 \qquad (27)$$

dividing by XY this separates into an r dependent equation and a θ and ϕ dependent equation.

$$\frac{d}{dr}\left(r^2\frac{dX}{dr}\right)+\frac{2mr^2}{\hbar^2}\left(\frac{c^2}{r}+E\right)X=AX \qquad (28)$$

and

$$\frac{1}{\sin\theta}\frac{\partial}{\partial\theta}\left(\sin\theta\frac{\partial Y}{\partial\theta}\right)+\frac{1}{\sin^2\theta}\frac{\partial^2}{\partial\phi^2}Y=-AY \qquad (29)$$

As (29) is independent of the total energy E and the potential energy V except through the separation constant A, (29) is valid for any central potential V = V(r), and any value of the total energy. Considering the angular part of the Schroedinger equation if we separate $Y(\theta,\varphi)$ into

$$Y(\theta,\varphi) = P(\theta)\phi(\varphi)$$

then the result is

$$\frac{\sin\theta}{P} \frac{\partial}{\partial\theta} (\sin\theta \frac{\partial P}{\partial\theta}) + A \sin^2\theta = -\frac{1}{\phi} \frac{\partial^2\phi}{\partial\varphi^2} \tag{30}$$

By convention the separation constant is named m^2, hence

$$\sin\theta \frac{d}{d\theta} (\sin\theta \frac{dp}{d\theta}) + AP \sin^2\theta = m^2 P \tag{31}$$

$$-m^2\phi = \frac{d^2\phi}{d\varphi^2} \tag{32}$$

Equation (32) can be integrated immediately to yield

$$\phi = \phi_o e^{\pm im\varphi}$$

where m is an integer. The integer m is called the magnetic quantum number.

Solving (31) using the substitutions

$$\xi = \cos\theta \frac{d}{d\theta} = -\sin\theta \frac{d}{d\xi}$$

yields

$$(1-\xi^2) \frac{d}{d\xi} ((1-\xi^2) \frac{dp}{d\xi}) + A(1-\xi^2)P = m^2 P$$

which is known as the associated Legendre equation, its solutions being the associated Legendre functions.

$$P_l^m = (\xi^2-1)^{m/2} \frac{d^m P_l}{d\xi^m}$$

m,l integers $m \leq l$

we can therefore state that the angular part of the Schrödinger equation for any potential depending only on the

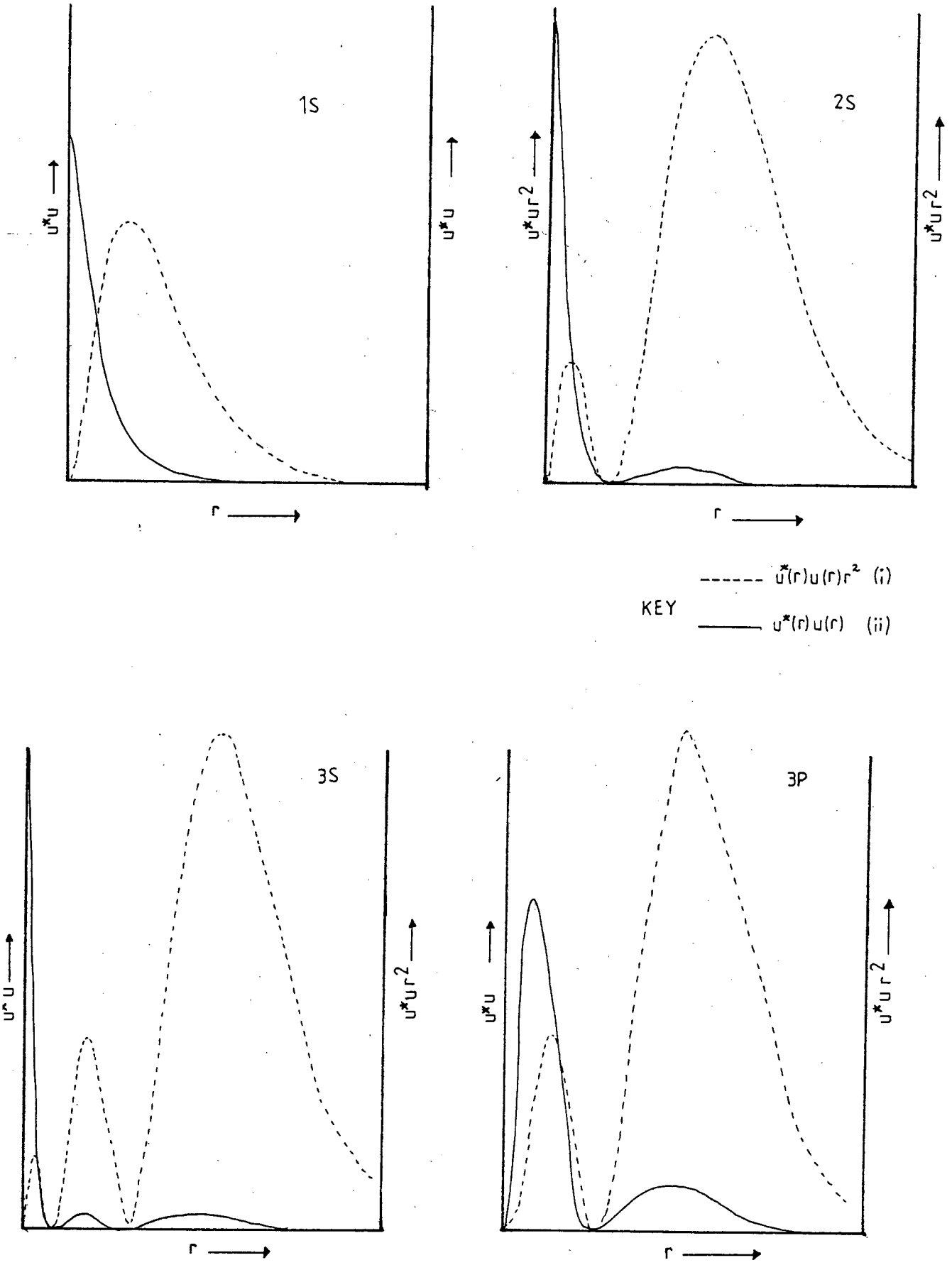

FIG 3 THE PROBABILITY(i) AND PROBABILITY DENSITY (ii) OF THE ELECTRON IN THE HYDROGEN ATOM AS A FUNCTION OF THE RADIUS, r.

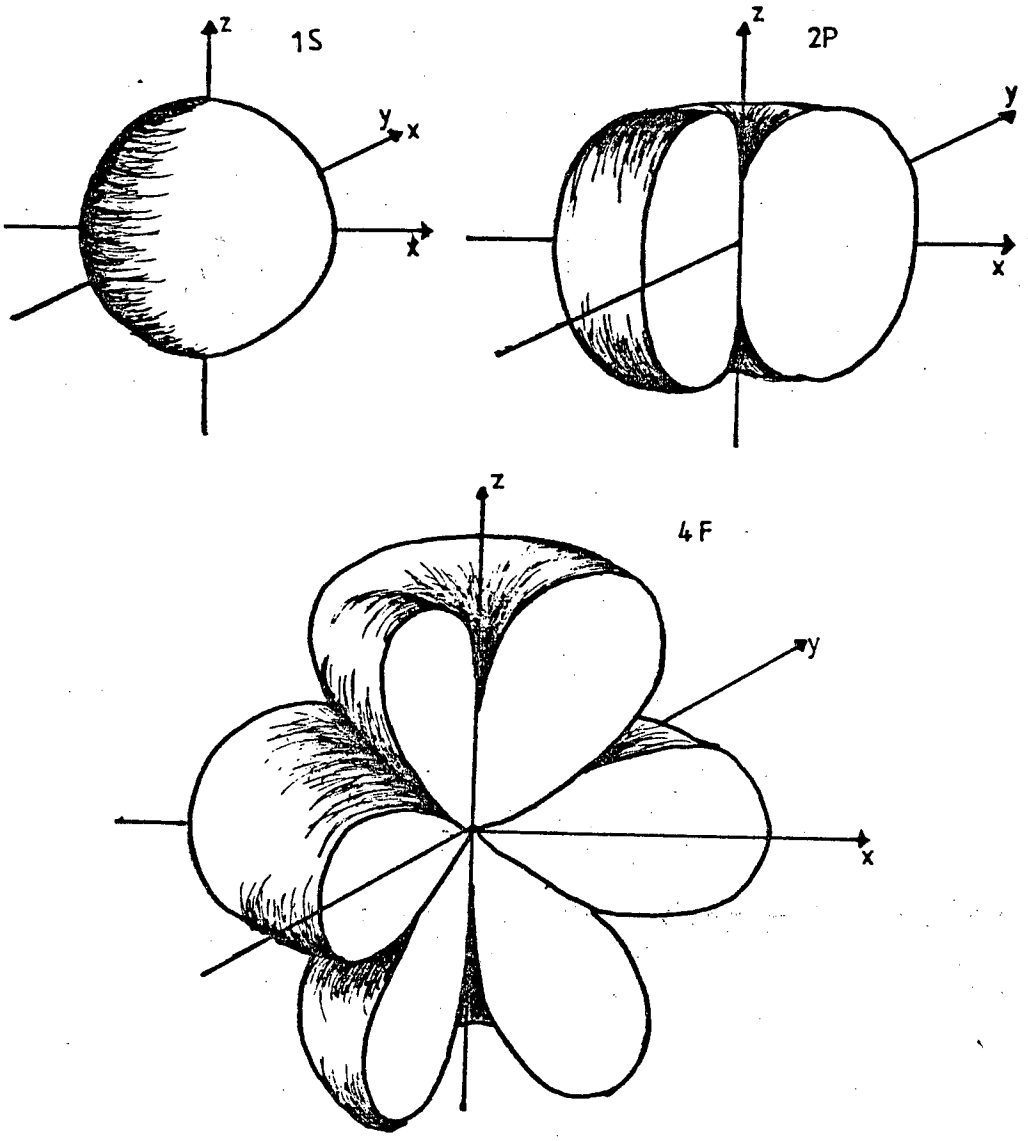

FIG 4 SPATIAL DISTRIBUTION OF THE ELECTRON PROBABILITY DENSITY U^*U IN A HYDROGEN ATOM.

magnitude of r is solved by the spherical Harmonics

$$Y_{lm} = N_{lm}\, e^{\pm im\varphi}\, P_l^{\,m}(\theta)$$

Nlm are normalization constants. Solution of the radial part of the Schroedinger equation yields

$$E = -\frac{me^4}{2n^2\hbar^2}$$

where n is the principal quantum number. Therefore the energy difference between two different states En_2, En_1 is given by

$$En_2 - En_1 = \frac{me^4}{2\hbar^2}\left(\frac{1}{n_1^{\,2}} - \frac{1}{n_2^{\,2}}\right)$$

This is the famous Rydberg formula for the spectral lines emitted by a hydrogen atom. Thus we have the following picture: The eigenfunctions of the hydrogen atom are

$$u_{nlm} = \frac{1}{r}\exp[-(me^2/n\hbar^2)r]\sum_{o}^{n} Ck\, r^k Y_{lm}$$

where Y_{lm} are the spherical harmonics.
Table 1 lists the complete hydrogen eigenfunctions $u(r,\theta,\varphi)$ for the four lowest values of n. The normalization constants have been determined such that $\int u^* u d\tau = 1$

Figure 3 shows the probability density $u^*(r)u(r)r^2$ and the probability density $u^*(r)u(r)$ of the electron in a hydrogen atom as a function of the radius. See also Figure 4.

TABLE 1 HYDROGEN EIGENFUNCTIONS

State	n	l	m	u
$1s$	1	0	0	$A_n e^{-x}$
$2s$	2	0	0	$A_n e^{-x}(1-x)$
$2p$	2	1	0	$A_n e^{-x} x \cos\vartheta$
$2p$	2	1	± 1	$A_n \frac{e^{-x}}{\sqrt{2}} x \sin\vartheta e^{\pm i\varphi}$
$3s$	3	0	0	$A_n e^{-x}\left(1-2x+\frac{2x^2}{3}\right)$
$3p$	3	1	0	$A_n e^{-x}\sqrt{\frac{2}{3}} x(2-x)\cos\vartheta$
$3p$	3	1	± 1	$A_n e^{-x}\frac{1}{\sqrt{3}} x(2-x)\sin\vartheta e^{\pm i\varphi}$
$3d$	3	2	0	$A_n e^{-x}\frac{1}{3\sqrt{2}} x^2(3\cos^2\vartheta-1)$
$3d$	3	2	± 1	$A_n e^{-x}\frac{x^2}{\sqrt{3}}\sin\vartheta\cos\vartheta e^{\pm i\varphi}$
$3d$	3	2	± 2	$A_n e^{-x}\frac{1}{2\sqrt{3}} x^2\sin^2\vartheta e^{\pm 2i\varphi}$
$4s$	4	0	0	$A_n e^{-x}\left(1-3x+2x^2-\frac{x^3}{3}\right)$
$4p$	4	1	0	$A_n e^{-x}\sqrt{5}x\left(1-x+\frac{x^2}{5}\right)\cos\vartheta$
$4p$	4	1	± 1	$A_n e^{-x}\sqrt{\frac{5}{2}} x\left(1-x+\frac{x^2}{5}\right)\sin\vartheta e^{\pm i\varphi}$
$4d$	4	2	0	$A_n e^{-x}\frac{1}{2} x^2\left(1-\frac{x}{3}\right)(3\cos^2\vartheta-1)$
$4d$	4	2	± 1	$A_n e^{-x}\sqrt{\frac{3}{2}} x^2\left(1-\frac{x}{3}\right)\sin\vartheta\cos\vartheta e^{\pm i\varphi}$
$4d$	4	2	± 2	$A_n e^{-x}\sqrt{\frac{3}{8}} x^2\left(1-\frac{x}{3}\right)\sin^2\vartheta e^{\pm 2i\varphi}$
$4f$	4	3	0	$A_n e^{-x}\frac{1}{6\sqrt{5}} x^3\cos\vartheta\,(5\cos^2\vartheta-3)$
$4f$	4	3	± 1	$A_n e^{-x}\frac{1}{6}\sqrt{\frac{3}{20}} x^3\sin\vartheta\,(5\cos^2\vartheta-1)e^{\pm i\varphi}$
$4f$	4	3	± 2	$A_n e^{-x}\frac{\sqrt{3}x^3}{6\sqrt{2}}\sin^2\vartheta\cos\vartheta e^{\pm 2i\varphi}$
$4f$	4	3	± 3	$A_n e^{-x}\frac{1}{18} x^3\sin^3\vartheta e^{\pm 3i\varphi}$

$x = \frac{rmc^2}{n\hbar^2}$

$A_n = \frac{1}{\sqrt{\pi}}\left(\frac{mc^2}{n\hbar^2}\right)^{3/4}$

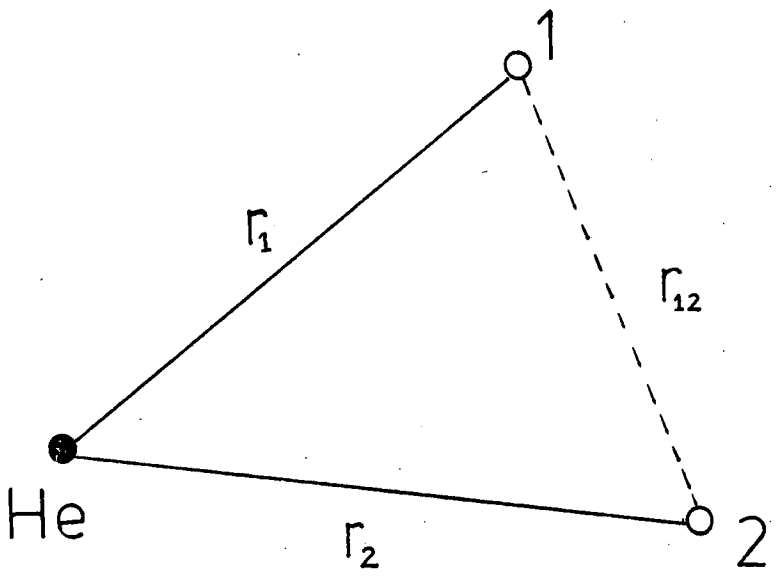

Fig 5a. Distances involved in Hamiltonian Operator for He.

Going beyond the H atom presented formidable many-body problems some of which still cannot be solved exactly. For over forty years approximate methods of solution, usually based on the variation principle, have been developed and refined. In the last decade high speed digital computers have made possible a breakthrough toward the goal of accurate wavefunctions for large molecules (about 50 atoms). But even so the Born-Oppenheimer approximation must be made and somewhat drastic orbital approximations must be accepted. The fact that molecular orbitals (MO) are used implies neglect of at least part of the correlation in the motion of the electrons. Beyond this, rather restricted mathematical expressions are generally used to describe the orbitals.

(v) Polyelectronic systems and the Slater Determinant

For the hydrogen atom the Schrödinger equation is simply given by

$$-[\tfrac{1}{2}\nabla^2 + \frac{1}{r}]\Psi = E\Psi \qquad (39)$$

For the helium atom, (see Fig 5a), containing two electrons, several other terms must be included in the Hamiltonian H.

$$[-\tfrac{1}{2}\nabla_1^2 - \tfrac{1}{2}\nabla_2^2 - \frac{2}{r_1} - \frac{2}{r_2} + \frac{1}{r_{12}}]\Psi = E\Psi \qquad (40)$$

here $-\tfrac{1}{2}\nabla_1^2$ = kinetic energy of electron 1.

$-\tfrac{1}{2}\nabla_2^2$ = kinetic energy of electron 2.

$\frac{2}{r_1}$ = coulomb attraction between the nucleus and electron 1.

$\frac{2}{r_2}$ = coulomb attraction between the nucleus and electron 2.

$\frac{1}{r_{12}}$ = coulombic repulsion between electrons 1 and 2.

Ψ will represent a varying number of electrons depending on the atom or molecule under consideration, and the total electronic structure can be obtained by building up those electrons in hydrogen-like orbitals. Taking the orbital energies as negative in the binding state, the lowest energy orbital i.e. greatest binding energy, is filled first, and as the quantum number increases, the binding energy decreases, or rather becomes less negative. The lowest energy orbital will then be with n = 1 and l = 0, the 1s orbital, and will contain two electrons of opposite spin. The helium atom containing two electrons, (1) and (2), will then have the $1s^2$ electrons as

$1s\alpha(1)$ and $1s\beta(2)$ or $1s\beta(1)$ and $1s\alpha(2)$

where α and β represent the spin. More conventionally the electrons are

$$1s(1),\ 1\bar{s}(2) \quad \text{or} \quad 1\bar{s}(1)\ 1s(2).$$

This implies that Ψ in equation (40) could be represented by a product of two one-electron wave functions namely

$$= \phi_{1s}(1)\ \bar{\phi}_{1s}(2) \tag{41}$$

However the Pauli Principle states that the total wave function must be antisymmetric with respect to electron permutation.

In (41), swapping electrons (1) and (2) would create a new wave function, and not the negative of the original. The problem is overcome by taking linear combinations of $\phi(1)$ and $\phi(2)$, to give two equivalent combinations Ψ_s and Ψ_a the symmetric and antisymmetric functions respectively.

$$\Psi_s = \phi_{1s}(1)\,\overline{\phi}_{1s}(2) + \phi_{1s}(2)\,\overline{\phi}_{1s}(1) \tag{42}$$

$$\Psi_a = \phi_{1s}(1)\,\overline{\phi}_{1s}(2) - \phi_{1s}(2)\,\overline{\phi}_{1s}(1) \tag{43}$$

The Pauli principle excludes (42), and so the wave function for the helium atom when normalized becomes:-

$$\Psi_{He} = \frac{1}{\sqrt{2}}\left[\phi_{1s}(1)\,\overline{\phi}_{1s}(2) - \phi_{1s}(2)\,\overline{\phi}_{1s}(1)\right] \tag{44}$$

where $1/\sqrt{2}$ is the normalizing factor.

The antisymmetric wavefunction can be represented in determinental form by the Slater[11] determinant (45), the general form of which is given in (46) for N electrons and N spin orbitals.

$$\Psi_{He} = \frac{1}{\sqrt{2}}\begin{vmatrix} \phi_{1s}(1) & \phi_{1s}(1) \\ \phi_{1s}(2) & \phi_{1s}(2) \end{vmatrix} \tag{45}$$

$$\Psi = \frac{1}{\sqrt{N}}\begin{vmatrix} \phi_1(1) & \phi_2(1) & \phi_3(1) & \cdots\cdots & \phi_N(1) \\ \phi_1(2) & \phi_2(2) & \phi_3(2) & \cdots\cdots & \phi_N(2) \\ \phi_1(3) & & & & \\ \vdots & & & & \\ \vdots & & & & \\ \vdots & & & & \\ \phi_1(N) & \cdots\cdots\cdots\cdots\cdots & & & \phi_N(N) \end{vmatrix} \tag{46}$$

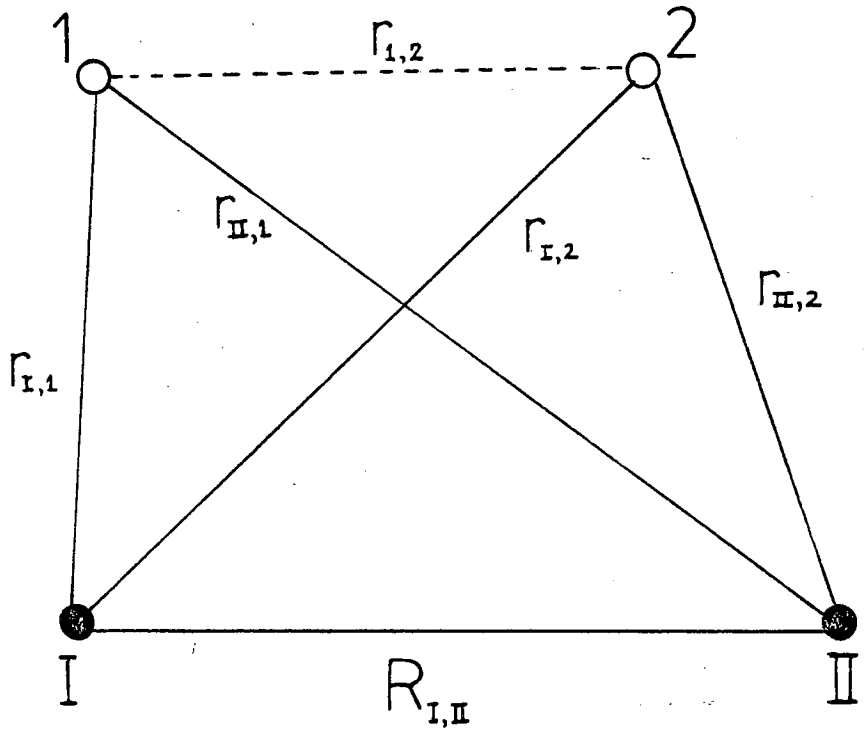

Fig 5b. Distances in H_2 which occur in the Hamiltonion Operator

The interchange of any pair of electrons corresponds to the interchange of two rows in the determinant, and has the effect of changing the sign but not the magnitude of the determinant. This satisfies the symmetry condition of the wave function, for if any two electrons have the same spin and the same orbital the determinant will have two identical columns and will therefore vanish. Thus we can see that the Pauli Exclusion Principle is also satisfied.

Before undertaking a more general treatment of molecular orbital calculations let us consider a polyatomic system, H_2, and begin by limiting ourselves to a single atomic orbital (AO) for each proton.

The total wavefunction can be written in the form of a Slater determinant

$$\Psi_{H_2} = \frac{1}{\sqrt{2}} \begin{vmatrix} \phi_{1s}(1) & \phi_{1s}(1) \\ \phi_{1s}(2) & \phi_{1s}(2) \end{vmatrix} \qquad (47)$$

We note however that ψ_{H_2} is an electronic wavefunction only and contains no information about the motion of the nuclei. The calculated Ψ_{H_2} therefore refers to a fixed nuclear arrangement (the Born-Oppenheimer approximation).

The electronic Hamiltonian for H_2 is

$$\hat{H}^e_{12} = -\tfrac{1}{2}\nabla_1^2 - \frac{1}{r_{I\,1}} - \frac{1}{r_{II\,1}} - \tfrac{1}{2}\nabla_2^2 - \frac{1}{r_{I\,2}} - \frac{1}{r_{II\,2}} + \frac{1}{r_{12}} \qquad (48$$

$-\tfrac{1}{2}\nabla_1^2$ = kinetic energy of electron 1

$-\tfrac{1}{2}\nabla_2^2$ = kinetic energy of electron 2

$\frac{1}{r_{I\,1}}$, $\frac{1}{r_{II\,1}}$, $\frac{1}{r_{I\,2}}$, $\frac{1}{r_{II\,2}}$ are the nuclear electron attraction energies.

$\frac{1}{r_{12}}$ is the electron-electron repulsion energy.

The various distances that occur in the Hamiltonian are illustrated in figure 5b.

Now the first three terms in expression (48) are associated with electron (1), and the second three with electron (2). These composite operators may be denoted h_1 and h_2 respectively. The last term is the electron-electron interaction and is frequently denoted $g_{1,2}$. Thus the Hamiltonian can be written as

$$\hat{H}^e_{1,2} = \hat{h}_1 + \hat{h}_2 + \hat{g}_{1,2} \qquad (49)$$

Now the electronic energy (E^e) is the expectation value of $\hat{H}^e_{1,2}$ over Ψ_{H_2}

$$E^e = \langle \Psi_{H2} \mid \hat{H}^e_{1,2} \mid \Psi_{H2} \rangle \qquad (50)$$

substituting eqn (47) for Ψ_{H2} gives

$$E_e = \tfrac{1}{2}\langle\{\phi_1(1)\overline{\phi}_1(2) - \phi_1(2)\overline{\phi}_2(2)\}|\hat{H}e_{1,2}|\{\phi_1(1)\overline{\phi}_1(2) - \phi_1(2)\overline{\phi}_2(2)\}\rangle \qquad (51)$$

the Hamiltonian operator we are using contains no spin operators and thus operates on the space functions only so that integration of the spin functions may be performed separately and since

$$\begin{aligned} \phi_1(1) &= \phi_1(1)\alpha(1) \\ \overline{\phi}_1(1) &= \phi_1(1)\beta(1) \end{aligned} \qquad (52)$$

$$E^e = \tfrac{1}{2} I_{spin} \langle \phi_1(1)\phi_1(2) | H^e_{1,2} | \phi_1(1)\phi_1(2) \rangle \qquad (53)$$

where $I_{spin} = 2$

$$E^e = \tfrac{1}{2}.2.\langle \phi_1(1)\phi_1(2) | \hat{H}^e_{1,2} | \phi_1(1)\phi_1(2) \rangle$$

$$= \langle \phi_1(1)\phi_1(2) | \hat{h}_1 + \hat{h}_2 + \hat{g}_{12} | \phi_1(1)\phi_1(2) \rangle \qquad (55)$$

now since h_1 operates on electron 1 and h_2 operates on electron 2 the above expression can be simplified to

$$E^e = \langle \phi_1(1) | \hat{h}_1 | \phi_1(1) \times \phi_1(2) | \phi_1(2) \rangle + \langle \phi_1(1) | \phi_1(1) \rangle$$

$$\langle \phi_1(2)\ \hat{h}_2 | \phi_1(2) + \langle \phi_1(1)\phi_1(2) | \hat{g}_{12} | \phi_1(1)\phi_1(2) \rangle \qquad (56)$$

Further, since $\hat{h}_1$ and $\hat{h}_2$ differ only in terms of the running index of the electron label the first two terms on the right hand side of the above equation are equal.

$$E^e = 2\langle \phi_1(1) | \hat{h}_1 | \phi_1(1) \rangle + \langle \phi_1(1)\phi_1(2) | \hat{g}_{1,2} | \phi_1(1)\phi_1(2) \rangle \qquad (57)$$

The first term in this expression is usually referred to as a one-electron integral since it involves integration over the spatial coordinates of only one electron. The second integral is a two electron integral since it involves integration over the spatial coordinates of two electrons.

(vi) Polyatomic systems

The search for accurate electronic wavefunctions of polyatomic molecules uses mainly the molecular orbital method. The ab initio method uses the correct Hamiltonian for the system and attempts a solution without the use of experimental data. A Hartree Fock SCF calculation seeks the antisymmetrized product $\mathcal{G}$ of one electron functions that minimizes $\int \mathcal{G}^* \hat{H} \mathcal{G} d\tau$ where $\hat{H}$ is the true Hamiltonian and is thus an ab initio calculation.

The Molecular Hartree-Fock Problem - (Roothaan's method)

Generalization of the concepts discussed in the previous section for the Helium atom leads to the following expressions.
(i) the wavefunction which describes the electronic ground state of a 2M electron system has the form of a 2M x 2M Slater determinant

$$\Psi_o \equiv \Psi_o(1,2,....2M) = \frac{1}{\sqrt{2M}} \begin{vmatrix} \phi_1(1)\ \overline{\phi}_1(1)\ ..... \phi_M(1)\ \overline{\phi}_M(1) \\ \phi_1(2)\ \overline{\phi}_1(2)\ ..... \phi_M(2)\ \overline{\phi}_M(2) \\ \\ \\ \phi_1(2M)\overline{\phi}_1(2M)..... \phi_M(2M)\overline{\phi}_M(2M) \end{vmatrix} \qquad (58)$$

(ii) the electronic Hamiltonian for a 2M electron system may be written as

$$\hat{H} \equiv \hat{H}(1,2,.....,2M) = \sum_{\mu=1}^{2M} \hat{h}\mu + \sum_{\mu>\nu}^{M(2M-1)} \hat{g}\mu\nu \qquad (59)$$

(iii) the energy value after substitution of Ψ_o and $\hat{H}$ into the expectation value equation is

$$E = \langle \Psi_o \mid \hat{H} \mid \Psi_o \rangle \tag{60}$$

and integrating out the spin variables has the form:

$$E = 2\sum_{p}^{M} \langle \phi_p(1) | \hat{h}_1 | \phi_p(1) \rangle + \sum_{p}^{M}\sum_{q}^{M} [2\langle \phi_p(1)\phi_q(2) | \hat{g}_{12} | \phi_p(1)\phi_q(2) \rangle - \langle \phi_p(1)\phi_p(2) | \hat{g}_{12} | \phi_q(1)\phi_q(2) \rangle] \tag{61}$$

where the two electron integrals (the last two terms in the above equation) are the Coulomb and Exchange integrals respectively. In the Coulomb integrals the electron (1) is associated with orbital ϕ_p, and electron (2) with orbital ϕ_q. This distinction between coulomb and exchange terms is clearer in electron density formalism where orbitals associated with electron (1) are collected in front of the operator while those associated with electron (2) are written behind the operator.

$$E = 2\sum_{p}^{M} \langle \phi_p(1) | \hat{h}_1 | \phi_p(1) \rangle + \sum_{p}^{M}\sum_{q}^{M} [2\{\phi_p(1)\phi_p(1) | \phi_q(2)\phi_q(2)\} - \{\phi_p(1)\phi_q(1) | \phi_q(2)\phi_q(2)\}] \tag{62}$$

The above expression (62) can conveniently be presented in abbreviated form

$$E = 2\sum_{p}^{M} h^{\phi}_{pp} + \sum_{p}^{M}\sum_{q}^{M} (2J^{\phi}_{pq} - K^{\phi}_{pq}) \tag{63}$$

where J_{pq} and K_{qp} symbolize the Coulomb and Exchange integrals respectively. The superscript ϕ indicates that these matrix representatives are over the MO basis. It should be noted that the diagonal elements of the Coulomb and Exchange integrals are identical

$$J_{pp} = K_{pp} \tag{64}$$

and that J_{pq} and K_{pp} are positive quantities. However K_{pq} has a negative sign in the energy expression and the term is therefore considered to be attractive. This is not a hard and fast point of view and has no unambiguous justification as the exchange term K_{pq} has no classical analogue, while the Coulombic term J_{pq} is analogous to the electrostatic Coulomb repulsion.

The J and K integrals are conveniently expressed as pseudo-one-electron integrals by defining pseudo-one-electron hermitian operators $\hat{J}_p$ and $\hat{K}_p$ such that:

$$\begin{aligned} J_{pq} &= \langle\phi_p|\hat{J}_q|\phi_p\rangle = \langle\phi_q|\hat{J}_p|\phi_q\rangle \\ K^{\phi}_{pq} &= \langle\phi_p|\hat{K}_q|\phi_p\rangle = \langle\phi_q|\hat{K}_p|\phi_q\rangle \end{aligned} \tag{65}$$

The energy expression may then be written as:

$$\begin{aligned} E &= 2\sum_{p}^{M}\langle\phi_p|\hat{h} + \sum_{q}^{M}{}''(2\hat{J}_q - \hat{K}_q)|\phi_p\rangle \\ &\equiv 2\sum_{p}\int\phi_p^*\{\hat{h} + \sum_{q}{}'(2\hat{J}_q - \hat{K}_q)\}\phi_p d\tau \end{aligned} \tag{66}$$

According to the Variation Theorem the energy may be optimized by variation of ϕ, hence we wish to minimize E with respect to ϕ_p. To do this we require δE, which will be set equal to zero. To obtain δE each ϕ_p is varied by an infinitesimal amount $\delta\phi_p$ and the variation in energy becomes:

$$\delta E = 2\sum_{p}^{M}\int(\delta\phi_p^*)\{h + \sum_{q}^{M'}(2J_q - K_q)\}\phi_p d\tau + 2\sum_{p}^{M}\int(d\phi_p)\{h^* + \sum_{q}^{M'}(2J_q^* - K_q^*)\}\phi_p^* d\tau = 0 \quad (67)$$

Introducing the orthonormality condition for the MO basis

$$S_{pq} \equiv \langle\phi_p|\phi_q\rangle \equiv \int\phi_p^*\phi_q d\tau = \delta_{pq} \quad (68)$$

permits us to introduce to orthonormality restriction on $\delta\phi_p$,

$$\delta S_{pq} \equiv \int(\delta\phi_p^*)\phi_q d\tau + \int(\delta\phi_q)\phi_p^* d\tau = 0 \quad (69)$$

The appropriate combination of these two equations leads to the following expression:

$$\{\hat{h} + \sum_{q}^{M}(2\hat{J}_q - \hat{K}_q)\}\phi_p = \phi_p\varepsilon_{pp} \quad (70)$$

where the operator, involving the one electron operator (h) and the two electron operators (J_q and K_q) is frequently called the Fock operator and abbreviated F.

$$\hat{F}\phi_p = \phi_p \varepsilon_{pp} \tag{71}$$

The elements of the diagonal matrix ε are in a sense the molecular orbital energies. This expression represents the Hartree-Fock integro-differential equation in matrix notation. To carry out the actual computation the matrix representative of the Fock operator must be generated over the MO basis.

The elements of the Fock matrix over the MO basis may be written as

$$F^{\phi}_{st} \qquad \langle \phi_s | F | \phi_t \rangle \tag{72}$$

and converting the Hartree-Fock operator equation to a matrix equation, we obtain

$$\underline{\underline{F}}^{\phi} = \underline{\underline{\varepsilon}} \tag{73}$$

since $$S^{\phi}_{st} = \langle \phi_s | \phi_t \rangle = \delta_{st} \tag{74}$$

Because ϕ is unknown we substitute

$$\phi = \underline{\underline{C}}\eta \qquad \phi^{\dagger} = \underline{\underline{C}}^{\dagger}\eta^{\dagger}$$

to obtain the Hartree-Fock matrix equation over the AO basis (η).

$$\underline{\underline{C}}\ \underline{\underline{F}}^{\eta}\underline{\underline{C}} = \underline{\underline{C}}\ \underline{\underline{S}}^{\eta}\underline{\underline{C}}\ \underline{\underline{\varepsilon}} \tag{75}$$

where

$$\underline{\underline{F}}^{\eta} = \underline{\underline{h}}^{\eta} + 2\underline{\underline{J}}^{\eta} - \underline{\underline{k}}^{\eta} \text{ and } S^{\eta}_{ij} = \langle \eta_i | \eta_j \rangle$$

These molecular integrals have the usual form

$$h^{\eta}_{ij}(1) = \langle \eta_i(1) | \hat{h} | \eta_j(1) \rangle \tag{76}$$

$$J^{\eta}_{ij}(1) = \sum_{k=1}^{N}\sum_{l=1}^{N} (\eta_i\{1\}\eta_j\{1\}|\eta_k(2)\eta_l(2))\rho_{kl}$$

$$K^{\eta}_{ij}(1) = \sum_{k=1}^{N}\sum_{l=1}^{N} \{\eta_i(1)\eta_k(1)|\eta_j(2)\eta_l(2)\}\rho_{kl} \qquad (77)$$

where ρ_{kl} is the k, l-th element of the density matrix

$$\underline{\underline{\rho}} = \underline{\underline{C}}_m \underline{\underline{C}}_m^{\dagger} \qquad (78)$$

Thus $$F^{\eta}_{ij} = h^{\eta}_{ij} + 2J^{\eta}_{ij} - K^{\eta}_{ij} \qquad (79)$$

Expressing E in terms of the AO integrals we get

$$E = 2\sum_{i=1}^{N}\sum_{j=1}^{N}\rho_{ij}h^{\eta}_{ji} + 2\sum_{i=1}^{N}\sum_{j=1}^{N}\rho_{ij}J^{\eta}_{ji} - \sum_{i=1}^{N}\sum_{j=1}^{N}\rho_{ij}K^{\eta}_{ji} \qquad (80)$$

or when the Fock matrix is explicitly used in the expression

$$E = \sum_{i=1}^{N}\sum_{j=1}^{N}\rho_{ij}(h^{\eta}_{ji} + F^{\eta}_{ji}) \qquad (81)$$

Note that the summation over j will eliminate the running index j and one is thus left with only i,i elements, and therefore the summation over i is simply the summation of the diagonal elements of a diagonal matrix i.e. it is the trace of the matrix

$$E = \sum_{i=1}^{N}\left(\sum_{j=1}^{N}\rho_{ij}(h^{\eta}_{ji} + F^{\eta}_{ji})\right) \qquad (82)$$

$$= \text{trace}\left\{\sum_{j=1}^{N}\rho_{ij}(h^{\eta}_{ji} + F^{\eta}_{ji}\right\}$$

$$= \text{trace}(\underline{\underline{\rho}}\{\underline{\underline{h}}^{\eta} + \underline{\underline{F}}^{\eta}) \qquad (83)$$

We saw in equation (65) that the matrix representative of the Fock operator over the MO basis is simply the MO energy matrix and when F_{pp} is transformed to the AO basis then

$$\varepsilon_p \equiv F^{\phi}_{pp} \equiv \langle\phi_p|\hat{F}|\phi_p\rangle = \sum_i^N \sum_j^N C_{ip}\langle\eta_i|\hat{F}|\eta_j\rangle C_{jp} \tag{84}$$

Summing up all of the occupied MO energies

$$\sum_{p=1}^{n} \varepsilon_p = \sum_{i=1}^{N} \sum_{j=1}^{N} \rho_{ij}\langle\eta_j|\hat{F}|\eta_i\rangle = \sum_{i=1}^{N} \sum_{j=1}^{N} \rho_{ij} F^{\eta}{}_{ji} \tag{85}$$

now $$h^{\eta}{}_{ji} = F^{\eta}{}_{ji} - (2J^{\eta}{}_{ji} - K^{\eta}{}_{ji})$$

and substituting into (81) gives

$$E = \sum_{i=1}^{N} \sum_{j=1}^{N} \rho_{ij} F^{\eta}{}_{ji} - \sum_{i=1}^{N} \sum_{j=1}^{N} \rho_{ij}(2J^{\eta}{}_{ji} - K^{\eta}{}_{ji}) \tag{86}$$

Relating E and $\Sigma\varepsilon_p$ through equations (85) and (86)

$$E = 2\sum_{i=1}^{n} \varepsilon_i - \sum_{i=1}^{N} \sum_{j=1}^{N} \rho_{ij}(2J_{ji} - K_{ji}) \tag{87}$$

Thus the total energy is twice the sum of the doubly occupied MO minus the electron electron repulsion. Now the basic problem is that, even when all of the integrals are known, we cannot directly find $\underline{\underline{F}}^{\eta}$ (required for the Hartree-Fock equation) and E because both depend on $\underline{\rho}$ which, in turn, is constructed from $\underline{\underline{C}}$ and it is this quantity which we want to obtain from the Hartree-Fock equation. This requires that the eigen problem equation be solved in an iterative manner

Fig 6: Flow Diagram Representing SCF Procedure

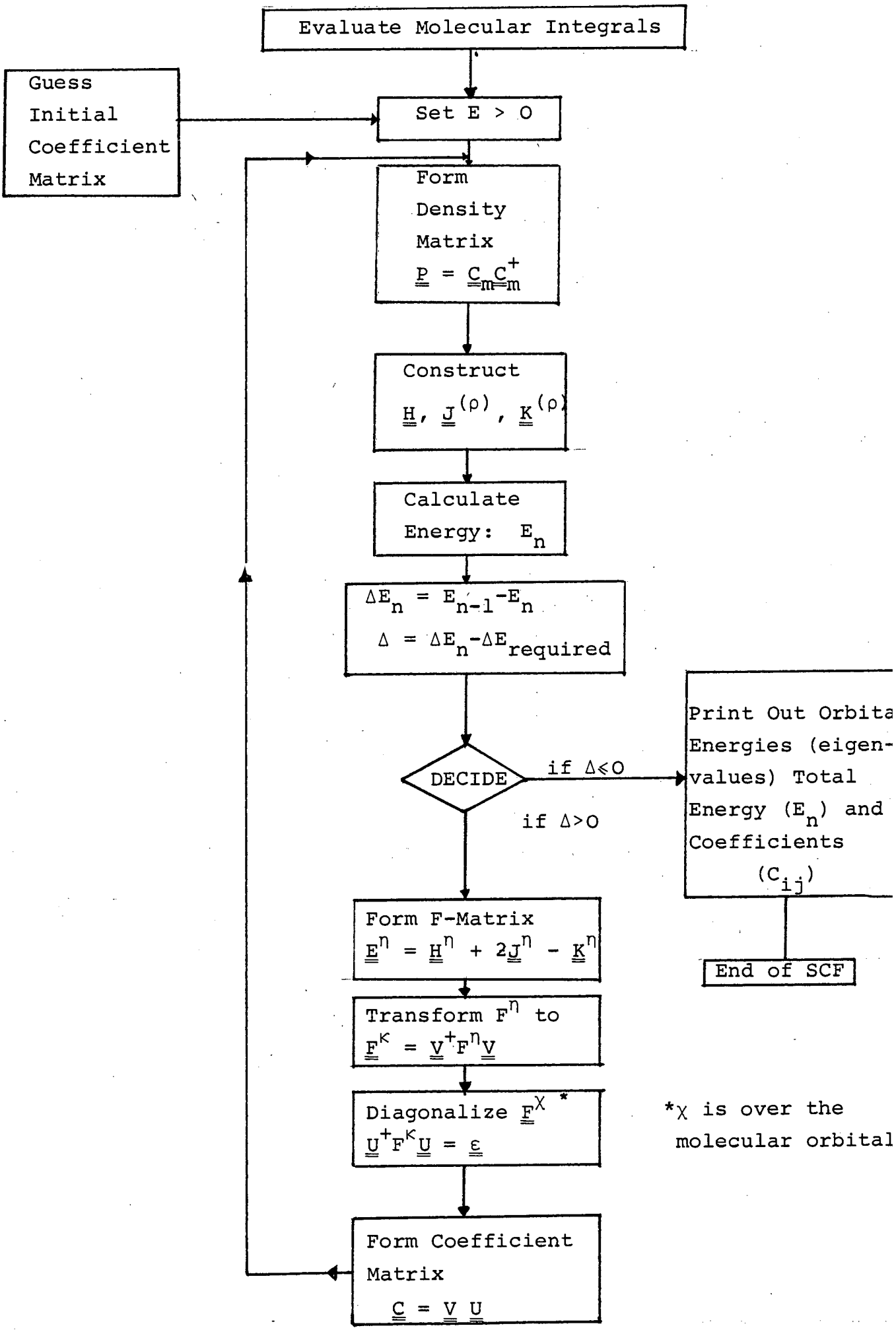

by the self consistent field method . The iterative process of solution must be started from an initial (physically realistic) trial set of coefficients $\underline{\underline{C}}$, which are used to generate a density matrix, the elements of which are related to the elements of the Fock operator matrix $\underline{\underline{F}}^n$ by equations (76) and (77). This allows the Fock matrix to be set up and E calculated. This in turn produces matrix $\underline{\underline{C}}$ of linear expansion coefficients. The process is then repeated using the new set of coefficients held in $\underline{\underline{C}}$, and successive iterations are performed until they no longer alter within a set limit (see figure 6) or convergence may be measured by the difference between the energy values associated with two successive iterations. See Figure 7 for a schematic illustration of the convergence of an SCF calculation.

From a calculation such as this electronic structure of molecules can be calculated.

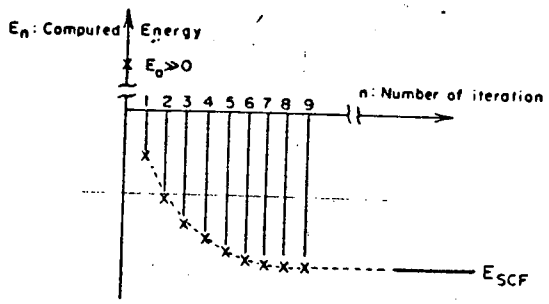

Figure 7 A schematic illustration for the convergenc of an SCF calculation

References

1. M. Planck, Ann. de Phys., 4, 553 (1900).
2. A. Einstein, Ann. de Phys., 17, 132, (1905).
3. E. Rutherford, Phil. Mag., 21, 669, (1911).
4. N. Bohr, Phil. Mag., 26, 1, (1913).
5. L. de Broglie, Ann. de Phys., 3, (1925).
6. W.Heisenberg, Z. Phys., 33, 879, (1925).
7. W. Born, S. Jordan, Z.Phys., 34, 858, (1925).
8. E. Schrö dinger, Ann. de Phys., 79, 489, (1926).
9. E. Schrö dinger, Ann. de Phys., 79, 734, (1926).
10. P. Dirac, Proc.Roy.Soc., 117, 610, (1928).
11. J.C. Slater, Phys.Rev., 35, 503, (1930).

CHAPTER 2

CALCULATIONS - PRACTICAL CONSIDERATIONS

(i) Atmol-3

Calculations of the LCGO-SCF type have been performed in this work using the Atmol-3[1] suite of programs mounted on the IBM 360/65, 370/168, ICL 4/75, and CDC 7600 machines.

Atmol-3 is composed of several packages which can be used independently or sequentially. A brief description of the packages most used is given below.

The integrals package is capable of evaluating Electron Repulsion, Nuclear Attraction (two electron integrals) Kinetic Energy, Overlap and Dipole moment (one electron) integrals, from a given basis set of A.O.s and the molecular structure of the system under investigation.

The two electron integrals are evaluated over the A.O. basis and are output to a disc or tape storage file called the main file. The integrals section uses a large amount of computer time (CPU) which can be reduced in two ways.

1) By the use of a facility which is available in the integrals package which indicates local centres of symmetry in the molecular geometry and enables two electron integrals equal, by symmetry, in absolute magnitude to be identified and calculated only once.

2) By the use of an Accuracy Factor which sets thresholds for the two electron integral evaluation e.g. an accuracy factor of (7 8) means that if the absolute value of an integral is less than 10^{-7} it will not be output to the main file and also if the estimated value of an integral over primitives is less than 10^{-8} it is not taken into account in the total integral over contracted functions.

All integrals of the form $< f_i f_j | f_k f_\ell >$ where f denotes the basis function, are evaluated and stored using the indices i,j,k,ℓ whose values are given by the basis function ordering where

$$\begin{matrix}\text{number of} \\ \text{basis function}\end{matrix} < \text{index} > 1.$$

These reference indices are stored along with the two electron integrals in the main file. Integrals estimated as zero by the limiting accuracy factor are not stored. To exploit this effect,the molecule should be orientated such that the number of two electron integrals whose values are likely to be zero by symmetry, is maximized.

The one electron integrals are evaluated and output to the Dump File.

The SCF section using the procedure outlined on page calculates iteratively the total energy eigenvalues and eigenvectors for the system under consideration. This iterative procedure uses the main file as a source of two electron integrals. The dump file is used as a source of the one electron integrals and also for the output of a copy of the current eigenvectors after each iterative cycle. The C.P.U. required for convergence is dependent on the number of basis functions used and their form.

A more detailed description of the Atmol-3 packages can be found in reference (1).

(ii) The Basis Set - Form and Size

Having so far outlined a practical procedure for obtaining molecular electronic wavefunctions, the final requirement for its execution is the choice of a basis set of functions to represent the atomic orbital basis.

We represent each molecular orbital ψ_i as a combination of atomic orbitals

$$\psi_i = \sum_k C_{ik} \eta_k$$

and each atomic orbital as a combination of basis functions b_i

$$\eta_k = \sum_j \alpha_{kj} b$$

Before any calculation is undertaken the number of basis functions to be used and their algebraic form must be considered.

a) Slater Functions

The use of hydrogen like orbitals of form (Section 1 eqn. 38) have several disadvantages when used for molecules or large atoms. They are based on the assumption that each electron moves in a field of nuclear charge, Ze. This only applies for single electron systems such as the hydrogen atom. In a molecule or large atom the inner electrons partially screen the nucleus so that the outer electrons are affected by a nuclear charge of less than Ze. Functions of form 1.38, therefore do not describe multielectron systems accurately.

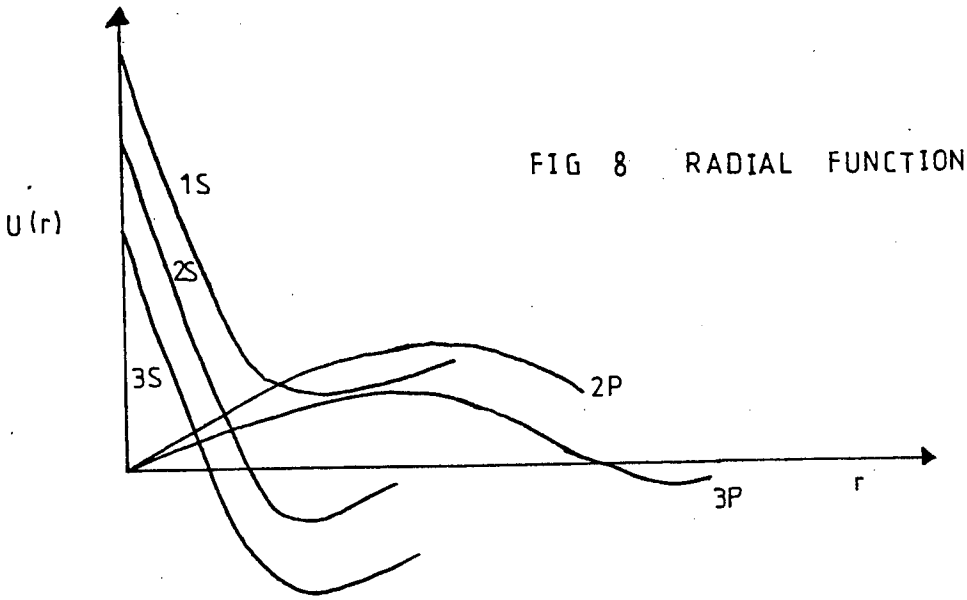

FIG 8 RADIAL FUNCTIONS U(r) v. r

FIG 9 SLATER ATOMIC ORBITALS FOR CARBON ALONG THE X AXIS

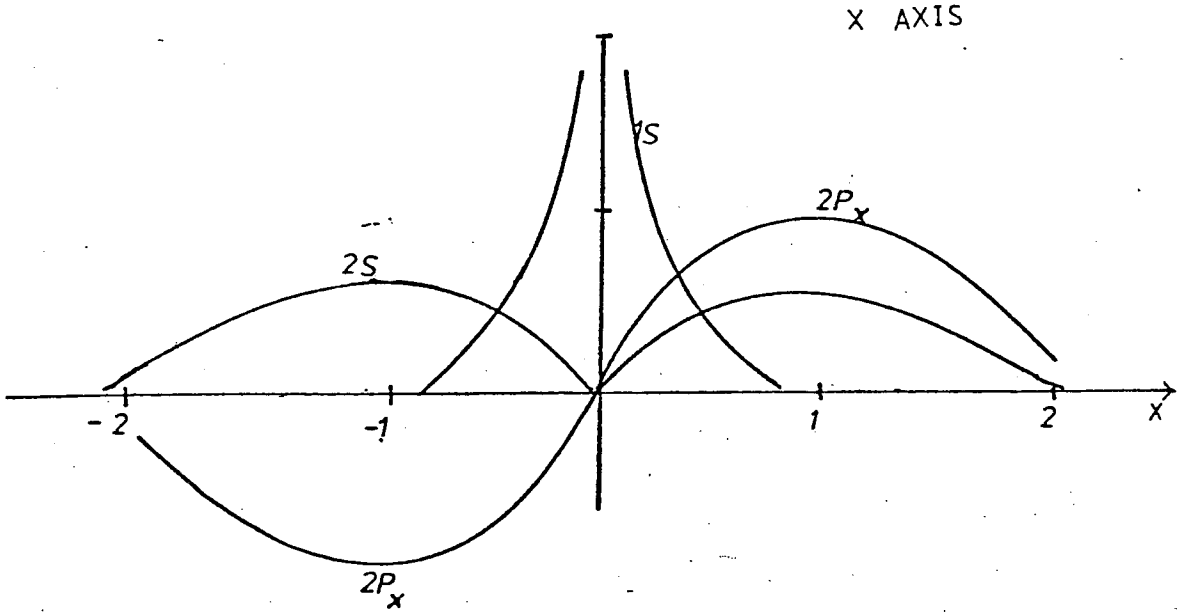

The second disadvantage of hydrogen-like orbitals is that when obtained from an SCF calculation, the A.O.'s are expressed in the form of a numerical table, and not as analytical functions. J.C. Slater[2] attempted to rectify these problems by devising approximate analytical functions which accounted for the fact that each electron moves in a field of effective nuclear charge, Z_{eff}. Slater[3] devised a set of rules for calculating Z_{eff} and called the difference between Z_{eff} and Z the shielding or screening constant, s. The radial function $R_{n\ell}(r)$ is given by

$$R_{n\ell}(r) = Nr^{n-\ell}e^{-\alpha r} \qquad (1)$$

where $\alpha = \frac{Z-s}{n}$ and N is the normalizing factor.

The approximate nature of the Slater orbital is shown by the fact that the radial functions for the 2s and 3s orbitals, which have nodes for the hydrogen like functions, are nodeless (See Fig. 8). The Slater orbitals for carbon, Z = 6, are shown in Table 2, and a plot of these is shown in Fig. 9. The values of α are obtained from SCF calculations on particular atoms by minimizing the total energy of the system. The optimized STO's are used for calculations on molecules containing these atoms.

For 1s to 3p functions, Slater orbitals provide a reasonable description of the atoms, giving better representation for the inner shells than for the valence shells. A better overall radial function can be obtained for functions beyond 3p, by using a linear combination of Slater type orbitals, (LCSTO) such that

$$M_{n\ell}(r) = \sum_i C_i R_{n\ell}(r) \qquad (2)$$

With a fixed STO basis the coefficients, C_i, are optimized to give a minimum total energy using Roothaan's method. In the LCSTO method only a few STO's are required to produce energies within 0.001% of the Hartree-Fock minimum. Generally a linear combination of two STO's per A.O. is sufficient to reproduce the atomic wavefunctions accurately. This is known as a double zeta basis, whereas a basis set consisting of one STO per occupied orbital is called a single zeta, or minimal basis set.

STO's however, suffer from the fact that the calculation of multicentre integrals for polyatomic systems using STO's is extremely difficult, and sometimes impossible. The major difficulty lies in the calculation of the inter electron repulsion integrals. This difficulty in calculating these multicentre integrals prompted the development of several techniques for integral evaluation using an STO basis viz.

a) The ζ-function method [4] which is based on the expansion of all orbitals about a single centre.

b) The axial expansion method [5] where each charge distribution is expanded as a series of exponentials with centres distributed on its axis.

c) Numerical integration. [6]

d) Gaussian expansion [7] where the STO is expanded, by a least squares fit in a number of gaussians.

e) Gaussian transform [8] which is based on the integral transform

$$e^{-\alpha r} = \frac{\alpha}{2} (\pi)^{\frac{1}{2}} \int_0^\infty s^{-3/2} e^{-\alpha^2/4s} e^{-sr^2} ds.$$

These techniques however although simplifying the multi-centre integral calculation, are time consuming and a calculation using an STO basis uses a large amount of CPU time which can be a limiting factor when available computer resources are considered. (It should be noted that the very possibility of performing an STO calculation basically depends on the number and arrangement of the different centres involved).

b) Gaussian Functions

To eliminate the large CPU involved in an STO calculation the use of the Gaussian function of the form

$$x^{\ell}y^{m}z^{n}e^{-\alpha r^2}$$

first suggested by Boys[9] has proved successful in ab initio calculations of polyatomic molecules. The product $x^{\ell}y^{m}z^{n}$ represents the angular distribution of the function and the coefficients ℓ,m,n can have any integral value. When a Basis Set of Gaussian functions is used, the necessary multi-centre integrals (for polyatomic molecules) are simpler to calculate than with STO's.

At this point it is instructive to demonstrate the methods of actual integral (i.e. overlap, kinetic energy, potential energy and electron repulsion) evaluation, and this is best done by example. Firstly, however we must note a very important property of gaussian functions namely that the product of any two gaussian functions is a third gaussian function, centred at a point on the line joining the centres

n	l	m	Orbital	Slater orbital
1	0	0	1s	$N_{1s}e^{-ar} = N_{1s}e^{-5.70r}$
2	0	0	2s	$N_{2s}r\,e^{-ar} = N_{2s}r\,e^{-1.625\,r}$
2	1	1	$2p_x$	$N_{2p_x}r\cos\Theta e^{-ar} = N_{2p_x}x\,e^{-1.625\,r}$

TABLE 2 SLATER ORBITALS FOR CARBON

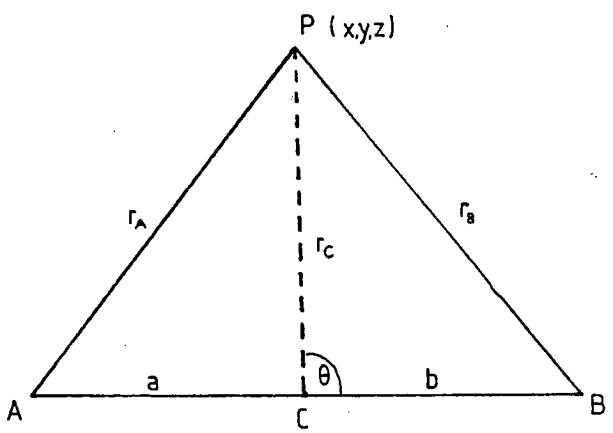

FIG 10

of the original functions, and multiplied by a constant factor.

$$G(A)\ G(B) = KG(C) \qquad (3)$$

Proof

Consider Fig. 10

If we apply the cosine rule to triangles APC and PCB

$$r_B^2 = b^2 - r_c^2 - 2br_c \cos\theta \qquad (4a)$$

$$r_A^2 = a^2 - r_c^2 + 2ar_c \cos\theta \qquad (4b)$$

eliminating $\cos\theta$ gives

$$ar_B^2 + br_A^2 = ab(a+b) + r_c^2(a+b)$$

$$a + b = \overline{AB}$$

$$ar_B^2 + br_A^2 = \overline{AB}(ab+r_c^2)$$

$$a = \overline{AC} = \frac{\alpha_j}{\alpha_i+\alpha_j}\ AB \quad b = \overline{BC} = \frac{\alpha_i}{\alpha_i+\alpha_j}\ \overline{AB}$$

substituting for a and b gives

$$\alpha_i r_A^2 + \alpha_j r_B^2 = \frac{\alpha_i\alpha_j}{\alpha_i+\alpha_j}\ \overline{AB}^2 + (\alpha_i+\alpha_j)r_c^2$$

Now let the Gaussian be

$$G(A) = \exp(-\alpha_A r_A^2)$$

$$G(B) = \exp(-\alpha_B r_B^2)$$

$$G(A)G(B) = \exp(-[\alpha_A r_A^2 + \alpha_B r_B^2])$$

$$= \exp(-[\frac{\alpha_A\alpha_B}{\alpha_A+\alpha_B} \overline{AB}^2 + (\alpha_A + \alpha_B) r_C^2])$$

$$= \exp(-\frac{\alpha_A\alpha_B}{\alpha_A\alpha_B} \overline{AB}^2) \exp[-(\alpha_A + \alpha_B) r_C^2] \quad (5)$$

from which equation (3) follows.

Overlap Integral, S

Consider the overlp between s-orbitals

$$S = \int_{-\infty}^{\infty} \exp(-\alpha_A r_A^2)\ \exp(-\alpha_B r_B^2)\, d\tau \qquad (6)$$

using the property of Gaussians described above

$$S = \int_{-\infty}^{\infty} \exp\left(-\frac{\alpha_A\alpha_B}{\alpha_A+\alpha_B}\overline{AB}^2\right)\ \exp(-(\alpha_A+\alpha_B) r_C^2)\, d\tau$$

changing the variable such that $\tau = \frac{4}{3}\pi r_C^3$

$d\tau = 4\pi r_C^2 dr_C$

$$S = 4\pi \int_{-\infty}^{\infty} \exp\left(-\frac{\alpha_A\alpha_B}{\alpha_A+\alpha_B}\overline{AB}^2\right) r_C^2\ \exp-(\alpha_A+\alpha_B) r_C^2\ dr_C$$

$$= 4\pi\ \exp\left(-\frac{\alpha_A\alpha_B}{\alpha_A+\alpha_B}\overline{AB}^2\right) \int_0^{\infty} r_C^2\ \exp-(\alpha_A+\alpha_B) r_C^2\ dr_C$$

using the general integral

$$\int_0^{\infty} r^{\lambda} \exp(-\alpha r^2)\, dr = \tfrac{1}{2}\alpha^{-(\lambda+1)/2}\ \Gamma\left(\frac{+1}{2}\right) \qquad (7)$$

derived from the integral representation of the Gamma function [8].

$$S = 4\pi\ \exp\left(-\frac{\alpha_A\alpha_B}{\alpha_A+\alpha_B}\overline{AB}^2\right) .\ \tfrac{1}{2}(\alpha_A+\alpha_B)^{-3/2}\Gamma(3/2)$$

since $\Gamma(\frac{3}{2}) = \tfrac{1}{2}(\pi)^{\frac{1}{2}}$

$$S = \exp\left(-\frac{\alpha_A\alpha_B}{\alpha_A+\alpha_B}\overline{AB}^2\right)\left(\frac{\pi}{\alpha_A+\alpha_B}\right)^{3/2} \qquad (8)$$

This is the expression for the overlap integral of two S type functions centred on A and B and is represented by S_{AB}^{OO}, where $S_{AB}^{OO} = \langle S_A|S_B\rangle$ the superscript representing the orbital angular momentum quantum number of the orbitals.

Higher order orbitals (e.g. p-type) can be derived from S-type Gaussian functions by differentiation using Shavitt's[7] method.

$$x_A \exp(-\alpha_A r_A^2) = \frac{1}{2\alpha_A}\frac{\partial}{\partial A_x}\exp(-\alpha_A r_A^2) \qquad (9)$$

where the Gaussian is centred at point A. The extension to d-type functions is obtained by successive differentiation.

As an example consider the overlap integral for two p-type functions

$$\phi_A = x_A \exp(-ar_A^2) \qquad \phi_B = x_B \exp(-br_B^2)$$

$$\langle P_A|P_B\rangle = S_{AB}^{11} = \int_{-\infty}^{\infty} x_A \exp(-ar_A^2)\, x_B \exp(-br_B^2)\, d\tau$$

now

$$x_A \exp(-ar_A^2) = \frac{1}{2a}\frac{\partial}{\partial A_x}\exp(-ar_A^2)$$

$$S_{ab}^{11} = \frac{1}{4ab}\int_{-\infty}^{\infty}\frac{\partial}{\partial A_x}[\exp(-ar_A^2)]\frac{\partial}{\partial B_x}[\exp(-br_B^2)]\,d\tau$$

$$= \frac{1}{4ab}\frac{\partial}{\partial A_x}\frac{\partial}{\partial B_x}(A_{ab}^{OO})$$

$$= \frac{1}{4ab}\left(\frac{\pi}{a+b}\right)^{3/2}\frac{\partial}{\partial A_x}\frac{\partial}{\partial B_x}\exp\left(-\frac{ab}{a+b}R^2\right)$$

where $R^2 = (A_x - B_x)^2 + (A_y - B_y)^2 + (A_z - B_z)^2$

$$S_{ab}^{11} = \frac{1}{4ab}\left(\frac{\pi}{a+b}\right)^{3/2} \frac{\partial}{\partial A_x}\frac{\partial}{\partial B_x} \exp\left[-\frac{ab}{a+b}(A_x^2+B_x^2)-2A_xB_x)+(A_y-B_y)^2 + (A_z-B_z)^2\right]$$

$$= \left(\frac{\pi}{a+b}\right)^{3/2} \exp\left(\frac{-ab}{a+b} R^2\right)\left[\frac{1}{2(a+b)} - \frac{ab}{(a+b)^2}(A_x - B_x)^2\right]$$

$$S_{ab}^{11} = \left[\frac{1}{2(a+b)} - \frac{ab}{(a+b)^2}(A_x-B_x)^2\right] S_{ab}^{oo} \qquad (10)$$

Hence we can see that overlap integrals involving higher order orbitals can be expressed in terms of S-type overlap integrals.

Kinetic Energy Integrals

This is represented by

$$< \psi_A | K | \psi_B > \qquad \text{where } \psi_A = \exp(-ar_A^2)$$

$$\psi_B = \exp(-br_B^2)$$

Now ψ_A can be written as $\psi_A = \exp(-ax_A^2 - ay_A^2 - az_A^2)$

and the kinetic energy operator is

$$K = -\tfrac{1}{2}\nabla^2 = -\tfrac{1}{2}\left(\frac{\partial}{\partial x^2} + \frac{\partial^2}{\partial y^2} + \frac{\partial^2}{\partial z^2}\right)$$

let K operate on ψ_B

$$K(\psi_B) = -\tfrac{1}{2}\nabla^2 \exp(-br_B^2)$$

$$= -\tfrac{1}{2}\left(\frac{\partial^2}{\partial x_B^2} + \frac{\partial^2}{\partial y_B^2} + \frac{\partial^2}{\partial z_B^2}\right) \exp\{-b(x_B^2+y_B^2+z_B^2)\}$$

$$= D_x + D_y + D_z \qquad (11)$$

$$D_x = -\tfrac{1}{2}\frac{\partial^2}{\partial x_B^2}\left(\exp\{-bx_B^2 - by_B^2 - bz_B^2\}\right]$$

but $-\tfrac{1}{2}\frac{2}{x_B^2}\left[\exp(-bx_B^2)\exp(-by_B^2 - bz_B^2)\right]$

$$= (b - 2b^2x_B^2)\exp(-bx_B^2 - by_B^2 - bz_B^2) \qquad (12)$$

Similarly the terms in y_B and z_B are

$$D_y = (b-2b^2y_B^2)\exp(-bx_B^2 - by_B^2 - bz_B^2)$$

$$D_z = (b - 2b^2z_B^2)\exp(-bx_B^2 - by_B^2 - bz_B^2)$$

$$-\tfrac{1}{2}\nabla\psi_B = [3b - 2b^2(x_B^2+y_B^2+z_B^2)]\ \exp(-bx_B^2-by_B^2-bz_B^2)$$

$$= (3b-2b^2r^2)\ \exp(-br_B^2) \qquad (13)$$

$$\langle\psi_A|K|\psi_B\rangle = \int_{-\infty}^{\infty} \exp(-ar_A^2)\ -\tfrac{1}{2}(3b-2b^2r^2)\ \exp(-br_B^2)\,d\tau$$

$$= \int_{-\infty}^{\infty} -\tfrac{1}{2}(3b-2b^2r^2)\ \exp(-ar_A^2-br_B^2)\,d\tau$$

$$= \int_{-\infty}^{\infty} (3b-2b^2r_B^2)\ \exp\left(\frac{-ab}{a+b}R^2\right)\ \exp(-(a+b)r_C^2)\,d\tau$$

$$= \exp\left(\frac{-ab}{a+b}R^2\right)\left[\int_{-\infty}^{\infty} 3b\ \exp(-(a+b)r_C^2)\,d\tau\right.$$

$$\left.-\int_{-\infty}^{\infty} 2b^2r_B^2\exp(-(a+b)r_C^2)\,d\tau\right]$$

$$= N[I_A + I_B] \qquad (14)$$

$$N = \exp\left(\frac{-ab}{a+b}R^2\right)$$

changing the variable $d\tau = 4\pi r_C^2 dr_C$ in I_A gives

$$I_A = \int_0^{\infty} 3b\ 4\pi r_C^2\ \exp(-(a+b)r_C^2)\,dr_C$$

$$= 12\pi b\ \tfrac{1}{2}(a+b)^{-3/2}\ \Gamma\left(\frac{3}{2}\right)$$

$$NI_A = 3b\ \exp\left(\frac{-ab}{a+b}R^2\right)\ \left(\frac{\pi}{a+b}\right)^{3/2} \qquad (15)$$

Consider I_B

$$I_B = 2b^2 \int_{-\infty}^{\infty} r_B^2 \exp(-(a+b) r_C^2) d\tau \qquad (16)$$

now from (4a)

$$r_B^2 = B^2 + r_C^2 + 2Br_C\cos\theta$$

$$\therefore I_B = -2b^2 [\int_{-\infty}^{\infty} B^2 \exp(-(a+b) r_C^2) d\tau$$

$$+ \int_{-\infty}^{\infty} r_C^2 \exp(-(a+b) r_C^2) d\tau$$

$$+ \int_{-\infty}^{\infty} 2Br_C\cos\theta \exp(-(a+b) r_C^2) d\tau]$$

Changing the variable such that $d\tau = 4\pi r_C^2 dr_C$

$$I_B = -8\pi b^2 B^2 \int_0^{\infty} r_C^2 \exp(-(a+b) r_C^2) dr_C$$

$$-8\pi b^2 \int_0^{\infty} r_C^4 \exp(-(a+b) r_C^2) dr_C \qquad (17)$$

$$+16\pi b^2 B \int_0^{\infty} r_C^3 \exp(-(a+b) r_C^2) dr_C \int_0^{2\pi} \cos\theta d\theta$$

$$= I_{B1} + I_{B2} + I_{B3}$$

$$I_{B3} = 0 \text{ since } \int_0^{2\pi} \cos\theta \, d\theta = 0$$

also $$I_{B1} = -8\pi b^2 B^2 \tfrac{1}{2}(a+b)^{-3/2} . \tfrac{1}{2} . \pi^{\frac{1}{2}}$$

$$NI_{B1} = -2b^4 \exp\left(\frac{-ab}{a+b} R^2\right) \left(\frac{\pi}{a+b}\right)^{3/2}$$

and

$$I_{B2} = -8\pi b^2 \int_0^\infty r_C^4 \exp(-(a+b) r_C^2) dr_C$$

$$= -8\pi b^2 \tfrac{1}{2}(a+b)^{-5/2} \Gamma\left(\frac{5}{2}\right)$$

$$= -3\pi^{3/2} b^2 (a+b)^{-5/2}$$

$$KI_{B2} = -3\left(\frac{\pi}{a+b}\right)^{3/2} \frac{b^2}{a+b} \exp\left(\frac{-ab}{a+b} \cdot R^2\right)$$

$$N(I_A + I_B) = \left(3b - 2b^2B^2 - \frac{3b^2}{a+b}\right) \left(\frac{\pi}{a+b}\right)^{3/2} \exp\left(\frac{-ab}{a+b} R^2\right) \qquad (18)$$

and since $B = \frac{a}{a+b} R$

$$\langle \psi_A | K | \psi_B \rangle = \frac{ab}{a+b}\left(3 - \frac{2ab}{a+b} \cdot R^2\right) \left(\frac{\pi}{a+b}\right)^{3/2} \exp\left(-\frac{ab}{a+b} R^2\right)$$

$$= \frac{ab}{a+b}\left(3 - \frac{2ab}{a+b} R^2\right) S_{ab}^{oo} \qquad (19)$$

This is a weighted sum of overlap integrals.

Potential Energy Integrals

These integrals represent the coulombic attraction between a charge distribution and a point charge at a point C.

$$I = \int_0^\infty \exp(-ar_{1A}^2)\ \frac{1}{r_{1C}}\ \exp(-br_{1B}^2)\,dr \tag{20}$$

using the transform

$$\frac{1}{r_{1C}} = \pi^{-\frac{1}{2}} \int_0^\infty s^{-\frac{1}{2}} \exp(-sr_{1C}^2)\,ds \tag{21}$$

and similar manipulations of the Gaussians (as shown in calculation of the Kinetic Energy Integral) we obtain

$$I = \frac{2\pi}{a+b} \exp\left(\frac{-ab}{a+b}\ \overline{AB}^2\right)\ F_o[\overline{PC}^2(a+b)]$$

$$= 2\left(\frac{\pi}{a+b}\right)^{-\frac{1}{2}}\ S_{ab}^{oo}\ F_o[\overline{PC}^2(a+b)] \tag{22}$$

where the function F_o is of the form

$$F_m(t) = \int_0^1 u^{2m} \exp(-tu^2)\,du \tag{23a}$$

and $$F_o(t) = \tfrac{1}{2}\sqrt{\frac{\pi}{t}}\ eA(\sqrt{t}\ ) \tag{23b}$$

This is the incomplete Gamma Function and has to be evaluated numerically.

Electron Repulsion Integrals

$$I = \langle aAbB \frac{1}{r_{12}} cCdD \rangle \qquad (24)$$

where $aA = \exp(-ar_A^2) = \phi_A$

The repulsion integrals I, represent the interaction of two charge distributions and can be classified as follows:

Coulomb Integrals - where both charge distributions are single centre. Here I is either

$$\langle \phi_A^2(1) | \frac{1}{r_{12}} | \phi_B^2(2) \rangle \qquad \text{1 centre}$$

or $$\langle \phi_A^2(1) | \frac{1}{r_{12}} | \phi_B(2)\ \phi_C(2) \rangle \qquad \text{2 centre}$$

Hybrid Integrals - where one charge distribution is single centre and the other two centre, and I is therefore either

$$\langle \phi_A^2(1) | \frac{1}{r_{12}} | \phi_A(2)\phi_B(2) \rangle \qquad \text{2 centre}$$

or

$$\langle \phi_A^2(1) | \frac{1}{r_{12}} | \phi_B(2)\phi_C(2) \rangle \qquad \text{3 centre}$$

Exchange Integrals - where both charge distributions are two centre and I is either

$$\langle \phi_A(1)\phi_B(1) | \frac{1}{r_{12}} | \phi_A(2)\phi_B(2) \rangle \text{ 2 centre}$$

$$\langle \phi_A(1)\phi_B(1) | \frac{1}{r_{12}} | \phi_A(2)\phi_C(2) \rangle \text{ 3 centre}$$

$$\langle \phi_A(1)\phi_B(1) | \frac{1}{r_{12}} | \phi_C(2)\phi_D(2) \rangle \text{ 4 centre}$$

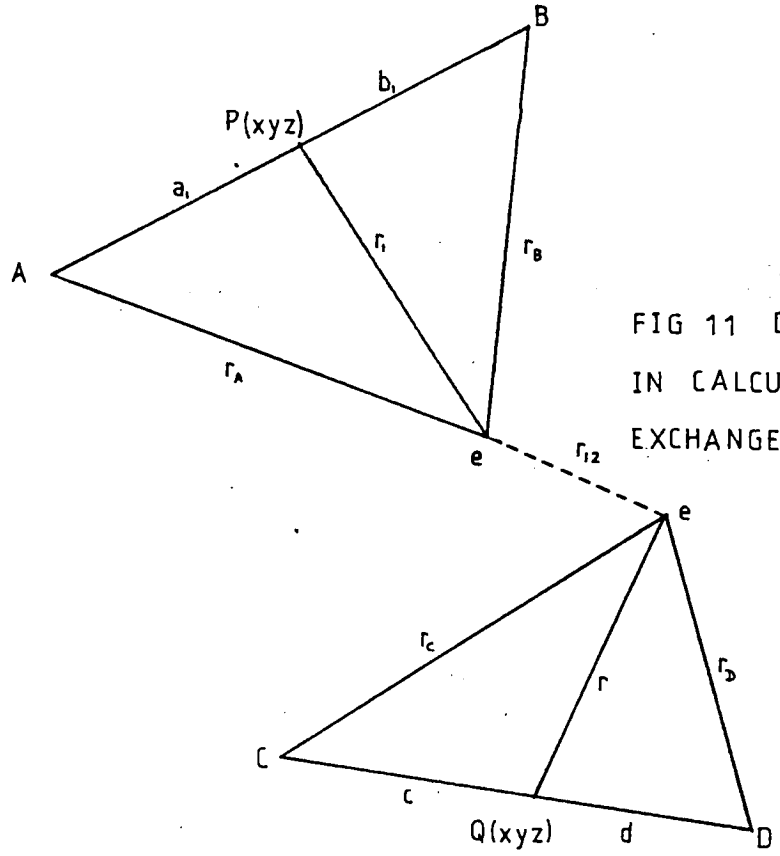

FIG 11 DISTANCES INVOLVED IN CALCULATION OF 4 CENTRE EXCHANGE INTEGRAL.

FIG 12 COMPARISON OF r DEPENDENCE FOR STO AND GTO

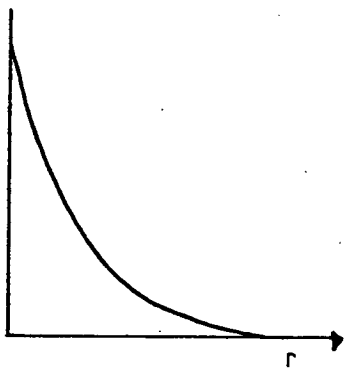

SLATER TYPE ORBITAL

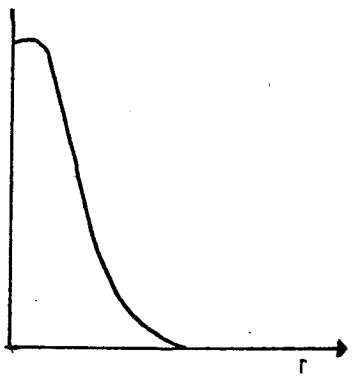

GAUSSIAN TYPE ORBITAL

As an example of electron repulsion integral calculation a 4 centre exchange integral is worked out below:

The required integral is

$$I = \langle \exp(-ar_A^2)\exp(-br_B^2)\left|\frac{1}{r_{12}}\right|\exp(-cr_C^2)\exp(-dr_D^2)\rangle \qquad (25)$$

(See fig. 11)

Applying the product of Gaussian theorem and introducing the integral transform of eqn (21)

$$I = \frac{1}{\sqrt{\pi}} \exp\left(-\frac{ab}{a+b}\overline{AB}^2 - \frac{cd}{c+d}\overline{CD}^2\right)\int_0^\infty I_x I_y I_z s^{-\frac{1}{2}} ds \qquad (26)$$

where

$$I_x = \int_{-\infty}^{\infty}\int_{-\infty}^{\infty} \exp[-p(x_1-P_x)^2 - q(x_2-Q_x)^2 - s(x_1-x_2)^2]\,dx_1 dx_2 \qquad (27)$$

and $a+b = p \quad q = c+d$

Let $u = x_1-P_x \quad v = x_2-Q_x \quad X = P_x-Q_x$

$$I_x = \int_{-\infty}^{\infty}\int_{\infty}^{\infty} \exp[-pu^2 - qv^2 - s(u-v+X)^2]\,du dv$$

$$= \exp[-sX^2]\int_{-\infty}^{\infty} \exp[-u^2(p+s) - 2sXu\,du \int_{-\infty}^{\infty} \exp[-v^2(q+s) + 2(x+u)sv]\,dv$$

using the relationship

$$\int_{-\infty}^{\infty} \exp(-\alpha x^2 + 2\beta x)\,dx = \sqrt{\frac{\pi}{\alpha}}\ \exp\left(\frac{\beta^2}{\alpha}\right) \qquad (28)$$

$$I_x = \exp[-sX^2] \int_{-\infty}^{\infty} \exp[-u^2(p+s)-2sXu] \sqrt{\frac{\pi}{q+s}} \exp[\frac{(X+u)^2 s^2}{q+s}] du$$

$$= \exp[-\frac{qsX^2}{q+s}] \sqrt{\frac{\pi}{q+s}} \int_{-\infty}^{\infty} \exp[u^2\{\frac{s^2-(p+s)(q+s)}{q+s}\} + 2u\{\frac{sXq}{q+s}\}] du$$

using the relationship given in equation (28)

$$I_x = \sqrt{\frac{\pi}{q+s}} \sqrt{\frac{\pi(q+s)}{pq+s(p+q)}} \exp\left[\frac{-qsX^2}{(q+s)} - \frac{s^2q^2X^2}{(q+s)(pq+sp+sq)}\right]$$

$$= \frac{\pi}{\sqrt{pq}} \left(1+\frac{p+q}{pq}.s\right)^{-\frac{1}{2}} \exp\{-\frac{sX^2}{1+\frac{s(p+q)}{pq}}\} \qquad (29)$$

The Integrals I_y, I_z give similar terms in y, z.

Hence equation (26) becomes

$$I = K \frac{\pi^3}{(pq)^{3/2}} \left(1+\frac{p+q}{pq}.s\right)^{-3/2} \int_0^{\infty} \exp[-\frac{s\overline{PQ}^2}{1+\frac{s(p+q)}{pq}}] s^{-\frac{1}{2}} ds \qquad (30)$$

where $K = \frac{1}{\sqrt{\pi}} \exp(\frac{-ab}{a+b}\overline{AB}^2 - \frac{cd}{c+d}\overline{CD}^2)$

Let $1 + \frac{p+q}{pq}.s = \frac{1}{1-t^2}$

$$I = \frac{2\pi^{5/2}}{pq\sqrt{p+q}} \exp[\frac{-ab}{a+B}\overline{AB}^2 - \frac{cd}{c+d}\overline{CD}^2] \int_0^1 \exp[\frac{-pq}{p+q}\overline{PQ}^2 t^2] dt \qquad (31)$$

$$= \frac{2\pi^{5/2}}{(a+b)(c+d)\sqrt{a+b+c+d}} F_o[\frac{(a+b)(c+d)\overline{PQ}^2}{a+b+c+d}] \exp[\frac{-ab}{a+b}AB^2 - \frac{cd}{c+d}\overline{CD}^2] \qquad (32)$$

Equation (31) gives the exchange integral for four s-type functions i.e. $\langle ss|\frac{1}{r_{12}}|ss\rangle$

extending this to $< ps|\frac{1}{r_{12}}|ss >$

$$< ps|\frac{1}{r_{12}}|ss > = \frac{1}{2a} < \frac{\partial}{\partial A_x} ss|\frac{1}{r_{12}}|ss > \qquad (32)$$

Differentiating equation (31) where

$$AB^2 = (A_x-B_x)^2 + (A_y-B_y)^2 + (A_z-B_z)^2$$

$$PQ^2 = (P_x-Q_x)^2 + (P_y-Q_y)^2 + (P_z-Q_z)^2$$

and

$$P_x = \frac{aA_x+bB_x}{a+b}$$

gives

$$\frac{1}{2a}\frac{\partial I}{\partial A_x} = \{\frac{-2^{5/2}}{(p+q)^{3/2}(a+b)} \exp[\frac{-ab}{a+b}\overline{AB}^2 - \frac{cd}{c+d}\overline{CD}^2]$$

$$(Px-Qx)F_1[\frac{pq}{p+q}\overline{PQ}^2] \frac{-2\pi^{5/2}b}{pq\sqrt{p+q}(a+b)} (Ax-Bx)F_o$$

$$[\frac{pq}{p+q}\overline{PQ}^2]\} \frac{(a+b)^{3/2}(c+d)^{3/2}}{\pi^3} S_{ab}^{oo} S_{cd}^{oo} \qquad (33)$$

now $S_{ab}^{1o} = \frac{-b}{a+b}(A_x-B_x)S_{ab}^{oo}$

$$\therefore \frac{1}{2a}\frac{I}{A_x} = M\{\frac{2\pi^{5/2}}{pq\sqrt{p+q}} F_o[\frac{pq}{p+q}\overline{PQ}^2]S_{ab}^{1o} S_{cd}^{oo}$$

$$\frac{2\pi^{5/2}}{(p+q)^{3/2}(a+b)} (Px-Qx)S_{ab}^{oo} S_{cd}^{oo} F_1[\frac{pq}{p+q}\overline{PQ}^2]\} \qquad (34)$$

where $M = \frac{(a+b)^{3/2}(c+d)^{3/2}}{\pi^3}$

This can be expressed as

$$\frac{1}{2a}\frac{}{A_x} I = M'[S^{10}_{ab} S^{00}_{cd} G^{0000}(t) - S^{00}_{ab} S^{00}_{cd} G^{1000}(t)] \qquad (35)$$

where

$$M' = 2[\frac{(a+b)(c+d)}{(a+b+c+d)}]^{\frac{1}{2}}$$

and the set of intermediate functions G is defined as

$$F_o(t) = G^{0000}(t)$$

$$G^{1000}(t) = \frac{(c+d)}{(a+b+c+d)} (P_x-Q_x)F_1(t)$$

It should be noted that integrals of all types use the overlap integral, and CPU time is saved by storing the overlap integrals. These integrals are over Gaussian functions and not contracted functions. "Contracted" integrals are obtained from weighted integrals over primitive Gaussian functions.

The main disadvantage of the Gaussian function is that it does not resemble very closely the form of real atomic orbital wave functions. In particular the Gaussian function lacks a cusp at the nucleus, and hence the region near the nucleus is described rather poorly unless a large number of functions are used. The behaviour at large distances is also very different from that of the exact atomic orbital wave functions. See Fig. 12.

A variational calculation of the energy of the hydrogen atom using a single Gaussian function gives only four fifths of the total energy exactly. This defect may be overcome by using a large number of Gaussian functions with suitably chosen exponents in the basis set, but it becomes very difficult to get the iterative self consistent field procedure to converge with a very large number of basis functions. Even if it is possible to obtain convergence, the time required to build up the matrix elements of the Hamiltonian, and diagonalize the resultant matrix increases enormously if a large basis set is used.

The problem of the size of the basis set required when Gaussian functions are used has been studied by Huzinaga et al.[10] It was found that the number of Gaussian basis functions necessary is more than twice as great as the number of Slater-type basis functions which give an identical energy. However, a method has been found to reduce the number of variables in the self consistent

field procedure with very little loss of accuracy. Instead of allowing all the coefficients of the basis function expansion to vary freely, certain coefficients are fixed relative to one another, thus forming groups of Gaussian functions, known as "contracted" Gaussians. The molecular orbital is then expressed as

$$\phi_i = \sum_k C_{ik} \vartheta_k \tag{36}$$

where ϑ_k is a small contraction of Gaussians of the same type on the same centre

$$\text{e.g.} \quad \vartheta_1 = C_1' B_1 + C_2' B_2 + C_3' B_3 \tag{37}$$

In this way a large basis set may be broken up into a much smaller number of groups. In the variational calculation of the molecular wave function only the coefficient of the contracted form (Ci) is allowed to vary, and not the relative proportions of the Gaussians within each group. The loss of accuracy depends on the skill with which the initial basis is contracted.

If a basis set is contracted to a minimal basis it can be too contracted. There is a procedure which splits the orbitals into portions i.e.

1s	1s'
↓	↓
Inner Part	Outer Part
↓	↓
High Exponents	Low Exponents

Figure 13

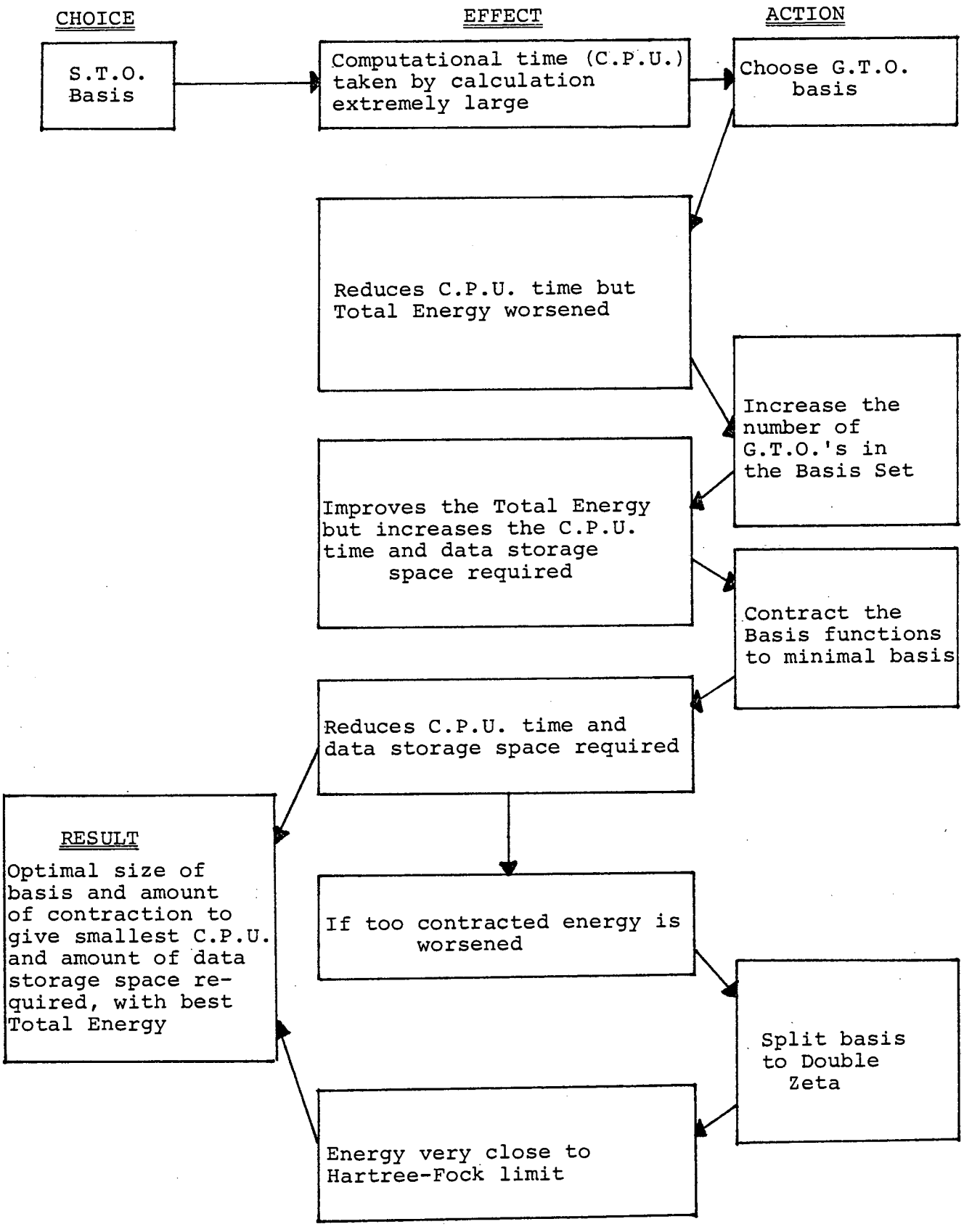
CHOICE
EFFECT
ACTION
S.T.O. Basis
Computational time (C.P.U.) taken by calculation extremely large
Choose G.T.O. basis
Reduces C.P.U. time but Total Energy worsened
Increase the number of G.T.O.'s in the Basis Set
Improves the Total Energy but increases the C.P.U. time and data storage space required
Contract the Basis functions to minimal basis
Reduces C.P.U. time and data storage space required
RESULT
Optimal size of basis and amount of contraction to give smallest C.P.U. and amount of data storage space required, with best Total Energy
If too contracted energy is worsened
Split basis to Double Zeta
Energy very close to Hartree-Fock limit

to give what is known as a Double Zeta basis, this splits the Gaussian type orbitals into orbital parts;

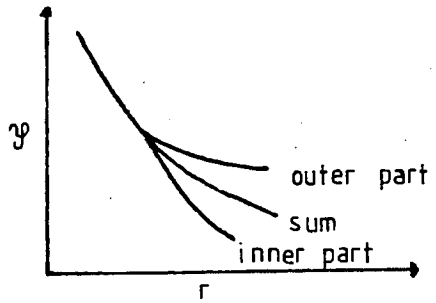

Such a basis gives better energies than the minimal basis.

If there are n functions in the primitive set then contraction to a set of m functions reduces the number of integrals to be manipulated by $(m/n)^4$. In practice it is found that little accuracy is lost if $m \approx n/2$, so that the contracted set contains 1/16 the number of integrals and will require only 1/16 of the time per iteration.

(iii) Choice of Basis Set - A Feasibility Study

The factors effecting the choice of optimal basis set are summarized in Fig. 13. There are however limitations on the basis set chosen by the procedure described in Fig. 13, namely the extent of computer resources; therefore before embarking upon a series of calculations, a study must be made to estimate the feasibility of performing calculations of a certain quality (i.e. with a particular size of basis set) under the restriction of computational resources available,

It is instructive, at this point, to give some consideration to calculations on atomic species and small molecules, as particular test cases.

The results of a literature survey produced four basis sets which were considered to be practicable for use on large molecular systems viz. Huzinaga's (14s/7p), (11s,7p) bases[11,12] and Dunning's (10s/6p) and (9s/5p) bases.[13,14] (The (7s/3p) basis scaled on ethylene[15], previously used by the Edinburgh Quantum Chemistry group has been extensively applied to the study of large molecules with 20 or more atoms. This is well within the limit of the available computer facilities).

Calculations with each of these double zeta quality basis sets (5,6,7,8) were performed on the carbon atom and a series of small molecules, as test cases. These results are tabulated in tables 7 to 9. Previous work[16] done by the group is given in Tables 3 to 6. These results show the effect of contraction on the total energy of the system under consideration, time taken for the calculation (CPU) and the amount of data storage space available, for Huzinaga's 11s/7p basis.

The less contracted the basis set the better the total energy but the disadvantage of the large amount of data storage space (DSS) and CPU required for the calculation outweighs the better total energy obtained. The optimum contraction for this basis set was found to be (6,2,2,1;5,2) with H(4,1). This was chosen taking total energy, DSS used and CPU taken for the calculation into consideration. Table 7 shows the effect of different accuracy factors on the total energy of the carbon atom. As can be seen the energy was unchanged until a relatively low accuracy factor was used. (A small change in the total energy

Total Energy (au)

Accuracy		Huzinaga 14s/7p	Huzinaga 11s/7p	Dunning 10s/6p	Dunning 9s/5p
10	11	-37.687533976	-37.587267842	-37.687164698	-37.684507821
9	10	-37.687533976	-37.687267847	-37.687164698	-37.684507821
8	9	-37.687533976	-37.687267842	-37.687164688	-37.684507821
7	8	-37.687533976	-37.687267842	-37.687164698	-37.684507821
6	7	-37.687533976	-37.687267842	-37.687164698	-37.684507821
5	6	-37.687533976	-37.687267842	-37.687164698	-37.684507821
4	5	-37.687533969	-37.687267842	-37.687164698	-37.684507821
3	4	-37.687533199	-37.687267842	-37.6871699372	-37.684507821
2	3	-37.687515662	-37.687096297	-37.686489131	-37.68445043

Table 7: Effect of Different Accuracy Factors on Total Energy of Carbon Atom (^3P)

Basis Set	Main File Size	Dump File Size	CPU(s) Integrals	CPU(s) S.C.F.	Energy (au)	Machine
[a]Huzinaga 14s/7p	2	6	169.3	10.3	-37.6875339	4/75
[b]Huzinaga 11s/7p	2	6	92.4	8.19	-37.6862578	4/75
[c]Dunning 10s/6p	8	7	101.8	128.9	-37.6871646	4/75
[d]Dunning 9s/5p	2	6	58.1	9.4	-37.6845078	4/75

a) contraction (4,4,3,2;4,3); b) contraction (6,2,2,1,5,2); c) contraction (6,2,1,1,1;3,1,1,1);
d) contraction (6,1,1,1;4,1)

Table 8: Table of Results of Calculations on Carbon Atom (Triplet State) for Different Basis Sets

of the atom brought about by the use of a lower accuracy factor would become more significant for low accuracy factor calculations on larger systems). On the basis of these results the (7 8)accuracy factor used extensively in prior calculations was once again adopted. It should be noted that the main file and dump file storage space required was not altered by the different accuracy factors.
The extent of the DSS required is given in Table 8 which shows the requirements for a calculation on the triplet state of the carbon atom using different basis sets.
The best total energy was obtained by employing Huzinaga's (14s/7p) basis, but this had an overall CPU requirement of almost three times that of the Dunning (9s/5p) basis.
The Dunning (10s/6p) basis had a large data storage space (DSS) requirement and took over ten times as long to reach convergence in the SCF section as the other calculations.
The total energy produced by the (10s/6p) basis was 0.0001 au worse than Huzinaga's (11s/7p) basis.

These results prompted further calculations on small molecules using the (9s/5p) and (11s/7p) bases only, the former having an overall CPU advantage; the 11s/7p basis giving a better total energy.

Table 9 shows the results of the calculations performed on Carbon Monoxide, methane, ethene and butadiene using the (9s/5p) and (11s/7p) bases. It is apparent that although Dunnings (9s/5p) basis used more DSS in the integrals calculation, the time taken per calculation is considerably lower than for the (11s/7p) set for all molecules considered.

Molecule/Basic	Main File Size	Dump File Size	CPU(s) Integrals	CPU(s) S.C.F.	Energy (au)	Machine
Carbon Monoxide 9s/5p[a]	22	8	700.5	90.82	-112.6850493	4/75
Carbon Monoxide 11s/7p[b]	18	8	1329.4	154.6	-112.60742800	4/75
Methane 9s/5p[c]	36	8	575.8	77.5	-40.18175324	4/75
Methane 11s/7p[d]	36	8	808.9	71.5	-40.170199	4/75
Methane 9s/5p[e]	36	8	438.9	78.3	-40.176511682	4/75
Methane 11s/7p[f]	36	8	631.9	71.3	-40.1769481	4/75
Ethene 9s/5p[c]	131	10	1077.3	237.3	-78.00785367	4/75
Ethene 11s/7p[d]	112	10	1737.1	171.9	-77.963665661	4/75
Ethene 9s/5p[e]	137	10	926.9	243.8	-78.00326361	4/75
Ethene 11s/7p[f]	123	10	1517	180.3	-77.9820079	4/75
Butadiene 9s/5p[e]	1497	22	23,494	3564	-154.8637072	4/75
Butadiene 11s/7p[f]	1081	22	38,613	747	-154.8056502	4/75
Butadiene 7s/3p[g]	1484	27	745	497,8	-154.73063865	4/75

Table 9: Table of Results for Different Molecules with Different Bases.

a) contraction C(6,1,1,1;4,1), O(6,1,1,1;4,1)

b) contraction C(6,2,2,1;5,2), O(6,2,2,1;5,2)

c) contraction C(6,1,1,1;4,1), H(2,3)

d) contraction C(6,2,2,1;5,2), H(2,3)

e) contraction C(6,1,1,1;4,1), H(3,1)

f) contraction C(6,2,2,1;5,2), H(3,1)

g) double zeta unscaled H(1,1,1).

e.g. for Butadiene the ratio of integrals CPU(s) is

$$\frac{(9s/5p)}{(11s/7p)} = \left(\frac{23,494}{38,613}\right) = 0.6$$

This would enable a great saving in CPU to be made if the 9s/5p set were used. Also in most cases the total energy for the 9s/5p basis was shown to be better than that for the 11s/7p basis. (It should be noted that the 11s/7p basis gave a better energy for the carbon atom calculation. This is an example showing that the results from calculations on atoms alone cannot be used to accurately predict molecular results).

Despite the 9s/5p basis requiring the larger amount of DSS it was considered that this disadvantage was outweighed by the lower CPU required and better total energies obtained. On this basis the 9s/5p basis was considered to be feasible within the CPU resources available and was chosen for use in future calculations.

To obtain a rough estimate as to the feasibility of the basis with respect to DSS available the fact that the integrals DSS required increases as (Number of basis functions)^4 then from the results given in table for butadiene.

DSS (integrals) = 1497

Number of basis functions = 52

for a molecule of say, 112 basis functions (which is of the size to be investigated) the estimated DSS is given by x

$$\left(\frac{112}{52}\right)^4 = \frac{x}{1497}$$

$$x = 32,216$$

A calculation of this size is within the limits of available resources.

References

1. V.R. Saunders, M.F. Guest, Atmol-3 Manual, Atlas Computing Division, Rutherford Laboratory, (1976).
2. J.C. Slater, Phys. Rev., 36, 57, (1930).
3. In C.A. Coulson, "Valence", Second ed., Oxford University Press.
4. M.P. Barnett, C.A. Coulson, Philos.Trans. R. Soc. London, Ser.A, 243, 221, (1951).
5. S.F. Boys, I. Shavitt, Technical Report, WIS-AF-13, University of Wisconsin Naval Research Lab.
6. E.A. Magnusson, C. Zauli, Proc.Phys.Soc. London, 78, 53, (1961).
7. I. Shavitt in "Methods of Computational Physics", edited by B. Alder, S. Fernbach, M. Rotenberg, Vol. 2, (1963), Acad. Press, (NY).
8. In H. Margenau, G.M. Murphy, "The Mathematics of Physics and Chemistry", Van Nostrand (1969).
9. S.F. Boys, Proc.R.Soc. London Ser.A, 200, 547, (1950).
10. S. Huzinaga, J.Chem.Phys., 42, 1293, (1965).
11. S. Huzinaga, J.Chem.Phys., 50, 1371, (1969).
12. S. Huzinaga, J.Chem.Phys., 52, 2224, (1970).
13. T. Dunning, J.Chem.Phys., 53, 2823, (1970).
14. T. Dunning, J.Chem.Phys., 55, 761, (1971).
15. See Appendix (A).
16. J. Nisbet, Unpublished work.

CHAPTER 3

The Experimental Method - Photoelectron Spectroscopy

Photoelectron spectroscopy (PES) is at present the best technique available for obtaining a direct measure of atomic and molecular energy levels. The information obtained by such measurements is greatly enhanced if a theoretical model is available for comparison and discussion of the results; Molecular Orbital theory provides a basis for interpretation of photoelectron spectra.

The complimentary nature of P.E. spectroscopic measurements and quantum chemical predictions constitutes what can be called a symbiosis; quantum chemical predictions provide models for spectral interpretation while the spectra serve as an excellent test for the theoretical procedures and reliability of the calculations. Having already outlined the theory and practical procedures involved in obtaining results from molecular orbital calculations we must now do the same for the experimental method.

(i) Theory

Photoelectron spectra are obtained by bombarding sample molecules with monochromatic photons. If the energy of the photons is greater than the electronic binding energies then photoelectrons are emitted with kinetic energies, E_k

$$E_k = h\nu - I_{1,2,3} \qquad (1)$$

where $I_{1,2,3}$ are the ionization energies for various molecular electronic orbitals.

$$I_n = E_j + E_{vib} + E_{ROT} \qquad (2)$$

where E_j is the adiabatic ionization energy for ejection of an electron from level j, and E_{vib} and E_{ROT} are the vibrational and rotational energies respectively of the positive ion. (Although vibrational structure is within the resolving power of the technique, rotational structure is much more closely spaced and is outwith experimental resolution). Thus by using monochromatic radiation and by precise measurement of the E_k of emitted electrons, a direct determination of the ionization energies of the molecular energy levels can be obtained. Through analysis of E_j and E_{vib} valuable information about the electronic structure of the molecular ions and their parent molecules can be obtained.

(ii) Direct Photoionization

Direct Photoionization is the process by which an electron is ejected from a molecule M(X; v") in its electronic ground state (X), vibrational level v", forming the molecular ion $M^+(x; v')$ in any one of the electronic states, x and vibrational levels, v' such that

$$M(X; v") + h\nu \rightarrow M^+(x; v') \qquad (3)$$

The probability of such a transition is determined by the square of the transition moment integral $\underline{M}$, where

$$\underline{M} = \langle \psi_i | \underline{p} | \psi_f \rangle$$

ψ_i and ψ_f are the eigenfunctions of the ground and final states respectively and $\underline{p}$ is the dipole moment operator.

Using the Born-Oppenheimer approximation, the eigenfunctions can be separated into the product of electronic and nuclear functions

$$\psi(r;\ R) = \psi_e(r;\ R)\ \psi_n(R) \tag{5}$$

where r and R are the electronic and nuclear coordinates respectively.

Neglecting interactions between vibrational and rotational motion, $\psi_n(R)$ can be expressed as a product of vibrational (ψ_v) and rotational (ψ_T) wavefunctions

$$\psi_r(R) = \frac{1}{R}\ \psi_v(R)\psi_T(R) \tag{6}$$

The dipole operator can be expressed as a sum of electronic and nuclear dependent terms

$$\underline{p} = \underline{p}_e + p_n \tag{7}$$

where $\underline{p}_e = \sum_i^{\text{all electrons}} \underline{p}_i$ and $\underline{p}_n = \sum_j^{\text{all nuclei}} \underline{p}_j$

substituting these results into (2) we obtain

$$m = \int \psi_e^{*''}(\tfrac{1}{R})\psi_v^{*''}(R)\psi_T^{*''}(R)\ |\ \underline{p}_e + \underline{p}_n\ |\ \psi_e'(r;R)\tfrac{1}{R}\psi_v'(R)\psi_T'(R)\,d\tau \tag{8}$$

but $d\tau = d\tau_e\ d\tau_R$, where $d\tau_e$ is the volume element of the

electron coordinates, and $d\tau_R = R^2 \sin\theta d\theta d\phi dR$ is the volume element of the nuclear coordinates substituting for $d\tau$ (8) becomes

$$m = \int \left(\frac{1}{R}\right)^2 \psi^{2''}_v(R)\psi^{*''}_T(R)\psi_v'(R)\psi_T'(R)d\tau_R \int \psi^{*''}_e(r;R)|p_e|\psi_e'(r;R)d\tau_e$$

$$+\int \left(\frac{1}{R}\right)\psi^{*''}_v(R)\psi^{*''}_T(R)\ |p_n|\ \frac{1}{R}\ \psi_v'(R)\psi_T'(R)d\tau_R \int \psi_e^{*''}(r;R)\psi_e'(r;R)d\tau_e \tag{9}$$

The second term vanishes since $\psi_e^{*''}$ and ψ_e' belong to different electronic states and are orthogonal using the substitution for $d\tau_R$, (9) becomes

$$m = \int \psi^{*'}_T(R)\psi_T'(R)\sin\theta\ d\theta d\phi \int \psi_v^{*''}(R)\psi_v'(R)dR \int \psi^{*''}_e(r;R)\times$$

$$|p_e|\psi_e'(r;R)d\tau_e \tag{10}$$

The first integral is constant for any combination of rotational levels, J, and to a good approximation the second and third integrals are independent of J. Therefore we can neglect the rotational part when ionization is applied to PES since rotational structure is unresolved.

$$m = K\int \psi^{*''}_v(R)\psi_v'(R)dR \int \psi^{*''}_e(r;R)|p_e|\psi_e'(r;R)d\tau_e \tag{11}$$

K = constant.

The second integral $m_e(r;R)$ is the matrix element of the electric dipole moment for a given configuration. As in most cases this varies only slightly with R, it can be expressed as a Taylor series about the R value corresponding to maximum

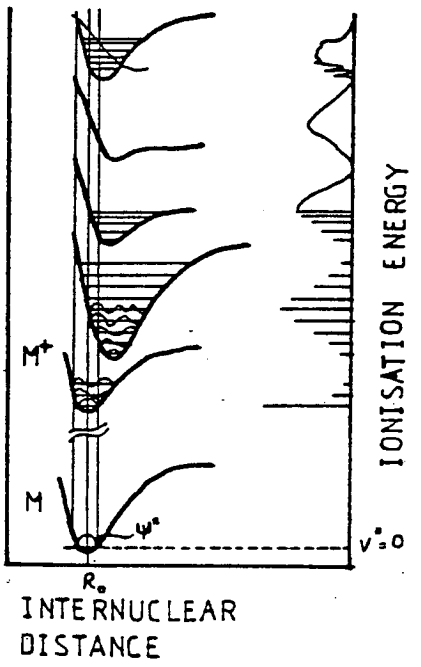

FIG 14 POTENTIAL ENERGY CURVES FOR MOLECULE M IN ITS GROUND STATE AND THE CORRESPONDING MOLECULAR ION M^+ IN VARIOUS IONIC STATES. THE FRANK-CONDON REGION IS BETWEEN THE VERTICAL LINES. PHOTOELECTRON BANDS RESULTING FROM TRANSITIONS ARE SHOWN ON THE RIGHT.

overlap of $\psi_v^{*"}\psi_v^{'}$ (usually R_o the ground state configuration).

$$m_e(r;R) = m_e(r;R_o) + \left(\frac{\delta m_e(r;R_o)}{\delta R}\right)_{R_o}(R-R_o) + \ldots\ldots \quad (12)$$

As the first term is the largest other terms can be neglected, and (9) becomes

$$m_e(r;\ R_o) = \int \psi_e^{*"}\ (r;\ R_o)\,|\ \underline{p}_e|\psi_e^{'}(r;R_o)\ d\tau_e \quad (13)$$

The photoionization transition probability can therefore be expressed as

$$\alpha|m_e(r;R_o)|^2(<\psi_v^{"}(R)\,|\psi_v^{'}(R)>)^2 \quad (14)$$

where the vibrational overlap integral is called the Franck-Condon factor, and is largely responsible for the relative intensities of the vibrational bands in the photoionization transition. This indicates that transitions are favoured when there is large overlap of the vibrational wavefunctions in the initial and final states. This is favoured when the nuclear positions are the same in the initial and final states, but is not an absolute requirement (See Fig (14)).

(iii) Adiabatic and Vertical Ionization Energies

Several different ionization energies can be measured, depending on the degree of vibrational excitation of the ions. Two types of ionization energies are usually considered.

1) Adiabatic ionization energy - this corresponds to the transition

$$m(X,v'' = 0) + h\nu \rightarrow m^+(x,v' = 0) + e^-$$

that is the minimum energy required to eject an electron from a molecule in its ground vibrational state and transform it into a positive ion in the lowest vibrational level of an electronic state of the ion.

2) Vertical Ionization Energy - this corresponds to the transition

$$m(X,v'' = 0) + h\nu \rightarrow m^+(x,v' = n) + e^-$$

where the value n of the vibrational quantum no v' corresponds to the vibrational level whose wavefunction gives the largest overlap with the v" = 0 wavefunction. This is the most probable transition and usually corresponds to the vertical transition where the internuclear separation of the ionic state is similar to that of the ground state. See Fig (1 4). In our investigation of ionization potentials we will normally consider the vertical ionization energies.

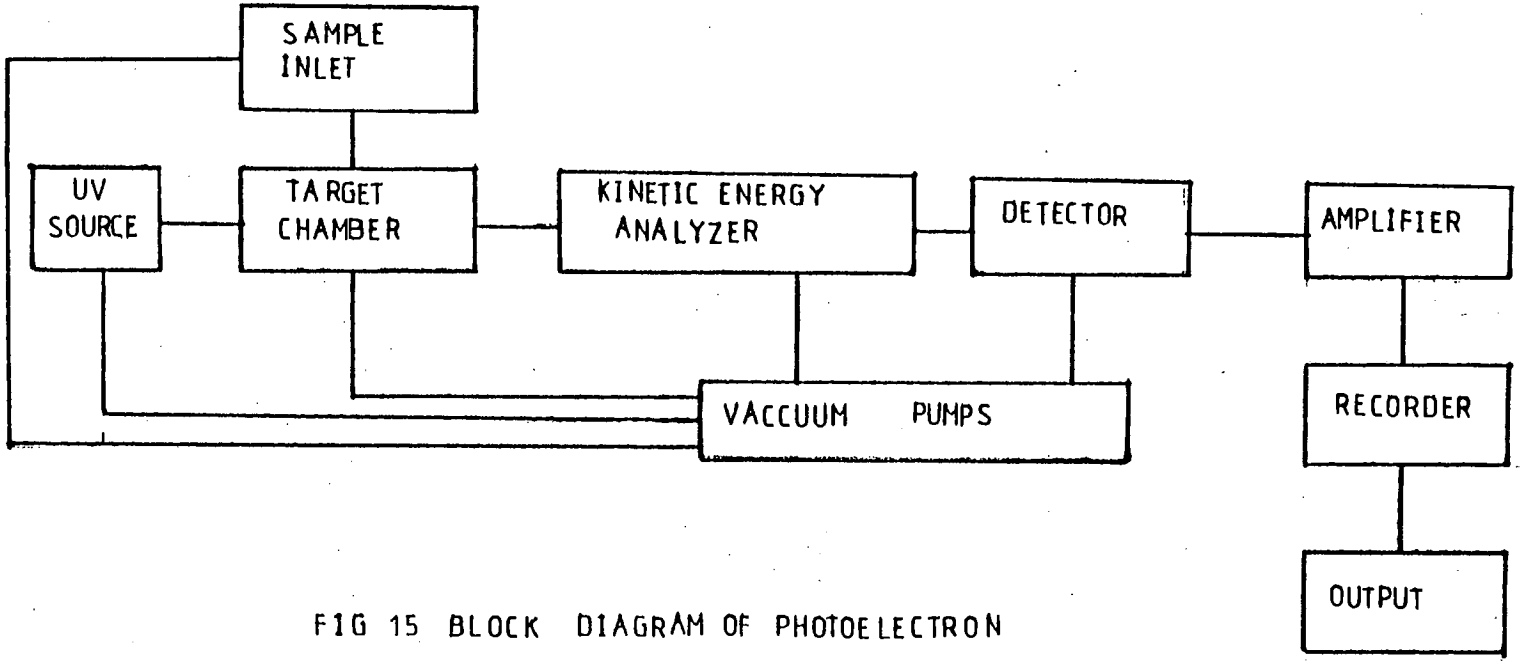

FIG 15 BLOCK DIAGRAM OF PHOTOELECTRON SPECTROMETER

(iv) Practical Considerations

A block diagram of the principal components of a PE spectrometer is given in Fig. (15). The spectrometer used in this study is a modified Perkin Elmer PS 16 UV photoelectron spectrometer based on the design of D.W. Turner[1], with an Helectros He(I)/He(II) UV photon source and alternative time averaging computer (CAT) recording system. The principle of operation is outlined below.

The ionizing source is an intense beam of photons produced by an electrical discharge in helium. The photons are directed into the target chamber through a capillary tube which collimates the photon beam and prevents contamination in the discharge by the sample. Photoelectrons produced by collisions of photons with vapourized sample molecules in the target chamber have kinetic energies E_k see equation (1). Those electrons ejected within the solid angle of acceptance of the target chamber exit slit enter the analyser where they are energy analysed by electrostatic deflection in a field produced between two concentric curved plates, Fig. (16). For a particular field only electrons of a particular energy are focussed onto the analyser exit slit. (A focussing lens is formed in the analyser by incorporating in each plate a small oppositely charged compensating electrode). The magnitude of the analysing potential is controlled by the recorder scanning mechanism. Electrons passing through the analyser exit slit are incident upon a "channeltron" detector in which

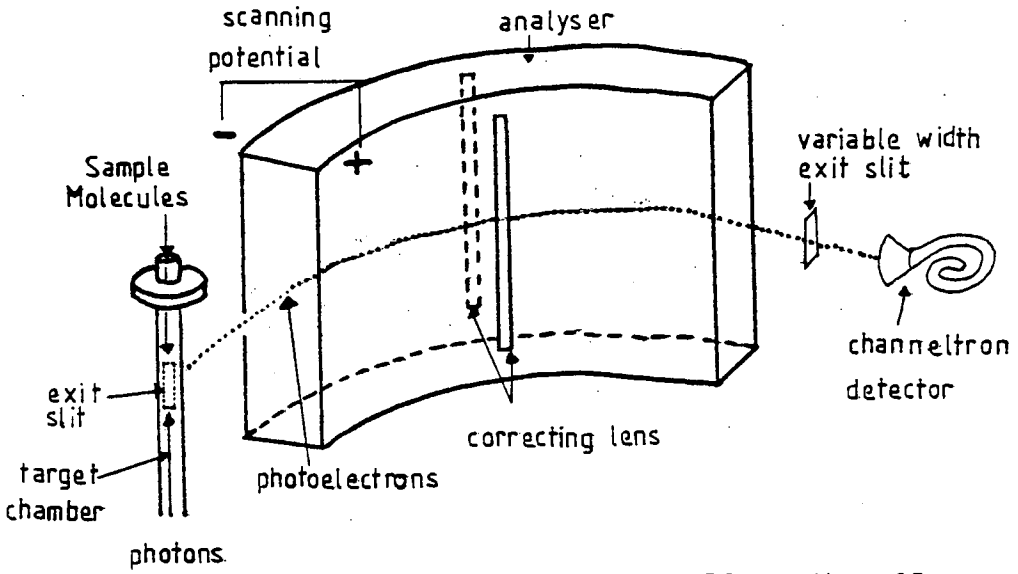

FIG 16 SCHEMATIC DIAGRAM OF ANALYZER AND OTHER BASIC COMPONENTS

a pulse is generated. The pulses from the detector, each corresponding to impact of an electron are converted by an amplifer and ratemeter to an output voltage proportional to the pulse frequency. The information is displayed as a differential spectrum by plotting the output detector voltage against the voltage applied to the analyser plates. The resulting analyser voltages can be converted by utilization of suitable internal calibrants into kinetic energy E_k or ionization energy E_I.

The following points must be noted (i) the internal calibrants most commonly used are the $^2P_{\frac{1}{2},\frac{3}{2}}$ doublets of Xenon and argon.

(ii) The ionizing photons must be monochromatic. In UV PES studies a helium resonance lamp is most often used. The principal resonance line in the helium spectrum is the $He(I)^*_\alpha$ at 584.334 Å, the "raie ultime", which corresponds to a transition from the first excited state to the ground state of the atom, $^1P_1 \rightarrow {}^1S_0$, this results for 98% of the emission intensity under normal operating conditions (∿ 2kV, 80 mA, 0.2 torr He). The He(II)* line at 303.781Å (40.8136 eV) results from resonance fluorescence of singly ionized He atoms. The intensity of this line is increased for lower He pressures and higher current density (∿ 5kV, 120 mA, 0.1 torr He). By utilization of both of these lines the valence shell orbitals up to 26 eV can be studied. It is not possible to extend the range up to 40 eV as the 30 to 40 eV region (9 to 10 eV E_k) is dominated by the He(I) spectra; the He(I) line being at least ten times

*Roman numerals indicate whether the emitting species is the neutral atom (I) or the singly ionized atom (II)

more intense than the He(II) line even under He(II) operating conditions.

(iii) Sample handling techniques - if the sample is non volatile and requires heating to obtain a sufficient sample vapour pressure, the design of the spectrometer is such that contamination of the analyser often takes place. This initially results in poorer resolution and eventually loss of signal. Therefore where possible it is best to attempt to increase the vapour pressure by alternative techniques. For solid samples this can be accomplished by grinding the sample to a fine powder which increases the surface area from whence molecules can "volatilise." For non volatile liquids the surface area can be increased by soaking the liquid into a plug of glass wool which increases the surface area. Non volatile samples are inserted directly into the target chamber in a sample holder using a heated probe accessory, whereas volatile samples enter the body of the instrument from an external reservoir.

(iv) Temperature control - the heated sample inlet (probe) accessory is in contact with the discharge lamp housing which is hot. The probe and hence sample temperature control on the PS16 is by water or air cooling of the lamp housing. This control system is very crude and often results in temperature changes of up to $\pm 5^{o}$ using water cooling, due to changes in mains water temperature. In an attempt at temperature stabilization various solvents were allowed to reflux in the vore of the heated probe accessory. This kept the sample

temperature constant to within $\pm 2^{o}$.

(v) Photoelectron spectra exhibit considerable random fluctuations and statistical noise due to low count rates and analysis of low energy electrons which are susceptible to stray electrostatic and electromagnetic fields and space charge effects. The peak intensities have an uncertainty which is equal to the square root of the total number of electrons counted at a given voltage. This can be reduced by increasing the product of the count rate and counting time, which is best achieved by increasing the count rate.

(vi) For extremely small amounts of sample or for low intensity spectra (either from non volatile samples or those obtained from the less intense He(II) radiation), a time averaging computer (CAT) was employed to reduce noise levels. This operates by scanning and storing the complete spectrum many times, adding each scan to the memory, and averaging over the number of scans. This results in reduction of noise, a reduction which increases as the number of scans increases.

(vii) The use of UV ionizing radiation limits one to a study of valence shell electrons, (6 → 30 eV), but it is possible to study core levels by X-ray irradiation (1000 → 1500 eV). The gap between low energy (UV) and high energy (X-ray) studies is likely to be bridged by utilization of "synchrotron radiation" produced by accelerating electrons in a magnetic field. This radiation potentially could be used to scan the 30 eV to 1000 eV region which is at present inaccessible by the two conventional methods.

Having now outlined the theory and practical procedures involved in obtaining an experimental measure of IP's and hence orbital energies, we must now consider how these are related to theoretical results obtained by the Hartree-Fock method.

(v) The Relationship between HF calculations and PES

The most rigorous approach for calculating ionization energies, within the Hartree-Fock approximation is the ΔE_{SCF} method. Here separate calculations are performed on the molecular ground state (m), and various states of the molecular ion (m^+). Since ionization energies correspond to transitions from the molecular ground state to the cationic states, differences in calculated total energies of these states should correspond to the experimental orbital energies.

$$\Delta E^{j}_{SCF} = E^{m}_{\text{ground state}} - E^{m+}_{\text{excited state: (singly occupied MO "j")}} = IP^{j}_{\text{corresponding to removal of electron from orbital j}}$$

Such calculations require an open shell treatment for the ion radical, which are unpopular as they often diverge or converge very slowly. For this reason calculated ionization energies are usually obtained by applying Koopman's Theorem[2] to a calculation on the ground state of the molecule.

(vi) Koopman's Theorem (KT)

KT states that "the molecular orbital energies are equal to the negatives of the calculated molecular orbital eigenvalues".

If we consider a closed shell molecule with n doubly occupied molecular orbitals ϕ_i. Then ψ for the ground state is

$$\psi = |\phi_1^2 \ldots \phi_{n-1}^2 \phi_n^2| \qquad (15)$$

the total energy of the system being given by the expression(ch1:87) This total energy is a sum of three terms.

a) ε_i the energy each electron would have alone in the nuclear framework, its kinetic and potential energy of nuclear attraction.

b) J_{ij} - a coulomb repulsion integral between every pair of electrons.

c) K_{ij} - an exchange interaction between every pair of electrons of the same spin.

The expression for the energy of the ion formed by removal of an electron from the orbital ϕ_n is similar to (ch1:eqn87), with the exception of missing terms in the summations due to the absence of electron n. If we assume $\varepsilon_j, J_{ij}, K_{ij}$ are the same in the molecule and the ion (Frozen core approximation) then the energy difference between the molecule and ion, hence the ionization energy is

$$\varepsilon_n + \sum_{i=1}^{n-1} (2J_{ni} - K_{ni}) + J_{nn} \qquad (16)$$

The orbital energy ε_n is determined by solution of the SCF equations (ch1;eqn 71). We can express ε_n from equations (ch1 eqn 85) as a sum of integrals

$$\varepsilon_n^{SCF} = \varepsilon_n + \sum_{j=1}^{n-1} (2J_{nj} - K_{nj}) + J_{nn} \qquad (17)$$

This sum being identical to that for the ionization energy expressed in (16). This is a general proof of Koopman s' Theorem which is better expressed as "the orbital energy ε_n^{SCF} for a closed shell molecule computed in an ab initio SCF calculation is exactly equal to the ionization energy of an electron from that orbital in the frozen core approximation.

When applying Koopman s' Theorem to general molecular photoionization phenomena, there are three additional approximations that are necessary, i.e.

1) The Reorientation, or Frozen Core Approximation. The general proof of Koopman s' theorem uses the assumption that all the orbitals $\phi_1 \ldots \phi_{n-1}$ are unaltered when going from molecule to ion. In order for the integrals of (16, 17) to be identical, it is essential that the orbitals of the ion be identical to those of the molecule, that is, there is no reorientation of orbitals upon ionization.

2) The Relativistic Energy Approximation. Since Hartree Fock theory does not consider relativistic effects, the use of Koopman s' Theorem is equivalent to assuming that the relativistic energy of both molecule and ion is the same, and that the orbital energy is given by a difference in electrostatic energy expressions.

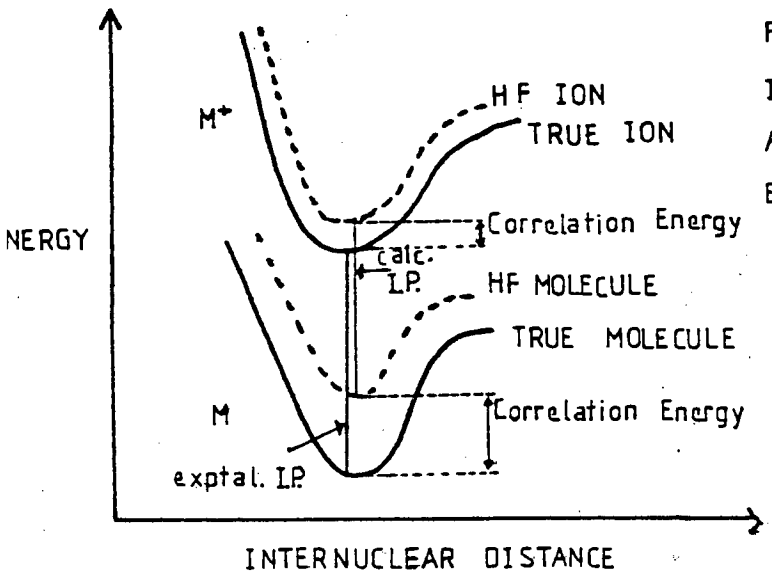

FIG 17 MOLECULAR AND IONIC POTENTIAL ENERGY AND HARTREE FOCK POTENTIAL ENERGIES

3) The Correlation Energy Approximation - Electrons tend to keep apart, that is, their motions are correlated. Koopman's theorem takes the difference between two energy expressions, neither of which include correlation effects. The assumption is made that the correlation energy is the same in both the molecule and ion. Correlation effects arise largely from pair interactions between electrons, and since the ion has less electrons than the parent molecule, this correlation energy will certainly be different and generally less in the ion than its parent molecule.

(vi) Spectral Assignment

The inherent approximations of Hartree Fock calculations lead to calculated orbital energies (OE) which are much larger than those obtained experimentally, although there is often an almost linear relationship between the two, Fig (17) Groupings of calculated IP's (or OE's) often match the observed groupings, and therefore by matching of these groupings spectral assignment can be achieved.

Since calculations provide calculated eigenvectors for particular eigenvalues the nature of each IP can be interpreted. Of course KT is not infallible and can be shown (see for example chapter (5)page) to give incorrect orbital ordering for closely lying levels. Indeed discrepancies in the relatively simple assignment of spectra by virtue of KT and those obtained using more sophisticated methods* have

*for example the ΔE_{SCF} or Green Functions method

prompted one group to comment, rather unjustly, that KT is "as useful as looking up a telephone directory!"[2] However KT has proved useful and appropriate, and indeed in the past, when computational facilities were considerably less sophisticated than those now available, provided the best available technique for spectral assignment.

Assignment can also be aided by relative peak intensity studies. Under He(II) conditions the photoionization cross section for lone pair and 'σ' type orbitals is larger than under He(I) conditions. This results in relatively larger He(II) peak intensities for these orbitals, and hence aids their identification. In addition peak shapes can provide useful information, see Fig. (14). Electrons from orbitals not strongly involved in bonding will have strong O → O transitions, whereas the envelope of a peak resulting from a bonding electron emission will have a Lorentzian shape.

Thus we can see that often a combination of interpretive techniques is best, and this is most often employed. We feel that absolute theoretical assignment of PES can be best achieved by the following

a) Use of a sufficiently large basis set (for example the double zeta basis given in Appendix A).

b) Optimization of the geometry of the molecular ground state.

c) Calculation of the total energies of the various geometrically optimized cationic (+1) states.

d) Employing the ΔE_{SCF} method

$$E_{ion} - E_{\substack{ground \\ state}} = -IP$$

With present computational facilities this technique would prove to be extremely lengthy and for larger structures, (for example $C_{10}H_8$), even impossible. However for future work using more powerful resources, it is possible that this technique will become routine.

In the following chapters where spectra are to be assigned, the techniques employed for interpretation will be fully discussed.

References

1. In: D.W. Turner, C. Baker, A.D. Baker, C.R. Brundle, "Molecular Photoelectron Spectroscopy". Wiley-Interscience, London (1970).

2. T. Koopmans, Physica, 1, 104, (1933).

3. W. Von Niessen, W.P. Kraemer, G.H.F. Kiercksen, Chem.Phys., 41, 113, (1979).

CHAPTER 4

Fig. 18

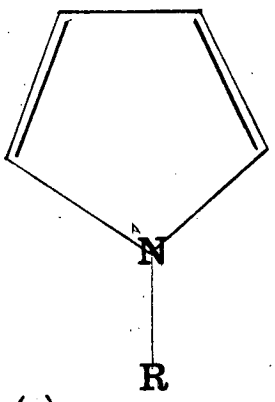

(1)
a) R = H
b) R = Me

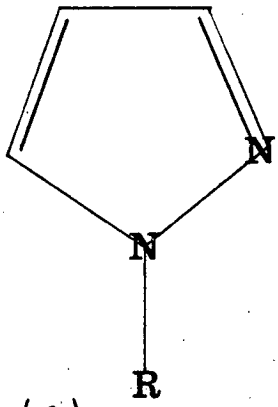

(2)
a) R = H
b) R = Me

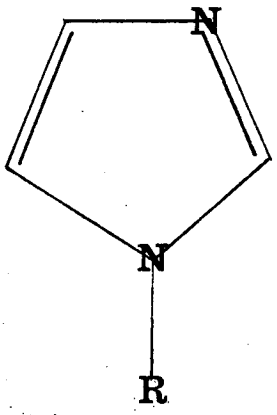

(3)
a) R = H
b) R = Me

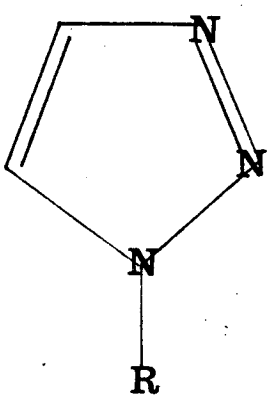

(4)
a) R = H
b) R = Me

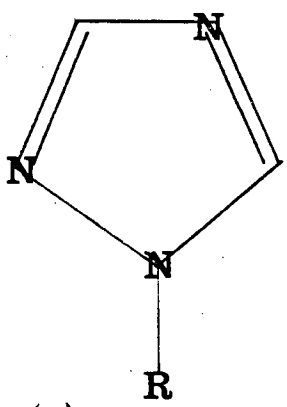

(5)
a) R = H
b) R = Me

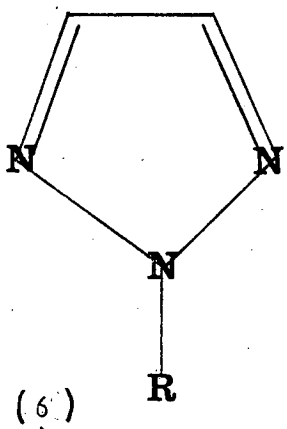

(6)
a) R = H
b) R = Me

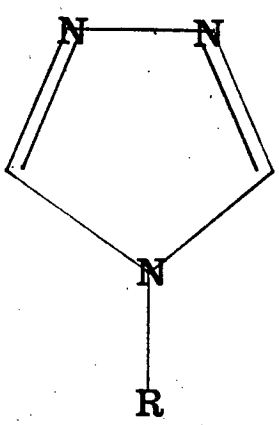

(7)
a) R = H
b) R = Me

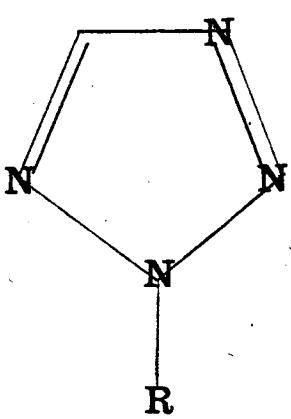

(8)
a) R = H
b) R = Me

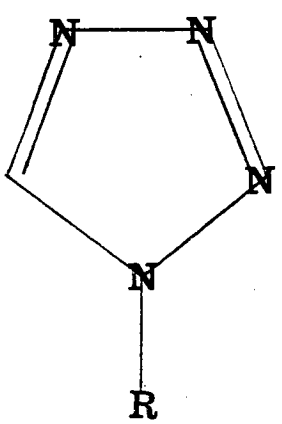

(9)
a) R = H
b) R = Me

THE AZOLES

In this Chapter ab initio calculations have been performed on a series of molecules (see Fig (18)). Calculated electric field gradients (and hence quadrupole coupling constants) have been obtained for comparison with experimental data. Herein is an extension of previous work done by the Edinburgh Quantum chemistry group[1] which provided a comparison of both Nuclear Quadrupole Resonance (NQR) and available Microwave (MW) data with that calculated using LCAO Hartree-Fock methods.

In addition the electronic structure of the molecules has been further studied by He(I)/He(II) photoelectron spectroscopy, and using the experimental and calculated data, we are able to ascertain the dominant vapour phase form of molecules capable of exhibiting tautomerism.

As an introduction to this work an investigation into the origins and theoretical background of the NQR phenomenon is instructive.

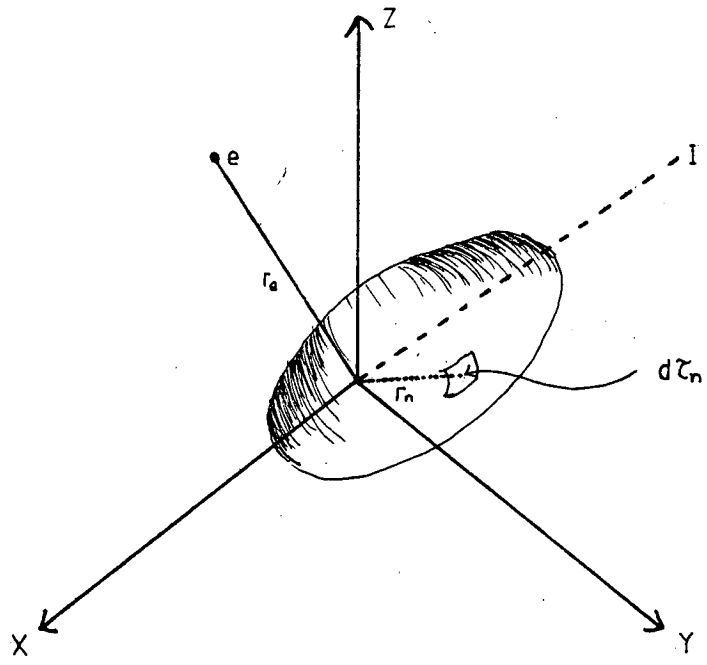

FIG 19 REFERENCE SYSTEM FOR NUCLEAR INTERACTION WITH EXTRANUCLEAR CHARGES.

Theoretical Background

(i) Pure NQR Phenomenon

The nuclear quadrupole interaction results from a nonspherical distribution of nuclear charge which gives rise to an NQR moment, and a nonspherical distribution of electronic charge about the nucleus which gives rise to an electric field gradient at the nucleus. (For spherically symmetric nuclear charge or electronic charge around the nucleus no such interaction is observed). The interaction puts a twisting torque on the nucleus tending to align its spin moment in the direction of the field gradient. As a result of this torque the spin axis will precess about the direction of the resultant field gradient, giving rise to precessional frequencies and NQR spectra. In solids the field gradients are fixed in direction and pure NQR spectra analogous to NMR spectra are observable. In the gaseous state the field gradient at the nucleus depends upon the rotational state of the molecule, and the NQR interaction differs for each rotational state and leads to hyperfine structure of the rotational levels.

Let us first consider the classical interaction energy of a nuclear charge with a static potential arising from extranuclear charges. Let $V(X,Y,Z)$ be the potential at (X,Y,Z) (which are cartesian coordinates fixed in space) which has its origin at the centre of the nucleus (see Fig19). The value of $V(X,Y,Z)$ at the origin is V_o. Because of the finite size of the nucleus the electrical energy is given by

$$E = \int \rho_n V \, d\tau_n \qquad (1)$$

where $\rho_n = \rho(X,Y,Z)$ represents the density of the nuclear

charge in the elemental volume $d\tau_n$, and the integral is over the nuclear volume. (ρ_n can be taken as uniform throughout this volume). To evaluate this integral we can express the potential, V as a Taylors expansion.

$$V = V_o + \left(\frac{\partial V}{\partial X}\right)_o X_n + \left(\frac{\partial V}{\partial Y}\right)_o Y_n + \left(\frac{\partial V}{\partial Z}\right)_o Z_n$$

$$+ \frac{1}{2}\left[\left(\frac{\partial^2 V}{\partial X^2}\right)_o X_n^2 + \left(\frac{\partial^2 V}{\partial Y^2}\right)_o Y_n^2 + \left(\frac{\partial^2 V}{\partial Z^2}\right)_o Z_n^2\right] \qquad (2)$$

$$+ \left(\frac{\partial^2 V}{\partial X \partial Y}\right)_o X_n Y_n + \left(\frac{\partial^2 V}{\partial X \partial Z}\right)_o X_n Z_n + \left(\frac{\partial^2 V}{\partial Y \partial Z}\right)_o Y_n Z_n$$

where $X_n = \Delta X$, $Y_n = \Delta Y$, $Z_n = \Delta Z$, represent the nuclear coordinates at the point of the elemental volume $d\tau_n$ in the nucleus.

If we substitute (2) into (1), the first term is

$$E_o = V_o \int \rho_n \, d\tau_n \qquad (3)$$

and this represents the monopole interaction which is independent of nuclear orientation. The second term, the dipole term

$$E_d = \left(\frac{\partial V}{\partial X}\right)_o \int X_n \rho_n d\tau_n + \left(\frac{\partial V}{\partial Y}\right)_o \int Y_n \rho_n d\tau_n + \left(\frac{\partial V}{\partial Z}\right)_o \int Z_n \rho_n d\tau_n$$

$$= 0 \qquad (4)$$

because $\rho_n(X,Y,Z)$ is a symmetric function, (this is shown by the absence of any experimentally observed electric dipole moment).

The term of next highest order, represents the quadrupole interaction

$$E_Q = \frac{1}{2}\left[\left(\frac{\partial^2 V}{\partial X^2}\right)_o \int \rho_n X_n^2 d\tau_n + \left(\frac{\partial^2 V}{\partial Y^2}\right)_o \int \rho_n Y_n^2 d\tau_n + \left(\frac{\partial^2 V}{\partial Z^2}\right)_o \int \rho_n Z_n^2 d\tau_n\right]$$

$$+ \left(\frac{\partial^2 V}{\partial X \partial Y}\right)_o \int \rho_n X_n Y_n d\tau_n + \left(\frac{\partial^2 V}{\partial X \partial Z}\right)_o \int \rho_n X_n Z_n d\tau_n + \left(\frac{\partial^2 V}{\partial Y \partial Z}\right)_o \int \rho_n Y_n Z_n d\tau_n \quad (5)$$

We now change the reference system from (X,Y,Z) to (x,y,z) where z lies along the spin axis I. As a consequence of rotational symmetry about the spin axis,(x,y,z) become the principal axes, and integrals containing cross terms vanish and

$$\int \rho_n x_n^2 \, d\tau_n = \int \rho_n \, y_n^2 \, d\tau_n$$

$$= \frac{1}{2} \int \rho_n (y_n^2 + x_n^2) d\tau_n$$

$$= \frac{1}{2} \int \rho_n (r_n^2 - z_n^2) d\tau_n \quad \text{since } r_n^2 = x_n^2 + y_n^2 + z_n^2$$

Hence equation (5) becomes

$$E_Q = \frac{1}{4}\left[\left(\frac{\partial^2 V}{\partial x^2}\right)_o + \left(\frac{\partial^2 V}{\partial y^2}\right)_o\right] \int \rho_n (r_n^2 - z_n^2) d\tau_n + \frac{1}{2}\left(\frac{\partial^2 V}{\partial z^2}\right) \int_o \rho_n z_n^2 d\tau_n \quad (6)$$

Now Laplaces equation $\nabla^2 V = 0$ holds as the charge giving rise to the field gradient, can be considered to be zero over the nuclear volume, therefore

$$\left(\frac{\partial^2 V}{\partial x^2}\right)_o + \left(\frac{\partial^2 V}{\partial y^2}\right)_o = -\left(\frac{\partial^2 V}{\partial z^2}\right)_o \quad (7)$$

and $$E_Q = \frac{1}{4}\left(\frac{\partial^2 V}{\partial z^2}\right)_o \int \rho_n (3z_n^2 - r_n^2) d\tau_n \quad (8)$$

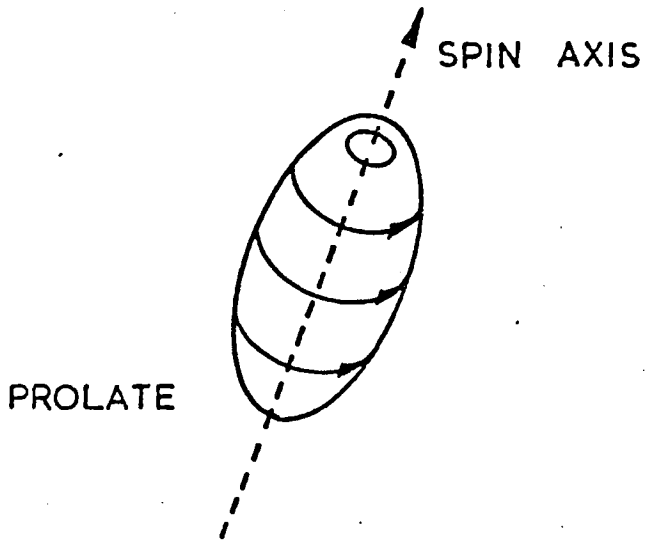

FIG. 20

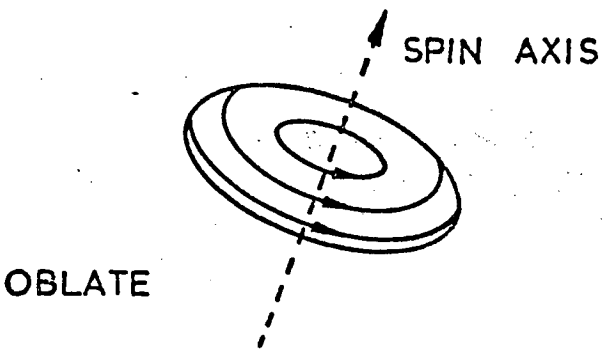

FIG. 20

we define

$$\frac{1}{e}\int \rho_n (3z_n^2 - r_n^2) d\tau_n = Q^* \qquad (9)$$

as the intrinsic nuclear quadrupole moment

$$E_Q = \frac{1}{4} \left(\frac{\partial^2 V}{\partial z^2}\right)_o eQ^* \qquad (10)$$

Q^* is a measure of the extent to which the nuclear charge distribution departs from spherical symmetry. A positive Q^* indicates the nucleus is elongated along the spin axis and is prolate. A negative Q^* indicates the nucleus is flattened along the spin axis i.e. oblate (see Fig. 20).

Q^* is not an observable, but can be obtained from the observable quantity Q, as

$$Q^* = \frac{2(I+1)}{2I-1} Q \qquad \text{(see below)} \qquad (11)$$

Now $-\left(\frac{\partial^2 V}{\partial z^2}\right) = q_{zz}$ is the electric field gradient or second derivative of the electrostatic potential. This is a tensor quantity and can be defined by its principal components and their direction cosines with respect to a set of space fixed orthogonal axes, $(X_p Y_p Z_p)$ originating at the centre of the nucleus such that these axes are the principal axes of the field gradient tensor. (These axes do not coincide with the principal inertial axes (x,y,z). Hence

$$\frac{\partial^2 V}{\partial Z^2} = \frac{\partial^2 V}{\partial X_p^2}\left(\frac{\partial X_p}{\partial Z}\right)^2 + \frac{\partial^2 V}{\partial Y_p^2}\left(\frac{\partial Y_p}{\partial Z}\right)^2 + \frac{\partial^2 V}{\partial Z_p^2}\left(\frac{\partial Z_p}{\partial Z}\right)^2 \qquad (12)$$

Also

$$\frac{\partial^2 V}{\partial Z^2} = \frac{\partial^2 V}{\partial X_p^2}\left(\frac{I_x}{|\underline{I}|}\right)^2 + \frac{\partial^2 V}{\partial Y_p^2}\left(\frac{I_y}{|\underline{I}|}\right)^2 + \frac{\partial^2 V}{\partial Z_p^2}\left(\frac{I_z}{|\underline{I}|}\right)^2 \qquad (13)$$

since $\underline{I}$ is along the Z axis and I_x, I_y, I_z are the components of $\underline{I}$, therefore the direction cosines are

$$\frac{\partial X_p}{\partial Z} = \cos(X_p, Z) = \frac{I_x}{|\underline{I}|} \text{ etc.} \qquad (14)$$

Now if the spin components are treated as quantum mechanical operators and if $I(I+1)$, the eigen value of $\underline{I}^2$, is substituted for $\underline{I}^2$ a spin Hamiltonian operator is obtained by substituting (13) into (10)

$$H_Q = \frac{eQ^*}{4I(I+1)}\left[\left(\frac{\partial^2 V}{\partial X_p^2}\right)_o I_x^2 + \left(\frac{\partial^2 V}{\partial Y_p}\right)_o I_y^2 + \left(\frac{\partial^2 V}{\partial Z_p}\right)_o I_z^2\right] \qquad (15)$$

When the field gradient is axially symmetric about Z_p, then using Laplaces equation

$$\left(\frac{\partial^2 V}{\partial X_p}\right)_o = \left(\frac{\partial^2 V}{\partial Y_p^2}\right)_o = -\frac{1}{2}\left(\frac{\partial^2 V}{\partial Z_p^2}\right)_o \qquad (16)$$

Now $I^2 = I_x^2 + I_y^2 + I_z^2$ and using this and equation (16), (15) becomes (for axially symmetric coupling)

$$H_Q = \frac{eQ^*}{8I(I+1)}\left(\frac{\partial^2 V}{\partial Z_p^2}\right)_o (3I_z^2 - I^2) \qquad (17)$$

and

$$E_Q = \frac{eQ^*}{8I(I+1)} \left(\frac{\partial^2 V}{\partial Z_p^2}\right)_o (3M_I^2 - I(I+1)) \qquad (18)$$

where M_I is the eigenvalue of I_z in units of $\hbar$. Eqn. (17) is the Hamiltonian for pure quadrupole resonance in the solid state.

Now comparing equation (17) with equation (10), Q is defined as the effective component for the most complete alignment along Z in other words the component for $M_I = I$, hence

$$(E_Q)_{M_I = I} = eQ^* \left(\frac{\partial^2 V}{\partial Z_p^2}\right)_o \frac{2I-1}{8(I+1)} \qquad (19)$$

also since

$$E_Q = \frac{1}{4} e \left(\frac{\partial^2 V}{\partial Z_p^2}\right)_o eQ^*$$

therefore $Q^* = \frac{2(I+1)}{2I-1} Q$

substituting this expression for Q^* into equation (15) the solid state operatore becomes

$$H_Q = \frac{1}{2I(2I-1)} (\chi_{xx} I_x^2 + \chi_{yy} I_y^2 + \chi_{zz} I_z^2) \qquad (20)$$

where $\chi_{xx} = eQq_{xx} = \left(\frac{\partial^2 V}{\partial Z_p^2}\right)_o$ A Quadrupole

resonance experiment yields the value of the quantity $\frac{e^2 q}{h} Q$ rather than q itself. If a precise value of the quadrupole moment, Q, is known, one may hence deduce the field gradient in the molecule directly. However nuclear quadrupole moments are difficult to measure, but have been obtained by several methc

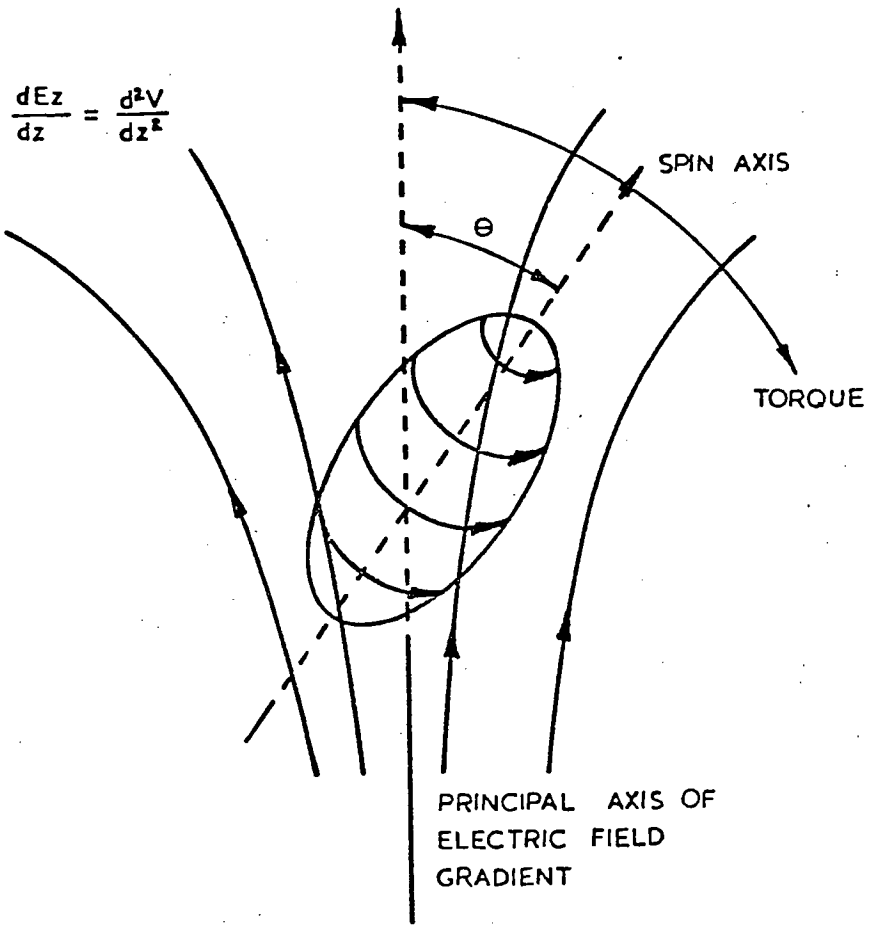
$\frac{dEz}{dz} = \frac{d^2V}{dz^2}$
SPIN AXIS
θ
TORQUE
PRINCIPAL AXIS OF
ELECTRIC FIELD
GRADIENT

FIG. 21

Now if the field gradient is almost axially symmetric about a bond to the coupling atom, the nearly symmetric axis is defined as the Z axis and the symmetry parameter (η) is

$$\eta = \frac{\chi_{xx} - \chi_{yy}}{\chi_{zz}} \qquad (21)$$

Because Laplaces equation holds

$\chi_{xx} + \chi_{yy} + \chi_{xx} = 0$, there are only two independent coupling parameters η and χ_{zz}.

As stated above the quadrupole experiences a torque in an electric field gradient, which tries to change the angle (θ) between the nuclear spin axis and the direction of χ_{zz} (see fig. The result of this for the case of axial symmetry is that the spin axis precesses about the direction of χ_{zz} at a frequency whic is the nuclear quadrupole resonance frequency of the nucleus in its electrostatic environment. Transitions between the quadrupole hyperfine levels in solids can be observed through coupling of the magnetic dipole moment of the nucleus to the applied radiation field (i.e.ofradio frequency). The selection rule for pure quadrupole absorption is $|\Delta M_I| = I$, therefore for an axially symmetric field i.e. $\eta = 0$ the resonant frequencies are

$$\nu = \left|\frac{\chi_{zz}}{\hbar}\right| eQ\left[\frac{3}{4I(2I-1)}\right][2|M_I|-1] \qquad (22)$$

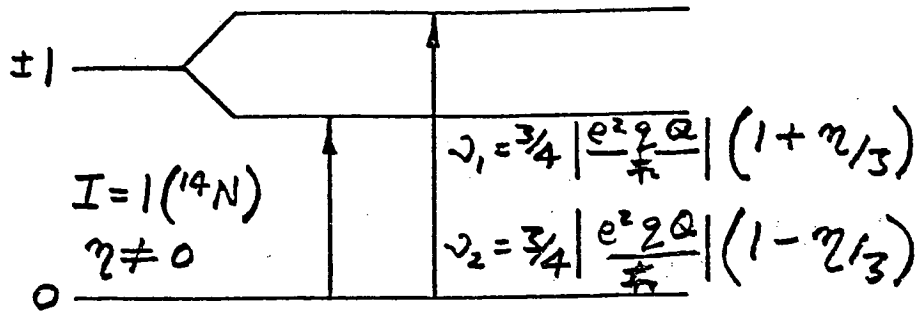

FIG. 23 .

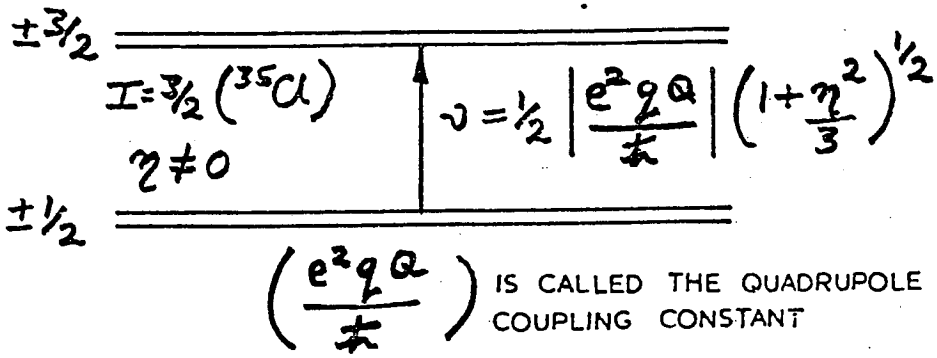

FIG. 23 .

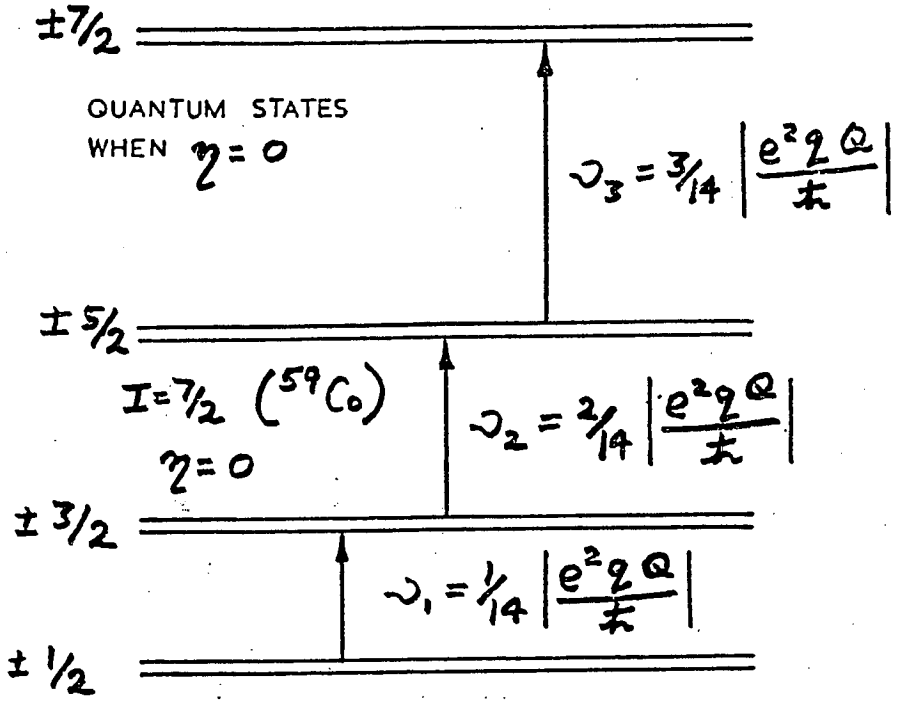

FIG. 22

In this case $\chi_{xx} = \chi_{yy}$, and the nuclear magnetic quantum numbers M_I can then be used to describe the energy levels. Relatively simple energy level diagrams are obtained (see Fig. 2
It is convenient to classify these according to the nuclear spin quantum number (I). For half integral I the energy levels grou together in pairs each remaining doubly degenerate (Kramers degeneracy). The magnitude of the coupling constant can be deduced directly from the spectrum. This is defined as $\frac{e^2qQ}{\hbar}$, and is quoted in units of Mc/s.

For a non axially symmetric field i.e. when $\eta \neq 0$ $\chi_{xx} \neq \chi_{yy}$. This is by far the most common case and the energy level diagrams become more complex than in(Fig. 23). A finite η means that the nuclear magnetic quantum numbers M_I, no longer provide a satisfactory description of the states. Now the energy level diagrams are assigned according to the value of I (see fig. 23).

In this case for I = 1 (eg. ^{14}N) three frequencies are expected.

$$\nu_{\frac{1}{2}} = \frac{3}{4} \left| \frac{e^2qQ}{\hbar} \right| \left(1 \pm \frac{\eta}{3}\right)$$

$$\nu_3 = \frac{1}{2} \left| \frac{e^2qQ}{\hbar} \right| \eta \qquad (23)$$

of which only the first two are commonly observed, the third be too small except when η is large. However knowing two frequen is sufficient since

$$\eta = \frac{3(\nu_1+\nu_2)}{(\nu_1-\nu_2)} \qquad (24)$$

and

$$3\,\frac{e^2Qq}{2\hbar} = \nu_1 + \nu_2 \qquad \text{hence } \nu_3 = \frac{13}{6}\,\frac{(\nu_1+\nu_2)^2}{(\nu_1-\nu_2)}$$

Both the quadrupole coupling constant and assymetry parameter can be deduced but the direction cosines cannot.

The above discussion has been for the case of frequencies obtained in the absence of an external magnetic field. When this restriction is removed, since in a small magnetic field the nuclear spins are quantized along the molecular axis and the applied field breaks the Kramers degeneracy and gives splitting of the quadrupole resonance lines.

Pure quadrupole resonance frequencies of solids, first detected by Dehmelt and Krüger[3] usually occur in the radio-frequency region. The values obtained for these coupling constants are very closely related to those which can be obtained from microwave spectroscopy of gases. Quadrupole resonance in solids is a simpler phenomenon than quadrupole resonance in gases when the field gradient is dependent on the rotational state of the molecule. This is particularly complicated for molecules containing more than one coupling nucleus. In solids the interaction of one nucleus does not perturb the field gradient at the other coupling nuclei. Thus plural coupling complicates the phenomenon in rotating molecules.

Although NQR is the most simple method available for the determination of quadrupole coupling constants we must note

1) NQR absorbtion is weak and many compounds having suitable nuclei give no detectable resonance due to relaxation time broadening.

2) Measurements are made on the crystalline solid, and charges on adjacent molecules can contribute to a field gradient on a resonant nucleus. Hence coupling constants differ by a small

amount from those which would be observed for an isolated molecule. This superimposed intermolecular field gradient gives rise to the relaxation time broadening as oscillating fields produced by vibration of the crystal lattice induce transitions between the quadrupole levels.

3) The molecular motion also makes the NQR frequencies temperature dependent, and most pure NQR measurements are made at 77^{o}K (boiling point of nitrogen) although such measurements are strictly comparable only at absolute zero.

(ii) NQR Data from Microwave (MW) Spectra

The only methods which yield nuclear quadrupole coupling constants for isolated molecules, are pure rotational (microwave) spectroscopy and various molecular beam methods. For brevity and since the vapour phase data referenced herein is from M.W. studies, the basic theoretical background to the analysis of fine structure in rotational spectra to give N.Q.C.C.'s is outlined below.

Now the presence of a quadrupolar nucleus in a molecule adds an additional set of terms to each rotational energy level which can be expressed as

$$E_{(J,K)} = E_{ROT}^{J,K} + E_{Q}^{I,J,K}$$

where I is the nuclear spin quantum number, J,K are the rotational quantum numbers, and E_Q represents the quadrupole coupling energy. The main difference between E_Q for the free molecule and E_Q for the fixed molecule is that in the former case the electrostatic field gradients must now be averaged over the molecular rotation, as described below.

It should be noted that the following theory applies to a molecule containing a single quadrupolar nucleus, and is presented as a simple example to show how N.Q.C.C.'s can be obtained from hyperfine structure in a microwave spectrum. Quadrupole coupling by two or three nucleii in a rotating molecule has been analysed,[4,5] and although molecules (2-9) fall into this category, the theoretical analysis is extremely complex and plural coupling has therefore not been used for the necessary example.

Considering the general expansion (5) for the classical quadrupole interaction. By addition and subtraction of $1/6\ \nabla^2 V \int \rho R_n^2 d\tau_n$

$$E_Q = 1/6\ [(\frac{\partial^2 V}{\partial X^2})_o \int (3X_n^2 - R_n^2)\rho_n d\tau_n + (\frac{\partial^2 V}{\partial y^2})_o \int (3y_n^2 - R_n^2)\rho_n d\tau_n$$

$$+ (\frac{\partial^2 V}{\partial Z^2})_o \int (3Z_n^2 - R_n^2)\rho_n d\tau_n$$

$$+ 6(\frac{\partial^2 V}{\partial X \partial Y})_o \int X_n Y_n \rho_n d\tau_n + 6(\frac{\partial^2 V}{\partial X \partial Z})_o \int X_n Z_n \rho_n d\tau_n$$

$$+6(\frac{\partial^2 V}{\partial Y \partial Z})_o \int Y_n Z_n \rho_n d\tau_n]$$

$$+ 1/6[(\frac{\partial^2 V}{\partial X^2})_o + (\frac{\partial^2 V}{\partial Y^2})_o + (\frac{\partial^2 V}{\partial Z^2})_o] \int R_n^2 \rho_n d\tau_n \qquad (24)$$

Since Laplaces equation holds over the nuclear volume the last term is small and can be ignored, hence (24) can be written as a scalar product

$$E_Q = -1/6\ \underline{Q}:\ \nabla\underline{E} = 1/6 \sum_{i,j=X,Y,Z} Q_{ij} V_{ij} \qquad (25)$$

where $V_{ij} = -\nabla E_{ij}$ (26)

and grad E, $(\nabla\underline{E})$, is given

by

$$\nabla E = e_x \frac{\partial E}{\partial X} + e_y \frac{\partial E}{\partial Y} + e_z \frac{\partial E}{\partial Z}$$

$\underline{Q}$ is the quadrupole moment tensor

$$\underline{Q} = \int \rho_n [3\underline{R}_n\underline{R}_n - \underline{W}R_n^2] d\tau_n \qquad (27)$$

$\underline{R}_n$ represents the vector locating points in the nuclear volume in the space fixed (XYZ) reference frame, and

$\underline{W} = \underline{e}_x\underline{e}_x + \underline{e}_y\underline{e}_y + \underline{e}_z\underline{e}_z$

where $\underline{e}_x$, $\underline{e}_y$, $\underline{e}_z$ are unit vectors along the XYZ axes.

Now the potential at the nucleus arises from the various extra nuclear charges of the molecules (here the other nuclei are ignored as they are well screened), and can be expressed as

$$V = \sum_k e\left(\frac{1}{R_e}\right)_k \qquad (28)$$

where $(1/R_e)_k$ is the reciprocal of the distance from the nucleus to the k^{th} electron. Substituting (28) into the tensor V_{ij} (26), and considering the X component only (since the Y and Z components are similar)

$$\frac{\partial^2}{\partial X^2}\left(\frac{1}{R}\right) = \frac{\partial^2}{\partial X^2}(X^2 + Y^2 + Z^2)^{-\frac{1}{2}}$$

$$= \frac{3X^2 - R^2}{R^5} \qquad (29)$$

Thus $$V_{xx} = \left(\frac{\partial^2 V}{\partial X^2}\right)_o = e\sum_k \left[\left(\frac{1}{R_e^3}\right)_k\right]\left[\left\{3\left(\frac{X_e}{R_e}\right)^2 - 1\right\}\right]_k$$

$$= e\sum_k \left[\left(\frac{1}{R_e^3}\right)_k\right]\left[(3\cos^2\theta_k - 1)_k\right] \qquad (30)$$

where θ_k is the angle between R_e and the X axis. Now $\left(\frac{1}{R_e^3}\right)_k$ is independent of the rotational state and can, for any one vibrational state, be considered a constant, therefore

$$V_{xx} = \sum_k C_k \left\langle \frac{3X_e^2}{R_e^2} - 1 \right\rangle_k \qquad (31)$$

Expressions for V_{yy} and V_{zz} are similar.

Now the angular dependence of the averaged sum of the molecular orbitals will the the same as that of $\underline{J}$, since the orbitals are fixed in the molecule and rotate with the molecular frame about the axis of $\underline{J}$.

The resultant field gradient of the electrons will therefore resolve along the (X,Y,Z) axes in the same proportions as the component of $\underline{J}$.

The rapid rotation about $\underline{J}$ averages out the components of the field gradient perpendicular to $\underline{J}$,and makes $\underline{J}$ the axis of symmetry for the gradient. Therefore equation (31) in operator form becomes

$$(V_{xx})_{OP} = C\left(3\frac{J_x^2}{\underline{J}^2} - 1\right) \qquad (32)$$

but the eigenvalues for $\underline{J}^2$ are $J(J+1)$, hence (32) can be written as

$$(V_{xx})_{OP} = \frac{C}{J(J+1)}\left(3J_x^2 - J(J+1)\right) \qquad (33)$$

where C is a proportionality constant which depends upon the electron distribution in the molecule, but mostly in the atom of the coupling nucleus.

The analogous off diagonal elements for the cross product terms are

$$V_{xy} = \sum_k C_k \left\langle \left(3\frac{X_e Y_e}{R^2_e}\right)_k \right\rangle \tag{34}$$

and the corresponding operator is

$$(V_{xy})_{OP} = \frac{C}{J(J+1)} \left(3\frac{J_x J_y + J_y J_z}{2}\right) \tag{35}$$

To evaluate C the coupling constant q_J is defined as that observed for the state $M_J = J$; hence from the ZZ component

$$q_J = \langle J,J|V_{zz}|J,J\rangle = \frac{C}{J(J+1)} [3J^2 - J(J+1)]$$

$$\text{therefore} \qquad C = \frac{J+1}{2J-1} q_J \tag{36}$$

Thus

$$(V_{zz})_{OP} = \frac{q_J}{J(2J-1)} [3J_z^2 - J(J+1)] \tag{37}$$

or more generally

$$(V_{ij})_{OP} = \frac{q_J}{J(2J-1)} \left[3 \frac{J_i J_j + J_j J_i}{2} - \delta_{ij} J^2)\right] \tag{38}$$

$$H_Q = \frac{1}{6} \frac{eq_J Q}{6J(2J-1)(2I-1)} \sum_{i,j=X,Y,Z} \left(3 \frac{I_i I_j + I_j I_i}{2} - \delta_{ij} \underline{I}^2\right)$$

$$x\left(3 \frac{J_j J_i + J_i J_j}{2} - \delta_{ij} \underline{J}^2\right. \tag{39}$$

where $\delta_{ij} = 1$ when $i = j$ and, 0 when $i \neq j$.

This Hamiltonian can be expressed in a more compact form,[6] by performing the multiplication indicated, and expressing the results in vector products

$$H_Q = \frac{eQq_J}{2J(2J-1)\ I(2I-1)} [3(\underline{I}\cdot\underline{J})^2 + \frac{3}{2}\ \underline{I}\cdot\underline{J} - I^2J^2] \qquad (40)$$

This Hamiltonian is applicable to a single nucleus in any type of molecule. The quantity q_j depends on if the molecule is a symmetric rotor, asymmetric rotor or linear.

To evaluate q_J the field gradient is transformed to the <u>principal inertial axes</u> a,b,c (since this is the reference frame in which components of the quadrupole coupling tensor are measured).

Now transforming to (a,b,c)

$$\frac{\partial^2 V}{\partial Z^2} = \frac{\partial^2 V}{\partial a^2}\left(\frac{\partial a}{\partial Z}\right)^2 + \frac{\partial^2 V}{\partial b^2}\left(\frac{\partial b}{\partial Z}\right)^2 + \frac{\partial^2 V}{\partial c^2}\left(\frac{\partial c}{\partial Z}\right)^2$$

$$+ 2\left[\frac{\partial^2 V}{\partial a \partial b}\left(\frac{\partial a}{\partial Z}\right)\left(\frac{\partial b}{\partial Z}\right) + \frac{\partial^2 V}{\partial a \partial c}\left(\frac{\partial a}{\partial Z}\right)\left(\frac{\partial b}{\partial Z}\right) + \frac{\partial^2 V}{\partial b \partial c}\left(\frac{\partial b}{\partial Z}\right)\left(\frac{\partial c}{\partial Z}\right)\right] \qquad (41$$

where $\frac{\partial a}{\partial Z} = \cos\theta_{z,a} = \phi_{z,a}$ etc. are the direction cosines of the principal axes, and

$\frac{\partial^2 V}{\partial a^2} = q_{aa}$ $\frac{\partial^2 V}{\partial a \partial b} = q_{ab}$ are the field gradient in the principal inertial axis system. To a first approximation they are independent of the rotational state, thus

$$\frac{\partial^2 V}{\partial Z^2} = q_{aa}\phi_{za}^2 + q_{bb}\phi_{zb}^2 + q_{cc}\phi_{zc}^2 + 2q_{ab}\phi_{za}\phi_{zb}$$

$$+ 2q_{ac}\phi_{za}\phi_{zc} + 2q_{bc}\phi_{zb}\phi_{zc} \qquad (42)$$

The diagonal terms q_{aa} etc are constants, the off diagonal terms are zero. Expressed in the principal inertial axes

$$q_J = \sum_{g=a,b,c} q_{gg} < J,J|\phi^2_{zg}| J,J > \quad (43)$$

where q_{aa} etc. are the molecular field gradients at the coupling nucleus with reference to the inertial axes.

eQq (referred to as the hyperfine coupling constant) is often written as χ, and therefore the general expression for the quadrupole coupling energy is, from equations (40) and (43)

$$E_Q = \sum_{g=a,b,c} \chi_{gg} < J,J|\phi^2_{zg}|J,J> \quad x[\frac{3/4\ C(C+1)-J(J+1)I(I+1)}{2J(2J-1)I(2I-1)}] \quad (4$$

where $\chi_{aa} = eQq_{aa}$ etc.

Again because Laplaces equation holds

$$\chi_{aa} + \chi_{bb} + \chi_{cc} = 0$$

there are only two independent coupling parameters, which are usually expressed as a coupling constant with reference to one of the axes (say c), and an asymmetry parameter where

$$\eta = \frac{\chi_{aa} - \chi_{bb}}{\chi_{cc}} \quad (45)$$

The reference axis is usually chosen to be the one which the coupling is closest to symmetric i.e. to minimize η.

Now the diagonal elements χ_{aa}, χ_{bb}, χ_{cc} are the coupling constants directly observable from rotational hyperfine structure and are with reference to the principal inertial axes (PIA). The most convenient reference frame for interpretation of results however are the principal axes of the field gradients (x,y,z). The transformation from PIA to (x,y,z) is given by

$$\chi_{xx} = \frac{\chi_{aa} \sin^2\theta_{ax} - \chi_{bb} \cos^2\theta_{ax}}{\sin^2\theta_{ax} - \cos^2\theta_{ax}}$$

$$\chi_{yy} = \frac{\chi_{aa} \cos^2\theta_{ax} - \chi_{bb}\cos^2\theta_{ax}}{\cos^2\theta_{ax} - \sin^2\theta_{ax}} \qquad (46)$$

$$\chi_{zz} = \chi_{cc}$$

where θ_{ax} is the angle between the a and x axes. This angle can only be found if the off diagonal elements χ_{ab}, χ_{bc} etc. are known.

These can only be measured approximately from second order displacements for nuclei with large quadrupole coupling. However several methods can be employed to ascertain θ using e.g. symmetry considerations and isotopic substitution.

Figure 24 Block Diagram of NQR Spectrometer

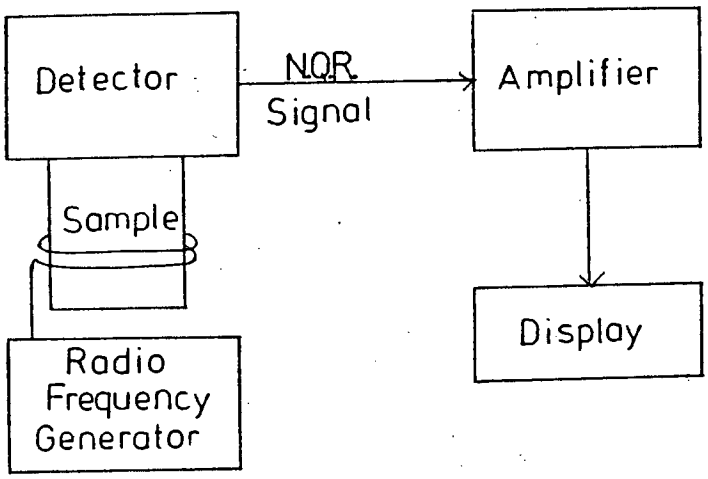

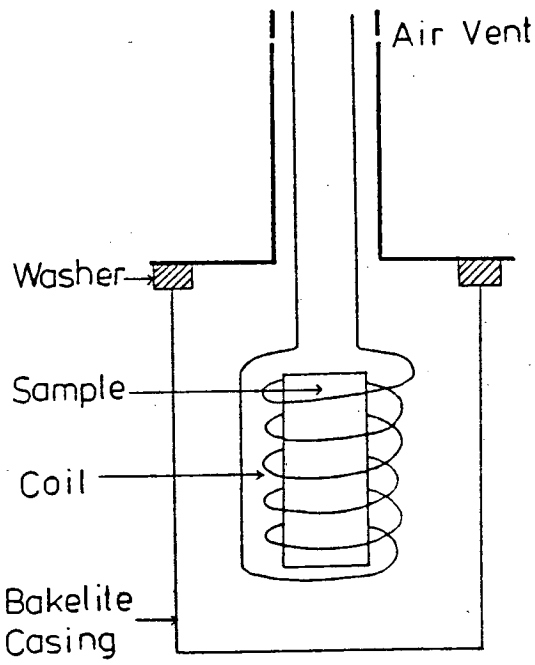

Figure 25. Sample Holder for NQR Experiment

(iii) The Pure Nuclear Quadrupole Resonance Experiment

We have now investigated the theoretical background of the NQR phenomenon for both vapour phase and solid phase studies. It is now appropriate to briefly mention the experimental technique which was used to obtain the experimental coupling constants quoted herein.

Compounds (1-9) were studied in a Decca Radar NQR spectrometer, a block diagram of which is shown in Fig.24 detail of the sample holder is shown in Fig. 25

Briefly in obtaining a spectrum the sample is first immersed completely in liquid nitrogen, as all reported signals are quoted at 77 K. The sample is allowed to crystallize slowly to prevent it supercooling to a glass, from which no measurable signal can be obtained, and when solidified a radio frequency signal is passed through the coil and hence through the sample. When resonance occurs this is detected, amplified and displayed, and Fig.(26) contains an example of the signals for 1-methyl-1,2,4-triazole. Different frequency ranges can be scanned using different coils, the greater the number of turns the lower the frequency emitted.

The observed frequencies ν_+ and ν_- are reported in Table (10).

These are related to the coupling constants by equation (22) which can be alternatively expressed as

$$\nu_+ = 0.5e^2Q \mid q_{zz} - q_{yy} \mid /\hbar$$

$$\nu_- = 0.5e^2Q \mid q_{zz} - q_{xx} \mid /\hbar \qquad (47)$$

FIG. 26. NQR SIGNALS FOR
1 METHYL 124 TRIAZOLE

(Reproduced with permission
of Dr. M Redshaw, Salford University)

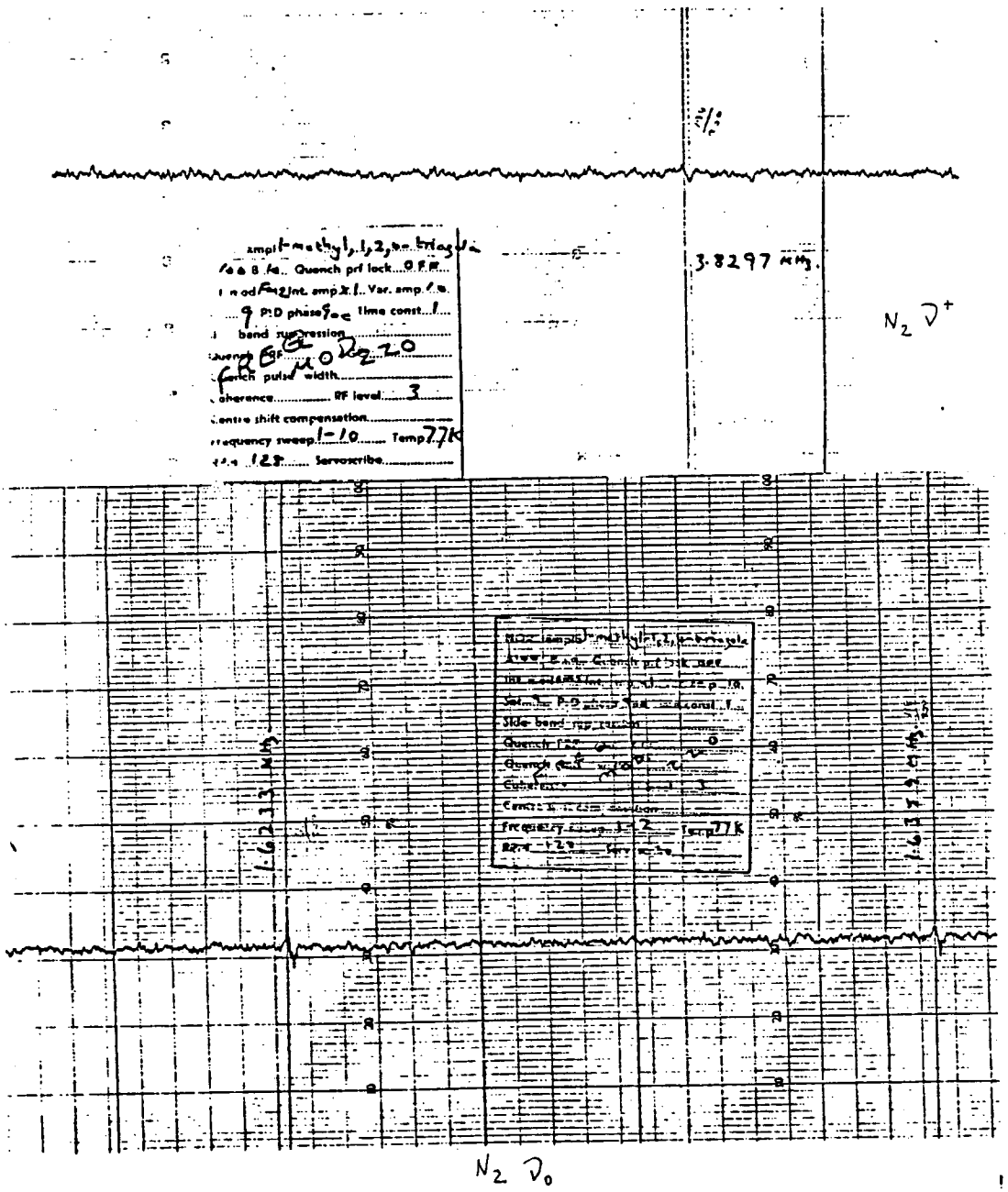

Table 10 Observed Frequencies from NQR Experiment (MHz)

Compound	N site	ν_+	ν_-	e^2Qq/h	η
pyrrole (1a)	N1	1.6850	1.4078	2.0618	0.2688
1-methylpyrrole (1b)	N1	2.175	1.68	2.57	0.385
pyrazole (2a)	N1	-	2.1181 2.0736	-	
	N2	3.6648 3.6396	2.3653 2.3148	3.9948	0.6572
1-methylpyrazole (2b)	N1	2.5786	2.1200	3.1324	0.2927
	N2	3.4969	2.2720	3.8459	0.6371
imidazole (3a)	N1	1.417	-	-	
	N2	2.559	2.348	3.271	0.126
1-methylimidazole (3b)	N1	-	-	-	
	N2	2.5416	-	-	
1H-1,2,3-triazole (4a)	N1	2.0872			
	N2	3.8040	2.3512	4.1034	0.7079
	N3	3.6750	3.3979	4.7152	0.1179
1-methyl-1,2,3-triazole (4b)	N1	2.0913	1.5300	2.4142	0.4651
	N2	3.7583	2.2581	4.0109	0.7482
	N3	3.8151	3.3776	4.7951	0.1825
1H-1,2,4-triazole (5a)	N1	-	-	-	
	N2				0.665
	N4				0.169
1-methyl-1,2,4-triazole (5b)*	N1	2.8569	2.2146	3.3810	0.3799
	N2	3.8297	2.1852	4.0099	0.8200
	N4	2.9218	2.8933	3.8766	0.0147
2-methyl-1,2,3-triazole (6b)	N1/N3	3.5330	2.7600	4.1953	0.3684
	N2	3.1611	2.3180	3.6527	0.4615
4-methyl-1,2,4-triazole (7b)	N1/N2	3.2472	2.2586	3.6705	0.5334
	N4	2.4123	2.3440	3.1708	0.0430

* Multiple resonances were observed for $\nu_o^{(m)}$ the average of which was 1.6450 MHz (1.6233, 1.6359, 1.6500, 1.6748 MHz).

Table 10 (contd.)

Observed Frequencies from NQR Experiment (MHz)

Compound	N site	ν_+	ν_-	e^2Qq/h	η
1H-tetrazole (9a)	N1	2.2400	1.5922	2.5548	0.5071
	N2	3.9023	2.7293	4.4210	0.5306
	N3	3.4436	2.7057	4.0995	0.3599
	N4	3.6572	3.0113	4.4457	0.2905
1-methyltetrazole (9b)	N1	2.1220 2.0926			
	N2	3.8160 3.7142	2.6523 2.6455	4.2760	0.5219
	N3	3.4525 3.4282	2.7133 2.6923	4.0954	0.3601
	N4	3.0765 3.0365	2.9626 2.8949	3.9901	0.0640
2-methyltetrazole (8b)	N1	3.6525	2.5555	4.1386	0.5301
	N2	2.5338	1.8030	2.8912	0.5054
	N3	3.7425*	3.0650	4.5383	0.2985
	N4	3.6278	2.9810	4.4058	0.2936

*Average of resonances 3.7572
3.7278 MHz

From equation (23)

$$\frac{3e^2Qq_{zz}}{\hbar} = 2(\nu_+ + \nu_-) \qquad (48)$$

hence all three coupling constants can be obtained from a measurement of two frequencies. {The third frequency, ν_o, was observed only for 1-methyl-1,2,4-triazole

$$\nu_o = 0.5e^2 \mid q_{yy} - q_{xx} \mid /\hbar \} \qquad (49)$$

In addition multiple resonances were obtained for some samples due to more than one crystal site being present in their unit cell. Such resonances were observed for N2 of pyrazole, 1-methyltetrazole (all resonances) and 1-methyl-1, 2,4-triazole; where several frequencies occurred the average value was taken for subsequent calculations. It is obvious that for molecules with more than one coupling nucleus several resonances will be obtained, and these must be assigned to particular coupling centres. This is obviously a difficult task and one must attempt to have some justification for assigning both ν^+ and ν^- (and hopefully ν^o) and these frequencies to particular centres.Obviously comparison with other experimental NWR data and assignments is useful, but relies on the veracity of the reported assignment. Where three resonances are observed for at least one coupling centre the problem is somewhat relieved, as ν_+, ν_- and ν_o

are numerically related and the group can be ascertained, but these three frequencies must be assigned to a particular nucleus. Alternatively working back from the calculated H.F.C.C's it is possible to obtain calculated frequencies and attempt assignment by comparison of experimental and calculated data; this must be done for cases where no other experimental data exists for comparison. The frequencies in Table (10) have been assigned by comparison with other reported experimental data and assignments (where information was available), and calculated values.

The principal axis coupling constants ($\frac{e^2Qq_{ii}}{\hbar}$, i = x,y,z) were evaluated from equations (47 and 48) and Table (11) contains the experimental N.Q.C.C.'s. The value of the nuclear quadrupole moment was taken as 0.0164 barn as was used in the previous work.

A comparison of these values with those calculated herein and other reported NQR and MW values is given in Table (19).

The experimental NQR data used in this chapter were kindly provided by Dr. Mavis Redshaw of the University of Salford, to whom we extend our grateful thanks.

Table 11 ^{14}N Nuclear Quadrupole Coupling Constants (MHz)

Compound	N site	e^2Qq_{zz}/h	e^2Qq_{yy}/h	e^2Qq_{xx}/h	η
pyrrole (1a)	N1	2.0618	1.3082	0.7538	0.268
1-methylpyrrole (1b)	N1	2.570	1.780	0.790	0.385
pyrazole (2a)	N1	-	-	-	-
	N2	3.9948	3.3096	0.6852	0.6572
1-methylpyrazole (2b)	N1	3.1324	2.0248	1.1076	0.2927
	N2	3.8459	3.1479	0.6981	0.6371
imidazole (3a)	N1				
	N2				
1-methylimidazole (3b)	N1				
	N2				
1H-1,2,3-triazole (4a)	N1				
	N2	0.5990	3.5046	-4.1034	0.7079
	N3	2.0806	2.6348	-4.7152	0.1176
1-methyl-1,2,3-triazole (4b)	N1	-2.4142	0.6458	1.7684	0.4651
	N2	0.5053	3.5057	-4.0109	0.7482
	N3	1.9601	2.8351	-4.7951	0.1825

Table II (contd.) N Nuclear Quadrupole Coupling Constants (MHz)

Compound	N site	e^2Qq_{zz}/h	e^2Qq_{yy}/h	e^2Qq_{xx}/h	η
1-methyltetrazole	N1				
	N2	4.2760	3.2542	1.0218	0.5219
	N3	4.0954	2.7852	1.3102	0.3601
	N4	3.9901	2.1229	1.8673	0.0641
2-methyltetrazole (8b)	N1	4.1386	3.1664	0.9724	0.5301
	N2	2.8912	2.1764	0.7148	0.5054
	N3	4.5383	2.9467	1.5916	0.2985
	N4	4.4058	2.8498	1.5562	0.2936

(iv) Discussion of Molecular Geometries Used in Calculations

The molecules whose structures are described below are given in Fig. (18). Experimental microwave structures are available for 1(a), 2(a), 3(a), 5(a),[7,8,9,10] and a crystal structure has been reported for 9(a).[11] It is worthwhile mentioning that the microwave structure is most relevant to NQR coupling data obtained from analysis of microwave spectra, whilst the crystal structure is most relevant to pure NQR data. The fine difference between the coupling constants obtained from the two experimental techniques is due to a slight change in geometry between the different states, and to intermolecular effects in the solid state.

Where no experimental structure was available it was necessary to use a geometry constructed as outlined below.

More detailed information on the geometries used can be found in Appendix (B), where bond lengths, and angles are given.

N-Methylpyrrole (1b)

Using the microwave ring geometry,[7] the 1H hydrogen was replaced by a methyl group, with the structure given below, along the external bisector the C5-N1-C2 angle.

N-C1 = 1.47Å < H-C1-N1 = 109.5°

C1-H = 1.1Å < H-C1-H = 120°

(Hereafter this methyl unit will be referred to as the standard methyl unit).

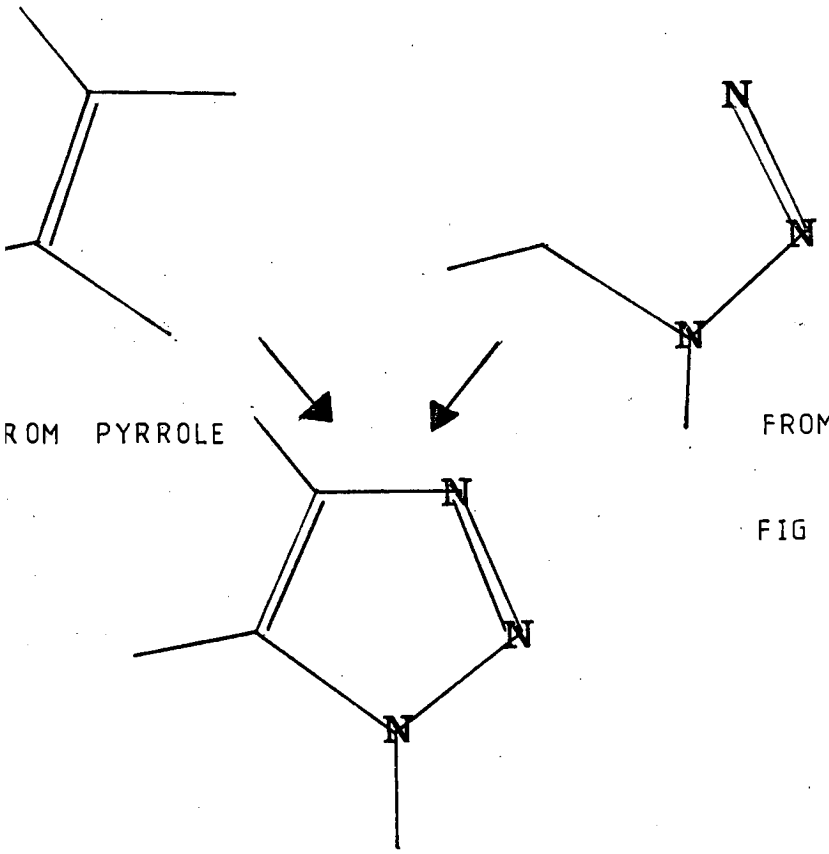

FIG 27 CONSTRUCTION OF GEOMETRY FOR 1-H-1,2,3-TRIAZOLE

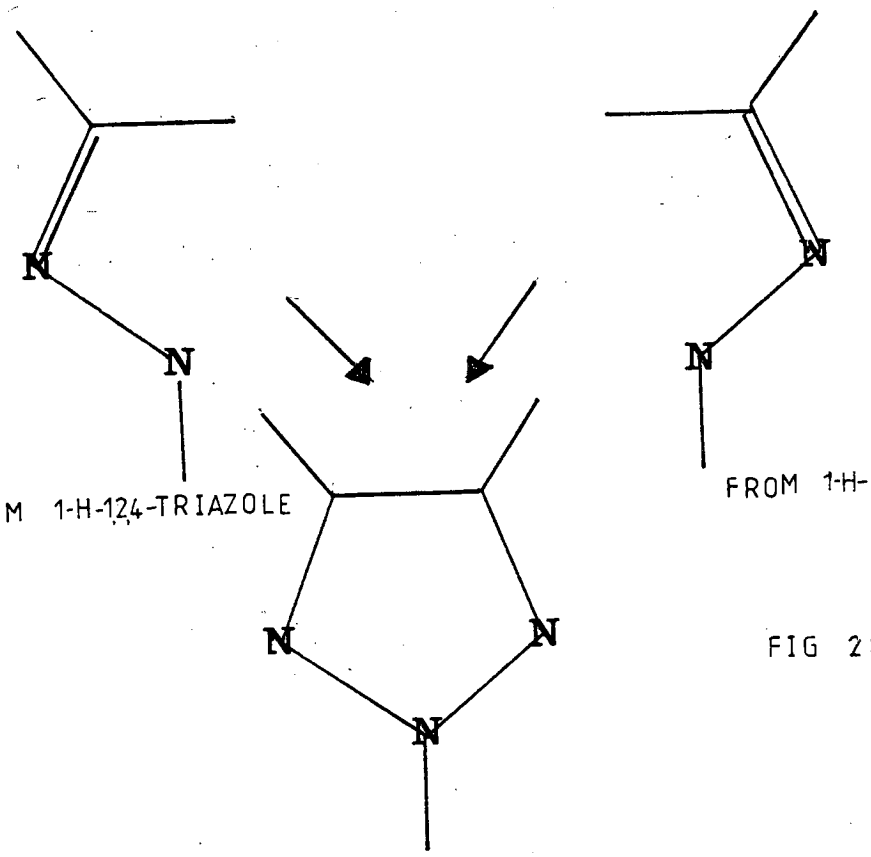

FIG 28 CONSTRUCTION OF GEOMETRY FOR 2-H-1,2,3-TRIAZOLE

These structural parameters were obtained from an incomplete Electron Diffraction study of N-Methyl-pyrrole.[12]

1-Methyl-pyrazole (2b)

Again the microwave ring structure [8] was used for the ring system. The 1H hydrogen was replaced by the standard methyl unit preserving the original C5-n1-H1 bond angle.

1-Methyl-imidazole (3b)

The geometry was constructred from the experimental ring structure, [9] replacing the 1H-hydrogen with the standard methyl unit. The original C2-N1-H1 bond angle was preserved.

1H-1,2,3-Triazole (4a)

Here the structure was obtained from a combination of parts of molecules for which experimental structure data was available The parts of the structures of 1H-tetrazole and pyrrole used to give the constructed geometry are shown in Fig. (27) The merging of these part structures was performed such as to preserve the bond lengths and as many of the existing angles as possible. The N3-C4 bond length was set at 1.32Å and the C4N3N2 angle adjusted accordingly.

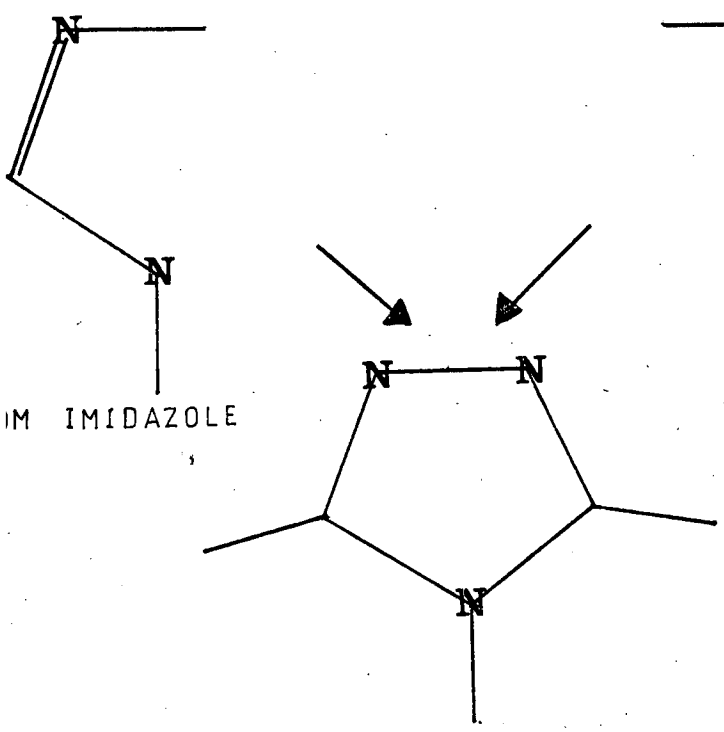

FIG 29 CONSTRUCTION OF GEOMETRY FOR 4H-1,2,4-TRIAZOLE

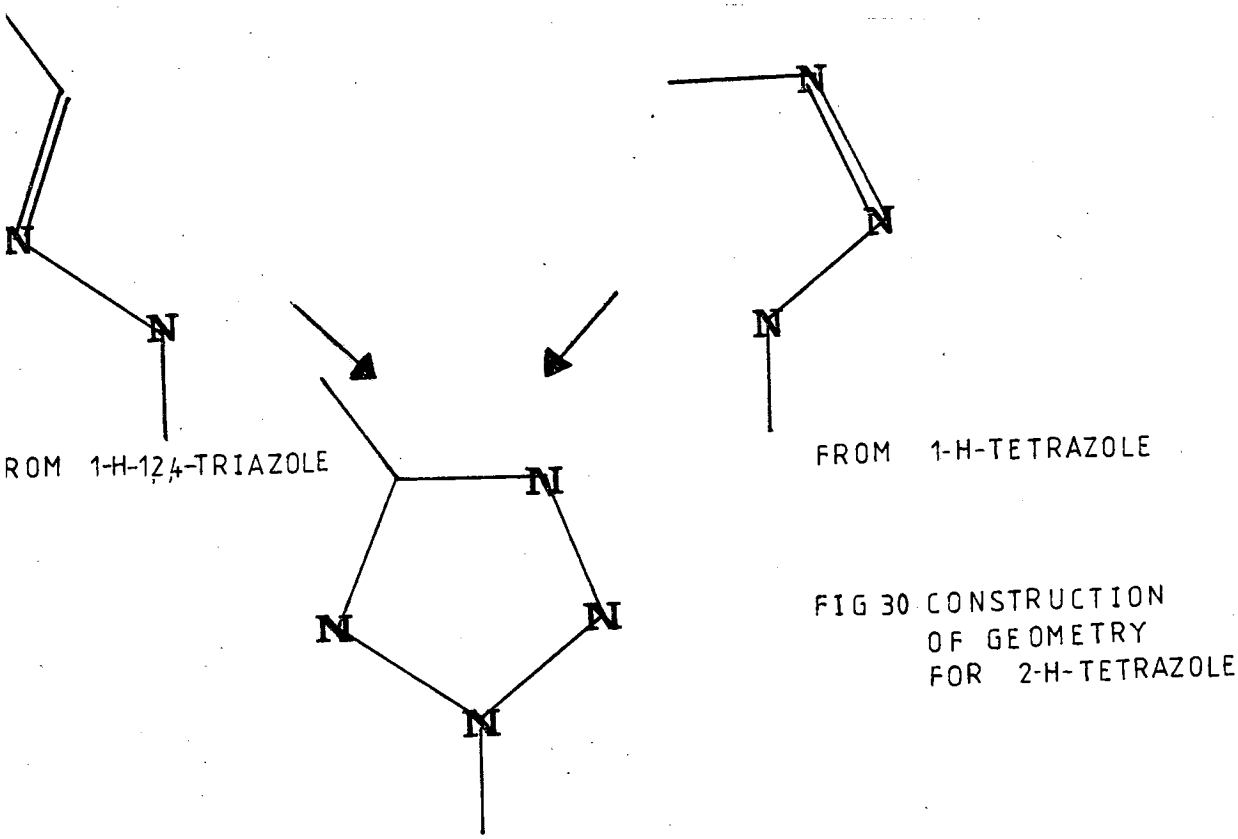

FIG 30 CONSTRUCTION OF GEOMETRY FOR 2-H-TETRAZOLE

1-Methyl-1,2,3-triazole (4b)

To the structure obtained above (4a) a standard methyl group was used to replace the 1H hydrogen along the external bisector of angle C5N1N2.

1-Methyl-1,2,4-triazole (5b)

The microwave ring structure [10] was used with the standard methyl group replacing the N-hydrogen preserving the C5N1H1 angle.

2H-1,2,3-triazole (6a)

This molecule has C_2V symmetry and for its geometry construction part of the 1H-1,2,4-triazole structure and the mirror image of that part were "fused" in the manner shown in Fig. 28). The C4-C5 bond length was set at 1.41Å (cf. pyrrole, pyrazole) and the CCN and NNC angles adjusted to values most closely comparable to similar angles in pyrazole.

2-Methyl-1,2,3-triazole (6b)

Here the standard methyl unit replaced the 2H hydrogen in the structure constructed for (6a). The N1N2H2 angle was preserved.

4H-1,2,4-triazole (7a)

As experimental data was again lacking this geometry was constructed from a part of the imidazole structure and, combined with its mirror image, (as shown in Fig (29)),

since the molecule has C_2V symmetry. This was adjusted to make the N1-N2 bond 1.35Å which is close to the value of the N-N bond in pyrazole.

4-Methyl-1,2,4-triazole (7b)

Using the structure obtained in (7a) the 4H hydrogen was replaced by the standard methyl unit, preserving the C3N4H4 angle.

1-Methyltetrazole (8b)

The reported crystal structure was used replacing the 1H hydrogen by a standard methyl unit and preserving the C5N1H1 angle.

2H-Tetrazole (9a)

In this case the geometry was constructed as shown in Fig. 30) from a combination of part of the 1H-tetrazole and 1H-1,2,4-triazole structures, preserving the existing bond lengths and making the N4C5 bond length 1.35Å by small sensible adjustments to the N4C5N1 and N3N4C5 angles.

2-Methyltetrazole (9b)

Again the structure for the unsubstituted tetrazole (9a) was used, replacing the 2H hydrogen with a standard methyl unit and preserving the C5N1H1 bond angle.

It should be noted that the above geometries were constructed in a manner that would enable the merge facility

available in the Atmol-3 service program to be used to its maximum advantage. By use of the merge facility existing mainfile integrals calculated for a particular system, can be re-used if part of that system occurs in another molecule.

For example for, 4a (Fig. (27)), all integrals obtained in a previous calculation on tetrazole, and which only refer to the centres N1, N2, N3, C5, H5 can here be used again as can those obtained for pyrrole which only refer to C4 and H4. This does not mean that no new integrals must be calculated since those integrals that involve centres N1, C4 etc. (i.e. those that involve centres in each part) must be computed and a new dumpfile is required.

(v) Synthetic Method

Having now discussed the experimental technique and the theoretical background to NQR we must now mention the synthetic methods which were used to prepare the samples whose NQR spectra were obtained. Pyrrole (1a), N-Methylpyrrole (1b), pyrazole (2a), imidazole (3a) and 1H-1,2,4-triazole (5a), were commercially available samples. All other compounds in the series, except 2H-tetrazole and 4H-1,2,4-triazole which are unstable, were prepared as described below, by Dr. M.H. Palmer.

1-Methylpyrazole(2b)

This was prepared from 1,1,3,3-tetramethoxypropane by addition of methylhydrazine.[13]

1-Methylimidazole (3b) was prepared by adding methyliodide to a solution of imidazole in benzene.[14]

1H-1,2,3-Triazole (4a) was obtained by decarboxylation of 4-carboxyl-1,2,3-triazole,[15] which was prepared by the reaction of propiolic acid with hydrazoic acid in boiling benzene.

1 Methyl-1,2,3-triazole (4b) and 2 methyl-1,2,3-triazole (6b) were prepared by addition of diazomethane to 1,2,3-triazole dissolved in ether. The resulting residue which was a mixture of the 1-methyl- and 2-methyl-isomers was separated by distillation and the composition of the fractions was checked from their proton NMR spectra.

1-Methyl-1,2,4-traizole (5b)

By treating 1H-1,2,4-triazole with diazomethane[16] only the 1-methyl isomer of 1,2,4-triazole was obtained, this was identified by its proton NMR. A more complicated method, outlined below, was required to obtain the 4-methyl-1,2,4-triazole.[15]

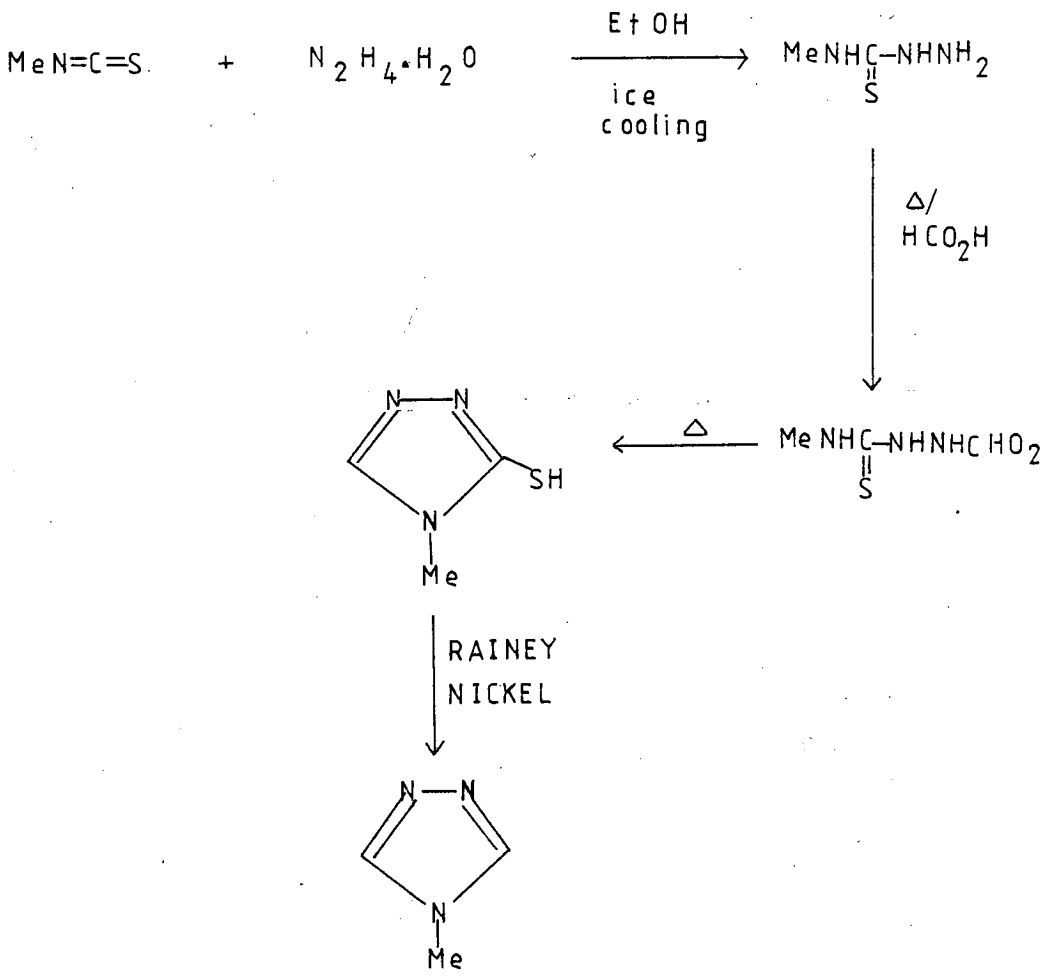

The product was identified from its proton NMR

1H-Tetrazole (9a) was prepared by deamination of commercially available 5-aminotetrazole.[17] 1-Methyltetrazole (9b) and 2-methyltetrazole (8a) were prepared in almost equal

proportions by methylation of alkaline tetrazole by methyl-iodide.[17] These isomers were separated by distillation and identified by comparison of their proton NMR spectral data with that previously reported.[17]

Fig 31

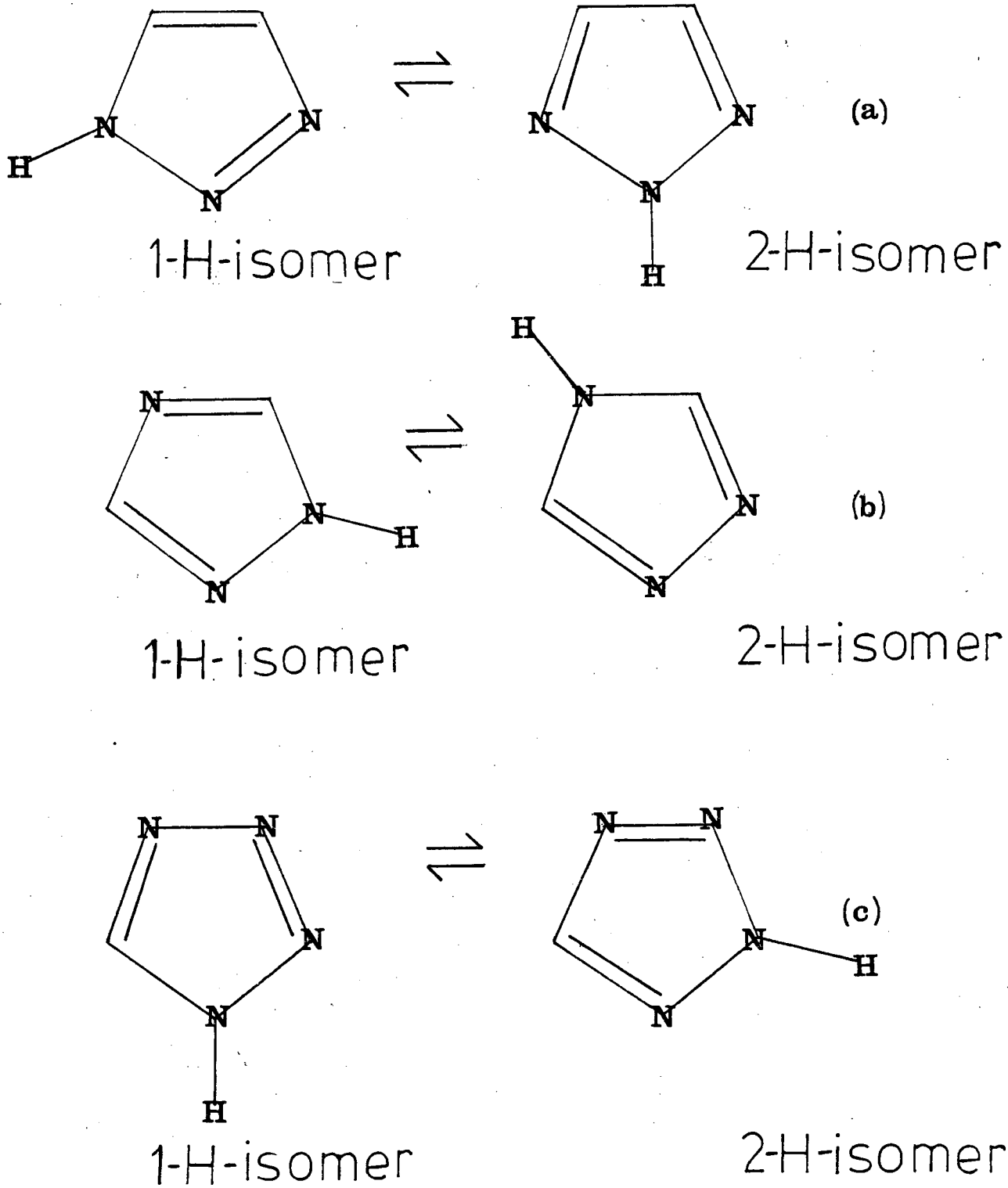
1-H-isomer
2-H-isomer
(a)
1-H-isomer
2-H-isomer
(b)
1-H-isomer
2-H-isomer
(c)

(vi) Tautomerism

Of the molecules studied herein the unsubstituted triazole and tetrazoles are capable of occurring as tautomers see Fig (31). For 1,2,3-triazole the 1H form is dominant in the solid phase and in solution [18]. The gas phase microwave spectrum of 1,2,3-triazole has been analysed in terms of the 1H tautomer [19], however the 2H tautomer has been observed [19] and since this has a very low dipole moment compared with the 1H tautomer it is considered that the ratio of 2H to 1H tautomers could be as high as 100:1 in the gas phase.[19b]

Studies have shown that the 1H isomer of 1,2,4-triazole [20] is dominant in the solid phase and in solution, as is the 1H isomer of tetrazole [21]. Several studies [22a,22b] have shown that only the unsymmetrical tautomer occurs in the vapour phase. This is in agreement with semi empirical calculations [22b] on the tautomerism of 1,2,4-traizole which concluded that the unsymmetrical form was favoured over the symmetrical tautomer.

The dominant tautomeric form of tetrazole in the gas phase has not been elucidated since it is reported that the dominant tautomer changes with deuteration.

The results of calculations and both NQR and photoelectron spectroscopic studies on the triazoles tetrazoles and their blocked methyl derivatives, (see below) will provide further evidence as to the dominant gas phase tautomeric forms of these molecules.

ii) Calculations - Results and Discussion

Ab Initio calculations were performed using the afore-described molecular geometries, Dunnings 9s/5p double zeta basis set (the numerical values of which are noted in appendix B), and the Atmol-3 programs. The resulting wave-functions, checked for the correct orbital occupancy, were used as input to the Atmol-3 Properties package which calculated electric field gradients and quadrupole moments, in the following manner. From the preceding theory, equations (29) and (9) represent Hamiltonian operators for the electric field gradients and quadrupole moments respectively. Now any observable quantity can be represented by a quantum mechanical operator and when this operates on a wavefunction the quantum mechanical expectation value of the observable is obtained. The operator must also be Hermitian hence

$$\int \psi_i^* \hat{M} \psi_j d\tau = \int \psi_j^* \hat{M} \psi_i d\tau$$
$$= \text{expectation value of M}$$

Therefore using this procedure, the calculated wavefunction and the operators (29), (9), a set of electric field gradients and quadrupole moments (and dipole moments) can be calculated for the systems under investigation. Hence the experimental results and calculated expectation values can be compared to estimate the quality of the calculation, or conversely to check the accuracy of the experiment. The latter is of importance since the experiment rarely leads directly to the results, but arrives at an assignment by an often difficult process.

Table (12) contains the calculated coupling constants (χ) for molecules (1-9). In order to obtain NQCC from

Table 12 Calculated ^{14}N Nuclear Quadrupole Coupling Constants (MHz)

Compound		Coupling Constants			Asymmetry Parameter
		χ_R	χ_T	χ_π	
Pyrrole (1a)		1.413	1.323	-2.736	0.0326
1-Methylpyrrole (1b)		1.594	1.237	-2.832	0.1258
Pyrazole (2a)	N-1	1.0143	2.0899	-3.1034	0.3465
	N-2	-3.938	3.208	0.731	0.6291
1-Methylpyrazole (2b)	N1	1.195	1.993	-3.188	0.2500
	N2	-3.824	3.184	0.639	0.6654
Imidazole (3a)	N1	1.352	1.290	-2.641	0.0235
	N3	-3.723	1.927	1.796	0.0351
1-Methylimidazole (3b)	N1	1.491	1.223	-2.714	0.0988
	N3	-3.735	1.925	1.81	0.0304
1 H-1,2,3-Triazole (4a)	N1	0.812	1.695	-2.507	0.3518
	N2	-4.095	3.534	0.561	0.7259
	N3	-4.721	2.616	2.105	0.1083
1-Methyl-1,2,3-triazole (4b)	N1	0.68	1.693	-2.372	0.4285
	N2	-3.979	3.447	0.533	0.7322
	N3	-4.719	2.663	2.056	0.1285
1H-1,2,4-traizole (5a)	N1	1.032	2.311	-3.343	0.3826
	N2	-4.0124	3.5176	0.4958	0.7926
	N4	-3.882	1.992	1.890	0.0262

'able 12 (contd.)

Calculated ^{14}N Nuclear Quadrupole Coupling Constants (MHz)

Compound		Coupling Constants			Asymmetry Parameter
		χ_R	χ_T	χ_π	
'-Methyltetrazole (8b)	N1	-4.178	3.195	0.983	0.5294
	N2	0.717	2.177	-2.893	0.5043
	N3	-4.511	2.907	1.604	0.2889
	N4	-4.407	2.846	1.561	0.2915
.H-Tetrazole (9a)	N1	0.668	1.858	-2.526	0.4714
	N2	-4.458	3.371	1.086	0.5124
	N3	-4.095	2.773	1.321	0.3546
	N4	-4.443	2.889	1.555	0.3000
.-Methyltetrazole (9b)	N1	0.489	1.864	-2.353	0.5842
	N2	-4.316	3.301	1.016	0.5296
	N3	-4.105	2.808	1.297	0.3680
	N4	-4.467	2.835	1.595	

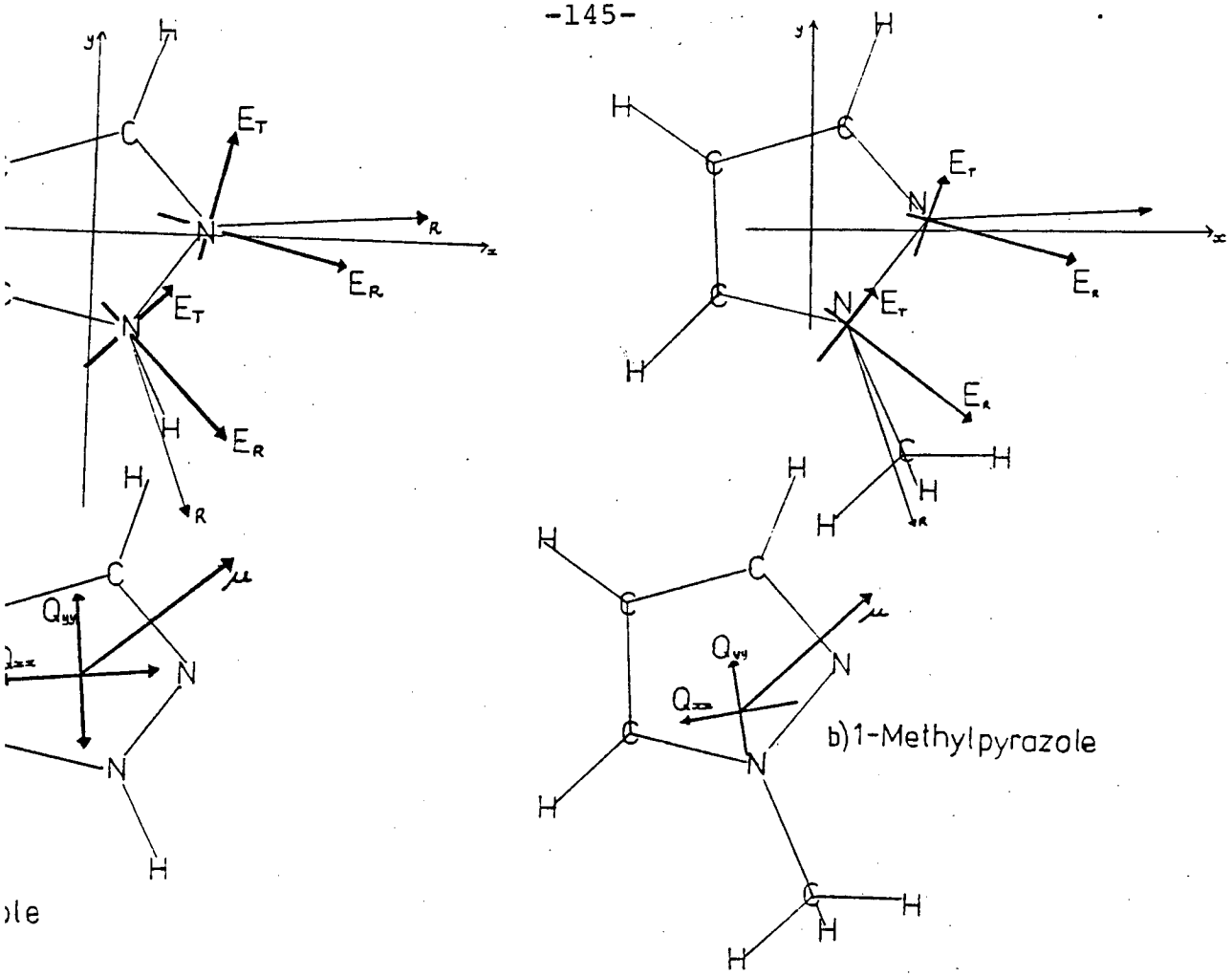

FIG 32 PRINCIPAL IN PLANE AXES FOR CALCULATED ELECTRIC FIELD GRADIENTS (E), QUADRUPOLE MOMENTS (Q), DIPOLE MOMENTS (μ) and COORDINATE AXES (x,y).

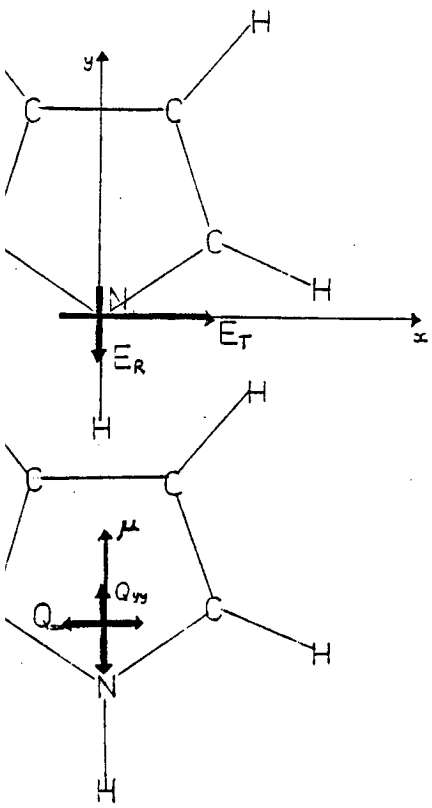

Pyrrole

FIG 32 (cont)

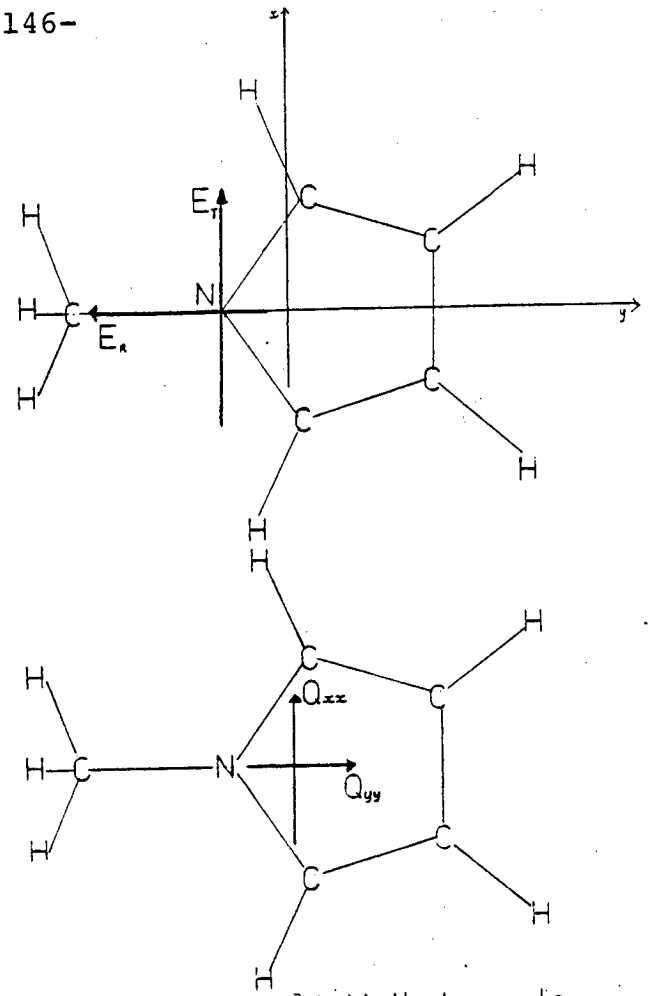

d) 1-Methylpyrrole

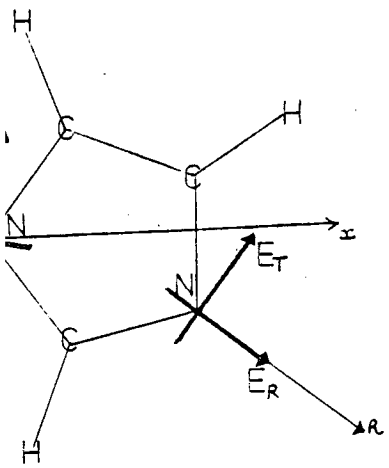

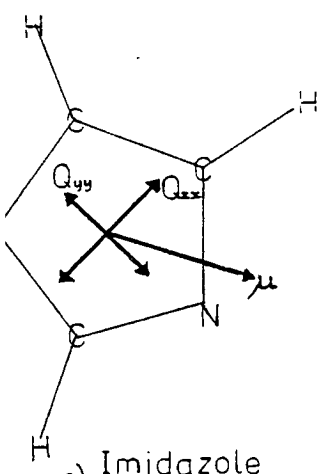

e) Imidazole

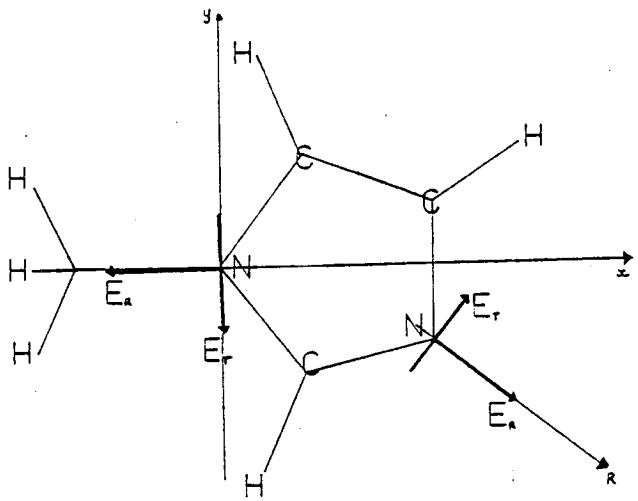

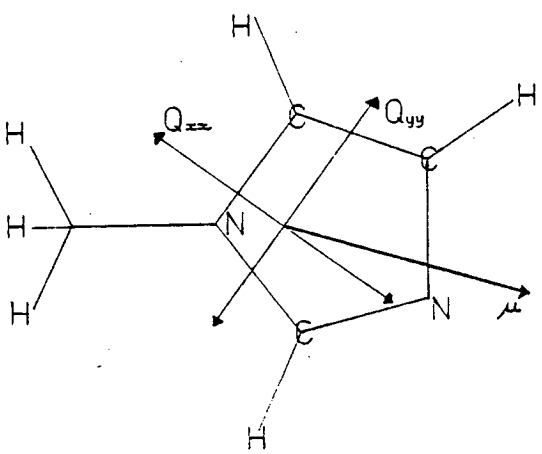

f) 1-Methylimidazole

FIG 32(cont)

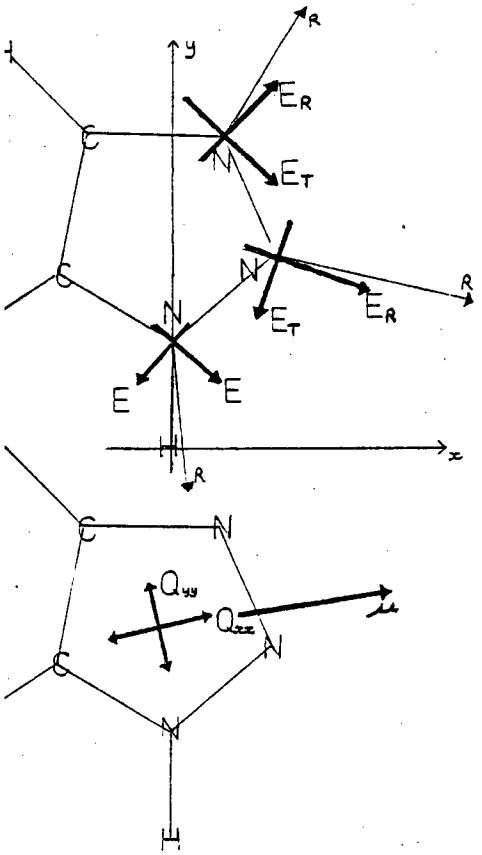

g) 1-H-1,2,3-Triazole

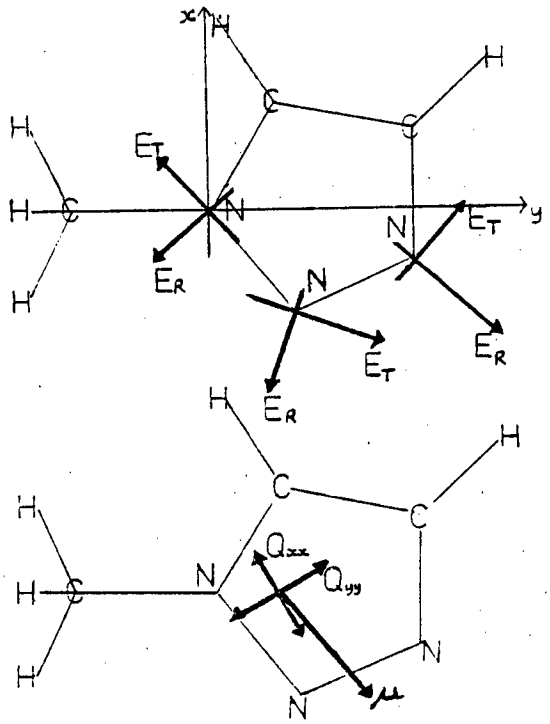

h) 1-Methyl-1,2,3-triazole

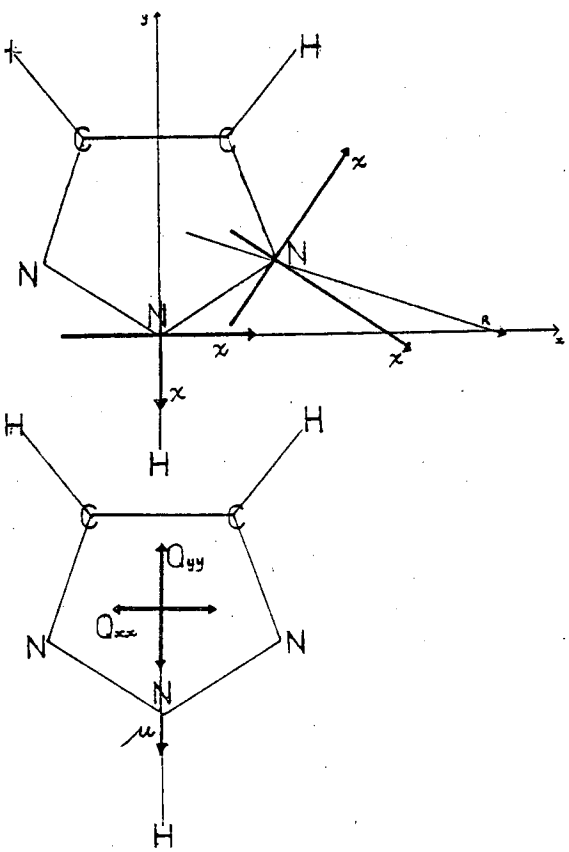

i) 2-H-1,2,3 Triazole

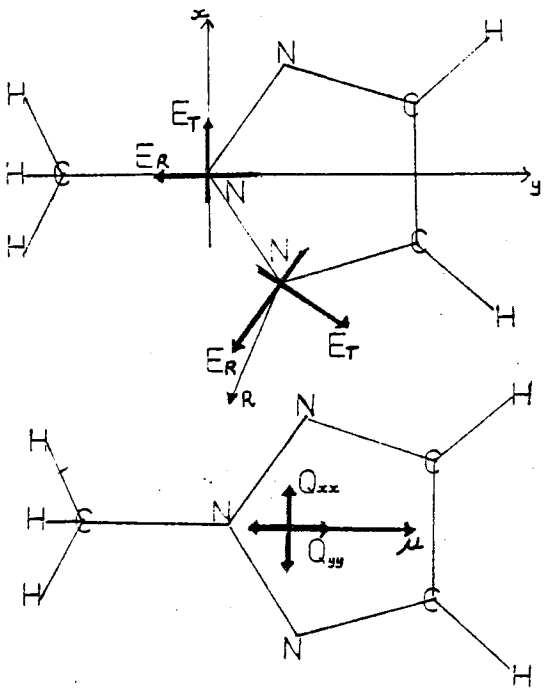

j) 2-Methyl-1,2,3-triazole

FIG 32 (cont)

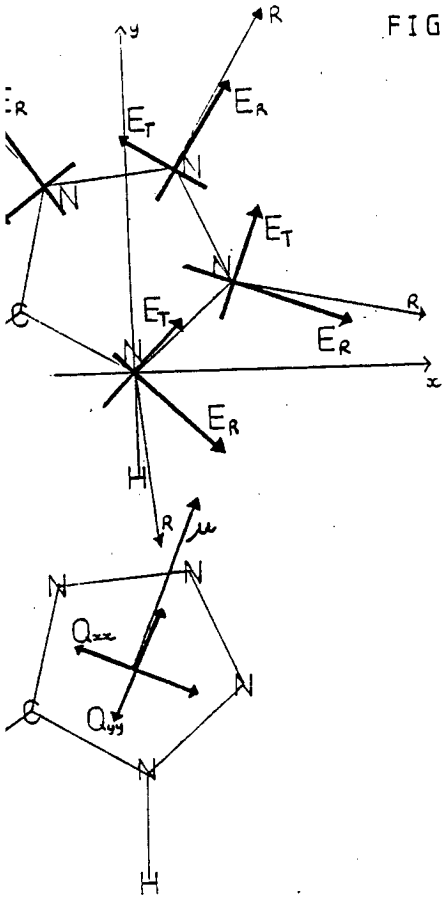

1-H-Tetrazole

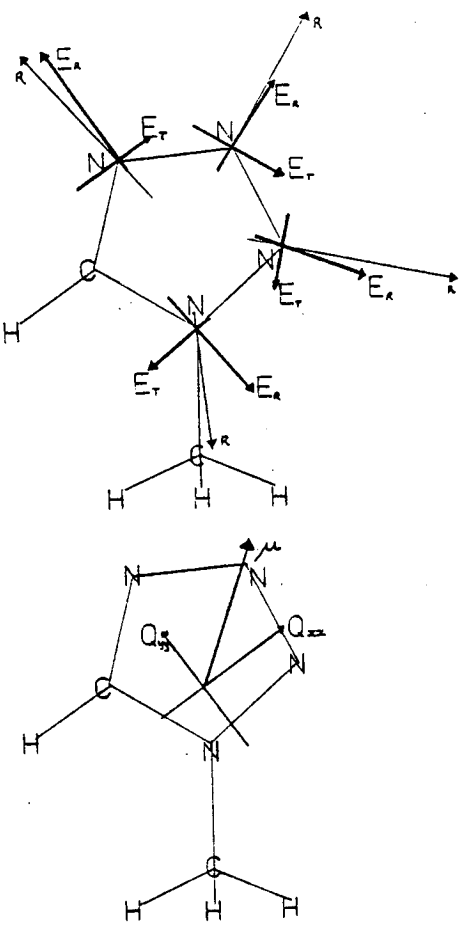

p) 1-Methyltetrazole

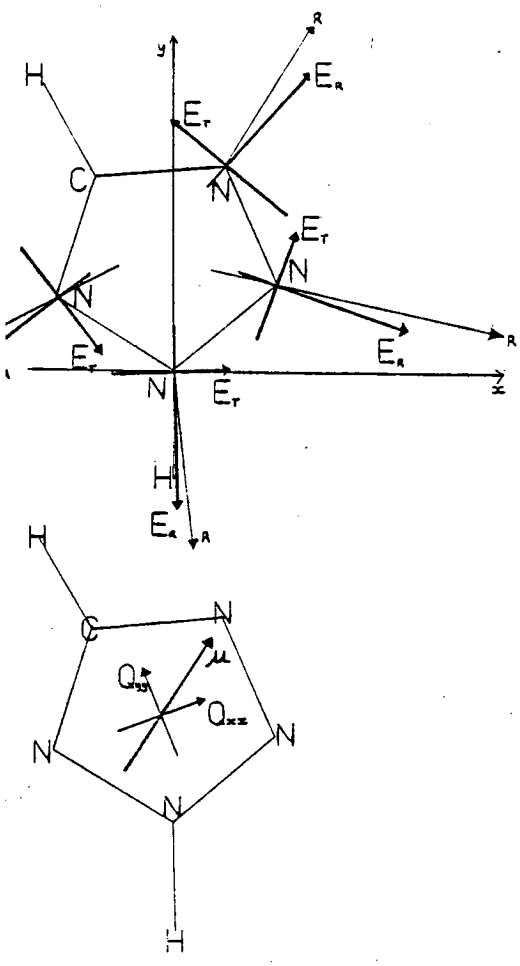

2-H-Tetrazole

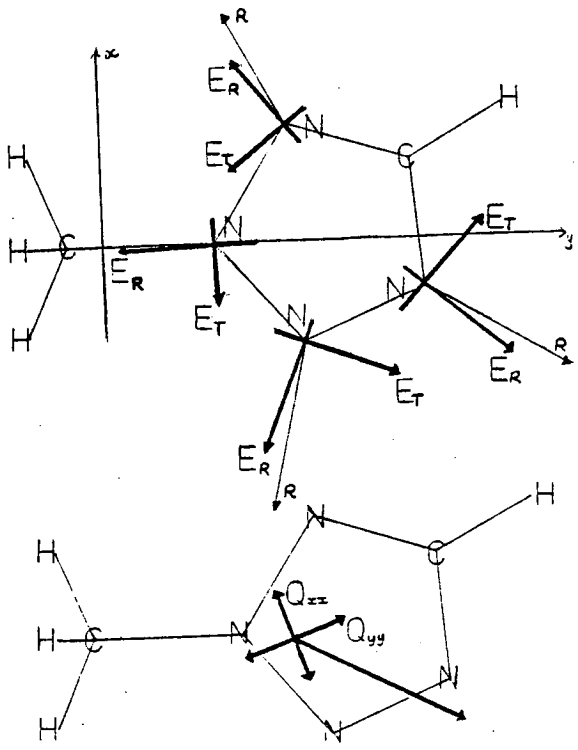

r) 2-Methyltetrazole

calculated electric field gradients a value for the ^{14}N atomic quadrupole moment (Q_N) is required. As stated above this is a difficult quantity to obtain experimentally, nevertheless various theoretical studies have been pursued and a value of 0.015 barn was chosen and scaled in previous work using the basis set used here; from a best fit of calculated and experimental NQCC's, which gave the optimum value of Q_N of 0.0164 barn and this is the value which was used here to obtain the calculated NQCC's given in table [The figures quoted are for the principle axis system].

It should be noted that if agreement between calculation and experiment is good, then calculations of this type can be used to predict with confidence coupling constants where data is lacking, and also to assign data which is open to more than one interpretation. Table (13) contains the calculated molecular quadrupole moments which are conventionally measured at the centre of mass, and in the case of symmetric molecules these must lie along the symmetry axes. See figs (32a to 32f) for the directions of the quadrupole moment axes. Unfortunately there is only experimental data for (1) in the azole series therefore no significant conclusions can be drawn from comparison of calculated and experimental data.

Directions of Principal Axes, Quadrupole Moments

Figures (32a to 32f) show schematically the principal in plane axes for the calculated Electric Field Gradients (E), Quadrupole Moments (Q), Dipole Moments (μ) and coordinate axes (x,y) for each of the molecules (1-9). 'R' represents the external bisector of the angle at the nitrogen atom.

Following the terminology of ref. (1) the in plane Electric Field Gradient axis lying closest to the external bisector at the N atom is defined as the radial axis (E_R) and the other as the tangential axis (E_T).

From these diagrams the following effects of adjacent centres and methyl substitution on the direction of the Principal Axes and Quadrupole Moments can be noted.

(i) E_R of imino nitrogens with two adjacent carbon atoms lies along the external bisector (R).

(ii) When the imino nitrogen is adjacent to one other nitrogen, the principal axes (E_R) direction is rotated towards the adjacent nitrogen by about 15^o for an amino nitrogen and slightly more for a pyrrolic nitrogen.

(iii) When a pyrrolic nitrogen is adjacent to one other nitrogen E_R is rotated towards the adjacent heteroatom by about 30^o.

(iv) If an imino or pyrrolic nitrogen is adjacent to two other nitrogens E_R lies along R.

(v) Methyl substitution has little effect on the directions of E_T and E_R at imino nitrogens, and only the E_R of the pyrrolic nitrogen in pyrazole is further rotated towards the adjacent heteroatom by methyl substitution.

(vi) The orientation of the Quadrupole Moment axes is related to the internal and external bisectors of the CH bond directions.

(vii) The principal magnitude of the QM lies very close to one of the CH bonds.

(vi) Methyl substitution rotates the Quadrupole Moment axes by 15^o-20^o in the asymmetrical molecules.

FIG 33 MOLECULAR ORBITALS AND PRINCIPAL EIGENVECTORS FOR PYRROLE.

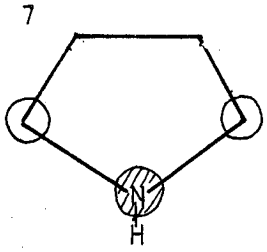

+0.44 1S(N)
−0.44 2S(C2+C5)

$\doteq \Psi_7$ a_1

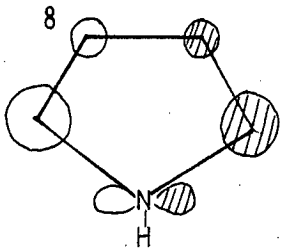

+0.27 $2P_x$(N)
+0.51 2S (C2 − C5)
+0.26 2S (C3 − C4)

$\doteq \Psi_8$ b_2

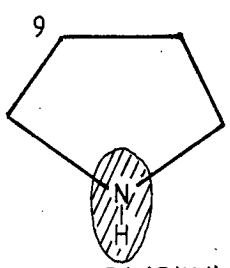

+0.31 1S(H1)
−0.42 $2P_y$(N)

$\doteq \Psi_9$ a_1

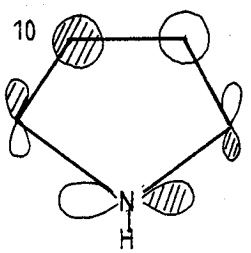

+0.38 $2P_x$(N)
−0.31 2S (C3 − C4)
−0.29 $2P_y$ (C2 − C5)

$\doteq \Psi_{10}$ b_2

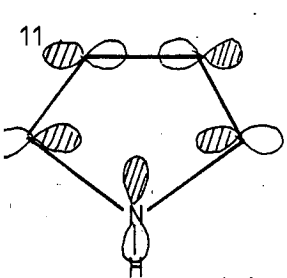

+0.22 $2P_y$ (N)
−0.31 $2P_x$ (C2−C5)
−0.2 $2P_x$ (C3−C4)

$\doteq \Psi_{11}$ a_1

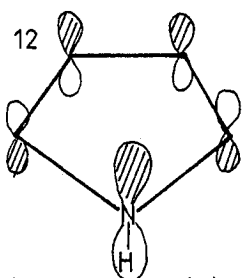

+0.4 $2P_y$(N)
−0.22 $2P_y$(C2+C5)
+0.35 $2P_y$(C3+C4)

$\doteq \Psi_{12}$ a_1

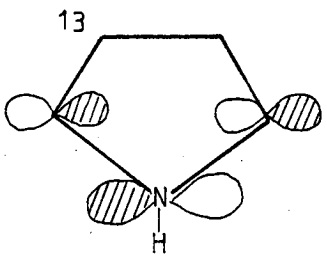

−0.46 $2P_x$(N)
+0.38 $2P_x$(C2+C5)

$\doteq \Psi_{13}$ b_2

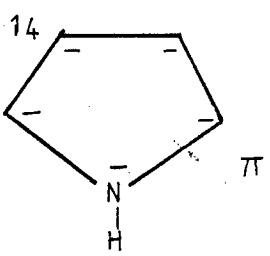

−0.51 $2P_z$(N)
−0.31 $2P_z$(C2+C5)
−0.21 $2P_z$(C3+C4)

$\doteq \Psi_{14}$ b_1

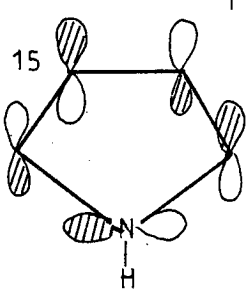

−0.24 $2P_x$ (N)
+0.3 $2P_y$ (C2−C5)
−0.39 $2P_y$ (C3−C4)
−0.39 1S (H3−C4)

$\doteq \Psi_{15}$ b_2

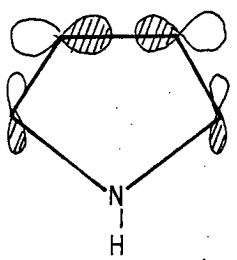

−0.47 $2P_x$ (C3−C4)
−0.25 $2P_y$ (C2+C5)

$\doteq \Psi_{16}$ a_1

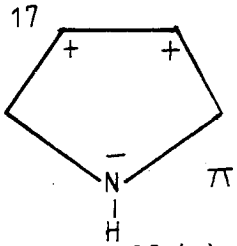

−0.73 $2P_z$(N)
+0.57 $2P_z$(C3+C4)

$\doteq \Psi_{17}$ a_2

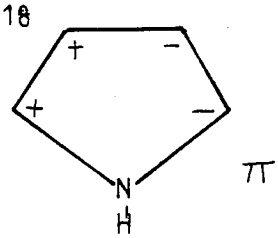

−0.67 $2P_z$(C2−C5)
0.39 $2P_z$(C3−C4)

$\doteq \Psi_{18}$ b_1

(HOMO)

(viii) Magnitudes of calculated coupling constants

It has been proposed that the EFG at a particular centre is due to electrons which reside in 'p' type orbitals at that centre, this is reasonable since 's' type orbitals at that centre are spherically symmetric and electrons residing therein can give no contribution to the variation of energy with nuclear orientation.

Various attempts have been made to interpret observed field gradients using approximate methods such as the Townes and Dailey theory,[23] Bond Polarization[2] (i.e. electronegativity).

These have been extensively used and since attempts at interpretation from earlier LCAO-SCF calculations were unreliable due to inconsistent theoretical results, and the simpler theory provided results of the same quality for considerably less trouble. The quality of contemporary calculations is such that a reliable interpretation can now be made on a molecular orbital basis.

Since the Electric Field Gradient is basically a measure of the asymmetry of the charge distribution of an atom, (the 'p' orbital electrons producing this to a great extent) then an orbital which contributes to the 'p' type character at that centre will increase the EFG. We illustrate by example: Figure (33) gives the valence shell orbitals for pyrrole and their symmetry type.

Orbital 7

Here the 's' type orbitals are symmetric with the C_2 axis and can in no way contribute to the 'p' type character at the nitrogen and hence will not alter the EFG appreciably.

TABLE 14 ***** EXPECTATION VALUES

IN ATOMIC UNITS

FOR PRINCIPAL AXIS COORDINATES
FOR PYRROLE N.

	FG(XX)	FG(YY)	FG(ZZ)	FG(XY)	FG(XZ)	FG(YZ)
AR	-0.4371	-0.5545	1.0416	0.0	0.0	0.0
RON	0.1116	0.1536	-0.2652	-0.0000	0.0	0.0
	-0.3755	-0.4009	0.7764	-0.0000	0.0	0.0

ETRY PARAMETER = 0.033

IN 10**16 ESU/CM**3

E_T	E_R	$E_{\pi\pi}$			
-0.1217	-0.1299	0.2517	-0.0000	0.0	0.0

INTEGRALS OVER MOLECULAR ORBITALS

O.						
1	0.0000	0.0000	-0.0001	-0.0000	0.0	0.0
2	0.0580	-0.0004	-0.0576	0.0000	0.0	0.0
3	0.0580	-0.0004	-0.0576	-0.0000	0.0	0.0
4	-0.0094	0.0229	-0.0135	0.0000	0.0	0.0
5	-0.0094	0.0229	-0.0135	0.0000	0.0	0.0
6	0.0055	0.0566	-0.0620	0.0000	0.0	0.0
7	-0.0390	0.0923	-0.0534	-0.0000	0.0	0.0
8	0.3030	-0.1334	-0.1697	0.0000	0.0	0.0
9	-0.3455	0.7026	-0.3571	0.0000	0.0	0.0
10	0.4749	-0.2296	-0.2453	-0.0000	0.0	0.0
11	-0.0705	0.1813	-0.1109	-0.0000	0.0	0.0
12	-0.2376	0.5003	-0.2626	-0.0000	0.0	0.0
13	0.5776	-0.2723	-0.3053	-0.0000	0.0	0.0
14	-0.4857	-0.4924	0.9781	-0.0000	0.0	0.0
15	0.1148	-0.0442	-0.0706	0.0000	0.0	0.0
16	0.0037	0.0145	-0.0181	-0.0000	0.0	0.0
17	-0.3588	-0.3422	0.7011	-0.0000	0.0	0.0
18	0.0162	-0.0016	-0.0146	-0.0000	0.0	0.0

TION MATRIX

GENVALUE	EIGENVECTORS		
.375545	1.000000	0.0	0.0
.400880	0.0	1.000000	0.0
.776419	0.0	0.0	1.000000

This is verified by inspection of Table (14) which shows the contribution of each molecular orbital to the calculated field gradient.

Orbital 8

There is a node along the C_2 axis and the combinations of SC_2 SC_5 orbitals effectively mimic a "p" type orbital, hence one would predict a positive contribution to E_T from this "pseudo" 'p' type orbital which is verified in table(14)

Orbital 9

This is mainly localized on $N(P_y)$ and 1H(1s) and thus is expected to produce a large positive contribution to E_R. Again this can be seen from Table (14)

Orbital 10

From inspection of Fig (33) one would expect this orbital to make a positive contribution to E_T and this is verified in Table (14).

Orbital 11

One would not expect the contribution of this orbital to E_T or E_R to be significant, since this does not affect the 'p' type character at the hetero atom and this is exhibited in Table (14)

Orbital 12

Here one would expect a positive contribution to E_R from this orbital since it contributes significantly to the 'p'-type character at N, and Table (14) confirms this.

Orbital 13

We can expect this orbital to contribute significantly to E_T, since the 2Py A.O.'s on the adjacent carbons additionally contribute to the overall 'p' type character at the heteroatom. In Table (14) we can indeed see that this orbital provides the largest positive contribution to E_T

Orbital 14

This π type orbital is expected to contribute significantly to the asymmetry of the out of plane charge distribution at the nitrogen atom, which explains its large positive contribution to E_π shown in Table (14).

Orbital 15

Consideration of this orbital leads to a prediction that it will have only a small contribution to E_T, since it is largely centred on C3 and C4 in the form of $2P_y$ components. The distance between the hetero atom and the charge density on the β carbons is such that its charge density as ymetry is unlikely to be affected. Inspection of Table (14) shows that this orbital does not contribute to E_T.

Orbital 16

The symmetry of this orbital is such that little contribution to the asymmetry of the charge distribution at the heteroatom is anticipated. The calculated contribution of this orbital to the field gradients is, as expected, very small and is shown in Table (14).

Orbital 17

π orbital 17 is such that one would expect a contribution to E_π and this is clearly in evidence upon inspection of the calculated orbital contributions. It is, perhaps, surprising that although this orbital has maximum amplitude on the heteroatom and the β carbons, it provides the maximum contribution to E_π despite the distance between the N and β carbon.

Orbital 18 (H.O.M.O)

This orbital has no electron density at the heteroatom (i.e. it is nodal) and therefore it is not surprising that it contributes almost nothing to the E.F.G. components (see Table (14)).

This analysis shows that it is possible to interpret the Electric Field gradients in terms of contributions from particular molecular orbitals, and their symmetry type.

This orbital by orbital analysis shows that, for pyrrole, E_T (and hence χ_T) has the greatest contribution from orbitals of b_2 symmetry type, E_R from a_1 type orbitals and E_π from b_1 type orbitals. It should be noted, however, that due to the traceless nature of the E.F.G. tensor, a large effect on one of the principal components induces an (opposite) effect in the other two. This explains why orbital 14, which is a π orbital, affects both E_T and E_R even though one would expect it to contribute to the out of plane component alone. Also noteworthy is that even for the

contributions to the E.F.G. from particular orbitals, the two smaller principal components are of opposite sign to (but not of equal magnitude) and their sum approximately equal (in absolute magnitude) to the larger component.

(Here it is appropriate to reiterate that in this discussion the electric field gradient (E) and the coupling constant (χ) are interchangeable since $KE = \chi$ where K is a constant.)

With reference to our results and analysis we can now critically comment on the approximate theories which have been extensively used for interpretation of N.Q.R. data in the past. We choose in particular the much applied Townes and Dailey theorem,[23] which interprets the E.F.G.'s observed for a centre, in terms of 'p' type orbitals on the centre alone, in the following manner: The field gradient at the nucleus of an atom produced by an electron in a p_z orbital is given by

$$E_z(P_z) = e \left\langle \frac{1}{r^3} \right\rangle \left\langle 3 \cos^2 \theta_z - 1 \right\rangle$$

cf. equation (30), where e is the electronic charge, and the average is taken over the P_z orbital which is symmetric about the z axis. Now with reference to another axis, g, E_g can be obtained by using the transformation

$$\langle 3 \cos^2\theta_g - 1 \rangle = \tfrac{1}{2}(3 \cos^2\alpha - 1) \langle 3 \cos^2\theta_z - 1 \rangle$$

where α is the angle between the symmetry axis and 'g'. Therefore

$$E_g(P_z) = e \left\langle \frac{1}{r^3} \right\rangle \left\langle 3 \cos^2\theta_g - 1 \right\rangle$$

$$= \tfrac{1}{2} e(3 \cos^2\alpha - 1) \left\langle \frac{1}{r^3} \right\rangle \left\langle 3 \cos^2\theta_z - 1 \right\rangle$$

or

$$E_g(P_z) = \tfrac{1}{2}(3 \cos^2\alpha - 1) E_z(P_z)$$

Now when x or y is chosen as the axis, g, $\alpha = 90^o$ hence

$$E_x(P_z) = E_y(P_z) = -\tfrac{1}{2}E_z(P_z)$$

Also

$$E_x(P_x) = E_y(P_y) = E_z(P_z) = E_{n1O}$$

where n1O represents the field gradient due to an electron in an atomic robital with $l = 1$, $m_l = 0$, n = total quantum number.

Thus the resultant field gradient due to all 'P' shell electrons is

$E_g = n_x E_g(P_x) + n_y E_g(P_y) + n_z E_g(P_z)$ where n_i represents the number of electrons in the P_i^{th} orbital. Hence

$$E_z(P_z) = -\left(\frac{n_x + n_y}{2} - n_z\right) E_{n1O}$$

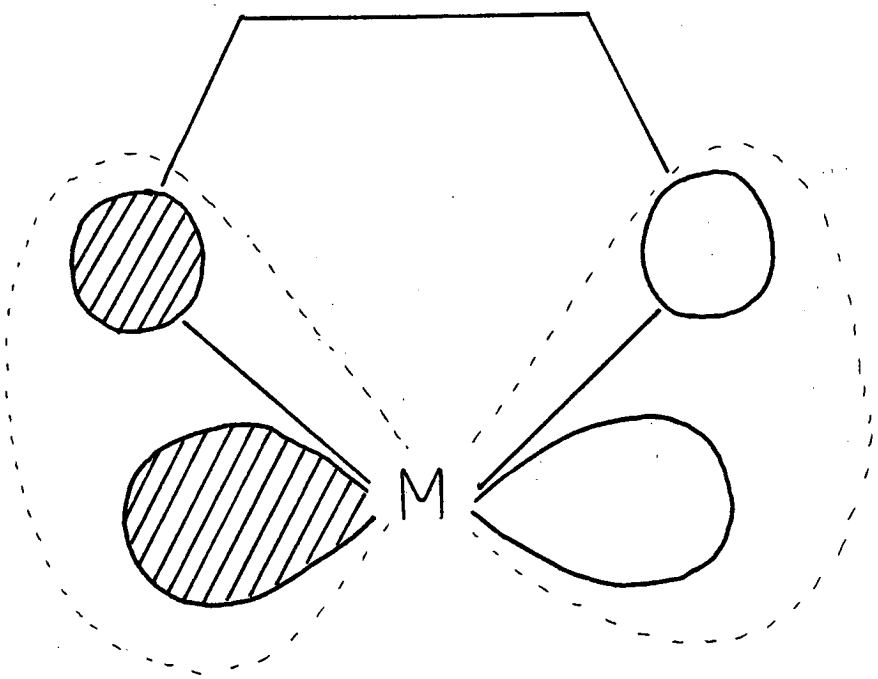

FIG 34 'M' IS THE COUPLING NUCLEUS. A COMBINATION OF THE P LOBES AND ADJACENT S ORBITALS CAN BE CONSIDERED TO EXTEND THE 'P' TYPE ORBITAL AT M AND HENCE CAN AFFECT THE ASYMMETRY OF THE CHARGE DENSITY AT M

$$E_y(P_y) = -(\frac{n_z+n_x}{2} - n_y)E_{n10}$$

$$E_x(P_x) = -(\frac{n_z+n_y}{2} - n_x)E_{n10}$$

Neglecting contributions from electronic charge in 's' type orbitals on the coupling nucleus, and neglecting contributions from 's' type and non-bonding orbitals on all other centres, the principal coupling constants are given by $\chi_x = eQE_x(P_x)$, $\chi_y = eQE_y(P_y)$, $\chi_z = eQE_z(P_z)$

This approximate method is here shown to be open to criticism on two main counts namely:

(i) Contributions to the EFG's are indeed significant from atomic orbitals on other centres, (even if they are of s-type), if combinations of these atomic orbitals in the molecular orbital extend the p-type character of the molecular orbital at the coupling nucleus (see Fig (34)).

(ii) The two smaller principal elements of the E.F.G. tensor, although of opposite sign to the largest element, are not equal in magnitude. Their sum, however, is equal in magnitude to the larger component.

The results of this study show that calculations of this type and quality, now provide the best fundamental method for interpretation of experimental electric field gradients.

FIG (35) Calculated Electric Field Gradients (au) for Pyrrolic Nitrogens

(i) X = H

(ii) X = Me

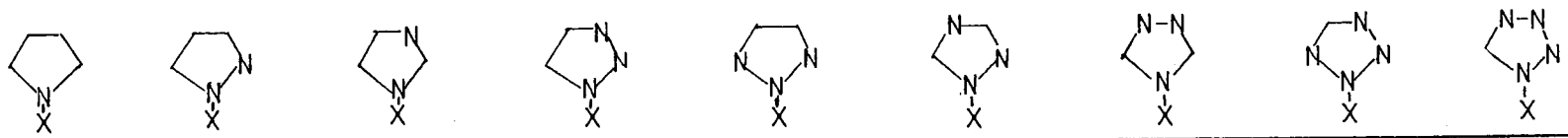

E_T(i)	-0.374	-0.5928	-0.3660	-0.4809	-0.736	-0.6557	-0.4818	-0.6126	-0.527
E_T(ii)	-0.3509	-0.565	-0.347	-0.4803	-0.8103	-0.6528	-0.4690	-0.6176	-0.5289
E_R(i)	-0.4009	-0.2877	-0.3836	-0.2304	-0.3445	-0.2928	-0.3992	-0.2745	-0.1895
E_R(ii)	-0.4523	-0.339	-0.4233	-0.1929	-0.2948	-0.2991	-0.4304	-0.2034	-0.1388
E_π(i)	0.7763	0.8805	0.7493	0.7113	1.080	0.9485	0.8809	0.8872	0.7167
E_π(ii)	0.8047	0.9045	0.7701	0.6003	1.045	0.9522	0.8992	0.8208	0.6676

(ix) Trends- Electric Field Gradients of Pyrrolic Nitrogens

Now from a M.O. analysis of the E.F.G.'s of pyrrole it is possible to predict the likely qualitative effects α or β nitrogen substitution will have on the E.F.G.'s of the pyrrolic nitrogen, if we assume that the aza substitution introduces a perturbation in the unsubstituted system.

This exercise has been performed, as outlined below, and inspection of the calculated and experimental E.F.G.'s of the relevant di-, tri- and tetra-azole will show if such a simple analysis is a valid method for prediction of trends.

For pyrrole, E_T of the pyrrolic nitrogen has maximum contributions from its molecular orbitals 10 and 13 (see Fig (33) and Table (14) for the molecular orbitals and the orbital contributions to the field gradients). (The large contribution from orbital 14 is neglected since it is induced by the large E_π component). Orbitals 10 and 13 are mainly centred on N1, C2, C5 therefore N substitution at an α position would affect E_T by causing a significant perturbation to orbitals 10 and 13. Using a similar argument one would not expect E_T to be significantly altered by methyl substitution at the pyrrolic nitrogen, or by β nitrogen substitution.

Gratifyingly, the above predicted trends appear to be verified by comparison of E_T for the pyrrolic nitrogens for the complete molecular series (see Fig (35)).

E_R in pyrrole has the largest contribution from orbital 9, (which is mainly centred on N1, H1), and from orbital 12 which is mainly centred on N1, C2, C5. This would tend to argue that aza substitution at the α position of pyrrole would alter E_R as would methyl substitution at the pyrrolic nitrogen. Again this predicted trend can be seen from our results, Fig (3 5).

using similar considerations E_π should be affected by α and β aza-substitution since π orbitals 14,17,18 which are those which contribute most to E_π in pyrrole have significant electron density on the α and β carbons.

It is reasonable to assume that β substitution would have a smaller effect (due to its increased distance from the pyrrolic nitrogen), since the E.F.G. is dependent on $1/R^3$, where R is the distance between the coupling nucleus and the electronic charge.

Again the predicted trend is observed from calculated results (Fig (3 5)).

At this point it is important to stress that the extent of perturbation of the principal components cannot be estimated for aza substitution from simple considerations such as these since the traceless nature of the E.F.G. tensor is such that perturbation of one component results in perturbation of the other two. In the light of such considerations it is perhaps surprising that first order approximations, such as those made above, do indeed predict and hence interpret, the qualitative observed trends.

It should also be noted that the E.F.G.'s quoted in Fig (3 5) are calculated values. This is justified since calculations exist for the complete series whereas experimental data is lacking for some molecules, and in a later section it is shown that calculated and experimental E.F.G.'s are in very close agreement.

TABLE 15 ***** EXPECTATION VALUES

IN ATOMIC UNITS

FOR PRINCIPAL AXIS COORDINATES

- PYRAZOLE N2

	FG(XX)	FG(YY)	FG(ZZ)	FG(XY)	FG(XZ)	FG(YZ
IUCLEAR	-0.3357	-0.6597	0.9954	0.0127	0.0	0.0
LECTRON	1.4532	-0.2506	-1.2026	-0.0127	0.0	0.0
OTAL	1.1175	-0.9103	-0.2073	0.0	0.0	0.0

SYMMETRY PARAMETER = 0.629

IN 10**16 ESU/CM**3

	E_R	E_T	E_π			
OTAL	0.3622	-0.2950	-0.0672	0.0	0.0	0.0

INTEGRALS OVER MOLECULAR ORBITALS

OCCUPIED M.O.S							
1	1	-0.0351	0.0954	-0.0604	0.0628	0.0	0.0
2	2	0.0000	-0.0000	-0.0000	-0.0000	0.0	0.0
3	3	0.0134	-0.0005	-0.0129	0.0180	0.0	0.0
4	4	0.0606	0.0024	-0.0629	-0.0898	0.0	0.0
5	5	0.0251	-0.0125	-0.0126	-0.0005	0.0	0.0
6	6	0.0648	0.0397	-0.1045	0.1038	0.0	0.0
7	7	0.0562	0.0416	-0.0979	-0.1262	0.0	0.0
8	8	-0.0179	0.0648	-0.0469	-0.0030	0.0	0.0
9	9	0.0220	0.0156	-0.0376	-0.0180	0.0	0.0
10	10	-0.1616	0.3716	-0.2100	-0.1136	0.0	0.0
11	11	0.0546	0.0037	-0.0583	0.0648	0.0	0.0
12	12	-0.0829	0.2523	-0.1694	-0.1239	0.0	0.0
13	13	-0.2124	-0.1814	0.3938	0.0180	0.0	0.0
14	14	-0.1137	0.2723	-0.1586	-0.0968	0.0	0.0
15	15	0.1479	-0.0636	-0.0842	-0.0088	0.0	0.0
16	16	1.3064	-0.6248	-0.6816	0.3125	0.0	0.0
17	17	-0.0712	-0.0636	0.1348	-0.0091	0.0	0.0
18	18	-0.3296	-0.3382	0.6678	0.0032	0.0	0.0

OTATION MATRIX

EIGENVALUE	EIGENVECTORS		
1.117516	0.970680	-0.240374	0.0
-0.910262	0.240374	0.970680	0.0
-0.207259	0.0	0.0	1.000000

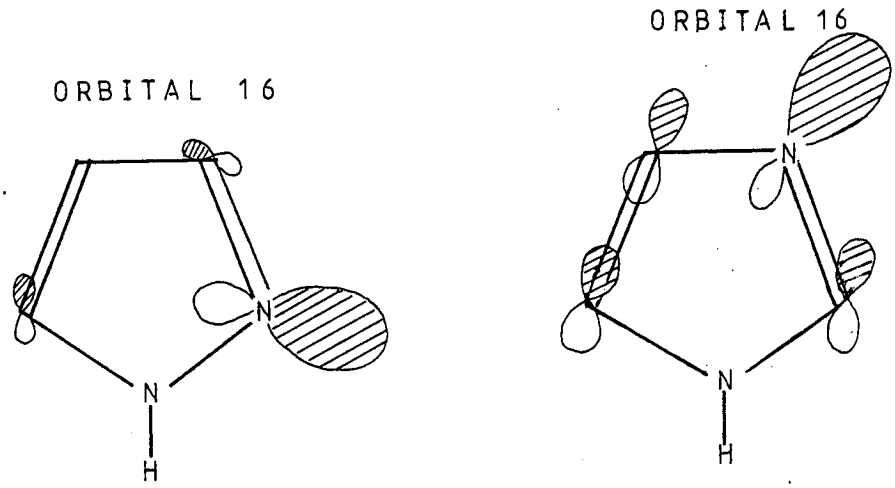

FIG 36 LONE PAIR ORBITALS* OF IMINO NITROGENS IN PYRAZOLE AND IMIDAZOLE.

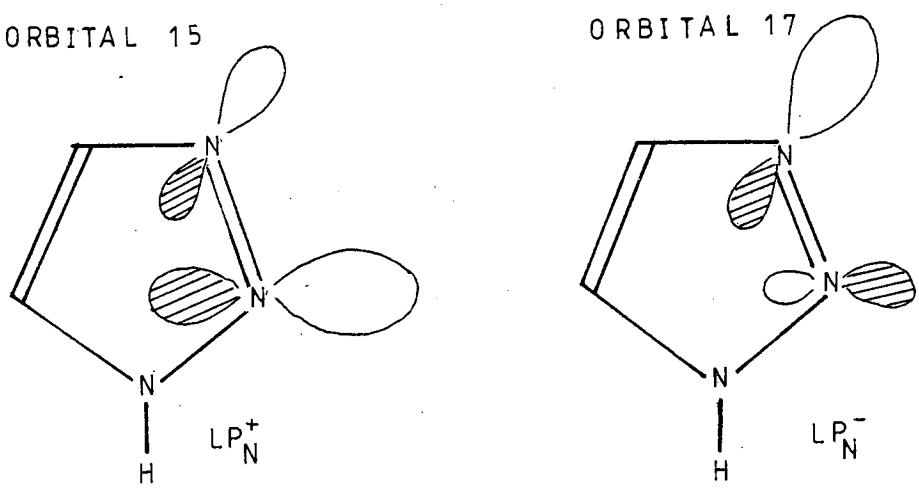

FIG 37 SEMILOCALIZED LONE PAIR ORBITALS* OF 1H-1,2,3-TRIAZOLE

* the size of the lobes indicates the relative magnitudes of the principal components of the orbital eigenvectors

(x) Electric Field Gradients of Imino Nitrogens

In agreement with the idea of a localized lone pair level at the imino nitrogens there is only a small variation in their electric field gradients (E_R); this can be seen in Table (12) where χ_R (and hence E_R by direct proportionality for imino nitrogens) lies in the range -3.625 and -4.721 MHz. As was noted in the earlier work,[1] the magnitude and direction of E_R is dependent on the nature of the adjacent centres.

To investigate this further we consider the orbital contribution to E_R of (a) pyrazole, (b) imidazole and (c) 1H-1,2,3-triazole for imino nitrogens with adjacent carbon/pyrrolic nitrogen, carbon/carbon, and pyrrolic nitrogen/nitrogen respectively.

a) Table (15) shows that orbital 16 in pyrazole contributes the most to E_R at the imino nitrogen, and it is obvious from inspection of the orbital eigenvectors that it is heavily localized, corresponding to the nitrogen lone pair. There is only a small contribution to this orbital from the adjacent carbons, hence one might expect E_R at the imino nitrogen to be only slightly affected by aza substitution at the adjacent β position (as would be the case for 1,2,3-triazole discussed above). See fig (36)

b) The major contribution to E_R (imino) in imidazole again comes from orbital 16 (see Table (16)) which is the LP_N orbital. It is important to note that LP_N in imidazole is more delocalized than that in pyrazole, see fig (36). This indicates that aza substitution at an adjacent position should affect E_R at the β imino nitrogen more than for that at the α imino nitrogen in pyrazole.

TABLE 16 ELECTRIC FIELD GRADIENTS
CALCULATED
WITH REFERENCE TO
THE POINT
N3 OF IMIDAZOLE
COORDINATES

X	Y	Z
3.951700	-1.452500	0.000000

IN ATOMIC UNITS

FOR PRINCIPAL AXIS COORDINATES

	FG(XX)	FG(YY)	FG(ZZ)	FG(XY)	FG(XZ)	FG(YZ)
R	-0.3604	-0.5661	0.9265	-0.0668	0.0000	0.0000
ON	1.4168	0.0193	-1.4361	0.0668	0.0000	0.0000
	1.0564	-0.5468	-0.5097	0.0000	0.0000	0.0000

TRY PARAMETER = 0.035

IN 10**16 ESU/CM**3

E_R	E_T	E_π			
0.3424	-0.1772	-0.1652	0.0000	0.0000	0.0000

ALS OVER MOLECULAR ORBITALS

PIED MOS						
1	0.0228	-0.0094	-0.0134	0.0120	0.0000	0.0000
2	0.0000	-0.0000	-0.0000	0.0000	0.0000	0.0000
3	0.0046	0.0584	-0.0630	0.0906	0.0000	0.0000
4	0.0221	-0.0093	-0.0127	-0.0108	0.0000	0.0000
5	0.0638	0.0479	-0.0567	-0.0827	0.0000	0.0000
6	0.0937	-0.0297	-0.0640	0.0294	0.0000	0.0000
7	0.0752	-0.0085	-0.0667	0.0004	0.0000	0.0000
8	-0.0348	0.1081	-0.0734	0.0064	0.0000	0.0000
9	-0.0796	0.1837	-0.1041	0.0200	0.0000	0.0000
10	-0.0623	0.1474	-0.0852	0.0047	0.0000	0.0000
11	0.0036	0.0720	-0.0755	-0.0715	0.0000	0.0000
12	0.0318	0.1196	-0.1516	0.1889	0.0000	0.0000
13	-0.0295	0.0845	-0.0550	-0.0001	0.0000	0.0000
14	-0.0931	-0.1065	0.1996	0.0089	0.0000	0.0000
15	-0.2439	0.5406	-0.2968	-0.1054	0.0000	0.0000
16 LPN	1.4590	-0.7264	-0.7325	-0.0539	0.0000	0.0000
17	-0.4236	-0.4224	0.8460	-0.0048	0.0000	0.0000
18	-0.0484	-0.0406	0.0870	0.0013	0.0000	0.0000

TABLE 17 ***** EXPECTATION VALUES

IN ATOMIC UNITS

FOR PRINCIPAL AXIS COORDINATES
FOR N3 IN 1,1H-1,2,3-TRIAZOLE

	FG(XX)	FG(YY)	FG(ZZ)	FG(XY)	FG(XZ)	FG(YZ
NUCLEAR	-0.3519	-0.7567	1.1086	0.0839	0.0	0.0
ELECTRON	1.5338	-0.2460	-1.2878	-0.0839	0.0	0.0
TOTAL	1.1819	-1.0026	-0.1592	0.0	0.0	0.0

ASYMMETRY PARAMETER = 0.726

IN 10**16 ESU/CM**3

	E_R	E_T	E_π			
TOTAL	0.3766	-0.3250	-0.0516	0.0	0.0	0.0

INTEGRALS OVER MOLECULAR ORBITALS

OCCUPIED MO's							
1	1		-0.0179	0.0809	-0.0630	0.0805	0.0	0.0
2	2		0.0000	-0.0000	-0.0000	-0.0000	0.0	0.0
3	3		0.0272	0.0402	-0.0675	-0.1010	0.0	0.0
4	4		0.0216	-0.0068	-0.0147	0.0169	0.0	0.0
5	5		0.0262	-0.0122	-0.0140	-0.0085	0.0	0.0
6	6		0.1397	-0.0214	-0.1183	0.0356	0.0	0.0
7	7		-0.0423	0.1746	-0.1324	-0.0993	0.0	0.0
8	8		0.0038	0.0309	-0.0348	0.0225	0.0	0.0
9	9		-0.0372	0.1067	-0.0695	0.0303	0.0	0.0
10	10		-0.1616	0.3689	-0.2073	-0.1076	0.0	0.0
11	11		0.0880	-0.0202	-0.0683	0.0563	0.0	0.0
12	12		-0.2278	-0.2084	0.4362	0.0152	0.0	0.0
13	13		-0.1673	0.3642	-0.1969	-0.0262	0.0	0.0
14	14		0.0123	0.0056	-0.0188	0.0048	0.0	0.0
15	15	$\angle P_N$+	1.2333	-0.6032	-0.6300	-0.1119	0.0	0.0
16	16		-0.0464	-0.0259	0.0724	-0.0122	0.0	0.0
17	17		0.2349	-0.0536	-0.1813	0.1609	0.0	0.0
18	18		-0.3317	-0.3431	0.6748	0.0020	0.0	0.0

ROTATION MATRIX

EIGENVALUE	EIGENVECTORS		
1.161854	0.941065	-0.338226	0.0
-1.002647	0.338226	0.941065	0.0
-0.159218	0.0	0.0	1.000000

TABLE 18 ***** EXPECTATION VALUES

IN ATOMIC UNITS

FOR PRINCIPAL AXIS COORDINATES

FOR N2 IN 1H-1,2,3-TRIAZOLE

	FG(XX)	FG(YY)	FG(ZZ)	FG(XY)	FG(XZ)	FG(YZ)
UCLEAR	-0.2495	-0.8046	1.0541	-0.0834	0.0	0.0
LECTRON	1.5690	0.0622	-1.6513	0.0334	0.0	0.0
OTAL	1.3395	-0.7423	-0.5972	0.0	0.0	0.0

SYMMETRY PARAMETER = 0.108

IN 10**16 ESU/CM**3

	E_R	E_τ	E_π			
OTAL	0.4342	-0.2406	-0.1936	0.0	0.0	0.0

INTEGRALS OVER MOLECULAR ORBITALS

OCCUPIED MO's						
1	1	0.0200	-0.0044	-0.0155	0.0198	0.0	0.0
2	2	-0.0335	0.1009	-0.0674	0.0756	0.0	0.0
3	3	0.0000	0.0000	-0.0000	0.0000	0.0	0.0
4	4	0.0292	-0.0142	-0.0151	-0.0057	0.0	0.0
5	5	0.0270	0.0330	-0.0600	-0.0899	0.0	0.0
6	6	0.0708	0.0186	-0.0894	0.0988	0.0	0.0
7	7	0.0474	0.0127	-0.0601	0.0300	0.0	0.0
8	8	-0.0346	0.1500	-0.1153	-0.0849	0.0	0.0
9	9	-0.0043	0.0335	-0.0292	0.0068	0.0	0.0
10	10	-0.1703	0.3835	-0.2132	-0.1019	0.0	0.0
11	11	0.0491	0.0075	-0.0566	-0.0543	0.0	0.0
12	12	-0.1160	-0.1124	0.2285	0.0153	0.0	0.0
13	13	-0.1949	0.4205	-0.2256	-0.0703	0.0	0.0
14	14	0.1118	-0.0390	-0.0726	-0.0280	0.0	0.0
15	15	0.3801	-0.0360	-0.3442	0.4403	0.0	0.0
16	16	-0.4304	-0.4272	0.3576	-0.0015	0.0	0.0
17	17 LP_N^-	1.0517	-0.5036	-0.5481	-0.2067	0.0	0.0
18	13	-0.0087	0.0078	0.0008	-0.0018	0.0	0.0

OTATION MATRIX

EIGENVALUE	EIGENVECTORS		
1.339518	0.674712	0.738081	0.0
-0.742325	-0.738081	0.674712	0.0
-0.697190	0.0	0.0	1.000000

A comparison of the relevant calculated E_R for pyrazole, imidazole, and 1H-1,2,3-triazole shows that E_R (N^{α}) in 1H-1,2,3-triazole is very similar to that of pyrazole whereas $E_R(N^{\beta})$ is significantly different (1MHz) from the corresponding imino nitrogen in imidazole. This can be seen from values of χ_R in Table (12). Hence the trend predicted from observation of the relevant molecular orbitals appears to be followed.

c) From an analysis of the molecular orbitals which contribute most to the E.F.G.'s imino nitrogens in 1H-1,2,3-triazole (see Tables (17 , 18)) it is obvious that $E_R(N^{\alpha})$ is mostly from the semi localized lone pair (LP_N^-) (orbital 17). $E_R(N^{\beta})$ comes mostly from the LP_N^+ combination (orbital 15), which is in fact more delocalized than the antisymmetric combination. (Diagrams of the LP_N^+ and LP_N^- orbitals are given in Fig. (37)). One might reasonably expect, therefore, that $E_R(N^{\beta})$ would be more perturbed by aza-substitution at the carbon adjacent to the β imino nitrogen. If such a substitution were performed, the molecule would be 1H-tetrazole. Upon inspection of the E_R(N3) in 1H-tetrazole it is found that this quantity differs by 0.7 MHz from E_R(N3) in 1H-1,2,3-triazole, this difference can be attributed to aza-perturbation of particular molecular orbitals as explained above.

It is evident, from the discussion given above that the relatively simple idea of aza substitution in a molecule

introducing a perturbation to that molecule (and its molecular orbitals), can be used to predict or interpret trends in the field gradients on a molecular orbital basis.

We can conclude that interpretation of E.F.G.s, and hence N.Q.C.C.s can be fundamentally performed by analysis of the molecular orbitals of the system under consideration given by ab initio calculations of the quality reported here. This is a valid conclusion since the comparison of calculated and experimental (from both N.Q.R. and M.W.) coupling constants shows a high level of agreement as is shown below.

(xi) Comparison of Calculated and Experimental Data

A summary of the magnitudes of N.Q.C.C.s obtained from microwave (MW), NQR and theoretical calculations is given in Table (19). It can be seen that there is generally good agreement of the data, hence we were able to assign the experimental couplings to χ_R, χ_T and χ_π.

There is, of course, a slight difference between the N.Q.C.C.'s obtained by the two different experimental methods since these values are obtained for molecules in different physical states. In the solid state it is reasonable to expect inter molecular forces to slightly affect the intra-molecular charge distribution.

There is some discrepancy between the M.W. data and the data obtained from the other two methods for 1-methylpyrrole. Since there is good agreement between the N.Q.R. and calculated data for the complete series, and also, especially, since the

Table 19 Comparison of ^{14}N Nuclear Quadrupole Coupling Constants (MHz) by Various Methods

Compound	N Site	Method	Coupling Constants			η	Ref.
			χ_R	χ_T	χ_π		
Pyrrole (1a)		(a) Calc	1.413	1.323	− 2.736	0.0326	
		(b) NQR	1.308	0.754	(−) 2.062	0.2688	
		(c) NQR	1.308	0.754	(−) 2.062		24, 25
		(d) MW	1.45	1.21	−2.66	0.0902	27
1-Methyl-pyrrole (1b)		(a) Calc	1.594	1.237	−2.832	0.1258	
		(b) NQR	1.780	0.790	(−) 2.570	0.385	
		(c) MW	1.97	−2.16	0.19		27
		(d) MW	2.05	−1.69	−0.37		26
pyrazole (2a)	N1	(a) Calc	1.0143	2.0899	−3.1034	0.3465	
		(b) NQR	—	—	—		
		(c) NQR					
		(d) MW	0.72	2.30	−3.02	0.5231	30 b
		(e) Calc	0.9586	2.398	−3.3567	0.4288	30 a
	N2	(a) Calc	−3.938	3.208	0.731	0.6291	
		(b) NQR	(−) 3.9948	3.3096	0.6852	0.6572	

Table 19 contd. Comparison of ^{14}N Nuclear Quadrupole Coupling Constants (MHz) by Various Methods

Compound	N Site	Method	Coupling Constants			η	Ref.
			χ_R	χ_T	χ_π		
pyrazole (2a)	N2	(c) NQR	(-)3.9948	3.3096	0.6852		28, 29
		(d) MW	-4.48	3.69	0.79	0.64732	30b
		(e) Calc	-3.8197	2.8995	0.9202	0.5182	30a
1-Methyl-pyrazole (2b)	N1	(a) Calc	1.195	1.993	-3.188	0.2500	
		(b) NQR	1.1076	2.0248	(-)3.1324	0.2927	
	N2	(a) Calc	-3.824	3.184	0.639	0.6654	
		(b) NQR	3.8172	3.0720	0.7452	0.6094	
Imidazole (3a)	N1	(a) Calc	1.352	1.290	-2.641	0.0235	
		(b) NQR	-	-	-		
		(c) MW	1.49	1.1	-2.159	0.123	32
		(d) Calc	1.5916	1.3037	-2.8953	0.0994	30a
	N3	(a) Calc	-3.723	1.927	1.796	0.0352	
		(b) NQR	3.271	1.847	1.425	0.129	
		(c) MW	-4.08	1.79	2.29	0.1215	32
		(d) Calc	4.0767	1.9116	2.1650	0.0622	30a

Table 19 (contd.) Comparison of ^{14}N Nuclear Quadrupole Coupling Constants (MHz) by Various Methods

Compound	N Site	Method	Coupling Constants			η	Ref.
			χ_R	χ_T	χ_π		
1-Methyl-imidazole (3b)	N1	Calc	1.491	1.223	-2.714	0.0988	
		NQR	-	-	-	-	
	N3	Calc	-3.735	1.925	1.810	0.0304	
		NQR	-	-	-	-	
1-H-1,2,3-Triazole (4a)	N1	Calc	0.812	1.695	-2.507	0.3518	
		NQR	-	-	-		
		MW	0.27	3.58	-3.86	0.858	31
	N2	Calc	-4.095	3.534	0.561	0.7259	
		NQR	-4.1034	3.5046	0.5990	0.7079	
		MW	-4.33	3.79	0.53	0.752	31
	N3	Calc	-4.721	2.616	2.105	0.1083	
		NQR	-4.7152	2.6348	2.0806	0.1176	
		MW	-4.87	2.19	2.19	0.101	31

Table 19 (contd.) Comparison of ^{14}N Nuclear Quadrupole Coupling Constants (MHz) by Various Methods

Compound	N Site	Method	Coupling Constants			η	Ref.
			χ_R	χ_T	χ_π		
1-H-1,2,4-Triazole (5a)	N2	Calc	-4.012	3.518	0.496	0.7926	
		NQR	-4.230	-	-	0.665	
		MW	-4.41	3.81	0.60	0.728	30c
	N4	Calc	-3.882	1.992	1.890	0.262	
		NQR	-3.220			0.169	
		MW	-4.01	1.80	2.21	0.102	30c
1-Methyl-1,2,4-triazole (5b)	N1	Calc	1.054	2.301	-3.356	0.3717	
		NQR	1.0482	2.3328	-3.381	0.3799	
	N2	Calc	-3.881	3.415	0.465	0.7601	
		NQR	-4.0099	3.6495	0.3605	0.8201	
	N4	Calc	-3.879	1.985	1.894	0.0236	
		NQR	-3.8766	1.967	1.9100	0.0147	

Table 19 (contd.) Comparison of ^{14}N Nuclear Quadrupole Coupling Constants (MHz) by Various Methods

Compound	N Site	Method	Coupling Constants			η	Ref.
			χ_R	χ_T	χ_π		
4-Methyl-1,2,4-triazole (7b)	N1/2	Calc	-3.639	2.785	0.855	0.5303	
		NQR	-3.6705	2.8239	0.8467	0.5334	
	N4	Calc	1.517	1.653	-3.169	0.0429	
		NQR	1.5172	1.6538	-3.1708	0.0430	
1H-Tetrazole (9a)	N1	Calc	0.668	1.858	-2.526	0.4714	
		NQR	0.6296	1.9252	-2.5548	0.5071	
	N2	Calc	-4.458	3.371	1.086	0.5124	
		NQR	-4.4210	3.3836	1.0376	0.5306	
	N3	Calc	-4.095	2.773	1.321	0.3546	
		NQR	-4.0995	2.7877	1.3119	0.3599	
	N4	Calc	-4.443	2.889	1.555	0.3000	
		NQR	-4.4457	2.8687	1.5769	0.2905	
1-Methyl-tetrazole (9b)	N1	Calc	0.489	1.864	-2.353	0.5842	
		NQR	-	-	-	-	
	N2	Calc	-4.316	3.301	1.016	0.5296	
		NQR	-4.2760	3.2542	1.0218	0.5219	

Table 19 (contd.) Comparison of ^{14}N Nuclear Quadrupole Coupling Constants (MHz) by Various Methods

Compound	N Site	Method	Coupling Constants			η	Ref.
			χ_R	χ_T	χ_π		
1-Methyl-tetrazole (9b)	N3	Calc	-4.105	2.808	1.297	0.3680	
		NQR	-4.0954	2.7852	1.3102	0.3601	
	N4	Calc	-4.467	1.595	2.8717	0.2857	
		NQR	-3.9901	2.1229	1.8673	0.0640	
2-Methyl-tetrazole	N1	Calc	-4.178	3.195	0.983	0.5294	
		NQR	-4.1386	3.1664	0.9724	0.5301	
	N2	Calc	0.717	2.177	-2.893	0.5043	
		NQR	0.7148	2.1764	-2.8912	0.5054	
	N3	Calc	-4.511	2.907	1.604	0.2889	
		NQR	-4.5383	2.9467	1.5916	0.2985	
	N4	Calc	-4.407	2.846	1.561	0.2915	
		NQR	-4.4058	2.8498	1.5562	0.2936	

microwave data for this molecule is contrary to the general trend that methyl substitution does not significantly affect the N.Q.C.C.'s, it is reasonable to propose that a re-estimation or reassignment of the M.W. data is required.

The trend $\chi_\pi > \chi_T > \chi_R$ for pyrrolic nitrogens has been used to remove the ambiguity in the calculated assignment of in plane E.F.G.s for 1-methyl-1,2,3-triazole (see Fig (32)) This is a reversal of the trend observed for the imino nitrogens $\chi_R > \chi_T > \chi_\pi$

The good agreement between the experimental and calculated data shows that

a) Assignment of the NQR data can be made with a high degree of certainty.
b) Calculations such as these are of sufficiently high quality to confidently predict N.Q.C.C.'s where data is lacking.

Total and Orbital Energies

(xii) Table (20) contains the calculated total energies for the complete series of molecules and other literature values. It can be seen that our results provide the best reported total energies to date for the complete series except pyrazole, for which a CI study using a double zeta basis has been performed.[33] This study is in fact the first complete study, (either ab initio or otherwise), for this series of molecules.

The total energies can be used to indicate which tautomeric form of the triazoles and tetrazoles might predominate in the gas phase since the calculations are for isolated molecules and the total energies are indicative of the relative stabilities of the structures.

Observation of Table (20) shows that the 2-H tautomers of both 1,2,3-triazole and tetrazole are energetically favoured, as is the 1-H form of 1,2,4-triazole. (A more lengthy disucssion of the predominant gas phase tautomers will be given below in the section devoted to P.E.S. spectroscopic studies of molecules 1 to 9).

Table (21) contains the orbital energies produced by the calculations and their symmetry type. Molecules (1a to 5a and 9a) have previously been investigated by MB ab initio calculations,[34] and Table (22) contains a comparison between the DZ orbital energies reported here and those produced by the minimal basis calculation.[34]

Inspection of Table (22) shows that DZ calculations produce lower orbital energies, as would be expected, and

Table of Total Energies (contd)

Molecule	Total Energy (au)	Other literature Values (au)
1-methyl-1,2,4-triazole (7b)	-279.68904	
1H-tetrazole (8a)	-256.60344	-255.8008[a]
1-methyltetrazole (8b)	-295.62796	
2H-tetrazole (9a)	-256.61827	
2-methyltetrazole (9b)	-295.64678	

a) M.H. Palmer, S. Cradock, R.H. Findlay, Tetrahedron, 29, 2173 (1973).

b) E. Clementi, H. Clementi, D.R. Davies, J.Chem.Phys. 46, 4725 (1967).

c) G. Berthier, L. Praud, J. Serre, In Quantum aspects of heterocyclic compounds in chemistry and biochemistry (E.D. Bergmann and B. Pullman Eds) Jerusalem Symposia 2, 40. N.Y. Academic Press 1970.

d) R.W. Kramling, E. Wagner, Theor.Chim.Acta., 15, 43 (1969).

e) H. Preuss, R. Janoscheck, J.Mol.Struct., 3, 423 (1969).

f) Tae Kyu Ha, J.Mol.Struct., 51, 87 (1979).

g) H.J.T. Preston, J.J. Kaufmann, Int.J.Quant.Chem., 7, 207 (1973).

h) All methyl hydrogen out of plane.

i) All methyl hydrogen out of plane.

Table 21 Orbital Energies (eV)

(C_2V)

pyrrole (1a)	pyrazole (2a)	imidazole (3a)	1H-1,2,3-triazole (4a)
-8.211 a_2	-9.678 a"(π)	-9.020 a"	-10.212 a"
-9.579 b_1	-10.248 a"	-11.065 a"	-11.782 a'(LP_N-)
-14.453 a_1	-12.456(LP_N) a'(σ)	-11.758 a' (LP_N)	-11.941 a"
-14.920 b_2	-15.624 a'	-15.724 a'	-13.873 a'(LP_N+)
-15.630 b_1	-16.200 a'	-16.586 a"	-17.297 a'
-15.942 b_2	-16.803 a"	-16.646 a'	-17.807 a'
-16.307 a_1	-16.904 a'	-16.778 a'	-18.033 a"
-20.181 a_1	-20.466 a'	-20.942 a'	-21.330 a'
-20.979 b_2	-22.033 a'	-21.991 a'	-23.612 a'
-21.794 a_1	-22.686 a'	-22.879 a'	-23.649 a'
-26.825 b_2	-29.113 a'	-27.857 a'	-30.335 a'
-28.647 a_1	-30.339 a'	-32.236 a'	-33.499 a'
-35.576 a_1	-38.155 a'	-37.204 a'	-40.557 a'
-305.358 a_1	-305.921 a'	-306.419 a'	-307.073 a'
-305.386 b_2	-306.654 a'	-307.085 a'	-307.531 a'
-306.634 a_1	-307.451 a'	-307.934 a'	-424.803 a'
-306.635 b_2	-424.599 a'	-423.480 a'	-425.976 a'
-424.787 a_1	-425.631 a'	-425.075 a'	-426.666 a'

1H-1,2,4-triazole (5a)	(C_2V) 2H-1,2,3-triazole (6a)	(C_2V) 4H-1,2,4-triazole (7a)	2H-tetrazole(8a)	1H-tetrazole (9a)
-10.728 a"	-10.885 a_2	-10.783 a_2	-11.990 a"	-11.809 a"
-11.841 a"	-11.181 b_1	-11.474 b_1	-12.720 a"	-12.636 a'(LP_N)
-12.173 a'(LP_N-)	-12.868 b_2(LP_N-)	-12.394 a_1(LP_N+)	-12.880 a'(LP_N)	-13.077 a"
-13.616 a'(LP_N+)	-13.741 a_1(LP_N+)	-12.558 b_2(LP_N-)	-13.545 a'(LP_N)	-13.319 a'(LP_N)
-16.687 a'	-17.035 b_2	-17.001 a_1	-15.686 a'(LP_N)	-15.443 a'(LP_N)
-17.651 a"	-17.323 a_1	-17.310 b_1	-18.366 a'	-19.185 a"
-18.072 a'	-17.491 b_1	-17.645 b_2	-19.025 a"	-19.458 a'
-21.364 a'	-20.335 a_1	-21.762 a_1	-21.460 a'	-21.945 a'
-22.654 a'	-22.719 b_2	-22.997 a_1	-24.082 a'	-24.929 a'
-24.159 a'	-23.437 a_1	-23.677 b_2	-25.585 a'	-25.404 a'
-31.081 a'	-30.320 a_1	-30.867 b_2	-33.39 a'	-33.568 a'
-33.479 a'	-32.911 b_2	-32.968 a_1	-34.98 a'	-35.273 a'
-39.392 a'	-39.413 a_1	-38.242 a_1	-42.239 a'	-42.497 a'
-307.841 a'	-307.357 a_2	-308.760 a_1	-308.366 a'	-307.073 a'
-308.641 a'	-307.386 a_1	-308.761 b_2	-425.367 a'	-307.531 a'
-423.769 a'	-425.675 a_1	-424.845 b_2	-425.973 a'	-424.803 a'
-425.359 a'	-425.695 b_2	-424.486 a_1	-427.173 a'	-425.975 a'
-426.188 a'	-426.777 a_1	-425.957 a_1	-427.822 a'	-426.665 a'

Table 22 Comparison of Valence Shell Orbital Energies

pyrrole (1a)		pyrazole (2a)		imidazole (3a)	
MB[a]	DZ[b]	MB	DZ	MB	DZ
-10.34 a_2	-8.21 1a	-11.32 3a"	-9.68 3a"	-11.17 3a"	-9.02 3a"
-11.65 b_1	-9.57 $2b_1$	-13.01 2a"	-10.24 2a"	-12.71 2a"	-11.07 2a"
-16.02 a_1	-14.45 $9a_1$	(LP_N)-13.84 15a'	(LP_N)-12.45 15a'	(LP_N)-12.83 15a"	(LP_N)-11.75 15a'
-16.37 b_2	-14.92 $6b_2$	-17.58 14a'	-15.62 14a'	-17.33 14a'	-15.72 14a'
-17.31 b_2	-15.63 $1b_1$	-18.59 13a'	-16.2 13a'	-17.60 13a'	-16.58 1a"
-17.68 a_1	-15.94 $5b_2$	-19.15 1a"	-16.80 1a"	-18.57 1a"	-16.64 13a'
-17.69 b_1	-16.30 $8a_1$	-19.24 12a'	-16.90 12a'	-18.59 12a'	-16.77 12a'
-21.29 a_1	-20.18 $7a_1$	-22.74 11a'	-20.46 11a'	-21.84 11a'	-20.942 11a'
-22.23 b_2	-20.97 $4b_2$	-24.07 10a'	-22.03 10a'	-23.71 10a'	-21.991 10a'
-22.93 a_1	-21.79 $6a_1$	-24.77 9a'	-22.69 9a'	-23.79 9a'	-22.879 9a'
-28.27 b_2	-26.82 $3b_2$	-30.81 8a'	-29.113 8a'	-29.39 8a'	-27.857 8a'
-30.01 a_1	-28.64 $5a_1$	-32.32 7a'	-30.339 7a'	-33.31 7a'	-32.236 7a'
-36.95 a_1	-35.57 $4a_1$	-39.95 6a'	-38.155 6a'	-38.69 6a'	-37.204 6a'

Table 22 (contd.) Comparison of Valence Shell Orbital Energies

1H-1,2,3-Triazole (4a)		1H-1,2,4-Triazole (5a)		1H-Tetrazole (9a)	
MB	DZ	MB	DZ	MB	DZ
-12.353 3a"	-10.21 3a"	-12.50 3a"	-10.73 3a"	3a"	-11.08 3a"
($\angle P_N^-$)-12.81 15a'	($\angle P_N^-$)-11.78 15a'	($\angle P_N^-$)-13.34 15a'	-11.84 2a"	($\angle P_N$)-13.5 15a'	($\angle P_N$)-12.63 15a'
-13.71 2a"	-11.94 2a"	-13.42 2a"	($\angle P_N$)-12.173 15a'	($\angle P_N$)-13.73 14a'	-13.077 2a"
($\angle P_N^+$)-15.16 14a'	($\angle P_N^+$)-13.87 14a'	($\angle P_N^+$)+14.92 14a'	($\angle P_N^+$)-13.616 14a'	-14.47 2a"	($\angle P_N$)-13.32 14a'
-18.47 13a'	-17.29 13a'	-18.76 13a'	-16.687 13a'	($\angle P_N$)-16.70 13a'	($\angle P_N$)-15.44 13a'
-18.85 12a'	-17.804 12a'	-19.02 12a'	-17.65 1a"	-19.56 12a'	-19.19 1a"
-19.9 1a"	-18.033 1a"	-19.72 1a"	-18.02 12a'	-20.46 1a"	-19.45 12a'
-27.85 11a'	-21.330 11a'	-22.90 11a'	-21.36 11a'	-23.26 11a'	-21.95 11a'
-24.09 10a'	-23.61 10a'	-24.68 10a'	-22.65 10a'	-25.35 10a'	-24.92 10a'
-25.18 9a'	-23.64 9a'	-25.07 9a'	-24.16 9a'	-26.08 9a'	-25.40 9a'
-31.98 8a'	-30.33 8a'	-32.73 8a'	-31.08 8a'	-34.55 8a'	-33.56 8a'
-34.69 7a'	-33.49 7a'	-34.4 7a'	-33.48 7a'	-35.80 7a'	-35.27 7a'
-42.03 6a'	-40.56 6a'	-41.13 6a'	-39.39 6a'	-43.09 6a'	-42.49 6a'

a) Minimal Basis Set E. Clementi "Tables of Atomic Functions". I.B.M. J. of Res. and Development 9, 2 (1965)

b) Double Zeta Basis set T.H. Dunning, J.Chem.Phys., 53, 2823 (1970).

that the double zeta basis does not produce any significant changes in either orbital orderings or groupings.

There is found to be a change in ordering of the 1a" and 12a' levels in imidazole which does not, however, alter the orbital groupings; a similar effect is found for 1-H-1,2,4-triazole, (where the DZ basis reorders the 15a' and 2a" levels), and 1-H-tetrazole which experiences reordering of the 14a' and 2a" levels, the orbital groupings being preserved in both cases, and it is generally true to say that the DZ basis effectively lifts degeneracy or near degeneracy of MB orbital energies.

From inspection of the contents of Table (2 1) the following trends are apparent:

(i) Introduction of a nitrogen atom into the pyrrole system results in general stabilization of the eigenvalues, which increases as the number of nitrogens increase.

(ii) The replacement of $\rangle\!\!\rangle$CH by $\rangle\!\!\rangle$N: results in transformation of a σ CH bonding orbital to one of lone pair character, which lies to lower binding energy. When more than one nitrogen is present in a symmetric molecule the lone pairs can exist as linear combinations, symmetric (LP_N^+) and antisymmetric (LP_N^-). For the asymmetrical molecules the LP_N exist as semi localized lone pairs and cannot be easily interpreted as combinations especially for the tetrazoles.

(iii) The valence orbital energies fall into distinct groupings for the azoles. The first band lies in the 8-10 eV region for pyrrole, moves to successively higher

binding energy upon successive aza substitution, and lies at 11-15.5 eV in tetrazole. It contains two levels for pyrrole and (2+n) levels in the other molecules, where n is the number of imino nitrogens.

The second region, (at 14-16 eV in pyrrole) again moves to higher binding energy on successive nitrogen substitution and contains (6-n) levels where n is the number of imino nitrogens.

The above trends have been reported in the literature where a more lengthy discussion ensues.[34]

Now inspection of Table (2 1) shows that methyl substitution produces an almost monotonic destabilization of the eigenvalues especially for the π level at 16 eV about which differs only slightly for particular orbitals. Methyl substitution also results in an additional π {Me(e)} in the 17-19 eV region (lying at higher binding energy as the number of nitrogens increases), but produces no reordering of the π, LP_N levels except for 1H-tetrazole where the LP_N of lowest binding energy is swapped with the adjacent π level.

(N.B. It should be noted that $LP_N^- < LP_N^+$ is the calculated ordering for all azoles except 4-H-1,2,4-triazole, where the LP_N^+ and LP_N^- levels are calculated to be almost degenerate. The extra destabilization of the symmetric combination has been attributed to a through bond interaction,[35,36] however results of chapter (5;p275) indicate that this can be more fundamentally explained by availability of orbitals with the correct symmetry in the unperturbed system).

(xiii) Photoelectron Spectra

Spectra were obtained for molecules (1-9) using the Perkin Elmer PS16 photoelectron spectrometer. The spectra were calibrated with the $^2P_{\frac{1}{2}}$, $^2P_{3/2}$ doublets of argon and xenon and He(II) spectra were recorded using a time averaging computer (CAT). The use of the CAT enabled us to obtain a very good signal to noise ratio for the He(II) spectra, but at the expense of some resolution. The slit to the detector was not opened (as is the usual practice to increase the signal) in an attempt to preserve resolution. The loss of resolution is inherent in the CAT which is unable to resolve <50 meV. However, the signal to noise ratio is so improved by its utilization that this compensates more than adequately for the loss of resolution.

General Considerations

Before attempting to assign the spectra the following points should be considered.

(i) Replacement of $\gg$CH by $\gg$N: results in the transformation of a σ CH bonding orbital to a lone pair orbital (LP_N) which can be expected to lie in the 9-12 eV region. Thus we can expect one IP attributed to an LP_N in this region of the spectrum per imino nitrogen.

(ii) Aza substitution results in a general shift of the photoelectron spectrum to higher binding energy. This stabilization increases as the number of imino nitrogens increases.

(iii) It is accepted that methyl substitution does not affect the general outline of the spectrum for the original

unsubstituted compound, but results in a general destabilization of the IP's.

It therefore follows that comparison of the PES of blocked methyl derivatives can indicate the dominant tautomeric gas phase form of the unsubstituted compound.

Having noted these points we must consider the methods available for spectral interpretation, which are

a) Koopman s' Theorem (K.T.).

b) Comparison of the spectra of the azasubstituted compounds with that of the unsubstituted parent compound.

c) Comparison of relative peak intensities of the He(I) and He(II) spectra. The cross section of LP_N and orbitals with 's' character increases under He(II) conditions, therefore the relative intensity of peaks resulting from ionizations from orbitals of this nature will increase for He(II) irradiation.

The use of K.T. relies on the correct calculation of orbital ordering for the theoretic orbital energies. Despite the high quality of the DZ calculations performed here, K.T. has been shown to give incorrect assignments, as was found for pyridine (Chapter 5 : page 309), and its predictions must therefore (i) be treated with a certain degree of scepticism, (ii) checked.

Comparison of the spectra for aza-substituted compounds with that of the parent compound (which here is pyrrole) relies on the latter's correct assignment; He(I)/He(II) relative intensity studies cannot conclusively indicate intensity increases for peaks which lie under the envelope of a broad band.

FIG 38 PHOTOELECTRON SPECTRA

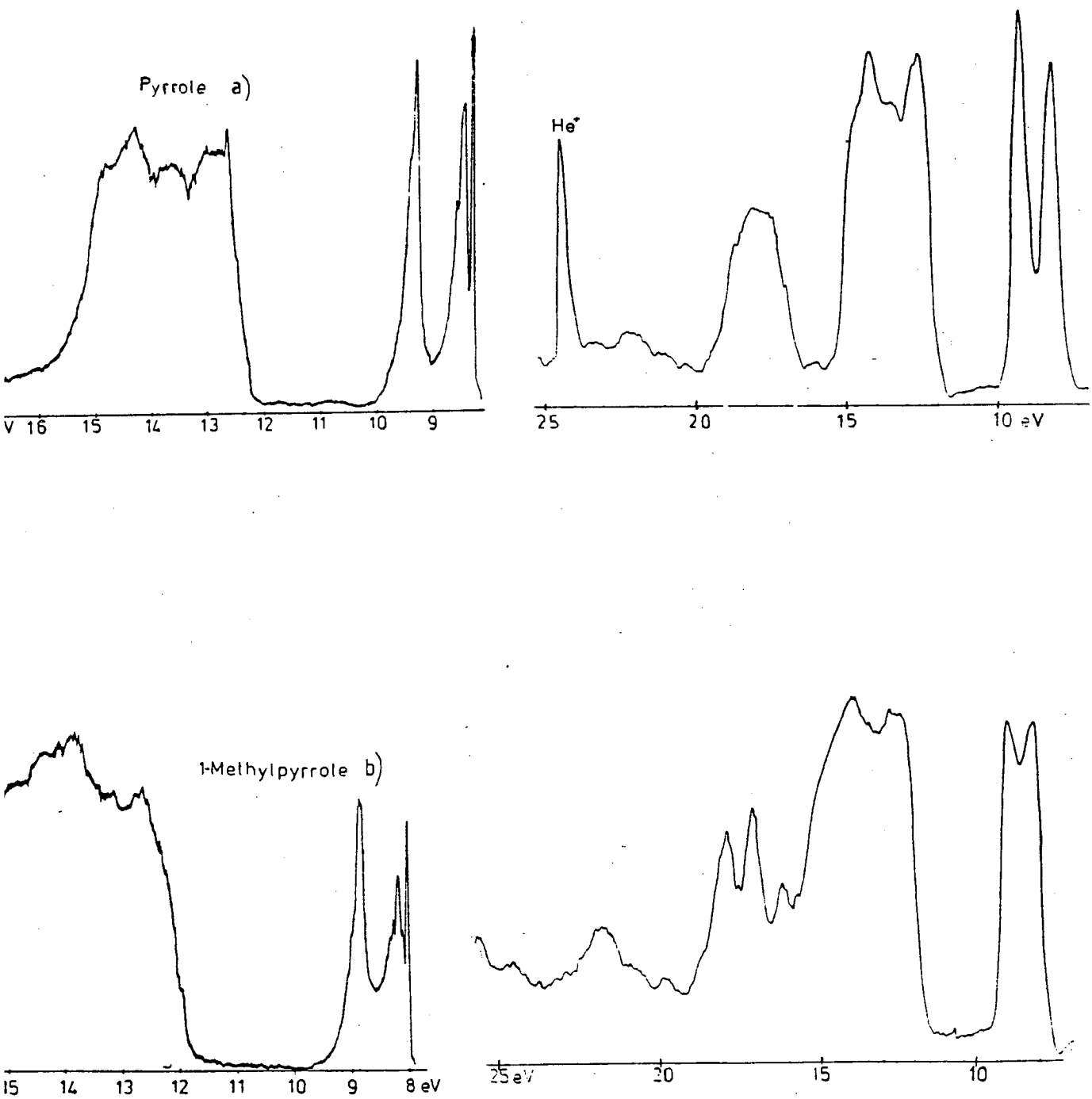

Therefore, although no one technique (a)-(c), is satisfactory on its own a combination of the three is acceptable (since they are often complementary) and this combination has been employed for spectral assignment, as indicated for each molecule below.

Spectral Analysis

Pyrrole/1-Methylpyrrole Figs(38 a,b)

The He(I) PES of pyrrole has been previously reported[37] and assigned by virtue of K.T. and the results of MB calculations. The spectrum we obtained is in agreement with the earlier work. If we are to use this spectrum for comparison with its aza analogues, it is essential that the correct assignment is given. We must, therefore check the previously reported assignment.

Comparison of the PES of pyrrole with that of cyclopentadiene (the parent hydrocarbon) which was reported by Lindholm et al[38] and assigned using a MB calculation[39] shows that the general envelopes outline of these spectra are similar. The second IP is destabilized in pyrrole and this is expected since replacement of $\rangle\!=\!\langle$CH by $\rangle\!=\!\langle$NH would cause some shifting of the π levels. If the assignment for cyclopentadiene is correct, then the first two IP's correspond to a_2 and b_1 respectively. This assignment is predicted by K.T. and our calculated orbital energies, and since these peaks are relatively no more intense under He(II) conditions, then within the limits of available information this assignment is probably correct.

Table 23 (contd.) Vertical Ionization Potentials (eV) and Their Assignment

1-Methyl-pyrrole (1b)		1-Methyl-pyrazole (2b)		1-Methyl-imidazole [40] (3b)		1-Methyl-1,2,3-triazole (4b)		1-Methyl-1,2,4-triazole (5b)	
8.006	4a"	8.85	4a"	8.69	4a"	9.88	4a"	10.11	4a"
8.83	3a"	9.54	18a'	9.75	18a'	10.25	18a'	10.84	18a'
12.67	2a"	10.56	3a"	9.75	3a"	10.54	17a'	11.00	17a'
13.15	18a'	12.89	2a"	13.12	2a"	11.85	3a"	12.53	3a"
13.81	17a'	13.87	17a'	14.01	17a'	14.20	2a"	14.37	2a"
14.5	16a'	14.50	16a'	14.74	16a'	14.30	16a'	15.15	16a'
15.48	15a'	14.78	15a'	15.37	15a'	15.4	15a'	15.72	15a'
15.95	14a'	15.48	14a'	17.28	14a'	15.6	14a'	17.08	14a'
16.94	12a"	16.87	1a"			17.81	1a"	18.15	1a"
17.80	13a'	18.13	13a'			19.68	13a'	19.73	13a'
19.65	12a'	19.10	12a'			20.97	12a'	19.84	12a'
21.23	11a'	20.085	11a'			22.37	11a'	23.16	11a'
24.32	10a'	22.25	10a'			23.56	10a'		
		23.56	9a'						

Table 23 (contd.) Vertical Ionization Potentials (eV) and their Assignment

2-Methyl-1,2,3-triazole (6b)		4-Methyl-1,2,4-triazole (7b)		2-Methyl tetrazole (8b)		1-Methyltetrazole (9b)	
9.61	4a"	9.75	4a"	10.79	4a"	10.87	4a"
10.59	18a'	9.9	18a'	11.01	18a'	11.18	18a'
10.73	17a'	10.64	17a'	11.61	17a'	11.36	17a'
11.8	3a"	11.32	3a"	13.35	3a"	13.07	3a"
13.81	16a'	14.2	2a"	14.62	16a'	14.76	16a'
14.73	2a"	14.8	16a'	15.61	15a'	15.05	2a"
15.45	15a'	15.74	15a'	15.61	2a"	15.46	15a'
16.66	14a'	16.1	14a'	16.82	14a'	16.2	14a'
19.00	1a"	17.91	1a"	18.76	1a"	17.25	1a"
20.26	13a'	18.33	13a'	20.43	13a'	18.80	13a'
22.69	12a'	19.81	12a'	21.64	12a'	20.5	12a'
22.69	11a'	20.37	11a'	22.71	11a'	21.4	11a'
		21.13	10a'				
		23.93	9a'				

The orbital energies are grouped (see Table 21)) such that five levels lie within the 14 → 16 eV range. Since the P.E.S. has a distinct broad band from 12 → 15 eV it is not unreasonable to expect, therefore, that five IP's lie within this band. The DZ calculation effectively lifts the degeneracy of the $5b_2$, $1b_1$ and $8a_1$ levels (given by the MB calculation) which produced a degree of ambiguity in the previous assignment. We must now decide if the $1b_1 < 5b_2 < 8a_1$ IP ordering given by KT and the DZ orbital energies is reasonable, and this can be attempted by inspection of relative peak intensities.

The He(II)/He(II) P.E.S. indicate that the peaks in the second band at 12.67 and 14.33 have a greater relative intensity under He(II) conditions than that at 13.65. This indicates that the assignment given by K.T. and our calculations is in fact correct and therefore the spectrum has been assigned accordingly. The bands at 17 → 19 eV and 21 → 24 eV have also been assigned by K.T.

Table 23 gives the experimental IP's and their assignment. It should be noted that our assignment differs from the previous one only in the ordering of the $1b_{1u}$, $5b_2$ and $8a_1$ levels.

Our spectrum for 1-methylpyrrole agrees with the literature spectrum.[37a] Comparison of this spectrum with that of pyrrole shows that the methyl substitution has little effect on the shape of the spectrum although the band at 16-19 eV is more resolved and the expected general destabilization of the IP's is in evidence.

Comparison shows that the groupings of the experimental IP's and orbital energies (OE's) is almost identical and since there is no reordering of the OE's on methyl substitution the spectrum of the 1-methylisomer has been assigned by virtue of K.T. and the DZ orbital energies.

FIG 39 PHOTOELECTRON SPECTRA

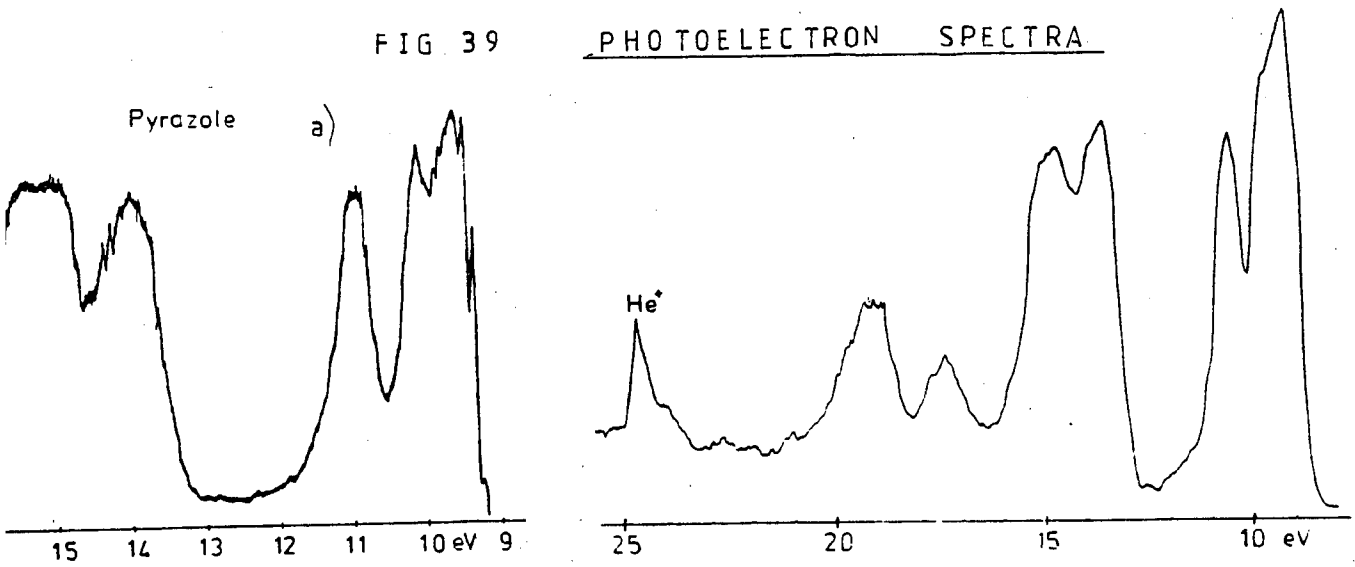

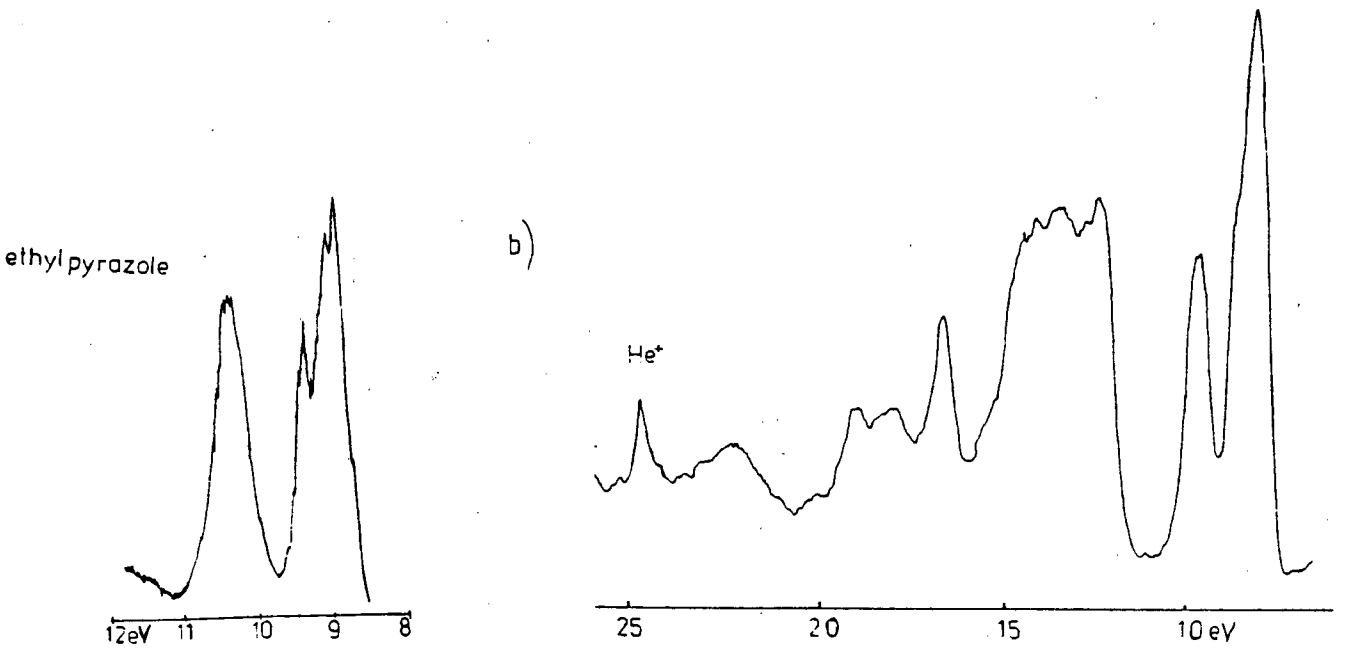

FIG 40

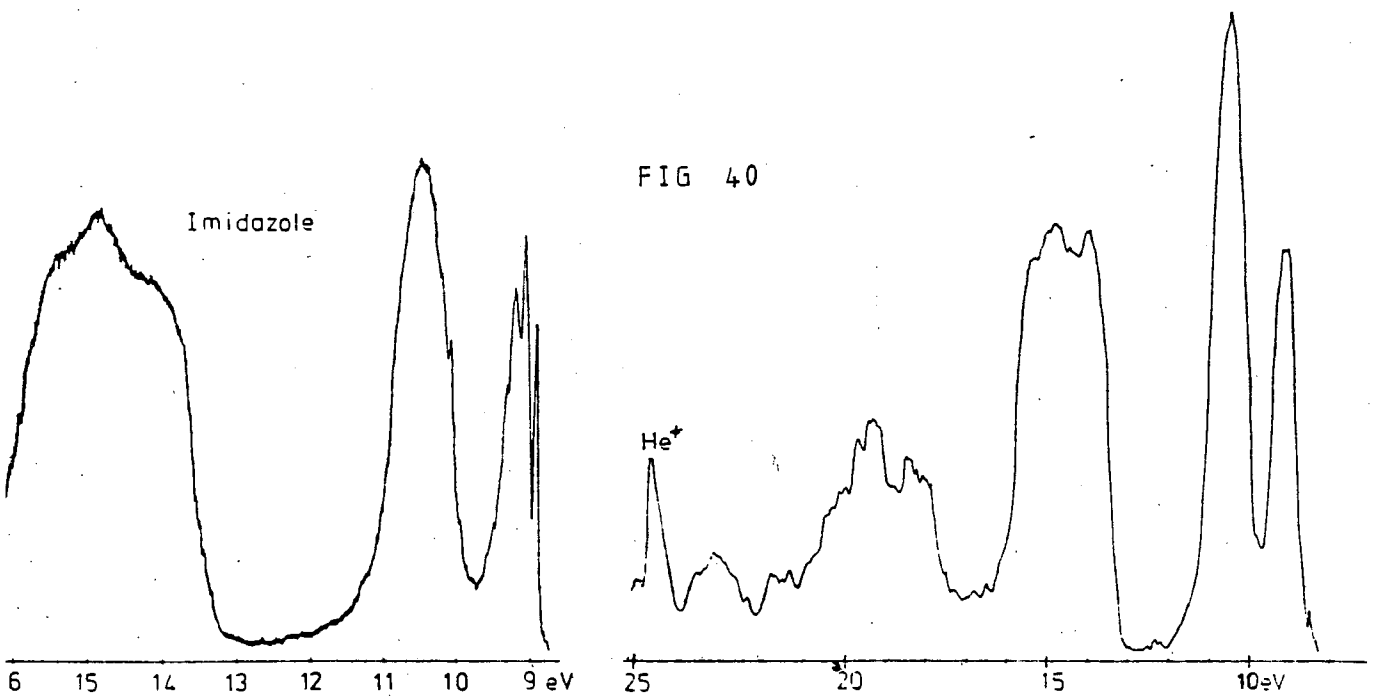

Pyrazole, Imidazole and their 1-Methyl Derivatives

Figs. (39 , 40)

The He(I) spectra of pyrazole and imidazole have been reported previously,[34] and assigned using KT and MB calculated orbital energies (OE's).

Introduction of the imino nitrogen in the pyrrole ring results in destabilization of one of the inner valence levels to the 9 → 12 eV region; comparison of the PES of imidazole with that of pyrrole indicates that this level lies under the second peak at 10.7 eV since this is significantly broader than in pyrrole, moreover its intensity increases under He(II) conditions indicating its LP_N character. Therefore the ordering proposed is $\pi < \pi < LP_N$ which is that predicted by the DZ calculations plus KT.

The assignment for pyrazole is not as clear cut, since the first peak is the envelope of two IP's and the second is broader than the corresponding peak in pyrrole. Therefore there is no assignment easily recognisable from a simple comparison of spectra, although it seems unlikely that the $2b_1$ level of pyrrole would be shifted so significantly towards the $1a_2$ level resulting in a $\pi < \pi < LP_N$ ordering. More likely, and as indicated by inspection of the He(II) relative peak intensities is a $\pi < LP_N < \pi$ assignment of the first three IP's, which has been adopted, although this is not predicted by KT. (This assignment does not agree with the earlier one given by KT.[34])

The bands of I.P.'s from 13 → 25 eV have been assigned using K.T., since groupings of I.P.'s and O.E.'s correlate favourably.

1-Methyl substitution for each isomer[40] leaves the original envelope of the spectrum unaltered, but results in almost monotonic destabilization of the original spectrum. The first three I.P.'s for each methyl isomer have therefore been assigned as those for the unsubstituted compounds. The remaining bands of I.P.'s have been assigned by K.T. and the calculated O.E.'s. There has been no spectrum for 1-Methyl pyrazole reported to date.

FIG 41 P.E.S.

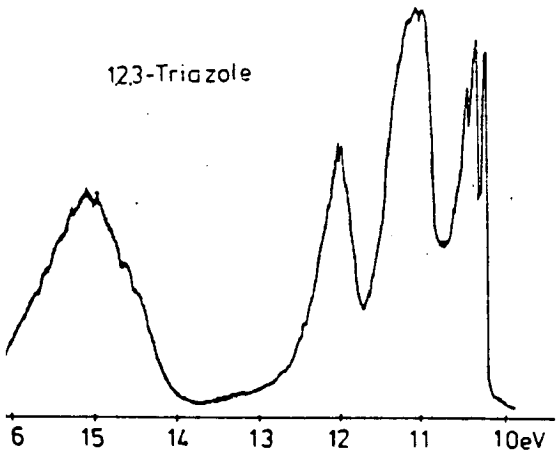
1,2,3-Triazole
6
15
14
13
12
11
10eV

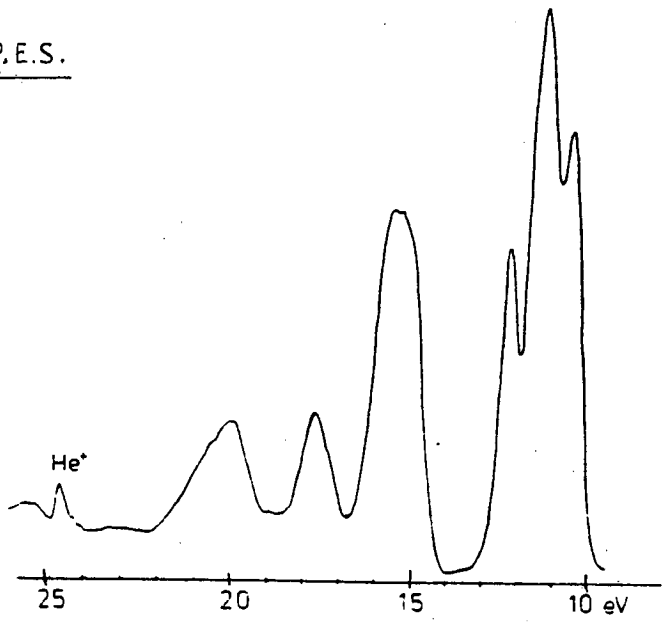
He+
25
20
15
10 eV

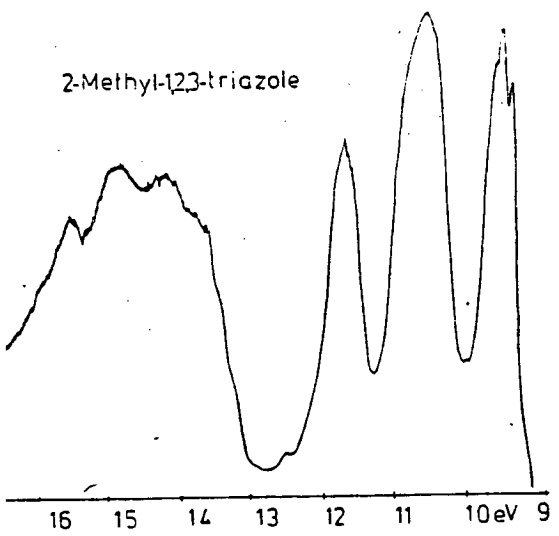
2-Methyl-1,2,3-triazole
16
15
14
13
12
11
10eV
9

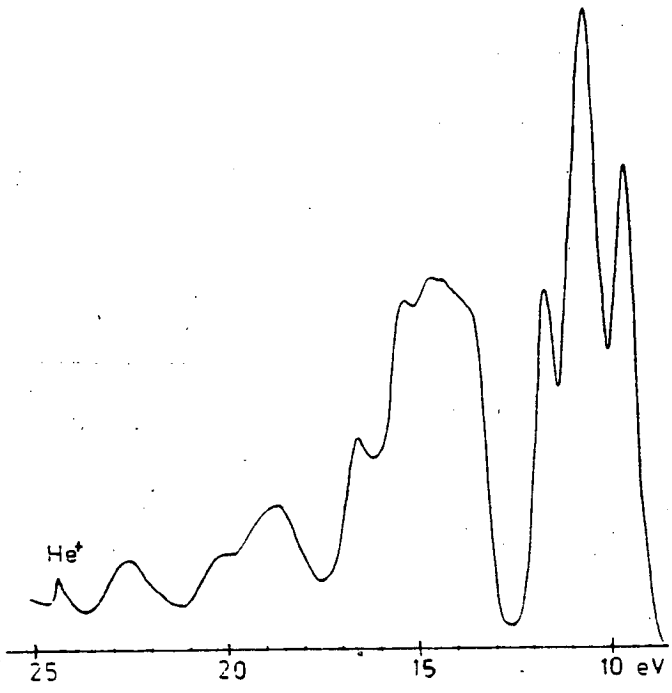
He+
25
20
15
10 eV

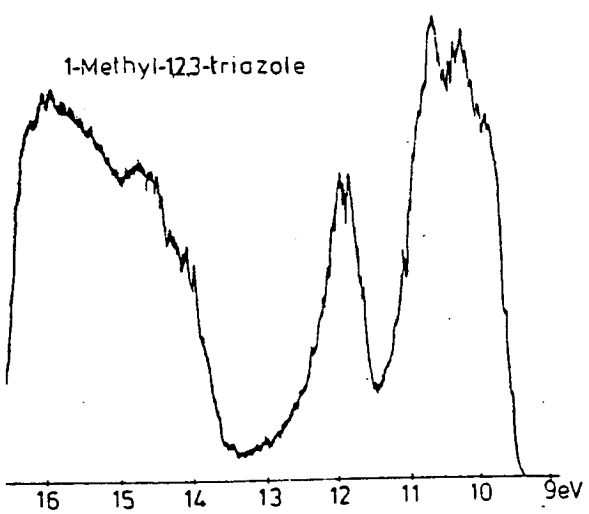
1-Methyl-1,2,3-triazole
16
15
14
13
12
11
10
9eV

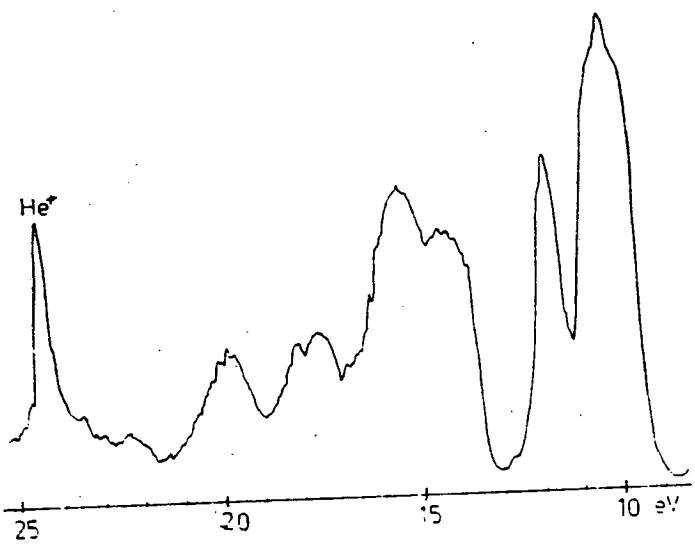
He+
25
20
15
10 eV

1,2,3-Triazoles Fig .(41)

In assigning the spectrum of 1,2,3-triazole we must take into account its ability to exhibit tautomerism. The spectrum could be from one dominant gas phase tautomer or a mixture of two.

Only the He(I) spectrum of 1,2,3-triazole has been reported[34] and assigned using K.T. and the results of a calculation on the 1-H tautomer. Recent[19b] investigations have indicated that the 2-H tautomer could be dominant in the gas phase, and indeed the calculated total energies favour the 2H-tautomer by 0.03 au (see Table (20)).

Two other methods are here available for elucidation of the dominant gas phase tautomer:

(i) by comparison of the calculated O.E.s for each tautomer and experimental I.P.'s via K.T. to observe which, if any, gives the closest correlation.

(ii) since methyl substitution does not alter the general shape of, but results in general destabilization of the spectrum of the original compound, comparison of the spectra for the 2-methyl and 1-methyl isomers with that of the unsubstituted traizole will indicate the original position of the pyrrolic hydrogen (and hence which tautomer predominates in the gas phase).

The calculated orbital energies for the 1H and 2H tautomers of 1,2,3-triazole give similar orbital groupings but different orbital ordering and it appears that those for

1H-tautomer give the closest correlation with the V.I.P.'s. This would argue that the 1-H tautomer is dominant in the gas phase. If the spectra of the 1-methyl and 2-methyl isomers are compared with that of the triazole it is obvious that the spectral envelope of 2-methyl-1,2,3-triazole more closely resembles that of the parent compound, although destabilized, thus indicating the predominance of the 2-H isomer. This experimental evidence for the predominance of the 2-H tautomer in the gas phase is more reliable than that provided by orbital energy groupings, and is in agreement with the evidence from our calculated total energies, and we can therefore conclude that the symmetric tautomer predominates in the gas phase.

Introduction of two imino nitrogens in the pyrrole system, as in 1,2,3-triazole, results in destabilization of two CH bonding levels to the 9 → 12 eV region. Comparison of the triazole spectrum with that of pyrrole shows that the first I.P. in each spectrum is similar in envelope and can therefore be attributed to a 'π' level. The second broader peak, whose intensity increases considerably under He(II) conditions can be assigned to two levels. The third peak whose relative intensity does not change under He(II) conditions can be thus assigned as the shifted 2b, π level of pyrrole.

Here the experimental peak intensity evidence argues that a $\pi < LP_N^- < LP_N^+ < \pi$ is the ordering whereas the orbital energies and K.T. order the levels as $\pi < \pi < LP_N^- < LP_N^+$. (this was the assignment reported previously).

However the experimental evidence has been used in the assignment of the first three bands as is shown in Table (23). The remaining bands have been assigned using K.T. and the orbital energies.

The He(I)/He(II) spectrum of the 2-methyl isomer, which is very similar to that of the unsubstituted triazole exhibited similar relative peak intensities and has therefore been assigned in the same manner as the triazole see Table (23).

The P.E.S. spectrum of the 1-methyl-1,2,3-triazole shows a broad peak at 9.5 - 11 eV whose intensity increases under He(II) conditions, whereas the relative intensity of the narrower second peak does not show a similar increase. It is likely, therefore, that the first broad peak is the envelope of three I.P.'s (π, LP_N^-, LP_N^+) and the second attributable to a 'π' level. It should be noted that the assignment of the first three I.P.'s can only be approximate since there is insufficient resolution to do so. The ordering of the levels has been given $\pi < LP_N^- < LP_N^+ < \pi$; the remaining I.P.'s have been assigned by virtue of K.T.

FIG 42 P.E.S.

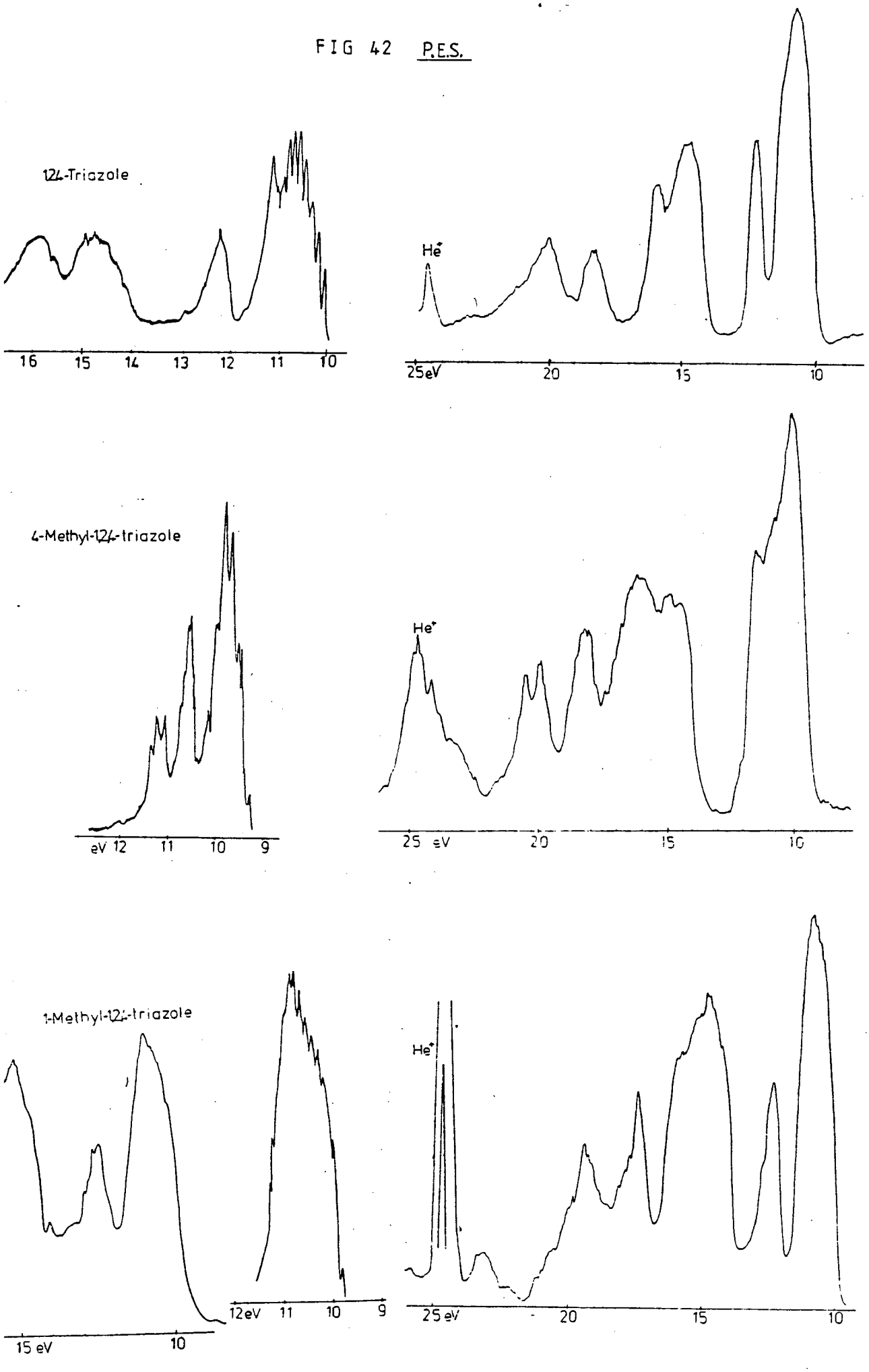
1,2,4-Triazole
16
15
14
13
12
11
10
He
25eV
20
15
10
4-Methyl-1,2,4-triazole
eV 12
11
10
9
He
25 eV
20
15
10
1-Methyl-1,2,4-triazole
15 eV
10
12eV
11
10
9
He
25 eV
20
15
10

1,2,4-Triazoles Fig (42)

To date only the He(I) spectrum of 1,2,4-triazole has been reported;[34] this was assigned using K.T. and the results of a M.B. calculation on the 1-H tautomer.

This triazole, like the 1,2,3-triazole, can exist in two tautomeric forms, and it is generally accepted that the 1-H tautomer predominates in the gas phase.[22] (This is in agreement with our calculated total energies which favour the unsymmetric tautomer by 0.02 au.)

Comparison of the grouping of calculated orbital energies with the groupings of experimental I.P.'s show that those of the 1-H isomer provide the best fit; the spectral envelopes of 1,2,4-triazole and its 1-methyl derivative are very similar and differ significantly from that of the 4-methyl isomer. This provides further confirmation of the gas phase predominance of the 1-H tautomer.

Assignment of the spectra is difficult since the first three I.P.'s lie under the envelope of a broad band in 1-methyl and 1H-triazole, with four I.P.'s under the first band in the 4-methyl isomer, and none of the spectra bear any similarities to that of pyrrole.

The relative intensity of the first band in 1,2,4-triazole (and its 1-methyl derivative) increases under He(II) conditions whereas that of the second peak is left unchanged but no one distinct peak can be assigned from this evidence as LP_N. It is likely that the first IP within the first

band can be assigned LP_N since its outline along the front edge of the peak shows fine structure which is generally associated with ionization of an LP_N level (i.e. no strong $0 \rightarrow 0$ band). Therefore the approximate assignment given to the first band of both 1H-1,2,4-triazole and its 1-methyl derivative is $LP_N^- < \pi < LP_N^+$. The second I.P. has been attributed to a π ionization, and the remaining bands of I.P.'s being assigned by virtue of K.T. and the calculated orbital energies. Again the ordering of the first I.P.'s predicted by K.T. does not appear to agree with experimental evidence.

Assignment of the P.E.S. of 4-methyl-1,2,4-triazole is equally difficult since the first four I.P.'s lie under the envelope of the first spectral band, which although resolved in the He(I) spectrum is poorly resolved under He(II) conditions, where the relative intensity of the peak at 11.32 eV only can be seen to increase, indicating LP_N character. Inspection of the first band under He(I) conditions shows a first peak broader than the following two, which therefore probably is the envelope of two almost degenerate levels π, LP_N^+. The assignment proposed in Table (23) is therefore $LP_N^+ < \pi < \pi < LP_N^-$ (which differs from that predicted by K.T.) the bands of I.P.'s from 15-25 eV being assigned by K.T. and the D.Z. orbital energies.

These assignments exemplify the difficulties experienced in interpreting spectra with broad unresolved bands, and show that even the combination of techniques used here cannot

FIG 43 P.E.S.

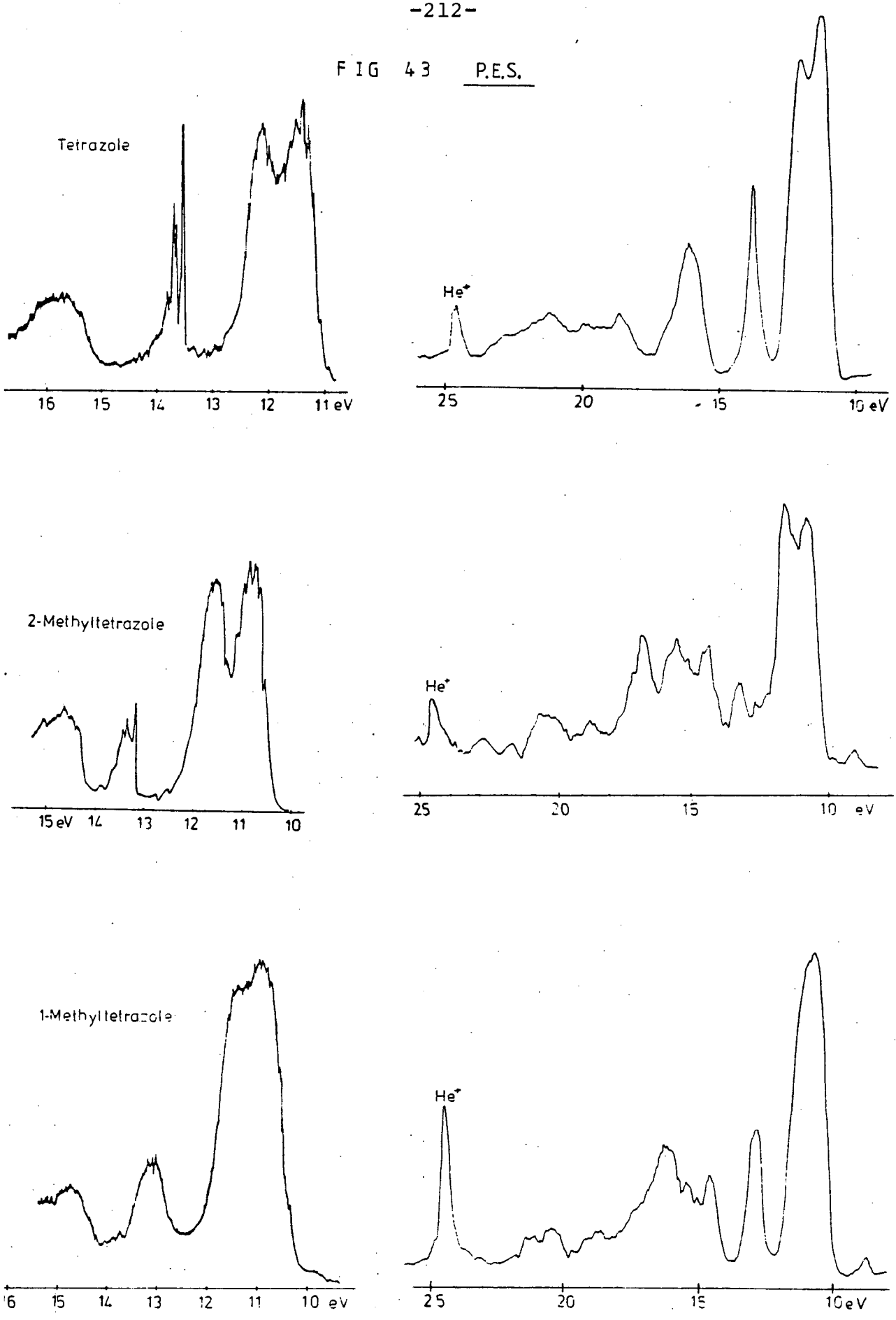
Tetrazole
He+
16 15 14 13 12 11 eV
25 20 15 10 eV
2-Methyltetrazole
He+
15 eV 14 13 12 11 10
25 20 15 10 eV
1-Methyltetrazole
He+
16 15 14 13 12 11 10 eV
25 20 15 10 eV

in these cases lead to unambiguous assignment. It should be stressed that we do not claim to give the correct spectral assignment but rather the assignment indicated by the calculated and experimental evidence available, and that the assignments proposed would be best checked by ΔE_{SCF} calculations.

The Tetrazoles Fig (43)

The He(I) spectrum of tetrazole has been reported before[34] and assigned using K.T. and the results of an ab initio M.B. calculation on the 1H-tautomer. The dominant tautomer in the gas phase has not yet been elucidated, and we must first attempt to ascertain its nature, before attempting assignment, by considering, as for the triazoles, calculated total energies, orbital energies and the spectral envelope of tetrazole and its 1-methyl and 2-methyl derivatives.

The calculated total energies favour the 2H tautomer by 0.01 au, see Table (20), indicating that the 2H tautomer is energetically more stable in the gas phase. However the groupings of calculated orbital energies for both tautomers correlate equally well with the groupings of observed I.P.s, thus giving no clear indication of the dominant tautomeric form.

The spectrum of the 2-methyl isomer is almost identical to that of tetrazole itself (although almost monotonically destabilized as expected), whereas the spectral envelope of the 1-methyl isomer differs in both the splitting of the peaks under the first band the shape of the peak at 13 eV. This evidence points to the predominance of the 2H tautomer in the gas phase.

Spectral assignment of the tetrazoles is complicated by the destabilization of now three CH bonding levels to the 9 → 13 eV region and therefore comparison of the spectrum of tetrazole and pyrrole is not instructive due to the complexity of its first broad band under which lie four I.P.'s. There is, however, a striking similarity in the tetrazole peak at ca. 13.5 eV and the first I.P. of pyrrole which exhibit, what is generally accepted as, the fine structure of a 'π' type orbital i.e. with a strong O → O band. Moreover, the relative intensity of this peak does not increase under He(II) conditions which indicates that its previous assignment,[34] as a lone pair level, is questionable. The relative intensities of the bands of I.P.'s at 10 → 12.5 eV for the tetrazoles studied herein, do increase under He(II) conditions although assignment of the I.P.'s therein can only be approximate due to their strong overlap.

It can be seen, however, that the intensity of the first peak in the band increases more than the second overlapping peak for both tetrazole and its 1- and 2-methyl derivatives. This points to a probable LP_N, $LP_N < \pi$, LP_N ordering for tetrazole and 2-methyl tetrazole where the peak at 13.5 eV can be attributed to ionization of a π level.

For 1-methyl tetrazole where the relative intensity of the second peak at 13 eV increases under He(II) conditions the assignment differs in that the first band could be the envelope of two LP_N levels and two π levels. (The ordering cannot be ascertained due to the complexity of the first band).

It should be noted that it is possible that the peak at 13 eV is the overlap of a π and LP_N level which would give the ordering LP_N, π, LP_N < LP_N, π. Due to this ambiguity, for which the orbital energies and K.T. offer no more conclusive clarification, the assignment proposed in Table (23) is approximate. The bands of I.P.'s from 14 → 25 eV have been assigned, as before, using K.T. and the calculated orbital energies.

FIG 44

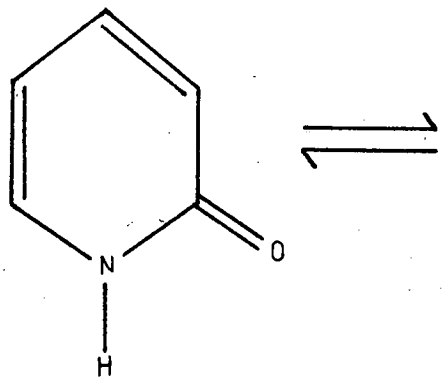

(1) 2-PYRIDONE

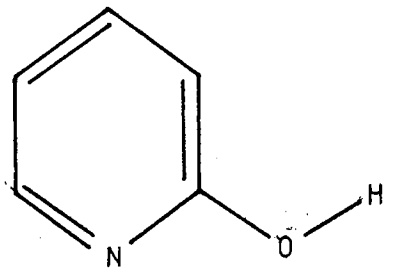

(2) 2-HYDROXPYRIDINE

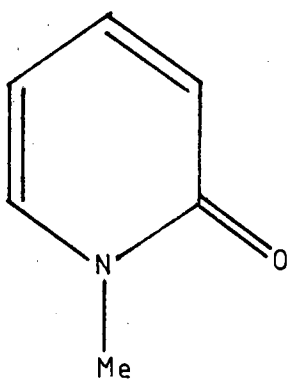

(3) 1-METHYL-2-PYRIDONE

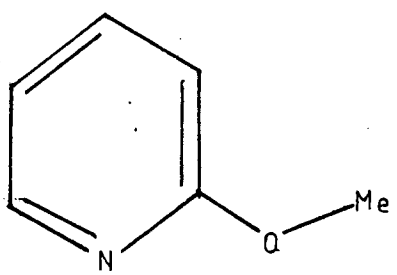

(4) 2-METHOXYPYRIDINE

(xiv) Tautomerism of 2-Pyridone

At this point it is appropriate to mention studies on 2-Pyridone which can exist in the tautomeric forms shown in Fig (44).

It is well established that in the solid state and in most solvents the pyridone[41] form predominates. For the vapour phase experimental evidence for the predominance of the hydroxy form (2) has been reported,[41] and recent ab initio (MB) calculations are in agreement with this.[42] We hoped that our DZ calculations would provide further theoretical evidence as to the predominant gas phase tautomer and would also provide a basis for assignment of the photoelectron spectrum. As an additional aid to interpretation comparison of the 2-pyridone PE spectrum with those of the blocked methyl derivatives, 2-methoxypyridine and 1-methyl-2-pyridone (assigned by calculations) has been employed.

Calculations

Double Zeta quality calculations were performed as structures (1-4), Fig (44). Of these molecules an experimental crystal structure is available for only (1).[43] The structure of 2-hydroxypyridine was constructed from the experimental geometry of pyridine[44] and an hydroxy group with C-O bond length was taken from the experimental MW structure of phenol.[45] These structures were used for the rings of (3), (4) with additional standard methyl units. Bond lengths and angles used are in Appendix B.

Table (25) Open Shell Total Energies

	2-Hydroxypyridine	2-Pyridone	2-Methoxypyridine	1-Methyl-2-Pyridone
Ground state	321.4247154	321.4563998	360.41624605	360.46686695
1st Ionized state	321.111652307	321.1647213	360.12372313	360.18289288
2nd Ionized state	*321.10965194	321.116293	*360.10773855	*360.
3rd Ionized state	*321.086359	*321.005462	*360.0643956	*360.00420388

* Full convergence not attained

Calculated total energies and orbital energies are given in Table (24), from which it can be seen that our calculations favour the pyridone form by 0.04 au. which is not in agreement with previous results.[42] This seeming anomaly could be explained by use of an incorrect constructed geometry for (2); indeed in reference [42] calculations showed the sensitivity of the total energy to the C-O bond length (a change of 0.03 Å resulted in a change of 0.04 au in total energy). The partially optimized C-O bond length they adopted was based on the experimental X-ray structure of 6-chloro-2-hydroxypyridine[46] which, in retrospect, is the better one to use. Therefore no conclusions about the energetically preferred tautomer can be made from our results, although it is important to note this example of the critical dependence of calculated total energies on geometry used. (It should be noted that the calculations of reference [42] favour the hydroxy form by 0.01 au).

To check the orbital ordering predicted by K.T. for these molecules(which is the same as reported in [42] for (1) and (2)), additional R.H.F. calculations have been performed on various cationic (+1) states. From these results ΔE_{SCF} calculations have been performed, see Table (25), and the orbital ordering therein predicted is found to be the same as that given by Koopman's Theorem. It should be noted that for the higher excited states, those corresponding to ionization from the third highest occupied orbital, full

FIG 45 PHOTOELECTRON SPECTRA

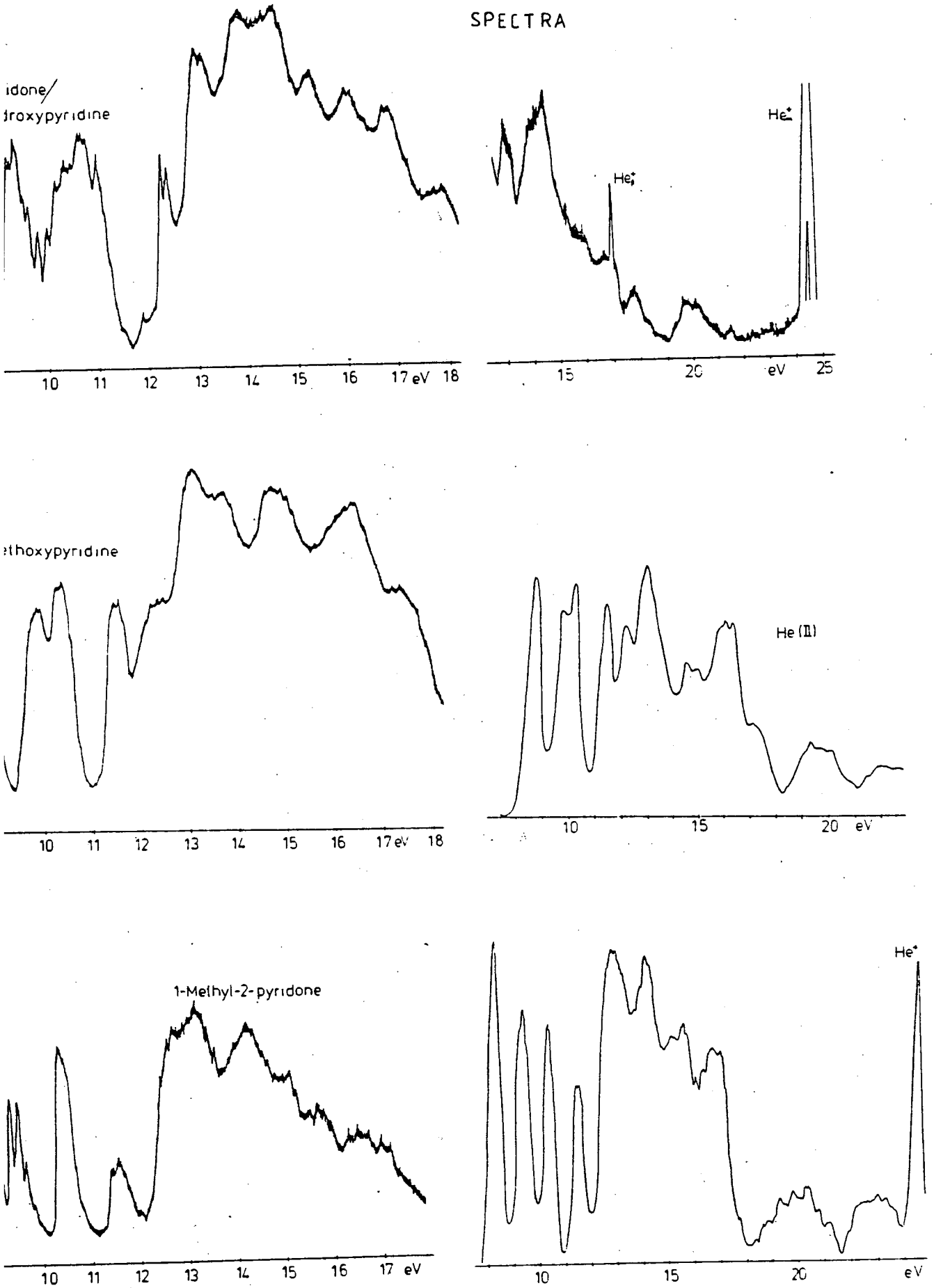

convergence could not be obtained for the accuracy initially desired (i.e. within 10^{-4} au) due to calculations which in many cases converged for several iterations but then became oscillatory or divergent. For these situations the RHF calculations were repeated to just before divergence, and the energy at that point adopted.

To date no calculations on 2-methoxypyridine and 1-methyl-2-pyridone have been reported.

Photoelectron Spectra

The He(I) and He(I) spectra obtained are given in Fig (45) Comparison of the spectrum of the parent compound with that of the methyl derivatives shows that spectrum (a) is in fact a mixture of the gas phase tautomers. Peaks which can be attributed to the lactim and lactam forms can be easily found by comparison with the blocked methyl derivatives, since as has been found with the azoles, (and as is widely accepted) methyl substitution leads to a general destabilization of the lower binding energy region. For example the first IP in spectrum a can be attributed to the pyridone form, as can the peak at 9.79 which exhibits almost the same vibrational splitting. By such comparisons the first four IP's of (1) and (2) can be identified. Having identified the peaks of (1) and (2) these can be assigned by virtue of our calculations and KT (since the ΔE_{SCF} calculations are in agreement with the KT orbital ordering). Due to the complex nature of spectrum (a) in the region above 12.5 eV, no assignment is attempted. See Table (26).

Assignment of the spectra of (3) and (4) however has been made up to 24 eV, Table (26) using the calculated results for each molecule respectively. The He(I) spectrum and assignment are in agreement with those reported for (1) and (3),[47] but our assignments of the spectra of (2) and (4)[47] are different. The spectra reported in reference [47] were assigned only by inspection and comparison with the PE spectrum of pyridine. Our He(I)/He(II) peak intensity studies for (3) and (4) indicate that our assignment is correct since the second peak in the former and the third peak in the latter have increased intensity under He(II) conditions.

We can conclude, as was noted before,[47] that in the gas phase 2-pyridone and 2-hydroxy-pyridine exist as a mixture, and at temperatures < 50°C (the temperature at which our spectra were obtained) no one tautomeric form is exclusively present.

It is probable that the hydroxy form is dominant since all peaks in spectrum (a) attributed to (2) are consistently larger than those attributed to (1).

Table (26) Vertical Ionization Potentials (eV)

2-Pyridone	2-Hydroxypyridine	1-Methyl-2-Pyridone	2-Methoxypyridine
8.7 π	9.2 π	8.31 π	8.77 π
9.77 LP_O	10.13 π	9.40 LP_O	9.77 π
10.8 π	10.65 LP_N	10.33 π	10.26 LP_N
11.85 π	12.23 π	11.57 π	11.65 σ
		12.63 σ	12.42 π
		13.12 σ	13.00 σ
		14.21 σ	13.69 π
		14. 4 π	14.69 σ
		15.00 σ	15.8 σ
		15.60 σ	16.00 σ
		16.3 σ	17.00 σ
		16.9 σ	17.5 σ
		19.5 σ	19.10 σ
		20.5 π	20.00 σ
		23.15 σ	21.66 π
		24.23 σ	22.5 σ

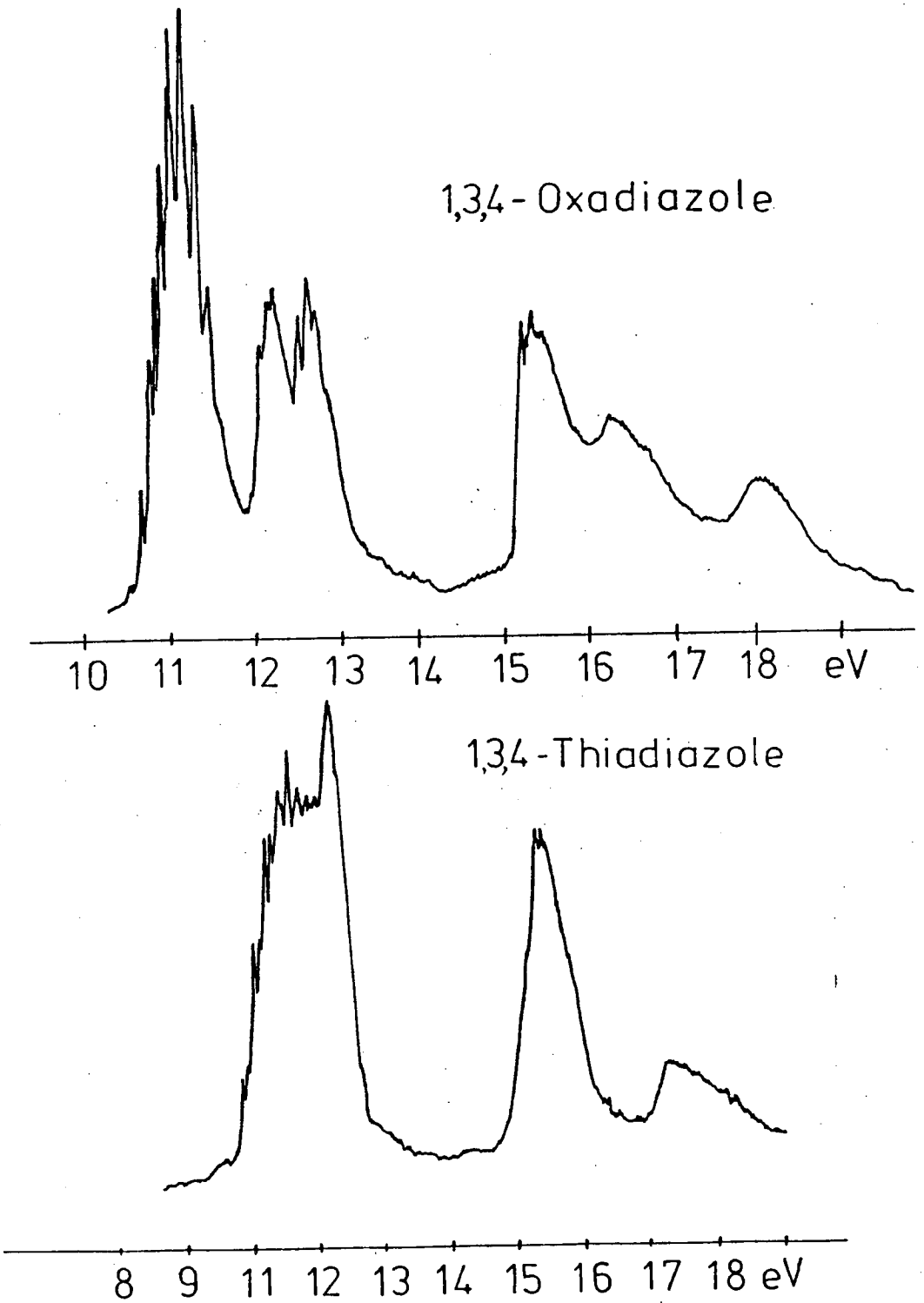

FIG 46 PHOTOELECTRON SPECTRA

(xv) Vibrational Structure

Only the bands in the lower binding energy region of the spectra show vibrational fine structure i.e. the upper π and N lone pair levels) and for pyrrole, pyrazole, imidazole 1,2,4-Traizole 1,2,3-Triazole + Tetrazole attempts have been made to assign this fine structure to vibrational modes by inspection of the spectra.[34] This method of assignment is somewhat empirical and it would possibly be more satisfactory if some theoretical information were available to assist the assignment. It is possible to obtain theoretical fine structure from ab initio calculations, but this procedure involves lengthy geometry optimization of the system under consideration. A theoretical investigation into the fine structure in the first ionization potentials in the P.E. spectrum of 1,3,4-Oxadiazole and 1,3,4-Thiadiazole was performed and is reported below. The results of this study indicated whether further theoretical investigations of the fine structure observed in PES of mols 1-9 is a worthwhile exercise.

Theoretical Investigation of Vibrational Fine Structure in Photoelectron Spectra

The experimental PES of 1,3,4-thiadiazole and 1,3,4-oxadiazole exhibit vibrational fine structure (Fig 46) and no previous attempt has been made to assign this fine structure to actual vibronic transitions, and what follows

in an attempt to do this by construction of Theoretical Photoelectron Spectra for 1,3,4-Thiadiazole and 1,3,4-Oxadiazole.

The procedure employed involves the calculation of equilibrium geometries from a minimization of the total energy of the molecule. Geometry optimization was imperative for only results obtained at the theoretical equilibrium geometry could be used for subsequent stages of the procedure. From equilibrium geometry data and a calculated force field the normal coordinates of the molecule and hence the frequencies of the vibrations described by the normal coordinates were obtained. Using the harmonic approximation (to obtain wavefunctions for the molecule in its ground and excited states) the vibrational coupling constants and hence information about the intensities of various vibrational transitions were obtained. From this data theoretical PE spectra could be constructed.

Procedure

From the atomic cartesian coordinates of the molecules, constructed from the M.W. geometries,[48] and a 7s/3p basis set[49] the existing Atmol suite of programs was employed to calculate the total energy of the systems.

Each of the molecules was then distorted by moving an atom by 0.01 au in say the 'X' direction, and obtaining the total energy for the distorted molecule. This process of distortion was repeated for each atom for $\pm$ 0.01 au in both the 'X' and 'Y' directions.

The results are tabulated as :

Atom	Total energy for 0.01 au 'x' distortion	for -0.01 au distortion
S	A_1	C_1
N	A_2	C_2
C	A_3	C_3
H	A_4	C_4

One can imagine A_i and C_i as points on an energy curve, which we assumed to be parabolic

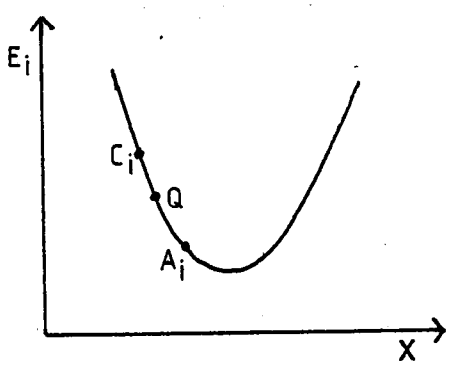

The gradient at Q (i.e. undistorted molecule) is given by

$$\left(\frac{\partial E}{\partial X}\right)_{E=Q} = \frac{C-A}{2 \times 0.01}$$

and gradients were obtained for all constituent atoms. The negative of these calculated gradient give the forces acting on the atoms in the molecule e.g.

$$\text{Force}_X = -\left(\frac{\partial E}{\partial X}\right)_{E=Q}$$

These forces indicate the directions in which each atoms is trying to move in order to get to its position of lowest energy, i.e. at its equilibrium position. It is apparent that to reduce the total energy of the molecule each atom should be moved along the direction of the force acting on it. This was implemented by adding increments of the

forces, F, for F = 0.5, 1.0, 1.5, 2.0, to the coordinates of the atoms. For each increment of F added, the total energy was calculated. There was a minimum value of total energy for a particular value of F. The value of F required to give the minimum total energy was obtained from the total energies for F = 0.5, 1.0, 1.5, 2.0 by Lagrange (cubic) Interpolation (see appendix C, and ref 51) when four values of E_{TOT} were known. An alternative method of obtaining the optimum F (F_{OPT}) using a computational curve fitting procedure was available.[50] This procedure, using existing library subroutines, also predicted the value of E_{TOT} at F_{OPT}.

The geometry for the F_{OPT} increment was then used to obtain a second set of gradients by the previously described procedure of distorting the molecule by moving each atom by $\pm$ 0.01 au.

At this stage it would have been possible to continue moving the atoms again by increments of the forces to obtain further F_{OPTs} and simply repeating this procedure until the gradients were negligibly small (i.e. < 0.0001 say), whereupon the molecule was at its equilibrium geometry. Such a procedure would be lengthy and excessive in computer time. Therefore a rapidly convergent descent method for minimization was adopted.[52] (This minimization procedure due to Fletcher and Powell is a powerful iterative descent method for finding a local minimum of a function of several variables). The procedure was executed computationally and required as input the two sets of gradients already evaluated and also a set of distortion amplitudes. The algorithm is explained below.

The Fletcher-Powell Procedure [52]

[N.B. Dirac notation is employed i.e. $|x\rangle$ is a column vector $(x_1, x_2, \ldots x_n)$. $\langle x|$ is a row vector with the same element].

Let f be the function of interest and $|x\rangle$ denotes the arguments. Let $|g\rangle$ denote the gradients. The standard notation of a quadratic function in 'n' dimensions is

(i) $f = f_o + \langle a|x\rangle + \frac{1}{2}\langle x|G|x\rangle$

(ii) also $|g\rangle = |a\rangle + \underline{G}|x\rangle$

If we consider the quadratic from (i) then given the matrix

$$G_{ij} = \frac{\partial^2 f}{\partial x_i \partial x_j}$$

we can calculate the displacement between the point $|x\rangle$ and minimum $|x_o\rangle$ as

(iii) $|x_o\rangle - |x\rangle = -\underline{G}^{-1}|g\rangle$

In this method the matrix $\underline{G}^{-1}$ is not evaluated directly, instead a matrix $\underline{H}$ is used which may initially be chosen to be any positive definite symmetric matrix. This matrix is modified after the i^{th} iteration using the information gained by moving down the direction, in

(iv) $|s^i\rangle = -\underline{H}^i|g^i\rangle$

accordance with (iii).

The modification is such that $|o^i\rangle$, the step to the minimum down the line,

(v) $|x\rangle = |x^i\rangle + \lambda|s^i\rangle$

is effectively an eigenvector of the matrix $\underline{H}^{i+1}\underline{G}$. This

ensures that as the procedure converges $\underline{H}$ tends to $\underline{G}^{-1}$ evaluated at the minimum.

It is convenient to take the unit matrix initially for H so that the first direction is down the line of steepest descent.

Let the current point be $|x^i\rangle$ with gradient $|g^i\rangle$ and matrix $\underline{H}^i$. The iteration can then be stated as follows.

Let $|s^i\rangle = -\underline{H}^i|g^i\rangle$

Obtain α^i such that $f(|x^i\rangle + \alpha^i|s^i\rangle)$ is a minimum with respect to λ along $|x^i\rangle + \lambda|s^i\rangle$ and $\alpha^i > 0$.

Set $|o^i\rangle = \alpha^i|s^i\rangle$

Set $|x^{i+1}\rangle = |x^i\rangle + |o^i\rangle$

Evaluate $f(|x^{i+1}\rangle)$ and $|g^{i+1}\rangle$ noting that $|g^{i+1}\rangle$ is orthogonal to $|o^i\rangle$ i.e. $\langle o^i|g^{i+1}\rangle = 0$

Set $|y^i\rangle = |g^{i+1}\rangle - |g^i\rangle$

$$\underline{H}^{i+1} = \underline{H}^i + \underline{A}^i + \underline{B}^i$$

$$\underline{A}^i = \frac{|o^i\rangle\langle o^i|}{\langle o^i|y^i\rangle}$$

$$\underline{B}^i = \frac{-\underline{H}^i|y^i\rangle\langle y^i|\underline{H}^i}{\langle y^i|\underline{H}^i|y^i\rangle}$$

set i = i+1 and repeat.

The practical output of this procedure is a set of "distortion amplitudes" s^i, which are used in exactly the same manner as a set of negative gradients i.e. forces. Increments of these "distortion amplitudes" are added to the last equilibrium geometry i.e. geom at last F_{OPT} A new F_{OPT} is obtained for

the distortion amplitudes and another third set of gradients were obtained at the new equilibrium geometry. This third set of gradients, the second set of gradients and the last set of distortion amplitudes were then used as input data for the Fletcher-Powell procedure and a second set of distortion amplitudes was obtained. This process was repeated until the gradients at the final optimal geometry were negligibly small (i.e. <0.0001. At this point the molecule was considered to be lying at its true theoretical equilibrium geometry.

The convergence of 1,3,4-Thiadiazole represented in Fig 47 where the 'gradients' obtained at each 'cycle' optimum geometry (a cycle is defined as the procedure employed in obtaining a value of F_{OPT}, and hence a minimum energy), are plotted v. cycle no.for each atom in the molecule.

(The 'gradients' plotted at cycle nos. 2 and 4 and 6 are in fact negative distortion amplitudes, which are not strictly gradients. They are, in fact, related to the gradients by

$$|s^i\rangle = -\underline{H}^i|g^i\rangle$$

For the purposes of fig. 47 the $|s^i\rangle$ can be considered as forces.)

The final equilibrium geometry gradient $\partial E_g/\partial X$, $\partial E_g/\partial Y$ and the occupied orbital energy gradients $\partial E_i/\partial X$, $\partial E_i/\partial Y$ were obtained for later use.

To construct a theoretical photoelectron spectrum for each orbital, showing vibrational transitions, we require the intensities of the peaks in the fine structure and the frequency spacing between these peaks.

An indication of the vibrational transition intensities can be obtained from a calculation of vibrational coupling constants. For this calculation we require the normal coordinates of the molecule at its equilibrium geometry.

Normal Coordinate Analysis

The relationship between cartesian coordinates and normal coordinates, and the relationship between normal coordinates and the frequency separation of the peaks in the fine structure of the PE spectra is described below.

In terms of cartesian coordinates of atoms arranged in a vector x with 3N components $\{x_A y_A z_A \ldots x_N y_N z_n\}$ the kinetic energy is given as

(i) $2\underline{T} = \underline{x}' \underline{M} \underline{x}$

where $\underline{M}$ is a diagonal matrix of order 3N whose elements are the masses of the atoms.

The internal coordinates of which there are 3N-6 in the case of a non-linear molecule, are arranged in a vector

$$r = \{r_1 r_2 r_3 \ldots r_{3N-6}\}$$

The internal and cartesian coordinates are related by the linear transformation

(ii) $$\underline{r} = \underline{B} \underline{x}$$

B is a rectangular matrix of dimension 3N x (3N-6) and therefore has no inverse. Thus the kinetic energy expression (i) cannot be transformed directly into internal coordinates. However by including the six conditions of zero linear and angular momentum [i.e. no translational or rotational motion] it can be shown that

(ii) $2\underline{T} = \underline{r}' \underline{K} \underline{r}$

(iii) where $\underline{K} = \underline{G}^{-1} = [\underline{B} \underline{M}^{-1} \underline{B}^{T}]^{-1}$

where $\underline{B}^{T}$ is the transpose of $\underline{B}$

$\underline{G}$ and $\underline{K}$ are square matrices of order 3N-6.

The potential energy of the molecule is the harmonic approximation is given by

(iv) $2\underline{V} = \underline{r}' \underline{F} \underline{r}$

where $\underline{F}$ is a symmetric square matrix of force constants of order 3N-6 whose elements are given by

(v) $$F_{ij} = \frac{\partial^2 V}{\partial r_i \partial r_j}$$

The application of Lagranges equation

(vi) $$\frac{d}{dt} \left(\frac{\partial T}{\partial r_i} \right) + \frac{\partial V}{\partial r_i} = 0$$

for each value of i results in the equations

(vii) $\underline{F} \underline{r} + \underline{K} \underline{r} = 0$

which are solved making the multiple substitutions

(viii) $r_i = l_{ik} \cos(2\pi\nu_k t + \rho)$

(ix) $r_i = -\lambda_k l_{ik} r_i$

There are 3N-6 equations such as (ix) one for each value of k. When these are substituted into (vii) there results

(x) $[\underline{F} - \lambda_k \underline{K}] l_{ik} = 0$

which, when multiplying by $\underline{K}^{-1} =$ becomes

(xi) $[\underline{G} \underline{F} - \lambda_k E] l_{ik} = 0$

$\underline{G} \underline{F} \underline{L} = \underline{L} \Lambda$

Λ is a diagonal matrix of 3N-6 eigenvalues and $\underline{L}$ is a square matrix of order 3N-6.

In solving the characteristic equations of GF it can be shown that

FIG 48 NORMAL COORDINATES FOR OBSERVED FREQUENCIES

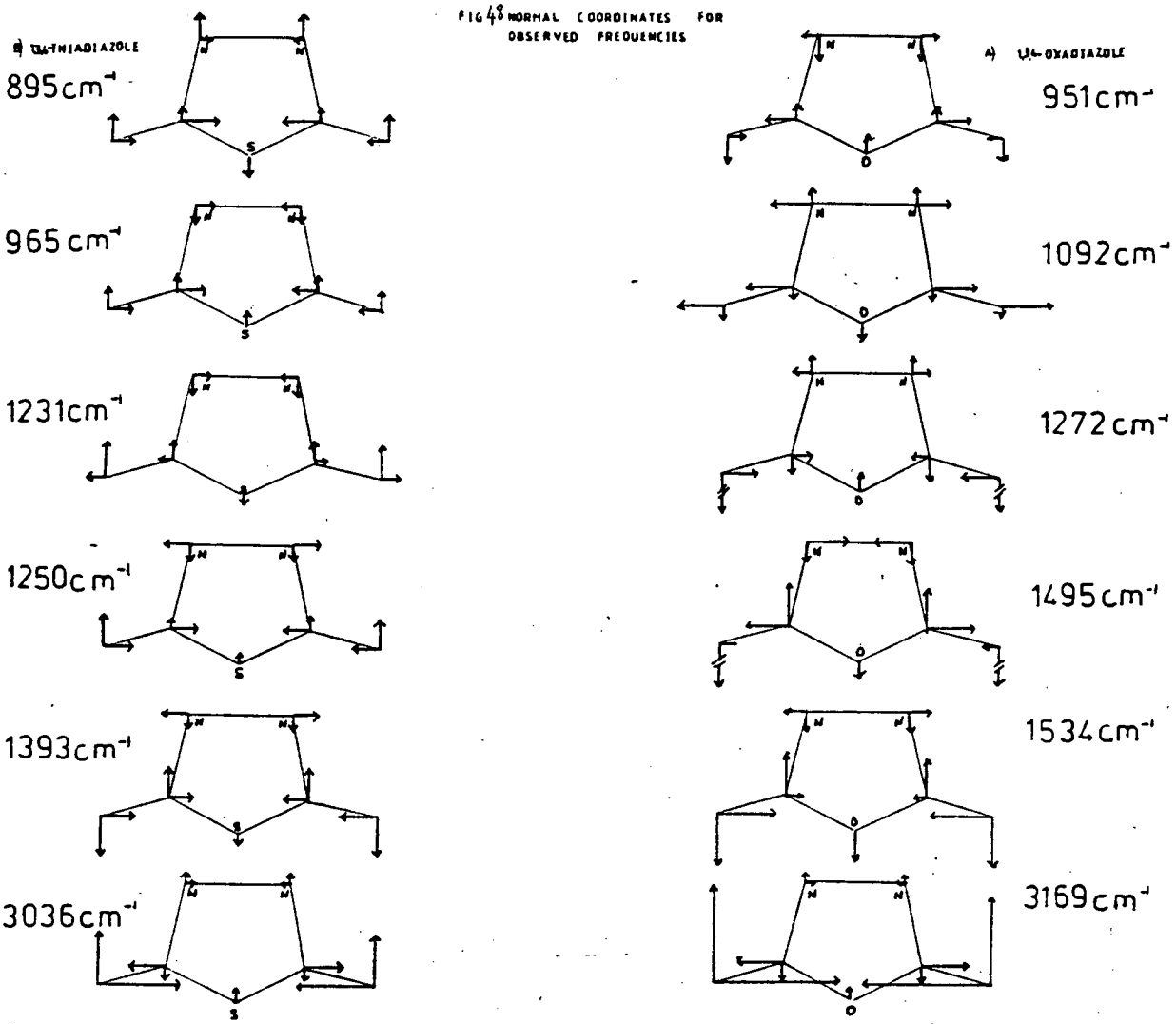

(b) (a)

(xii) $\underline{L}\,\underline{L}^{T}\,\underline{G}$

(xiii) and $\underline{L}^{T}\underline{F}\,\underline{L} = \underline{\Lambda}$

If we define a vector Q of 3N-6 coords $[Q_1 Q_2 \ldots Q_{3N-6}]$, related to the internal coordinates by

(xiv) $\underline{r} = \underline{L}\,\underline{Q}, \quad Q = \underline{L}^{-1}\underline{r}$

and substitute these relations into the expression for the potential energy

$$2V = \underline{Q}^{T}\,\underline{L}^{T}\,\underline{F}\,\underline{L}\,\underline{Q}$$

$$= \underline{Q}^{T}\,\underline{\Lambda}\,\underline{Q}$$

(xv) $$= \Sigma_i Q_i^{2} \lambda_i$$

The coordinates Q_i are the normal coordinates.

The normal coordinates Q_i, give the relative displacements of all the atoms in that vibration.

λ_i indirectly gives the frequency of that vibration for $\lambda_i = 4\pi^2 \nu_i^{2}$ where ν_i is the frequency of the vibration. There is one normal mode of vibration described by its normal coordinate corresponding to each observed vibrational frequency. Figures (48a and 48b) show the normal coordinates of 1,3,4-Oxadiazole and 1,3,4-Thiadiazole respectively.

Force Field Analysis

i.e. construction of force constant matrix F. The harmonic force field used was that developed by Cyvin and Cyvin.[53] [A unique force field for each molecule at its experimental geometry was not constructed, for the procedure would have been complicated and lengthy for the length of this project].

The force field used were developed by an iterative procedure employing successive fitting to observed frequencies by means of L matrices. [These force fields were unique for the geometries adopted by Cyvin].[53]

The frequencies of vibration and normal coordinates obtained from the above procedure were used as input for a program which calculated the vibrational coupling constant. The gradients $\partial E_g/\partial X$, $\partial E_g/\partial Y$, $\partial \varepsilon_i/\partial X$, $\partial \varepsilon_i/\partial Y$ which are used to provide an estimate of $E_{\text{excited state}}$ (i.e. E_{exs} see below) are also used as input data.

The theory used in the existing program used is best described by a 1-D model for Franck-Condon Factors (i.e. vibrational coupling constants).

We assume

a) Vibrational frequencies in the ground and excited state are identical.

b) The normal coordinates of the excited state are parallel to the ground state.

$$\text{i.e. } Q^* = Q-a$$

[where * indicates the excited state] a is a geometry shift.

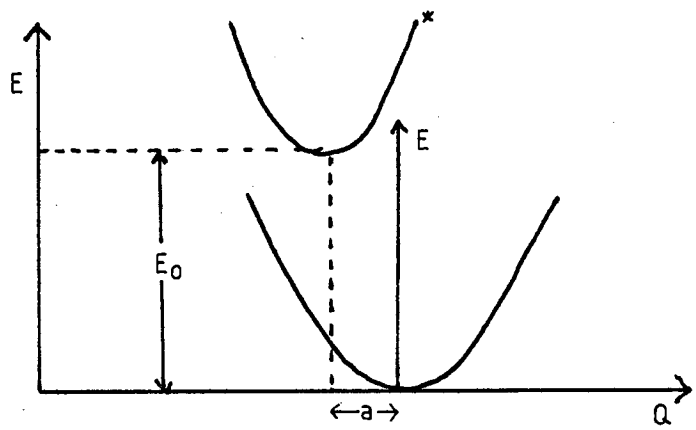

We use the harmonic approximation which allows the energy of the two states to be written as

$$E_{gs} = \frac{1}{2}\lambda Q^2$$

$$E_{exs} = \frac{1}{2}\lambda (Q-a)^2 + E_o \qquad \text{(xvi)}$$

$$\lambda = \nu^2$$

i.e. the potential wells are parabolic 'a' should not be large.

The wavefunctions are

$$\psi_{gs} = \left(\frac{\gamma}{\pi}\right)^{1/4} e^{-\frac{1}{2}\gamma Q^2} \qquad \gamma = \frac{\nu}{h}$$

$$\psi_{exs} = \left[\left(\frac{\gamma}{\pi}\right)^{\frac{1}{2}} \frac{1}{2^n n!}\right]^{\frac{1}{2}} e^{-\frac{1}{2}\gamma Q^{*2}} \quad Hn(\gamma^{\frac{1}{2}} Q^*)$$

i.e. Hermite orthogonal functions.

The un-normalized Franck-Condon factor is given by

$$\left| \int_{-\infty}^{\infty} dQ \; e^{-\frac{1}{2}Q^2} e^{-\frac{1}{2}(Q-a)^2} \; H_n(\gamma^{\frac{1}{2}}Q - \gamma^{\frac{1}{2}}a) \right|^2$$

$$(xvii) \quad = \gamma^{\frac{1}{2}} \int dz \; e^{-\frac{1}{2}z^2} \; e^{-\frac{1}{2}(z-b)^2} \; H_n(z-b)$$

where $b = \gamma^{\frac{1}{2}}a$

$z = \gamma^{\frac{1}{2}}Q.$

From standard texts on Hermite polynomials

$$C^{-\frac{1}{2}(z-b)^2} \; H_n(z-b) = e^{1/4 \; b^2 - \frac{1}{2}z^2}$$

$$x \left\{ \sum_{m=o}^{n} H_m(z) \; \frac{n!(-b)^{n-m}}{m!(n-m)!} \; F(n+1 \,|\, n-m+1 \,|\, -\tfrac{1}{2}b^2) \right.$$

$$\left. + \sum_{m=n+1}^{\infty} H_m(z) \; \frac{(b/2)^{m-n}}{(m-n)!} \; F(m+1 \,|\, m-n+1 \,|\, -\tfrac{1}{2}b^2) \right\}$$

where $F(a|c|z) = 1 + \frac{a}{c} z + \frac{1}{2!} \frac{a(a+1)}{c(c+1)} z^2 + \ldots$

is the confluent hypergeometric function. It then follows that integral (ii) becomes

$$\gamma^{-\frac{1}{2}}\ 1/4\ b^2 \int dz e^{-z^2} \{ \sum_{m=o}^{n} H_m(z)\ \frac{n!(-b)^{n-m}}{m!(n-m)!}\ F(n+1|n-m+1|^{-\frac{1}{2}})$$

$$+ \sum_{m=n+1}^{\infty} H_m(z)\ \frac{(b/2)^{m-n}}{(M-n)!}\ F(m+1|m-n+1|-\tfrac{1}{2}b^2)\}$$

By the orthonormality of Hermite polynomials only the term with m = o contributes.

Therefore the normalized Franck-Condon factor is the square of

$$(\frac{\gamma}{\pi})^{1/4} (\frac{\gamma}{\pi})^{1/4} (\frac{1}{2^n n!})^{\frac{1}{2}}\ \gamma^{-\frac{1}{2}} e^{1/4b^2} (-b)^n F(n+1|n+1|-\tfrac{1}{2}b^2)\ \sqrt{\pi}$$

but $F(n|n|z) = e^z$

therefore integral (ii) becomes

$$\int_{-\infty}^{\infty} e^{-1/4\ b^2} (-b)^n (\frac{1}{2^n n!}) dz$$

and the Franck Condon factor is then

$$\left| \int_{-\infty}^{\infty} e^{-1/4\ b^2} (-b)^n (\tfrac{1}{2}^n n!) dz \right|^2$$

$$= \frac{e^{-\frac{1}{2}\ b^2} (b^2)^n}{2^n n!}$$

Thus if we measure the vibrational peak intensity relative to the O→O line the intensity of O→n is

$$\frac{(b^2)^n}{2^n n!}$$

and from equation (xvi)

$$b = (\frac{\nu}{h})^{\frac{1}{2}} a$$

and

$$\frac{\partial E_{exs}}{\partial Q} = \lambda (Q-a)$$

$$\frac{\partial E_{exs}}{\partial Q} \Big|_{Q=O} = -\lambda a = -\nu^2 a = d$$

thus $b^2 = \frac{\nu}{h} a^2 = \frac{\nu}{h} \{\frac{d}{\nu 2}\}^2$

we define the dimensionless normal coordinate Q as

$$Q = (\frac{\nu}{h})^{\frac{1}{2}} Q$$

$$g = \frac{1}{\sqrt{2}} \frac{\partial E_e}{\partial Q} \; ; \quad f = (\frac{g}{h\nu})^2 \qquad \text{N.B. f is dimensionless}$$

giving the intensity of O→n as

$$I(O \rightarrow n) \alpha \frac{f^n}{n!} \text{ - a Poisson distribution}$$

Note

(1) The larger 'a' the larger $\frac{\partial E_{exs}}{\partial a}\Big|_{a=o}$ and vice versa.

This fits qualitatively with the prediction of progression in the P.E. spectra.

(2) Using Koopmanns theorem

$$E^{k}_{exs} = E_{gs} - \varepsilon_k, \text{ for ionization from orbital k.}$$

$$\frac{\partial E^{k}_{exs}}{\partial Q}\Big|_{Q=0} = -\frac{\partial \varepsilon_k}{\partial Q}\Big|_{Q=0}$$

(3) For many modes, the model decouples the normal coordinate such that

$$I\left(\begin{matrix}0\to n\\ 0\to m\end{matrix}\right) \alpha \frac{f_1^{\,n} f_2^{\,m}}{n!m!} \qquad \text{combination bands.}$$

frequency split of combination

$$n\nu_1 + m\nu_2$$

(4) The appearance of the spectrum in this model is independent of the sign of a.

(5) The values of f for each orbital and the vibrational frequency of each mode were obtained from the computational calculation, therefore for each orbital plot of $f^n/n!$ ($n = 1,2,3,4\ldots$) for each mode were plotted the $0\to0$ being unity in magnitude. These plots were then compared with existing experimental P.E. spectra, see Figs. (50,52,46)

(6) The $\frac{f^n}{n!} \alpha I(0\to n)$ for different orbitals cannot be compared directly as the intensity of a peak is dependent on the cross section of the orbital. Cross section differs vastly for different orbitals, therefore the intensity of the theoretical peaks cannot be directly compared to experimental peaks.

(7) An alternative method of obtaining peak intensities and frequency splits is to use Greens Functions.

FIG 49

MICROWAVE GEOMETRY *

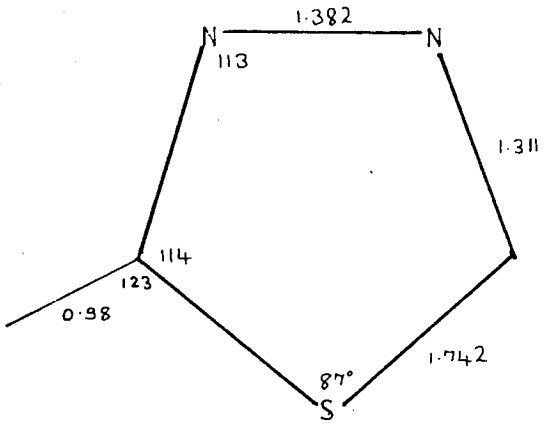

THEORETICAL GEOMETRY *

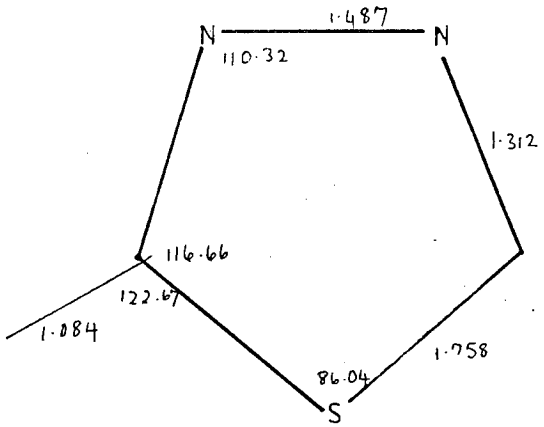

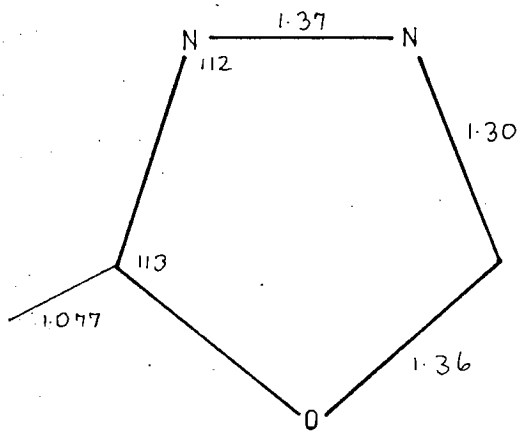

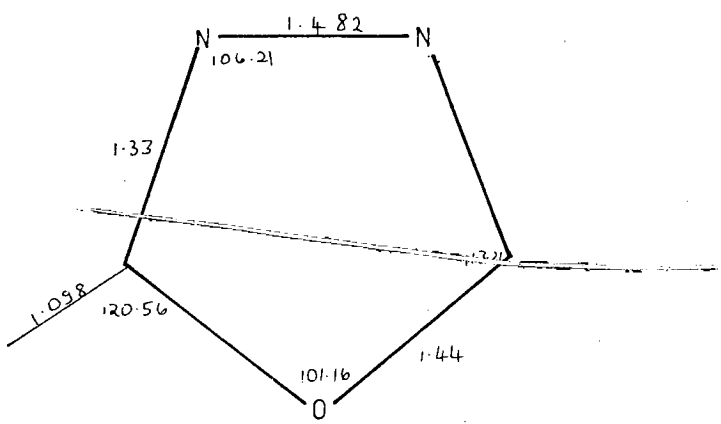

* BOND LENGTHS IN Å

BOND ANGLES IN DEGREES

Results

Tables (27) to (30) give the total energies for each cycle and gradients at the final cycle.

Although the gradients were not as small as initially intended at the final cycle, it was considered that, see Fig. (49) the gradients were too small to alter the bond lengths significantly. Hence the calculations were curtailed at cycles 3 and 2 for the thiadiazole and oxadiazole respectively.

It should be noted that the cause of the discrepancy in the bond lengths is due to the inadequacy of the basis set used which was scaled on ethylene. Hence a larger basis such as Dunnings 9s/5p double zeta basis would have produced a better theoretical geometry. However calculations with this basis for geometry optimization would have been too lengthy due to the excessive amount of CPU and data storage space required.

Cycle Number	Total Energy
0	-581.99924198
1	-582.00403784
2	-582.00736811
3	-582.0087146

Table 27 Results for 1,3,4-Thiadiazole

Atom		Gradient at Final Equilibrium Geometry
	X	0.0000000
	Y	0.00167
N3	X	0.0165455
	Y	-0.006318
C2	X	-0.011339
	Y	0.0014415
H2	X	-0.003188
	Y	0.004039

Table 28 Gradients at Final Equilibrium Geometry for 1,3,4-Thiadiazole

Cycle Number	Total Energy (a.u)
0	-259.81197986
1	-259.83154071
2	-259.83217698

Table 29 Results for 1,3,4-Oxadiazole

Atom		Gradients
O	X	0.000000
	Y	0.0055955
N3	X	0.000013
	Y	-0.0045525
C2	X	0.0019165
	Y	0.0087145
H2	X	0.003496
	Y	-0.006952

Table 30 Results at final equilibrium geometry for 1,3,4-Oxadiazole

FIG 50 PLOTS OF $f^n/n!$

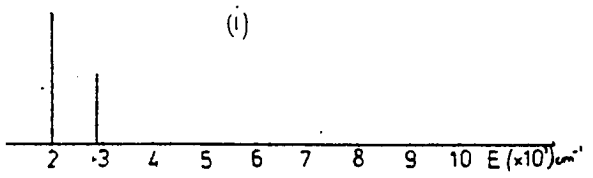

orbital 1
calc I.P 11.28 eV

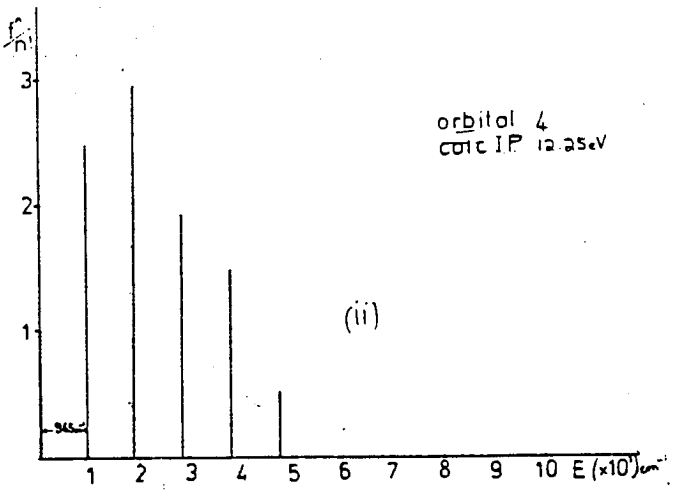

orbital 4
calc I.P 12.25 eV

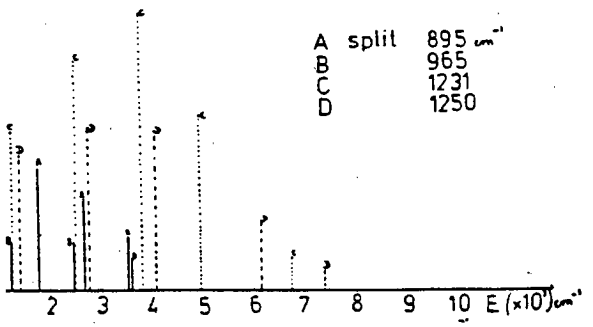

orbital 2
calc I.P 11.56 eV

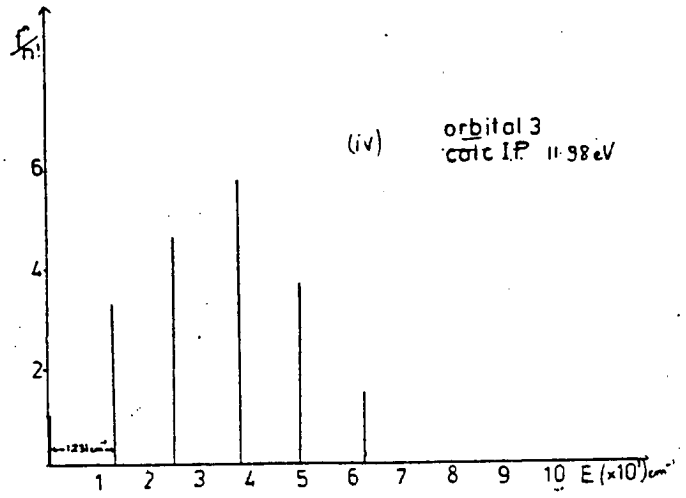

orbital 3
calc I.P 11.98 eV

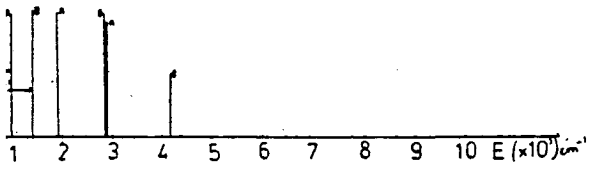

orbital 5
calc I.P 15.63 eV

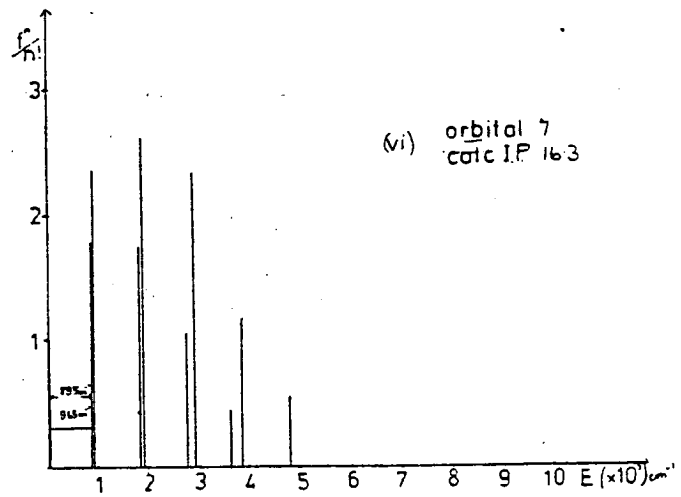

orbital 7
calc I.P 16.3

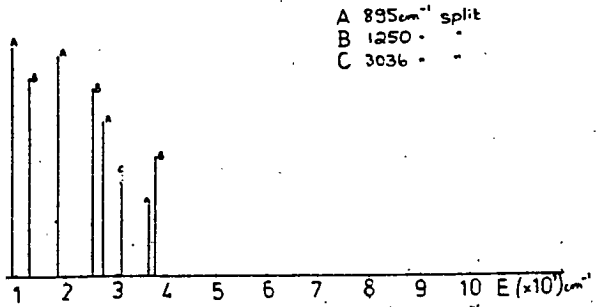

orbital 6
calc I.P 16.3 eV

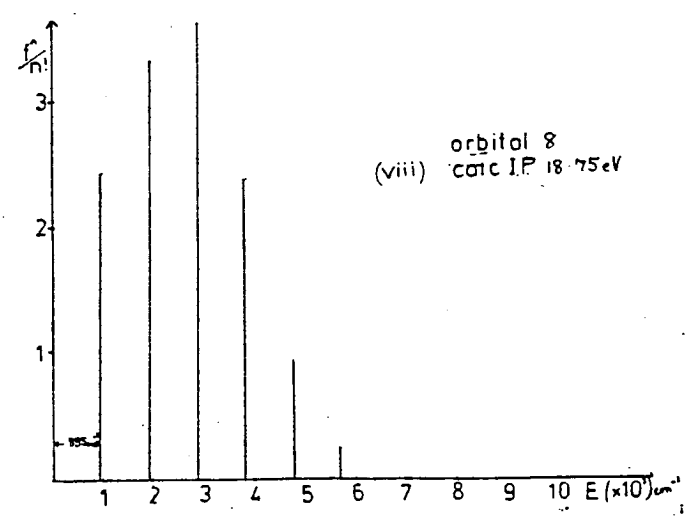

orbital 8
calc I.P 18.75 eV

Assignment of P.E. Spectra

1,3,4-Oxadiazole

Figure (4 6) shows the He(I) P.E. spectrum of 1,3,4-Oxadiazole scanning electron energies from 10-20 eV.

Figures (50 (i) to (viii))

Are plots of $f^n/n!$ for n = 1,2..v frequency split in eV for each of the frequency splits and for each orbital.

(Table 31 shows f for each frequency split for each orbital). When figures 50 (i) to (viii) are compared with figure 46 it can be seen that the general shape of each peak for each orbital are clearly represented by the theoretical plots for each orbital. Fig 50(ii) predicts much fine structure and this is clearly seen in the peak for orbital 1 in Fig. (4 6) Similarly the predicted shapes of peaks in other plots (Figs. 50 iii to viii) closely resemble the experimental P.E. spectrum i.e. the overall theoretical representation closely resembles the experimental P.E. spectrum.

Figures (51 a to g)

The upper portions of these figures shows an expanded version of peak 1 in figure (4 6) The lower portion of the figure shows the plots of $f^n/n!$ for orbitals 1-3 for different frequency separations. [The X scale of both experimental and theoretical plots are identical, therefore a direct comparison and assignment can be made].

The initial problem is to identify the (0→0) peak for each orbital, different assignments can be made choosing different (0→0) peaks.

Frequency split	'f' for orbital 1	2	3	4	5	6	7	8
951	2.513779	0.02372	0.314253	0.807813	0.007448	0.72795	0.009958	0.115996
1092	0.189111	0.161925	2.519886	2.429948	0.541355	0.523239	4.873288	4.067111
1272	0.423712	0.046643	0.275564	0.009630	0.008339	0.000171	0.294841	0.191646
1495	0.996042	1.219698	0.004559	0.138801	0.002840	0.451501	0.958109	0.051551
1534	1.873196	0.445188	0.169844	0.000084	0.09585	1.001886	0.249004	0.060635
3169	0.083900	0.083848	0.046387	0.118426	0.206895	1.428639	0.049893	0.319450

Table 31 Showing f for each frequency split for orbitals 1-8 of 1,3,4-Oxadiazole

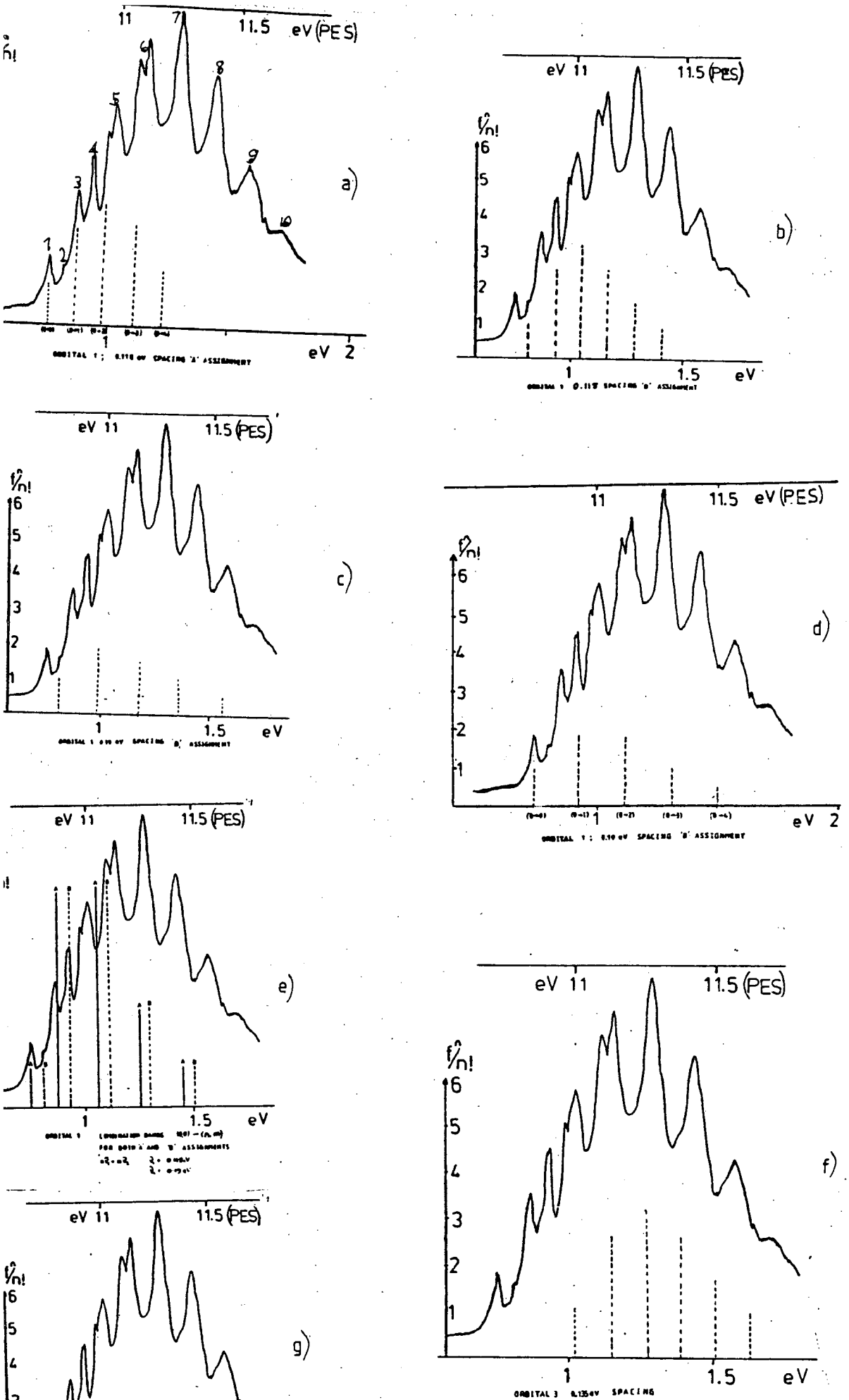

FIG 51 Experimental and Theoretical PES of 1,3,4-Oxadiazole around 11eV

Assignment 'A' - This assignment choses peak 1 in Fig.(51a) as the (O→O) peaks for orbital 1.

Assignment 'B' - choses peak 2 in fig(51a) as the (O→O) transition for orbital 1.

Both assignments have their own merits, consider Figs.(51 a and f) for assignment 'A.' In this assignment peaks 5,6,7,8,9,10 are accounted for by the orbital 3 progression which has peak 5 as its (O→O) transition. This assignment however leads to difficulties in assigning the peaks originally thought to be for orbitals 3 and 4 which lie around 13 eV in the experimental P.E. spectrum.

For Assignment 'B' then orbital 2 is placed before orbital 1. This assignment does not require the orbital 3 progression to account for peaks 8,9,10. The disadvantage of this assignment lies in its inadequacy to assign peak 3 in fig(51a) 1,3,4-Thiadiazole.

Fig.(46)

Shows the P.E. spectrum of 1,3,4-Thiadiazole from 8-20 eV.

Figs (52 i to viii)

Are plots of $f^n/n!$ n = 1,2,3 v frequency split (in eV) for each of the 8 orbitals considered for each mode frequency (Table 32) shows f for each frequency split and these for each orbital). When figures (52 i to viii) are compared with fig (46) it is found that the general shape of each theoretical orbital plot closely resembles the general shape for each experimental peak i.e. theoretical overall shapes of peaks closely resemble those in the experimental spectrum.

FIG 52 PLOTS OF $f_{n'}$

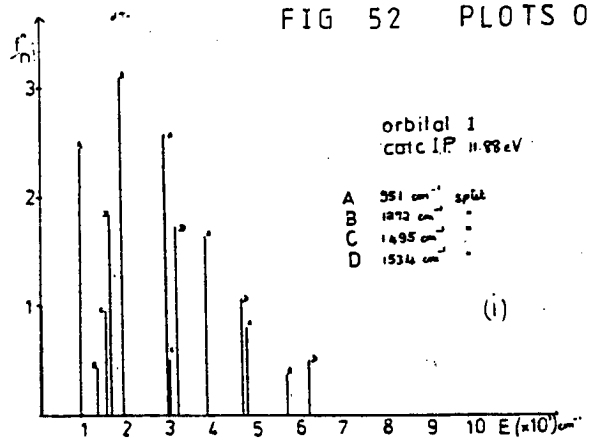

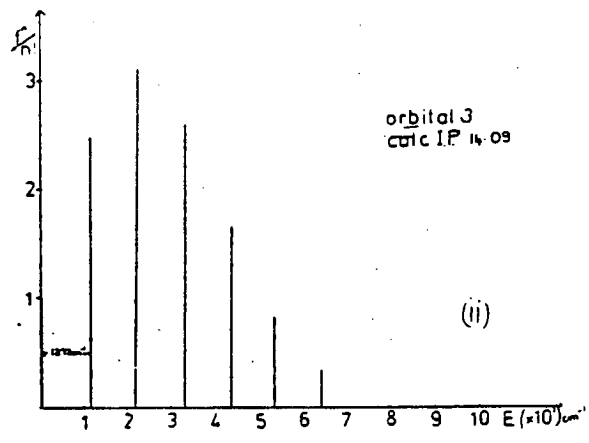

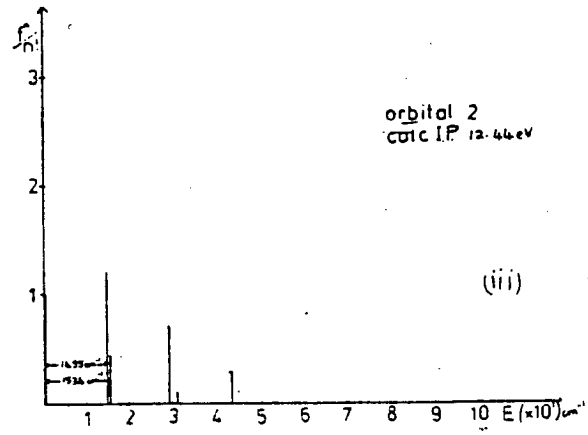

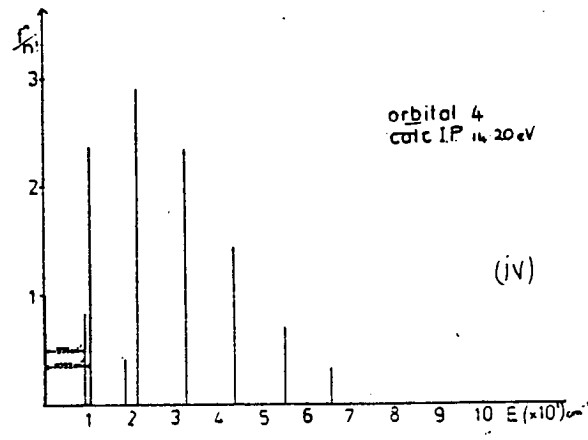

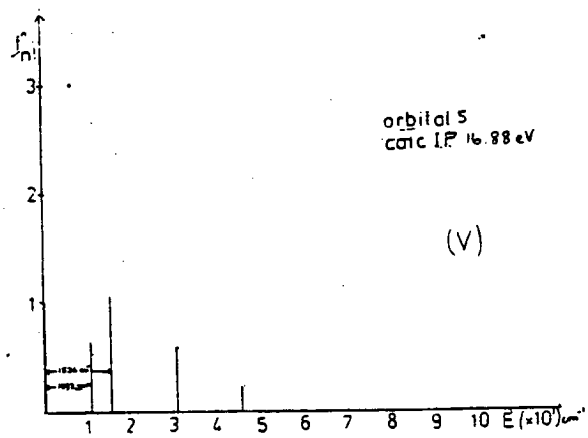

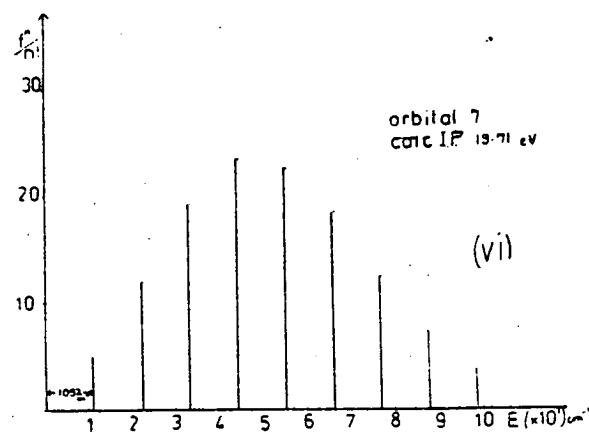

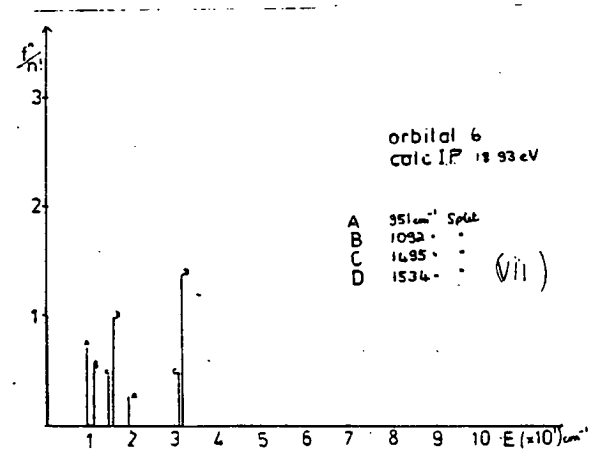

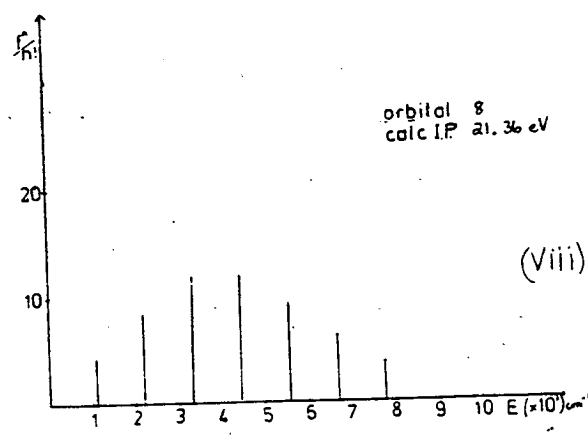

Frequency split	'f' for orbital 1	2	3	4	5	6	7	8
895	0.022648	2.232828	0.003563	0.161597	0.068674	1.844884	1.706266	0.277897
965	1.511608	0.00087	0.201104	2.606096	1.030714	0.426780	2.427304	3.088332
1231	0.005467	1.113728	0.180299	0.005608	0.112491	0.252182	0.359678	0.131526
1250	0.050524	3.174744	3.22884	0.099207	0.00387	1.580718	0.179825	0.142809
1393	0.000577	2.684089	0.200985	0.042978	1.06874	0.471971	0.269286	0.342092
3036	0.014308	0.050377	0.050935	0.079960	0.102225	0.729117	0.032833	0.300011

Table 32 Showing f for each frequency split for orbitals 1-8 of 1,3,4 Thiadiazole

Figs.(5 3 a to h)

Contain an expanded P.E. spectrum for the peak at about 11 eV in fig.(4 6) The lower portion of the figures show the plots for orbitals 1-3 for different frequency separations. [The X scale for both theoretical and experimental P.E. spectra are identical therefore a direct comparison can be made]. The O→O transition peaks are as indicated. The nature of peaks 9,10,11 in fig.(5 3a) are such that there can be no apparent identification as to where orbital 4 should be. It is obvious from the plots (5 3 a , b and c) that it is impossible to be certain that any one assignment of peaks is unique as there is no way to identify with certainty the O→O transition for any one orbital. This is exemplified by assignments A and B in figs.(5 3 a, b) where one assignment is just as adequate as the other.

There is, in fact, as much ambiguity in assigning peaks in the fine structure of such complex spectra, by this procedure, as there is in assigning the peaks intuitively by inspection of the experimental spectra. It seems that further work, such as this, on similar molecules with complex P.E. spectra would not be justified.

The inability of any one assignment, e.g. A or B for 1,3,4-Oxadiazole, to identify exactly all the fine structure peaks for the orbitals discussed could be due to one of several points.

(i) The assignment of the O→O peak was incorrect.

(ii) Neither of the molecules considered had converged on their theoretical equilibrium geometries when $\partial Eg/\partial X$ etc. were calculated.

(iii) The geometries upon which the molecules were converging were incorrect due to the inadequacy of the basis set.

(iv) The force field used was not unique.

(v) The Potential Energy curves were all assumed to be harmonic - no attempt was made to account for anharmonicity in the simple models used.

It should be noted that if finer resolution for spectra were available then it might be possible to identify with more confidence the fine structure peaks of the spectra.

(Note

No comparison between intensities of peaks in different orbitals can be made as there is here for photon absorbtion no account taken of the different cross sections of different orbitals.)

Thus we can conclude that these results indicate that a theoretical investigation of fine structure for the azoles molecules (1-9) would provide no more unambiguous assignment than by inspection alone. No further calculations were therefore attempted.

References

1. M. Redshaw, M.H. Palmer, R. Findlay, Z. Naturforsch, 34, 220, (1979).
2. In E.A.C. Lucken, Nuclear Quadrupole Coupling Constants, Acad.Press, London 1969.
3. H.G. Dehmelt, H. Kruger, Naturwiss, 37, 111, (1950).
4. J. Bardeen, C. Townes, Phys.Rev., 173, 97, (1948).
5. M. Mizushima, T. Ito, J.Chem.Phys., 19, 739, (1951).
6. H.B.G. Casimir, 'On the Interaction Between Atomic Nucleii and Electrons', Teyler's Tweede Genootschap, E.F. Bohn, Haarlem, (1936).
7. L. Nygaard, J.T. Neilsen, J. Kircheiner, G. Maltesen, G.O. Sørensen.
   J. Rastrup-Andersen, J.Mol.Struct., 3, 491, (1969).
8. L. Nygaard, D. Christen, J.T. Neilsen, E.J. Pedersen, O.Snerling, E. Vestergaard, G.O. Sørensen, J.Mol.Struct., 22, 401, (1974).
9. B.M. Craven, R.K. McMullan, J.D. Bell, H.C. Freeman, Acta Cryst., B33, 2585, (1977).
10. K. Bolton, R.D. Brown, F.R. Burden, A. Mishra, J.Mol.Struct. 27, 261, (1975).
11. N. Van der Putten, D. Heijdenrijk, H. Schenk, Cryst.Struct., Comm., 3, 321, (1974).
12. L.V. Vilkov, P.A. Akishim, V.N. Presnyohova, J.Struct. Chem.USSR, 3, 5, (1962).
13. D.M. Burness, J.Org.Chem., 21, 97, (1956).

14. Following the preparation for 4-Methylimidazole in F.L. Pyman, J.Chem.Soc.London, Ser A 121, 2616, (1922).

15. C. Pedersen, Acta.Chem.Scand., 13, 888, (1959).

16. G. Pulvermacher, Chem.Ber., 27, 613, (1

17. R.A. Henry, W.G. Finnegan, J.Am.Chem.Soc., 76, 290, (1954).

18. T.L. Gilchrist, G.E. Gynerin "Advances in Heterocyclic Chemistry", 16, 33 (1974) Ed. by E.R. Katritzky and A.J. Bouton.

19. a) C.J. Neilsen, L. Nygaard, G.O. Sørensen, IVth European Microwave Spectroscopy Conference, Tubingen, (1977).

b) L. Nygaard private communication.

20. L.T. Creagh, P. Truitt, J.Org.Chem., 30, 1892, (1968).

21. M.F. Kaufman, F.M. Ernsberger, W.S. McEwan, J.Am.Chem.Soc., 78, 4197, (1956).

22. For Example a) B.B. Makarsii, B.A. Zubon, Khim.Geterosikl Soedin, 4, 540, (1977); b) C. Guimon, G. Pfister-Guillouzo, Tetrahedron, 36, 1071, (1980).

23. C.H. Townes, B.P. Dailey, J.Chem.Phys., 17, 782, (1949).

24. L. Guibe, E.A.C. Lucken, Proc. (XIII) Colloque Ampere, (North Holland Publishing Company), (1965).

25. L. Guibe, E.A.C. Lucken, Mol.Phys., 14, 73, (1968).

26. K. Bolton, R.D. Brown, Aust. J. Phys., 27, 143, (1974).

27. W. Arnold, H. Driezler, H.D. Rudolph, Z. Naturforsch, 23, 301, (1968).

28. E. Schempp, P.J. Bray, Phys.Lett., 25A, 414, (1967).

29. E. Schempp, P.J. Bray; Ann.Meeting of Am.Phys.Soc., 1967; Bull.Am.Phys.Soc., 12, 59, (1967).

30. a) Tae Kyu-Ha, J.Mol.Struct., 51, 87, (1979).
b) G.L. Blackman, R.D. Brown, F.R. Burden, A. Mishra, J.Mol.Struct., 9, 465, (1971); c) J.Mol.Spectros., 57, 294, (1975).

31. G.L. Blackman, R.D. Brown, F.R. Burden, W. Garland, J.Mol.Spectros., 65, 313, (1977).

32. J. Sheridan in "Physical Methods in Heterocyclic Chemistry", 6, Ed. by A.R. Katritzky, Acad.Press, (1974).

33. H.J.T. Preston, J.J. Kaufmann, Int.J.Quant.Chem. 7, 207, (1973).

34. M.H. Palmer, S. Cradock, R.H. Findlay, Tetrahedron, 29, 2173, (1973).

35. J.M. Foster, S.F. Boys, Rev.Mol.Phys., 32, 300, (1960).

36. D. Deeters, Q.C.P.E., 330, (1977).

37. a) A.D. Baker, D. Beteridge, N.R. Kemp, R.E. Kirby, J.Chem.Soc., 286, (1970).
b) M.H. Palmer, A.J. Gaskell, Theor.Chim.Acta, 23, 51, (1971)
c) P.J. Derrick, L. Åsbrink, E. Lindholm, Int. J.Mass Spectrom. Ion.Phys., 6, 191, (1971).

38. C. Fridh, L. Åsbrink, E. Lindholm, Chem.Phys.Lett., 15, 408, (1972).

39. S. Cradock, R.H. Findlay, M.H. Palmer, J.Chem.Soc. Dalton Trans., 1650, (1974).

40. The Spectrum of 1-Methylimidazole used was reported by: L. Klasnic, B. Russic, F. Kajfee, V. Sunjic, Int. J. Quant. Chem. Biol. Symp., 5, 367, (1978).

41. P. Beak, F.S. Fry, J.Am.Chem.Soc., 95, 1700, (1973).

42. J.S. Kwiatowski, Acta.Phys.Pol., A55, 923, (1979).

43. B.R. Penfold, Acta.Cryst., 6, 591, 1953.

44. F. Mata, M.J. Quintana, G.O. Sørensen, J.Mol.Struct., 42, 1, (1977).

45. In: "Microwave Molecule Spectra", Techniques of Organic Chemistry Volume (IX), part 2. (1970). W. Gordy and R. Cook, Wiley Interscience, (1970).

46. J. Almlöf, A. Kvick, J. Olovsson, Acta Cryst., B27, 1201, (1971).

47. M.J. Cook, S.El Abbady, A.R. Katritzky, C. Guimon, G.Pfister-Guillouzo, J.Chem.Soc., Perkin Trans.Ser 2, 1652, (1977).

48. a) L. Nygaard, R.L. Hansen, J.Mol.Struct., 12, 59, (1972).
b) P. Markov, R. Stoelevick, Acta.Chem.Scand., 24, 2525, (1970).

49. See Appendix A.

50. Edinburgh Regional Computer Centre, 'NAG' programme Library.

51. See for example "Handbook of Mathematical Functions", Ed. M.Abramowitz, I.A. Stegun.Dover Publications (NY), (1965)

52. R. Fletcher, M.J.D. Powell, Computer Journal, 6, 163, (1963).

53. B.N. Cyvin, S.J. Cyvin, Acta.Chem.Scand., 23, 3139, (1969).

CHAPTER 5

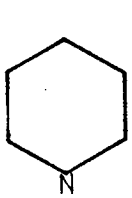
1

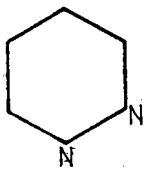
2

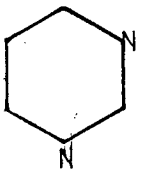
3

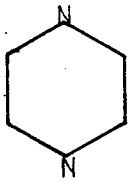
4

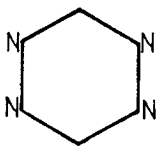
5

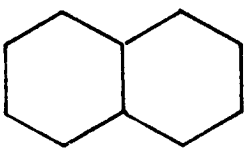
6

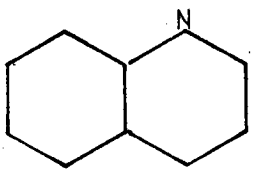
7

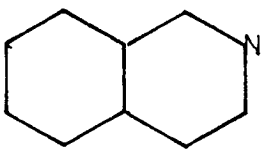
8

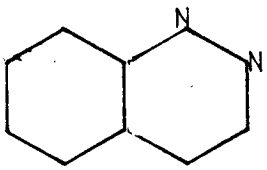
9

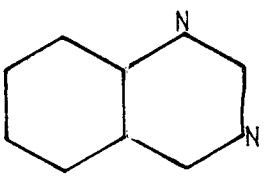
10

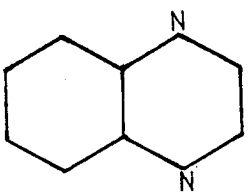
11

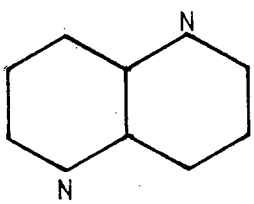
12

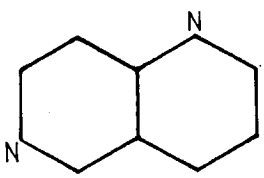
13

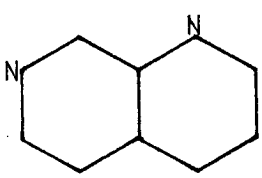
14

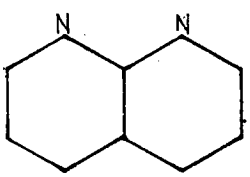
15

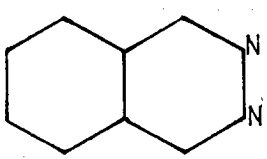
16

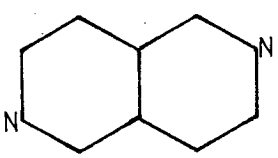
17

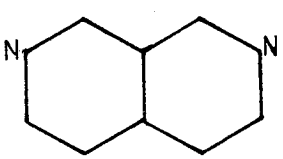
18

FIG 54 MOLECULES STUDIED IN CHAPTER 5

THE AZINES AND AZANAPHTHALENES

This chapter contains the results of investigations of the electronic structure of the series of molecules shown in Fig (54), with particular reference to the positions of the nitrogen lone pair levels, by closed shell ab initio LCAO-SCF calculations using both Minimal Basis and Double Zeta quality basis sets.

He(I) and He(II) Photoelectron spectra were also obtained where samples were available. In addition open shell unrestricted Hartree Fock calculations have been performed for each molecule, using both basis sets, to obtain theoretical ^{1}H and ^{14}N spin densities for a critical comparison with hyperfine coupling constants (and hence spin densities) obtained experimentally from Electron Spin Resonance studies.

A CLOSED SHELL CALCULATIONS

The azines have been the subject of many previous semi empirical[1] and ab initio[2] investigations, since a thorough understanding of the simple six membered ring systems gives an insight into the nature of more complicated heteroaromatic compounds in general, especially large biochemical molecules for which azines are fundamental building blocks.

Recently calculations using the 9s/5p DZ basis set used here have been reported,[3] but to date no complete ab initio study for the Azanaphthalenes, either using MB or DZ basis sets have been reported.

An ab initio calculation has been reported for Naphthalene[4] as have semi-empirical calculations for the complete azanaphthalene series.[5]

(i) Molecular Geometries Used in Calculations

Where possible experimental structures were used for the calculations performed and where experimental data is lacking geometries were constructed as described below.

Azines

Experimental microwave gas phase structures are available for pyridine[6] and pyridazine.[8] The structure used for pyrimidine was constructed from the results of a nematic phase NMR study[7a] and the crystal structure.[7b] An Electron Diffraction structure is available for pyrazine,[9] whereas a UV/rotational gas phase structure is available for S-tetrazine.[10] More detailed information of these geometries can be found in Appendix (B).

FIG 55 CONSTRUCTION OF GEOMETRIES

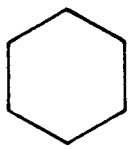

FROM $C_{10}H_8$

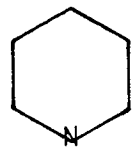

FROM PYRIDINE

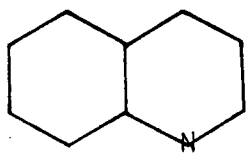

QUINOLINE

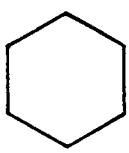

FROM $C_{10}H_8$

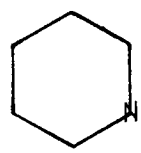

FROM PYRIDINE

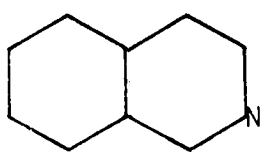

ISOQUINOLINE

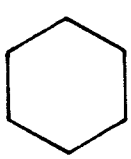

FROM $C_{10}H_8$

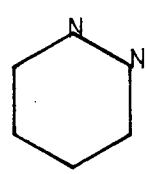

FROM PYRIDAZINE

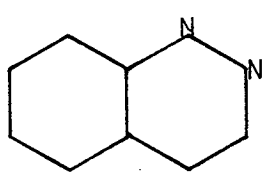

CINNOLINE

Naphthalene and the Azanaphthalenes

A neutron diffraction structure is available for Naphthalene[1] whereas crystal structures are available for Phthalazine,[12] 1,5-Diazanaphthalene,[13] 2,6-Diazanaphthalene,[13] Quinazoline,[15] Quinoxaline,[14] and 1,8-Diazanaphthalene.[16] The positions of the protons in 2,6- and 1,5-Diazanaphthalene were chosen using the results of nematic phase studies.[17]

The crystal data for Phthalazine, Quinazoline and 1,8-Diazanaphthalene show that these structures are in fact slightly non planar in the solid state, however since these deviations from planarity are small, for the purpose of this work the molecules were assumed to be planar and hence a "flattened out" crystal structure was used.

There is no experimental data available for the remaining molecules and it was therefore necessary to construct geometries as outlined below.

Although an early X-ray diffraction study has been performed for Quinoline, no structural parameters were reported and the theoretical structure was constructed from half of a naphthalene molecule fused to the C_2-C_3 bond of a pyridine molecule, modifying the pyridine structure to preserve the naphthalene bridging C-C bond length (Fig. (55)).
Similarly for isoquinoline the half naphthalene molecule was fused onto the C3-C4 bond of pyridine again modifying the pyridine molecule to preserve the naphthalene C9-C10 bridge bond length (Fig. (55)).

In constructing the geometry of cinnoline a modified pyrid azine structure was fused along its C3-C4 bond to half

FIG 56 CONSTRUCTION OF GEOMETRIES

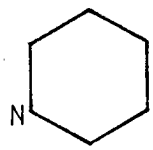

FROM ISOQUINOLINE

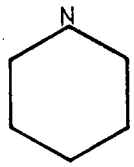

QUINOLINE

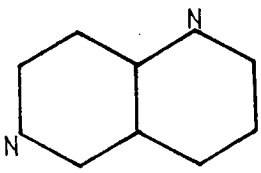

1,6-DIAZANAPHTHALENE

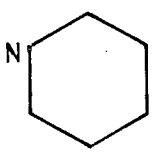

ROM ISOQUINOLINE

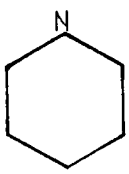

FROM QUINOLINE

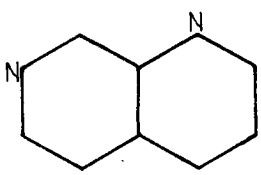

1,7-DIAZANAPHTHALENE

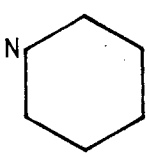

IM ISOQUINOLINE

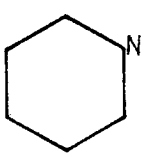

FROM ISOQUINOLINE

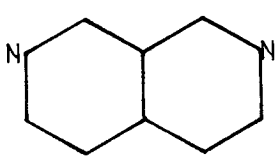

2,7-DIAZANAPHTHALENE

of a naphthalene molecule, preserving the C9-C10 bridge bond (Fig. (55)).

For construction of the theoretical geometry of 1,6-Diazanaphthalene parts of the Quinoline and Isoquinoline moleucles were fused as shown in Fig (56), the same parts being used to construct the geometry of 1,7-Diazanaphthalene only in different orientations Fig (56). The structure of 2,7-Diazanaphthalene was constructed from two Isoquinoline rings fused as shown in Fig (56).

Bond lengths and angles are given in Appendix B

(ii) Calculations

Calculations were performed on the complete series of molecules (1 to 18) using the aforedescribed geometries, a 7s/3p minimal basis (MB)*, and a 9s/5p double zeta* (DZ) quality basis set, as input to the Atmol-3 programs. The MB calculations were performed on the IBM 370 as were the DZ calculations for the azines. The faster CDC7600 was used for the DZ calculations for the bicyclic systems due to their considerable size. For example, the estimated size of the mainfile for naphthalene (116 basis functions DZ) using the relationship mainfile blocks written α (number of basis functions)^4, is 33,000 blocks (in practice this was ca. 28,000 blocks). Such a calculation was considered too large to undertake on the IBM 370 which is a factor of four slower than the CDC7600. Nevertheless the DZ calculation on phthalazine was performed on the IBM 370 and took over four months (real time), that is 56,280s C.P.U., to attain convergence of the ground state and radical anion.

* see appendix(A)

Table (33) Job Statistics

Molecule	Machine	CPU integrals	Blocks in mainfile	CPU SCF (closed shell)	CPU UHF (open shell)	start date	finish date
Phthalazine C_{2V}	IMB370	200 min	23,282	487 min	251 min	8/12/78	26/4/79
Quinoxaline C_{2V}	CDC7600	54 min	23,004	37 min	123 min	1/11/79	7/1/80

A comparable calculation on the CDC7600 took only two months (real time) to complete (12,900s C.P.U.) and was limited by the then relatively meagre resources of CPU available and excessive number of mainfile data storage tape failures. This tape fail limitation was also experienced on the IBM370 for large jobs, but these proved disastrous since regeneration of a complete tape full of two electron integrals on this machine required four times as much CPU as on the CDC7600.

In all, a series of very large calculations such as this is outwith the scope of the IBM 370 and just within, but encroaching on the limits of, our presently available CPU resources on the CDC7600. It is true to say that for large calculations such as these the data storage system, on both machines, is at present sufficiently unreliable to be a major limiting factor. The statistics for two comparable calculations performed on the different systems are given in Table (33).

Table (34) Total Energies (au) and other Reported ab initio Total Energies

molecule	MB	DZ	(a)	(b)	(c)	(d)	(e)	(f)
pyridine	-246.0153	-246.6053	-245.7649	-245.622	-246.327	-246.417		-246.54907
pyridazine	-261.8922	-262.5429	-261.685			-262.31		-262.4744
pyrimidine	-261.9138	-262.5785	-261.6787			-262.361		-262.5132
pyrazine	-261.9045	-262.5513		-261.554	-262.255	-262.352	-262.57306	-262.5107
s-tetrazine	-293.6675	-294.4516	-293.4748			-294.15		294.36608

a) M.H. Palmer, A.J. Gaskell, R.H. Findlay, Journal of the Chemical Society Perkin (II), 778, (1974).

b) E. Clementi, Journal of Chemical Physics, 46, 4731, (1967).

c) J.D. Petke, J.L. Whitten, J.A. Ryan, Journal of Chemical Physics, 48, 953, (1968).

d) J. Almlof, B. Roos, U. Wahlgren, H. Johansen, Journal of Electron Spectroscopy and Related Phenomena, 2, 51, (1974).

e) S. Canuto, O. Goscinski, M. Zerner, Chemical Physics Letters, 68, 232, (1979).

f) W. Von Niesen, W.P. Kraemer and G.H. F. Diercksen, Chemical Physics, 41, 113 (1979).

Table (35) Total Energies (au)

Molecule	7s/3p Mimal Basis	9s/5p Double Zeta Basis
Naphthalene	-382.37043	-383.23229
Quinoline	-398.27300	-399.20821
Isoquinoline	-398.27179	-399.20669
Cinnoline	-414.15090	-415.14598
Quinazoline	-414.10530	-415.13982
Quinoxaline	-414.17298	-415.17317
1,5-Diazanaphthalene	-414.16992	-415.18241
1,6-Diazanaphthalene	-414.17222	-415.18142
1,7-Diazanaphthalene	-414.17173	-415.17998
1,8-Diazanaphthalene	-414.08244	-415.15561
Phthalazine	-413.96740	-415.01532
2,6-Diazanaphthalene	-414.02482	-415.05853
2,7-Diazanaphthalene	-414.17041	-415.17878

Results of Closed Shell Calculations

(iii) Total Energies

Tables (34) and (35) contain the calculated total energies for the azines and azanaphthalenes respectively, with a selection of other reported total energies given for the former.

The most recently reported azine total energies [3] result from calculations which used the same DZ basis and contraction as employed herein. Despite this, they obtain slightly poorer total energies for all molecules, even though identical structures were used for pyrimidine, pyridazine and s-tetrazine (for which our calculations gave energies 0.07 au, 0.07 au and 0.08 au better respectively). No such comparison can be made for pyridine and pyrazine since different structures were used. It is interesting that they report the literature gas phase electron diffraction structure for pyrazine gave a worse energy than the crystal structure, although our calculation using the gas phase structure gives a significantly better energy than their best. One might reasonably expect that calculations using the same structure and basis set would give effectively identical total energies, since use of an identical basis set ensures that the electron-nuclear attraction and electron-electron repulsion integrals are identical, and use of the same structure produces identical nuclear-nuclear repulsion integrals.

The significant difference in the total energies for identical structures, cannot be attributed to convergence of their[3] wavefunction on a doubly excited state since the reported orbital energies[3] match ours very closely. The literature structures used, however, do not give C-H bond

lengths and it is possible that discrepancies in the total energy could be due to our better estimation of these lengths (from Nematic phase NMR studies[17]); this is somewhat unlikely, since the positions of the hydrogen atoms are considered to be relatively unimportant. Equally unlikely is the possibility that their criterion for convergence is any less stringent than ours, and we must therefore postulate that their programs might calculate the integrals either to an artificially high level of accuracy or not accurately enough. Both 'underestimation' and 'overestimation' would cause similar effects since too high a level of accuracy overestimates the repulsion integrals thereby worsening the energy, whereas too low a level of accuracy underestimates the attraction integrals producing the same effect.

The DZ calculations reported here provide the best calculated total energies, to date, for the complete series, including the azanaphthalenes, bar pyrazine. For pyrazine a configuration Interaction study [26] using the same basis set and the crystal structure provides a total energy better by 0.02 au than ours.

There have been no reported total energies for the azanaphthalenes, although a calculation, using the same MB basis set and structure as used here, has been reported and gives the same total energy.[4]

FIG 57 HOMO'S of benzene

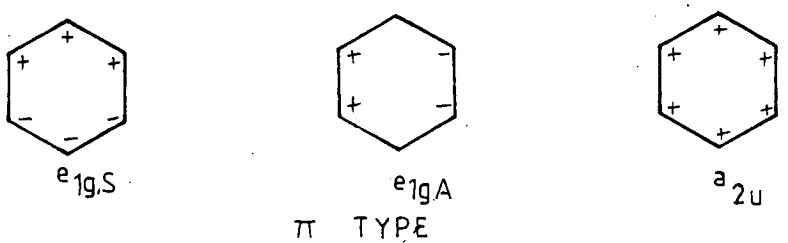

π TYPE

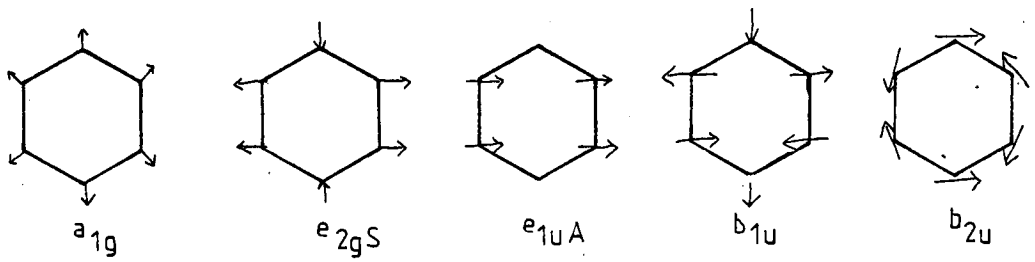

σ TYPE (CH bonding)

A — asymmetric
S — symmetric

(iv) Orbital Energies - Azines

The azines can be regarded as a perturbation of the benzene system by replacement of $\gg$CH by $\gg$N: and detailed analysis of the effect of aza-substitution on the calculated molecular orbitals of benzene have been discussed at length in the literature[2k] where the following points were noted.

1) There is a shift to higher binding energy for all orbitals as the number of nitrogen atoms introduced increases.

2) The introduction of a nitrogen atom has a small perturbation when introduced on a nodal plane in an orbital.

3) Large and medium perturbations occur when the nitrogen atom is introduced in non-nodal positions either at the maximum of the wave or adjacent to the nodal position.

4) When a study of the eigenvectors for the azines is made, with regard to the sign rather than the magnitude of the components it is found that the perturbed systems have apparent D_6h symmetry, which enables correlation of particular levels to be made throughout the series.

5) The highest occupied molecular orbitals (HOMO's) for benzene are given in Fig (58) and the orbital ordering is $1e_{1g} < 3e_{2g} < 1a_{2u} < 3e_{1u} < 1b_{2u} < 2b_{1u} < 3a_{1g} < 2e_{1u} < 2e_{2g}$. Now replacement of $\gg$CH by $\gg$N: removes a CH bonding orbital and introduces a destabilized lone pair orbital (LP_N) per nitrogen atom, which is characterized by large coefficients for $2S_N$ and $(2P_x, 2P_y)_N$ in the eigenvector.

For the diazines the LP_N exist as linear combinations viz.

$$aLP_{N1} + bLP_{N2} \text{ - symmetric combination, } LP_N^+$$
$$bLP_{N1} - aLP_{N2} \text{ - antisymmetric combination, } LP_N^-$$

with the antisymmetric combination lying at lower binding energy for all the diazines except pyrazine.

6) The extent of shifting of the LP_N is affected by several factors viz.

$$\Delta E_{SHIFT} = E_{\substack{ORIGINAL \\ HYDROCARBON \\ ORBITAL}} + K + \emptyset$$

where K = a factor which depends on the electron density* or amplitude of the wave at the position of N substitution

$\emptyset$ = a positive amount for LP_N^- and a negati amount for LP_N^+

*N.B. The electron density is proportional to the coefficient of the eigenvector squared.

7) The seeming anomaly in the ordering of the lone pair combinations for pyrazine can be explained as follows; the e_{2gA} and e_{1uA} are nodal at the N atoms and hence cannot be lone pair orbitals, but the lone pair combinations are satisfied by e_{2gS} and e_{1uS}. Now e_{2gS} is at lower binding energy then e_{1uS} in benzene and, although accommodating the symmetric combination, provides the first accessible level for anylone pair combination - hence the LP_N ordering is interpretable.

Table (36) Orbital Energies (eV)

Pyridine		Pyridazine		Pyrimidine	
MB	DZ	MB	DZ	MB	DZ
-10.34 π $1a_2$	-9.80 π $1a_2$	-10.59 LP_N^- $8b_2$	-10.83 π $1a_2$	-11.30 LP_N^- $7b_2$	-10.80 π $3b_1$
-10.99 π $2b_1$	-10.67 π $2b_1$	-11.30 π $1a_2$	-11.01 LP_N^- $8b_2$	-11.38 π $2b_1$	-11.43 LP_N^- $7b_2$
-11.06 LP_N $11a_1$	-11.27 LP_N $11a_1$	-11.77 π $2b_1$	-11.43 π $2b_1$	-11.91 π $1a_2$	-11.67 π $1a_2$
-14.21 $7b_2$	-14.22 $7b_2$	-13.03 LP_N^+ $10a_1$	-13.20 LP_N^+ $10a_1$	-12.79 LP_N^+ $11a_1$	-12.92 LP_N^+ $11a_1$
-15.53 π $1b_1$	-15.00 π $1b_1$	-16.34 $9a_1$	-16.05 π $1b_1$	-16.51 $10a_1$	-16.03 π $1b_1$
-15.96 $10a_1$	-15.87 $10a_1$	-16.49 $1b_1$	-16.24 $9a_1$	-16.57 π $1b_1$	-16.49 $10a_1$
-16.74 $6b_2$	-16.59 $6b_2$	-16.80 $7b_2$	-16.71 $7b_2$	-16.76 $6b_2$	-16.61 $6b_2$
-17.83 $9a_1$	-17.87 $9a_1$	-18.21 $6b_2$	-18.29 $6b_2$	-18.44 $9a_1$	-18.32 $9a_1$
-18.10 $5b_2$	-18.25 $5b_2$	-19.10 $8a_1$	-19.40 $8a_1$	-19.23 $5b_2$	-19.46 $5b_2$
-20.06 $8a_1$	-19.92 $8a_1$	-20.49 $7a_1$	-20.34 $7a_1$	-20.83 $8a_1$	-20.73 $8a_1$
-23.25 $4b_2$	-23.55 $4b_2$	-24.06 $6a_1$	-24.43 $6a_1$	-24.36 $7a_1$	-24.65 $7a_1$
-23.39 $7a_1$	-23.60 $1a_1$	-24.72 $5b_2$	-25.04 $5b_2$	-24.70 $4b_2$	-24.97 $4b_2$
-28.33 $3b_2$	-28.55 $3b_2$	-30.43 $4b_2$	-30.83 $4b_2$	-29.87 $6a_1$	-30.00 $6a_1$
-29.87 $6a_1$	-30.11 $6a_1$	-30.85 $5a_1$	-31.07 $5a_1$	-32.79 $3b_2$	-33.17 $3b_2$
-34.54 $5a_1$	-34.95 $5a_1$	-37.07 $4a_1$	-37.60 $4a_1$	-36.32 $5a_1$	-36.61 $5a_1$
-307.35 $4a_1$	-306.51 $4a_1$	-308.27 $3b_2$	-307.28 $3b_2$	-308.02 $4a_1$	-306.89 $4a_1$
-307.35 $2b_2$	-306.51 $2b_2$	-308.27 $3a_1$	-307.31 $3a_1$	-309.04 $3a_1$	-308.07 $2b_2$
-307.66 $3a_1$	-306.91 $3a_1$	-308.69 $2a_1$	-307.69 $2a_1$	-309.04 $2b_2$	-308.07 $3a_1$
-308.10 $2a_1$	-307.27 $2a_1$	-308.69 $2b_2$	-307.69 $2b_2$	-309.54 $2a_1$	-308.32 $2a_1$
-308.11 $1b_1$	-307.27 $1b_2$	-424.69 $1a_1$	-425.37 $1b_2$	-423.99 $1b_2$	-424.47 $1a_1$
-423.25 $1a_1$	-423.95 $1a_1$	-424.72 $1b_2$	-425.38 $1a_1$	-423.99 $1a_1$	-424.47 $1b_2$

Table (36) cont.

Pyrazine						s-Tetrazine					
MB			DZ			MB			DZ		
-11.10	LP_N^+	$6a_{1g}$	-10.79	π	$1b_{3g}$	-10.93	LP_N	$3b_{1g}$	-11.45	LP_N	$3b_{1g}$
-11.13	π	$1b_{2g}$	-11.30	π	$1b_{2g}$	-13.16	π	$1b_{3g}$	-12.65	π	$1b_{2g}$
-11.28	π	$1b_{3g}$	-11.65	LP_N^+	$6a_{1g}$	-13.94	π	$1b_{2g}$	-13.89	π	$1b_{2g}$
-12.96	LP_N^-	$5b_{2u}$	-13.33	LP_N^-	$5b_{2u}$	-14.29	LP_N	$6a_{1g}$	-14.54	LP_N	$6a_{2g}$
-14.16		$4b_{1g}$	-14.56		$4b_{1g}$	-14.38		$5b_{2u}$	-14.74		$5b_{2u}$
-15.93	π	$1b_{1u}$	15.62	π	$1b_{1u}$	-15.55		$4b_{3u}$	-15.56		$4b_{3u}$
-17.23		$3b_{3u}$	-17.27		$3b_{3u}$	-18.57	π	$1b_{1u}$	-18.18	π	$1b_{1u}$
-18.04		$4b_{2u}$	-18.25		$3b_{1g}$	19.77		$4b_{2u}$	-19.80		$4b_{2u}$
-18.63		$2b_{3u}$	-19.14		$3b_{3u}$	-21.05		$5a_{1g}$	-20.83		$5a_{1g}$
19.82		$5a_{1g}$	-19.84		$5a_{1g}$	-21.33		$3b_{3u}$	-22.01		$3b_{3u}$
-23.25		$3b_{1g}$	-23.78		$2b_{1g}$	-26.18		$4a_{1g}$	-26.74		$4a_{1g}$
-24.81		$4a_{1g}$	-25.33		$4a_{1g}$	-27.96		$2b_{1g}$	-28.61		$2b_{1g}$
-29.19		$2b_{1g}$	-29.58		$2b_{3u}$	-33.24		$3b_{2u}$	-33.62		$3b_{2u}$
-32.08		$3b_{2u}$	-32.77		$3b_{2u}$	-36.85		$2b_{3u}$	-37.41		$2b_{3u}$
-35.07		$3a_{1g}$	-35.64		$3a_{1g}$	-40.18		$3a_{1g}$	-40.63		$3a_{1g}$
-308.53		$2b_{2u}$	-307.87		$1b_{1g}$	-310.91		$2a_{1g}$	-309.47		$2a_{1g}$
-308.53		$1b_{1g}$	-307.87		$2b_{2u}$	-310.91		$2b_{2u}$	-309.47		$2b_{2u}$
-308.53		$2a_{1g}$	-307.91		$2a_{1g}$	-426.45		$1b_{3u}$	-426.83		$1b_{2u}$
-308.54		$1b_{2u}$	-307.91		$1b_{3u}$	-426.46		$1a_{1g}$	-426.83		$1b_{1g}$
-423.84		$1a_{1g}$	-425.16		$1a_{1g}$	-426.48		$1b_{1g}$	-426.86		$1a_{1g}$
-423.84		$1b_{2a}$	-425.16		$1b_{2u}$	-426.48		$1b_{2u}$	-426.86		$1b_{3u}$

Orbital energies for the MB and DZ calculations are given in Table (36)- it is noteworthy that the trends in orbital energies observed before, for the MB calculations, are exhibited by the DZ orbital energies. The ordering of the LP_N levels remains unchanged as is the ordering of the π levels although the LP_N/π ordering is changed where energy levels are very close, for example in pyridazine.

It is appropriate to extend this study to naphthalene and the diazanaphthalenes to see if similar trends exist.

Orbital Energies - Naphthalene and the Diazanaphthalenes

The calculated orbital energies for naphthalene and the diazanaphthalenes are given in Table (37).

The azanaphthalenes can be considered as a perturbation of the naphthalene system and, as for the azines, the following trends are immediately apparent from inspection of their orbital energies and eigenvectors.

a) There is a general stabilization of the orbital energies with nitrogen substitution, which increases with the number of substituent nitrogens.

b) Inspection of the diazanaphthalene eigenvectors with regard to sign, and not magnitude, shows that they have a perturbed or apparent D_{2h} $(C_{10}H_8)$ symmetry.

It should be noted that these trends are directly comparable with those noted for the azines, but a more detailed investigation of the positions of the N atom substituents and their corresponding perturbation of the $C_{10}H_8$ levels, must be made to elucidate if the orbital ordering for this series of molecules can be interpreted in a similar manner to that of the azines.

Table (37) Orbital Energies (eV)

Naphthalene				Quinoline				Isoquinoline			
MB		DZ		MB		DZ		MB		DZ	
ε_i	D_2h	ε_i	D_2h	ε_i	*A.S.	ε_i	*A.S.	ε_i	*A.S.	ε_i	*A.S.
-8.47	π $1a_{1u}$	-7.97	π $1a_{1u}$	-8.90	π $1a_{1u}$	-8.49	π $1a_{1u}$	-8.81	π $1a_{1u}$	-8.36	π $1a_{1u}$
-9.47	π $2b_{1u}$	-8.99	π $2b_{1u}$	-9.84	π $2b_{1u}$	-9.27	π $2b_{1u}$	-10.33	π $1b_{1u}$	-9.84	π $2b_{1u}$
-11.29	π $1b_{3g}$	-10.63	π $1b_{3g}$	-11.10	LP_N $9a_{1g}$	-11.27	LP_N $9a_{1g}$	-11.14	LP_N $6b_{1g}$	-11.22	π $1b_{3g}$
-13.09	π $1b_{2g}$	-12.41	π $1b_{2g}$	-12.05	π $1b_{3g}$	-11.53	π $1b_{3g}$	-11.79	π $1b_{3g}$	-11.24	LP_N $6b_{1g}$
-13.17	$9a_{1g}$	-13.12	$9a_{1g}$	-13.46	π $1b_{2g}$	-12.87	π $1b_{2g}$	-13.74	$9a_{1g}$	-13.31	π $1b_{2g}$
-13.44	$6b_{1g}$	-13.22	$6b_{1g}$	-13.89	$6b_{1g}$	-13.77	$6b_{1g}$	-13.86	π $1b_{2g}$	-13.65	$9a_{1g}$
-14.48	$7b_{3u}$	-14.48	$7b_{3u}$	-14.34	$7b_{3u}$	-14.17	$7b_{3u}$	-14.63	$7b_{3u}$	-14.51	$7b_{3u}$
-15.48	π $1b_{1u}$	-14.77	π $1b_{1u}$	-15.94	$5b_{1g}$	-15.63	π $1b_{1u}$	-15.43	$7b_{2u}$	-15.35	$7b_{2u}$
-15.54	$7b_{2u}$	-15.41	$7b_{2u}$	-16.03	$7b_{2u}$	-15.84	$7b_{2u}$	-16.23	π $1b_{1u}$	-15.60	π $1b_{1u}$
-16.24	$6b_{3u}$	-16.09	$6b_{3u}$	-16.24	π $1b_{1u}$	-15.93	$5b_{1g}$	-16.68	$6b_{3u}$	-16.51	$5b_{1g}$
-16.80	$5b_{1g}$	-16.09	$5b_{1g}$	-16.66	$6b_{3u}$	-16.53	$6b_{3u}$	-16.71	$5b_{1g}$	-16.56	$6b_{3u}$
-17.12	$6b_{2u}$	-16.99	$8a_{1g}$	-16.98	$6b_{2u}$	16.91	$6b_{2u}$	-17.51	$6b_{2u}$	-17.41	$6b_{2u}$
-17.14	$8a_{1g}$	-17.09	$6b_{2u}$	-17.67	$8a_{1g}$	-17.52	$8a_{1g}$	-17.69	$8a_{1g}$	-17.63	$8a_{1g}$
-18.78	$7a_{1g}$	-18.69	$7a_{1g}$	-19.26	$7a_{1g}$	-19.19	$7a_{1g}$	-19.11	$7a_{1g}$	-19.03	$9a_{1g}$
-19.18	$4b_{1g}$	-19.31	$4b_{1g}$	-19.65	$5b_{3u}$	-19.52	$5b_{3u}$	-19.79	$4b_{1g}$	-19.84	$4b_{1g}$
-19.54	$5b_{3u}$	-19.33	$5b_{3u}$	-19.89	$4b_{1g}$	-19.98	$4b_{1g}$	-19.96	$5b_{3u}$	-19.91	$5b_{3u}$
-22.31	$6a_{1g}$	-22.40	$6a_{1g}$	-22.77	$6a_{1g}$	-22.80	$6a_{1g}$	-22.88	$6a_{1g}$	-22.94	$6a_{1g}$
-22.88	$5b_{2u}$	-22.93	$5b_{2u}$	-23.45	$5b_{2u}$	-23.68	$5b_{2u}$	-23.55	$5b_{2u}$	-23.73	$5b_{2u}$
-23.27	$4b_{3u}$	-23.97	$4b_{3u}$	-24.06	$4b_{3u}$	-24.22	$4b_{3u}$	-24.27	$4b_{3u}$	-24.44	$4b_{3u}$
-26.94	$3b_{1g}$	-26.97	$3b_{1g}$	-27.59	$3b_{1g}$	-27.74	$3b_{1g}$	-27.39	$3b_{1g}$	-27.57	$3b_{1g}$
-27.56	$5a_{1g}$	-27.82	$5a_{1g}$	-28.07	$5a_{1g}$	-28.25	$5a_{1g}$	-28.89	$5a_{1g}$	-29.09	$5a_{1g}$
-27.73	$4b_{2u}$	-28.84	$4b_{2u}$	-30.08	$4b_{2u}$	-30.27	$4b_{2u}$	-29.52	$4b_{2u}$	-29.69	$4b_{2a}$
-30.48	$3b_{3u}$	-30.63	$3b_{3u}$	-31.48	$3b_{3u}$	-31.67	$3b_{3u}$	-32.04	$3b_{3u}$	-32.24	$3b_{2u}$
-32.33	$4a_{1g}$	-32.44	$4a_{1g}$	-34.71	$4a_{1g}$	-35.10	$4a_{1g}$	-34.61	$4a_{1g}$	-34.97	$4a_{1g}$
-306.8	$3a_{1g}$	-306.11	$3b_{2u}$	-306.96		-306.14		-307.19		-306.42	
-306.8	$3b_{2u}$	-306.11	$2b_{1g}$	-307.07		-306.14		-307.19		-306.44	
-306.8	$2b_{1g}$	-306.11	$3a_{1g}$	-307.09		-306.31		-307.25		-306.52	
-306.8	$2b_{3u}$	-306.11	$2b_{3u}$	-307.12		-306.42		-307.29		-306.59	
306.8	$2a_{1g}$	-306.11	$2b_{2u}$	-307.24		-306.58		-307.34		-306.63	
-306.8	$1b_{3u}$	-306.11	$1b_{1g}$	-307.56		-306.59		-307.71		-306.66	
-306.8	$2b_{2u}$	-306.11	$2a_{1g}$	-307.67		-306.89		-307.91		-306.92	
-306.9	$1b_{1g}$	-306.11	$1b_{3u}$	-308.08		-307.23		-308.02		-307.13	
-307.32	$1b_{2u}$	-306.31	$1b_{2u}$	-308.41		-307.41		-308.14		-307.35	
-307.32	$1a_{1g}$	-306.34	$1a_{1g}$	-423.49		-423.88		-423.6		-423.83	

*Apparent D_2h symmetry

Table (37) (contd.) Orbital Energies(eV)

Cinnoline				Quinazoline				Quinoxaline				
MB		DZ		MB		DZ		MB		DZ		
	*AS	ε_i	*AS	ε_i	*AS	ε_i	*AS	ε_i	*AS	ε_i	*AS	C_2V
π	$1a_{1u}$	-8.93	π $1a_{1u}$	-9.96	π $1a_{1u}$	-9.18	π $1a_{1u}$	-9.21	π $1a_{1u}$	-8.86	π $1a_{1u}$	a_2
2 LP_N^-	$9a_{1g}$	-10.18	π $2b_{1u}$	-10.97	π $2b_{1u}$	-10.15	π $2b_{1u}$	-10.35	π $2b_{1u}$	-9.76	π $2b_{1u}$	b_1
1 π	$2b_{1u}$	-10.98	LP_N $9a_{1g}$	-11.40	LP_N^- $9a_{1g}$	-11.24	LP_N^- $9a_{1g}$	-11.04	LP_N^+ $9a_{1g}$	-11.42	LP_N^+ $9a_{1g}$	a_1
7 π	$1b_{3g}$	-12.02	π $1b_{3g}$	-12.87	LP_N^+ $6b_{1g}$	-12.21	π $1b_{3g}$	-12.87	π $1b_{3h}$	-12.58	π $1b_{3g}$	a_2
8 LP_N^+	$6b_{1g}$	-13.05	LP_N^+ $6b_{1g}$	-12.91	π $1b_{3g}$	-12.71	LP_N^+ $6b_{1g}$	-13.38	LP_N^- $5b_{1g}$	-13.17	π $1b_{2g}$	b_1
4 π	$1b_{2g}$	-13.72	π $1b_{2g}$	-14.76	π $1b_{2g}$	-13.84	π $1b_{2g}$	-13.78	π $1b_{2g}$	-13.61	LP_N^- $5b_{1g}$	b_2
6	$7b_{3u}$	-14.61	$7b_{3u}$	-15.42	$7b_{3u}$	-14.89	$7b_{3u}$	-14.29	$6b_{1g}$	-14.26	$6b_{1g}$	b_2
2	$5b_{1g}$	-15.18	$5b_{1g}$	-15.91	$5b_{1g}$	-15.48	$5b_{1g}$	-14.71	$7b_{3u}$	-14.56	$7b_{3u}$	a_1
5	$7b_{2u}$	-16.41	$7b_{2u}$	-17.19	$7b_{2u}$	-16.46	$1b_{1u}$	-16.38	$7b_{2u}$	-16.33	$7b_{2u}$	b_2
8 π	$1b_{1u}$	-16.44	$1b_{1u}$	-17.30	π $1b_{1u}$	-16.85	$7b_{2u}$	-16.89	π $1b_{1u}$	-16.37	π $1b_{1u}$	b_1
2	$6b_{3u}$	-16.98	$6b_{3u}$	-17.69	$6b_{3u}$	-17.40	$6b_{3u}$	-16.92	$6b_{3u}$	-16.85	$6b_{3u}$	a_1
1	$6b_{2u}$	-17.32	$6b_{2u}$	-18.22	$6b_{2u}$	-17.78	$6b_{2u}$	-17.09	$6b_{2u}$	-17.03	$6b_{2u}$	b_2
1	$8a_{1g}$	-18.15	$8a_{1g}$	-18.79	$8a_{1g}$	-18.43	$8a_{1g}$	-18.21	$8a_{1g}$	-18.14	$8a_{1g}$	a_1
3	$7a_{1g}$	-19.53	$7a_{1g}$	-20.14	$7a_{1g}$	-19.85	$7a_{1g}$	-19.57	$7a_{1g}$	-19.46	$5b_{3u}$	a_1
9	$4b_{1g}$	-20.26	$4b_{1g}$	-21.13	$5b_{3u}$	-20.85	$5b_{3u}$	-20.01	$5b_{3u}$	-20.12	$7a_{1g}$	a_1
5	$5b_{3u}$	-20.51	$5b_{3u}$	-21.53	$4b_{1g}$	-21.38	$4b_{1g}$	-20.33	$4b_{1g}$	-20.45	$4b_{1g}$	b_2
9	$6a_{1g}$	-23.33	$6a_{1g}$	-23.96	$6a_{1g}$	-23.78	$6a_{1g}$	-23.12	$6a_{1g}$	-23.19	$6a_{1g}$	a_1
8	$5b_{2u}$	-24.45	$5b_{2u}$	-24.81	$5b_{2u}$	-24.76	$5b_{2u}$	-23.89	$5b_{2u}$	-24.23	$5b_{2u}$	b_2
4	$4b_{3u}$	-25.46	$4b_{3u}$	-25.66	$4b_{3u}$	-25.63	$4b_{3u}$	-25.21	$4b_{3u}$	-25.47	$4b_{3u}$	a_1
1	$3b_{1g}$	-28.28	$3b_{1g}$	-28.94	$3b_{1g}$	-28.78	$3b_{1g}$	-28.03	$3b_{1g}$	-28.21	$3b_{1g}$	b_2
9	$5a_{1g}$	-29.94	$5a_{1g}$	-29.75	$5a_{1g}$	-29.61	$5a_{1g}$	-28.59	$3b_{3u}$	-28.83	$5a_{1g}$	a_1
0	$4b_{2u}$	-31.17	$4b_{2u}$	-32.50	$4a_{1g}$	-32.38	$4a_{1g}$	-31.65	$4b_{3u}$	-31.83	$3b_{3u}$	a_1
9	$4a_{1g}$	-32.66	$4a_{1g}$	-33.32	$4b_{2u}$	-33.40	$4b_{2u}$	-33.31	$5a_{1g}$	-33.85	$4b_{2u}$	b_2
0	$3a_{1g}$	-37.58	$3a_{1g}$	-36.67	$3a_{1g}$	-36.74	$3a_{1g}$	-35.86	$4a_{1g}$	-36.29	$4a_{1g}$	a_1
2		-306.66		-307.80		-306.17		-307.27		-306.49		a_1
3		-307.71		-307.98		-306.34		-307.27		-306.50		b_2
3		-306.82		-308.01		-306.45		-207.37		-306.57		a_1
9		-306.88		-308.02		-306.79		-307.37		-306.59		b_2
4		-307.14		-308.34		-306.90		-308.46		-306.67		b_2
6		-307.21		-309.21		-307.73		-308.46		-307.71		a_1
1		-307.55		-309.22		-307.87		-308.85		-307.75		b_2
8		-307.60		-309.65		-307.92		-308.85		-307.79		a_1
5		-425.22		-424.28		-424.10		-424.35		-424.86		a_1
2		-425.38		-424.40		-424.18		-424.35		-424.94		b_2

rent D_2h Symmetry

Table (37) contd Orbital Energies (eV)

1,5-Diazanaphthalene				1,6-Diazanaphthalene				1,7-Diazanaphthalene			
MB		DZ		MB		DZ		MB		DZ	
	*AS	ε_i	*AS	ε_i	*AS	ε_i	*AS	ε_i	*AS	ε_i	*AS
π	$1a_{1u}$	-9.45 π	$1a_{1u}$	-9.31 π	$1a_{1u}$	-8.94 π	$1a_{1u}$	-9.29 π	$1a_{1u}$	-8.89 π	$1a_{1u}$
π	$2b_{1u}$	-9.68 π	$2b_{1u}$	-10.61 π	$2b_{1u}$	-10.16 π	$2b_{1u}$	-10.60 π	$2b_{1u}$	-10.15 π	$2b_{1u}$
LP_N^+	$9a_{1g}$	-10.89 LP_N^+	$9a_{1g}$	-11.32 LP_{N1}	$9a_{1g}$	-11.45 LP_{N1}	$9a_{1g}$	-11.07 LP_{N1}	$9a_{1g}$	-11.28 LP_{N1}	$9a_{1g}$
LP_N^-	$7b_{3u}$	-11.96 π	$1b_{3g}$	-11.55 LP_{N2}	$6b_{1g}$	-11.72 LP_{N2}	$6b_{1g}$	-11.86 LP_{N2}	$6b_{1g}$	-11.98 LP_{N2}	$6b_{1g}$
π	$1b_{3g}$	-12.42 LP_N^-	$7b_{3u}$	-12.56 π	$1b_{3g}$	-12.02 π	$1b_{3g}$	-12.64 π	$1b_{3g}$	-12.14 π	$1b_{3g}$
π	$1b_{2g}$	-13.83 π	$1b_{2g}$	-14.39 π	$1b_{2g}$	-13.67 π	$1b_{2g}$	-14.32 π	$1b_{2g}$	-13.87 π	$1b_{2g}$
	$6b_{1g}$	-14.45	$6b_{1g}$	-14.26	$7b_{3u}$	-14.66	$7b_{3u}$	-14.85	$7b_{3u}$	-14.80	$7b_{3u}$
	$5b_{1g}$	-15.75	$5b_{1g}$	-15.86	$7b_{2u}$	-15.85	$7b_{2u}$	-15.68	$7b_{2u}$	-15.62	$7b_{2u}$
	$7b_{2u}$	-16.18	$7b_{2u}$	-16.35	$1b_{1u}$	-16.28	$6b_{3u}$	-16.36	$5b_{1g}$	-16.27	$5b_{1g}$
	$6b_{2u}$	-16.25 π	$1b_{1u}$	-16.90	$6b_{3u}$	-16.31 π	$1b_{1u}$	-16.91 π	$1b_{1u}$	-16.32 π	$1b_{1u}$
π	$1b_{1u}$	-16.55	$6b_{2u}$	-17.18	$5b_{1g}$	-17.11	$5b_{1g}$	-17.16	$6b_{3u}$	-17.08	$6b_{3u}$
	$6b_{3u}$	-17.27	$6b_{3u}$	-17.45	$6b_{2u}$	-17.35	$6b_{2u}$	-17.54	$6b_{2u}$	-17.52	$6b_{3u}$
	$8a_{1g}$	-17.85	$8a_{1g}$	-17.94	$8a_{1g}$	-17.87	$8a_{1g}$	-17.88	$8a_{1g}$	-17.71	$8a_{1g}$
	$7a_{1g}$	-19.71	$7a_{1g}$	-19.65	$4b_{1g}$	-19.64	$7a_{1g}$	-19.73	$7a_{1g}$	-19.77	$7a_{1g}$
	$5b_{3u}$	-20.03	$5b_{3u}$	-20.11	$7a_{1g}$	-20.08	$4b_{1g}$	-20.16	$5b_{3u}$	-20.06	$5b_{3u}$
	$4b_{1g}$	-20.78	$4b_{1g}$	-20.49	$5b_{3u}$	-20.64	$6a_{1g}$	-20.44	$4b_{1g}$	-20.58	$4b_{1g}$
	$6a_{1g}$	-23.32	$6a_{1g}$	-23.34	$6a_{1g}$	-23.43	$5b_{3u}$	-23.33	$6a_{1g}$	-23.42	$6a_{1g}$
	$5b_{2u}$	-24.36	$5b_{2u}$	-24.14	$5b_{2u}$	-24.41	$5b_{2u}$	-24.13	$5b_{2u}$		
	$4b_{3u}$	-24.87	$4b_{3u}$	-24.93	$4b_{3u}$	-25.17	$4b_{3u}$	-24.99	$4b_{3u}$	-24.42	$5b_{2u}$
	$5a_{1g}$	-28.78	$5a_{1g}$	-28.23	$3b_{1g}$	-28.42	$3b_{1g}$	-28.26	$3b_{1g}$	-25.20	$4b_{3u}$
	$3b_{1g}$	-29.73	$3b_{1g}$	-29.69	$5a_{1g}$	-29.91	$5a_{1g}$	-29.40	$5a_{1g}$	-28.45	$3b_{1g}$
	$4b_{2u}$	-30.69	$4b_{2u}$	-30.69	$4b_{2u}$	-30.95	$4b_{2u}$	-30.99	$4b_{2u}$	-29.63	$5a_{1g}$
	$3b_{3u}$	-34.66	$3b_{3u}$	-34.35	$3b_{3u}$	-34.81	$3b_{3u}$	-34.24	$3b_{3u}$	-31.23	$4b_{2u}$
	$4a_{1g}$	-35.79	$4a_{1g}$	-35.4	$4a_{1g}$	-35.77	$4a_{1g}$	-35.47	$4a_{1g}$	-34.69	$3b_{3u}$
		-306.66		-307.33		-306.37		-307.46		-35.83	$4a_{1g}$
		-306.66		-307.62		-306.89		-307.74		-306.64	
		-306.91		-308.05		-306.94		-307.94		-307.09	
		-306.91		-308.08		-307.31		-308.26		-307.11	
		-307.44		-308.22		-307.42		-308.27		-307.25	
		-307.44		-308.44		-307.67		-308.29		-307.33	
		-307.55		-308.58		-307.73		-308.48		-307.38	
		-307.55		-309.01		-307.93		-308.83		-307.49	
		-424.08		-423.84		-424.08		-423.83		-307.78	
		-424.08		-423.86		-424.22		-423.99		-424.11	
										-424.38	

arent D_{2h} Symmetry

Table (37) contd Orbital Energies (eV)

1,5-Diazanaphthalene				1,6-Diazanaphthalene				1,7-Diazanaphthalene			
MB		DZ		MB		DZ		MB		DZ	
	*AS	ε_i	*AS	ε_i	*AS	ε_i	*AS	ε_i	*AS	ε_i	*AS
π	$1a_{1u}$	-9.45 π	$1a_{1u}$	-9.31 π	$1a_{1u}$	-8.94 π	$1a_{1u}$	-9.29 π	$1a_{1u}$	-8.89 π	$1a_{1u}$
π	$2b_{1u}$	-9.68 π	$2b_{1u}$	-10.61 π	$2b_{1u}$	-10.16 π	$2b_{1u}$	-10.60 π	$2b_{1u}$	-10.15 π	$2b_{1u}$
P_N^+	$9a_{1g}$	-10.89 LP_N^+	$9a_{1g}$	-11.32 LP_{N1}	$9a_{1g}$	-11.45 LP_{N1}	$9a_{1g}$	-11.07 LP_{N1}	$9a_{1g}$	-11.28 LP_{N1}	$9a_{1g}$
P_N^-	$7b_{3u}$	-11.96 π	$1b_{3g}$	-11.55 LP_{N2}	$6b_{1g}$	-11.72 LP_{N2}	$6b_{1g}$	-11.86 LP_{N2}	$6b_{1g}$	-11.98 LP_{N2}	$6b_{1g}$
π	$1b_{3g}$	-12.42 LP_N^-	$7b_{3u}$	-12.56 π	$1b_{3g}$	-12.02 π	$1b_{3g}$	-12.64 π	$1b_{3g}$	-12.14 π	$1b_{3g}$
π	$1b_{2g}$	-13.83 π	$1b_{2g}$	-14.39 π	$1b_{2g}$	-13.67 π	$1b_{2g}$	-14.32 π	$1b_{2g}$	-13.87 π	$1b_{2g}$
	$6b_{1g}$	-14.45	$6b_{1g}$	-14.26	$7b_{3u}$	-14.66	$7b_{3u}$	-14.85	$7b_{3u}$	-14.80	$7b_{3u}$
	$5b_{1g}$	-15.75	$5b_{1g}$	-15.86	$7b_{2u}$	-15.85	$7b_{2u}$	-15.68	$7b_{2u}$	-15.62	$7b_{2u}$
	$7b_{2u}$	-16.18	$7b_{2u}$	-16.35	$1b_{1u}$	-16.28	$6b_{3u}$	-16.36	$5b_{1g}$	-16.27	$5b_{1g}$
	$6b_{2u}$	-16.25 π	$1b_{1u}$	-16.90	$6b_{3u}$	-16.31 π	$1b_{1u}$	-16.91 π	$1b_{1u}$	-16.32 π	$1b_{1u}$
π	$1b_{1u}$	-16.55	$6b_{2u}$	-17.18	$5b_{1g}$	-17.11	$5b_{1g}$	-17.16	$6b_{3u}$	-17.08	$6b_{3u}$
	$6b_{3u}$	-17.27	$6b_{3u}$	-17.45	$6b_{2u}$	-17.35	$6b_{2u}$	-17.54	$6b_{2u}$	-17.52	$6b_{3u}$
	$8a_{1g}$	-17.85	$8a_{1g}$	-17.94	$8a_{1g}$	-17.87	$8a_{1g}$	-17.88	$8a_{1g}$	-17.71	$8a_{1g}$
	$7a_{1g}$	-19.71	$7a_{1g}$	-19.65	$4b_{1g}$	-19.64	$7a_{1g}$	-19.73	$7a_{1g}$	-19.77	$7a_{1g}$
	$5b_{3u}$	-20.03	$5b_{3u}$	-20.11	$7a_{1g}$	-20.08	$4b_{1g}$	-20.16	$5b_{3u}$	-20.06	$5b_{3u}$
	$4b_{1g}$	-20.78	$4b_{1g}$	-20.49	$5b_{3u}$	-20.64	$6a_{1g}$	-20.44	$4b_{1g}$	-20.58	$4b_{1g}$
	$6a_{1g}$	-23.32	$6a_{1g}$	-23.34	$6a_{1g}$	-23.43	$5b_{3u}$	-23.33	$6a_{1g}$	-23.42	$6a_{1g}$
	$5b_{2u}$	-24.36	$5b_{2u}$	-24.14	$5b_{2u}$	-24.41	$5b_{2u}$	-24.13	$5b_{2u}$		
	$4b_{3u}$	-24.87	$4b_{3u}$	-24.93	$4b_{3u}$	-25.17	$4b_{3u}$	-24.99	$4b_{3u}$	-24.42	$5b_{2u}$
	$5a_{1g}$	-28.78	$5a_{1g}$	-28.23	$3b_{1g}$	-28.42	$3b_{1g}$	-28.26	$3b_{1g}$	-25.20	$4b_{3u}$
	$3b_{1g}$	-29.73	$3b_{1g}$	-29.69	$5a_{1g}$	-29.91	$5a_{1g}$	-29.40	$5a_{1g}$	-28.45	$3b_{1g}$
	$4b_{2u}$	-30.69	$4b_{2u}$	-30.69	$4b_{2u}$	-30.95	$4b_{2u}$	-30.99	$4b_{2u}$	-29.63	$5a_{1g}$
	$3b_{3u}$	-34.66	$3b_{3u}$	-34.35	$3b_{3u}$	-34.81	$3b_{3u}$	-34.24	$3b_{3u}$	-31.23	$4b_{2u}$
	$4a_{1g}$	-35.79	$4a_{1g}$	-35.4	$4a_{1g}$	-35.77	$4a_{1g}$	-35.47	$4a_{1g}$	-34.69	$3b_{3u}$
		-306.66		-307.33		-306.37		-307.46		-35.83	$4a_{1g}$
		-306.66		-307.62		-306.89		-307.74		-306.64	
		-306.91		-308.05		-306.94		-307.94		-307.09	
		-306.91		-308.08		-307.31		-308.26		-307.11	
		-307.44		-308.22		-307.42		-308.27		-307.25	
		-307.44		-308.44		-307.67		-308.29		-307.33	
		-307.55		-308.58		-307.73		-308.48		-307.38	
		-307.55		-309.01		-307.93		-308.83		-307.49	
		-424.08		-423.84		-424.08		-423.83		-307.78	
		-424.08		-423.86		-424.22		-423.99		-424.11	
										-424.38	

nt D_2h Symmetry

Table (37) contd. Orbital Energies (eV)

2,7-Diazanaphthalene						
MB			DZ			
ε_i	*AS		ε_i	*AS		C_2V
-9.23	π	$1a_{1u}$	-8.84	π	$1a_{1u}$	a_2
-11.04	π	$2b_{1u}$	-10.61	π	$2b_{1u}$	b_1
-11.21	LP_N^-	$6b_{1g}$	-11.36	LP_N^-	$6b_{1g}$	b_2
-11.91	LP_N^+	$7b_{2u}$	-11.89	π	$1b_{3g}$	a_2
-12.44	π	$1b_{3g}$	-12.03	LP_N^+	$7b_{2u}$	a_1
-14.63		$9a_{1g}$	-14.28	π	$1b_{2g}$	b_1
-14.69	π	$1b_{2g}$	-14.56		$9a_{1g}$	b_2
-15.38		$7b_{3u}$	-15.32		$7b_{3u}$	a_1
-16.90	π	$1b_{1u}$	-16.29	π	$1b_{1u}$	b_1
-17.11		$5b_{1g}$	-16.95		$5b_{1g}$	b_2
-17.22		$6b_{3u}$	-17.21		$6b_{3u}$	a_1
-17.63		$8a_{1g}$	-17.48		$8a_{1g}$	a_1
-18.16		$6b_{2u}$	-18.14		$6b_{2u}$	b_2
-19.87		$7a_{1g}$	-19.92		$7a_{1g}$	a_1
-20.04		$5b_{3u}$	-20.07		$5b_{3u}$	a_1
-20.49		$4b_{1g}$	-20.51		$4b_{1g}$	b_2
-23.41		$6a_{1g}$	-23.52		$6a_{1g}$	a_1
-24.27		$5b_{2u}$	-24.513		$5b_{2u}$	b_2
-25.19		$4b_{3u}$	-25.44		$4b_{3u}$	a_1
-28.21		$3b_{1g}$	-28.41		$3b_{1g}$	b_2
-29.65		$4b_{2u}$	-29.85		$4b_{2u}$	b_2
-31.09		$5a_{1g}$	-21.32		$5a_{1g}$	a_1
-34.61		$3b_{3u}$	-35.08		$3b_{3u}$	a_1
-35.311		$4a_{1g}$	-35.67		$4a_{1g}$	a_1
-307.54			-306.71			
-307.548			-306.71			
-308.135			-306.87			
-308.49			-307.34			
-308.49			-307.54			
-308.49			-307.65			
-308.67			-307.87			
-308.67			-307.87			
-424.01			-424.37			
-424.01			-424.33			

*Apparent D_{2h} Symmetry

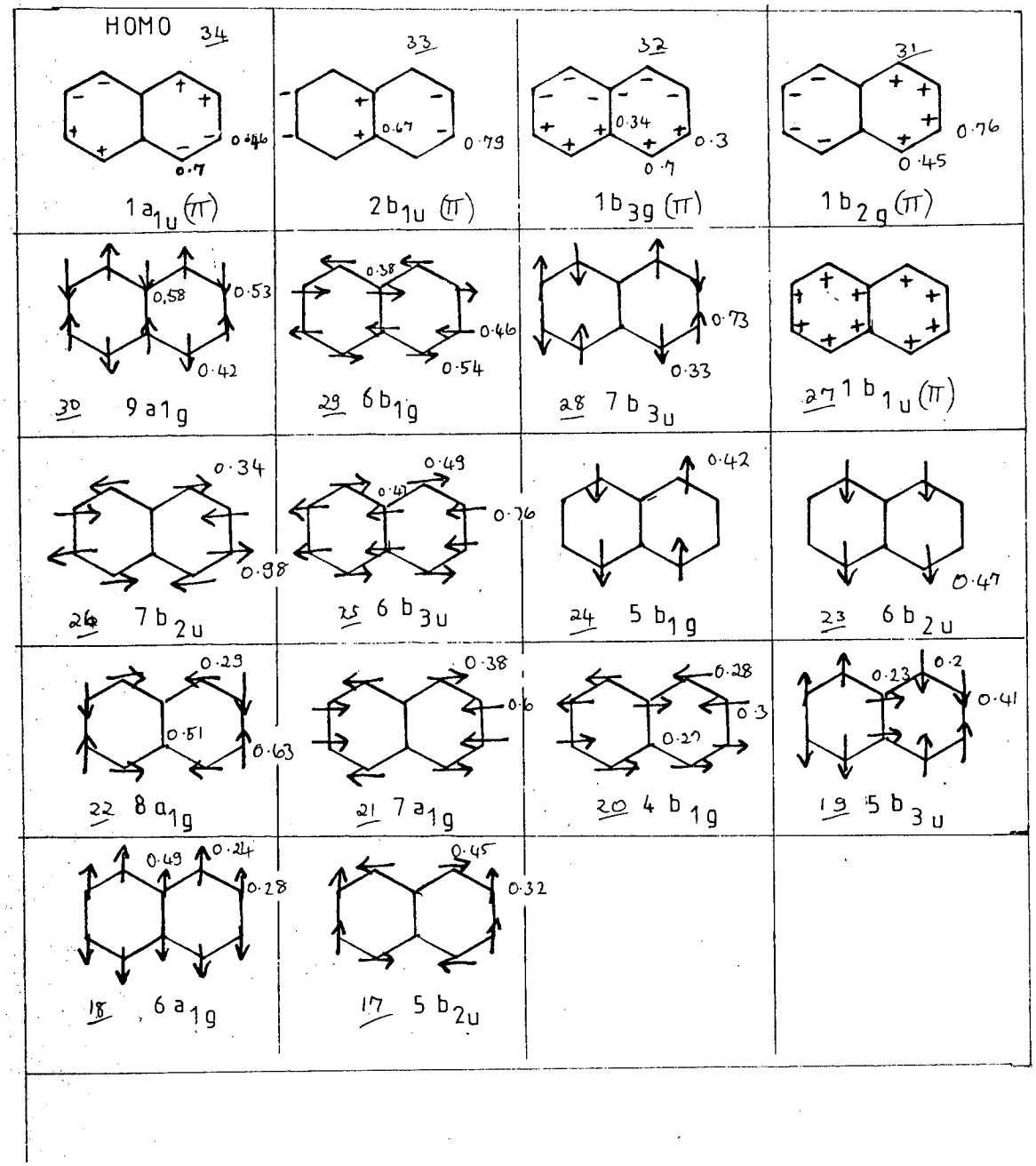

FIG 58 HOMOS OF NAPHTHALENE AND THIER SYMMETRY TYPES

(The numbers indicate the relative magnitudes of the electron densities at each centre; the direction of the arrows represent the sign of the 'p' orbitals ie → positve 'x', ↑ positve 'y')

The monoazanaphthalenes and diazanaphthalenes must be considered in separate groups (A and B respectively) since the occurrence of delocalized lone pair combinations in the diazanaphthalenes make a comparison of the monoaza and diaza compounds inappropriate.

Group A

The symmetry of the a_{1u} HOMO [see Fig(5%)] is such that introduction of either an α or β nitrogen is at a non nodal position, the former being at a position of higher electron density. Hence it is reasonable to expect a similar perturbation of a_{1u} for both quinoline and isoquinoline, being slightly larger for the former.

The nitrogen is at a node in the $2b_{1u}$ orbital in quinoline, but is at the position of maximum electron density for this orbital in isoquinoline. One, therefore might anticipate the large and small perturbations of $2b_{1u}$ observed for isoquinoline and quinoline respectively.

Similarly the nitrogen in quinoline is at the position of maximum electron density for $1b_{3g}$ and although a β nitrogen is non nodal in this orbital it is at a position of lower electron density. This explains the slightly larger shift of $1b_{3g}$ observed for quinoline from inspection of the orbital energies. A larger shift of $1b_{2g}$ observed for isoquinoline can be interpreted if similar criteria are applied.

Almost monotonic stabilization of the $1b_{1u}$ level is expected and is observed from the orbital energies, since this orbital is nodal only in the molecular plane and has equivalent electron density at each ring centre.

Now inspection of the $C_{10}H_8$ HOMO's (fig 58) shows that the first orbital of suitable symmetry for a LP_N in quinoline is the $9a_{1g}$ level which we would therefore expect to be destabilized, since LP_N levels lie in the 9-12.5 eV region. Similarly for isoquinoline the LP_N level is expected to be of $6b_{1g}$ symmetry since this $C_{10}H_8$ orbital is the first HOMO of suitable symmetry. Inspection of the LP_N for both isomers shows that they do adopt the predicted symmetry orbital. As the $6b_{1g}$ and $9a_{1g}$ levels are almost degenerate in naphthalene and introduction of a (β,α) nitrogen in ($6b_{1g}$,$9a_{1g}$) respectively is at a position of very similar electron density, the destabilization of these levels should be almost the same; this is found to be so upon inspection of the orbital energies.

Group B

Similar shifting of the $1a_{1u}$ orbital is expected for the $\alpha\alpha$ substituted diazanaphthalenes where both nitrogen atoms are introduced at positions of maximum electron density. Similarly a smaller shifting of this π orbital can be anticipated for the (α,β) substituted isomers with one nitrogen at the maximum of the wave and the other non nodal but in a position of smaller amplitude (or lesser electron density), and by analogy the smallest shift might be expected for $\beta\beta$ substitution.

The calculated a_{1u} orbital energies are given below:

Position of 'N' atoms	($C_{10}H_8$)	1,2	1,3	1,6	1,7
$-\varepsilon_i(1a_{1u})$ eV	7.97	8.93	9.18	8.94	8.89

2,3	2,6	2,7	1,5	1,8	1,4	Position of 'N' atoms
9.42	9.03	8.84	9.45	9.48	8.86	$-\varepsilon i\,(1a_{1u})$

And we can see that the predicted trends are, in general, observed but it appears that αα and ββ substitution in the same ring the simple concept of first order perturbation is inadequate for interpretation, and some secondary interaction takes place, probably due to the orbitals having two nodal planes.

No perturbation of the $2b_{1u}$ level is predicted for N substitution in the 1,4-, 1,5-, 1,8- positions since these are nodal and this trend is in evidence from the calculated orbital energies:

Position of 'N' atoms	Naphthalene	1,5	1,4	1,8	1,2	1,3	1,6
$2b_{1u}$ $-\varepsilon_i$ (eV)	8.99	9.76	9.68	9.63	10.18	10.15	10.11

1,7	2,3	2,6	2,7	Position of the 'N' atoms
10.15	10.96	10.93	10.61	$-\varepsilon_i\,(2b_{1u})$ eV

A medium perturbation is expected for molecules with one nitrogen nodal and the other in the β position of maximum amplitude whereas for two β nitrogens a large perturbation

is expected. Again these trends are in evidence from the orbital energies (see above), and hence the simple perturbation interpretation works well.

For the $1b_{3g}$ level, with one nodal plane parallel to the molecular axis, similar perturbation is expected and found for the (2,3), (2,6), 2,7) ββ isomers. By analogy we might expect that for αα substituted isomers the perturbation would be similar, but observation of the calculated results show that the shift for 1,4-diazanaphthalene is significantly larger than for the 1,5- and 1,8-isomers (which have similar shifts). Comparable shifts are found (see below) for the unsymmetrical isomers (with both α and β nitrogen) as would be expected.

Again the simple perturbation concept breaks down for the (1,4) isomer, and it is interesting to note that this orbital like the $1a_{1u}$ orbital where the (1,4) and (2,3) isomers were exceptional, has a node parallel to the long molecular axis.

Position of 'N' atoms	Naphthalene	1,2	1,3	1,6	1,7
$-\varepsilon_i(b_{3g})$ eV	10.63	12.02	12.21	12.02	12.14

1,4	1,5	1,8	2,3	2.6	2,7	Position of 'N' atoms
12.58	11.96	12.15	11.91	11.79	11,89	$-\varepsilon_i(b_{3g})$ eV

The $1b_{2g}$ orbital has one nodal plane perpendicular to the long molecular axis with maximum electron density at the β positions.

We would therefore expect maximum perturbation for N substitution at two β positions, with smaller perturbations for α,β substitution and α,α substitution . The orbital energies given below, from Table (37), do show the larger perturbation for the β,β substituted isomers, with the smallest shift for 1,4-diazanaphthalene.

Position of 'N' atoms	$C_{10}H_8$	1,2	1,3	1,6	1,7	1,4	1,5
$-\varepsilon_i(1b_{2g})$ eV	12.41	13.72	13.84	13.67	13.87	13.17	13.83

1,8	2,3	2,6	2,7	Position of 'N' atoms
13.62	14.14	14.42	14.28	$-\varepsilon_i(1b_{2g})$ eV

The inner $1b_{1u}$ level is shifted almost monotonically for all diaza-isomers which is expected since the orbital is nodal in the plane of the molecule.

Position of 'N' atoms	$C_{10}H_8$	1,2	1,3	1,4	1,5	1,6	1,7
$-\varepsilon_i(1b_{1u})$ eV	14.77	16.44	16.46	16.37	16.25	16.31	16.32

1,8	2,3	2,6	2,7	Positions of 'N' atoms
16.23	16.47	16.35	16.29	$-\varepsilon_i(1b_{1u})$ eV

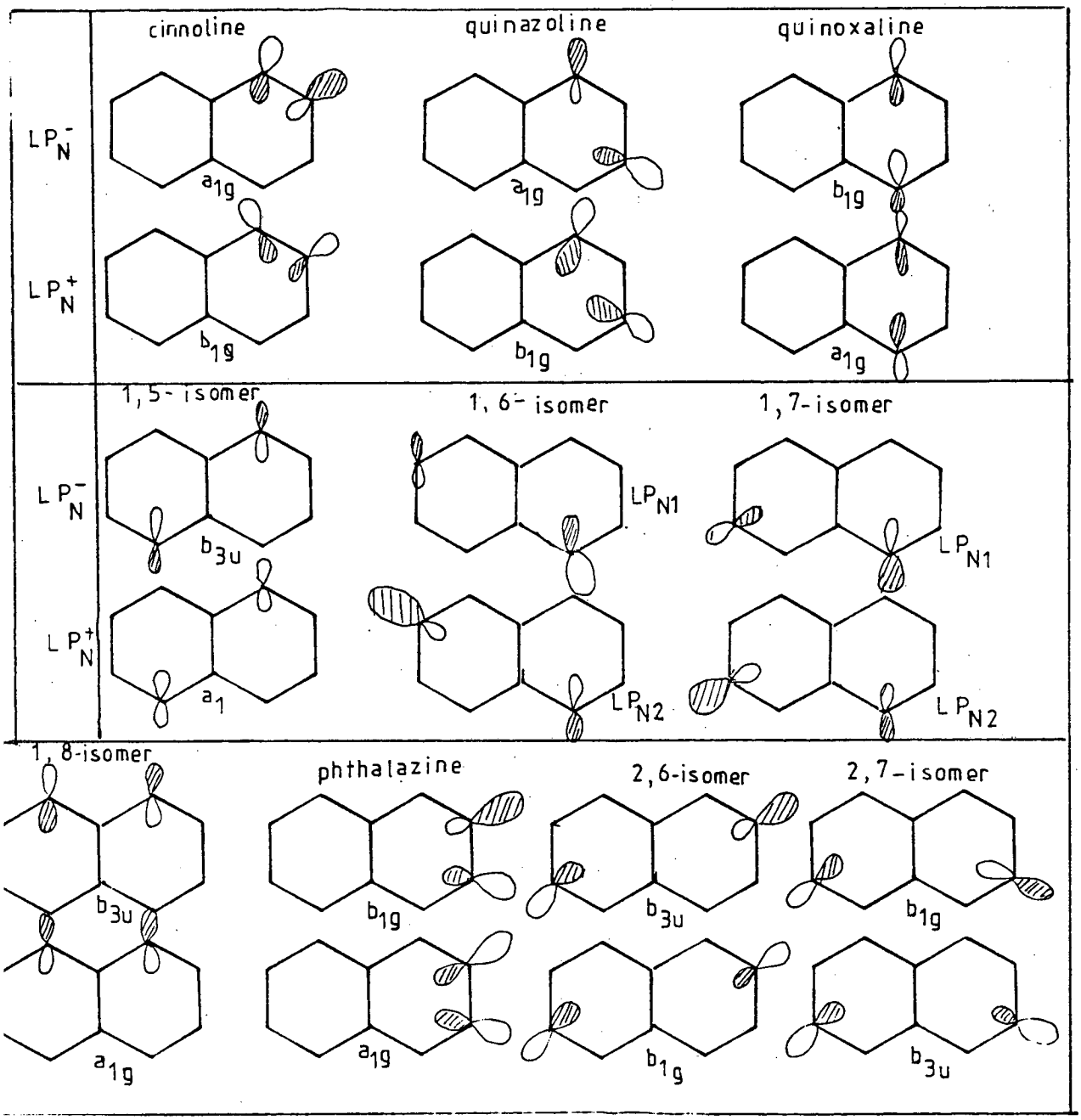

FIG 59 LONE PAIRS FOR THE DIAZANAPHTHALENES

For the lone pair levels (LP_N) replacement of $\gg CH$ by $\gg N:$ will result in destabilization of one σ CH bonding level (of $C_{10}H_8$) per N atom introduced (the destabilization being superimposed on the monotonic stabilization due to introduction of an N atom into the system). Again the extent of destabilization or perturbation of the $C_{10}H_8$ type level depends on whether the N atom is introduced at a position of maximum electron density (i.e. position of maximum amplitude of the wave) or at a node.

The diazanaphthalene lone pair levels are, again, capable as existing as linear combinations,

$$LP_N^+ = aLP_{N1} + bLP_{N2} \qquad \text{symmetric}$$

$$LP_N^- = bLP_{N1} - aLP_{N2} \qquad \text{antisymmetric}$$

with the symmetric combination at higher binding energy and with the coefficients 'a' and 'b' equal for the symmetric isomers. (The very unsymmetric isomers may exist as semi localized lone pairs and analysis of the coefficients in the molecular wave functions must be made for elucidation). Plots of the lone pair orbitals for the diazanaphthalenes and their calculated apparent symmetry types is given in Fig. (59). It can be seen that the lone pair orbitals generally exist as "radial" type orbitals at the nitrogen i.e. with the P_N lobes lying very closely to the external bisector at the N atom. Bearing this in mind, analysis of the first several HOMO σ orbitals of naphthalene indicate that, from first principles one would expect the $9a_{1g}$ orbital to be the first orbital of correct symmetry for the LP_N^+

orbital of the (1,4), (1,8) and (1,5) isomers, and the $7b_{3u}$ ($C_{10}H_8$) orbital to be of correct symmetry for the antisymmetric combination for the (1,5) and (1,8) isomers. The first available $C_{10}H_8$ orbital of correct symmetry type for LP_N^- for 1,4-diazanaphthalene is $5b_{1g}$, which lies to considerably higher binding energy than $9a_{1g}$. Hence we can predict that since, as discussed above, the amount of destabilization of the original $C_{10}H_8$ orbital is dependent on

$$E_{\text{destabilization}} = E_{\substack{\text{original} \\ C_{10}H_8 \\ \text{level}}} + K + \emptyset$$

where K = a factor which depends on electron density or amplitude of wave at position of N substitution.

$\emptyset$ = a +ve amount for LP_N^- and -ve amount for LP_N^+

it is reasonable to expect that:

a) the LP_N^+ level will lie at lower binding energy for the (1,8) and (1,5) isomers since the N perturbation is at a position of higher electron density/maximum amplitude of the wave, in $9a_{1g}$ than in $7b_{3u}$ (which is at higher binding energy in $C_{10}H_8$ anyway).

b) The LP_N^+ level will be at lower binding energy for 1,4-diazanaphthalene because the first orbital of the correct symmetry for LP_N^-, $5b_{1g}$, is at considerably higher binding energy in $C_{10}H_8$.

It is gratifying to note that the calculated LP_N orbital ordering and symmetries is as predicted: Table (37).

For the β,β substituted isomers viz. (2,3), (2,6), (2,7) $6b_{1g}$ provides the first orbital of correct symmetry for an LP_N combination (LP_N^+ for the (2,7) and LP_N^- for the (2,3), (2,6) isomers) with $7b_{2u}$ the next available orbital for the remaining LP_N combination. Inspection of the calculated orbital ordering and symmetries of the LP_N combinations shows that these interpretations are apparently correct with phthalazine providing the exception to the trend. It should however be pointed out that the HOMO σ orbitals of phthalazine are very distorted* and therefore the reported ordering is only approximate.

For the unsymmetric isomers [(1,2), (1,3), (1,6), (1,7)] which have both α and β nitrogens, we cannot predict the symmetries of the lone pair orbitals since the LP_N may not now exist as combinations. Inspection of the eigenvectors show that for αβ N substitution in the same ring the lone pairs exist very nearly as linear combinations whereas for αβ N substitution in different rings they exist as semi localized lone pairs, see fig(59).

In all four unsymmetric isomers the $9a_{1g} < 6b_{1g} < 7b_{3u}$ $C_{10}H_8$ orbital ordering is preserved with the antisymmetric combination at lower binding energy for cinnoline and quinazoline as is the semi localized LP_N in the α position.

It is interesting to note that, as was shown for pyrazine reference [2k] the idea of a 'through bond' interaction proposed by Heilbronner et al [21] where the $LP_N^+ < LP_N^-$ ordering is explained by a symmetry allowed interaction of the LP_N^+ orbital with a low lying σ orbital does not apply here. The effect can be more fundamentally explained by

---

* from the apparent D_{6h} symmetry

Fig: 60

Correlation of the Diazanaphthalene Orbital Energy Levels with Naphthalene

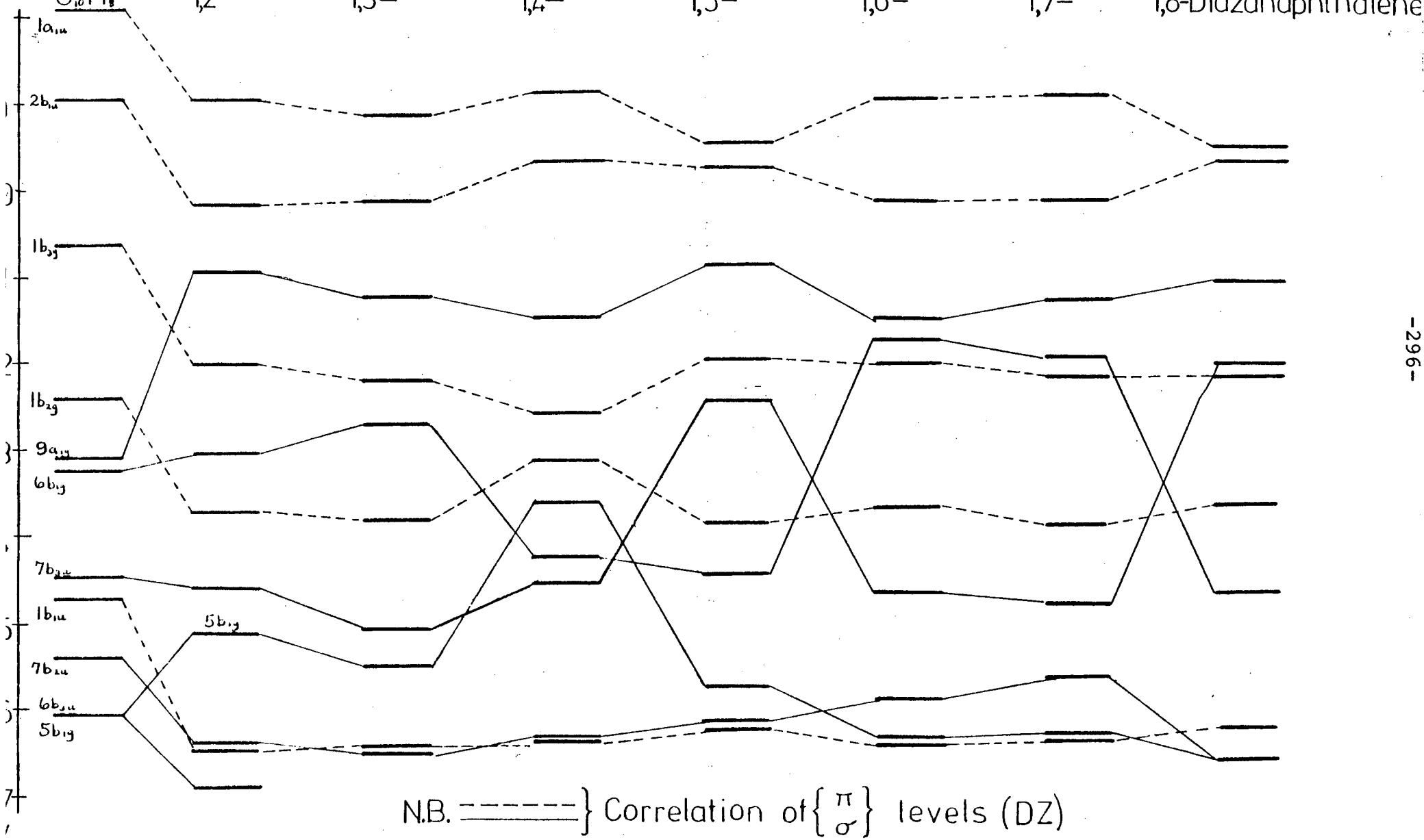

considerations of availability of orbitals, for the LP_N, of the correct symmetry type in the unperturbed parent hydrocarbo

Hence these results, for both LP_N and π orbitals, provide a corollary of the trends observed earlier for the azines and reiterate the fact that nitrogen heterocycles can be considered as perturbations of the parent hydrocarbon.

The correlation of the orbital energy levels for the $(1,N)_{N = 1 \text{ to } 8}$ isomers is shown pictorially in Fig (60) The splitting of the upper π levels ($1a_{1u}$ and $2b_{1u}$) is similar for all isomers except those with $\alpha\alpha$ nitrogens in different rings, whereas the $1b_{3g}$ π level has higher binding energy for the isomers with both nitrogens in the same ring than for those with nitrogens in different rings. Almost uniform stabilization of the $1b_{2g}$ level is observed (except for quino-xaline) and this trend is repeated for the inner b_{1u} level.

The $9a_{1g}$ level appears to be destabilized by an amount which decreases as distance between the heteroatoms increases for isomers with both nitrogens in the same ring and apart from the (1,5) isomer this trend is also found for isomers with nitrogen atoms in different rings.

The correlation of the other σ type orbitals is more complicated, and can be explained by the interpretation of the symmetries and ordering of the LP_N levels as discussed above.

In general the groupings of the orbital energies of the (1,2) and (1,3) isomers are very similar, as are those of the (1,7) and (1,6) unsymmetrical isomers (i.e. for those isomers with semi localized lone pairs; the only difference between the orbital energy levels of the αβ and αβ' isomer (β' represents β substitution in different ring) is in the position of the $6b_{1g}$ level, which is destabilized and lies between the $9a_{1g}$ and $1b_{3g}$ levels in the αβ' isomers.

The αα' isomers have very similar groupings of orbital energies but these are significantly different from those of 1,4-diazanaphthalene (αα substituted) for which no αα isomer exists for comparison.

FIG 61

PHOTOELECTRON SPECTRA

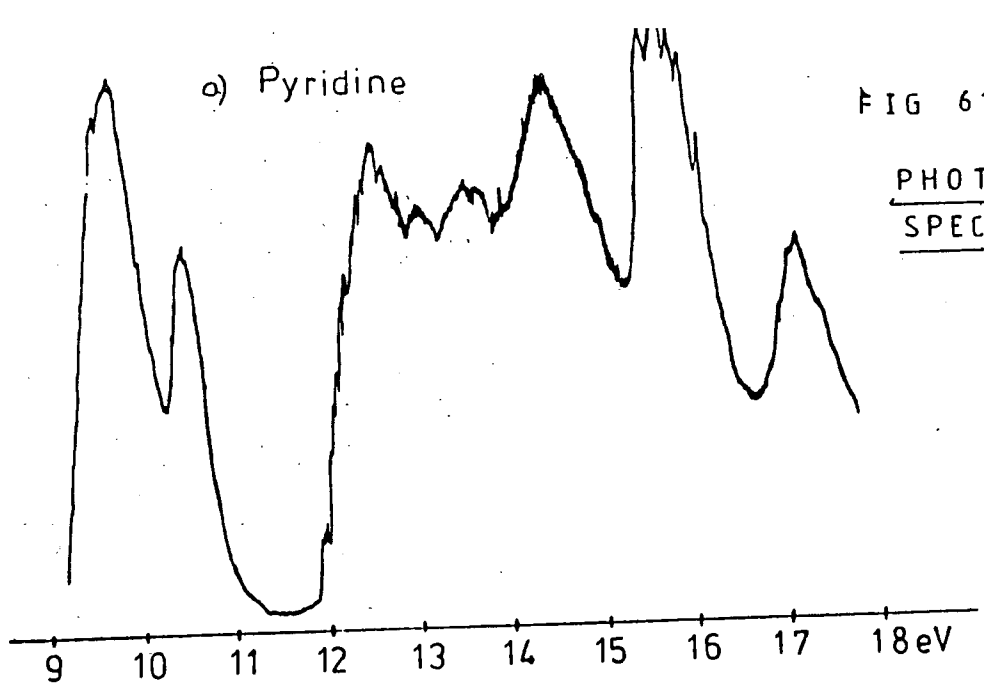

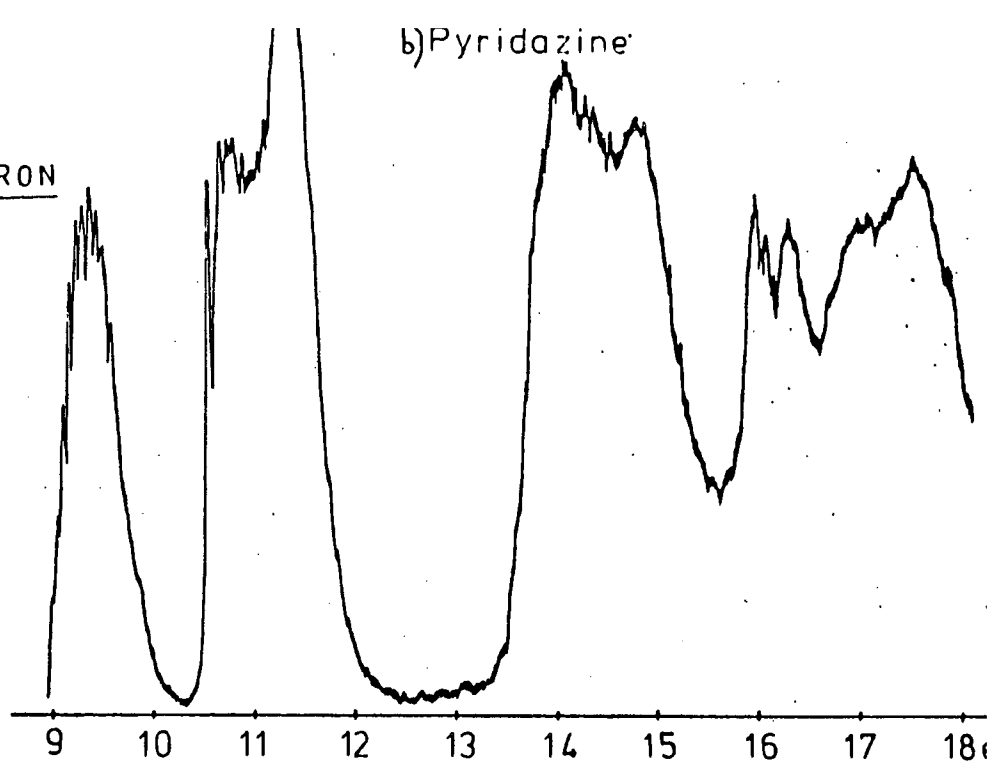

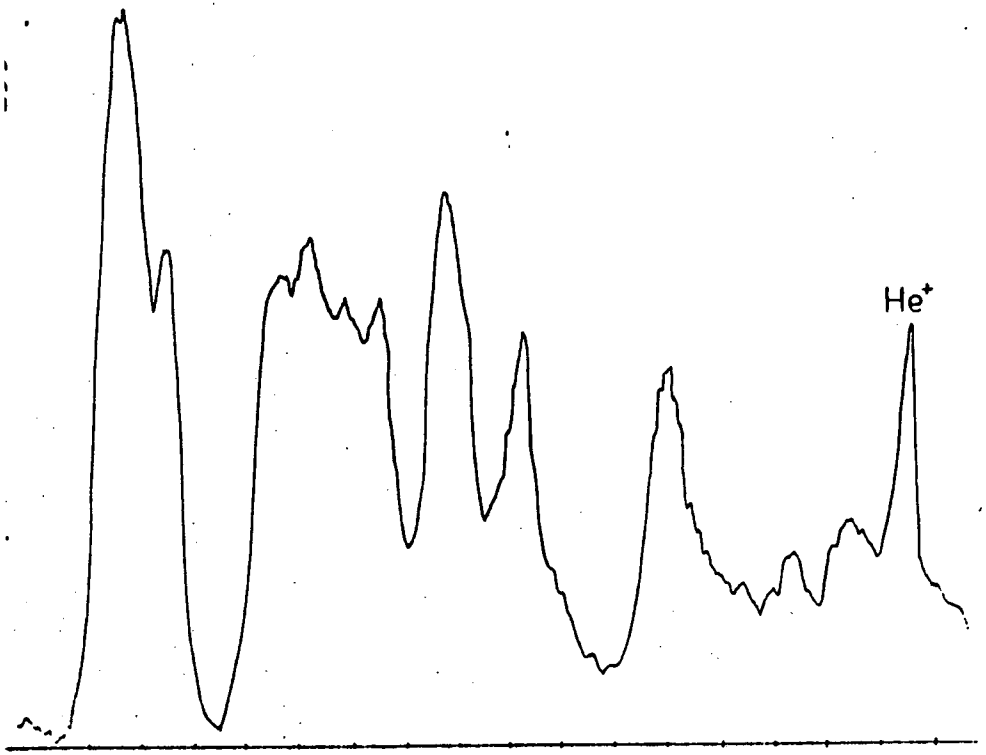

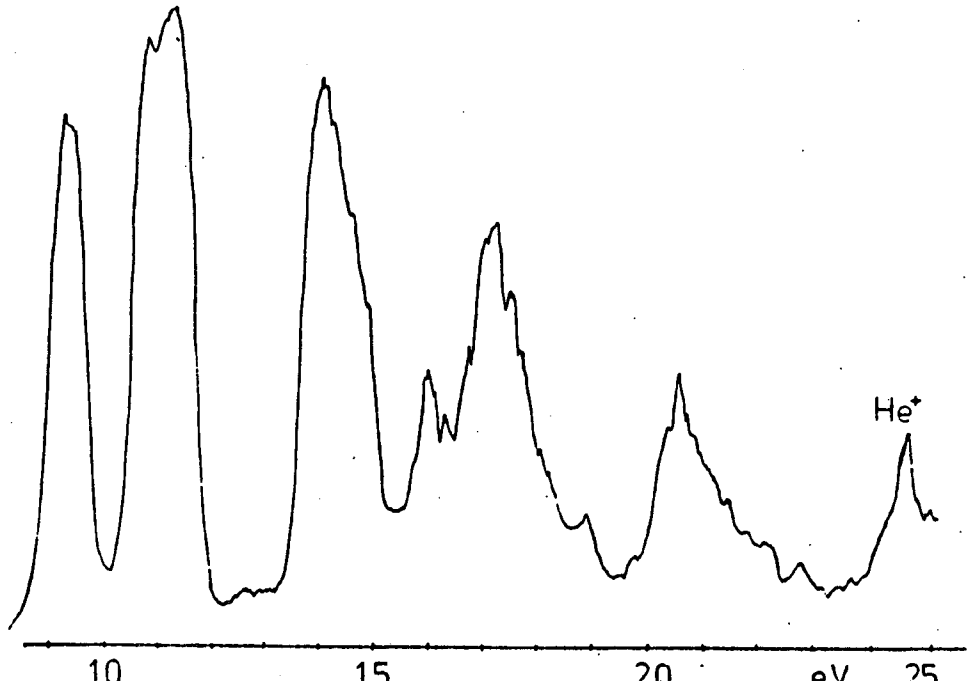

FIG. 61 (CONT)

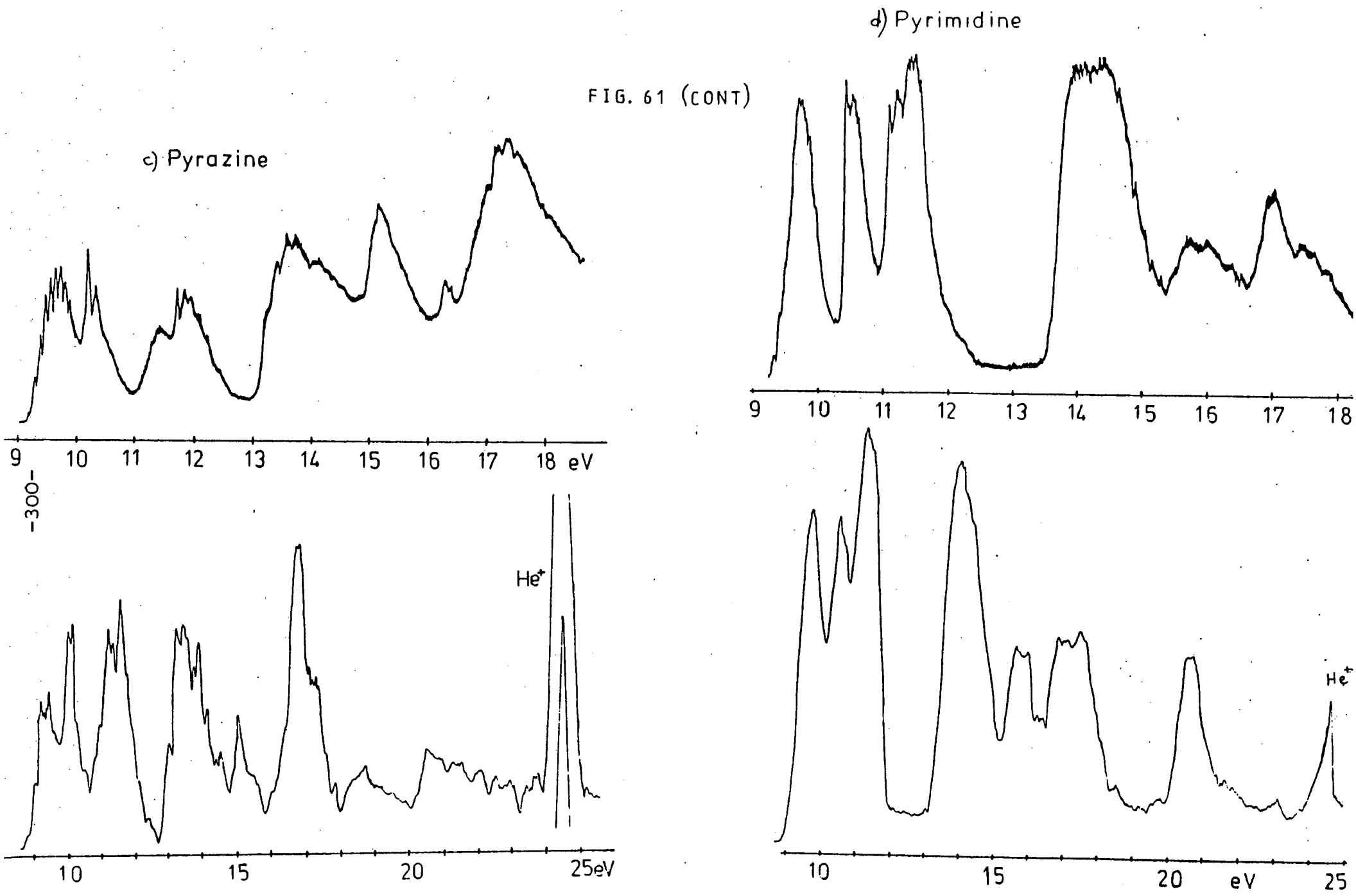
c) Pyrazine
9 10 11 12 13 14 15 16 17 18 eV
-300-
He+
10 15 20 25eV
d) Pyrimidine
9 10 11 12 13 14 15 16 17 18
He+
10 15 20 eV 25

FIG 61 (CONT)

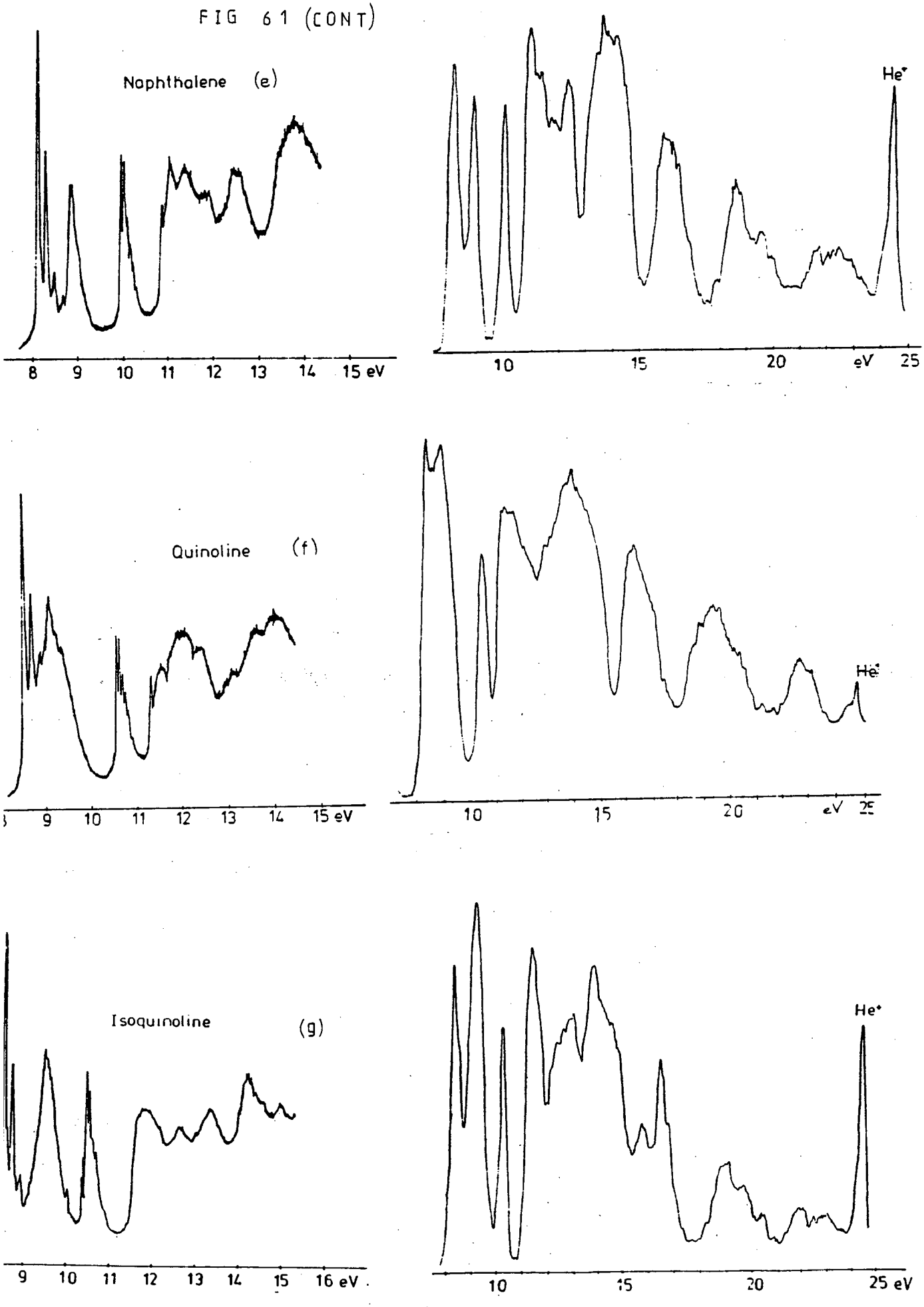
Naphthalene (e)
8 9 10 11 12 13 14 15 eV
He*
10 15 20 eV 25
Quinoline (f)
9 10 11 12 13 14 15 eV
He*
10 15 20 eV
Isoquinoline (g)
9 10 11 12 13 14 15 16 eV
He*
10 15 20 25 eV

FIG. (6 1) CONT

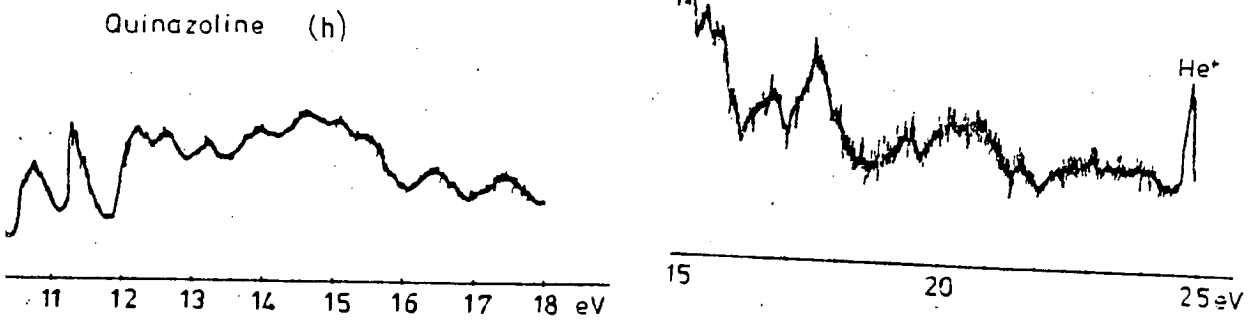
Quinazoline (h)
He+
11 12 13 14 15 16 17 18 eV
15 20 25eV

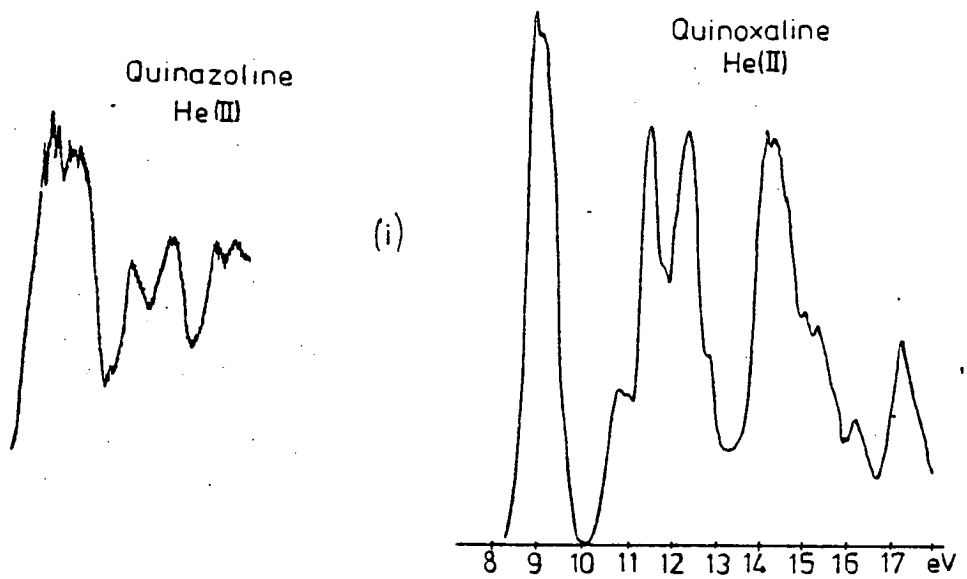
Quinazoline
He(II)
(i)
Quinoxaline
He(II)
8 9 10 11 12 13 14 15 16 17 eV

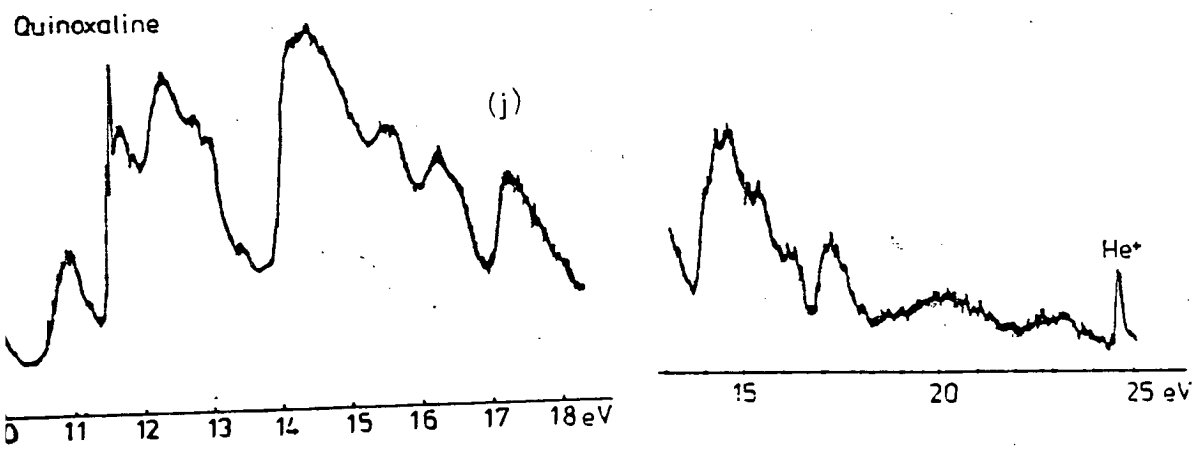
Quinoxaline
(j)
He+
0 11 12 13 14 15 16 17 18eV
15 20 25 eV

FIG 61 (CONT)

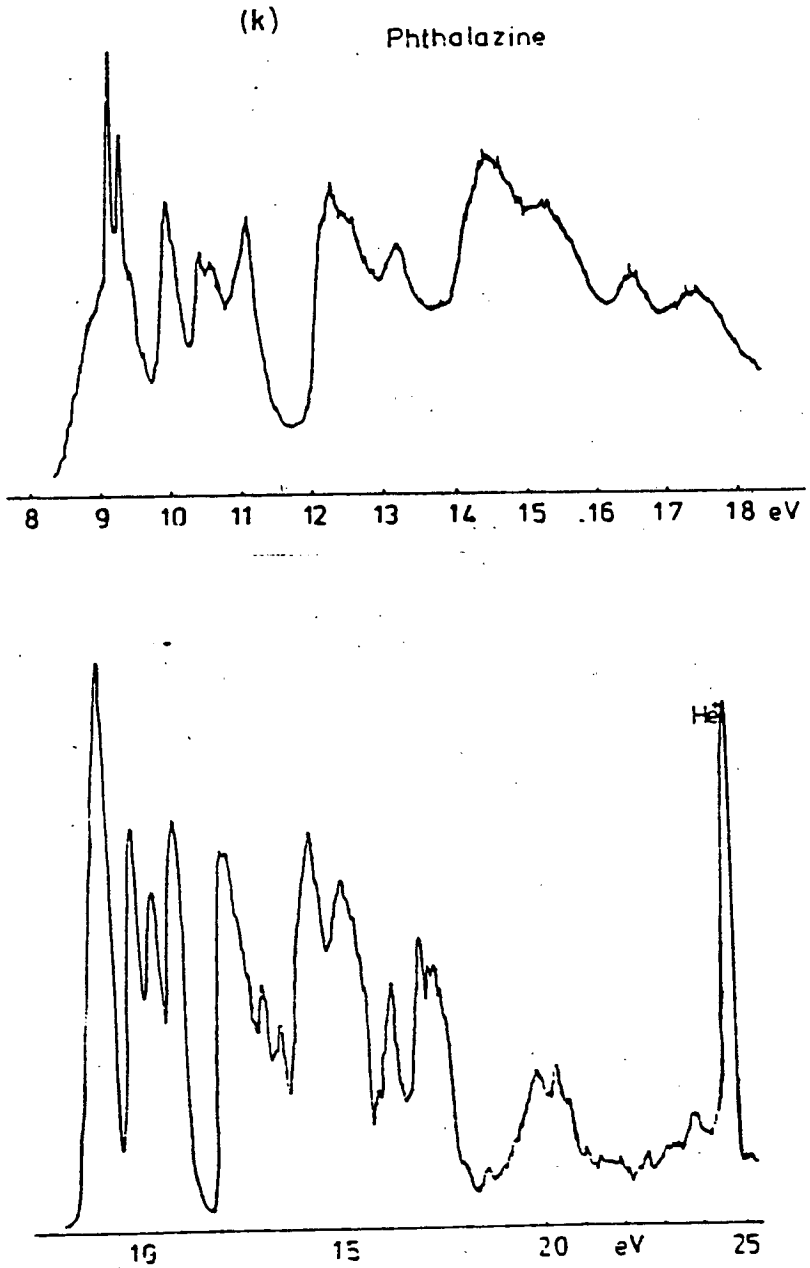

(v) PHOTOELECTRON SPECTRA

He(I) and He(II) photoelectron spectra have been obtained for pyridine, pyrdiazine, pyrimidine, pyrazine, naphthalene, quinoline, isoquinoline, quinoxalene, quinazoline and phthalazine. Figs. (61a to k). Using the Perkin Elmer PS16 spectrometer with Argon and Xenon as internal calibrants. He(II) spectra for all molecules except quinazoline were obtained with the aid of a time averaging computer.

He(I) photoelectron spectra for the azines[18 to 21] and for naphthalene[22,23], quinoline and isoquinoline[22] and the diazanaphthalenes[24] have been previously reported, but He(II) spectra have only been reported for the azines[19 to 21] and naphthalene.[22] In addition ionization potentials for the complete series from electronic transitions observed in the vapour phase have been reported.[25]

Table (38) contains our observed Vertical Ionization potentials (VIP's) and their assignments made using Koopman's Theorem and the calculated orbital energies from Table 37 and also additional information described in more detail for each molecule below.

Azines

General Considerations and Principles

The azines can be considered as a perturbation of the benzene system by replacement of $\rangle\!=\!\langle CH$ by $\rangle\!=\!\langle N:$ Thus there is removal of one σ level of C_6H_6 and replacement by a lone pair (LP_N) nitrogen level or more than one of these for the

Table (3.8) Observed Vertical Ionization Potentials (eV) and their Assignments

Pyridine	Pyridazine	Pyrimidine	Pyrazine
9.6 LP_N $11a_1$ 9.8 π $1a_2$	9.31 LP_N^- $8b_2$	9.71 LP_N^- $7b_2$	9.65 LP_N^+ $6a_{1g}$
10.63 π $2b_1$	10.58 π $2b_1$	10.43 π $2b_1$	10.2 π $1b_{2g}$
	11.09 LP_N^+ $10a_1$	11.19 LP_N^+ $11a_1$	11.37 LP_N^- $5b_{2u}$
12.71 $7b_2$	11.49 π $1a_2$	11.48 π $1a_2$	11.81 π $1b_{3g}$
13.23 π $1b_1$	13.94 $9a_1$	13.98 $10a_1$	13.49 $4b_{1g}$
13.75 $10a_1$	14.39 π $1b_1$	14.01 π $1b_1$	13.97 $1b_{1u}$
14.63 $6b_2$	14.73 $7b_2$	14.34 $6b_2$	15.09 $3b_{3u}$
15.62 $9a_1$	15.85 $6b_2$	15.65 $9a_1$	17.07 $3b_{1g}$
15.99 $5b_2$	17.43 $8a_1$	16.95 $5b_2$	17.52 $3b_{2u}$
17.25 $8a_1$	18.71 $7a_1$	17.41 $8a_1$	18.74 $5a_{1g}$
20.05 $4b_2$	20.38 $6a_1$	20.65 $7a_1$	20.8 $2b_{1g}$
20.49 $7a_1$	21.04 $5b_2$	20.89 $4b_2$	21.00 $4a_{1g}$
22.32 $3b_2$	23.06 $5a_1$	23.2 $6b_1$	22.5 $2b_{3u}$

FIG 62 P.E.S OF BENZENE

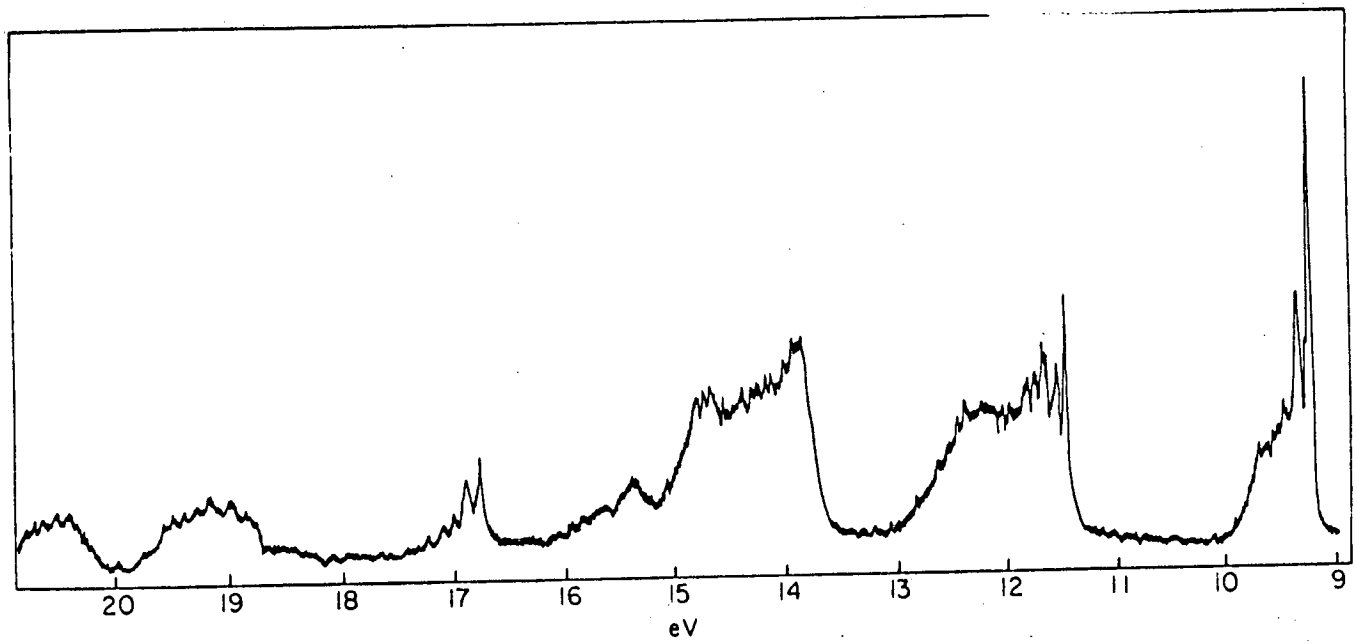

multiaza-substituted compounds. For example, with each of the diazines we can expect linear combinations of LP_N.

a) $LP_{N1} + LP_{N2}$ symmetric.

b) $LP_{N1} - LP_{N2}$ antisymmetric.

In benzene the highest occupied levels are the (π) e_{1g} degenerate pair. Clearly in pyridine the perturbation wrought by the N will lead to a splitting of these into the symmetric π level (b_1) and the antisymmetric (a_2). From first principles we can expect the level of splitting of the e_{1g}-C_6H_6 type levels in the azines to vary with the relative portions of the N atoms. For instance in pyrazine [see also Fig 57] the N atoms are nodel in $1a_2$ whereas they are at the maximum of electron density of orbital $2b_1$. Hence the perturbation of the benzene e_{1g} level (9.23 eV) will be small for (iii) and large for (iv). These effects have been fully discussed in the literature [2k].

Given that LP_N in simple alkylamines [in the 8 - 11 eV region] (e.g. NH_3 10.85 eV, Me_2NH 8.94 eV Me_3N 8.46 eV) we can expect the two π-levels and the LP_N to lie close to 9-11 eV, or slightly higher when symmetry adapted LP_N occur.

If we consider the photoelectron spectrum of benzene, we see the e_{1g} level (9.23 eV) with a high 0→0 band and weaker progression followed by the e_{2g} (σ) and a_{2u}(π) levels at 11.8 and 12.1 eV respectively.

The envelope of pyridine shows two main bands between 9 and 11 eV with an approximate intensity of 2:1 (low:high binding energy). The principles discussed above would predict the binding energy order of $1a_2$ and LP_N (9.2-9.6 eV), $2b_1$ (ca 10 eV). For pyrimidine, where the N atoms are meta, and in classical organic chemical terms interact the least, we have four bands

in the 9-11.5 eV region to be assigned to two π and two LP_N levels. Here the N atoms are not nodal in either π level so that a shift of $2b_1$ and $1a_2$ to higher binding energy can be expected. However the LP_N levels can be expected to be split (symmetric and antisymmetric), but the degree cannot be determined from first principles. There is some evidence of vibrational coupling (high O→O band) on the second and third IP's which are hence probably π levels.

For pyridazine and pyrazine the spectra are more complicated and hence assignment should be made using other available techniques, as described below.

Pyridine Fig. (61a)

For this molecule the MB calculation gives an orbital ordering of $\pi(a_2)$, $\pi(b_1)$, $LP_N(a_1)$, $\sigma(b_2)$ with the b_1 and a_1 levels almost degenerate. The DZ calculation splits these levels leaving the orbital ordering unchanged.

However, investigation of peak intensities in the photoelectron spectrum of pyridine indicates that the first peak corresponds to ejection of an electron from a $\sigma(LP_N)$ type orbital since its intensity and hence cross section increases under He(II) conditions (See Fig. 61a).

The first five IP's of the previously reported spectrum,[18] assigned using the results of HMO calculations, gave orbital ordering of $n(a_1)$, $\pi(a_2)$, $\pi(b_1)$, $\sigma(b_2)$. Other semi empirical calculations are in agreement with this[1,2] as does a recent Greens function/ab initio many body calculation.[3] Due to the

discrepancy in the results, Double Zeta Δ SCF type calculations on the radical cation of pyridine, forcing different singly occupied cationic states by virtue of RHF formalism were performed. (See section 3B). For these calculations the geometry of the cation was assumed to be the same as for the ground state, which was used as the starting point for the open shell calculations. The results of this investigation are given below:

ΔSCF (eV)	orbital type
8.58	a_1
9.053	a_2
9.81	b_1
13.52	b_2

These results support the orbital ordering proposed earlier and indicated by the P.E.S. peak intensity investigations, and not that predicted by Koopman's Theorem. This indicates that Koopman's Theorem should not be taken per se (particularly when the orbital energies are close) even when used in conjunctio with very high quality calculations, and points to the necessity of ΔSCF calculations to check orbital ordering. However the ionization energies predicted by the ΔSCF procedure are no closer to the VIP's experimentally observed. This is probably due to the ground state geometry used for the open shell calculations not being a sufficiently accurate approximation for the geometry of the cation. The ΔSCF

procedure, however, is extremely costly in terms of CPU since convergence in open shell calculations such as these is very slow, and becomes increasingly difficult (and hence costly) for the calculations corresponding to removal of electrons from inner orbitals (i.e. those increasingly more strongly bound). Therefore such calculations should be embarked upon only after careful consideration of the CPU required and CPU available. It is also interesting to note that this shows that comparison of He(I)/He(II) peak intensities in P.E.S. can indeed be usefully employed for assignment of lone pair type peaks.

The IP's from 13.23 eV to 23 eV have been tentatively assigned using Koopman's Theorem and the groupings of the experimental IP's and orbital energies matched well. Despite the scepticism of the validity of KT evident in ref. [3] it should be noted that our assignment of these peaks does in fact compare favourably with their's. For Pyridazine, Fig. (61 b) again the MB and DZ calculations give differing orbital orderings, although the former gives almost degenerate $1a_2$ and $8b_2$ orbital energies corresponding to a destabilization of the LP_N^- orbital from MB to DZ. However the relative increase in intensity of the first IP and peak at 11.09 eV under He(II) conditions indicates their 'N' type character. Indeed the reported assignments of $LP_N^-(b_2)$, $\pi(a_2)$, $LP_N^+(a_1)$, $\pi(b_1)$ [1,2] seem resonable in the light of the intensity results, and our assignment has been made accordingly.

The remaining IP's have been assigned using Koopman s'Theorem and the orbital energies obtained from the DZ calculation. Again despite the discrepancy in the ordering of ionic states predicted by our calculations and Koopman s'Theorem, and the results of Von Niessen et al [3] for the first four IP's, our assigment of the remaining peaks compares favourably . The groupings of experimental IP's and calculated orbital energies correlate well.

Pyrimidine Fig.(61 d)

Since the orbital ordering calculated by the two basis sets differ, a comparison of the relative peak intensities was used to obtain an ordering of LP_N^- (b_2), $\pi(b_1)$, $LP_N^+(a_1)$, $\pi(a_2)$ which is in fact the ordering of the ionic states reported in the literature,[1,12] and is that used here. The remaining IP's have been assigned using Koopman s' Theorem and the DZ orbital energies and again there is reasonable agreement with the assignment given in ref.[27]

Pyrazine Fig.(61c)

Due to the poor quality of the He(II) spectrum obtained, no significant conclusions can be drawn as to the relative intensities of the peaks. The calculated orbital ordering again differs for the two basis sets, although both basis sets show the symmetric lone pair combination has a lower binding energy than the antisymmetric combination. This lone pair ordering which makes pyrazine unique (in this respect) in the azabenzenes has been reported beofre[1,2,3,26,27] although the most recent work[26] again gives different ordering of the ionic states (i.e. LP_N^+, π, $LP_N^-\pi$) than that predicted

Isoquinoline Fig (61g)

Again comparison of the He(I)/He(II) spectra shows an increase in the intensity of the peak at 9.5 eV indicating that it is best assigned as due to electrons from an LP_N type orbital. The MB and DZ calculations, however, give the orbital ordering of the HOMO's as π, $LP_N\pi$ and thus the assignment given by Koopman's Theorem is again questionable. The other reported assignments[22,27] are in agreement with our assignment for the first four IP's from experimental peak intensities, which are adopted in Table (38) the remaining ionization energies being assigned by virtue of Koopman's Theorem and the DZ orbital energies.

Quinazoline Fig (61h)

It is again appropriate to compare spectra of the diaza-substituted compounds with that of naphthalene and by such observation the assignment of the first four IP's is shown to be π, π, LP_N^-, LP_N^+ which is the assignment predicted by Koopman's Theorem and the DZ orbital energies. Comparison of the He(I)/He(II) peak intensities also indicates that this ordering is in fact possible, although the resolution of the He(II) spectrum is not sufficient to clearly indicate whether the peak at 9.34 or 9.75 has increased intensity. Previous work by Heilbronner et al[22] and Spanget-Larsen[27] reports the assignment as π, LP_N^-, π, LP_N^+, π. Therefore there is an added degree of uncertainty here in the assignment for the second and third IP's. The peaks from 12.15 eV to 24 eV have been assigned using Koopman's Theorem and the DZ orbital energies.

by our calculations and others [2c,f] and Koopman's Theorem. On the basis of the good agreement between the assignment of Von Niessen et al [3] the spectrum has been assigned as $LP_N^+(a_1)$, $\pi(b_{3g})$, $LP_N^-(b_2)$, $\pi(b_{2g})$, the remaining peaks being assigned using Koopman's Theorem and the calculated orbital energies.

It is interesting to note that the first peaks of both pyrazine and pyridazine are very similar in outline, and although this does not prove that the peaks are due to electrons from the same type of orbital it is probable that both are due to removal of an electron from an LP_N orbital since the 0→0 transition is not the most intense. This indicates that the ionization is accompanied by a large change in interatomic distances, as is reasonable for removal of electron from the 'σ' framework of the molecule.

Also noteworthy is the fact that the IP's of the azines fall into definite bands as is shown in Table (38) , and that there is general stabilization of these upon nitrogen substitution as would be expected. The VIP's given in Table (38) are in extremely good agreement with those reported earlier.[18 to 21]

Naphthalene and the Azanaphthalenes

General Considerations and Principles

The general principles outlined in the previous section for aza substitution in the monocyclic systems again apply, and we can compare the PES of the azanaphthalenes with that of the parent hydrocarbon to obtain an indication of assignment from first principles.

In naphthalene the highest occupied orbitals are the $1a_{1u}$, $2b_{1u}$, $1b_{3g}$ and $1b_{2g}$ π levels and $9a_{1g}(\sigma)$ level shown below

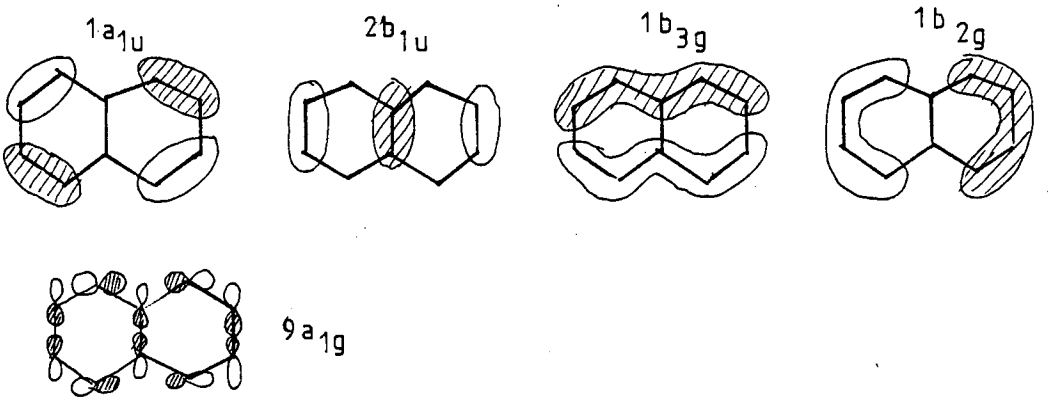

and therefore in quinoline and isoquinoline the perturbation by N will lead to a similar shifting of the $1a_{1u}$ level, since the nitrogen is, in both cases perturbing a position of high electron density. Similarly the $2b_{1u}$ level would be expected to be more stabilized in isoquinoline than in quinoline. This interpretation becomes more complicated for the diaza-naphthalenes where alternative methods must be used for assignments.

However as for the azines we can expect the first five levels, both π and σ (LP_N) levels, to lie within a certain range (8 → 12 eV) in quinoline and isoquinoline, and slightly higher for the diazanaphthalenes where symmetry adapted LP_N occur. Also comparison of the spectra of all of the aza-naphthalenes with that of naphthalene give evidence of two peaks with a strong (0 → 0) bands, assinged as the la_{1u} and $1b_{3g}$ π levels in naphthalene.

Again the IP's from these spectra can be divided into six distinct bands, see Table (38), the difference between the parent hydrocarbon and the mono- and di-azasubstituted compounds being in the number of IP's falling in the first four bands. Also there is a general stabilization of the first IP, and indeed the positions of the bands, upon nitrogen substitution in both α and β positions in the parent compound. This stabilization increases for the third, fourth and fifth bands as the number of nitrogens increases. As with the azines there is good agreement of our experimental IP's and those reported in the literature. However the calculations reported in the literature on the bicyclic series of molecules are far fewer than for the azines; the only ones available for comparison are semi empirical[23,24,27], with no reported sophisticated calculations such as the Greens Function calculations for the azines. Therefore the only methods available for interpretation, other than from general considerations, are thus Koopman's Theorem and relative peak intensities.

ΔE_{SCF} calculations on this series of molecules, due to their size, are outside the scope of available resources within the time available for this project.

It should be noted that some difficulty was experienced in actually assigning bands of orbital energies to bands of IP's since in some cases alternative groupings would be equally plausible. However it is felt that our assignment is the most likely, but we do not claim that it is conclusive.

It should be reiterated that these assignments would best be checked by ΔE_{SCF} calculations when facilities become available.

Naphthalene Fig (61e)

The photoelectron spectrum reported earlier[23,24] has been assigned[23,27] and both DZ and MB calculations herein reported give orbital energies and an orbital ordering, which, when used with Koopman's Theorem, provide an assignment in full agreement with that previously reported. This can be seen in Table (38)

Quinoline Fig (61f)

Comparison of the He(I)/He(II) spectra shows conclusively that the intensity of the peak at 9.06 eV increases under He(II) conditions, indicating its LP_N type character. Again Koopman's Theorem does not give the correct ordering but since the lowest energy LP_N and π levels are assigned as experimentally degenerate this discrepancy is not significant. Hence the assignment proposed is $\pi < LP_N < \pi$ and this agrees with the earlier assignment of Heilbronner et al.[22] The remaining IP's have been assigned by virtue of Koopman's Theorem and the DZ orbital energies.

Quinoxaline Fig. (61j)

One might expect that the calculations would give the symmetric lone pair combination of higher orbital energy than the antisymmetric combination as is evidenced by pyrazine which is very similar to quinoxaline, and indeed both MB and DZ calculations show this orbital ordering for the lone pair levels.

Comparison of this PES with that of naphthalene indicates that the first IP, a broad band, is in fact the overlap of the two peaks assigned to orbitals a_{1u}, b_{1u} in Naphthalene, and the peak at 10.00 eV can be assigned to an LP_N orbital since its cross section increases under He(II) conditions (Fig. This assignment for the first three IP's is in fact that predicted by Koopman's Theorem and the DZ orbital energies, which have been used to assign the spectrum. It should be noted, however, that this assignment does not agree with the π, LP_N^-, π, LP_N^+ ordering proposed by Heilbronner.[22]

Phthalazine Fig. (61k)

A rather poor quality He(I) spectrum has been reported and assigned by comparison with that of naphthalene given in reference (28). This assignment for phthalazine gave the first five IP's as LP_N^-, π, π, $LP_N^+\pi$ but comparison of the He(I)/He(II) spectra (Fig. 61k) does not give the same assignment since the relative intensities of peaks at 8.9 and 11 eV increase under He(II) conditions, indicating an LP_N^-, π,π,π,LP_N^+ assignment.

The MB and DZ calculations however, give different orbital orderings, both of which when used with Koopman s' Theorem give assignments which do not agree with experimental evidence. Therefore the assignment indicated by relative peak intensities has been adopted for the first five IP's those remaining being assigned by Koopman s'Theorem and the DZ orbital energies. It should be noted that the orbital energies fall into bands which well match the observed bands of IP's.

Table (39) Calculated and Experimental* Splitting of the LP_N Levels

Molecule	Separation of N atoms (au)	CALCULATED LP_N^+ (eV)	CALCULATED LP_N^- (eV)	CALCULATED $\|\Delta LP_N\|$ (eV)	EXPERIMENTAL LP_N^+ (eV)	EXPERIMENTAL LP_N^- (eV)	EXPERIMENTAL ΔLP_N (eV)
1,2-Diaza-naphthalene	2.48	MB 12.98 DZ 13.05	10.62 10.18	2.36 2.87	(11.05)	(8.90)	(2.15)
1,3-	4.49	MB 12.87 DZ 12.71	11.40 11.24	1.47 1.47	10.67 (10.7)	9.30 (9.5)	1.37 (1.2)
1,4-	5.44	MB 11.04 DZ 11.42	13.38 13.61	2.34 2.19	9.75 (9.30)	11.5 (10.9)	1.75 (1.6)
1,5-	6.95	MB 10.70 10.89	12.34 12.42	1.64 1.53	(9.20)	(10.40)	(1.20)
1,6-	7.83	MB 11.55 DZ 11.72	11.32 11.45	0.23 0.27	(9.90)	(9.50)	(0.4)
1,7-	6.78	MB 11.86 DZ 11.98	11.07 11.28	0.79 0.70	(9.30)	(10.00)	(0.7)
1,8	4.34	MB 11.29 DZ 11.08	12.44 12.04	1.15 0.96	(10.10)	(9.20)	(0.9)
2,3-	2.55	MB 11.17 DZ 10.96	13.24 12.72	2.07 1.76	11.15 (10.60)	8.87 (8.7)	2.28 (1.90)
2,6-	9.51	MB 10.89 DZ 11.40	11.76 12.18	0.87 0.78	(9.4)	(10.00)	(0.6)
2,7-	9.11	MB 11.21 DZ 11.36	11.91 12.03	0.7 0.67	(9.35)	(10.10)	(0.75)

*Experimental values in brackets taken from reference [24]

TABLE (39b) VALUES OF LP_N

molecule		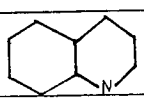	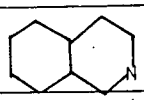
LP_N (eV)	9.6 (11.27)*	9.06 (11.27)	8.47 (11.24)
molecule		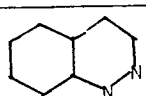	
LP_N^- (eV)	9.31 (11.01)	8.9 (10.62)	
LP_N^+ (eV)	11.04 (13.2)	11.02 (12.98)	
molecule	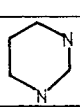	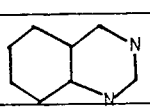	
LP_N^- eV	9.71 (11.43)	9.3 (11.24)	
LP_N^+ eV	11.19 (12.92)	10.67 (12.71)	
molecule	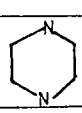	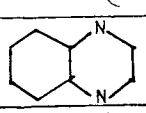	
LP_N^- eV	11.37 (13.33)	11.51 (13.61)	
LP_N^+ eV	9.65 (11.65)	9.75 (11.42)	

* Calculated values in brackets

(vi) Comparison of the Lone Pair Levels

Table (39a) contains a summary of the experimental values of the LP_N combinations for the monocyclic and bicyclic systems studied, and it is immediately obvious that fusion of a benzene ring to the heterocyclic system does not apparently alter the positions of the LP_N levels for the diaza isomers and hence does not alter the splitting of these levels. This indicates that the splitting and hence interaction is predominantly affected by the relative positions of the nitrogen atoms in the structure, a 'through space' interaction. It is interesting that the LP_N level in the mono-aza substituted compounds does indeed shift when a benzene ring is fused to the monocyclic heterocycle (i.e. pyridine), and is dependent on the position of fusion, and this dependence is not apparent for the pyridazine phthalazine cinnoline series where the LP_N levels remain apparently unaffected by addition of the bicyclic system. For the mono azasubstituted isomers a large shift is expected since addition of the second ring radically changes the geometry and symmetry of the original heterocycle.

Splitting of the Lone Pair Levels

One might expect that the interaction or rather splitting of the LP_N of the diazanaphthalenes to vary in some way which is dependent upon the distance between the N atoms. Now although the positions of the LP_N levels in this series of molecules have been reported, [24] the relative splitting of these levels has not been discussed. Therefore we have plotted the LP_N splitting (both theoretical and experimental) v separation of N atoms (from the values given in Table 39b)

Fig 63

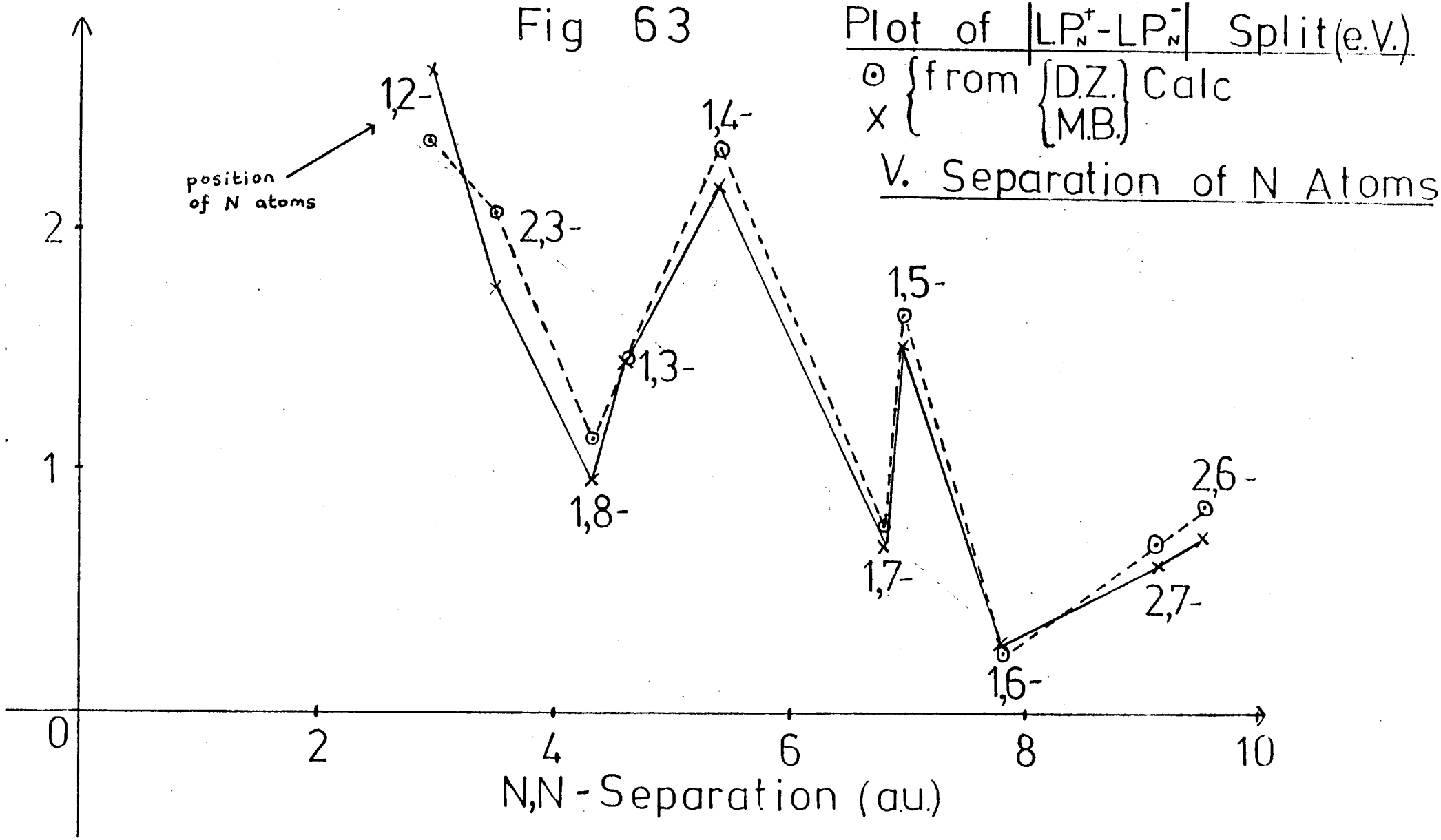
Plot of |LP$_N^+$-LP$_N^-$| Split (e.V.)
⊙ {from {D.Z.} Calc
× {{M.B.}
V. Separation of N Atoms
position of N atoms
1,2-
2,3-
1,8-
1,3-
1,4-
1,5-
1,7-
1,6-
2,7-
2,6-
0
1
2
2
4
6
8
10
N,N - Separation (a.u.)

to see if any trends are apparent.

Fig (63) is a plot of the calculated splitting (both MB and DZ) v the distance between the N atoms. It is immediately obvious that no simple relationship exists, although it can be noted that there is an overall reduction in the LP_N splitting with increasing separation. It can also be seen that the splitting is greater for $[^{\alpha\alpha}_{\beta\beta}]$ nitrogens in the same ring, than for $[^{\alpha\alpha}_{\beta\beta}]$ nitrogens in different rings. However, for the asymmetrical molecules i.e. 1,2-, 1,3-, 1,6-, 1,7 isomers where semi localized LP_N's exist for the (1,6), (1,7) isomers, the splittings lie approximately on a straight line. This is reasonable since the lone pairs of these molecules are $9a_{1g}$ for the semi localized α LP_N [for the (1,6), 1.7) isomers] and perturbed LP_N^- for the (1,2) and 1,3 isomers, whereas the β LP_N and LP_N^+ orbitals are $6b_{1g}$. Hence the only variable within this series of molecules is the separation of the N atoms (and of course small alterations in bond lengths and angles), and it would appear that there is a direct relationship between theoretical splitting and the separation (r).

$$\Delta E_{splitting} = Kr^{-n}$$ where K is a constant.

For the symmetrical (α,α) (β,β) isomers no such trend is in evidence.

Fig (64) gives a plot of the experimental splitting v separation of N atoms, where the experimental lone pair splittings for molecules not experimentally studied herein were taken from reference [24]. It should be noted that

Fig 64 Plot of Exptal $|LP_N^+ - LP_N^-|$ Split (e.V.) V. Separation of N Atoms

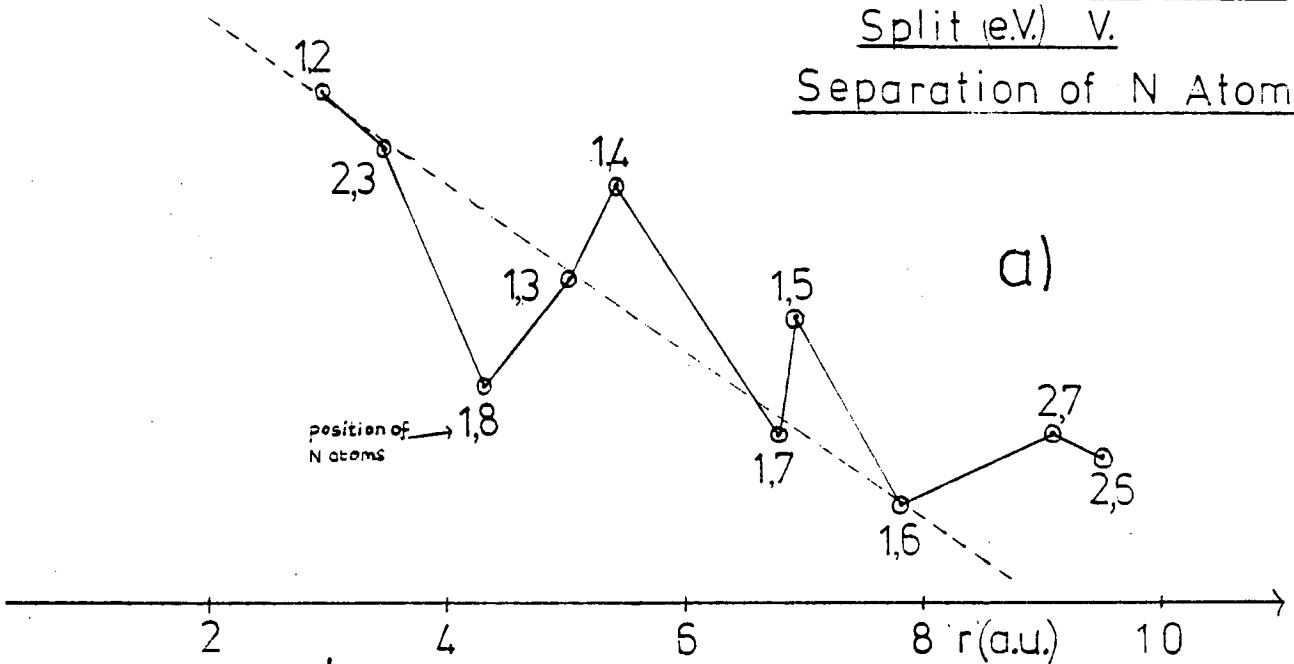

Plot as above with error bars

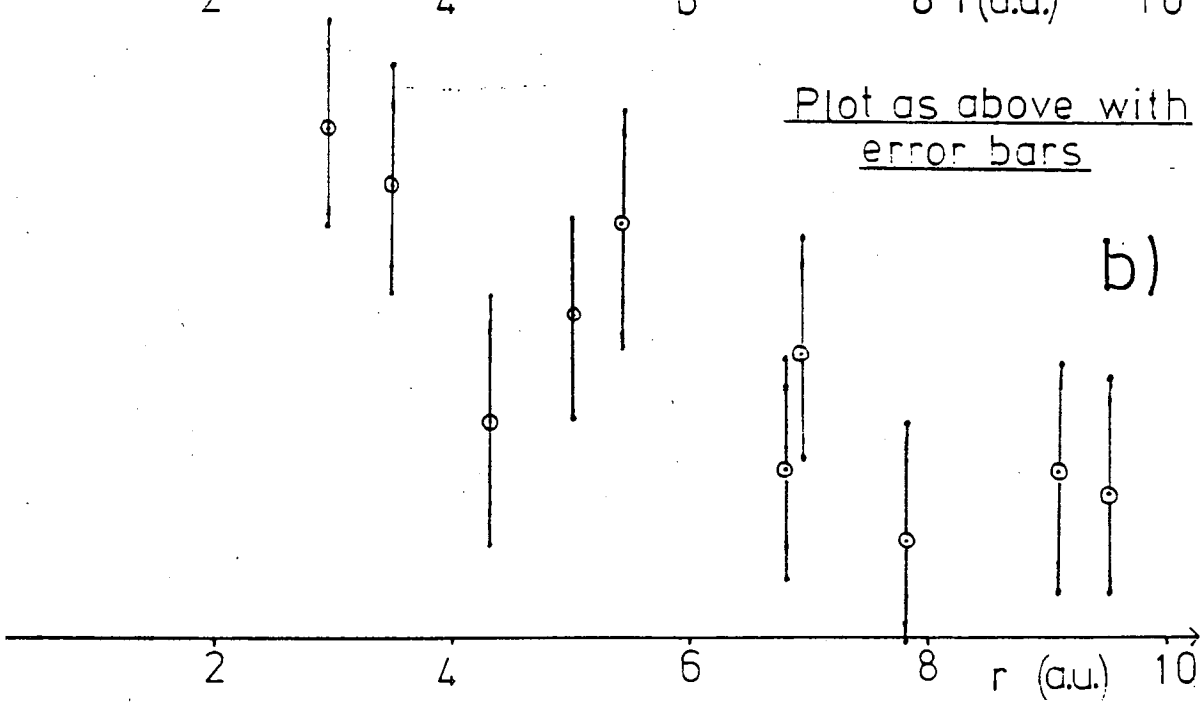

the splittings therefore rely on the veracity of the assignments proposed in reference [24]. The general outline of this plot is almost identical to that given in Fig. (63) for the variation of the calculated splitting. Again the splitting of the LP_N of the unsymmetrical molecules apparently has a linear relationship with 'r', (the splitting decreasing with increasing 'r'), as the dashed line in Fig (64a) indicates.

It must be pointed out that the uncertainty in measurement of experimental IP's especially when the IP's in question lie under the envelope of a broad band, can be greater than $\pm$ 0.5 eV, therefore, strictly, one should introduce error bars in the plot of experimental data Fig. (64 b) is the plot of experimental data with error bars estimated from an uncertainty in the measurement of LP_N of approximately $\pm$ 0.25 eV (hence up to $\pm$ 0.5 eV for splitting). Introduction of the error bars shows that it is possible to draw a straight line and several curves (e.g. for a 1/r relationship) through the points within experimental error, hence no conclusive interpretation can be made here, although it is unlikely that a simple linear relationship holds for the splitting of lone pair combinations (in the symmetric molecules) versus the separation of the nitrogen atoms, but this may be true for semi localized lone pairs. Before any conclusive interpretation of the data can be made it is necessary to:

a) Obtain better resolved He(I) and He(II) experimental data for the complete series.

b) Obtain ΔE_{SCF} calculations to check calculated orbital ordering, whereupon there will be a sufficient information to correctly interpret the spectra and hence obtain more accurate experimental LP_N splitting.

With the calculated information available here we can only conclude that no simple overall trend was observed for the complete series, for LP_N splitting.

B. Open Shell Calculations

(vii) Introduction

In 1953 isotropic hyperfine structure due to ring protons in aromatic anions was observed by Weissmann et al[29] in Electron Spin Resonance (E.S.R.) experiments. This was quite unexpected since the conventional simple model of an aromatic molecule, where the odd electron is thought to reside in a π orbital, is unable to explain a finite spin density at the proton position. Experiments by Fraenkel et al[30] eliminated the possibility that bending vibrations of the CH bond were mechanisms producing the hyperfine structure by showing that splitting constants on deuterated compounds were not inversely proportional to the square root of the nuclear masses which would be expected for such a mechanism (even the order of magnitude of the splittings could be explained by the vibrational mechanism). These negative results prompted the suggestion that the unpaired electron is not solely in a π state but that some spin density could perhaps be transferred to the σ bond by configuration interaction between σ and π states.

Various quantum mechanical approaches [e.g. Unrestricted Hartree-Fock (UHF) and Valence Bond] have been used to describe the σ π interaction and to a first order approximation, all of these methods lead to the conclusion that the ring proton splitting is proportional to the calculated spin density at the adjacent carbon atom (McConnell's relationship).

In the mid-sixties much attention was focussed on hyperfine interactions from nuclei other than ring protons. In particular splittings due to the intracyclic nuclei ^{13}C and ^{14}N were studied extensively. Karplus and Fraenkel[31] provided a detailed treatment for ^{13}C coupling constants, which showed that the ^{13}C hyperfine splittings are dependent on π spin density both at the nucleus under consideration and at nearest neighbour atoms. (Similar conclusions apply also to ^{14}N hyperfine splittings).

In the present study U.H.F. wavefunctions have been constructed for the radical anions of pyridine, the diazines, s-tetrazine, naphthalene, quinoline, isoquinoline and the diazanaphthalenes. The objective of this study is to show the qualitative and quantitative properties of UHF ab initio wavefunctions for predicting ^{1}H and ^{14}N hyperfine coupling constants (H.F.C.C.) and the dependence of the results on the size of the basis set used.

To date no ab initio study of this kind for these molecules has been reported although several semi empirical studies have been made[32-40] using different theoretical techniques. Amos and Snyder[34] noted that the simple Hückel MO method was inadequate, as is the Restricted Hartree Fock method, since these procedures cannot give negative spin densities which are known to occur; They therefore used the UHF procedure. The UHF method is capable of predicting negative spin densities but results of the semi empirical UHF calculations were not completely

satisfactory, since the UHF wavefunction is inherently contaminated by low lying virtual components. It was found that calculated spin densities were in better agreement with experimental results if annihilation of the contaminating spin component was performed, therefore the annihilation technique was also applied to our calculated UHF wavefunctions.

(viii) E.S.R. Spectra

Origins of the Hyperfine Structure

The electron has a non-classical, intrinsic angular momentum (spin) characterized by the quantum number $S = \frac{1}{2}$, its component along a defined axis, say z, being characterised by $M_S = \pm \frac{1}{2}$. The electron thus has two spin states which are described by convention

$$M_S = \frac{1}{2} : \text{Spin up or } \alpha$$
$$M_S = -\frac{1}{2} : \text{Spin down or } \beta$$

The spin of the electron gives rise to a magnetic moment μ_E, whose z component (μ_E^z) has two values corresponding to the two spin quantum numbers ($M_S = -\frac{1}{2}$) where

$$\mu_E^z = -M_S \cdot g_E \cdot \beta_E \qquad (1)$$

β_E is the Bohr magneton (9.2733×10^{-21} erg/gauss)

g_E is a dimensionless constant (2.0023 for free electrons)

If the z axis is defined as that of an applied magnetic field, then μ_E^z is responsible for the behaviour of the electron in the magnetic field. Now in the absence of a magnetic field the two states with $M_S = \pm\frac{1}{2}$ are degenerate, and this degeneracy is lifted upon application of an external magnetic field (Zeeman effect). The energy of interaction (E) is given by

$$E = \mu_E^z , \underline{H} = (M_S \, g_e \, \beta_E) \cdot \underline{H} \qquad (2)$$

The difference in energy for the two spin states E_1, E_2 is given by

$$E_1 - E_2 = g_E \beta_E H \qquad (3)$$

and transitions between the Zeeman levels (E_1, E_2) occur when the system is exposed to radiation of frequency ν where $h\nu = g_E \beta_E H$.

Similarly for a nucleus in an applied magnetic field the component of the nuclear magnetic moment μ_N in the direction of the field (μ_N^z) is given by

$$\mu_N^z = +M_I g_N \beta_N \qquad (4)$$

where M_I is the nuclear spin quantum number

β_N is the nuclear magneton (5.0493×10^{-24} erg/gauss)

and g_N is characteristic of the nucleus in question.

In a strong magnetic field, H, the interaction between an unpaired electron and a magnetic nucleus can be seen from a small perturbation of the Zeeman levels (i.e. hyperfine structure). This perturbation (δ_E) is made up of two terms

$$\delta E = (\delta E)_{\text{anisotropic}} + (\delta E)_{\text{isotropic}} \qquad (5)$$

The anistropic term represents the dipole-dipole interaction, which depends upon the relative positions of the magnetic moments of the unpaired electron and the nucleus. In single

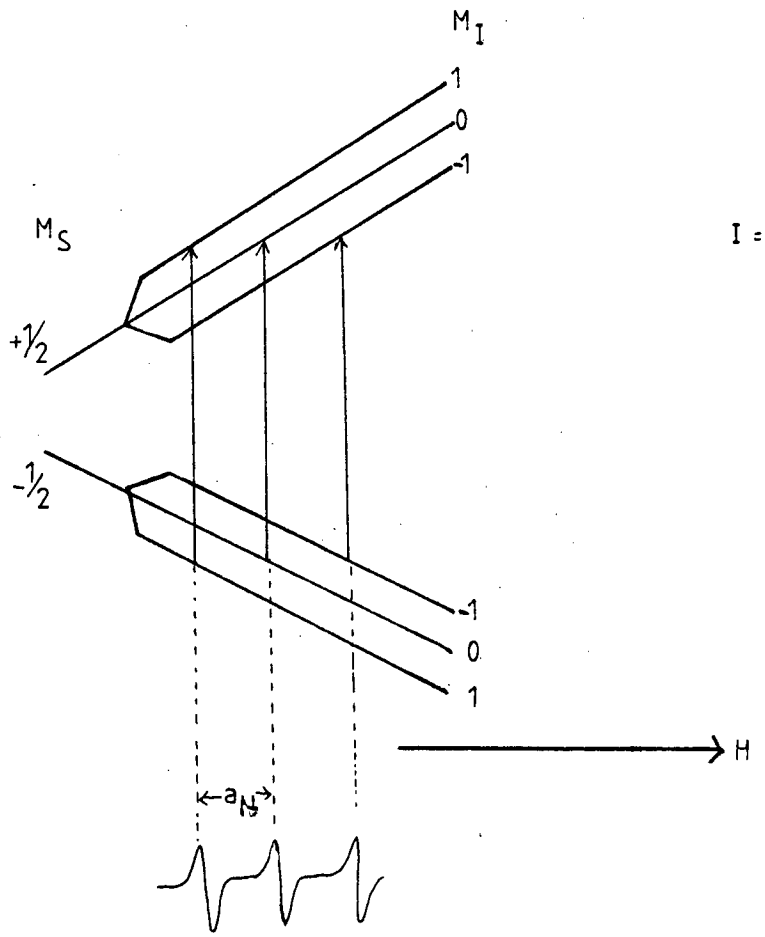

FIG. 65 ENERGY LEVEL DIAGRAM SHOWING SPLITTING OF AN ESR SIGNAL

A_N DENOTES THE COUPLING CONSTANT

crystals this interaction provides useful information, but in amorphous and polycrystalline substances it causes line broadening which rends the hyperfine structure unresolvable. However for liquids, where the molecular motion continuously changes the relative positions of the magnetic moments the dipole-dipole interactions average out (except for a small amount which depends on the viscosity of the solvent). Hence the anisotropic term contributes to the line width of the signal at resonance but not to δE, since the time average of $(\delta E)_{aniso}$ is zero. The hyperfine structure of radicals in solution is therefore only due to the direction independent Fermi[41] contact term, which for a strong field is given by

$$(\delta E)_{isotropic} = -\frac{8\pi}{3}(\mu_E^z \mu_N^z)\rho'(0) \qquad (6)$$

where $\rho'(0)$ is the spin density at the nucleus (which is chosen as the coordinate origin). Fig (65) refers to a radical in which the unpaired electron interacts with a single nucleus of spin quantum number I = 1 e.g. ^{14}N. The levels of the electron spin states, E_1 and E_2, ($M_S = \pm \frac{1}{2}$) are each split into three sub-levels corresponding to the quantum numbers M_I = 1,0,-1 of the ^{14}N nucleus. The ordering of the M_I levels for E_2, E_1 is reversed as can be deduced from equation (6) as can the fact that the sub levels with M_I = 0 always have the same position as the unperturbed levels since $(\delta E)_{isotropic}$ vanishes.

The selection rules which apply here are $\Delta M_S = \pm 1$ $\Delta M_I = 0$, consequently three hyperfine resonance lines are expected, the separation between the adjacent lines giving the coupling constants (a_N measured in gauss). These are independent of the applied field and are characteristic of the electron-nucleus interaction in the radical.

Now the coupling constant of any nucleus depends only on the spin density, $\rho'(0)$ at that nucleus and for nitrogen the coupling constant can be ascertained from the equation

$$a_N = K_N . \rho'(0)$$

where

$$K_N = \frac{2}{g_E \beta_E} \left| \frac{(\delta E)_{\text{isotropic}}}{\rho'(0)} \right| = 2 . \frac{2\pi}{3} g_N \beta_N |M_S M_I| \qquad (7)$$

From this brief introduction we can see the origins of the hyperfine structure and the dependence of the H.F.C.C.'s on the nuclear spin density. Although no E.S.R. experiments were carried out during the course of this work, and literature data only are reported, it is considered appropriate to briefly mention the methods by which experimental data is obtained.

(ix) Obtaining a Spectrum

To obtain an E.S.R. spectrum it is essential to

(a) have a radical to study,

(b) have an instrument to study it with.

A brief description of each of these necessities is given below in turn.

(a) Doublet state paramagnetic molecules, such as the π aromatic radical anions which are the basis of this study, have an unpaired electron, are therefore unstable with high reactivity and a short lifetime. They can however be stabilized by restricting their mobility, for example by freezing them into a solid matrix. This, however, results in $(\delta E)_{anisotropic}$ becoming significant and hence the hyperfine lines are broadened considerably; for the best resolution of the hyperfine structure, radical ions are usually studied in solution where sufficient stability is ensured.

The most frequently used method for preparation of heteroaromatic radical anions is reduction with alkali metals. This is carried out in a solvent such as 1,2-dimethoxyethane (D.M.E.) or tetrahydrofuran (T.H.F.) in the absence of air and water

$$Ar + Me \rightarrow Ar^{\ominus\cdot} + Me^{\oplus}$$

and formation of the radical is often indicated by appearance of a bright colour.

The reaction between aromatic hydrocarbons and an alkali, or alkaline earth metal in liquid ammonia also leads to production of radical anions.

Electrolytic methods, where the radicals are formed on the surface of a pool of mercury which is used as a reducing cathodic electrode, also exist for radical anion production. This method has the advantage that the anions can be produced continuously actually in the E.S.R. measuring cell which ensures a high concentration of these short-lived species.

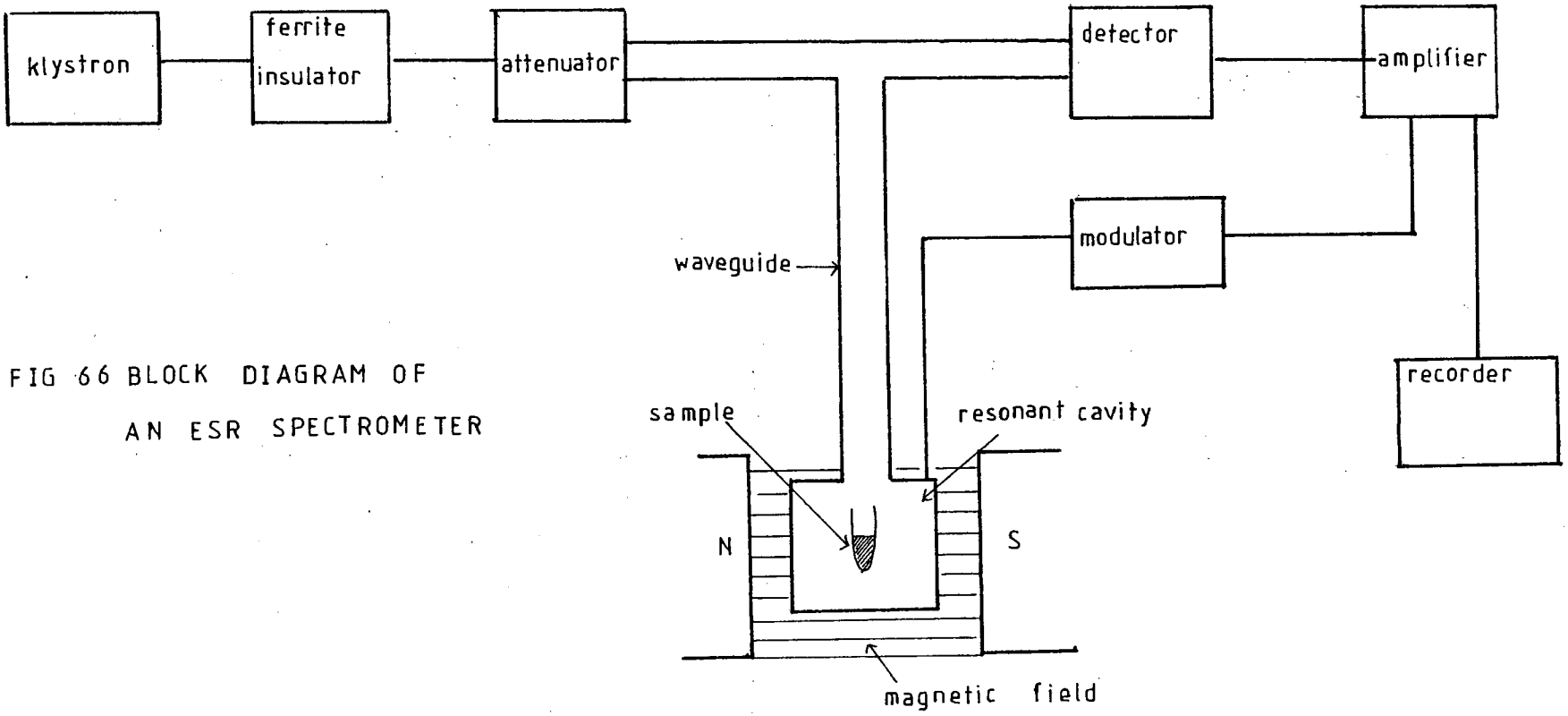

FIG 66 BLOCK DIAGRAM OF
AN ESR SPECTROMETER

(b) Having prepared the radical, the E.S.R. spectrum is obtained in an ESR spectrometer, a block diagram of which is shown in Fig (66). The mode of operation is as follows: microwave frequency radiation is taken to the resonant cavity via a wave guide, from a klystron valve.

Interposed between the Klystron and wave guide is the attenuator to regulate power input, and an insulator to protect the klystron from reflected radiation. The radiation reaches the detector by a 'T' shaped bridge which can be adjusted so that no radiation reaches the detector if no absorbation of microwaves occurs in the resonator. The applied magnetic field is modulated (hence the modulator) to improve the signal to noise ratio. The appearance of the ESR signal is characterized by absorption of microwaves at a particular field strength.

Analysis of a spectrum obtained in this manner, to obtain coupling constants and assign these to particular centres, becomes increasingly complicated as the number of coupling nuclei increases. It is basically performed by consideration of relative peak intensities of the hyperfine components.

Having now established the origins of the hyperfine structure and how it is experimentally studied we must now consider how experimental and calculated data are connected - the theoretical interpretation of results.

(x) Theoretical Interpretation

As mentioned above the coupling constant due to any nucleus (M) is directly proportional to the spin density $\rho'(0)$ at this nucleus.

$$a_M = K_M \rho'(0) \qquad (8)$$

The spin density $\rho'(0)$ is the difference between the α and β electron densities $P_\alpha(r)$ and $P_\beta(r)$ made up where the α and β electrons differ in their spin quantum number M_S

$$\rho'(0) = P_\alpha(r) - P_\beta(r) \qquad (9)$$

In a diamagnetic substance the spin density $\rho'(r)$ is zero everywhere as electrons of different spins occupy orbitals in pairs. In a paramagnetic species the unpaired electron is in a singly occupied orbital, and therefore the spin density does not vanish everywhere.

It is important at this point to distinguish between the related quantities, the spin density $\rho'(r)$ and the spin population density $\rho(r)$. $\rho'(r)$ is a probability density measured in electrons per cubic metre. The spin population (often confusingly called the spin density) is a number representing the fractional population of unpaired electrons on an atom in a <u>particular</u> <u>orbital</u>. ρ_M^ψ denotes the spin population density obtained by summation of $\rho'(r)$ over the ψ type atomic orbitals centred on atom M; for example ρ_H^{1s} is the spin population density in the 1s orbital of the hydrogen atom and its value is 1. For π molecular orbitals which

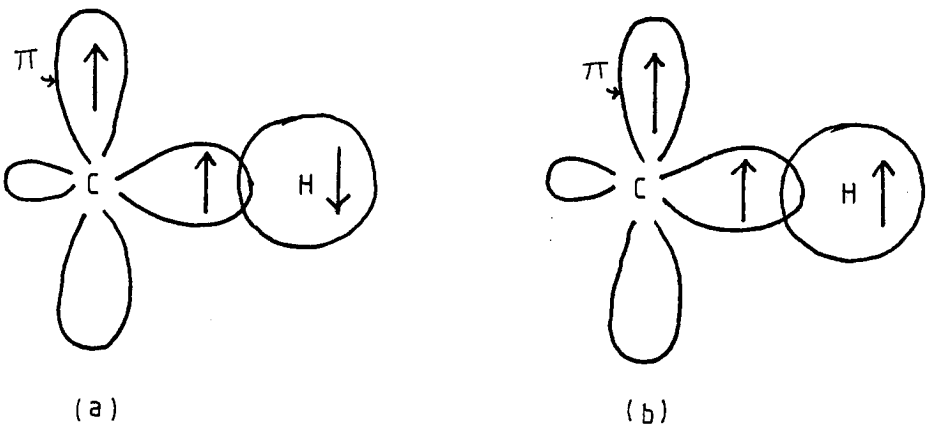

FIG.67 THE >C–H FRAGMENT

↑, ↓ represent electrons of opposite spins.

are delocalized over several centres (M) and constructed as linear combinations of $2P_Z$ A.O.'s (ϕ_M), ρ_M^π is defined as the contribution of the A.O.'s to the total π spin population density. Summation of ρ_M^π over all centres in the system must give the total spin population density.

$$\sum_M \rho_M^\pi = 1$$

In most aromatic anions the odd electron occupies a π M.O. delocalised over the ring atom framework and formed by overlap of the $2P_Z$ orbitals. However coupling due to ring protons is experimentally observed, which indicates that the spin density at the proton is not zero (as is expected). The apparent spin density at the proton can be explained, since exchange forces between electrons couple the spin of the σ electron in the CH bond and the π electrons in the ring. We illustrate by example; consider the GH fragment with an π electron in the $2P_z$ orbital, see Fig (67). in the approximation of perfect pairing (a) and (b) could be considered to be of equal importance. If exchange interactions between the σ and π electrons are taken into account (a) is preferred. The spins of the electron in the C-H bond are therefore polarised slightly. By convention the odd electron is of α spin, and therefore there is a slight excess of α spin in the carbon π orbital which induces an excess of β spin in the hydrogen 1s orbital. (For this

reason the spin density at the proton and hence the H.F.C.C.'s are conventionally negative). This mechanism is called σ-π spin polarization. According to McConnell's relationship[42] the coupling constants observed for ring protons in aromatic radical ions are proportional to the π spin population density on the adjacent carbon atom.

$$a_{H_m} = Q_{CH}\ \rho^{\pi}_{M} \qquad (10)$$

where Q_{CH} is a proportionality constant whose value lies between 20 and 30 gauss. By virtue of this simple relationship both calculable spin population densities and hydrogen H.F.C.C.'s can be compared, but for ^{14}N nuclei in aromatic rings the relationship is thought to be more complicated.

In nitrogen heteroaromatic radical ions the nitrogen atom lies in the nodal plane of the π orbitals. It was proposed by Karplus and Fraenkel[31] that the finite spin density on the ^{14}N nuclei is due not only to the polarization of the paired spins of the bonding σ electrons by the unpaired π electrons, but also to an interaction between the electrons in the atomic orbitals of the ^{14}N centre and the unpaired electron. The latter interaction is primarily a σ-π spin polarization and an LP_N-π spin polarization. The theory used in reference [31] to derive the coupling constants for ^{14}N coupling constants is bot lengthy and complicated and is outwith the scope of this work. The complicated formulae derived for a_N therein, can be reduced to the simpler expression

$$a_N = Q_N\ \rho^{\pi}_{N} + \sum_{\mu} Q_{\mu N}\ \rho^{\pi}_{\mu} \qquad (11)$$

in which the first term on the R.H.S. is proportional to the π spin population density (ρ_N^π) at the nitrogen while the second term depends on the spin population density (ρ_μ^π) at the adjacent atoms μ.

This expression has been used[43-47] for semi empirical investigations of H.F.C.C.s for nitrogen centres with two adjacent carbons, for which equation (11) becomes

$$a_N = Q_N \rho_N^\pi + Q_{CN} (\rho_{C_1}^\pi + \rho_{C_2}^\pi) \qquad (12)$$

The range of reported empirical estimates of Q_N and Q_{CN} vary considerably, although it is generally accepted that $|Q_{CN}|$ is much smaller than $|Q_N|$. For this reason the contribution of the spin population density from the adjacent centres is often neglected so that equation (12) can be written

$$a_N \approx Q_N \rho_N^\pi \qquad (13)$$

which is comparable with the McConnell relationship (10). This was proposed by Carrington et al,[43] but Henning[47] in a statistical analysis of eight heteroaromatic anions reported from Hückel calculations that this simple expression is statistically insufficient and the Karplus and Fraenkel relation is required.

Calculations - Obtaining Spin Densities

(xi) The Unrestricted Hartree-Fock Method

Having outlined the theory and practical procedures involved in obtaining H.F.C.C.'s from E.S.R. spectra, we must now investigate the methods used herein to obtain calculated spin population densities, for the radical anions under consideration, to enable comparison of experimental and calculated data to be made.

Now a radical anion is a system with a charge of -1, i.e. it has a single unpaired electron, which must be accommodated in a molecular orbital. A calculation on such a system may be carried out in two ways.

(i) by the restricted Hartree-Fock (RHF) procedure where the electron lies in a singly occupied molecular orbital (called the open shell), all other occupied M.O.'s containing both an α and β spin electron. (The theoretical background to this procedure is basically the same as that considered in chapter 1 only with additional terms in equation (1. 66) for the unpaired electron). This procedure is not useful here since it can give only positive spin densities, and negative spin densities are known to exist, for example for the allyl and benzyl radicals.

(ii) by the unrestricted Hartree-Fock (U.H.F.) procedure, which predicts both positive and negative spin densities, and has therefore been adopted here, for calculation of spin population densities (S.P.D.).

The U.H.F. wavefunction is constructed using different spatial orbitals for electrons of different spin. For a system with A α spin electrons and B, β spin electrons (A $\geq$ B) the general form of the U.H.F. wavefunction is

$$\psi_{UHF} = \left|\psi_1^{\alpha}(1)\alpha(1)\psi_2^{\alpha}(2)\alpha(2) \ \ldots\ldots \ \psi_A^{\alpha}(A)\alpha(A)\psi_1^{\beta}(A+1)\beta(A+1) \ \ldots\ldots \right.$$

$$\left. \ldots\ldots \ \psi_B^{\beta}(A+B)\beta(A+B)\right| \qquad (14)$$

where ψ_i^{α} and ψ_i^{β} are taken as linear combinations of valence shell atomic orbitals ϕ_u

$$\psi_i^{\alpha} = \sum_{\mu} C_{\mu i}^{\alpha} \phi_u$$

$$\psi_i^{\beta} = \sum_{\mu} C_{\mu i}^{\beta} \phi_u \qquad (15)$$

where $C_{\mu i}$ are linear expansion coefficients. Here there are two Hartree Fock problems (cf. Chapter 1 equation (71)).

$$F^{\alpha} \sum_{\mu} C_{\mu i}^{\alpha} \phi_u = \sum_{\mu} C_{\mu i}^{\alpha} \varepsilon^{\alpha}$$

$$F^{\beta} \sum_{\mu} C_{\mu i}^{\beta} \phi_u = \sum_{\mu} C_{\mu i}^{\beta} \varepsilon^{\beta} \qquad (16)$$

The two Fock matrices can be written as

$$\underline{F}^{\alpha} = \underline{H} + \underline{J} - \underline{K}^{\alpha}$$
$$\underline{F}^{\beta} = \underline{H} + \underline{J} - \underline{K}^{\beta} \qquad (17)$$

where $\underline{K}^{\alpha}$ and $\underline{K}^{\beta}$ depend on the density matrices P^{α} and P^{β}

respectively where

$$P^{\alpha}_{\mu\nu} = \sum_{i}^{A} C^{\alpha}_{\mu i} C^{\alpha}_{\nu i}$$

$$P^{\beta}_{\mu\nu} = \sum_{i}^{B} C^{\beta}_{\mu i} C^{\beta}_{\nu i} \qquad (18)$$

The total energy, minimized using the standard SCF Procedure Fig (6), of the system is given by

$$E = \sum_{i}^{\alpha+\beta} H_i + \tfrac{1}{2} \sum_{i}^{\alpha+\beta} \sum_{j}^{\alpha+\beta} J_{ij} - \tfrac{1}{2}\left(\sum_{i}^{\alpha} \sum_{j}^{\alpha} k_{ij} - \sum_{i}^{\beta} \sum_{j}^{\beta} k^{\beta}_{ij}\right) \qquad (19)$$

one electron term — coulomb term — exchange term

The unpaired electronic population matrix, which is what we require, is given by

$$\rho_{\mu\nu} = P^{\alpha}_{\mu\nu} - P^{\beta}_{\mu\nu} \qquad (20)$$

Now the classification of open shell systems is in terms of the spin multiplicity

$$\text{spin multiplicity} = 2 \mid S_z \mid + 1 \qquad (21)$$

where S_z is the expectation value of the total spin angular momentum operator with respect to axis (z); S_z is given by

$$S_z = \sum_{i=1}^{\text{all electrons}} S_z(i) \qquad (22)$$

where $S_z(i)$ are the spin eigenvalues ($-\frac{1}{2}$ or $+\frac{1}{2}$) of the electrons of the system.

The UHF wavefunction is not a pure spin state since it is inherently contaminated by spin states of higher multiplicity; as a consequence the energy computed in the UHF method is not a quantum mechanically rigorous upper bound for the energy of the molecular state. Although the UHF wavefunction is an eigenfunction of S_z it is not in general an eigenfunction of S_z^2 (often referred to as S^2) for which eigen are $S_z(S_z+1)$. It is reasonable, therefore, to assume that deviation of the expectation value of the S^2 operator, for a UHF wavefunction, from $S_z(S_z+1)$ can be used as an indication of the quality of that wavefunction (i.e. how physically realistic it is).

The UHF wavefunction contains contributions from components of several spin states

$$\psi_{UHF} = \sum_{M=O}^{B} C_{S'+M}\, \psi_{S'+M} \qquad (23)$$

where the lowest spin component has $S_z = S' = \frac{1}{2}(A-B)$ while the highest value of spin is $S_z = S' + B$.

For π electron UHF wavefunctions, where $s' = \frac{1}{2}$, spin multiplicity = 1, (such as the radical anions studied herein) it has been shown[48] that the major spin component of ψ_{UHF}

is that of lowest spin multiplicity, and the coefficients of the normalized components of higher multiplicity rapidly decrease. Therefore a practical procedure to improve ψ_{UHF} is to remove the largest unwanted component as was proposed by Amos et al.[33] They found that this can be performed by operating on ψ_{UHF} with the annihilator $\alpha_{S'+1}$

$$\alpha_{S'+1} = S^2 - (S'+1)(S'+2) \qquad (24)$$

The new wavefunction is (from equations (23) and (24)

$$\alpha_{S'+1}\ \psi_{UHF} = \sum_{M=O}^{B} C_{S'+M}(M-1)(2S'+M+2)\psi_{S'+M} \qquad (25)$$

This is referred to as the annihilated UHF wavefunction ψ_{AUHF}. It is usual that annihilation improves the expectation value of the S^2 operation (i.e. gives a value closer to $S_z(S_z+1)$, hence the wavefunction can be considered as more physically realistic, and can therefore be expected to produce improved spin population densities.

The integrated spin densities here reported were obtained from UHF and annihilated UHF wavefunctions (AUHF) constructed for the radical anions (-1) of the azines, naphthalene, quinoline, isoquinoline and diazanaphthalenes, using both M.B. and D.Z. basis sets. In addition UHF and AUHF wavefunctions were constructed for the azine radical cations (+1)

for both σ and π cationic (+1) states. The geometries used for these calculations were the same as those used for ground state (GS) closed shell calculations (see above). This approximation is justified since it is not expected that introduction of the electron into the GS system would substantially alter its geometry, and also since geometry optimization of the radicals would have been so lengthy as to be impractical.

The computer program used for construction of the wave-functions was the ATMOL 3 UHF module, for which a lengthy description of data input can be found in reference

Table (40) UHF Total Energies (au) for Radical Ions of Azines

(i) Radical Anions

Molecule	Minimal basis (MB)	Double Zeta basis (DZ)
Pyridine	-245.9021773	-246.5374283
Pyridazine	-261.81411196	-262.50842470
Pyrimidine	-261.8397398	-262.5360434
Pyrazine	-261.7864292	-262.54286498
S-Tetrazine	-293.6540046	-294.3400739

Table (41) UHF Total Energies (au) for Radical Ions of Azines and Expectation Values of S^2 Operator

Radical Cations (π open shell)

Molecule	DZ (au)	$\langle S^2 \rangle$ B.A.*	$\langle S^2 \rangle$ A.A.*
Pyridine	-246.2651007	1.0799	0.8196
Pyridazine	-262.1815164	0.8061	0.7505
Pyrimidine	-262.22010121	0.8821	0.7603
Pyrazine	-262.20191917	0.9533	0.7727

Radical Cations (σ open shell)

Molecule	DZ (au)	S^2 B.A.*	S^2 A.A.*
Pyridine	-246.3018703	1.2669	0.9852
Pyridazine	-262.22338686	1.4215	1.1604
Pyrimidine	-262.2234767	1.4779	1.2926
Pyrazine	-262.16786525	0.7816	0.7507

*B.A. = Before Annihilation

A.A. = After Annihilation

Results and Discussion

(xii) Total Energies

Tables (41) and (42) contain the calculated UHF total energies for the radical anions. Comparison of these values with the ground state total energies Tables (34 , 35) show that, for every case, the radical anions are less stable than the ground states indicating their negative electron affinities. Analysis of the UHF wavefunctions showed that all radical anions had the unpaired electron in a delocalized π state (except S-tetrazine where it resided in a delocalized σ orbital).

Table (41) gives the total energies of the diazine radical cations for both π and σ open shells respectively. These additional calculations were prompted by the results of recent ESR and optical studies on the azine[49] radical cations prepared in frozen solution from intermolecular charge transfer induced by γ-ray irradiation. In these studies the azine cations formed were found to have unpaired spin density localized in the LP_N in plane orbitals. This is in agreement with our PES studies of the azines (see above) which predict that the first IP is of LP_N character. Now the technique used in reference [49] gives results for effectively isolated cations and therefore calculations on the isolated structures are directly comparable. UHF calculations (using the ground state geometry) initially converged, in all cases, on states with the unpaired

Table (42) UHF Total Energies (au) for Radical Anions

Anion of	Minimal Basis	Double Zeta Basis
Naphthalene	-382.2907492	-383.17753368
Quinoline	-398.2099344	-399.1735181
Isoquinoline	-398.2137350	-399.1729348
Cinnoline	-414.1179443	-415.1403735
Quinazoline	-414.0685507	-415.1198415
Quinoxaline	-414.1439144	-415.1743317
1,5-Diazanaphthalene	-414.1155034	-415.1566845
1,6-Diazanaphthalene	-414.1317649	-415.1682377
1,7-Diazanaphthalene	-414.1314339	-415.165929
1,8-Diazanaphthalene	-414.0410964	-415.0903125
2,3-Diazanaphthalene	-413.9261216	-414.9791243
2,6-Diazanaphthalene	-413.9729275	-415.0461776
2,7-Diazanaphthalene	-414.1343413	-415.1649212

electron in a π orbital. Now the UHF module of Atmol -3 has the facility for forcing the unpaired electron to reside in a chosen orbital and this was utilized to attain convergence for cations with the unpaired electron in an orbital of LP_N character. From Table (4 1) it can be seen that in all cases the LP_N radical cation is energetically more stable than the π cation, which is in full agreement with the experimental findings of Kato and Shida[49] and our experimental PES studies.

Table (43) Calculated Spin Population Densities (ρ_c^π) and Experimental Hydrogen HFCC's (a_H) for Radical Anions

Molecule		Minimal Basis		Double Zeta Basis		Experimental
		ρ_c^π B.A.*	ρ_c^π A.A.*	ρ_c^π B.A.*	ρ_c^π A.A.*	HFCC's (a_H)
Naphthalene	C1	0.301	0.225	0.301	0.224	4.84[a]
	C2	0.013	0.044	0.016	0.047	1.83
Quinoline	C2	0.029	0.058	0.170	0.131	3.29[b]
	C3	-0.013	0.035	-0.122	-0.004	1.26
	C4	0.36	0.274	0.468	0.360	7.80
	C5	0.249	0.188	0.283	0.181	3.90
	C6	-0.018	0.034	-0.071	0.001	1.14
	C7	-0.0005	0.042	0.095	0.068	2.02
	C8	0.265	0.182	0.432	0.113	3.46
Isoquino-line	C1	0.268	0.215	0.341	0.264	5.38[b]
	C3	-0.147	-0.033	-0.118	-0.031	0.37
	C4	0.339	0.231	0.269	0.181	4.01
	C5	0.163	0.145	0.087	0.102	3.95
	C6	0.183	0.139	0.275	0.187	3.26
	C7	-0.165	-0.034	-0.239	-0.063	0.04
	C8	0.381	0.268	0.437	0.295	6.26
Quinoxaline	C2	-0.005	0.038	0.015	-0.048	2.38[b]
	C5	0.165	0.110	0.128	0.107	3.33
	C6	-0.001	0.024	0.007	-0.002	1.45
1,5-Diazan naphthalene	C2	0.091	0.088	0.117	0.102	293[a]
	C3	-0.065	0.008	-0.057	0.015	1.66
	C4	0.337	0.245	0.361	0.265	5.72
Phthalazine	C1	0.266	0.203	0.319	0.247	5.91[c]
	C5	0.291	0.224	0.279	0.201	4.64
	C6	0.035	0.058	0.038	0.063	2.14
1,8-Diaza-naphthalene	C2	0.020	0.052	0.151	0.113	2.04[d]
	C3	-0.002	0.037	-0.092	0.003	0.70
	C4	0.295	0.217	0.391	0.280	6.54
2,7-Diaza-naphthalene	C1	0.229	0.172	0.156	0.122	4.02[d]
	C3	0.078	0.067	0.107	0.076	3.40
	C4	0.389	0.289	0.409	0.351	4.95
Pyridine	C2	0.089	0.062	0.150	0.112	3.14[b]
	C3	-0.092	0.018	-0.117	-0.004	0.88
	C4	0.500	0.401	0.537	0.-43	9.10
Pyrdiazine	C3	-0.255	-0.078	-0.242	-0.075	0.16[a]
	C4	0.290	0.218	0.310	0.231	6.47
Pyrimidine	C2	-0.269	-0.082	-0.152	-0.048	(-)0.72[e]
	C4	0.379	0.299	0.497	0.384	9.78
	C5	-0.253	-0.083	-0.341	-0.108	(-)1.31
Pyrazine		0.0395	0.024	-0.006	0.040	(-)2.63[a]
		-0.282	-0.267	-0.276	10.086	0.21[c]

*B.A. = Before Annihilation A.A. = After Annihilation

for references (a→d) see Table(45)

FIG 68 PLOTS OBTAINED USING THE MC CONNEL RELATIONSHIP

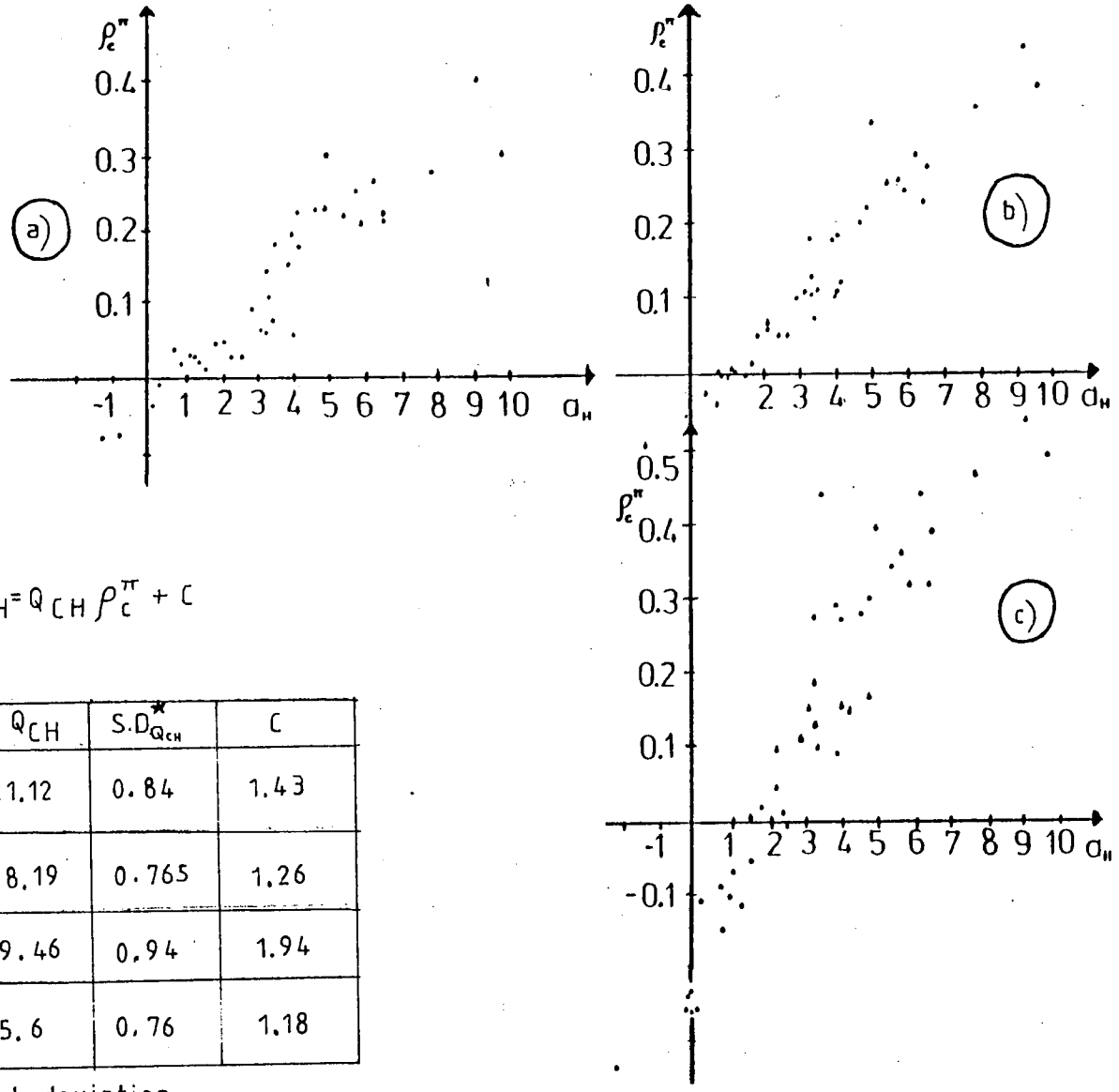

$$a_H = Q_{CH}\,\rho_c^\pi + C$$

	Q_{CH}	$S.D^{*}_{Q_{CH}}$	C
a)	21.12	0.84	1.43
b)	18.19	0.765	1.26
c)	9.46	0.94	1.94
ref[52] (UHF)	15.6	0.76	1.18

* Standard deviation

Calculated Spin Population Densities

ρ_C^π

From the calculated values of ρ_C^π and the experimental HFCC's, see Table (43) by virtue of the Established McConnell relationship we can investigate.

a) The effect of size of basis set on the calculated spin densities.

b) The effect of annihilation on the calculated spin densities. The latter has been studied by semi empirical methods* where it was found that annihilation caused a reduction in the original ρ_C^π of about 30%, attributed to a reduction in the σ-π polarization[50,51]. Both a) and b) have been studied by ab initio methods but for small radicals only;[50,51] for example $.CH_3$, $.C_2H_5$ where the use of basis sets (of a comparable size to the 7s/3p basis used here), and annihilation were shown to be essential in obtaining accurate spin densities. It is therefore interesting to extend this study to the large anions studied here, to see if the same requirements are in evidence.

Assuming a McConnell relationship the following graphs were plotted see Fig (68).

a) ρ_C^π (aa) (7s/3p) v. a_H

b) ρ_C^π (aa) (9s/5p) v. a_H

c) ρ_C^π (ba) (9s/5p) v. a_H

From a) and b) Fig (68) we can see that the use of the larger basis set has the effect of reducing the scatter of the points around the best straight line, but this is only a small effect, as is indicated by the values of the standard deviation (obtained from a least squares fit). It is also

noteworthy that the graphs do not pass through the origin and that the intercept, c, is larger for the smaller basis set.

The presence of a finite intercept indicates that a_H is not solely dependent on ρ^π on the adjacent carbon since this predicts a finite a_H even for zero ρ^π_C. The finite intercept indicates that a_H is made up of contributions not only from the adjacent carbon ρ^π but also smaller contributions from all other centres in the system.

$$a_H = \sum_{X}^{\text{all ring centres}} Q_{XH}\, \rho^\pi_X$$

their contributions decreasing with increasing distance from the coupling centre. The small value of the intercept c however is an indication that the major contribution is from the adjacent centre and therefore, to a first approximation, as is adequate for the basis set comparisons made in this study, McConnell's relationship holds. The value of Q_{CH} is slightly smaller using the larger basis set, and is outwith the accepted value of 20 to 30 gauss (It should be noted that Q_{CH} has a negative sign by convention). The values of Q_{CH}, C and the standard deviations given in Fig (68) are comparable, but not identical to those reported by Zeiss and Whitehead using semi empirical methods. This indicates that if calculated spin population densities are to be used for prediction of a_H where experimental data is lacking, or alternatively if ESR spectra are to be assigned by

comparison with calculated ρ^{π}, then it is essential to obtain values of Q_{CH} and C from plots such as those in Fig (6 8) since the values of these constants appear to depend on the theoretical method used.

Comparing b) and c) we can see that annihilation has the effect of reducing the scatter about the best straight line and increases the absolute value of Q_{CH} by reducing the magnitudes of the spin population densities.

It is noteworthy that both M.B. and D.Z. calculations give almost identical ρ_C^{π} before and after annihilation, and that in general the two basis sets give very similar ρ_C^{π}. This coupled with the fact that the $\langle S^2 \rangle$ (expectation value of the S^2 operator) is similar for both basis sets is an indication that beyond a certain limit ρ_C^{π} are not very sensitive to basis set, but that annihilation makes a more marked improvement on ρ_C^{π}.

The relatively good fit of ρ_C^{π} and a_H (a.a.) is an indication that the geometry used for the anions is good. The initial dependence of spin population densities (ρ_C^{π}) on structure has been noted before,[50,51] and is a consequence of the dependence of the UHF wavefunction on structure. (This will be further discussed in the next section).

It is noteworthy that our calculations lead to a reassignment of the experimental data for 2,7-diazanaphthalene and 1,8-diazanaphthalene where comparison of the HFCC's for ρ_C^{π} and ρ_N^{π} lead to the assignments given in Table (4 3).

Table (4 4) Calculated Spin Population Densities (ρ_μ^π) (μ = N,C) (Anions for which no experimental data is available

Molecule		Minimal Basis		Double Zeta Basis	
		ρ_μ^π B.A.	ρ_μ^π A.A.	ρ_μ^π B.A.	ρ_μ^π A.A.
Cinnoline	N1	0.402	0.311	0.400	0.320
	N2	0.316	0.222	0.333	0.244
	C3	-0.213	-0.063	-0.241	0.074
	C4	0.339	0.223	0.356	0.241
	C5	-0.102	0.001	-0.083	0.0003
	C6	0.304	0.173	0.271	0.152
	C7	-0.295	-0.085	-0.243	-0.071
	C8	0.423	0.243	0.375	0.210
Quinazoline	N1	0.388	0.269	0.242	0.166
	N2	0.160	0.134	0.077	0.085
	C2	-0.127	-0.022	-0.023	0.011
	C4	0.360	0.285	0.515	0.407
	C5	0.408	0.236	0.438	0.240
	C6	-0.289	-0.084	-0.345	-0.104
	C7	0.309	0.179	0.371	0.208
	C8	-0.077	0.016	-0.182	-0.031
1,6-Diaza-	N1	0.229	0.1819	0.182	0.144
naphthalene	N2	0.101	0.083	0.016	0.036
	C2	0.438	0.314	0.521	0.390
	C3	-0.208	-0.047	-0.262	-0.064
	C4	0.234	0.167	0.326	0.227
	C5	0.208	0.189	0.159	0.111
	C7	-0.079	-0.009	-0.004	0.013
	C8	0.260	0.196	0.321	0.219
1,7-Diaza-	N1	0.416	0.293	0.356	0.268
naphthalene	N2	0.179	0.120	0.124	0.088
	C2	0.256	0.207	0.352	0.275
	C3	0.173	0.133	0.004	0.099
	C4	-0.154	-0.025	-0.035	0.029
	C5	0.194	0.163	0.225	0.177
	C6	-0.158	-0.038	-0.128	-0.032
	C8	0.326	0.211	0.256	0.161
2,6-Diaza-	N1	0.375	0.246	0.319	0.219
naphthalene	C1	0.045	0.085	0.111	0.125
	C3	-0.317	-0.097	-0.279	-0.088
	C4	0.417	0.249	0.365	0.219

This molecule has not been investigated theoretically before and it was previously assigned by inspection. In addition our calculations indicate that for quinoline it is likely that a_H for C_3 and C_6 would be better exchanged and also that a_H C_5 of pyrimidine is negative.

Table (45) Calculated Spin Population Densities (ρ_N^π) and Experimental Nitrogen HFCC's (a_N)

Molecule	Minimal Basis		Double Zeta Basis		a_N
	ρ_N^π BA	ρ_N^π AA	ρ_N^π BA	ρ_N^π AA	
Quinoline N	0.356	0.265	0.284	0.219	3.95[b]
Isoquinoline N	0.181	0.128	0.149	0.112	1.92[b]
Quinoxaline N	0.465	0.360	0.440	0.331	5.70[b]
1,5-Diaza-naphthalene N	0.269	0.200	0.224	0.165	3.37[a]
Phthalazine N	-0.020	0.051	-0.018	-0.025	0.876[c]
1,8-Diaza-naphthalene N	0.324	0.236	0.198	0.149	4.07[d]
2,7-Diaza-naphthalene N	-0.061	0.012	-0.095	-0.007	0.43[d]
Pyridine N	0.512	0.437	0.397	0.342	6.28[b]
Pyridazine N	0.464	0.359	0.432	0.343	5.29[a]
Pyrimidine N	0.382	0.282	0.249	0.193	3.26[e]
Pyrazine N	0.551	0.451	0.501	0.418	7.18[a]
S-tetrazine N	0.391	0.384	0.388	0.293	5.27[c]

a) J. Henning, J.Chem.Phys., 44, 2139, (1966).

b) S. Kume, J. Jagur-Grodzinki, M.S warc, J. Chaudhari, J.Am.Chem.Soc., 90, 642 , (1968).

c) E.W. Stone, A.H. Maki, J.Chem.Phys., 39, 1635, (1963)

d) F. Gerson, Fundamentals of Electron Spin Resonance Spectroscopy, John Wiley, London (1970).

e) L. Myers, C.L. Talcott, Mol. Phys., 12, 549, (1967).

Table (46)

Calculation of Q_N^N and Q_X^N and Standard Deviations using the following Expressions

(i) $a_N = Q_N^N \rho_N^\pi + C$

Method	Basis Set	Q_N^N	Standard Deviation	C
UHF_{ba} *	7s/3p	10.33	0.955	0.681
UHF_{aa}	7s/3p	14.34	0.913	0.107
UHF_{ba}	9s/5p	11.01	0.937	1.06
UHF_{aa}	9s/5p	14.65	0.894	0.87
Reference(52) Semi Empirical		17.3	0.79	1.03

(ii) $a_N = Q_N^N \rho_\pi^N + Q_X^N \sum_i \rho_{X_i}^\pi$ (type 1)

Method	Basis Set	Q_N^N	Q_C^N	Standard Deviation
UHF_{ba} *	9s/5p	12.23	1.343	0.903
UHF_{aa}	9s/5p	15.48	2.63	0.876
Reference(52) Semi Empirical		17.7	1.97	0.79

(iii) $a_N = Q_N^N \rho_N^{TOT} + C$

Method	Basis Set	Q_N^N	Standard Deviation	C
UHF_{aa}	9s/5p	13.6	1.33	0.979

Values of ρ_N^{TOT} ($9s/5p_{aa}$) and a_N used for (iii) above

Anion	ρ_N^{TOT}	a_N
Quinoline	0.23	3.95
Isoquinoline	0.11	1.92
Quinoxaline	0.377	5.70
1,5-Diaza-naphthalene	0.177	3.37
Phthalazine	-0.02	0.876
1,8-Diaza-naphthalene	0.154	4.07
2,7-Diaza-naphthalene	-0.01	0.43
Pyridine	0.36	6.28
Pyrimidine	0.23	3.26
Pyrazine	0.44	7.18
Pyridazine	0.36	5.29

*ba = before annihilation

aa = after annihilation

$\underline{\rho_N^\pi}$

The following relationships have been investigated

$$a_N = Q_N^N \rho_N^\pi \qquad \text{(i)}$$

$$a_N = Q_N^N \rho_N^\pi + Q_X^N \sum_i \rho_{X_i}^\pi \qquad \text{(ii)}$$

Least squares fitting of the calculated spin population densities to a_N using expression (i) has been performed for each basis set before and after annihilation, and resulting values of Q_N^N are given in Table (4 6). As above, for the ρ_C^π, the use of the larger basis set improves the standard deviation slightly but improves this more significantly. From these calculations the larger basis set has been used to further investigate (ii) to see if any statistical improvement is made upon using this more complicated expression for anions with a nitrogen adjacent to two carbon atoms. See Table (4 6).

The expression (ii) is more complex for anions with nitrogen coupling centres adjacent to both a carbon and nitrogen viz.

$$a_N = Q_N^N \rho_N^\pi + Q_{N_2}^N \rho_{N_2}^\pi + Q_C^N \rho_C^\pi$$

The values of $Q_{N_1}^N$, $Q_{N_2}^N$, Q_C^N cannot be obtained with any degree of accuracy for this set of molecules as the $N \diagup N \diagdown C$

structure arises in only cinnoline, phthalazine, s-tetrazine and pyridazine. Experimental data is not available for cinnoline, and s-tetrazine is a σ anion. Since then only two sets of data are available no least squares fitting has been performed as this would not provide results of any statistical significance.)

In agreement with the semi empirical findings of Zeiss and Whitehead[52] our results show that a small statistical improvement is made using the more complicated expression (ii), but not to the extent reported by Dunning. It is noteworthy that our results give poorer standard deviations than those obtained by semi empirical methods and that as was noted for Q_{CH}, the ab initio constant Q_N^N is lower than other reported values. The standard deviations obtained from (i) and (ii) are only slightly poorer than those obtained from the McConnell relationship (see above). We therefore feel that the simple expression (i) is adequate for interpretation of the results, and can be used to estimate a_N for molecules for which experimental data is lacking, and alternatively to assign experimental data where there is no clear indication to which centre a particular coupling constant refers.

It is important to note that since the values of Q_N^N depend on the theoretical technique used before any estimation of a_N from theoretical spin population densities can be made a least squares fit should be made for a series of previously studied radicals using information calculated by the same theoretical technique to obtain compatible Q_N^N.

Since the spin density at the ^{14}N site in heterocyclic anions is thought to be due not only to σ-π polarization but also to n-π and N_{1S}- polarization the total spin density (ρ_N^{tot}) has been used in expression (i) to see if a better relationship exists between this quantity and a_N. The results of least squares fitting of the DZ calculated ρ_N^{tot} after annihilation see Table (4 6), and a_N are given in Table (4 6) where it is found that the standard deviation was considerably worse. This indicates that a_N is more closely related to ρ_N^{π} and that ρ_N^{σ} is not related to a_N by any such simple expression.

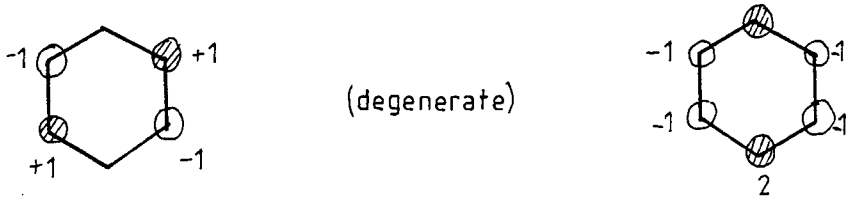

(i) $e_{2u(A)}$ (ii) $e_{2u(S)}$

FIG 69 TWO LOWEST UNNOCUPIED M.O.'s IN BENZENE

b_{2g} b_{3g}

FIG 70 TWO LOWEST UNNOCUPIED M.O.'s IN NAPHTHALENE

TABLE 47

anion	SOMO symmetry	a_N
pyridine	symm	6.28
pyridazine	assymm	5.29
pyrimidine	asymm	3.26
pyrazine	symm	7.18
s-tetrazine	asymm	5.27

If we regard aza substitution in the azines as a perturbation of the benzene system, for which the two lowest unoccupied M.O.'s are degenerate, see Fig (69) then the singly occupied molecular orbital (SOMO) of the azine anions will have the symmetry of either i) or ii). Table (47) shows the symmetry of the calculated azine SOMO, and the experimental coupling constants, a_N. It can be seen that in general the anions with the unpaired electron in e_{2UA} have smaller a_N (and ρ_N^π) than those with the symmetric e_{2US} SOMO. This is interpretable in terms of the electron density of the positions of substitution in the unperturbed C_6H_6 virtual orbital; $\propto$ nitrogen centres in e_{2US} are at positions which have relatively larger electron density than those at positions of maximum electron density in e_{2UA}.

We can extend this to the bicyclic anions; the two lowest unoccupied MO's of $C_{10}H_8$ are b_{2g} and b_{3g} which are energetically close ($|b_{3g}|-|b_{2g}|$ = 0.03 au for DZ calculation). See Fig.(70).

Inspection of the calculated eigenvectors of the radical anions show that in all cases the unpaired electron is in an orbital of apparent b_{2g} symmetry, which has maximum electron density in the α position and slightly less in the β position in $C_{10}H_8$. If we again regard aza substitution as a perturbation of $C_{10}H_8$ then we can expect that the electron density (and hence the SPC and HFCC's) to be greatest at positions where b_{2g} has highest electron density that is at the α positions. Table (48) gives the ρ_N^π and a_N and the positions (α,β) of aza substitution in the azanaphthalene

Table (48) Comparison of Experimental Nitrogen Coupling Constants and ρ_N^π with Position of N Substitution

	Positions of N Substitution	$\rho_N^\pi(9s/5p)_{aa}$	a_N experimental
Quinoline	α	0.219	3.95
Quinoxaline	α,α	0.331	5.70
1,5-Diazanaph-thalene	α,α'	0.165	3.37
1,8-Diazanaph-thalene	α,α'	0.149	2.4
Isoquinoline	β	0.112	1.92
Phthalazine	β,β	-0.025	0.876
2,6-Diazanaph-thalene	β,β'	0.219	-
2,7-Diazanaph-thalene	β,β'	-0.007	0.43
Cinnoline	α β	0.320 0.244	-
Quinazoline	α β	0.166 0.085	-
1,6-Diazanaph-thalene	α β'	0.144 0.036	-
1,7-Diazanaph-thalene	α β'	0.268 0.088	-

It would appear that in general α nitrogens have larger ρ_N^π (and a_N) than β nitrogens as is expected. However there are exceptions viz. cinnoline and 2,6-diazanaphthalene where although $\rho_N^\pi(\alpha) > \rho_N^\pi(\beta)$ is still observed for the former, the $\rho_N^\pi(\beta)$ in both cases is considerably larger than all other calculated $\rho_N^\pi(\beta)$. This could be due to

a) The trend not being generally adopted.

b) The calculated spin population densities being incorrect.

Unfortunately there is no experimental data with which i) or ii) can be proved or disproved. However it should be noted that $\langle S^2 \rangle_{aa}$ (expectation value of S^2 operator after annihilation for both cinnoline and 2,6-diazanaphthalene exhibits the largest deviation from the ideal value of 0.75 in the complete series of anions; $\langle S^2 \rangle_{aa}$ for all other anions is very close to 0.75. It has been noted[53] that spin population densities from UHF wavefunctions which gave too large values of $\langle S^2 \rangle_{aa}$, were poor. Therefore it is not unreasonable to assume that the trend we predict is general and that the large values of $\langle S^2 \rangle_{aa}$ for cinnoline and 2,6-diazanaphthalene anions is an indication of the inaccuracy of the calculated UHF wavefunction. (This is probably due to our using an unrealistic geometry for these particular anions).

It is interesting to note the effect on a_N/ρ_N^π of addition of a second ring to an azine structure. For example the quinoline anion, which effectively is a pyridine anion fused to a benzene ring, has a_N which is

2.33 gauss less than a_N in the pyridine anion. Similarly a_N for the quinoxaline anion is 2.51 gauss less than for the pyrazine anion. Unfortunately no other comparison of a_N can be made since no experimental data exists for cinnoline and quinazoline anions. However comparison of the 'α' ρ_N^π for these anions and those of pyridazine and pyrimidine shows that there is a reduction of about 0.03 upon addition of benzene ring. Using the best calculated value at Q_N^N and C from equation (13) this corresponds to a change of approximately 1.23 gauss. Therefore we can say that for azine anions with the unpaired electron in e_{2US}, addition of second ring to the system has a greater effect on $a_N(\alpha)$ than it has for $a_N(\alpha)$ of e_{2UA} azine anions. This indicates that in both cases the added benzene ring "drains" electron density from the N centres, the effect being greater for α nitrogens with greater initial spin population density, that is the α nitrogens in e_{2US} anions. (This comparison has been made assuming that the calculated ρ_N^π are accurate for cinnoline and quinazoline). No such comparison can be made for the β nitrogens since N centres only occur at positions of maximum electron density in the azine anions.

Although no firm conclusion can be made in the absence of experimental evidence we feel that it is likely:
a) that the absolute values of the spin densities are very sensitive to deviations of $\langle S^2 \rangle_{aa}$ from the ideal value (and hence to inaccuracies in ψ_{UHF}). This would account for

$\rho_N^\pi(\beta)$ in cinnoline and 2,6-diazanaphthalene being larger than our $\rho_N^\pi(\beta)$ but still allows for $\rho_N^\pi(\alpha)$ being relatively larger than $\rho_n^\pi(\beta)$ for cinnoline.

b) that aza substitution can be regarded as a perturbation to the original hydrocarbon system.

c) that the relative magnitudes of a_N (and hence ρ_N^π) can be interpreted in terms of electron density in the 'parent' unoccupied orbital.

Table (49) Expectation Value of S^2 Operator

(i) Radical Anions

Molecule	Minimal Basis		Double Zeta Basis	
	$\langle S^2 \rangle$ B.A.*	$\langle S^2 \rangle$ A.A.*	$\langle S^2 \rangle$ B.A.*	$\langle S^2 \rangle$ A.A.*
Naphthalene	0.8392	0.7561	0.8355	0.7555
Quinoline	0.8495	0.7575	0.8678	0.7609
Isoquinoline	0.8832	0.7645	0.8877	0.7649
Cinnoline	1.0095	0.8096	1.0005	0.8019
Quinazoline	0.9732	0.7915	0.9491	0.7851
Quinoxaline	0.8635	0.7579	0.8486	0.7558
1,5-Diazanaphthalene	0.8556	0.7588	0.8539	0.7584
1,6-Diazanaphthalene	0.8866	0.7652	0.8949	0.7653
1,7-Diazanaphthalene	0.8893	0.7656	0.8520	0.7581
1,8-Diazanaphthalene	0.8527	0.7579	0,8734	0.7616
2,3-Diazanaphthalene	0.8226	0.7539	0.8280	0.7544
2,6-Diazanaphthalene	1.0652	0.8495	0.9573	0.7905
2,7-Diazanaphthalene	0.8602	0.7592	0.8759	0.7616
Pyridine	0.8153	0.7510	0.8315	0.7539
Pyridazine	0.8930	0.7629	0.8673	0.7592
Pyrimidine	0.8866	0.7613	0.8678	0.7574
Pyrazine	0.8433	0.7508	0.8361	0.7516
S-tetrazine	0.8895	0.7617	0.7787	0.7506

*B.A. = Before Annihilation

A.A. = After Annihilation

(xiv) The Expectation Value of the S^2 Operator, $\langle S^2 \rangle$

$\langle S^2 \rangle$ is an indication of the goodness of the UHF wavefunction, ψ_{UHF}; values of $\langle S^2 \rangle$ before (b.a.) and after annihilation (a.a.), for the complete series of molecules, are given in Table (49). Since doublet open shell systems ($S_z = \frac{1}{2}$) have been studied here, $\langle S^2 \rangle$ should ideally have a value of 0.75.

There are three factors which can cause an increase in $\langle S^2 \rangle$ by affecting ψ_{UHF}

(i) Intrinsic contamination of ψ_{UHF} by higher multiplets.

(ii) The basis set used.

(iii) The geometry of the system under consideration.

Taking each in turn:

(i) ψ_{UHF} is not a pure spin state and is contaminated by higher multiplets. The largest contamination, by the next highest state, can be removed by the use of the annihilation operator, as shown above. The extent to which the contaminating multiplets cause an increase in the value of $\langle S^2 \rangle$ has been investigated in reference [54] where it was shown that percentage contamination of ψ_{UHF} by higher multiplets can be investigated as follows:

Let ψ_{UHF} be made up of three parts, doublet (D), quartet (Q), and sextet (X) respectively

$$\psi_{UHF} = a(D) + b(Q) + c(X)$$

and $$a^2 + b^2 + c^2 = 1 \qquad (26)$$

Let $$S^2 = \langle S^2 \rangle = a^2 \tfrac{1}{2}(\tfrac{1}{2} + 1) + b^2 \tfrac{3}{2}(\tfrac{3}{2} + 1) + c^2 \tfrac{5}{2}(\tfrac{5}{2} + 1)$$

$$= \frac{3}{4} a^2 + \frac{15}{4} b^2 + \frac{35}{4} c^2 \qquad (27)$$

Now let the annihilation operator, $\alpha_{\frac{1}{2}+1}$ work on ψ_{UHF}

$$\alpha_{\frac{1}{2}+1} = S^2 - (\tfrac{1}{2}+1)(\tfrac{1}{2}+2) \qquad (28)$$

This removes the contaminating quartet component.

$$\alpha_{\frac{1}{2}+1}|\psi_{UHF} = S^2|\psi_{UHF} - \frac{15}{4}|\psi$$

$$= \frac{3}{4}a + \frac{15}{4}b + \frac{35}{4}c - \frac{15}{4}a - \frac{15}{4}b - \frac{15}{4}c$$

$$= -3a + 5c = \psi' \qquad (29)$$

but ψ' is not normalized therefore we let

$$9a^2 + 25c^2 = N^2 \qquad (30)$$

and

$$\psi'|S^2|\psi' = N^2 S^2_{\text{after annihilation}} \qquad (31)$$

$$S_{aa} = \frac{1}{N^2}\left[\frac{27a^2}{4} + \frac{875c^2}{4}\right] \qquad (32)$$

This leaves us with a set of four equations in three unknown

$$S^2_{ba} = \frac{3}{4} a^2 + \frac{15}{4} b^2 + \frac{35}{4} c^2$$

$$S^2_{aa} = \frac{1}{N^2}\left(\frac{27}{4} a^2 + \frac{875}{4} c^2\right) \qquad (33)$$

$$a^2 + b^2 + c^2 = 1$$

$$9a^2 + 25c^2 = N^2$$

These have solutions

$$c^2 = \frac{Q(-\frac{15+4S^2_{ba}}{12})}{920-72S^2_{aa}} \qquad Q = 27-36S^2_{aa} \qquad b^2 = \frac{4S^2_{ba} - 3 - 32c^2}{12} \tag{34}$$

$$a = 1 - b^2 - c^2$$

This analysis enables us to ascertain the percentage multiplet contamination, and this has been done for a selection of molecules as shown in Table (50). When applied to the flavin radicals in reference [54], where values of 1.20 were obtained for $\langle S^2 \rangle$ after annihilation, this analysis showed that multiplet contamination of ψ_{AUHF} could not solely account for gross deviations of $\langle S^2 \rangle$ from the required 0.75.

(ii) Our results indicate that $\langle S^2 \rangle$ is not very sensitive to the basis set used since MB and DZ calculations give such similar results.

It is appropriate to mention the open shell investigations of Hinchliffe whose earlier work[53] on approximate structures (that is, not using experimental or optimized structures) such as the pentadienyl, benzyl, anilino and phenoxyl radicals[55] gave large values of $\langle S^2 \rangle$; for example 1.3027_{ba}, 0.9431_{aa} for the pentadienyl radical. His later work using large uncontracted basis sets gave better $\langle S^2 \rangle$ values, (for example 0.82_{ba}, 0.7513_{aa} for pyrazine[56] using 114 basis functions), which he initially attributed

to the sensitivity of $\langle S^2 \rangle$ to the basis set used. It should be noted, however, that $\langle S^2 \rangle$ improved not only as he increased the size of basis set, but also adopted the use of optimized geometries for the structures under investigation.

We feel that our results indicate that there is a limit to the improvement larger basis sets can make to $\langle S^2 \rangle$, and beyond that limit other factors become more significant.
(iii) Since the values of $\langle S^2 \rangle$ in Table (49) are relatively close to 0.75, and we can assume that the basis set is adequate, the contamination from higher multiplets small, we must conclude that the structures used are relatively close to the theoretical optimum geometry. This means that the initial assumption, that the ground state and anionic structures are similar, was valid.

Now the importance of the geometry factor for obtaining good $\langle S^2 \rangle$ values was indicated indirectly by Hinchcliffe's work and we are able to investigate this yet further: For radical anions where the unpaired electron resides in a delocalised π orbital, the introduction of this electron is expected to have only a small effect on the geometry of the structure, since the π orbital framework is not strongly involved in bonding. (This assumption is valid since π electrons have been shown from PES studies to generally produce peaks which have strong $0 \rightarrow 0$ transitions which indicate a small change in geometry in going from the neutral molecule to the π cation. It follows that outer valence π electrons are not considered to contribute

significantly to the bonding). Calculations on the azine radical cations, see Table (41), shows that for π cations $\langle S^2 \rangle_{aa}$ is again generally close to 0.75; for σ(LP_N) cations where the electron is removed from an orbital which can be considered to be heavily involved with the bonding σ framework of the molecule, there is a large deviation of $\langle S^2 \rangle_{aa}$ for all cations except pyrazine. (This exception indicates that the geometry used here for pyrazine must be closer to that of the theoretical geometry of the σ cation).

It should be noted that although $\langle S^2 \rangle$ for the σ cations is high, the total energies are lower than for the π cations, indicating their greater stability. If a geometry optimization were performed it is likely that this would improve both $\langle S^2 \rangle$ and further decrease the total energy of 'σ' cation reiterating the σ character of the highest occupied MO.

The $\langle S^2 \rangle_{aa}$ for the σ cations of the azines are equally as large as those reported in reference [54] for the flavin radicals where it was considered that geometry optimization alone would not be able to improve $\langle S^2 \rangle$ to the extent needed. They concluded that the use of a single determinantal wavefunction for large molecules was not adequate. There is, however, a comparably large difference between $\langle S^2 \rangle$ for the azine π and σ cations which is attributable to small changes in geometry.

From the evidence herein obtained we consider that large deviations in the value of $\langle S^2 \rangle_{aa}$ can be attributed to the geometry factor (iii) which contributes most to ψ_{UHF} when using basis sets of this quality and multiplet annihilation;

but for absolute verification of this, a UHF geometry optimization on both σ and π azine cations should be performed.

We can conclude that for calculations using basis sets of this quality, and annihilation $\langle S^2 \rangle_{aa}$ is a sensitive test of the quality of the UHF wavefunction.

References

1. For example a) R. Pariser, R.G. Parr, J.Chem.Phys., 21, 767 (1953).
   b) T. Yonezawa, H. Kato, Theor.Chim.Acta, 13, 125, (1969).
2. a) E. Clementi, J.Chem.Phys., 46, 4737, (1967).
   b) J.D. Petke, J.L. Whitten, J.A. Ryan, BullChem.Soc.Jpn, 48, 953, (1968).
   c) M. Hackmeyer, J.L. Whitten, J.Chem.Phys., 54, 3739, (1971).
   d) D.W. Genson, R.E. Christoffersen, J.Am.Chem.Soc., 94, 6904, (1972).
   e) T. Kyu-Ha, C.T. O'konski, Int.J.Quantum.Chem., 7, 609, (1973).
   f) J. Almlöf, B.Roos, U.Wahlgren, H. Johonsen, J.Electron.Sepctr.Relat.Phenom, 2, 51, (1973).
   g) M.H. Palmer, A.J. Gaskell, R.H. Findlay, J.Chem.Soc., Perkin Trans. 2, 778, (1974).
3. W.Von Neissen, W.P. Kraemer, G.H.F. Kiercksen, Chem.Phys., 41, 113, (1979).
4. M.H. Palmer, S.M.F. Kennedy, J.Chem.Soc., Perkin Trans., 1893, (1974).
5. R.W. Wagner, P. Hackmaan, M.Ashraf El Byournd, J.Mol.Spectrosc., 54, 167, (1975).
6. a) G.O. Sørensen, L. Mahler, N. Rastrup Andersen, J.Mol.Struct., 20, 119, (1974).
7. W.A. Yeranos, C.W. Spangler, J.Mol.Spectrosc., 24, 247, (1967).
8. W. Werner, R. Dreïzler, A. Rudolf, Z. Naturforsch, 22a, 531, (1967).
9. B.J. Bormans, G. Dewith, F.C. Mijhoff, J.Mol.Struct., 42, 121, (1977).

10. A.J. Merer, K.K. Innes, Proc.R.Soc.London, Ser.A, 302, 271, (1968).

11. G.S. Pawley, E. Yates, Acta.Crystallogr., B25, 2009, (1969).

12. C. Huiszoon, B.W. Van der Waal, A.B. Van Egmond, S. Vlakenia, Acta Crystallogr., B28, 3415, (1972).

13. M. Brufani, W. Fedeli, G. Giacomello, F.M. Riccieri, A. Vaciago, Atti.Acad.Nazi.Lincei.Rend.Classe Sci.Mat. Nat., 40, 187, (1966).

14. G.J. Visser, A.Vor, Acta.Crystallogr., B27, 1793, (1971).

15. C. Huiszoon, Acta.Crystallogr., B32, 998, (1976).

16. A. Clearfield, M.J. Sims, P. Singh, Acta.Crystallogr., B28, 350, (1972).

17. Y.P. Lee, D.F.R. Gilson, Can.J.Chem., 54, 2783, (1976).

18. R. Gleiter, E. Heilbronner, V. Hornung, Helv.Chim.Acta, 55, 255, (1972).

19. B.O. Jonsson, E. Lindholm, Int.J.Mass.Spectrom.Ion Phys., 3, 385, (1969).

20. C. Fridh, L. Asbrink, B.O. Jonsson, E. Lindholm, Int.J. Mass.Spectrom.Ion. Phys., 8, (1972), a) 85; b) 101; c) 215; d) 229; e) 485.

21. E. Heilbronner, V. Hornung, F.H. Pinkerton, S.F. Thames, Helv.Chim.Acta, 55, 289, (1972).

22. F. Brogli, E. Heilbronner, T. Kobayashi, Helv.Chim.Acta, 55, 274, (1972).

23. E. Lindholm, C. Fridh, L. Asbrink, Discuss.Farad.Soc., 54, 127, (1972).

24. D.M.W. Van Den Ham, D.Van Der Meer, Chem.Phys.Lett., 12, 447, (1972).

25. J.P. Bryne, I.G. Ross, Aust.J.Chem., 24, 1107, (1971).

26. S. Canuto, O. Gosunski, M.Zerner, Chem.Phys.Lett., 68, 232, (1979).

27. J. Spanget-Larsen, J.Electron.Spectros.Relat. Phenom, 3, 369, (1974).

28. J.H. Eland, C.J. Danby, Z.Naturforsch., Teil A, 23, 355, (1968).

29. S.I. Weissmann, J. Townsend, D.E. Paul, G.E. Pake, J.Chem.Phys., 21, 2227, (1953).

30. B. Venataraman, G.K. Fraenkel, J.Chem.Phys., 24, 737, (1956).

31. G.K. Fraenkel, M. Karplus, J.Chem.Phys., 35, 1312 (1961)

32. A. McLauchlin, Mol.Phys., 3, 233,(1960).

33. A.T. Amos, G.G. Hall, Proc. R. Soc., London, Ser. A. 263, 483, (1961).

34. L.C. Snyder, A.T. Amos, J.Am.Chem.Soc., 86, 1647 (1964).

35. B.T. Sutcliffe, J.Chem.Phys., 39, 3322, (1963).

36. J.A. Pople, J.Am.Chem.Soc., 90, 4201, (1968).

37. P.J. Black, C.A. McDowell, Mol.Phys., 12, 233, (1967).

38. J. Tino, Theoret.Chim.Acta, 18, 119, (1970).

39. J. Colpa, J. Bolton, Mol.Phys., 6, 273, (1963).

40. G. Giarometti, Theoret. Chim.Acta, 1, 404, (1963).

41. E. Fermi, Z.Physik, 60, 320, (1930).

42. H.M. McConnell, J.Chem.Phys., 24, 632, (1956).

43. A. Carrington, J.dos.Santos Viega, Mol.Phys., 5, 21, 1962.

44. R.L. Ward, J.Am.Chem.Soc. 84, 332, (1962).

45. N.M. Atherton, F. Gerson, J.N. Murrel, Mol.Phys., 5, 509, (1962).

46. C.A. McDowell, K.F.G. Paulus, Mol.Phys., 7, 541, (1963).

47. J.C.M. Henning, J.Chem.Phys.,44, 2139, (1966).

48. T. Amos, L.C. Snyder, J.Chem.Phys., 41, 1773, (1962).

49. T. Kato, T. Shida, Chem.Phys.Lett., 68, 106, (1979).
T. Kato , T. Shida, J.Am.Chem.Soc., 101, 6869, (1979).

50. C. Thom son, in Specialist Periodical Reports, ESR vol 3, The Chemical Society, (1974).

51. J. Ålmlof, A. Lund, K:Å-Thomas, Chem.Phys.Lett., 28, 179, (1974).

52. G.D. Zeiss, M.A. Whitehead, J.Chem.Soc., Faraday Trans 2, 68, 526 (1972).

53. A. Hinchcliffe, Chem.Phys.Lett., 13, 594, (1972).

54. R.J. Platenkamp, M.H. Palmer, A.J.W.G. Visser, in Press.

55. A. Hinchcliffe, J.Cobb, J.Mol.Struct., 23, 273, (1974).

56. A. Hinchcliffe, Int.J.Quant.Chem., 11, 767, (1977).

CHAPTER 6

GROUP(A)	GROUP(B)	GROUP(C)	GROUP(D)	GROUP(E)
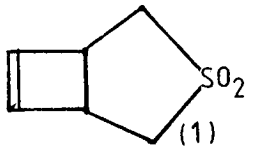 (1)	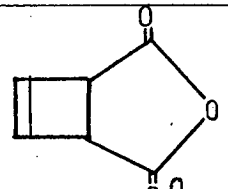 (13)	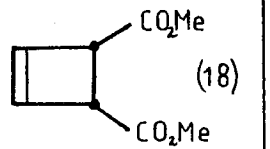 (18)	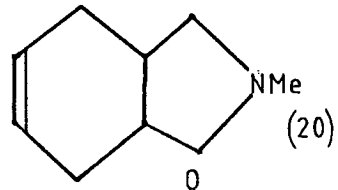 (20)	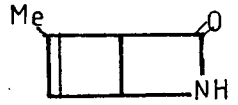 (22)
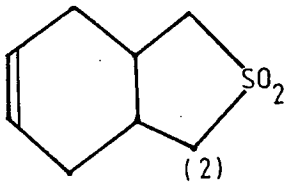 (2)	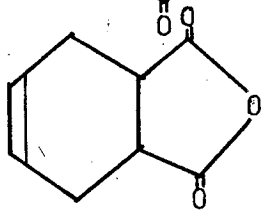 (14)	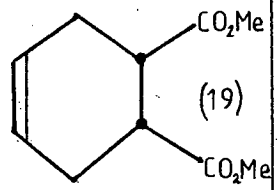 (19)	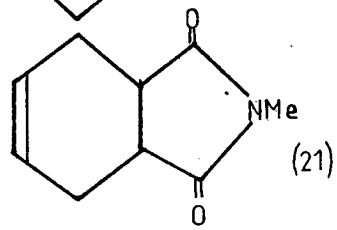 (21)	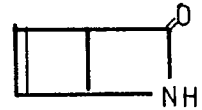 (23)
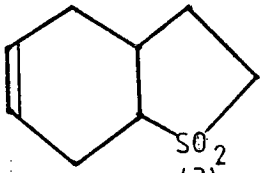 (3)	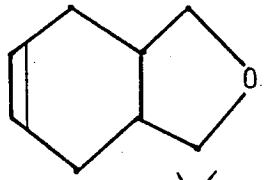 (15)			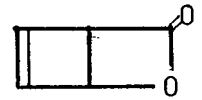 (24)
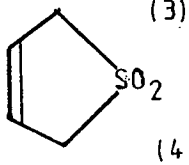 (4)	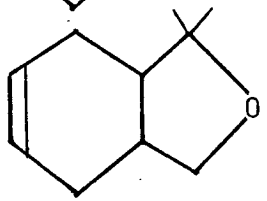 (16)			 (25)
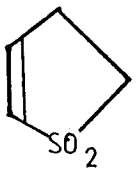 (5)	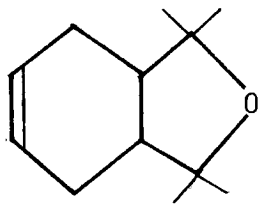 (17)			 (26)
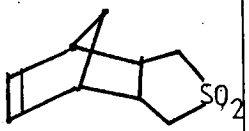 (6)				
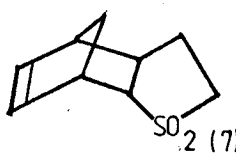 (7)				
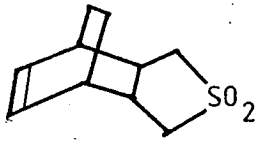 (8)				
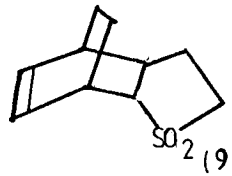 (9)				
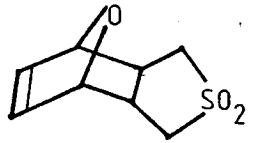 (10)				
Ai 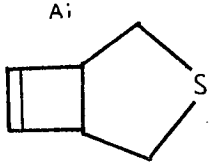 (11)				
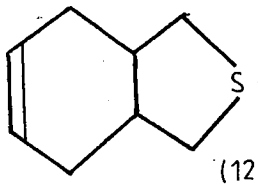 (12)				

Table (51) Nomenclature

(1) 3-Thiabicyclo[3,2,0]hept-6-ene-3,3-dioxide

(2) 3-Thiabicyclo[4,3,0]non-7-ene-3,3-dioxide

(3) 2-Thiabicyclo[4,3,8]non-7-ene-2,2-dioxide

(4) 2,5-Dihydrothiophen-1,1-dioxide

(5) 2,3-Dihydrothiophen-1,1-dioxide

(6) Endo-4-thiatricyclo[5,2,1,$O^{2,6}$]dec-8-ene-4,4-dioxide

(7) Endo-3-thiatricyclo[5,2,1,$O^{2,6}$]dec-8-ene-3,3-dioxide

(8) Endo-4-thiatricyclo[5,2,2,$O^{2,6}$]undec-8-ene-4,4-dioxide

(9) Endo-3-thiatricyclo[5,2,2,$O^{2,6}$]undec-8-ene-3,3-dioxide

(10) Exo-10-oxa-4-thiatricyclo[5,2,1,$O^{2,6}$]dec-8-ene-4,4-dioxide

(11) 3-Thiabicyclo[3,2,0]hept-6-ene

(12) 3-Thiabicyclo[4,30]non-7-ene

(13) 3-Oxabicyclo[3,2,0]hept-6-ene-2,4-dione

(14) 3-Oxabicyclo[4,3,0]non-7-ene-2,4-dione

(15) 3-Oxabicyclo[4,3,0]non-7-ene

(16) 2,6'-Dimethyl-3-oxabicyclo[4,3,0]non-7-ene

(17) 2,2',4,4'-Tetramethyl-3-oxabicyclo[4,3,0]non-7-ene

(18) 1,2-Dimethoxycarbonylcyclobut-3-ene

(19) 1,2-Dimethoxycarbonylcyclohex-4-ene

(20) 3-Methyl-3-azabicyclo[4,3,0]non-7-ene

(21) 3-Methyl-3-azabicyclo[4,3,0]none-7-ene-2,4-dione

(22) 5-Methyl-3-azabicyclo[4,3,0]none-7-ene-2,4-dione

(23) 2-azabicyclo[2,2,0]hex-5-en-3-one

(24) 2-Oxabicyclo[2,2,0]hex-5-en-3-one

(25) Cyclobutene

(26) Bicyclo[2,2,0]hexa-2,5-diene (Dewar benzene)

PHOTOELECTRON SPECTROSCOPY - REACTIVITY STUDIES

(i) Introduction

This chapter is primarily concerned with experimental studies (PES) of the series of molecules* given in Fig (71). The initial aim of this work was to estimate the IP of the olefinic double bond, $IP\pi_{C=C}$, present in each molecule, to see if this matched the observed reactivities of these molecules. Ab initio calculations have been performed on selected molecules of the series primarily as an aid to spectral interpretation.

The initial interest in this molecular series was prompted by the lack of reactivity of the cyclobutene molecules 1, 13, 18, (when compared with the reactivity of the cyclohexene analogs we 2, 14, 19) for nitrene addition across the double bond, see Fig. (72). The lack of reactivity was evidenced by smaller percentage yield of the product. This was unexpected since in classical organic chemical terms four membered rings are considered less stable than six membered rings due to increased ring strain, and therefore this double bond might reasonably be expected to be more reactive.

Initially the percentage yield for nitrene addition in 1,13,18 was found to be almost zero, but during the course of this work this was found to be incorrect (the nitrene product was found to be very insoluble and had been accidentally filtered off). A re-estimate of the percentage yield for these molecules was < 13%. Percentage yields for 2,14,19 were about 26%. It should be noted that although relative

*Samples and other synthetic experimental results were kindly provided by Dr. I. Gosney, Department of Chemistry, University of Edinburgh.

FIG 72 NITRENE ADDITION.

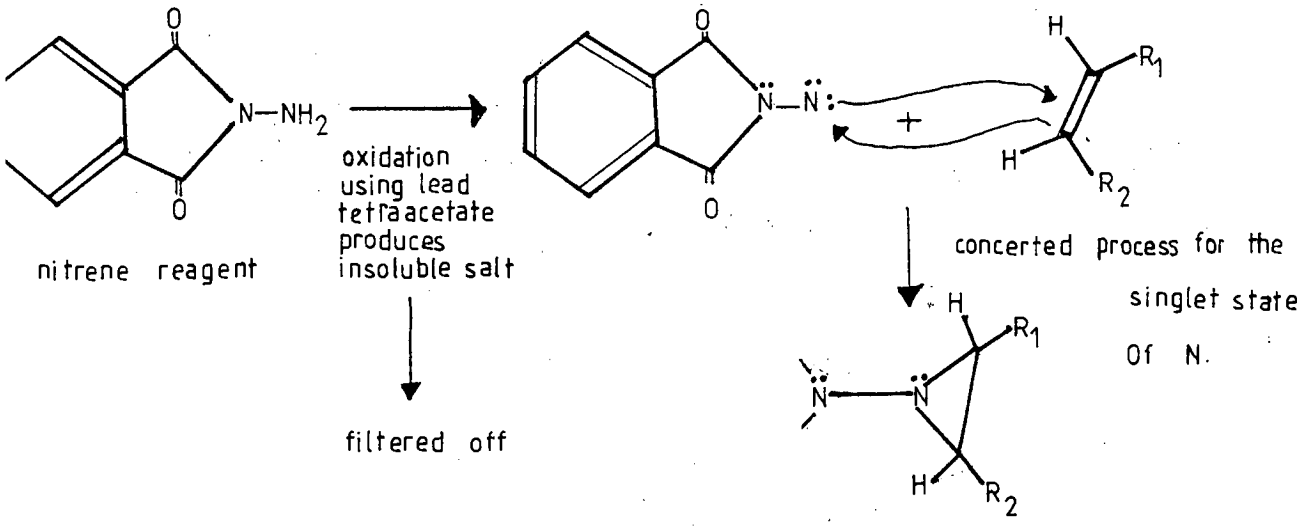

3) THE OTHER NITRENE USED WAS $EtO-\overset{\overset{O}{\|}}{C}-\ddot{N}:$

WHICH IS LESS ELECTROPHILIC THAN (A)

FIG 73 REACTIVITY OF OLEFINIC GROUP REPORTED IN REFERENCE [2].

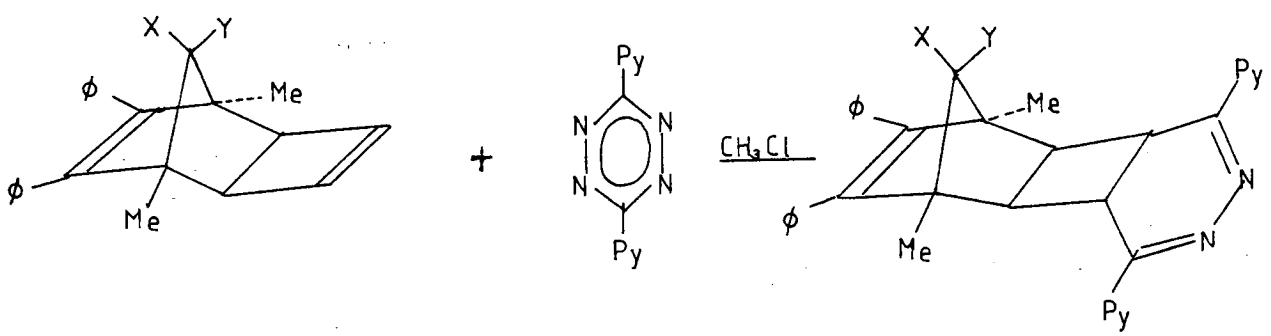

a) X = Y = H

b) X = Y = O

c) X = H, $Y = OCH_3$

REACTION RATE IN CHLOROFORM c >> a > b

Py = 2'- pyridyl

percentage yield is not a satisfactory measure of reactivity, since it is sensitive to many other effects, it is considered that large differences in percentage yield are indicative of a difference in reactivity.

The relative lack of reactivity of molecules 1,13,18 could be due to several factors:

a) As the nitrene is electrophilic it is possible that some intermolecular intereaction was taking place which results in stabilization of the double bond.

b) It is possible that since addition of the nitrene results in formation of a strained three membered ring system across the double bond, its formation in an already strained system would be energetically less favourable.

If b) were the case we would not expect any trend in $IP\pi_{C=C}$ to be observed. If, however, some stabilization of the olefinic double bond, which resulted in reduced reactivity, were taking place then this would be evidenced by a stabilization of $IP\pi_{C=C}$.

Warrener[1,2] et al have noticed sensitivity of olefinic bond reactivity in the series of molecules given in Fig (7 3) to remote substituents. They attributed these effects to "through space" intereactions between substituent and double bond. The PES and ab initio calculations reported here can provide information about the extent and type of interactions which result from different five membered ring substituents, from an investigation of the relative magnitudes of $IP\pi_{C=C}$ and appropriate molecular orbital analyses.

FIG 74 CONSTRUCTION OF MOLECULAR GEOMETRIES *

a) molecule 13

from Dewar benzene

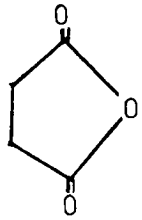

from Succinic anhydride

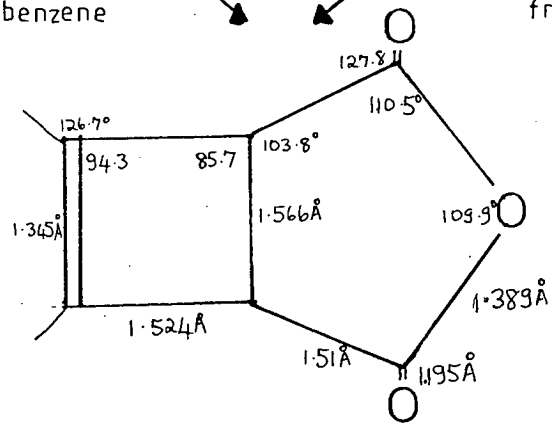

interplanar angle = 117.25Å

C-H = 1.118Å

α = 52.3° (angle between the intersection of the planes through C5, C6, C3 ; HCH and C6-C5 bond. $\angle C3C2H2 = 48.99°$)

b) cyclohexene

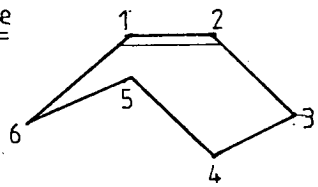

half chair

conformations of cyclohexene

boat

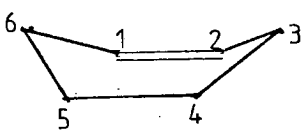

c) molecule 14

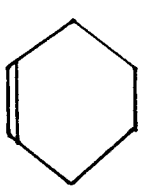

boat conformation of cyclohexene

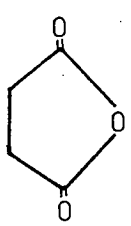

from succinic anhydride

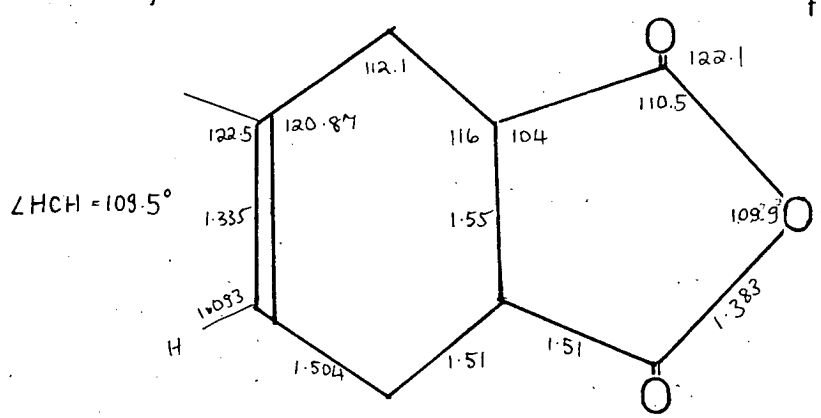

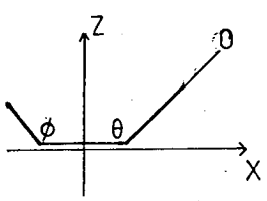

cross section of molecule 14

ϕ = 118.25°

θ = 117.25°

C=O = 1.194

* Bond Lengths in Å

Bond Angles in Degrees

Calculations

Calculations were performed for structures 1,2,11,12, 13,14,20,23,24,25,26 using a 7s/3p minimal basis set (see Appendix A), the Atmol-3 suite of programs, and molecular geometries constructed as described below

(ii) Molecular Geometries

Of the molecules studied, experimental structures exist for only (25)[3] and (26)[4], and these were adopted for calculation. Geometries were constructed for the remaining structures by fusing experimental geometries for the five membered heterocyclic systems to a cyclobutene or cyclohexene ring.

The molecule (13) was constructed by the fusion of half a Dewar benzene system to the crystal structure of succinic anhydride.[5] The bridging bond C3-C6 was assumed to be 1.55Å which is the average of the bridge bond in Dewar benzene and C3-C4 bond in succinic anhydride. The molecule is not planar and the equilibrium interplanar angle of Dewar benzene[4] was adopted.

An electron diffraction structure is available for cyclohexene[6] where the molecule is shown to be in the half chair conformation. However when a second ring is fused to this structure as in (14), this constrains the C5-C6 and C4-C5 bond orientations such that they lie in the same plane; the cyclohexene structure therefore adopts the boat conformation, see Fig. (7 4). For molecule (14) the succinic anhydride structure[5] was fused to this boat conformation of cyclohexene, preserving its C4-C5 bond length. The bond lengths of the C1,C2,C3,C6 section were assumed

FIG 74 CONT*

d) molecule 1

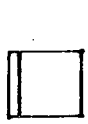

from Dewar benzene

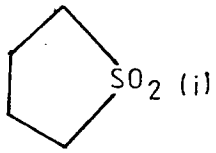

tetrahydrothiophene-1,1-dioxide

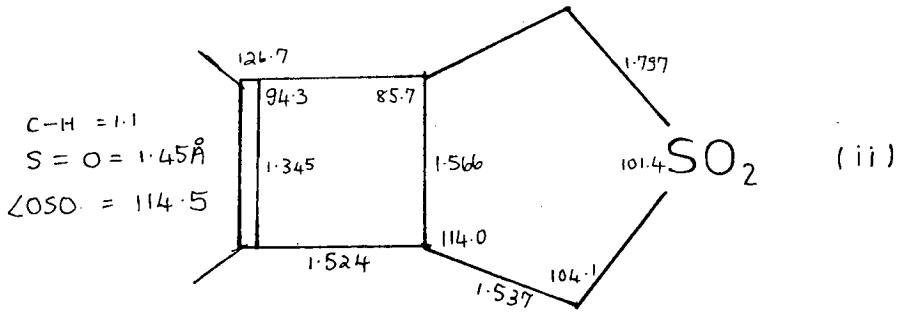

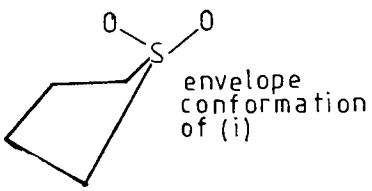

envelope conformation of (i)

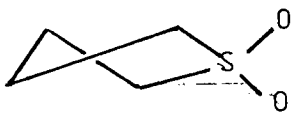

half chair conformation of (i)

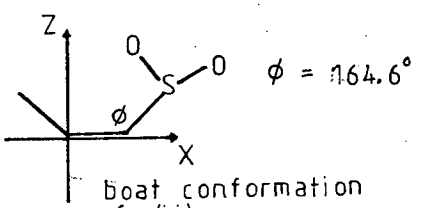

ϕ = 164.6°

boat conformation of (ii)

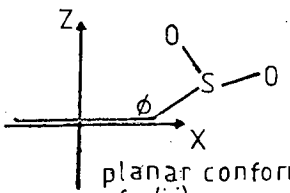

planar conformation of (ii)

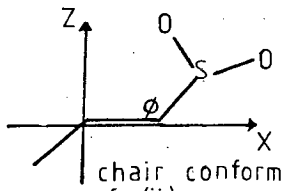

chair conformation of (ii)

e) molecule 2

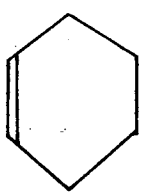

'boat' cyclohexene

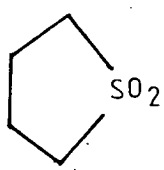

tetrahydrothiophene-1,1-dioxide

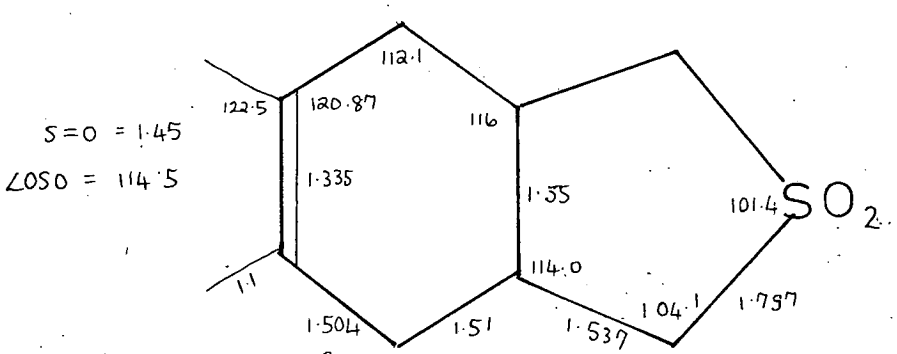

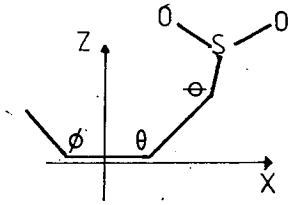

cross section of molecule 2

ϕ = 118.25°
θ = 117.25°
$\ominus$ = 164.6°

* Bond Lengths in Å

identical to those of the half chair structure, and the azimuthal angle was 118.25°. The resulting system can adopt the boat or chair conformations. Previous ab initio calculations[7] on both of these conformations have shown that the boat form is energetically preferred. The interplanar angle was taken as 117.25° (that of Dewar benzene).

The electron diffraction structure of tetrahydrothiophen-1,1-dioxide[8] was fused to a half Dewar benzene structure to construct the geometry of molecule (1). The five membered ring can exist in the envelope or half-chair conformation, but the former must be used here since the bonds from the C-C bridge are locked by the presence of the second ring. The bridging bond length was taken as 1.566Å, and the interplanar angle used was 117.25°. Calculations on both the boat, planar and chair conformations[7] (Fig (7 4)) of this molecule showed that the boat form is energetically preferred.

For molecule (2), the tetrahydrothiophene-1,1-dioxide structure[8] was fused to the boat cyclohexene structure, being modified to allow a bridging bond length of 1.55Å, (the length of the corresponding bond in cyclohexene). The interplanar angle was assumed to be 117.25°, and the boat molecular conformation was used.

The structures of molecules (11) and (12) were assumed to be those of (1) and (2) without the sulphone oxygens.

No structure is available for N-methyl-tetrahydropyrrole, therefore in constructing the geometry of molecule (20) the five membered ring structure was taken as that of tetrahydrofuran[9] with the oxygen replaced by an N-methyl group with

FIG 74 CONT

f) molecule 20*

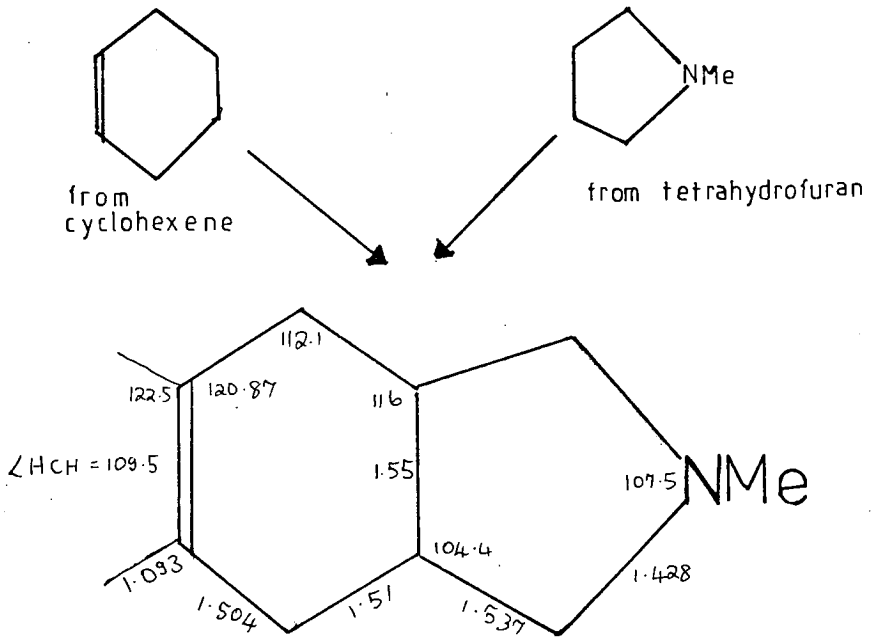

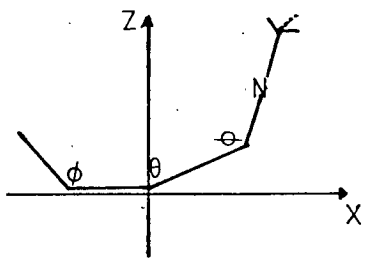

cross section of molecule 20

$\phi = 118.25°$

$\theta = 117.25°$

$\Theta = 164.6°$

g) molecule 23*

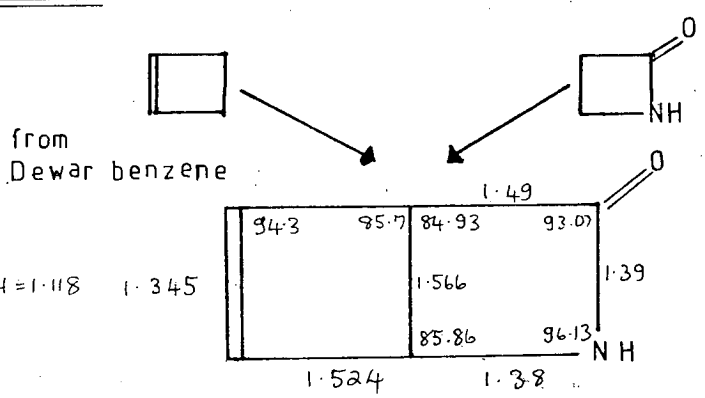

h) molecule 24*

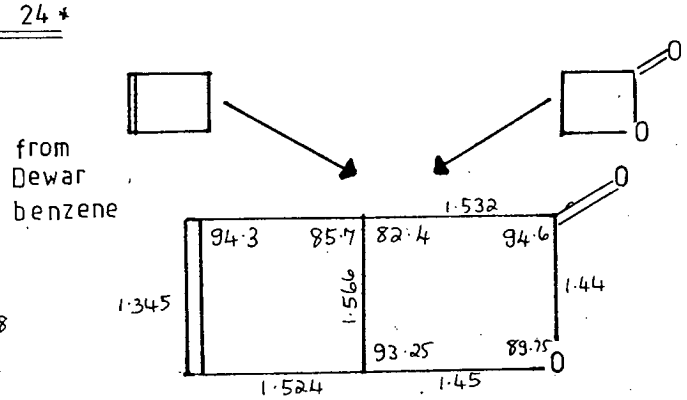

* Bond Lengths in Å
Bond Angles in Degrees.

N-C bond length 1.47Å. Tetrahydrofuran was shown to be non-planar in reference [7], but the conformation was not ascertained. We assume an envelope structure with azimuthal angle of 164.6°. This five membered ring structure was fused to the boat conformation of cyclohexene preserving the C4-C5 1.55Å bond length.

The crystal structures of propiolactone[10] and azetidine[11] were fused to the half Dewar benzene system in forming structures of (24) and (23) respectively. The Dewar benzene C3-C6 bridging bond length and interplanar angles were adopted.

Additional Calculations

To check the orbital ordering predicted by Koopman's Theorem, ΔE_{SCF} calculations, see page (9 1), have been performed for molecules (2) and (25) using ground state structures for each ionized state.

Analysis of the four highest occupied molecular orbitals was performed by utilization of the "Mulliken Analysis" facility available in the Atmol-3 suite of programs. Briefly this analysis takes any chosen calculated molecular orbital and estimates its electron density at each centre in the molecule on a percentage basis, i.e. assuming one electron in the orbital.

Table (52) contd. Total Orbital Energies

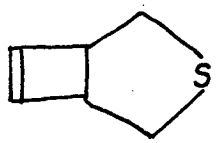	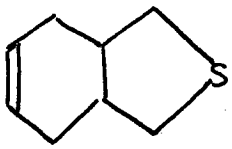	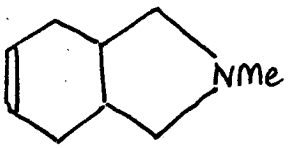
Total Energy -628.0128914	Total Energy -705.927618553	Total Energy -402.92286215 au
Orbital Energie(eV)	Orbital Energies(eV)	Orbital Energies(eV)
-8.95 a'	-8.65 a'	-8.22 a'
-9.86 a'	-9.87 a'	-9.71 a'
-11.64 a'	-11.05 a'	-11.75 a"
-12.56 a"	-12.03 a"	-12.36 a'
-13.03 a'	-12.71 a"	-12.55 a"
-13.45 a"	-12.99 a'	-13.48 a"
-14.32 a"	-13.84 a"	-13.68 a'
-14.86 a'	-14.54 a'	-14.07 a"
-16.37 a"	-14.64 a'	-14.25 a'
-16.65 a'	-15.26 a'	-14.96 a"
-17.67 a'	-15.42 a'	-14.99 a'
-18.92 a'	-15.52 a"	-15.39 a'
-18.98 a"	-17.13 a'	-16.09 a"
-21.28 a'	-17.35 a"	-16.25 a'
-22.339 a"	-18.16 a'	-16.77 a"
-24.182 a'	-18.45 a"	-17.76 a'
-27.23 a"	-18.99 a'	-17.99 a'
-28.72 a'	-21.45 a'	-18.34 a"
-32.56 a'	-21.51 a"	-18.97 a'
-177.84 a'	-23.26 a'	-21.08 a'
-177.91 a'	-25.54 a"	-21.46 a"
-177.94 a"	-26.35 a'	-22.96 a'
-235.36 a'	-28.88 a"	-25.25 a'
-306.58 a"	-29.05 a'	-25.42 a"
-306.61 a'	-31.82 a'	-27.82 a'
-306.68 a'	-177.63 a'	-28.27 a"
-306.69 a"	-177.70 a'	-30.48 a'
-306.88 a'	-177.73 a"	-33.16 a'
-306.88 a"	-235.16 a'	-305.88 a"
-2492.01 a'	-306.10 a"	-305.90 a'
	-306.11 a'	-306.05 a'
	-306.28 a'	-306.05 a"
	-306.28 a"	-306.28 a'
	-306.68 a'	-306.29 a"
	-306.69 a"	-306.56 a'
	-306.74 a'	-306.56 a"
	-306.74 a"	-306.66 a'
	-2491.79 a'	-420.85 a'

Table (52) contd. Total and Orbital Energies

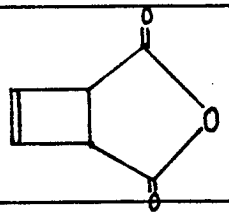	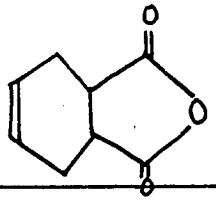	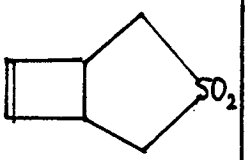	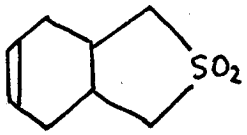
Total Energy -452.7117702au	Total Energy -530.6598259au	Total Energy -777.7874516au	Total Energy -855.0905481au
Orbital Energies(eV)	Orbital Energies(eV)	Orbital Energies(eV)	Orbital Energies(eV)
-11.68 a'	-10.83 a'	-10.94 a'	-10.22 a'
-13.05 a"	-12.81 a"	-11.63 a"	-11.34 a"
-13.57 a'	-13.26 a'	-11.77 a'	-11.70 a'
-13.47 ap	-13.33 a"	-12.54 a"	-12.35 a"
-14.41 a"	-13.56 a'	-12.65 a'	-12.45 a'
-15.55 a'	-14.49 a'	-13.53 a"	-12.83 a"
-16.64 a"	-15.36 a"	-14.01 a'	-13.66 a'
-16.86 a'	-16.02 a'	-14.89 a'	-14.20 a"
-17.45 a'	-16.14 a"	-15.09 a"	-14.82 a'
-17.56 a"	-16.55 a'	-16.11 a'	-15.46 a"
-18.57 a"	-16.81 a"	-16.86 a'	-15.54 a'
-18.92 a'	-17.41 a'	-17.50 a"	-15.66 a"
-19.56 a'	-17.85 a"	-17.91 a"	-15.97 a'
-20.78 a'	-17.95 a'	-18.28 a'	-16.33 a'
-21.58 a"	-18.54 a"	-18.61 a'	-17.06 a'
-22.38 a'	-18.97 a'	-19.56 a'	-17.95 a"
-24.50 a"	-19.46 a'	-20.20 a"	-18.23 a"
-27.40 a"	-20.54 a'	-22.07 a'	-18.46 a"
-27.93 a'	-20.57 a"	-23.52 a"	-18.8 a'
-34.22 a'	-22.44 a'	-24.86 a'	-19.28 a"
-38.36 a'	-23.81 a"	-28.62 a"	-19.82 a'
-39.79 a"	-25.07 a'	-29.45 a'	-22.14 a'
-42.03 a'	-25.84 a"	-33.50 a'	-22.54 a"
-308.41 a"	-29.50 a"	-35.66 a'	-23.89 a'
-308.42 a'	-29.55 a'	-39.08 a'	-26.65 a"
-308.82 a'	-32.79 a'	-188.27 a"	-26.88 a'
-308.84 a"	-38.24 a'	-188.31 a'	-29.69 a'
-314.04 a'	-39.74 a"	-188.35 a'	-29.82 a"
-314.05 a"	-41.83 a'	-245.53 a'	-32.64 a'
-561.38 a'	-307.03 a"	307.32 a"	-35.56 a'
-561.38 a"	-307.05 a'	307.32 a'	-38.97 a'
-562.33 a'	-307.56 a'	307.68 a'	-188.12 a"
	-307.57 a"	307.70 a"	-188.15 a'
	-308.62 a'	307.81 a'	-188.19 a'
	-308.63 a"	307.81 a"	-245.38 a'
	-313.85 a'	557.32 a'	-306.54 a"
	-313.85 a"	557.41 a'	-306.55 a'
	-561.19 a'	-2504.90 a'	-306.88 a'
	-561.19 a"		-306.88 a"
	-562.11 a'		-307.58 a'
			-307.58 a"
			-307.58 a'
			-307.59 a'
			-557.19 a"
			-557.317 a'
			-2504.73 a'

Table (52) Total and Orbital Energies

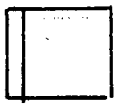	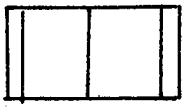	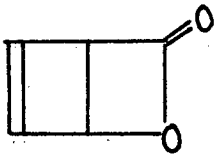	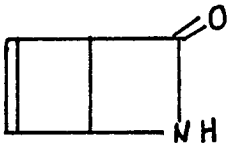
Total Energy -154.5063299	Total Energy -229.9447749	Total Energy -340.27589312	Total Energy -320.516234941
Orbital Energies(eV)	Orbital Energies(eV)	Orbital Energies(eV)	Orbital Energies(eV)
-10.06 $2b_1$	-9.89 $5b_2$	-11.18	-10.39
-12.76 $5b_2$	-10.47 $8a_1$	-12.69	-10.56
-13.12 $7a_1$	-11.47 $7a_1$	-12.96	-12.06
-14.13 $1a_2$	-12.28 $3a_2$	-13.18	-12.71
-14.81 $6a_1$	-13.43 $5b_1$	-15.18	-14.24
-18.08 $1b_1$	-15.02 $4b_2$	-15.80	-14.48
-18.65 $5a_1$	-16.41 $6a_1$	-16.26	-15.21
-19.10 $4b_2$	-17.58 $4b_1$	-17.81	-16.91
-23.86 $3b_2$	-17.88 $3b_2$	-18.54	-17.44
-23.47 $4a_1$	-18.71 $5a_1$	-19.16	-19.02
-31.67 $3a_1$	-20.28 $2a_2$	-19.87	-19.59
-306.17 $2b_2$	-23.07 $4a_1$	-20.20	-20.12
-306.18 $2a_1$	-23.97 $3b_1$	-21.95	-21.91
-306.28 $1a_1$	-28.53 $2b_2$	-24.85	-24.76
-306.29 $1b_2$	-33.26 $3a_1$	-26.78	-26.29
	-306.21 $2a_1$	-32.81	-31.29
	-306.22 $2b_2$	-38.59	-34.99
	-306.38 $1b_1$	-40.31	-36.68
	-306.38 $1a_2$	-307.77	-307.24
	-306.38 $1a_1$	-307.79	-307½42
	-306.40 $1b_2$	-308.07	-307.50
		-309.32	-308.41
		-313.34	-311.24
		-560.80	-424.30
		-561.18	-557.48

(iii) Results

Calculated total and orbital energies are given in Table (52). Of the molecules studied, only (25) and (26) have had previously reported theoretical studies.[12,13]

Results of the ΔE_{SCF} calculations are given in Table (53) and give the same orbital orderings as KT. ΔE_{SCF} calculations were attempted for (24) but convergence could only be attained for the first ionized state. For other states, although the configuration locking procedure available in Atmol-3, iterated molecular orbitals to be selected on the principle of maximum overlap with the trial molecular orbitals), was used for the second and third ionized states, reversal to the first ionized state was always obtained. This indicates that the energy surfaces for both the second and third ionized states must be somewhere degenerate with the energy surface of the first ionized state. At these points the configuration initially forced by the lock directive, can revert to that preferred by the Aufbau principle whence the energy is minimized along the most steeply descending surface.

The results of the Mulliken Analyses of the highest occupied molecular orbitals for each molecule theoretically studied, are given in Table (54).

Table (53) Results of ΔE_{SCF} Calculations

8-Thiabicyclo[4.3.0]non-3-ene-8,8-dioxide (2)

Molecular/Ionic State	Total Energy (au)
Ground State	-855.0905
First Ionized	-854.7549
Second Ionized	-854.7351
Third Ionized	-854.6526

$IP_I = E_{\text{"I"th ionized state}} - E_{\text{Ground state}}$

$IP_1 = 9.13$ eV

$IP_2 = 9.67$ eV $\quad IP_1 < IP_2 < IP_3 \equiv$ ordering predicted by KT

$IP_3 = 11.92$ eV

Molecule 23

Molecular/Ionic State	Total Energy (au)
Ground State	-320.5162
First Ionized	-320.2189
Second Ionized	-320.1875
Third Ionized	-320.1514

$IP_1 = 8.08$ eV

$IP_2 = 8.94$ eV $\quad IP_1 < IP_2 < IP_3 \equiv$ ordering predicted by KT

$IP_3 = 9.93$ eV

Table (54) Mulliken Analyses of the Three Highest Occupied Molecular Oribtals

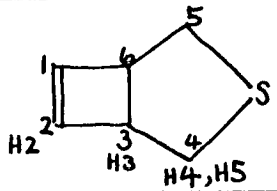

	HOMO	HOMO-1	HOMO-2
C2	0.0017	0.284	0.167
C3	0.002	0.037	0.052
C4	0.014	0.051	0.054
S	0.872	0.191	0.434
H2	0.00008	0.0002	0.002
H3	0.00004	0.031	0.0004
H4	0.016	0.00001	0.0006
H5	0.028	0.0000	0.005

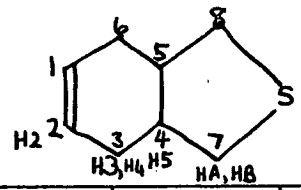

	HOMO	HOMO-1	HOMO-2
C2	0.04	0.319	0.065
C3	0.006	0.021	0.033
C4	0.006	0.015	0.046
C7	0.016	0.013	0.082
S	0.76	0.175	0.575
H2	0.0000	0.0000	0.0000
H3	0.002	0.005	0.0005
H4	0.006	0.032	0.0000
H5	0.0000	0.0001	0.012
HA	0.025	0.003	0.0008
HB	0.016	0.0008	0.0000

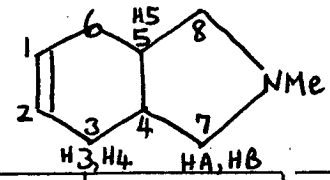

	HOMO	HOMO-1	HOMO-2
C2	0.011	0.403	0.08
C3	0.004	0.021	0.13
C4	0.007	0.01	0.111
C7	0.025	0.002	0.019
N	0.645	0.032	0.0001
CN	0.016	0.003	0.0000
HX	0.04	0.003	0.000
HY	0.01	0.0004	0.0001
HZ	0.01	0.0004	0.0001
H2	0.000	0.00003	0.052
H3	0.001	0.007	0.0008
H4	0.004	0.033	0.002
H5	0.0003	0.0003	0.066
HA	0.053	0.001	0.013
HB	0.029	0.0008	0.010

Table (54) contd.

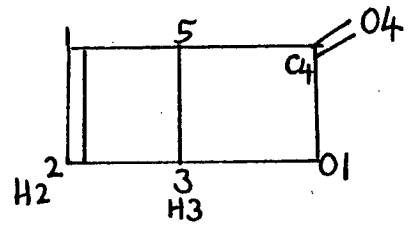

	HOMO	HOMO-1	HOMO-2
C1	0.331	0.140	0.032
C2	0.265	0.074	0.064
C3	0.074	0.084	0.258
C4	0.052	0.012	0.013
C5	0.022	0.086	0.187
O4	0.175	0.197	0.07
O1	0.056	0.326	0.313
H1	0.002	0.030	0.010
H2	0.000	0.011	0.021
H3	0.013	0.20	0.020
H5	0.005	0.015	0.006

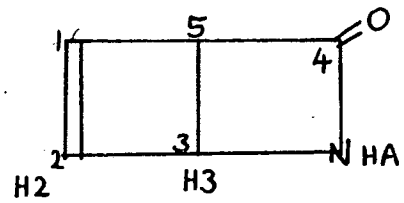

	HOMO	HOMO-1	HOMO-2
C1	0.0823	0.213	0.222
C2	0.038	0.165	0.260
C3	0.012	0.070	0.048
C4	0.022	0.034	0.002
C5	0.019	0.021	0.002
N	0.368	0.060	0.091
O4	0.42	0.409	0.416
H1	0.004	0.003	0.0001
H2	0.003	0.0001	0.0007
H3	0.008	0.006	0.0013
HA	0.0002	0.002	0.008
H5	0.01	0.01	0.005

Table (54) Mulliken Analysis of Three Highest Occupied Molecular Orbitals

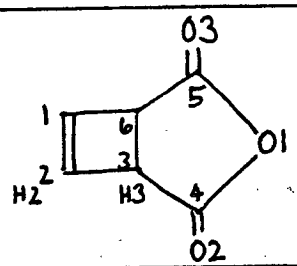

HOMO		HOMO-1	HOMO-2
C2	0.383	0.016	0.004
C3	0.027	0.062	0.006
C4	0.021	0.018	0.038
O1	0.053	0.112	0.357
O2	0.046	0.339	0.271
H2	0.001	0.004	0.0001
H3	0.005	0.002	0.0003

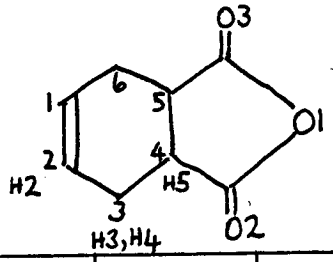

HOMO		HOMO-1	HOMO-2
C2	0.416	0.006	0.027
C3	0.023	0.0169	0.022
C4	0.01	0.056	0.096
C7	0.002	0.023	0.024
O1	0.005	0.113	0.17
O2	0.001	0.320	0.216
H2	0.009	0.001	0.001
H3	0.035	0.000	0.021
H4	0.0031	0.009	0.0009
H5	0.0003	0.009	0.002

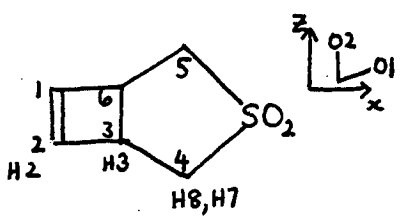

C2	0.384	0.012	0.002
C3	0.02	0.03	0.0002
C4	0.03	0.139	0.004
S	0.02	0.09	0.055
O1	0.02	0.203	0.44
O2	0.04	0.314	0.47
H2	0.001	0.002	0.00004
H3	0.03	0.003	0.00002
H7	0.03	0.001	0.003
H8	0.005	0.003	0.000025

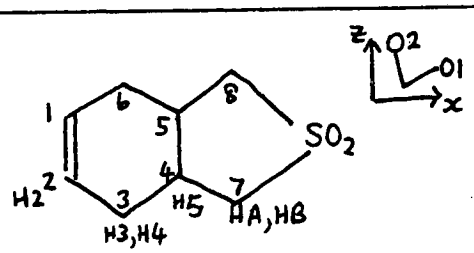

C2	0.397	0.0008	0.014
C3	0.0235	0.011	0.0006
C4	0.012	0.03	0.0003
C7	0.003	0.144	0.003
S	0.0025	0.09	0.05
O1	0.01	0.226	0.465
O2	0.02	0.259	0.426
H2	0.0000	0.0000	0.0000
H3	0.008	0.002	0.0000
H4	0.036	0.006	0.0007
H5	0.0002	0.009	0.00004
HA	0.0005	0.0011	0.0041
HB	0.0008	0.0015	0.0019

FIG 76

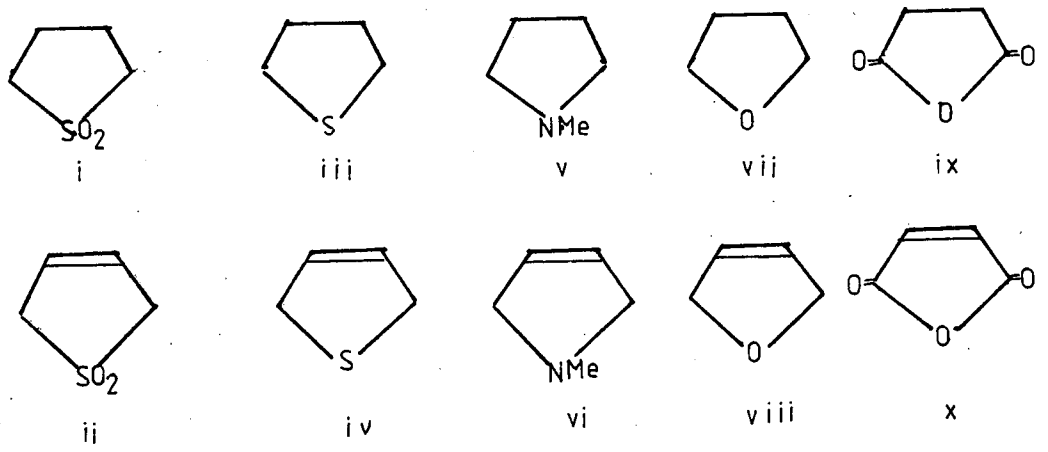

FIG 76 CORRELATION DIAGRAM REPRESENTING INTERACTION OF π LEVEL OF CIS BUT-2-ENE WITH THE NON BONDING LEVEL OF TETRAHYDRO -1,1'-DIOXIDE.

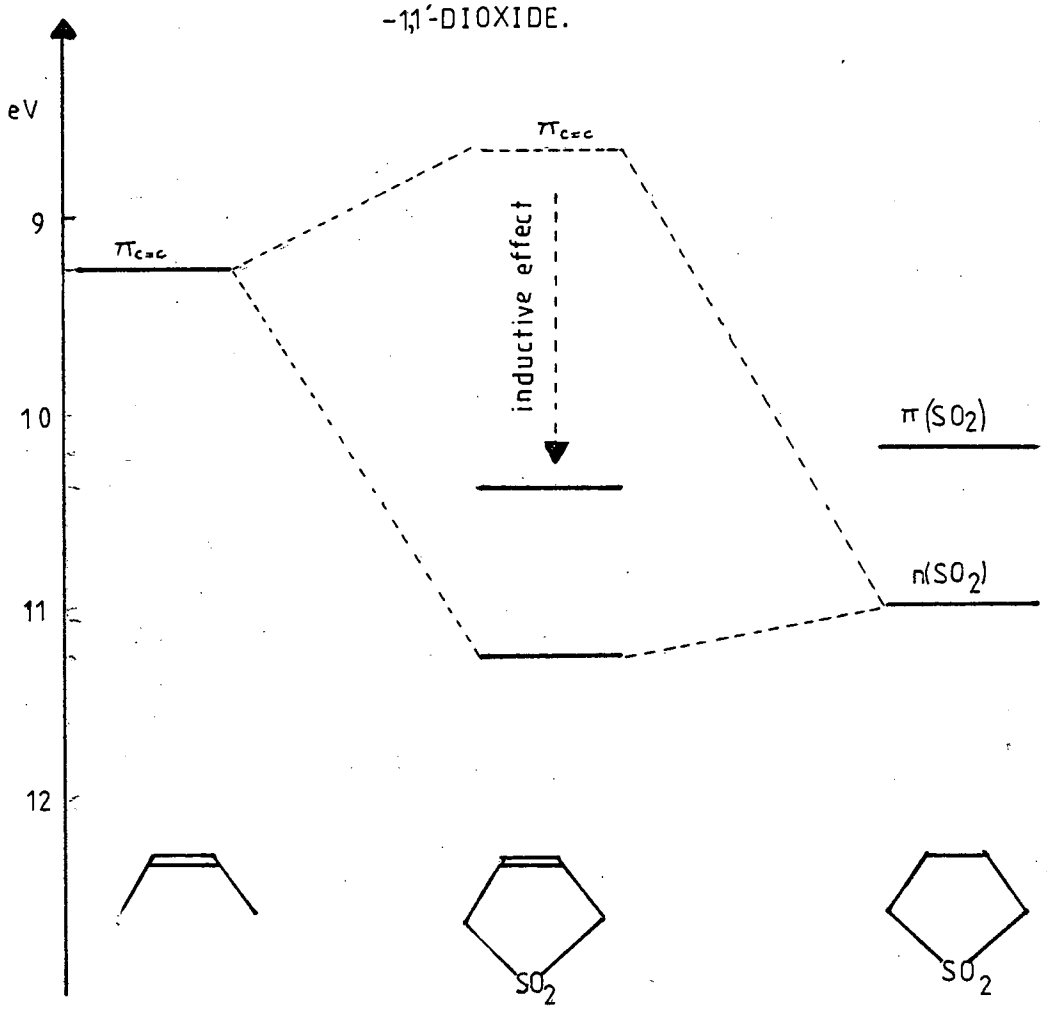

(iv) Photoelectron Spectra

He(I) photoelectron spectra were obtained for molecules (1-24) on the Perkin Elmer PS 16 spectrometer, see Figs (82a to 82w). The Xenon and Argon $^2P_{\frac{1}{2},\frac{3}{2}}$ were used as internal calibrants. In addition He(II) spectra were obtained for selected molecules as a complementary aid to spectral assignment. He(II) spectra were only made available by use of the Time Averaging Computer (CAT) since the He(II) count rates for all molecules were extremely low (< 15 counts per second). Since the initial aim of this work was to study the variation of $IP\pi_{C=C}$ for the complete series of molecules, we attempt no complete spectral assignment, but rather assignment of the first three IP's.

General Considerations

Before attempting assignment of PES for the bicyclic systems (1 to 24), it is appropriate to consider the positions of $IP\pi_{C=C}$ and the substituent levels in the monocyclic series of molecules (i) to (X) given in Fig (75), of which (i)[14] and (ii)[15] have been experimentally studied herein. The PES of (iii) to (x) have been reported elsewhere.[16,17,18,19].

Spectral interpretation can be done from first principles using the "composite molecule" approach. This is based on the assumption that a large molecule may be hypothetically fragmented into smaller molecular sub units, and information concerning these simpler sub units may be used to provide a picture of the whole molecule. This approach is used as a standard interpretive technique.[20] We illustrate by example: we can imagine the olefinic level in (ii), (iv), (vi), (viii), (x) to be the perturbed $\pi_{C=C}$ level of but-2-ene,

perturbed by an interaction with a low lying level of the substituent. This substituent level can be represented by the lowest (binding energy) level in the tetrahydro structure.

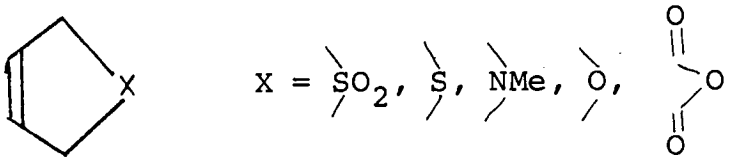

The interaction results in destabilization of the lower binding energy level of the pair, and stabilization of the higher. This effect can be interpreted by first order perturbation theory,[21] which gives the energy of the i^{th} level, upon interaction with the j^{th} level, (where $\varepsilon_i < \varepsilon_j$) as

$$\varepsilon_i' = \varepsilon_i(\text{unperturbed}) + \sum_{j \neq i} \frac{|\underline{H}'_{ij}|^2}{\varepsilon_i - \varepsilon_j}$$

where $\underline{H}'$ is the perturbation operator. Similarly

$$\varepsilon_j' = \varepsilon_j + \sum_{j \neq i} \frac{|\underline{H}'_{ij}|^2}{\varepsilon_j - \varepsilon_i}$$

Since $\varepsilon_i < \varepsilon_j$, and $\underline{H}'_{ij} = \langle \phi_i | \underline{H}' | \phi_j \rangle$ is positive, it follows that when two levels interact the lower binding energy level is destabilized and the higher stabilized.

The energy level diagram representing this interaction for X = SO_2 is given in Fig (76). The apparent stabilization of the $\pi_{C=C}$ level is due to the additional, and greater "inductive" effect caused by σ bond polarization induced by addition of the SO_2 group.

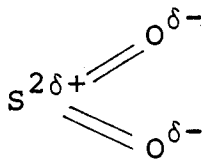

This results in the σ electron framework being "pulled" towards the sulphone group which leads to overall stabilization of the σ molecular energy levels. The π electrons are "pulled" closer to the carbon nucleii, (which become less screened as a result of σ electron polarization), and are hence stabilized.

The $\pi_{C=C}$ level does not mix with the $\pi(SO_2)$ level, since it is of the wrong symmetry, but mixes rather with the $n(SO_2)$ orbital, Fig. (80). Interaction of the antibonding $\pi(SO_2)$ will obviously be small as there are no occupied orbitals of the correct symmetry with which it can mix.

Taking the above points into consideration we would expect the PES of (i) and (ii) to be similar, but with an additional (destabilized) level in the 9.5 to 10.5 eV region. This would correspond to removal of two CH bonding levels, and their replacement by a $\pi_{C=C}$ level. Comparison of the spectra, Figs (82e) and (82f), show that this is apparently so, the extra peak lying at about eV. It should be noted that the simple composite molecule approach gives no unambiguous assignment of the first three peaks, for which calculations are required; Muller et al[15] have assigned the spectrum of (ii) as $\pi_{C=C} < \pi(SO_2) < n(SO_2)$ using CNDO calculations and KT. For the bicyclic systems containing both olefinic and sulphone groups, we can use this assignment as

COMPOSITE MOLECULE CORRELATION DIAGRAMS FOR VARIOUS STRUCTURES

FIG 77

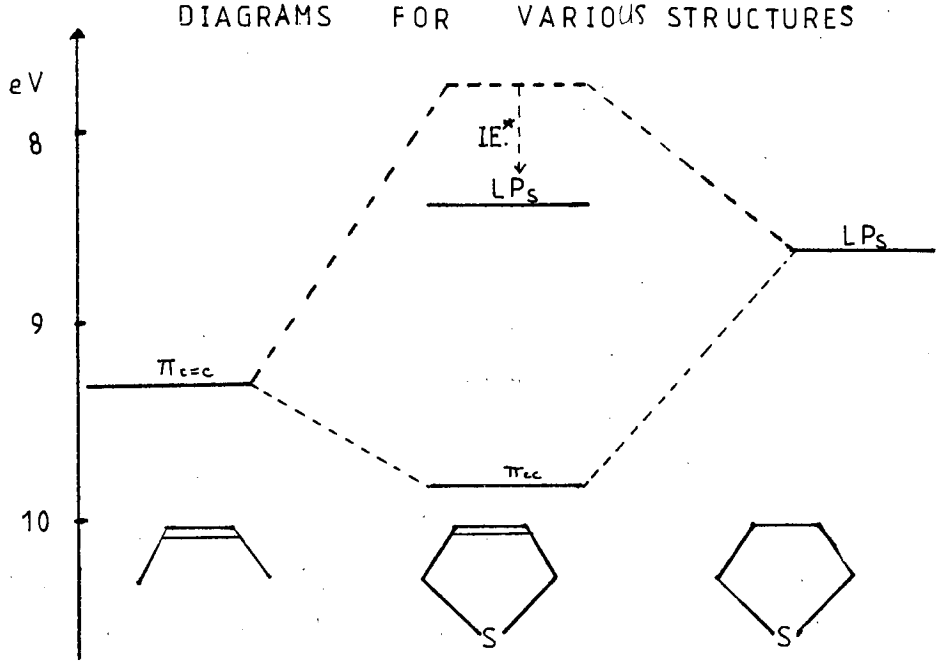

FIG 78

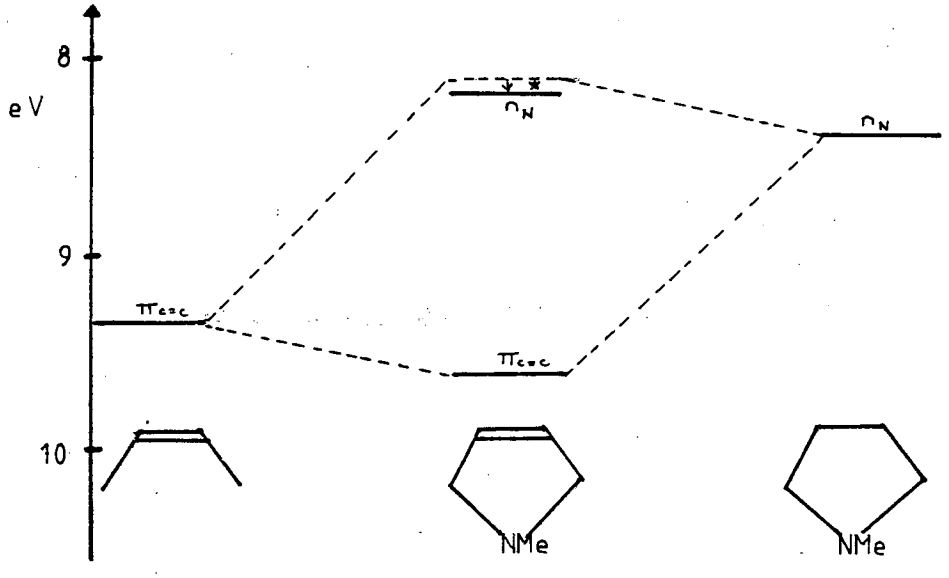

FIG 79

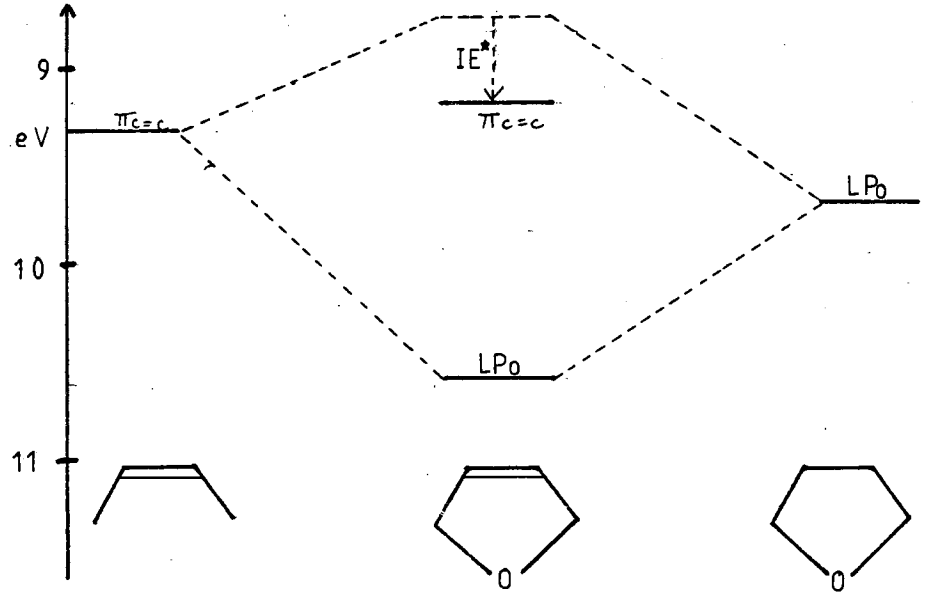

* IE INDUCTIVE EFFECT

an indication of the likely orbital ordering but as $\pi_{C=C}$ and $\pi(SO_2)$ are likely to be close, unambiguous spectral assignment can only be obtained by comparison with calculation.

Using the PES data from reference [17] a similar energy level diagram can be drawn representing the interaction of the sulphur lone pair (LP_S) and $\pi_{C=C}$ in molecule (iv). Fig(77).The splitting is uneven due to the inductive effect which additionally stabilizes $\pi_{C=C}$. (It should be noted that the inductive effect of the sulphur atom is less than that of the sulphone group). Extrapolating this to the bicyclic systems (11), (12), Fig (77), it is likely that ionization from LP_S corresponds to the first IP and $\pi_{C=C}$ to the second.

Similar diagrams can be drawn for (v) and (vi), Fig. (78), which lead to the prediction that the nitrogen non bonding level, n_N, will be of lower binding energy than $\pi_{C=C}$ in (vi), whereas LP_O will be of higher Fig 79 binding energy in (viii). These orbital orderings have been checked by CNDO calculations on N-methylpyrrolidine[17] and 2,5-dihydrofuran[18] respectively. It is possible that similar orbital orderings will be observed for the bicyclic systems (13), (14) and (20) which have these substituents.

Assignment of the PES of maleic anhydride (x) by virtue of KT with calculated ab initio orbital energies has been previously reported;[19] this gave the first two IP's as $LP_O < \pi_{C=C}$. However by drawing an energy level diagram for the interaction of orbitals, Fig (81), using the experimental data given in reference [19], it seems more likely from first principles, that $\pi_{C=C} < LP_O$ is the correct ordering. Therefore for assignment of the comparable

FIG 80 HOMOS OF SULPHONE GROUP

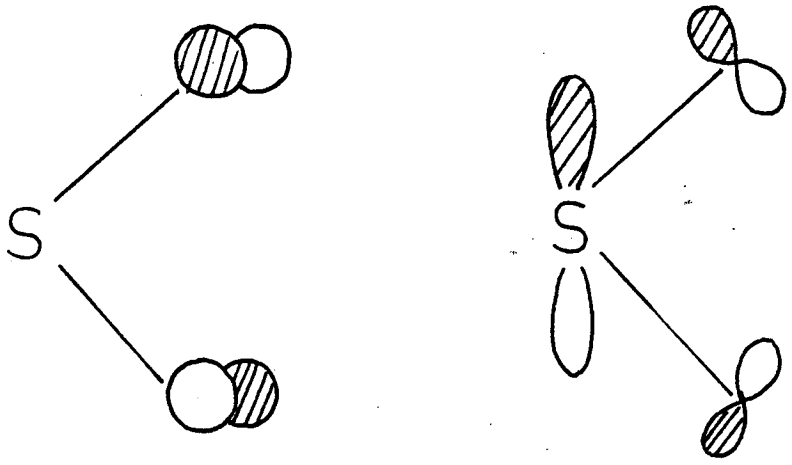

$\pi (SO_2)$ $n(SO_2)$

FIG 81 "COMPOSITE MOLECULE" CORRELATION DIAGRAM FOR MALEIC ANHYDRIDE

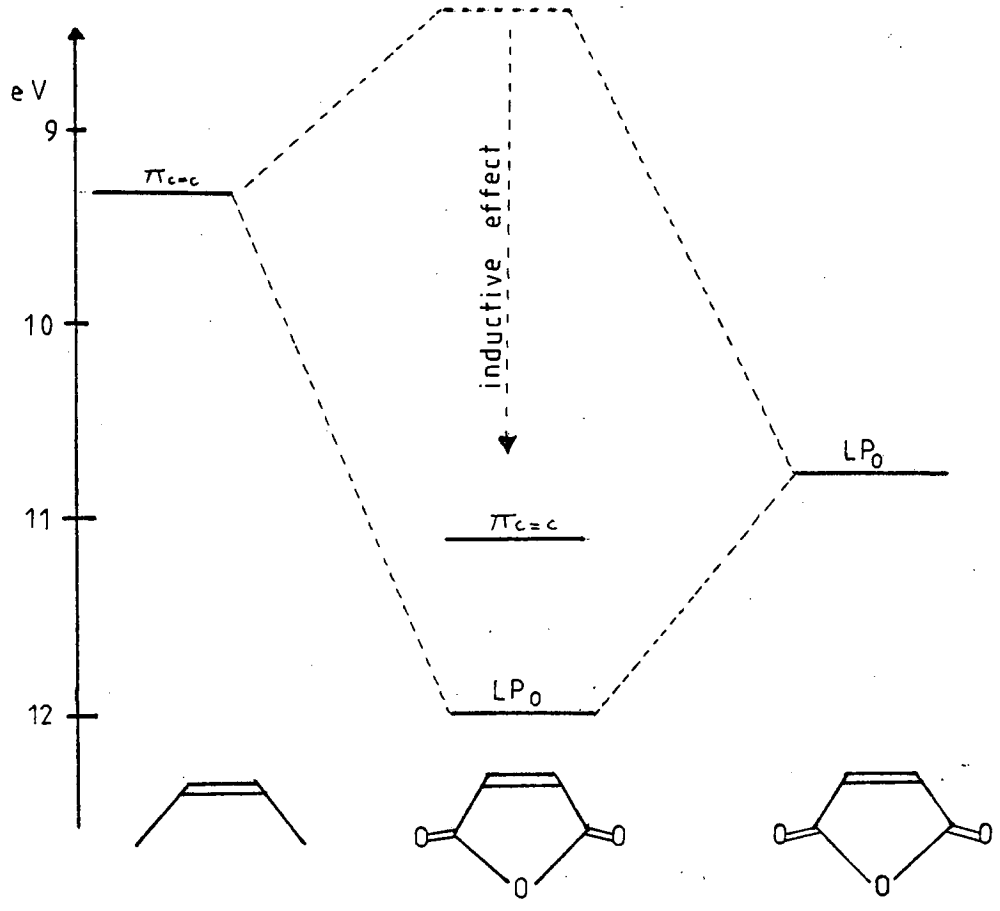

bicyclic systems, (13) and (14), calculations and He(I)/He(II) peak intensity studies have been made to ensure that the correct ordering is adopted.

The ordering for the monocyclic alkenes, given by the composite molecule approach, can be summarized as shown below:

Substituent	1st IP	2nd IP
$>SO_2$	$\pi_{C=C}/\pi(SO_2)$	$\pi_{C=C}/\pi(SO_2)$
>S	LP_S	$\pi_{C=C}$
>NMe	n_N	$\pi_{C=C}$
>O	$\pi_{C=C}$	LP_O
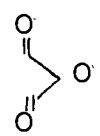	$\pi_{C=C}$	LP_O

These orderings can be used as an initial indication of the likely ordering of the IP's in the corresponding bicyclic systems.

It should be noted that these orderings are compatible with synthetic results for the bicyclic systems since the nitrene adds at the sulphur and nitrogen in molecules (12) and (20) respectively.

FIG 82 PHOTOELECTRON SPECTRA

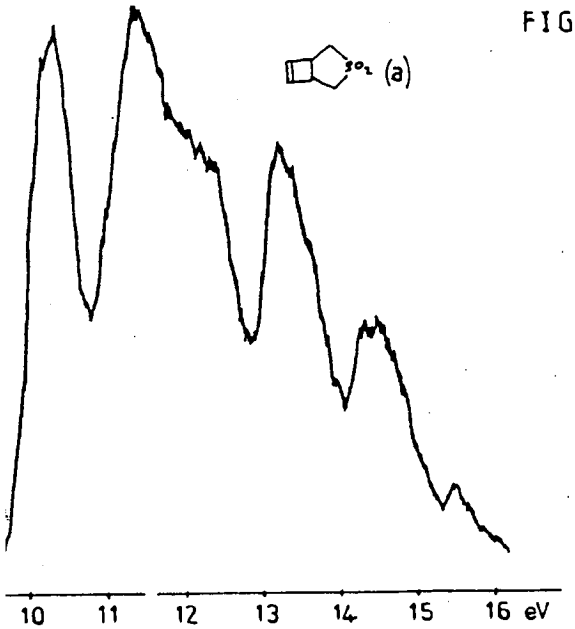

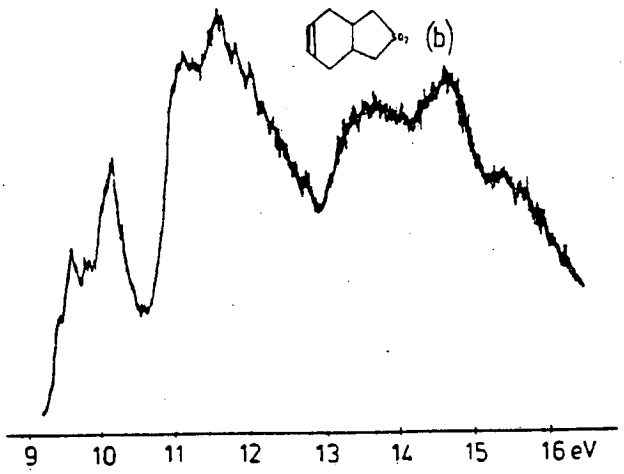

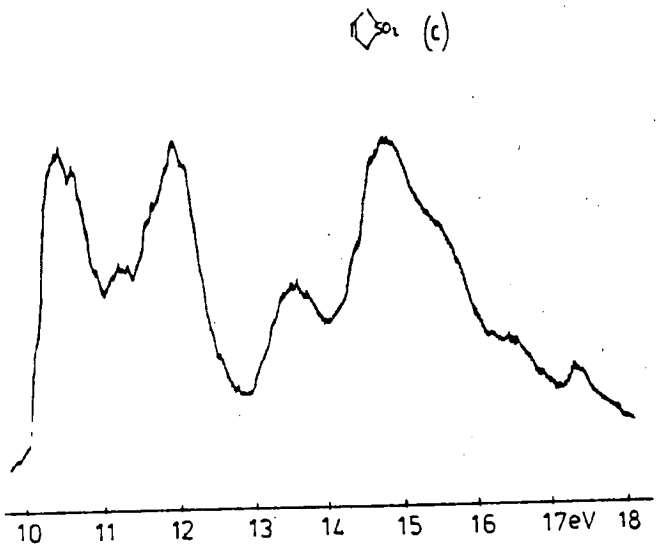

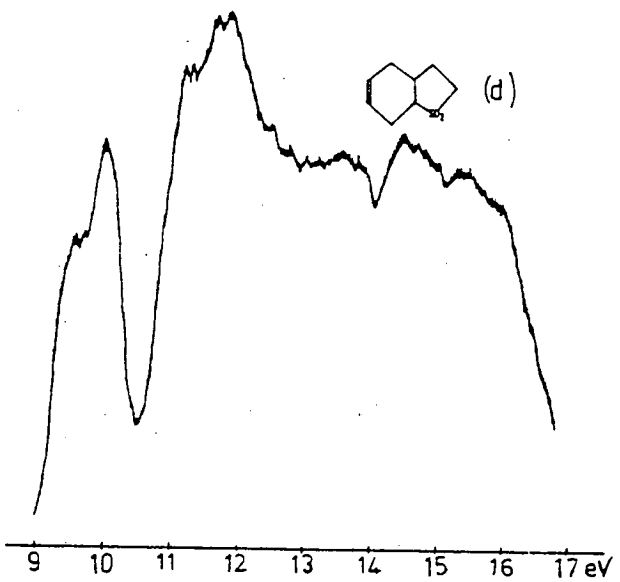

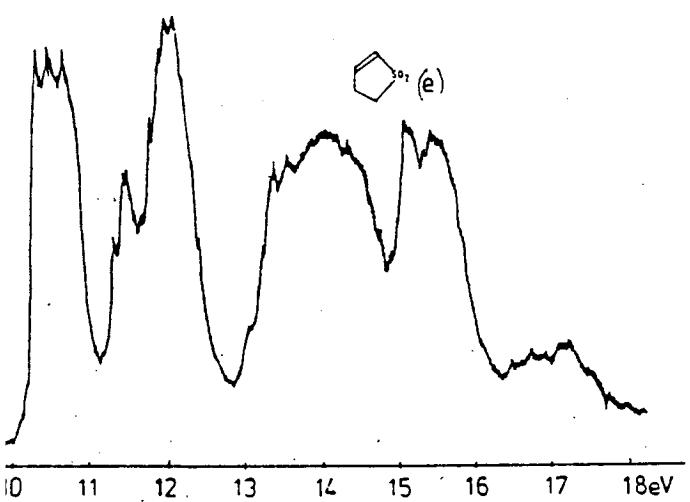

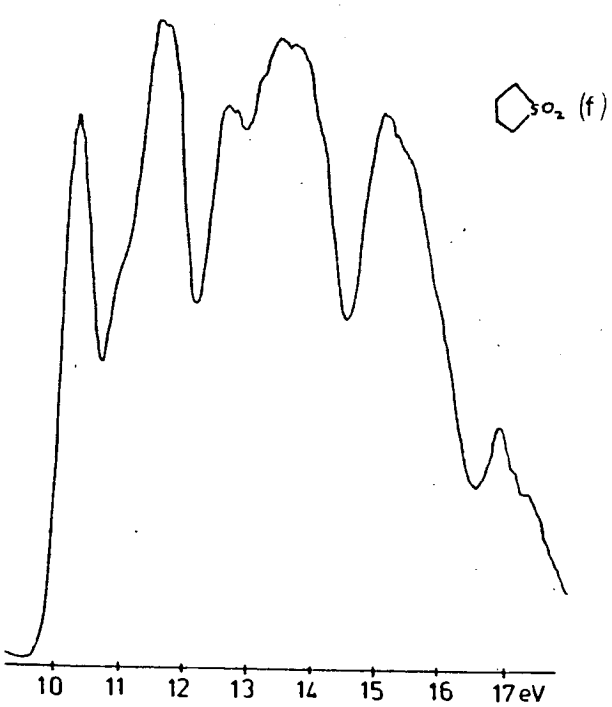

FIG 82 CONT

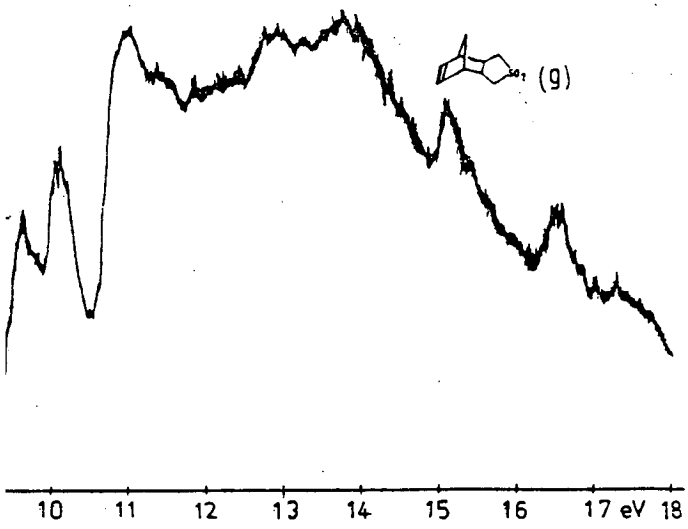
(g)
10 11 12 13 14 15 16 17 eV 18

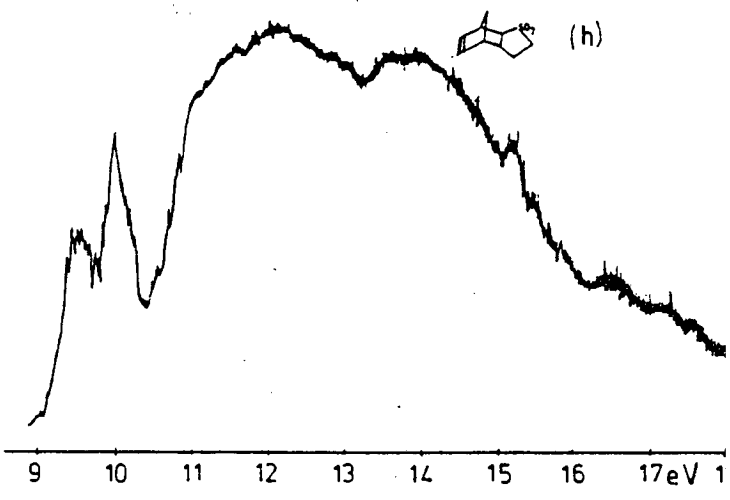
(h)
9 10 11 12 13 14 15 16 17eV 1

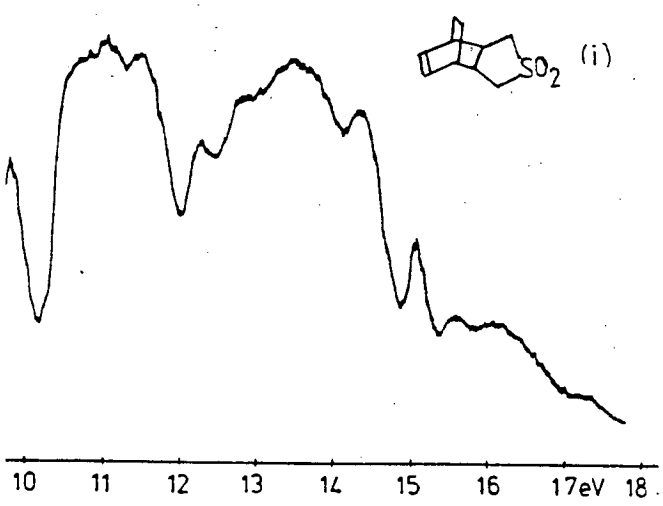
SO2
(i)
10 11 12 13 14 15 16 17eV 18

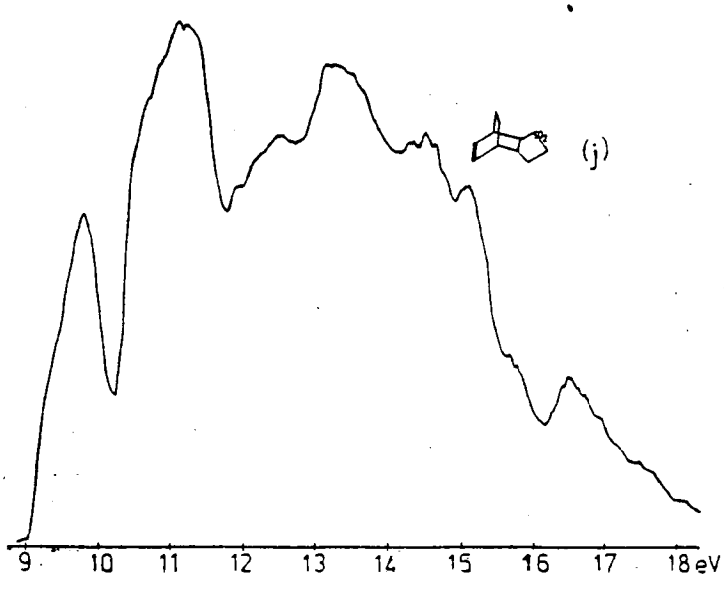
(j)
9 10 11 12 13 14 15 16 17 18eV

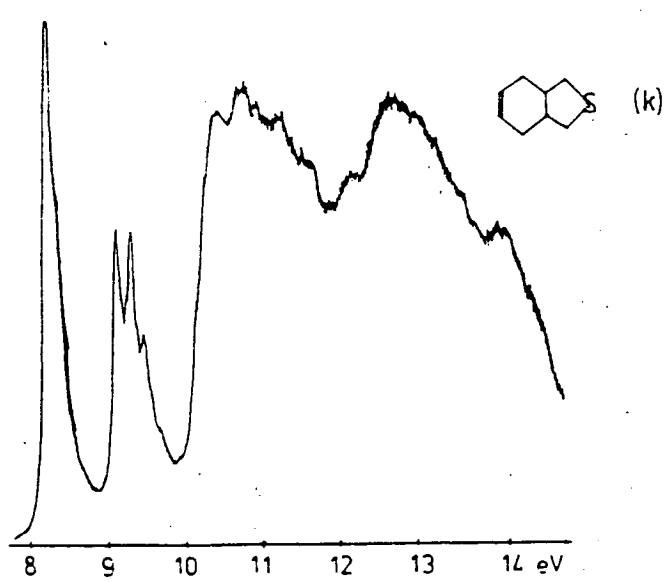
S
(k)
8 9 10 11 12 13 14 eV

FIG 82 CONT.

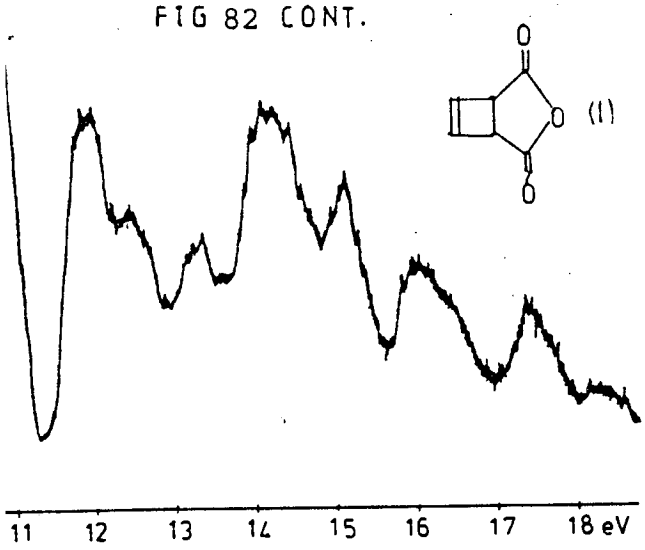
(l)
11 12 13 14 15 16 17 18 eV

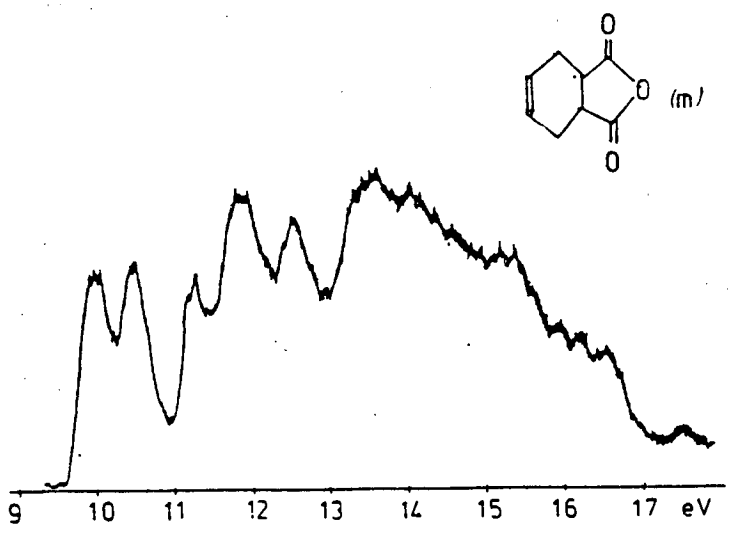
(m)
9 10 11 12 13 14 15 16 17 eV

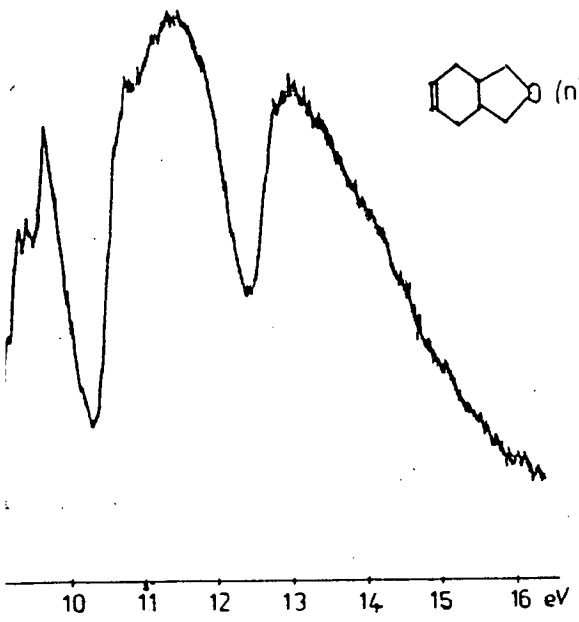
(n)
10 11 12 13 14 15 16 eV

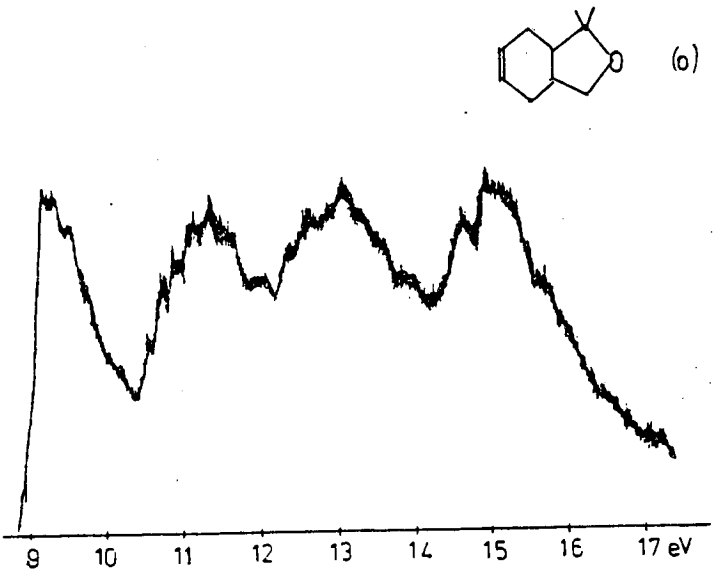
(o)
8 10 11 12 13 14 15 16 17 eV

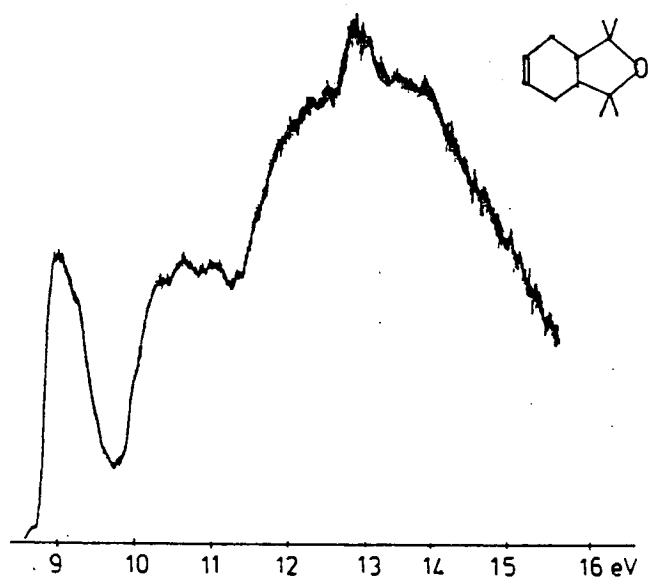
(p)
9 10 11 12 13 14 15 16 eV

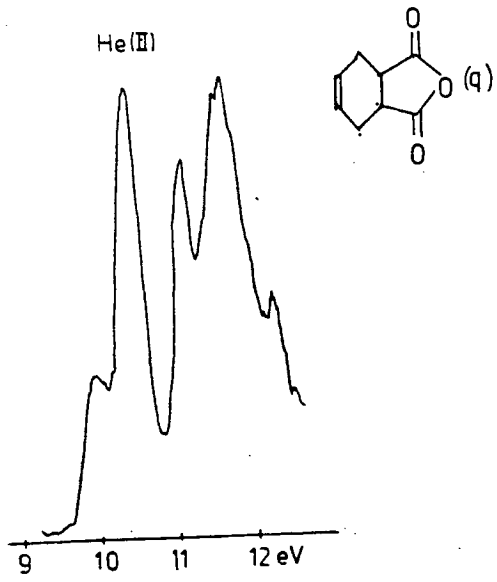
He(II)
(q)
9 10 11 12 eV

FIG CONT
82

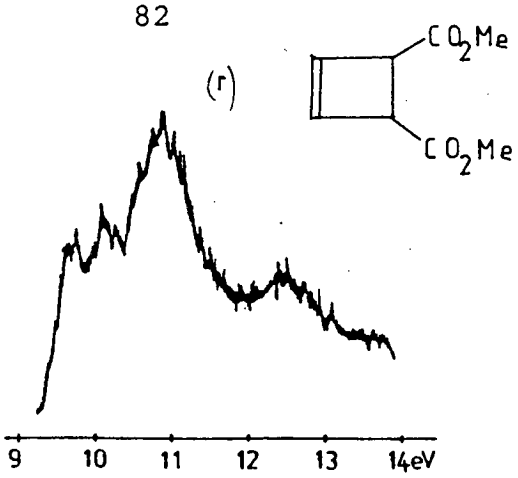
(r)
CO_2Me
CO_2Me
9 10 11 12 13 14eV

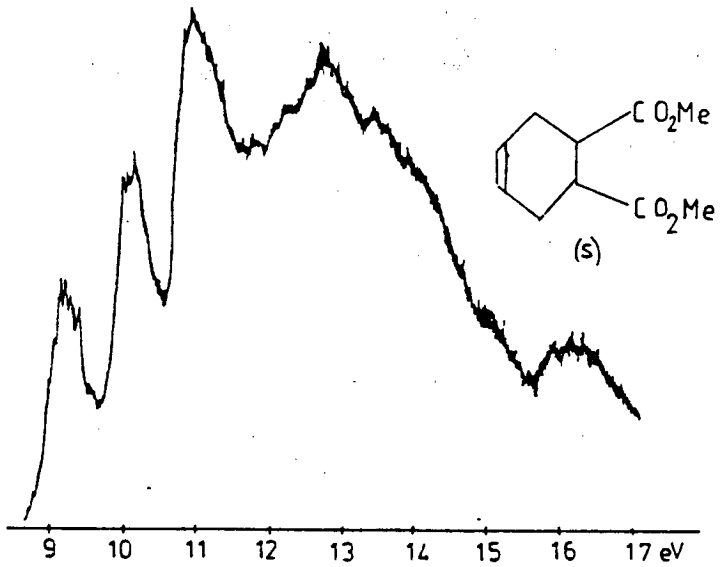
CO_2Me
CO_2Me
(s)
9 10 11 12 13 14 15 16 17 eV

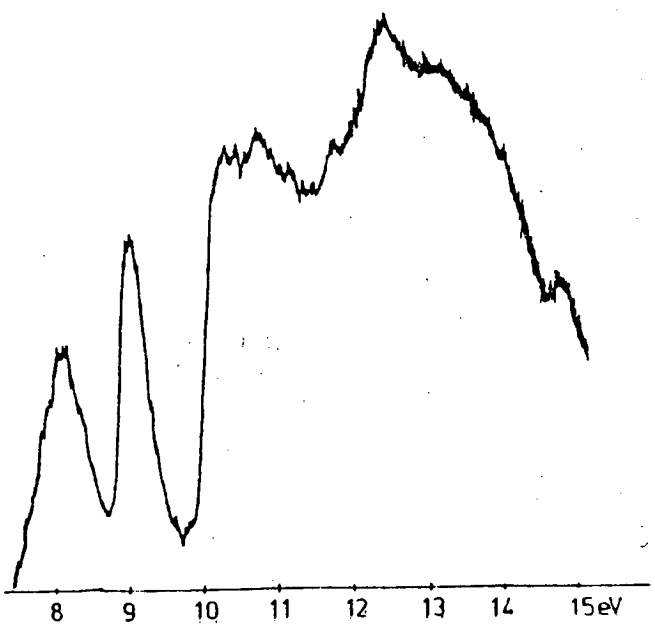
8 9 10 11 12 13 14 15eV

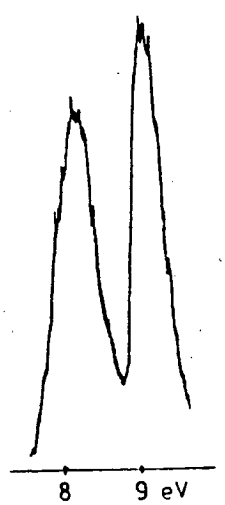
He(II)
8 9 eV

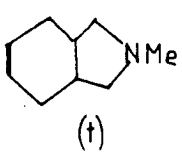
NMe
(t)

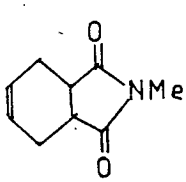
O
NMe
O

(u)

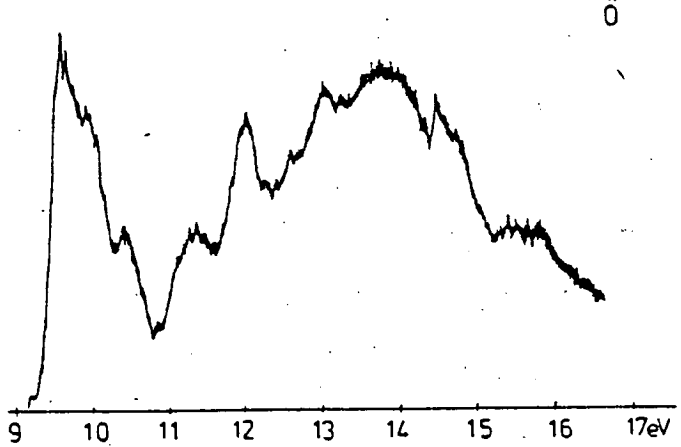
9 10 11 12 13 14 15 16 17eV

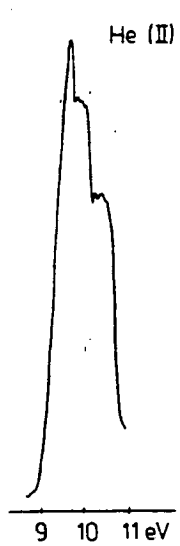
He (II)
9 10 11eV

FIG 82 CONT

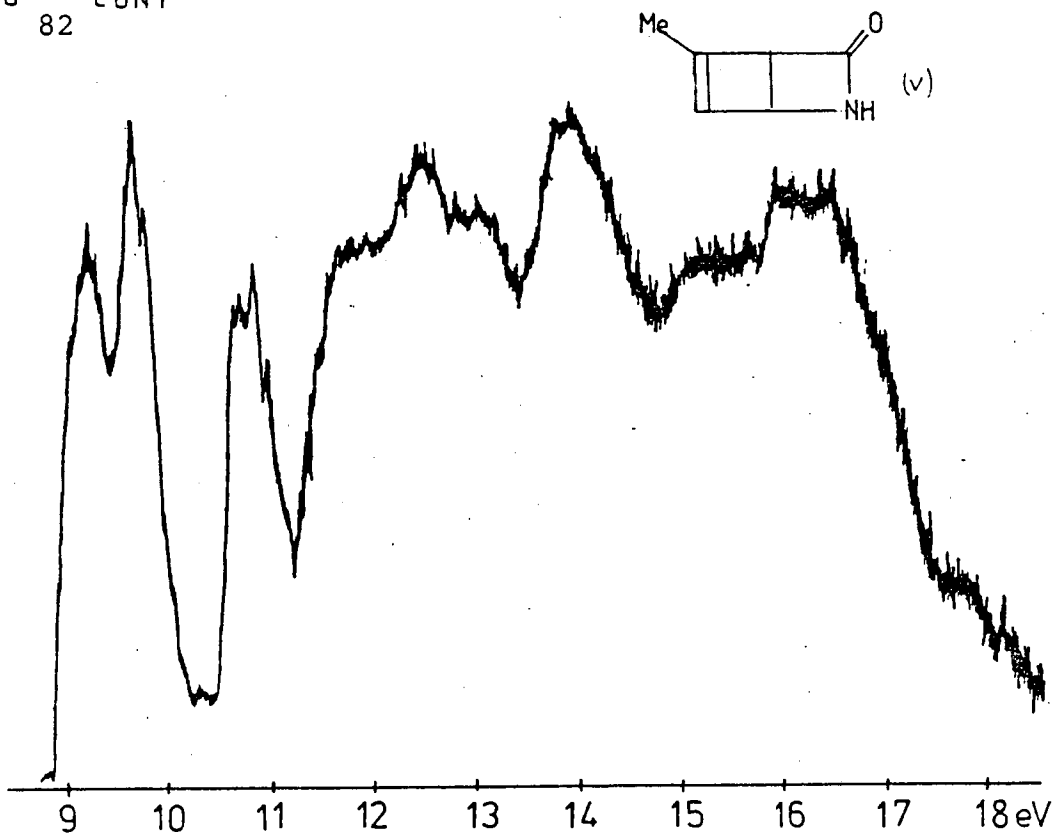

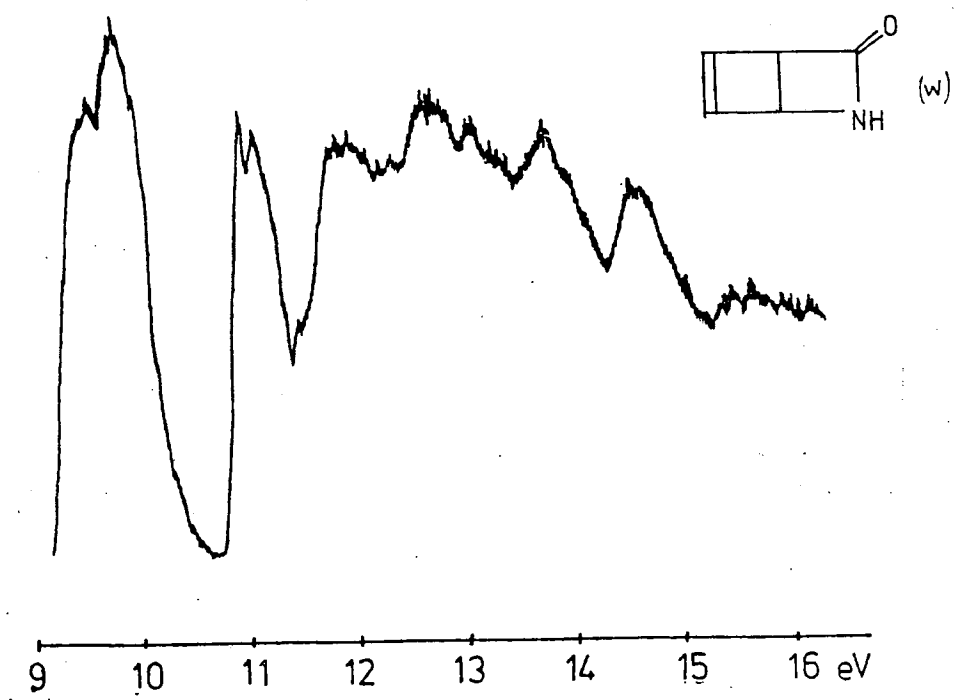

Assignment of Spectra

Group (A) Fig (82 a to i)

The Calculations for molecules (1) and (2), see Tables (52) and (53), give an orbital ordering of $\pi_{C=C} < \pi(SO_2) < n(SO_2)$. He(I) and He(II) peak intensity studies provided no additional information, as no observable difference in peak intensities was apparent, see Fig (82). The aforementioned assignment was adopted and was used also for the spectra of other molecules containing the sulphone group.

Group (Ai) Fig (82k)

As was predicted for the monocyclic thiophene from the composite molecule approach, the orbital ordering given by KT and calculated orbital energies for molecules (11), (12), Table (52), is:-

$$LP_S < \pi_{C=C} < \sigma$$

Since synthetic evidence (i.e. the nitrene adds at the sulphur for molecule (12)) provides a corrolary this ordering it has been used for spectral assignment.

Group (D) Fig (82t,u)

The calculations for molecule (20) indicate that the HOMO is of non bonding nitrogen character, n_N, Table (53). The relative intensity of the first peak in the PES of molecule (20) increases under He(II) conditions, Fig (82t,u), therefore the assignment $n_N < \pi_{C=C} < \sigma$ has been adopted. For molecule (21), relative peak intensity studies, Fig. (82t), indicate an ordering of $n_N < \pi_{C=C} < LP_O$ and this has been

adopted for spectral assignment.

Group(B) Fig (821 to q)

The PES of the furan type molecules (15-17) have been assigned as $\pi_{C=C} < LP_O < \sigma$ in accordance with the assignment of dihydrofuran from first principles. It is interesting to note that the envelope of the spectra of the methyl substituted compounds, Fig. (82o) and (82p), are similar to that of the parent compound, Fig (82m), but destabilized as is expected with methyl substitution.

Calculations performed for molecules (13) and (14), Table (52) give the KT ordering as $\pi_{C=C} < LP_{O1} < LP_{O2,3}$. This ordering is also indicated by relative peak intensity studies as is evidenced by the substantial increase in the intensity of the second IP under He(II) conditions, see Fig 82q This ordering has therefore been adopted for spectral assignment.

Group (E). Fig (82v,w)

The spectra of molecules (22) and (23), Figs. (82v) and (82w), can be assigned by virtue of the ΔE_{SCF} calculation on the former. Inspection of the Mulliken analysis for (23), Table (53), shows that the second and third HOMOs cannot easily be assigned as a particular type (e.g. lone pair, π) as these orbitals are heavily delocalized. Characterization of these orbitals has been made by identification of their greatest atomic orbital contributions from an analysis of the eigenvectors.

Table (55) First Three IP's (eV) and Their Assignment

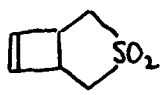	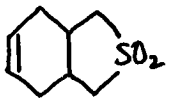	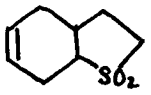	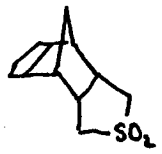	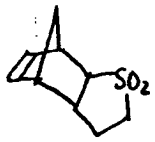	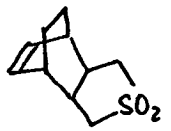	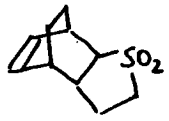
0.25 π	9.69 π	9.59 π	9.6 π	9.55 π	9.75 π	9.8 π
0.4 π(SO_2)	10.1 π(SO_2)	10.00 π(SO_2)	10.15 π(SO_2)	10.00 π(SO_2)	10.4 π(SO_2)	10.4 π(SO_2)
1.25 n(SO_2)	11.2 n(SO_2)	11.5 n(SO_2)	11.00 n(SO_2)	11.05 n(SO_2)	10.99 n(SO_2)	11.1 n(SO_2)

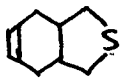	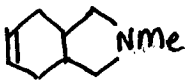	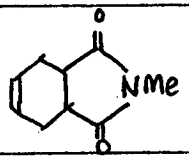	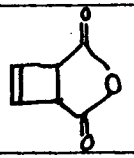	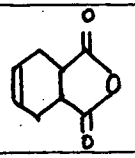	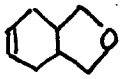	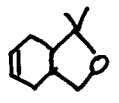	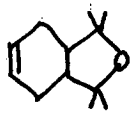	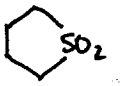
8.22 LP_S	8.20 LP_N	9.62 π	10.49 π	10.00 π	9.5 π	9.29 π	9.03 π	10.75π(SO_2
9.2 π	9.1[illegible] π	10.00 LP_N	10.95 LP_{O1}	10.6 LP_{O1}	9.95 LP_O	9.59 LP_O	9.25 LP_O	11.4
0.67 σ	10.53 σ	10.5 LP_O	11.8 $LP_{O2,3}$	11.3 $LP_{O2,3}$	10.99 σ	10.7 σ	10.25 σ	11.8 σ

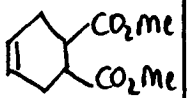	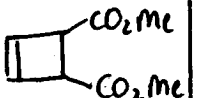	 [a]	 [a]	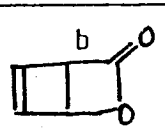 [b]	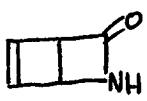	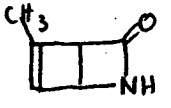	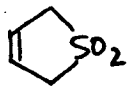	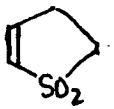
9.25π	9.76 π	8.94 π	9.43π	10.06 π	9.39 πNO	9.22 πNO	10.35π	10.28π
0.1 LP_O	10.00 LP_O	10.1 σ	10.6 σ	11.02 LP_O	9.9 π/LP_O	9.7 π/LP_O	10.85π(SO_2)	10.56π(SO_2
1.06 σ	10.58 σ	10.3 σ	10.9 σ	11.48π_{OCO}	11.0 LP_O	10.8 LP_O	11.32n(SO_2)	11.43n(SO_2

a) From Reference [25]

b) From Reference [22]

Previous semi-empirical calculations by Schweig et al[22] for molecule (24) gave the same ordering and hence assignment as our ab initio calculations.

It should be noted that for nitrene addition to molecules (22) and (23) the nitrene adds at the nitrogen. This synthetic result provides additional evidence that our calculated assignment of the character of the first IP is correct as the HOMO is heavily localized on this centre and the oxygen.

Table (55) contains the values of the first three IP's for each molecule and their assignment.

Having now established the positions of the π levels we can now comment on the relative magnitudes of their IP's in the various structures (1-26).

(v) Magnitude of Ionization Potential of the Unsaturated Level ($IP\pi_{C=C}$)

(a) A comparison of its value in four and six membered ring systems

Analysis of Table (55) shows that $IP\pi_{C=C}$ for molecules in which the olefinic group is contained in a four membered ring system, is higher than the corresponding level in the six membered analogues. For example

$$\Delta IP\pi = IP\pi_{C=C}(\text{cyclobutene}) - IP\pi_{C=C}(\text{cyclohexene})$$
$$\simeq +0.49 \text{ eV}$$

and for the following pairs of molecules (1)(2), (13)(14), (18)(19) $\Delta IP\pi$ is +0.56, +0.49, +0.51 eV respectively. This trend, in fact, matches the reactivity pattern of the molecules to nitrene addition. (Cyclobutene[23] and cyclohexene[24] show 1.5 and 45 percent yields respectively for addition of nitrene (B) ethoxycarbonylnitrene. We can therefore say that the energetic availability of the electrons in the double bond probably contributes to the relative reactivities of these systems for electrophilic addition; it should again be stressed that this cannot be held as the only contributing factor since percentage yield is not a sufficiently stringent criterion for absolute measurement of reactivity.

The relative positions of the IP's of the unsaturated level in cyclobutene and cyclohexene and in all of the membered analogues, is surprising. In classical organic chemical terms the strain in the less thermodynamically stable small ring might be expected to lead to general destabilization of the orbitals and not the observed stabilization. We must therefore attempt to identify the possible causes of this unexpected trend, and an appropriate starting point is with the monocyclic alkenes, C_mH_{2m-2}. Analysis of the $IP\pi_{C=C}$ for this molecular series will indicate if the trend observed for the bicyclic molecules can be attributed to a residual effect in the parent cycloalkenes.

A literature survey showed that for the cycloalkenes C_mH_{2m-2} (m = 3 to 8) the IP of the olefinic level is in fact destabilized as the ring size increases[25] cf. cyclopropene

(9.7 eV), cyclobutene ((.42 eV), cyclopentene (9.01 eV), cyclohexene (8.94 eV). This trend can be attributed to inductive and hyperconjugative effects.[25] (Hyperconjugation[26] refers to delocalization that occurs when an alkyl group is conjugated with an unsaturated group).

The decrease of $IP\pi_{C=C}$ with increasing alkyl substitution has also been noted[27] also for the comparable open chain molecules "substituted ethylenes" i.e. propene, butene, pentene, hexene and again, has been attributed to hyperconjugative and inductive effects. It should be noted, however, that the decrease in $IP\pi_{C=C}$ for both the alkenes and cycloalkenes with increasing alkyl substitution is non linear, becoming smaller as the size of the molecule increases.

The trends of $IP\pi_{C=C}$ for both the open chain and ring alkenes indicate that introduction of an alkyl group stabilizes the ground state of the ion more than that of the molecule. This stabilization can be thought of as the result of easier delocalization of the ionic positive charge; the greater the electron density in the vicinity of the ionized orbital the more easily the electron deficiency in the ion can be delocalized. This leads to stabilization of the ion and hence a reduction in $IP\pi_{C=C}$.

We must also consider that as m increases for both the alkenes (C_mH_{2m}) and cycloalkenes (C_mH_{2m-2}), the molecules become increasingly "floppy", and hence the number of alkyl groups which can get close to the olefinic group increases.

FIG 83 I.P.π FOR SOME STRAINED SYSTEMS

	STRAINED SYSTEMS	STRAIN "FREE" SYSTEMS
a)	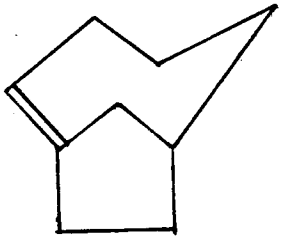	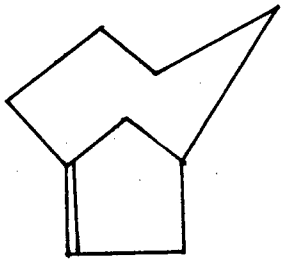
$IP\pi_{C=C}$ (eV)	8.45	8.37
b)	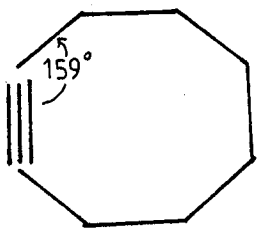	Bu — C ≡ C — Bu
$IP\pi_{C\equiv C}$ (eV)	9.2	9.02
c)	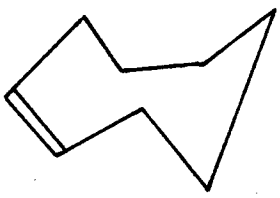	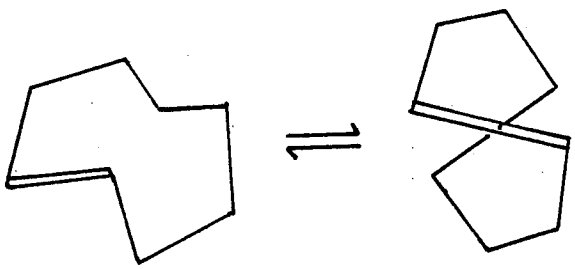
$IP\pi_{C=C}$ (eV)	8.98	8.69

a) from Ref[29]
b) from Ref[30]
c) from Ref[31]

This would lead to greater electron density in the vicinity of the olefinic group and possibly easier delocalization of the positive charge in the ion by what can be called a"through space" effect. This effect, if it exists, must be small since the destabilization of $IP\pi_{C=C}$ gets progressively smaller as 'm' increases.

Rodwell et al[28] have theoretically optimized the geometry of $C_2H_4^+$, and have shown that the C-C bond length is longer in the cation than in the molecular ground state by (0.1Å). Hence removal of a π bonding electron can be expected to lead to a lengthening of the bond from whence it came. In the smaller cycloalkenes for example cyclopropene and cyclobutene, as these molecules are forced to be planar, lengthening of the double bond is more "difficult" than in the larger, more floppy cycloalkenes where such an effect can be more easily accommodated. (This is effectively representative of the strain in the molecule). The ease with which the olefinic bond can lengthen could possibly effect the energy "barrier" for removal of an electron, and would also contribute to the relatively smaller $IP\pi_{C=C}$ for the larger cycloalkenes. This effect, although small, is in evidence for other strained systems, see Fig. (83), where in all cases $IP\pi_{C=C}$ is slightly higher for the more strained systems.

It could be anticipated that the relative positions of $IP\pi_{C=C}$ for the cyclobutene and cyclohexene analogues might reflect the relative thermodynamic stabilities of these molecules. This, however, is untrue, and the seeming anomally

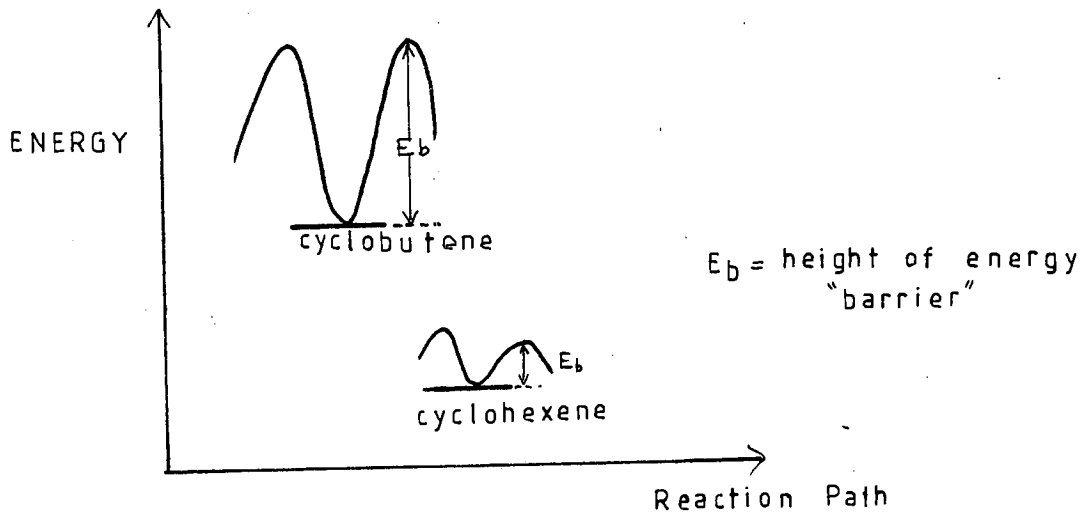
ENERGY
E_b
cyclobutene
E_b
cyclohexene
E_b = height of energy "barrier"
Reaction Path

FIG 84

can be accounted for in the following manner taking cyclobutene and cyclohexene as our example. Although cyclobutene is thermodynamically less stable than cyclohexene, it is possible that thermodynamic energy surface is such that the molecule lies in a very steep potential well. Even if the minima for cyclobutene is at a higher absolute level than that of cyclohexene, the relative energy "barriers" for a deformation, say removal of a π electron could be larger for the smaller ring system, Fig. (84). If this is so we can conclude that the height of the energy "barrier" for removal of an electron, (and hence the IP), for the monocyclic systems must be determined by several factors viz.:

(1) Induction.

(2) Hyperconjugation.

(3) Through space effects.

(4) Strain.

No quantitative estimate of these individual effects can be made for this molecular series since $\Delta IP\pi$ will be a combination of all four. Since $\Delta IP\pi$ is approximately the same for the monocycles (18) and (19), a cyclobutene and cyclohexene the bicyclic sulphones (1) and (2) and anhydrides (13) and (14) it is reasonable to conclude that the overriding trend in $IP\pi_{C=C}$ for the bicycles can be attributed to residual effects (1)-(4) in the parent cycloalkenes. Any variation of $IP\pi_{C=C}$ within a cyclobutene or cyclohexene molecular series can be attributed to substituent effects.

It is noted that the existence of the hyperconjugative effect is evidenced by the Mulliken analyses, Table (54), for the sulphones (1), (2) and anhydrides (13), (14). These results show that delocalization of the π level on the alkyl groups occurs preferentially in the cyclohexenes (2) and (14). Now the extent of delocalization is a measure of destabilization of the π level; although this is slightly greater for the cyclobutenes (1), (13), the additional larger inductive effects of the extra alkyl groups in the cyclohexenes (2), (14) result in greater destabilization of $IP\pi_{C=C}$ for the latter pair.

(b) Substituent Effects

Substituent effects for the molecular series can be attributed to stabilizing inductive effects. As was observed for the monocyclic series, Fig (75), the anhydride group produces the largest inductive effect and this gradually decreases for different substituents as is indicated below. This is evidenced by variations in $IP\pi_{C=C}$ for the cyclohexene series.

molecule	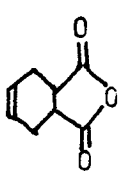	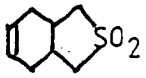	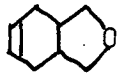	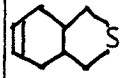	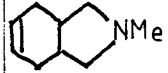
$IP_{C=C}$ (eV)	10.00	9.59	9.5	9.2	9.1

The results of the Mulliken analyses show that some additional through space mixing occurs, Table (54), which appears as delocalization of the HOMO 'π' level in

the sulphone (1) and anhydride (13), resulting in finite electron density on the substituent atoms. This is effectively the same for both cyclobutenes but $IP\pi_{C=C}$ is greater for the anhydride therefore we can conclude that the substituent inductive effect is the overriding factor.

It is obvious that the position of the olefinic level in this series of molecules is dependent on several factors, and this can be summarized in the following expression

$$IP\pi_{C=C} = IP\pi_{intrinsic} - \Delta_{\substack{\text{destabilization due to alkyl induction and hyperconjugation}}} + \delta_{\substack{\text{inductive stabilization of substituents}}} - \emptyset_{\substack{\text{destabilization due to through space interaction}}}$$

(c) Other Comparisons

It is interesting to compare $IP\pi_{C=C}$ for the sulphones (2) and (3), see Table (55). The $IP\pi_{C=C}$ of the unsymmetrical molecule is slightly lower than that of the symmetric molecule, but for both IPπ, Δ and δ will be identical. ø will differ since in the unsymmetrical molecule the sulphone and olefinic groups are slightly closer, and this could possibly explain the small destabilization observed. (It should be noted however that such small differences in IP are approaching the limit of accuracy of measurement by PES and therefore no absolute conclusions must be drawn).

Of the molecules given in group A, Fig (71), sulphones (6), (7), (8) and (9) are forced to be in the boat (or endo) conformation, due to the presence of the transannular bridge. The $IP\pi_{C=C}$ of the symmetric and asymmetric sulphones are almost identical for all comparable pairs of molecules except (2) and (3) where they differ by 0.1 eV. Now if this difference in IP were due to a through space interaction it would be in evidence for molecules (6) and (7), (8) and (9). This difference could therefore be indicative that these molecules have different vapour phase conformations which would lead to a greater difference in ø.

Estimations of 'δ' the inductive effect of various substituents can be obtained from the comparisons made below:

(1)	(2)	$\Delta I P\pi(eV) = I.P\pi_1 - I.P\pi_2$
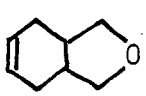	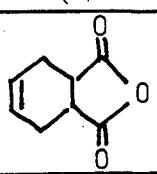	0.55
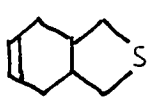	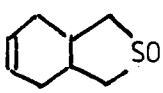	0.49
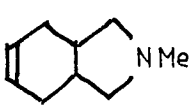	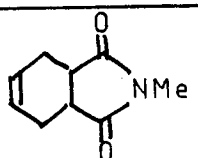	0.52
		0.33
	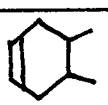	0. 31
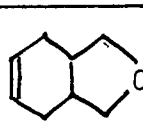	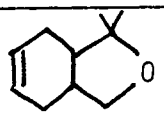	0.21
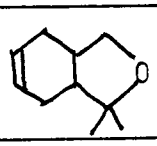	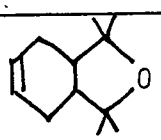	0.22

$\delta(20) = +0.5eV$; $\delta(CO_2Me) = +0.32eV$; $\delta(Me) = -0.1eV$

FIG 85

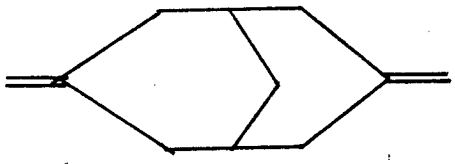

3,7-Dimethylene bicyclo[3,3,1] nonane

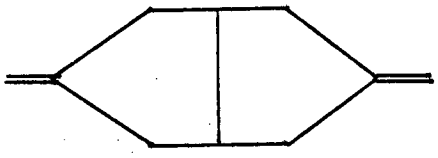

3,7-Dimethylenebicyclo[3,3,0]octane

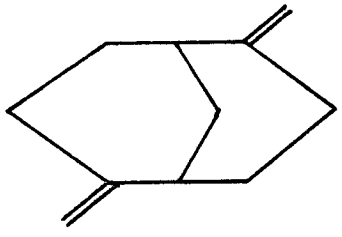

2,6-Dimethylenebicyclo[3,3,1]nonane

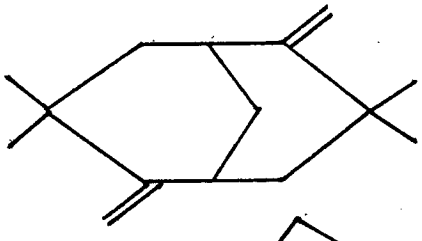

3,3,7,7-Tetramethyl-2,6-dimethylene-
bicyclo[3,3,1]nonane

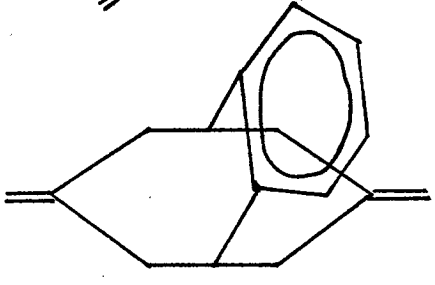

3,7-Dimethylenebicyclo[3,3,2]dec-9-ene

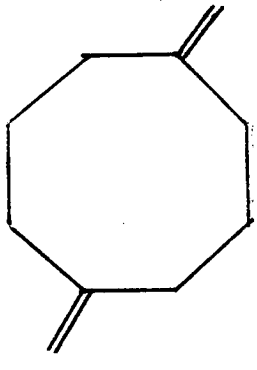

1,5-Dimethylenecyclooctane

(vi) Other Reactivity/Conformational Studies

At this point it is appropriate to mention other photoelectron spectroscopic studies which were embarked upon in an attempt to gain some information of the possible reactivity and conformation of the very unusual molecules shown in Fig. (85)*.

Now in molecules containing two olefinic groups, if the σ-π separation is reasonable then interaction results in the olefinic π levels existing as linear combinations.

$$\pi^{+} = a\pi_1 + b\pi_2 \qquad \text{symmetric}$$
$$\pi^{-} = b\pi_1 - a\pi_2 \qquad \text{antisymmetric}$$

with the antisymmetric level normally lying to lower binding energy. It was hoped that this work would show

a) if any π-π interaction of the dienes would be evidenced by a splitting of their IP's.

b) if the positions of the IP's in any way matched the observed reactivities of these molecules. Of the molecules studied F undergoes, photochemical cycloaddition to [3.3.2] propellane

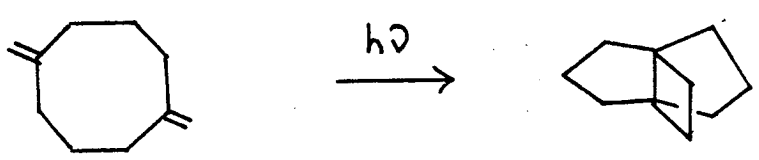

*Samples of these molecules, and some experimental data were provided by Dr. Roger Bishop, School of Chemistry, The University of New South Wales, Australia.

Table 56 Reactivity, First IP's (eV) and Splitting of the $\pi_{C=C}$ Levels

Molecule	Reactivity	First IP (eV)	Splitting of $\pi_{C=C}$ levels (eV)
A. 3,7-Dimethylenebicyclo [3.3.1]nonane	Irradiation causes photocyclization	8.54	0.1
B. 3,7-Dimethylenebicyclo [3.3.0]octane	Photochemical properties not yet studied	9.17	no observable split
C. 2,6-Dimethylenebicyclo [3.3.1]nonane	Does not undergo photocyclization	8.89	0.165
D. 3,3,7,7-Tetramethyl-2,6-dimethylenebicyclo[3.3.1] nonane	Photochemical properties not yet studied	8.71	0.145
E. 3,9-Dimethylenebenzobicyclo [3.3.2]dec-9-ene	Irradiation causes photocyclization (not as efficient as A or F	8.32	0.1
F 1,5-Dimethylenecyclo-octane	Irradiation causes photocyclization	8.51	0.23

and transannular cyclization under acidic conditions.

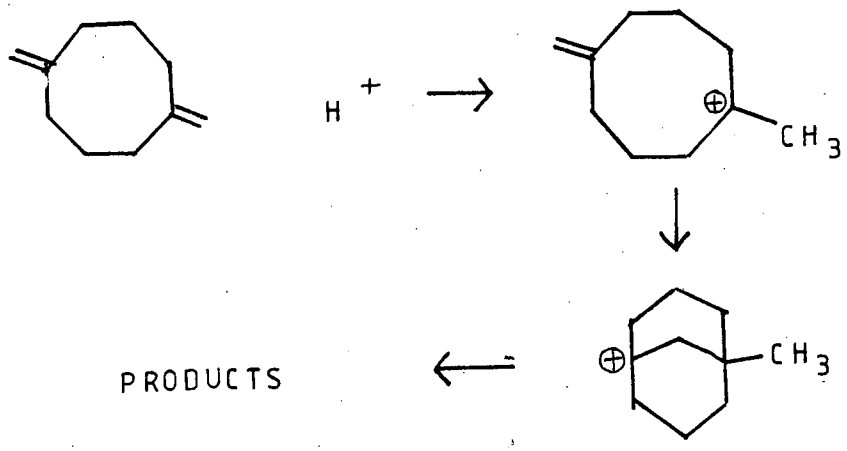

Also molecules A and E undergo photocyclization although this is less efficient process in the latter.

Table (56) gives a synopsis of the first IP's for the complete series of molecules, indication of the experimental reactivity and any observed splitting of the $\pi_{C=C}$ levels (which are taken as the first two IP's). The He(I) photoelectron spectra are given in Fig (86).

Inspection of Table (56) shows that the molecules which undergo cycloaddition have IP's approximately 0.4 eV lower than that of (C) which is unreactive. The relatively high first IP's of molecule (B) is probably indicative that it will not undergo cycloaddition.

The first IP of molecule (D) is only slightly higher than that of the reactive molecules therefore it is possible that this molecule will undergo photocyclization.

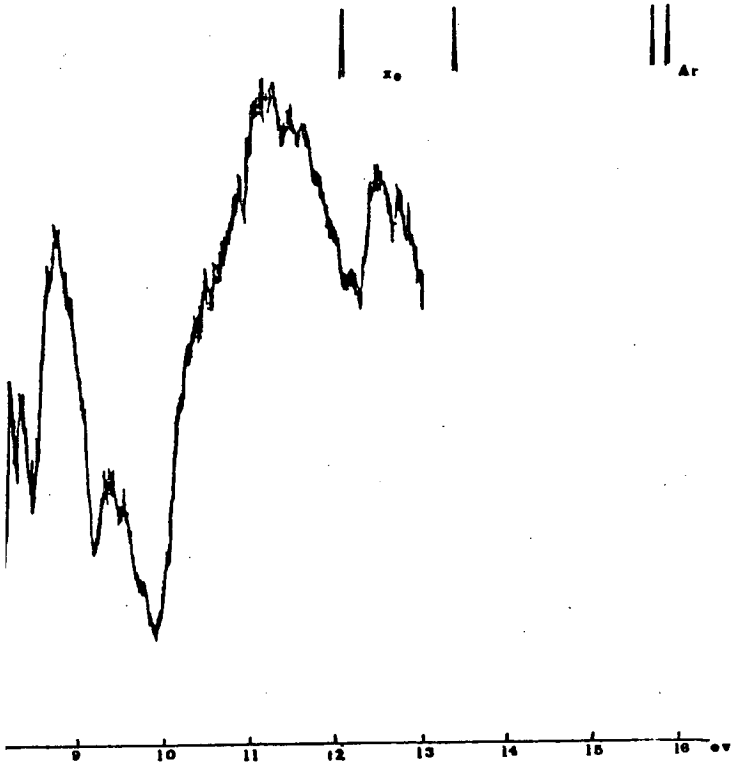

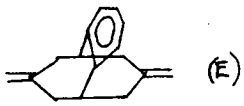

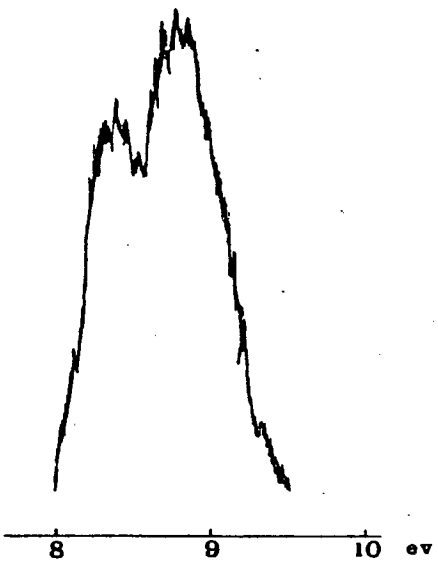

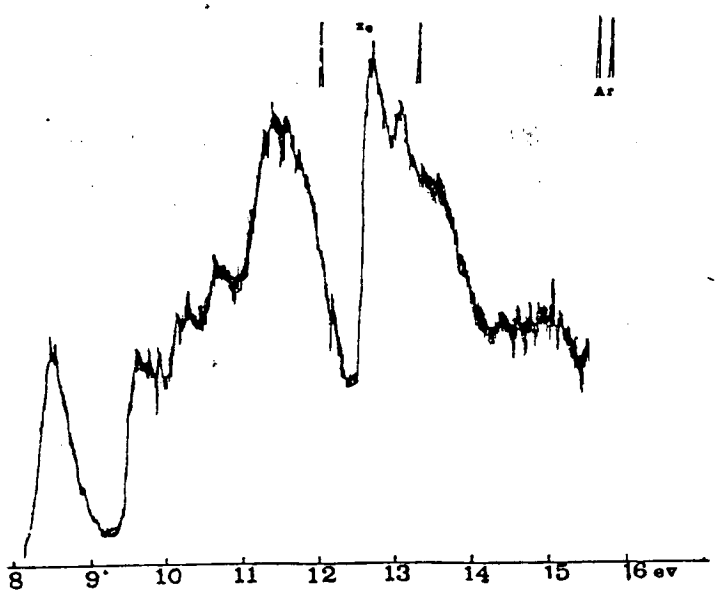

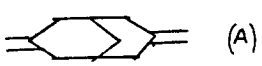

FIG 86 PHOTOELECTRON SPECTRA

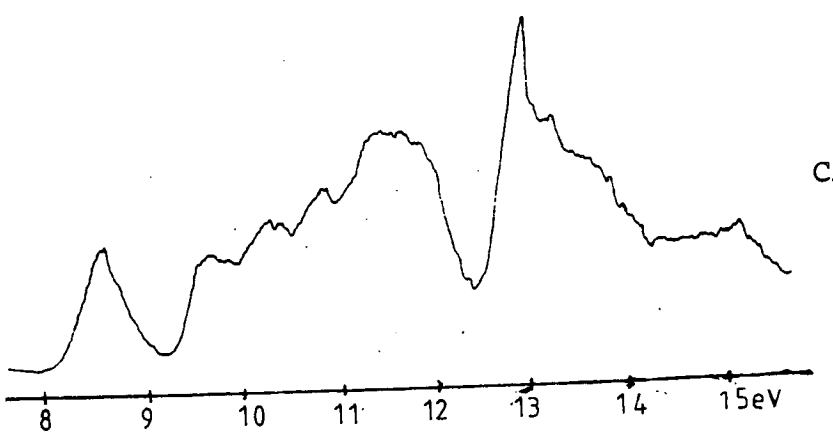

CAT Spectrum

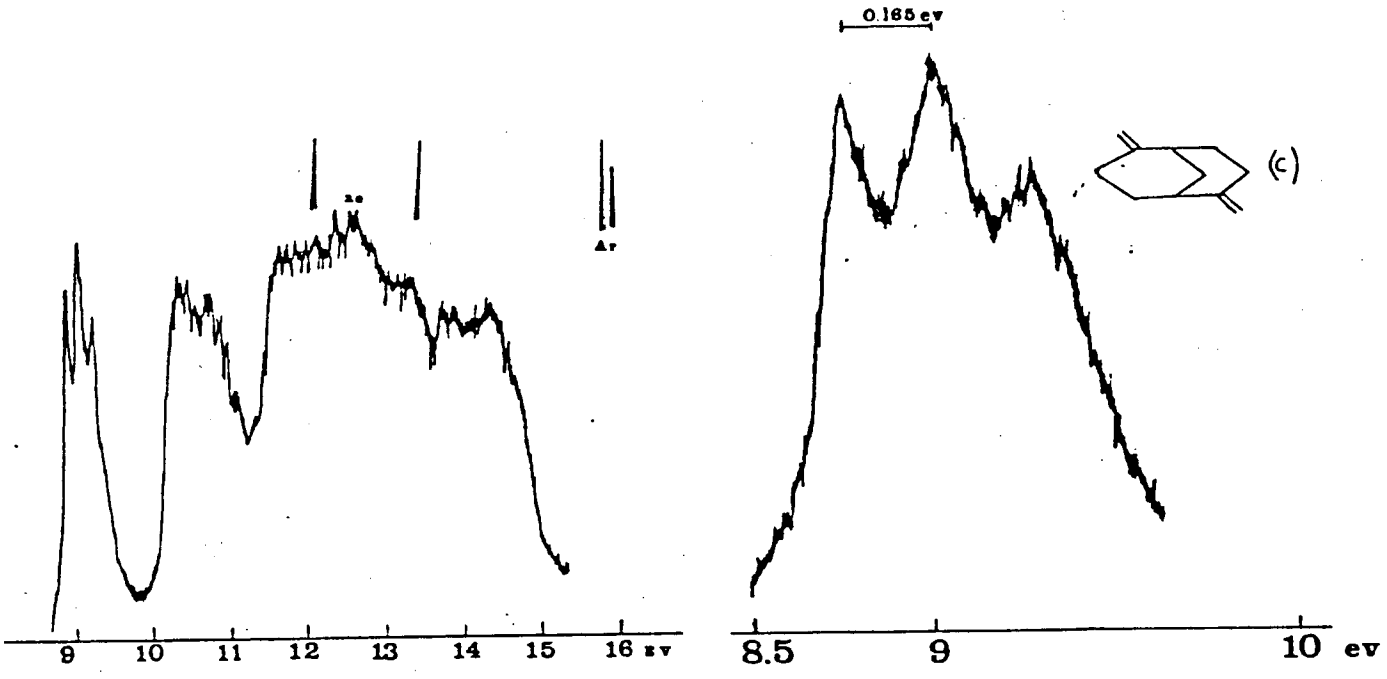
0.165 ev
Xe
Ar
(C)
9
10
11
12
13
14
15
16 ev
8.5
9
10 ev

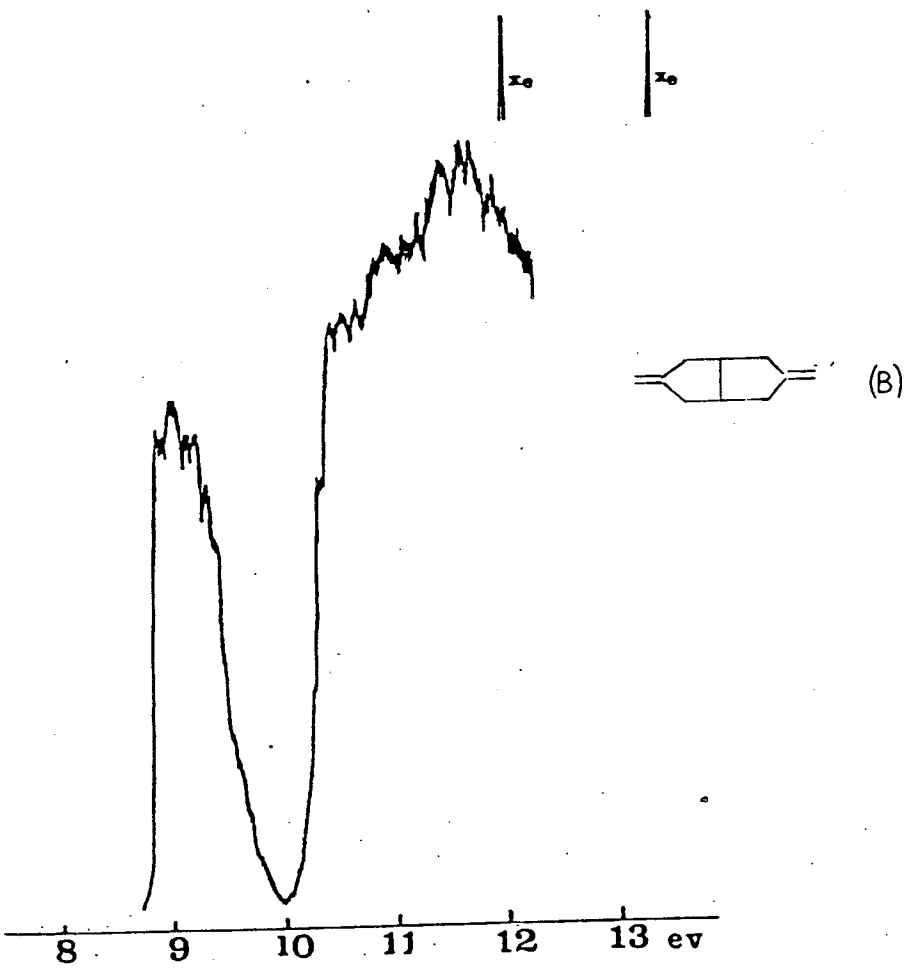
Xe
Xe
(B)
8
9
10
11
12
13 ev

FIG CONT
86

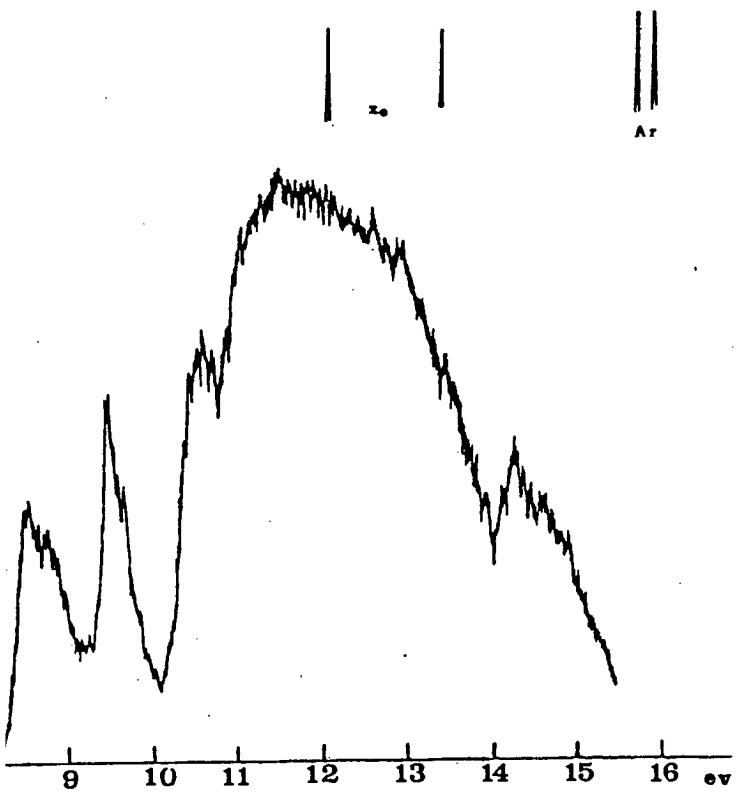
Xe
Ar
9
10
11
12
13
14
15
16 ev

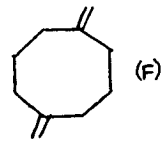
(F)

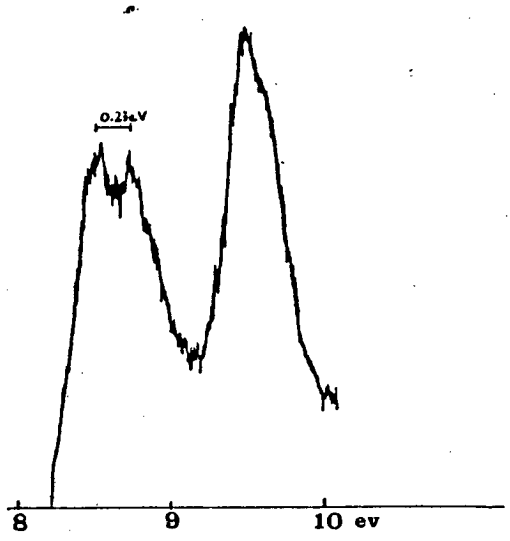
0.21eV
8
9
10 ev

FIG CONT
86

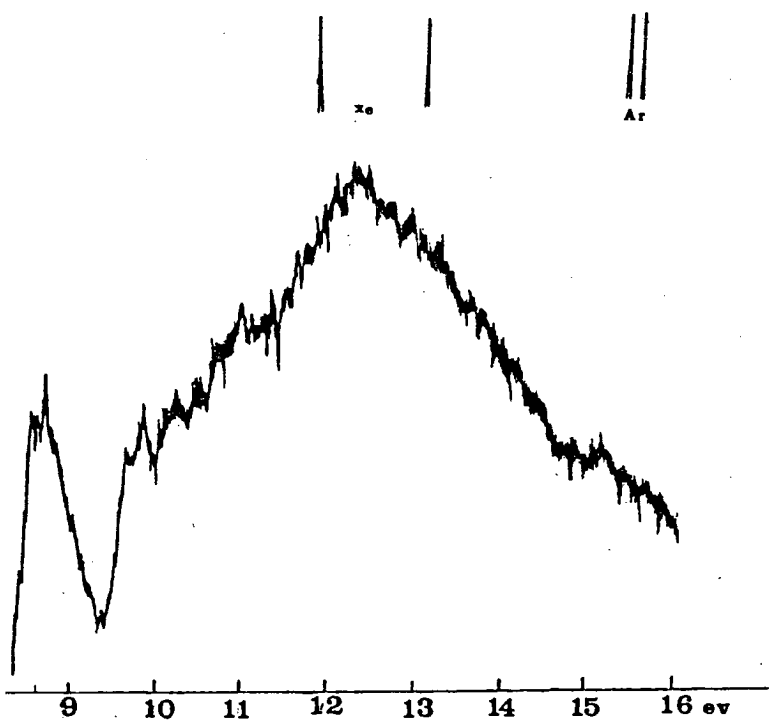
Xe
Ar
9
10
11
12
13
14
15
16 ev

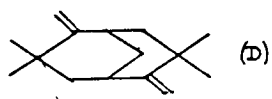
(D)

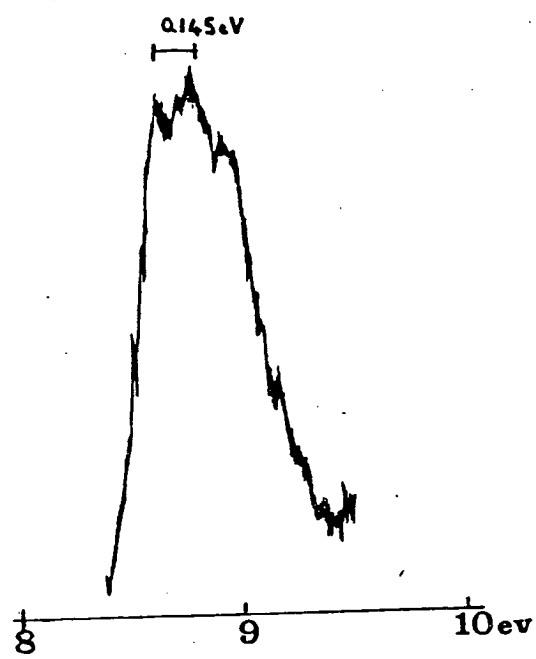
0.145eV
8
9
10ev

FIG 87 PROBABLE MOLECULAR CONFORMATIONS

twin chair (A)

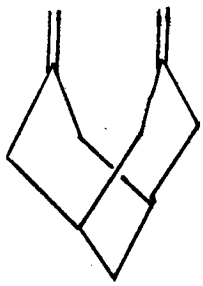

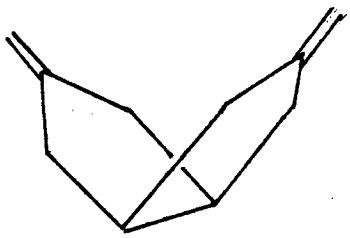

(B) butterfly

twin twist boat (C)

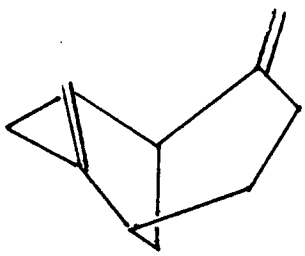

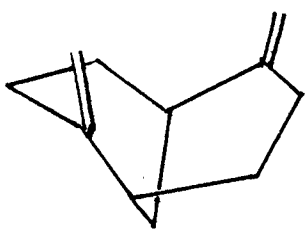

(D) twin twist boat

twin chair (E)

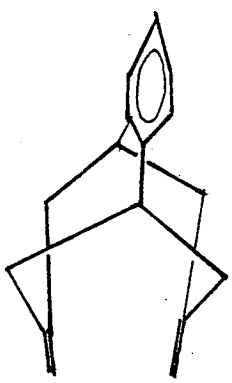

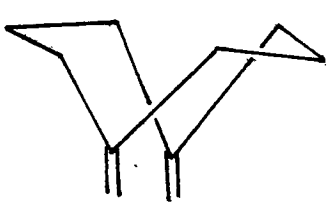

(F) boat

The splittings of the olefinic levels can give some information as to the relative conformations of the molecules; the greater the interaction the larger the splitting. If any interaction takes place this indicates that the $\pi_{C=C}$ levels are favourably orientated (i.e. not orthogonal) with respect to each other, and that they are reasonably close. Inspection of the experimental splittings in Table (56) shows that in all cases the interaction of the $\pi_{C=C}$ levels is small since all splittings are < 0.5 eV. The largest splitting 0.23 eV is exhibited by molecule F; this is a floppy molecule which can exist in numerous conformations. The relatively large split however indicates that the predominant gas phase conformation is one with the dienes close together and possibly eclipsed, see Fig (87). The PES of (A) shows only a small splitting of $\pi_{C=C}$; this is surprising since the molecule is expected to be in the twin chair conformation as it readily undergoes cycloaddition. It is possible however that even in the twin chair conformation the distance between the olefinic double bonds could be too large for a significant through space interaction and this would account for the relatively small observed splitting. Other molecular conformations for this structure are twin boat and chair/boat, however as the molecule readily undergoes cycloaddition, the twin chair conformation is the most likely.

The presence of the methyl groups in molecule (D) prevents it existing in the twin chair conformation. More likely is the twin twist boat conformation, shown in Fig. (87), since there is a splitting of 0.15 eV observed for the $\pi_{C=C}$ levels. In this conformation the olefinic bonds are close and favourably orientated for interaction, whereas in the chair boat and other twist boat conformations they are distant and co-linear.

The first IP in the PES of (B) is effectively the degenerate pair of $\pi_{C=C}$ levels, with associated vibrational structure. This is indicative that no π-π interaction is taking place, and that the butterfly conformation of the molecule is fixed such that the double bonds are distant, Fig. (87).

The observed splitting of the $\pi_{C=C}$ levels in the PES of molecule (C) is almost identical to that of molecule (D), and again is considered to be too large to atribute to vibrational structure. The similarity in the shape and splitting of the first two IP's for these molecules, Fig (87), indicates that their conformations are the same, twin twist boat.

The presence of the benzene ring in molecule (E) results in an extra peak in the 8 to 10 eV region, which can be attributed to the two benzene e_{1g} π levels. This, of course, brings an additional degree of uncertainty to the assignment of the diene levels, and calculations are necessary for a

more conclusive assignment. The best we can say is that the splitting is small, about 0.15 eV, if we assign the first two peaks to the $\pi_{C=C}$ combinations. This indicates that the molecule is in the twin chair conformation, since no interaction could take place in the boat chair conformation. That the olefinic bonds are photochemically cyclized is further indication that the twin chair conformation is the most probable.

It should be noted that great difficulty was experienced in obtaining some of the spectra since several of the compounds, although not sufficiently volatile to give good count rates when inserted into the spectrometer through the volatile sample inlet system, were too volatile to input with the heated sample probe, hence the poor signal to noise ratio. These spectra could not be repeated when the CAT became available as the amounts of the samples initially available were so small as to be depleted in the first analysis. However, some of sample (A) remained and an improved (CAT) spectrum was obtained, see Fig (86(A)).

To date no photoelectron spectra for these molecules have been reported.

References

1. M. Paddon-Row, R. Warrener, Tet.Lett.15, 1405, (1972).
2. M. Paddon-Row, R. Warrener, J.Chem.Soc.Chem.Comm., 78, (1978).
3. B. Bak, J.J. Led, E.J. Pedersen, J.Mol.Struct., 3, 369, (1969).
4. E.A. McNeil, Z.R. Scholer, J.Mol.Struct., 31, 65, (1976).
5. K. Brendhaugen, M. Fikee, H.M. Seup, Acta.Chem.Scand., 27, 1107, (1973).
6. F. Chionig, S.H. Bauer, J.Am.Chem.Soc., 91, 1898, (1969).
7. H. Farries, Fourth Year Chemical Physics Project Report, University of Edinburgh, (1979).
8. U.A. Maumov, U.N. Semashko, S.A. Sohaidalin, Zh. Strukt.Khim, 14, 595, (1973).
9. H.J. Heise, W.J. Adams, L.S. Bartell, Tetrahedron, 25, 3045, (1969).
10. J. Bregman, S.H. Bauer, J.Am.Chem.Soc., 77, 1955, (1955).
11. Crowfoot in Clare, Johnson, Robinson, "The Chemistry of Pennicilin", Princetown University Press (NY), (1949).
12. J.S. Binkley, J.A. Pople, W.J. Hehre, Chem.Phys.Lett., 36, 1 (1975).
13. G. Bieri, E. Heilbronner, M.J. Goldstein, R.S. Leight, M. Lipton, Tetrahedron Lett., 581, 1975.
14. B. Solouki, H. Boch, R. Appel, Chem.Ber., 108, 897, (1975).
15. C. Muller, A. Schweig, J.Am.Chem.Soc., 96, 280, (1974).

16. H. Schmidt, A. Schweig, Tet.Lett., 16, 1437, (1973).

17. K. Yoshuhawa, M. Hashimoto, I. Morishama, J.Am.Chem.Soc., 97, 4283, (1975); 96, 288, (1974).

18. H. Schmidt, A. Schweig, Chem.Ber. 107, 725, (1974).

19. M. Alemark, J.E. Backvall, C. Moberg, B. Akermark, L. Åsbrink, B. Roos, Tetrahedron, 30, 2503, (1974).

20. For example see W.J. Rabalais, Principles of Photoelectron Spectroscopy, Wiley Interscience, (1977).

21. R. Hoffmann, Account Chem. Res., 4, 1, (1971).

22. A. Schweig, V. Eck, C. Muller, R. Schulz, H. Verneer, J.Electron.Spectros. and Related Phenom., 17, 67, (1979).

23. A.G. Anderson, D.R. Fagerburg, Tetrahedron, 29, 2873, (1973).

24. W. Lwowski, T.W. Mattingly, J.Am.Chem.Soc., 87, 1947, (1965).

25. P. Bischoff, E. Heilbronner, Helv. Chim.Acta, 53, 195, (1970).

26. R.S. Mulliken, J.Chem.Phys., 7, 539, (1939).

27. G. Bien, F. Burger, E. Heilbronner, J.P. Mair, Helv.Chim.Acta, 60, 2213, (1977).

28. W.R. Rodwell, M.F. Guest, D.T. Clark, D. Shuttleworth, Chem.Phys.Lett., 45, 50, (1977).

29. C. Batich, O. Ermer, E. Heilbronner, J.R. Wiseman, Angew.Chem. 12, 312, (1973).

30. O. Ermer, E. Heilbronner, J.R. Wiseman, Angew.Chem., 85, 302, (1972).

31. C. Batich, P. Bischoff, E. Heilbronner, J.Electron. Spectros. Relat.Phenom., 1, 333, (1973).

APPENDIX A

Double Zeta Basis Set*

	OXYGEN		NITROGEN		CARBON	
	coefficients	exponents	coefficients	exponents	coefficients	exponents
1s	0.002031	7816.54	0.002004	5909.440	0.002029	4232.61
	0.015436	1175.82	0.015310	887.451	0.015535	634.882
	0.073771	273.188	0.074293	204.749	0.075411	146.097
	0.247606	81.1696	0.253364	59.5878	0.257121	42.4974
	0.611832	27.1836	0.600576	19.9981	0.596555	14.1892
	0.241205	3.4136	0.245111	2.8864	0.242517	1.9666
1s′	1.000000	9.5322	1.0	7.1927	1.0	5.1477
2s	1.000000	2.9393	1.0	0.7	1.0	0.4962
2s′	1.000000	0.2846	1.0	0.2133	1.0	0.1533
2p	0.019580	35.1832	0.018257	26.786	0.018534	18.1557
	0.124139	7.9040	0.116407	5.9564	0.115442	3.9864
	0.394727	2.3051	0.390111	1.7074	0.396206	1.1429
	0.627375	0.7171	0.637221	0.5314	0.640089	0.3594
2p′	1.000000	0.2137	1.0	0.1654	1.0	0.1146

	HYDROGEN	
	coefficients	exponents
1s	0.032828	13.3615
	0.231208	2.0133
	0.817238	0.4539
1s′	1.0	0.1233

*The Gaussian Basis Sets given in this Appendix are from T.H.Dunning, Journal of Chemical Physics, 53, 2823, (1970) (Double Zeta), and see below.

APPENDIX(A) Minimal Basis Set*

	OXYGEN		NITROGEN		CARBON	
	coefficients	exponents	coefficients	exponents	coefficients	exponents
1s	Ø.004324	2714.89	Ø.004479	2038.41	Ø.ØØ4813	1412.29
	Ø.032265	415.725	Ø.034581	3Ø1.629	Ø.Ø37267	2Ø6.885
	Ø.156410	91.9805	Ø.164263	66.463	Ø.172403	45.8498
	Ø.447813	24.4515	Ø.453898	17.8Ø81	Ø.459261	12.3887
	Ø.481602	7.22296	Ø.463979	5.3Ø452	Ø.456185	3.72337
2s	Ø.524708	Ø.955612	Ø.513598	Ø.756202	Ø.522342	Ø.557981
	Ø.616734	Ø.29Ø043	Ø.6Ø5721	Ø.23173	Ø.594186	Ø.174021
2p	Ø.129373	7.65485	Ø.119664	6.29636	Ø.112194	4.74919
	Ø.481269	1.60223	Ø.474629	1.3Ø369	Ø.466227	Ø.966859
	Ø.6Ø4484	Ø.36Ø279	Ø.611142	Ø.3Ø3209	Ø.622569	Ø.226177

	SULPHUR	
	coefficients	exponents
1s	Ø.ØØ1575	25506.3
	Ø.Ø12217	3812.82
	Ø.Ø61166	86Ø.556
	Ø.211761	242.94Ø
	Ø.452Ø13	79.Ø448
	Ø.4ØØ193	27.5705
2s	Ø.382204	6.49476
	Ø.657797	2.41078
3s	Ø.579568	Ø.152296
	Ø.463545	Ø.412644
2p	Ø.Ø29Ø69	129.089
	Ø.179893	29.63Ø5
	Ø.47817	8.84715
	Ø.496736	2.85576
3p	Ø.441Ø37	Ø.65Ø366
	Ø.664344	Ø.182Ø22
3d	1.Ø	Ø.541

	HYDROGEN	
	coefficients	exponents
1s	Ø.Ø7Ø48	6.99357
	Ø.40789	1.0587
	Ø.64767	Ø.235235

*From B.Roos, P.Seigbahn
Theor. Chim. Acta, 17, 209, (1970)

APPENDIX (B)**

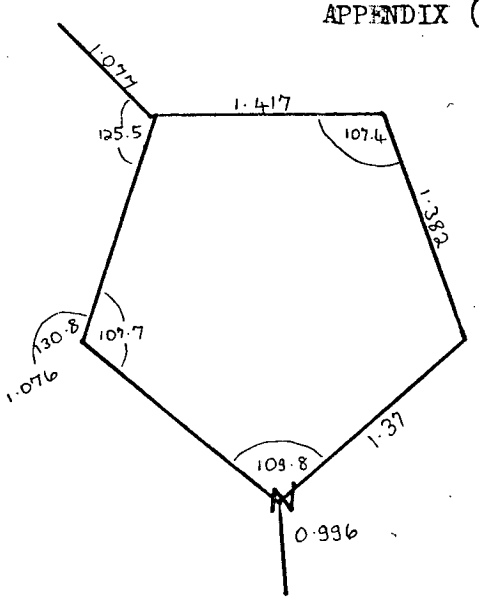

PYRROLE

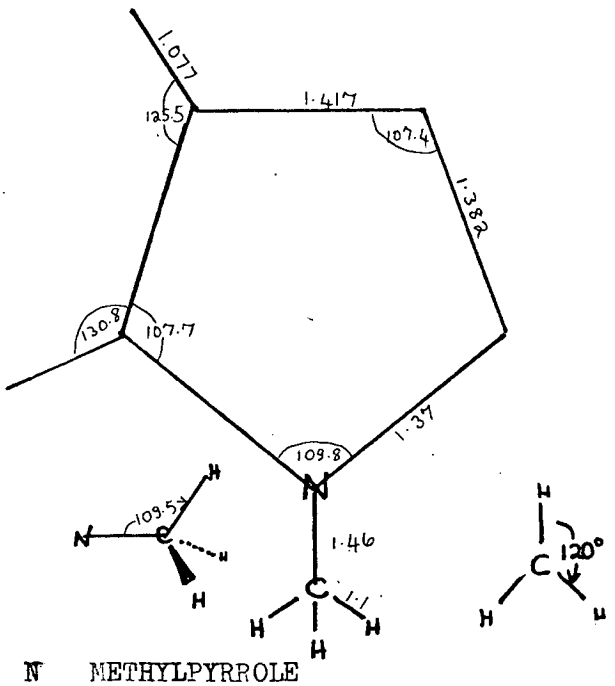

N METHYLPYRROLE

(The geometric parameters of the methyl group were used for all methyl isomers)

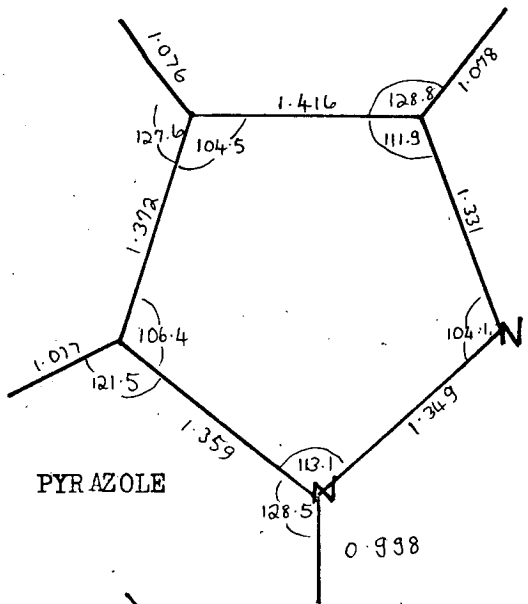

PYRAZOLE

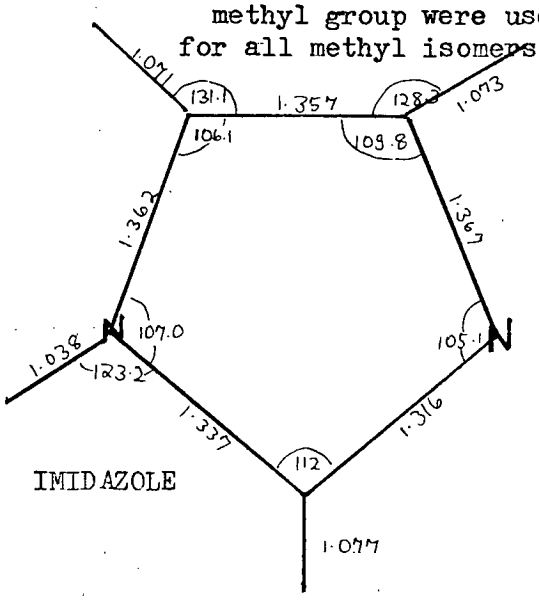

IMIDAZOLE

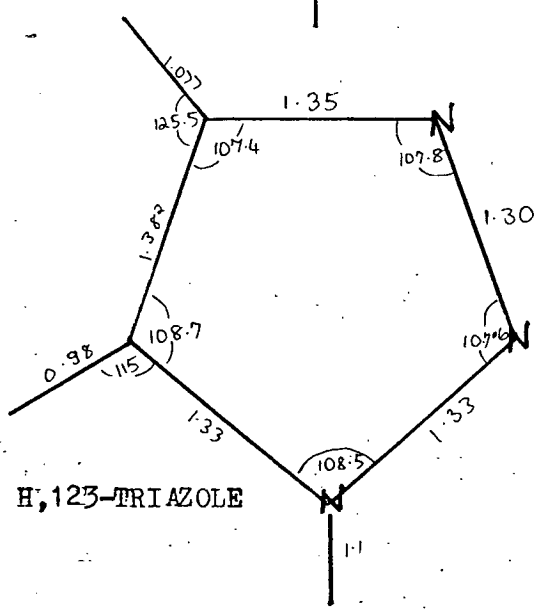

1 H,123-TRIAZOLE

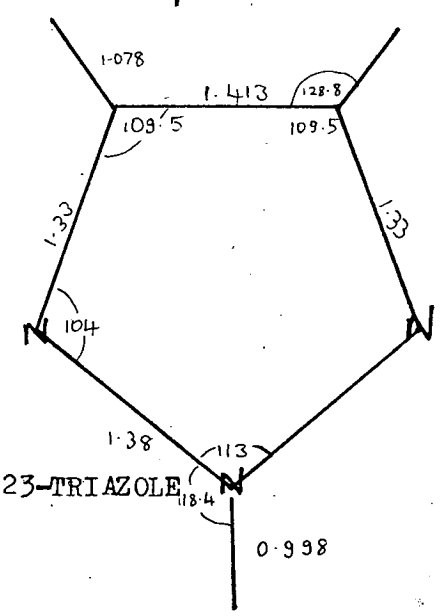

2H-123-TRIAZOLE

**All bond angles in ; all bond lengths in angstrom(A).

APPENDIX (B) Cont.**

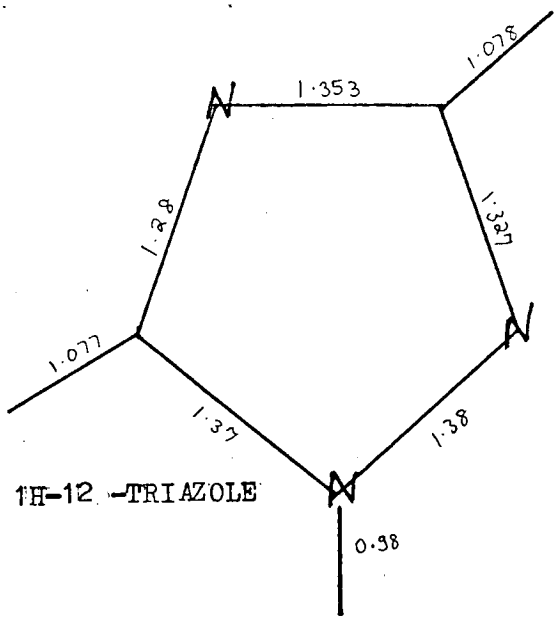

1H-12 -TRIAZOLE

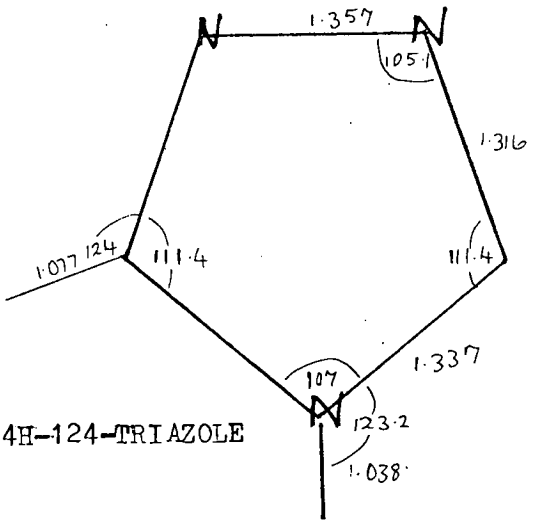

4H-124-TRIAZOLE

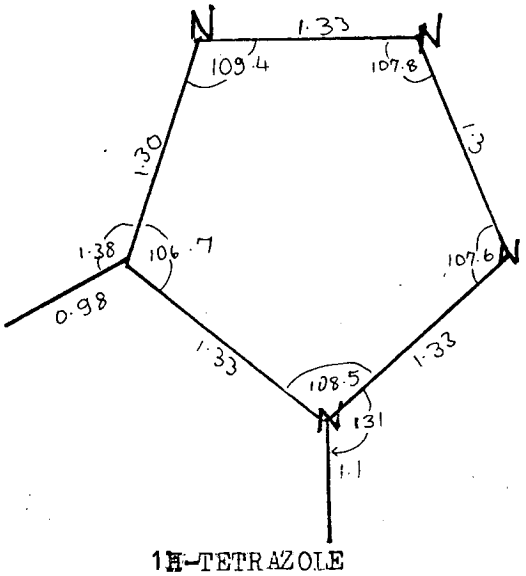

1H-TETRAZOLE

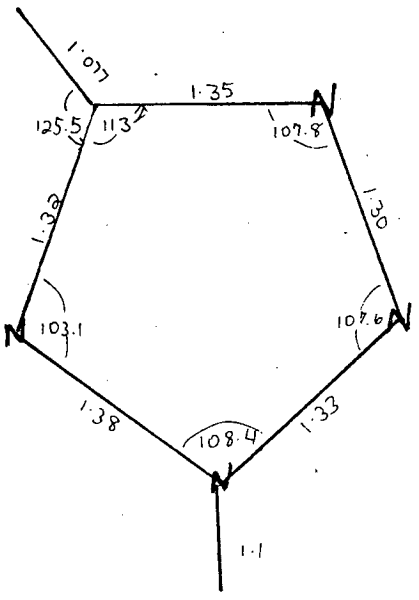

2-H-TETRAZOLE

*All methyl substituted compounds geometries were constructed using the standard methyl unit along the N-H bond.

**All bond angles in degrees; All bond lengths in Angstrom.

APPENDIX (B) Cont.**

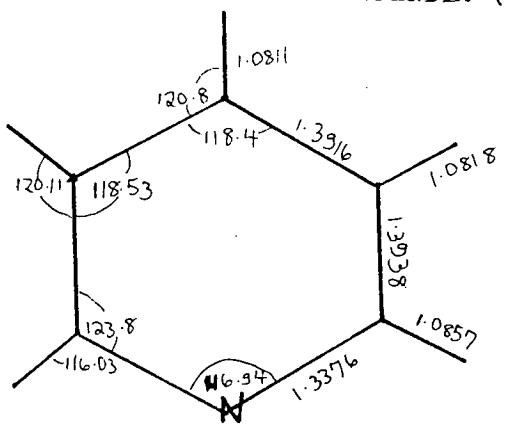

PYRIDINE

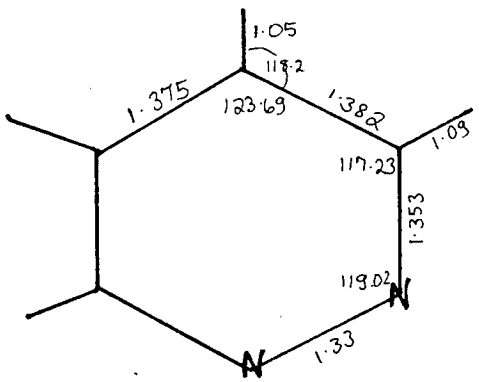

PYRIDAZINE

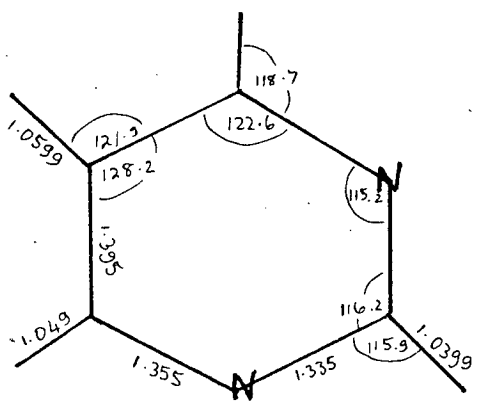

PYRIMIDINE

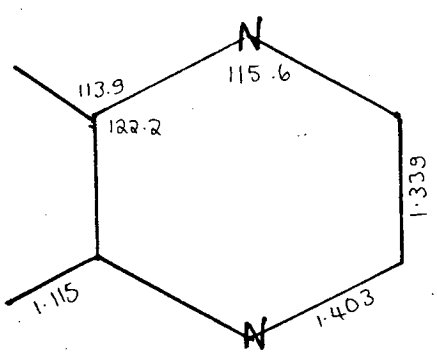

PYRAZINE

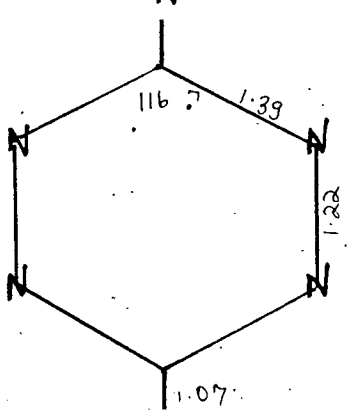

S-TETRAZINE

**All bond angles in degrees

APPENDIX (B) Cont.**

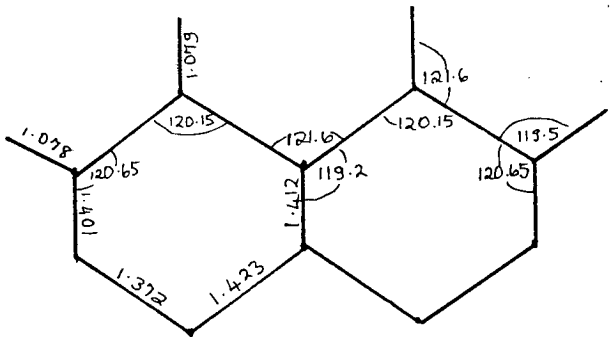

NAPHTHALENE

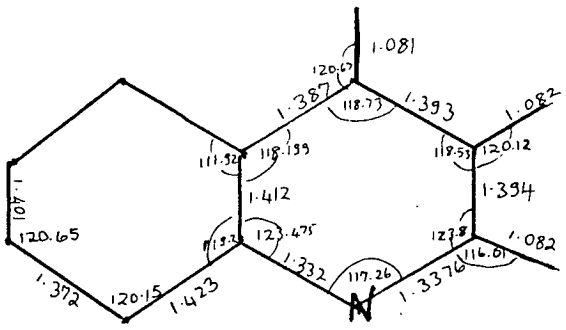

QUINOLINE

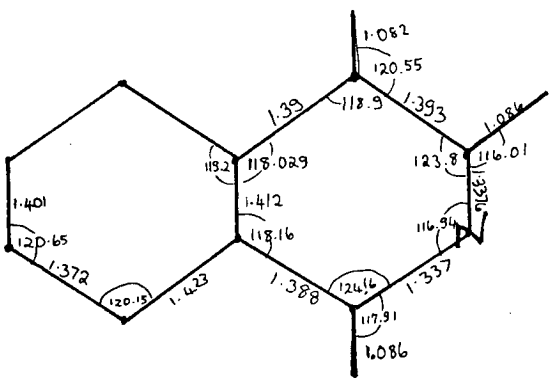

ISOQUINOLINE

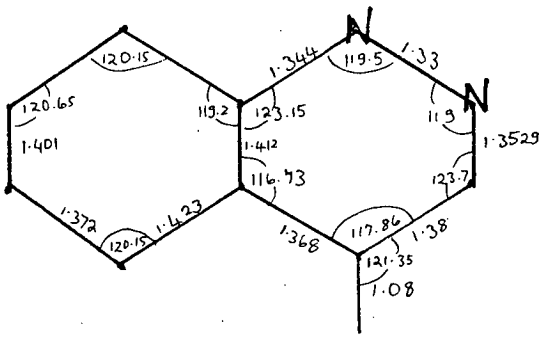

CINNOLINE

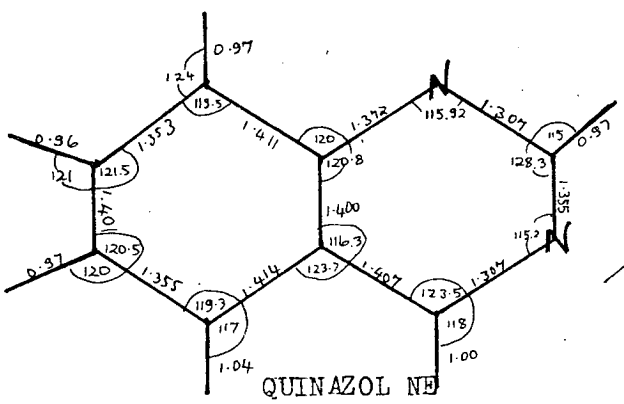

QUINAZOL NE

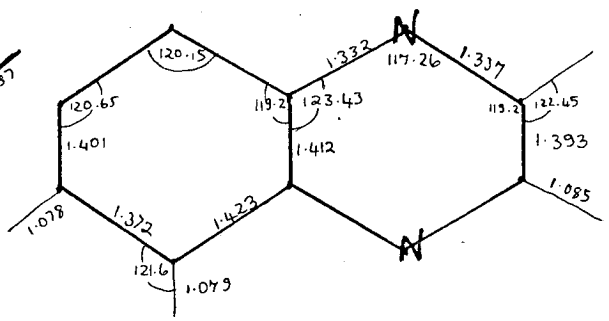

QUINOXALINE

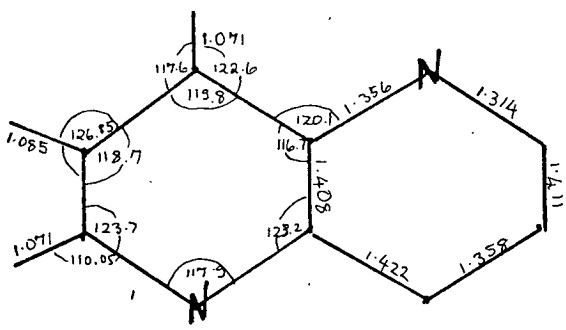

1,5-DIAZANAPHTHALNNE

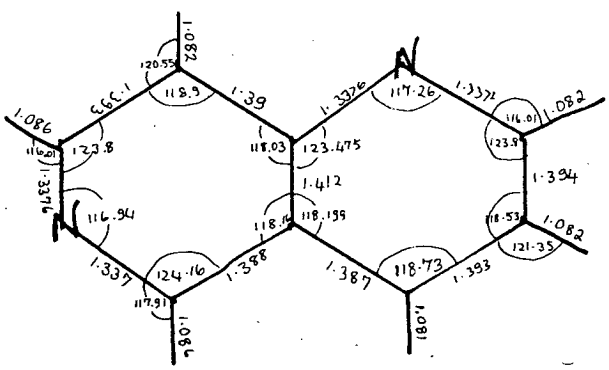

1,6-DIAZANAPHTHALENE

**All bond angles in degrees; All bond lengths in Angstrom.

APPENDIX (B) Cont.**

1,7-DIAZANAPHTHALENE

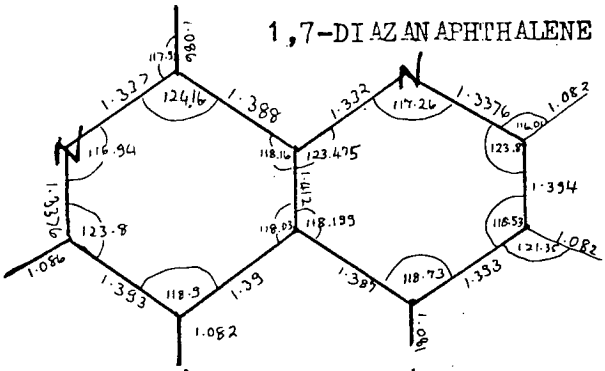

*1,8-DIAZANAPHTHALENE

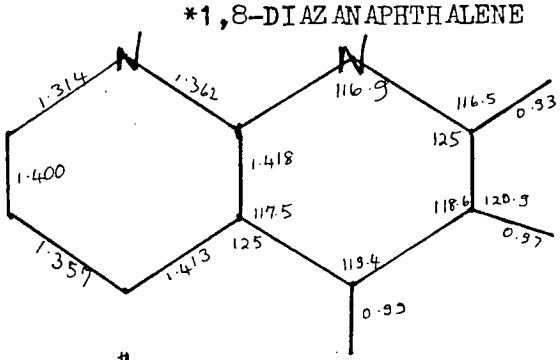

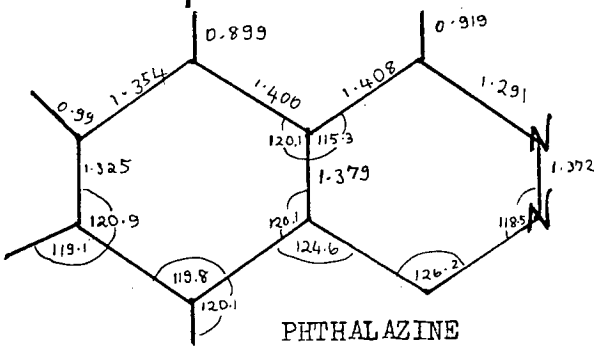

PHTHALAZINE

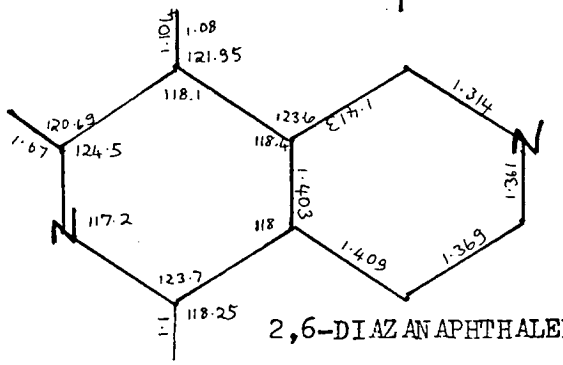

2,6-DIAZANAPHTHALENE

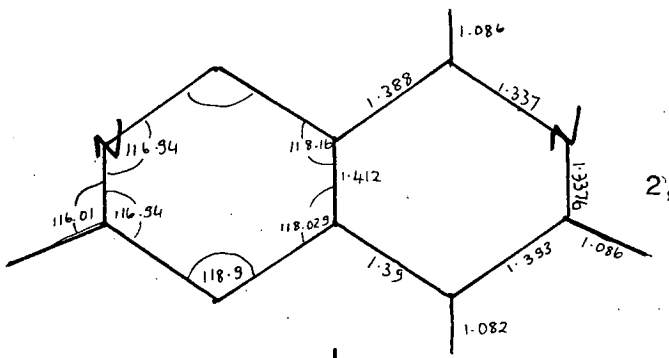

2,7-DIAZANAPHTHALENE

**All angies in degrees; All bond lengths in Angstrom.

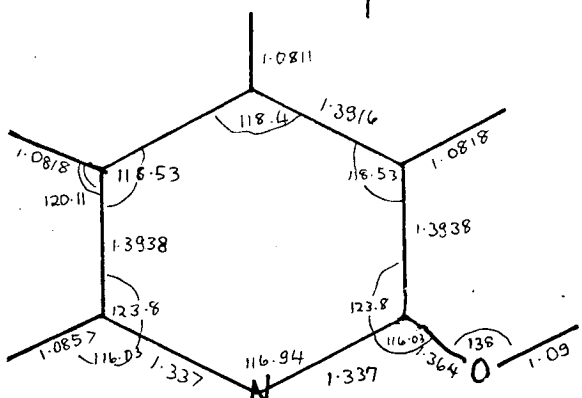

2-HYDROXYPYRIDINE

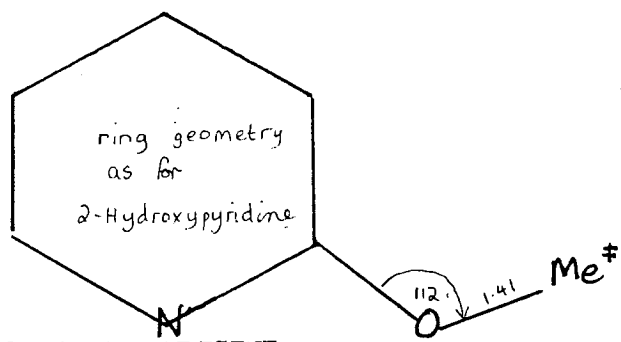

2-METHOXYPYRISINE

‡(standard methyl unit as above)

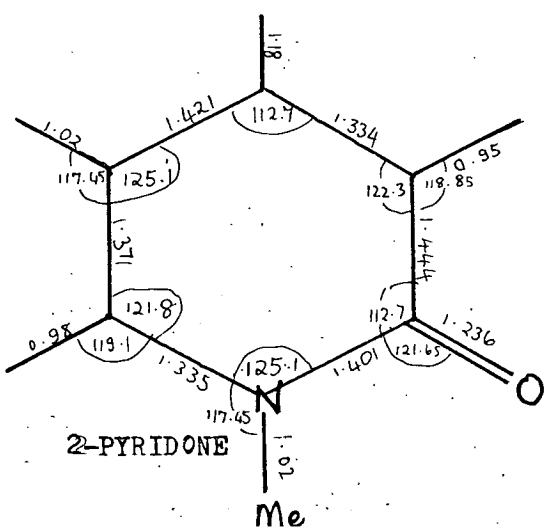

2-PYRIDONE

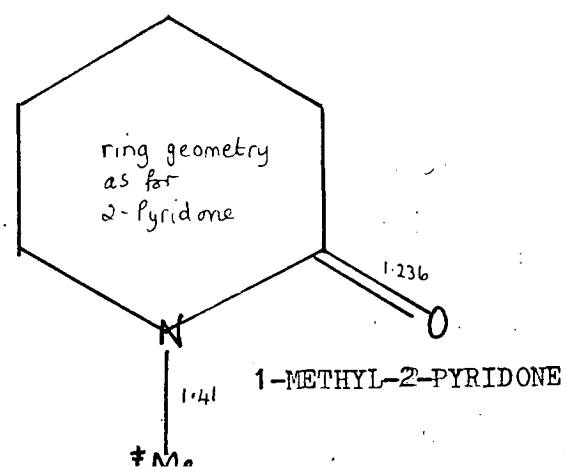

1-METHYL-2-PYRIDONE

Appendix C

Lagrange Four Point Interpolation

The formula is

$$f(x_o + ph) = A_{-1}f_{-1} + A_o f_o + A_1 f_1 + A_2 f_2 + R_3(P)$$

$$\frac{-p(p-1)(p-2)f_{-1}}{6} + \frac{(p^2-1)(p-2)f_o}{2}$$

$$\frac{-p(p+1)(p-2)f_1}{2} + \frac{p(p^2-1)f_2}{6} \qquad \text{(i)}$$

For our example page ( )

f_{-1} = Energy at F = 0.0; f_o = Energy at F = 0.5; f_1 = Energy at F = 1.0 etc.

h is the step length

x_o is the value of 'F' at the second point (= 0.5)

By differentiation of (i) a turning point can be found at value(of p given by solutions of the quadratic equation

$$(-\tfrac{1}{2}f_{-1} + \tfrac{3}{2}f_o - \tfrac{3}{2}f_1 + \tfrac{1}{2}f_2)p^2 + (f_{-1} - 2f_o + f_1)p$$

$$+ (-\tfrac{1}{3}f_{-1} - \tfrac{1}{2}f_o + f_1 - \tfrac{1}{6}f_2) = 0$$

EPILOGUE

A thesis is never finished - just abandoned.